NASA TM X-71996

NASA TECHNICAL MEMORANDUM

NASA TM X-71996

COPY NO.

CLASSIFICATION CHANGE

TO = UNCLASSIFIED [redacted]

N/S-5

By authority of [redacted] NASA HG Ltr 10/9/80

Changed by Galenik Merrill Date 11/18/80

WIND TUNNEL INVESTIGATION OF SEVERAL HIGH ASPECT-RATIO SUPERCRITICAL WING CONFIGURATIONS ON A WIDE-BODY-TYPE FUSELAGE [redacted]

By Dennis W. Bartlett

(NASA-TM-X-71996) WIND-TUNNEL INVESTIGATION OF SEVERAL HIGH ASPECT-RATIO SUPERCRITICAL WING CONFIGURATIONS ON A WIDE-BODY-TYPE FUSELAGE (NASA) 407 p HC A18/MF A01 CSCL 01A G3/02

N83-11070

Unclas 31564

[redacted]AL SECURITY IN ..MATION
Unau[redacted] Subject to
Cri[redacted]

This informal documentation mediu
special release of technical informa
may not meet NASA formal editing
vised, or may be incorporated in a

ORIG... OF POOR Q...

National Aeronautics and Space Administration

Langley Research Center
Hampton, Virginia 23665

ORIGINAL PAGE IS
OF POOR QUALITY

1. Report No. NASA TM X-71996	2. Government Accession No.	3. Recipient's Catalog No.
4. Title and Subtitle Wind-Tunnel Investigation of Several High Aspect-Ratio Supercritical Wing Configurations on a Wide-Body-Type Fuselage		5. Report Date July 1977
		6. Performing Organization Code
7. Author(s) Dennis W. Bartlett		8. Performing Organization Report No.
		10. Work Unit No. 516-53-01-11
9. Performing Organization Name and Address NASA Langley Research Center Hampton, VA 23665		11. Contract or Grant No.
		13. Type of Report and Period Covered Technical Memorandum
12. Sponsoring Agency Name and Address National Aeronautics & Space Administration Washington, DC 20546		14. Sponsoring Agency Code

15. Supplementary Notes

16. Abstract

An investigation has been conducted in the Langley 8-foot transonic pressure tunnel on two aspect-ratio 11.95 supercritical wings that were tested in combination with a representative wide-body-type fuselage. The two supercritical wings have identical planforms for equal sweep angles and differ only in thickness. Each wing was tested at quarter-chord sweep angles of 27° and 30°, and at the higher sweep angle, the aspect ratio is reduced to 11.36. At 27° of quarter-chord sweep, the thicker supercritical wing (SCW-1) has maximum streamwise thickness-to-chord ratios of 0.16 at the wing-fuselage juncture, 0.14 at the planform break station and 0.12 at the tip. The thinner wing (SCW-2) has maximum streamwise thickness-to-chord ratios of 0.144, 0.12 and 0.10 at the same stations respectively. Tests were also conducted on the thinner supercritical wing at the 27° sweep angle with a 15.24 cm (6.0 in.) shorter span which results in an aspect ratio of 10.25. For comparison, data were obtained on a current wide-body transport wing (AR=7) that was tested on the same fuselage used with the supercritical wings.

17. Key Words (Suggested by Author(s)) Supercritical wings; Supercritical airfoil application; Subsonic transport design	18. Distribution Statement [redacted]

19. Security Classif. (of this report) [redacted]	20. Security Classif. (of this page) U	21. No. of Pages	22. Price

Unauthorized Di... Criminal Sanctions

SUBJECT TO GE... SIFICATION SCHEDULE OF EXECUTIVE ... AUTOMATICALLY DOWNGRADED AT ... ERVALS AND DECLASSIFIED ON DEC 31 1983

WIND-TUNNEL INVESTIGATION OF SEVERAL HIGH ASPECT-RATIO SUPERCRITICAL WING CONFIGURATIONS ON A WIDE-BODY-TYPE FUSELAGE

Dennis W. Bartlett

NASA Langley Research Center
Hampton, VA 23665

SUMMARY

An investigation has been conducted in the Langley 8-foot transonic pressure tunnel on two aspect-ratio 11.95 supercritical wings that were tested in combination with a representative wide-body-type fuselage. The two supercritical wings have identical planforms for equal sweep angles and differ only in thickness. Each wing was tested at quarter-chord sweep angles of 27^o and 30^o, and at the higher sweep angle, the aspect ratio is reduced to 11.36. At 27^o of quarter-chord sweep, the thicker supercritical wing (SCW-1) has maximum streamwise thickness-to-chord ratios of 0.16 at the wing-fuselage juncture, 0.14 at the planform break station and 0.12 at the tip. The thinner wing (SCW-2) has maximum streamwise thickness-to-chord ratios of 0.144, 0.12 and 0.10 at the same stations respectively. Tests were also conducted on the thinner supercritical wing at the 27^o sweep angle with a 15.24 cm (6.0 in.) shorter span which results in an aspect ratio of 10.25. For comparison, data were obtained on a current wide-body transport wing (AR=7) that was tested on the same fuselage used with the supercritical wings.

Longitudinal force and moment data were obtained over a Mach number range that generally varied from 0.60 to 0.82 for the supercritical-wing configurations and from 0.60 to 0.90 for the simulated wide-body configuration. The angle-of-attack range varied from about -2^o to $+8^o$ and all results were obtained at a unit Reynolds number of [redacted] (5 X 10^6ft).

At a lift coeficient of 0.60, the thicker supercritical wing has drag-rise Mach numbers (point where $\partial C_D/\partial M = 0.1$) of 0.783 and 0.802 at quarter-chord sweep angles of 27° and 30° respectively, whereas the thinner supercritical wing has drag-rise Mach numbers of 0.802 and 0.811 for the same conditions. The simulated wide-body configuration, with 35° of sweep at the quarter chord, has a drag-rise Mach number of 0.835 at a lift coefficient of 0.45. Range factors, computed at the drag-rise Mach number ($M_{DR}(L/D)/sfc$), vary between 21-percent and 27-percent higher for the supercritical-wing configurations as compared to the range factor for the simulated wide-body configuration.

Based on the breaks in the lift and pitching-moment curves at Mach numbers near drag-rise, the thinner supercritical wing would have a higher buffet-onset lift coefficient than the thicker supercritical wing. Furthermore, compared with the simulated wide-body configuration, the thinner supercritical wing has approximately the same buffet margin (≈0.4g above cruise lift coefficient) at Mach numbers near the drag rise.

Maximum lift-curve slopes for the supercritical-wing configurations vary between 0.185 and 0.20 at a lift coefficient of 0.60, while the maximum lift-curve slope for the simulated wide-body configuration is about 0.14 at a lift coefficient of 0.45. In addition, the pitching-moment coefficients at zero lift ($C_{m,o}$) are considerably more negative for the supercritical wing configurations than for the simulated wide-body configuration. This is a reflection of both the higher camber and larger aspect ratios of the supercritical wings.

INTRODUCTION

Early NASA emphasis on supercritical airfoil application to subsonic transport wing design was directed toward increasing the cruise Mach number of

 [redacted]L-this class of airplanes. This work involved the flight-testing of an advanced transport-type supercritical wing on a TF-8A test-bed airplane (ref. 1) and the follow-on ATT studies (ref. 2).

Since that time and primarily because of increased fuel costs, the emphasis for supercritical airfoil application to transports has shifted to allow for an increase in lift-to-drag ratios rather than cruise Mach number. To accomplish this, these types of supercritical wings relative to current transport-type wings would have increased aspect ratios, increased thickness-to-chord ratios, increased design lift coefficient, and reduced sweepback.

As part of this effort, tests have been conducted in the Langley 8-foot transonic pressure tunnel on two aspect-ratio-11.95 wings incorporating NASA supercritical airfoils. Each wing was tested in combination with a representative wide-body-type fuselage. The two supercritical wings have identical planforms for equal sweep angles and differ only in thickness. For 27° of quarter-chord sweep, the thicker wing (SCW-1) has maximum streamwise thickness-to-chord ratios of 16-percent at the wing-fuselage juncture, 14-percent at the planform break and 12-percent at the tip. The thinner wing (SCW-2) has maximum streamwise thickness-to-chord ratios of 14.4-percent, 12-percent and 10-percent at the same stations respectively. In addition to 27°, each wing was tested with 30° of quarter-chord sweep. Tests were also conducted on the thinner supercritical wing with the span reduced by 15.24 cm (6.0 in.) which produces an aspect ratio of 10.25. For comparison, data were obtained on a current wide-body transport wing (AR=7) in conjunction with the same fuselage used for the supercritical-wing tests.

Results of the present investigation are for wing-body combinations only. Longitudinal force and moment data are presented over a Mach number range that generally varied from 0.60 to 0.82 for the supercritical-wing configurations and from 0.60 to 0.90 for the simulated current wide-body configuration. Limited pressure data were obtained from two rows of surface static pressure orifices positioned on the fuselage side above and below the wing root for the supercritical-wing configurations. In addition, lateral-directional data are presented for supercritical wing-1 ($\Lambda_{c/4} = 30^{\circ}$) at a sideslip angle of -2.5°. All data were obtained at a unit Reynolds number of 16.4×10^{6}/m (5×10^{6}/ft).

SYMBOLS

Results presented herein are referred to the stability-axis system for the longitudinal aerodynamic characteristics and to the body-axis system for the lateral-directional aerodynamic characteristics. Force and moment data for all configurations have been reduced to conventional coefficient orm based on the geometry of the trapezoidal planform of the aspect-ratio-11.95 supercritical wing at 27° quarter chord sweep (fig. 1(b)). Moments are referenced to the quarter-chord point (fuselage station 84.605 cm (33.309 in.)) of the mean geometric chord of the trapezoidal planform at the 27° quarter-chord sweep angle. Although a common reference area was used for all configurations in reducing the force data to coefficient form, the pitching moments for several configurations were computed about a second reference point. Increasing the quarter-chord sweep to 30° (SCW-1b and SCW-2b) translates the quarter-chord point aft, and therefore the pitching moments for these configurations were computed about an additional reference point-fuselage station 86.068 cm (33.885 in.). (See fig. 1(c)). Also, the pitching moments for the aspect-ratio-10.25 supercritcal wing were computed about a second reference point (fuselage station 83.409 cm (32.838 in.)), since reducing the span would translate the quarter-chord point of the mean geometric chord forward. (See fig. 1(e).)

It should be noted that the trapezoidal-wing area for both the simulated wide-body configuration and the aspect-ratio-11.95 supercritical wing are equal, and the quarter-chord point of the mean geometric chord for the simulated wide-body configuration is also located at fuselage station 84.605 cm (33.309 in.). (See fig. 1(e).)

All dimensional values are given in both the International System of Units (SI) and U. S. Customary Units; however, measurements and calculations were made in U. S. Customary Units.

b	wing span of aspect-ratio-11.954 supercritical wing, 151.821 cm (59.772 in.)
C_D	drag coefficient, Drag/qS
C_L	lift coefficient, Lift/qS
C_l	rolling-moment coefficient, Rolling moment/qSb
C_m	pitching-moment coefficient, Pitching-moment/qS$\bar{c}$
$C_{m,o}$	pitching-moment coefficient at zero lift
C_n	yawing-moment coefficient, Yawing moment/qSb
c_p	pressure coefficient, $\dfrac{p_l - p_\infty}{q}$
C_y	side-force coefficient, Side Force/qS
C_{L_α}	lift-curve slope, $\partial CL/\partial\alpha$, per degree
$C_{m_{C_L}}$	longitudinal-stability derivative, $\partial Cm/\partial CL$
c	local streamwise chord of wing
$\bar{c}$	mean geometric chord of the trapezoidal planform of the aspect-ratio-11.95 supercritical wing ($\Lambda_{c/4} = 27^{o}$) 13.757 cm (5.416 in.)

i_w wing-to-fuselage mounting angle, positive for leading edge up, deg.

M free-stream Mach number

M_{DR} drag-rise Mach number (point where $\partial C_D / \partial M = 0.1$)

P_l local static pressure

P_∞ free-stream static pressure

q free-stream dynamic pressure

R Reynolds number

S area of trapezoidal planform of aspect-ratio-11.95 supercritical wing ($\Lambda_{c/4} = 27^o$) including fuselage intercept, 0.193 m^2 (2.0754 ft^2)

SS_r structural span from wing root to tip, measured along wind midchord

SS_b structural span from wing planform break station to wing tip, measured along wind midchord

t maximum local wing thickness

x streamwise distance measured from leading edge of wing parallel to waterline, positive toward wing trailing edge

y spanwise distance measured normal to model plane of symmetry, 0 at fuselage centerline

z vertical distance measured normal to x, positive up

α angle of attack, referred to fuselage waterline, deg.

β angle of sideslip, referred to fuselage centerline, positive when nose is left, deg.

ε local streamwise wing section incidence angle referred to fuselage waterline, positive for leading edge up, deg.

λ taper ratio of wing trapezoidal planform, c_{tip}/c_{root}

Γ wing dihedral angle, deg.

Subscripts:

b wing planform break station

r wing root (fuselage-juncture) station

T location of wing boundary-layer grit trips

Abbreviations:

c.g.	assumed center of gravity for pitching-moment reference
F.S.	fuselage station (Fuselage station of nose is 14.704 cm (5.789 in.))
M. G. C.	mean geometric chord, $\bar{c}$
sfc	specific fuel consumption
SCW	supercritical wing
L.S.	lower surface
U.S.	upper surface

TEST FACILITY

The investigation was conducted in the Langley 8-foot transonic pressure tunnel. (See ref. 3.) This facility is a continuous-flow single-return rectangular slotted-throat tunnel having controls that allow for independent variation of Mach number, density, stagnation temperature, and dewpoint temperature. The test section is approximately 2.2 m (7.1 ft.) square (same cross-sectional area as that of a circle with a 2.4-m (8 ft.) diameter) with the upper and lower walls axially slotted to permit the test-section Mach number to be changed continuously throughout the transonic speed range. The slotted top and bottom walls each have an average open ratio of approximately 0.06. The stagnation pressure in the tunnel can be varied from a minimum of 0.25 atm (1 atm = 0.101 MN/m^2) at all Mach numbers to a maximum of approximately 2.00 atm at Mach numbers less than 0.40. At transonic Mach numbers, however, the maximum stagnation pressure that can be obtained is about 1.5 atm.

MODEL DESCRIPTION

Drawings of the model are presented in figures 1 and 2, and photographs of the model installed in the 8-foot transonic pressure tunnel are shown in figure 3. Streamwise airfoil coordinates for supercritical wings 1 and 2 are presented in tables 1 and 2 respectively, and streamwise coordinates for the simulated wide-body configuration are presented in Table 3. It should be noted that these coordinates include the twist that was built into each wing. In addition, the maximum wing thickness-to-chord ratios and local section incidence angle for the wings are presented in figure 4 as a function of span. A schedule of the configurations tested is presented in Table 4.

Fuselage

The fuselage used for the present investigation has a maximum diameter of 14.582 cm (5.741 in.) and is 125.885 cm (49.561 in.) long. The fineness ratio of the fuselage is equal to that of current wide-body transports. The fuselage wetted area is approximately 0.523 m^2 (5.630 ft^2).

Cross sections of the fuselage with the thicker supercritical wing (SCW-1) are shown in figure 2. The wing lower surface was faired into the fuselage to provide a relatively flat bottom that extended from near the wing leading edge to approximately 15.24 cm (6.0 in.) aft of the wing trailing edge at the side of the body. (See fig. 2.) A wing upper-surface, fuselage fillet was also employed with the supercritical wings (except 1a*). This fillet, originating at about the midchord of the wing root was largest at the wing trailing edge (fig. 1(b)) and then, merging with the wing lower-surface fuselage fillet, faired into the basic circular fuselage between stations 102.616 cm (40.400 in.) and 111.76 cm (44.00 in.) (fig. 2). At the wing trailing-edge, this fillet extended up the side of the fuselage to the point of maximum width (fig. 2). Neither the upper or lower surface fillet increased the maximum diameter of the fuselage. Although shown only in the planform of figure 1(b), this upper-surface fillet was used with all the supercritical-wing configurations except SCW-1a*. (Since the results for configuration 1a* were from the initial series of tests, the wing upper-surface fuselage fille had not been included on the model. Only a minimum of filleting was employed in this region for this configuration.)

For the representative wide-body configuration, the wing lower-surface, fuselage fillet was very similar to that used with the supercritical-wing configurations in that the bottom of the fuselage was relatively flat in the region of the wing. The wing upper-surface fuselage fillet, however, was kept to a minimum to be more consistent with what is used on the current wide-body aircraft.

Wings

Supercritical.- The supercritical airfoils used at the planform break and tip stations (references 4 and 5) are designed for a two-dimensional normal-force coefficient of 0.70 and were oriented in a streamwise direction with the wing at 27^{o} of quarter-chord sweep. For the three-dimensional case the wing sweep and finite aspect ratio of the wing and the fuselage all contribute to a loss in lift as compared to the basic airfoil and, consequently, the three-dimensional design lift coefficient is reduced to about 0.60. The airfoil employed at the wing-fuselage juncture is not a typical supercritical airfoil, however, it does utilize some aft camber. (See fig. 1(f).) In addition, the upper surface at the wing-fuselage juncture has significantly reduced curvature as compared to a conventional supercritical airfoil; in fact, the last 20-percent of the airfoil upper surface has zero curvature (straight line). Furthermore, the location of maximum thickness for the wing-fuselage-juncture airfoil is about 30-percent chord while the supercritical airfoils at the planform break and tip stations have their maximum thickness at about 40-percent chord. These modifications to the airfoil shape at the side of the fuselage are necessary to compensate for the adverse interference of the fuselage which tends to move the wing isobars aft (unsweeps shock wave) in this region.

The two supercritical wings tested have identical planforms for equal sweep angles and differ only in thickness (fig. 4). For 27° quarter-chord sweep, supercritical wing-1 (SCW-1) has maximum streamwise thickness-to-chord ratios of 0.16 at the side of the fuselage, 0.14 at the planform break and 0.12 at the tip. The thinner supercritical wing (SCW-2) has maximum streamwise thickness-to-chord ratios of 0.144, 0.12 and 0.10 at the same stations respectively. The two wings were tested at quarter-chord sweep angles of 27° (SCW-1a and SCW-2a) and 30° (SCW-1b and SCW-2b) with the wing pivot point located 3.81 cm (1.5 in.) off the model centerline at fuselage station 84.605 cm (33.309 in.). (See fig. 1(c)).

The wings were designed with aspect-ratio-12 trapezoidal planforms at 27° quarter-chord sweep for 0° dihedral. However, the wings were installed on the fuselage with 5° of dihedral and this slightly alters the projected planform geometric characteristics. With 5° of dihedral at 27° quarter-chord-sweep the trapezoidal planform has an aspect ratio of 11.954, an area of 0.193 m^2 (2.0754 ft^2), a span of 151.821 cm (59.772 in.), a mean geometric chord of 13.757 cm (5.416 in.) and a taper ratio of 0.333. The supercritical-wing dimensional characteristics are given in Table 4 for 5° of dihedral, and all the dimensions on the drawings in figure 1 are for the wings with 5° of dihedral as tested. In addition to the 5° of dihedral, the supercritical wings were mounted on the fuselage with -1° of incidence, i_w (not reflected in coordinates of tables 1 and 2). (Note: An initial set of results was obtained for configuration 1a* in which the incidence was set at 0°.)

The supercritical wings also incorporate a trailing-edge extension which originates 29.098 cm (11.456 in.) from the model centerline. At the centerline, the trailing-edge extension increases the theoretical root chord by 40 percent (fig. 1(b)).

The wetted area for the aspect-ratio 11.95 supercritical wing (to side of fuselage) including the trailing-edge extension is approximately 0.369 m^2 (3.976 ft^2). This is the wetted area computed for the thicker supercritical wing (SCW-1), however, the thinner wing wetted area would be very close to the same value since the effect of thickness on wetted area is relatively small (i.e., the arc length for a 10-percent-thick supercritical airfoil is 2.035, and the arc length for a 14-percent-thick airfoil is 2.056).

Supercritical wing-2 was also tested with a 15.240 cm (6.0 in.) shorter span at only the 27^o quarter-chord sweep angle (fig. 1(e)). (This configuration is designated SCW-2'.) This reduction in span, which increases the taper ratio to 0.4 and reduces the aspect ratio to 10.25, was made in anticipation of adding winglets (ref. 6) to this configuration at a later date. The trapezoidal planform area of this wing is 0.182 m^2 (1.961 ft^2) which is approximately a 5.5 percent reduction in area as compared to the aspect-ratio 11.95 wing.

<u>Wide-Body</u>.- Planform characteristics for the simulated current wide-body configuration are shown in figure 1(d), and a comparison with the supercritical wing planforms ($\Lambda_{c/4} = 27^o$) is shown in figure 1(e). This wing has an aspect ratio of 7, a mean geometric chord of 18.225 cm (7.175 in.) and a span of 116.119 cm (45.716 in.). The area of the trapezoidal planform is 0.193 m^2 (2.0754 ft^2). This is identical to the area of the trapezoidal planform of the aspect-ratio 11 supercritical wings, and, as a result, the wetted areas

are also very close. The maximum streamwise thickness-to-chord ratios for this wing are approximately 0.12 near the fuselage side and a constant 0.09 from the planform break to the tip (fig. 4). Coordinates for this wing are presented in Table 3.

MEASUREMENTS AND TEST CONDITIONS

Six-component force and moment data were obtained with an electrical strain-gage balance housed within the fuselage cavity, and two streamwise rows of surface static-pressure orifices were positioned on the left fuselage side 1.27 cm (0.5 in.) above and below the wing-root section. Although located on the fuselage, these pressures would be representative of the wing flow field at the fuselage juncture. The surface pressures were recorded by differential-pressure scanning-valve units mounted in the nose section of the model.

For determination of the base drag, the static- pressure in the balance chamber and in the plane of the model base were recorded with differential pressure transducers referenced to the free-stream static pressure. The model attitude in the tunnel was determined from an accelerometer attached to the balance block.

Longitudinal force and moment data were obtained over a Mach number range that generally varied from 0.60 to 0.82 for the supercritical-wing configurations and from 0.60 to 0.90 for the simulated wide-body configuration. In addition, limited results were obtained for supercritical-wing configuration 1b at a sideslip angle of -2.5°. The angle-of-attack range for most tests varied from about -2° to $+8^{\circ}$. The fuselage pressure data (around wing root) were obtained only for the supercritical-wing configurations over a limited Mach number range near the design lift coefficient of 0.60.

The entire investigation was conducted at a Reynolds number of 16.4×10^6/m (5.0×10^6/ft) and at a stagnation temperature of 322K (120°F). Dewpoint temperature was maintained low enough to avoid significant condensation effects.

Boundary-Layer Transition

Boundary-layer transition was fixed on all model components for the entire investigation with carborundum grit set in a plastic adhesive. All model transition strips were 0.127 cm (0.05 in.) wide, and the carborundum grit sizes were selected by using the techniques of ref. 7.

Longitudinal-aerodynamic data were obtained for all configurations with the wing upper-surface grit located at both a forward position (#150 carborundum grit at $x_T/c = 0.05$) and an aft position (fig. 5). The wing lower-surface grit was maintained in an aft position for all tests (fig. 5) except for configuration 2b when it was also located forward ($x_T/c = 0.05$) at Mach numbers 0.60 and 0.70. The wing aft grit location was employed in order to simulate a higher effective Reynolds number (ref. 8). The aft position of the wing upper-surface grit along the span was determined primarily from analysis of oil-flow photographs taken near the drag-rise Mach number at approximately 0.6 lift coefficient. A more complete discussion of wing boundary-layer transition location and its effect on the longitudinal aerodynamic characteristics are contained in a later section. Number 120 carborundum grit was located on the fuselage 2.54 cm (1.00 in.) from the nose.

Corrections

Drag results presented herein have been adjusted to correspond to free-stream static pressure acting in the balance chamber and at the fuselage base. Corrections have been made to the measured angle of attack to account for tunnel airflow angularity. This angularity was determined from a comparison of results for upright and inverted configurations. No corrections have been applied to the data to account for any type of wind-tunnel boundary interference.

PRESENTATION OF RESULTS

Results are presented herein for five supercritical-wing configurations (SCW-1a*, SCW-1a, SCW-1b, SCW-2a and SCW-2c) and a representative wide-body configuration. (See table 4.) Results for SCW-1a* were obtained in the initial series of tests of the present program and were included to demonstrate the effects of wing boundary-layer transition location at the higher Mach numbers. This configuration (1a*) was the only one tested with the wing-to-fuselage mounting angle at 0°; the wing mounting angle was -1° for all other configurations (table 4). In addition, the wing upper-surface fuselage fillet (figure 2) was not included on configuration 1a*.

The results of this investigation are presented in the following figures:

Figure

Figure

DISCUSSION

Comments on Reynolds Number Effects

The two-dimensional supercritical airfoils used for the wings of the present investigation were designed at an effective Reynolds number of around 40 million (ref. 5). This was obtained by testing at a chord Reynolds number of 7.6 million with the wing upper- and lower-surface boundary-layer transition strips at 28-percent of the chord. This combination of Reynolds number and transition location provides the same relative trailing-edge, boundary-layer-displacement thickness as full-chord turbulent flow for about 40 million Reynolds number (full-scale large transport condition). Of course, the 40 million Reynolds number case would be simulated only as long as laminar flow is maintained from the leading edge to the transition strip. For this reason, the high Reynolds number simulation is usually obtained on the upper surface only in the vicinity of the design point when the shock wave is aft of the transition strip. Even at low, off-design Mach numbers (i.e., M = 0.60) before the upper-surface shock wave has formed, the supercritical airfoil exhibits a pressure peak near the leading edge that would prematurely trip the flow. (See 2-D pressure distributions of references 4 and 5.)

For three-dimensional wings and particularly those with high aspect ratios, the model chords and consequently the local Reynolds numbers are significantly lower than those usually obtained in wind-tunnel tests of two-dimensional airfoils. As a result, the maximum Reynolds numbers that can be simulated by locating the transiton point aft are considerably reduced as compared to the two-dimensional case. For the present investigation, the Reynolds numbers based on the mean geometric chord and tip chord were 2.26 million and 1.04 million, respectively. With the 35- to 40-percent chord transition-strip location, the simulated Reynolds number at the design conditions ($M \approx 0.78 - 0.81$ @ at $C_L = 0.60$) is thought to be no larger than about 8-11 million. This is based on analysis of a 12-percent-thick supercritical airfoil using the viscous theory of reference 9. Full-scale Reynolds numbers for most airplanes would be even higher.

The high-aspect-ratio supercritical wings of the present investigation, relative to current transports, have increased thickness-to-chord ratios and higher design lift coefficients and, consequently, are more sensitive to Reynolds number. However, the simulated Reynolds number ($\approx$8-11 million) is large enough to keep the boundary-layer attached through the weak upper-surface shock wave to the trailing edge for the design point. With the transition grit strip located near the leading edge ($x_T/c = 0.05$), oil-flow photographs indicate that the flow was separated at the shock wave on the upper surface (fig. 6) and also in the lower-surface "cusp" area. Although the lower surface is subcritical, there is an adverse pressure gradient entering the "cusp" region.

Longitudinal Aerodynamic Characteristics

Summary figures for the longitudinal aerodynamic characteristic are presented in figures 21 through 26 and a summary of the performance parameters is given in table 5. The values used for specific fuel consumption vary linearly from 0.638 at a Mach number of 0.75 to 0.678 at 0.85 Mach number. These values are typical of those for current high bypass ratio, turbofan engines. Performance parameters for configuration 2c are presented at a lift coefficient of 0.55 in addition to 0.60. If these lift coefficients were based on the actual reference wing area of configuration 2c, they would correspond to 0.58 and 0.64 respectively. In addition, since the wide-body configuration was designed to fly optimally at a lower lift coefficient, the performance parameters for this configuration are presented at a lift coefficient of 0.45.

The wind-tunnel results presented herein are intended to show only relative differences between the various configurations. No increments have been applied to the data to account for things such as tail surfaces and nacelles nor has any correction been included to account for the Reynolds number difference between tunnel and full-scale conditions. It is interesting, though, that the L/D's measured for the simulated wide-body configuration are close to those obtained in flight for this type of airplane. In this particular case, the effect of Reynolds number on drag has apparently offset the drag increments due to tails, engines, pylons, etc.

Cruise performance characteristics.- As evidenced by the drag-rise Mach numbers (table 5 and figures 21-26) the supercritical-wing configurations are designed for slightly lower cruise speeds than the current wide-body configuration. Drag-rise Mach numbers (point where $\partial C_D/\partial M = 0.1$, see figures 21-26) vary from 0.783 for configuration 1a to 0.811 for configuration 2b at a lift coefficient of 0.60, while the wide-body configuration has a drag-rise Mach number of 0.835 at a lift coefficient of 0.45.

The grit forward data (lower effective Reynolds number) exhibits a rather large drag-creep prior the drag-rise (figures 21-26) however, the grit-aft results show a dip prior the drag-rise. This dip is a result of the transition point moving aft to the transition strip as Mach number is increased. A similar trend is seen in the two-dimensional results of reference 5.

Increasing the quarter-chord sweep angle from 27° to 30° increases the drag-rise Mach number from 0.783 to 0.802 for the thicker supercritical-wing (SCW-1), however, for the thinner wing (SCW-2), this same increase in sweep results in only an 0.01 increment in drag-rise Mach number. (See table 5.) The reasons for this are not known at this time. It is interesting to note, though, that the thicker supercritical wing (SCW-1b) at 30° quarter-chord sweep has about the same drag-rise Mach number as the thinner supercritical wing (SCW-2a) at the 27° sweep angle.

The aspect-ratio 10.25 supercritical wing (SCW-2c) does pay a small penalty in drag-rise Mach number as compared to the aspect-ratio 11.95 wing (SCW-2a) at a lift coefficient of 0.60. However, as pointed out earlier, this would correspond to a lift coefficient of about 0.64 if based on the actual reference area of configuration 2c. At a lift coefficient of 0. 55, configuration 2c has a drag-rise Mach number of 0.80.

In comparing the range factors ($M_{DR}(L/D)/sfc$) at the drag-rise Mach number for each configuration (table 5), those for the supercritical-wing configurations vary from about 21 percent (SCW-2c) to 27 percent (SCW-2a and

SCW-2b) higher than the range factor for the simulated wide-body configuration. In addition L/D's for the supercritical-wing configurations at the drag-rise Mach number vary from 22-percent to 29-percent higher than the L/D for the simulated wide-body configuration (table 5). Detailed structural trade-offs between the various configurations have not been made, however, a brief discussion on relative wing weights is presented in a later section.

Stability characteristics.- Maximum lift-curve slopes for the supercritical-wing configurations (@ $C_L = 0.60$) vary from about 0.185 to slightly over 0.20 while the simulated wide-body configuration (@ $C_L = 0.45$) has maximum lift-curve slopes of about 0.14. (See figures 21-26). These maximum values of C_{L_α} occur approximately 0.02 to 0.03 in Mach number before the drag-rise. (See figures 21-26.) The higher lift-curve slopes for the supercritical wings are probably associated with the larger thickness and aspect ratios, the lower sweep angles, and the greater extent of local supersonic flow.

Lift-curve slopes with the wing upper-surface transition grit located forward ($x_T/c = 0.05$) are significantly reduced at the higher Mach numbers as compared to the grit-aft results. This is due to shock-induced separation of the thicker turbulent boundary-layer which results from the lower effective Reynolds number with the forward grit location. (See oil-flow photographs of figure 6.) It is not certain though why the results for the grit-aft configurations have reduced lift-curve slopes at the lower Mach numbers. A possibility, though, is that a laminar separation bubble occurs on the upper surface near the leading edge. At the lower Mach numbers (i.e., $M = 0.60$), the supercritical airfoil has a leading-edge pressure peak (ref. 5) which tends to trip the laminar flow if the transition strips are located aft and in the transition process a laminar separation bubble probably occurs. It is also interesting to note that the differences between the forward and aft grit locations for all the parameters presented in figures 21-26 are much larger for the supercritical-wing configurations than the simulated wide-body configuration. Again, this is due to the increased sensitivity to low Reynolds number of the thicker, higher cambered supercritical wings.

The pitching-moment coefficients at zero lift ($C_{m,o}$) are considerably more negative for the supercritical-wing configurations than for the representative wide-body configuration. This is a reflection of both the higher camber and larger aspect ratios of the supercritical wings.

Near the drag-rise Mach number for each configuration, the supercritical wings have about the same longitudinal stability as the simulated wide-body configuration ($C_{m_{C_L}} \approx -0.1$). (i.e., The supercritical-wing configurations with 27° of quarter-chord sweep have $C_{m_{C_L}}$ values slightly greater than -0.1 while the supercritical-wing configurations with 30° of quarter-chord sweep have $C_{m_{C_L}}$ values slightly less than -0.1.) (See figures 21-26.)

Both the s percritical-wing configurations and the simulated wide-body configuration exhibit an increase in longitudinal stability (more negative trend of $C_{m_{C_L}}$) as Mach number is increased, however, this trend is reversed near the drag-rise Mach number with the longitudinal stability decreasing above this point.

Estimated buffet onset.- Breaks in the lift and pitching-moment curves are usually indicative of the onset of buffet and stability problems. For the thicker supercritical wing (SCW-1) at Mach numbers near the drag rise, the break in the lift and pitching-moment curves occurs at a lift coefficient of about 0.75 for SCW-1a (@M = 0.78) and about 0.77 for SCW-1b (@M = 0.80). (See figs. 8(f) and 10(d).) For the thinner supercritical wing (SCW-2), the break in the lift and pitching-moment curves occurs at a lift coefficient of about 0.85 for SCW-2a (@ M - 0.80) and about 0.82 for SCW-2b (@M = 0.81). (See figs. 12(f) and 14(g).)

Of course, at Mach numbers below the drag rise the break in the lift and pitching-moment curves occurs at higher lift coefficients while at Mach numbers beyond the drag rise, the break occurs at slightly lower lift coefficients. However, the degradation in buffet-onset lift coefficient beyond the drag-rise Mach number appears to occur much faster for the thicker supercritical wing (SCW-1). (See figs. 8 and 10.)

For the simulated current wide-body configuration at a Mach number of 0.84, the break in the lift and pitching-moment curves occurs at a lift coefficient of about 0.62. Therefore based on the present data, the thinner supercritical wing (SCW-2a) has approximately the same buffet margin ($\approx 0.4g$ above cruise lift coefficient) as the simulated wide-body configuration for Mach numbers near the drag rise. However, for the supercritical-wing configurations, the present data does not go high enough in Mach number to fully evaluate the overspeed condition.

Lateral-Directional Aerodynamic Characteristics for SCW-1b

The lateral-directional aerodynamic coefficients for configuration SCW-1b are presented in figure 27 as a function of angle of attack for 0° and -2.5° of sideslip. The wing upper-surface transition grit strip was located in the forward position ($x_T/c = 0.05$) for Mach numbers 0.60 to 0.77 and in the aft position (fig. 5(b)) for Mach numbers 0.79 through 0.82. The wing lower-surface transition grit strip was located aft (fig. 5(b)) at all Mach numbers.

Near the design lift coefficient of 0.60 ($\alpha \approx 2.2^{\circ}$), the configuration is laterally stable (positive effective dihedral) up to a Mach number of 0.81, however, at 0.82 Mach number the configuration becomes unstable at a lift coefficient of about 0.54 ($\alpha \approx 1.7^{0}$). The angle of attack at which the configuration becomes laterally unstable decreases as Mach number is increased. At a Mach number of 0.60, the configuration is laterally stable over the complete angle-of-attack range, however, at 0.80 Mach number the configuration has become unstable at an angle-of-attack of 2.4^{0}.

Although lateral aerodynamic data are not currently available on the thinner supercritical wing (SCW-2), the lateral stability margins should be larger for this wing. This assumption is based on a comparison of the breaks in the lift and pitching moment curves as discussed in the previous section on buffet onset.

Fuselage Pressure Distributions

Pressure distributions on the fuselage side around the wing root are presented in figures 28 through 32 for all the supercritical-wing configurations. Although these pressures were measured on the fuselage, they are indicative of the flow on the adjacent wing section. These pressures were utilized in developing the wing upper-surface fuselage fillet and in refining the wing-root airfoil.

Comments on Relative Wing Weights

In comparing the aerodynamic characteristics of the supercritical-wing configurations with the representative wide-body configuration, the indicated performance increases would be degraded if there was an accompanying increase in wing weight. One of the parameters that has been used as an indication of relative wing box weight is the ratio of structural span (distance measured along wing midchord) to wing maximum thickness (the higher the ratio, the heavier the wing box). These ratios are presented in table 6 at the wing-root (fuselage side) and planform-break stations for supercritical-wing configurations 1a, 2a and 2c, and for the simulated current wide-body configuration. The ratios are based on separate span lengths that were computed from both the root and break stations for each wing. At the root, the ratios for the supercritical-wing configurations vary from 16.9 to 31.4 percent higher than the ratio for the wide-body configuration, while at the break station, percent increase is considerably lower, particularly for configurations 1a percent) and 2c (8.2 percent). (See table 6.) Another thing that should be taken into consideration, however, when comparing the supercritical wings with the wide-body configuration is that the lower sweep of the supercritical wings should allow for a lighter wing carry-through (across-fuselage) structure. In addition, the optimum wing loading is expected to be higher for aircraft with the supercritical wings than for current aircraft not only because of their higher design lift coefficient for cruise, but also because of the expected gain in takeoff and landing performance achievable with their higher aspect ratio and lower sweep angle. The corresponding reductions in wing size should result directly in lower wing weight. As a result of these considerations, it is estimated that the supercritical-wing configurations would not necessarily be heavier than the representative wide-body configuration.

SUMMARY OF RESULTS

The present wind-tunnel investigation of several high aspect-ratio supercritical-wing configurations and a simulated current wide-body configuration has shown the following results:

1. At a lift coefficient of 0.60, the thicker supercritical-wing (SCW-1), with maximum streamwise thickness-to-chord ratios of 0.16 at the wing-fuselage juncture, 0.14 at the planform break and 0.12 at the tip, has drag-rise Mach numbers (point where $\partial C_D/\partial M = 0.1$) of 0.783 and 0.802 for 27^o and 30^o of quarter-chord sweep respectively. The thinner supercritical wing (SCW-2), with maximum thickness-to-chord ratios of 0.144 at the wing-fuselage juncture, 0.12 at the planform break and 0.10 at the tip, has drag-rise Mach numbers of 0.802 and 0.811 (@C_L = 0.60) for 27^o and 30^o of quarter-chord sweep respectively. The simulated wide-body configuration, with 35^o of sweep at the quarter-chord, has a drag-rise Mach number of 0.835 at a lift coefficient of 0.45.
2. Range factors computed at the drag-rise Mach number for each configuration ($M_{DR}(L/D)/sfc$), are 21-percent to 27-percent higher for the supercritical-wing configurations as compared to the range factor for the simulated wide-body configuration.
3. Based on the breaks in the lift and pitching-moment curves at Mach numbers near drag-rise, the thinner supercritical wing (SCW-2) would have a higher buffet-onset lift coefficient than the thicker supercritical wing (SCW-1). In addition, at Mach numbers near the drag-rise, the thinner supercritical-wing has approximately the same buffet margin (≈ 0.4g above cruise lift coefficient) as the simulated wide-body configuration.

4. Maximum lift-curve slopes for the supercritical-wing configurations vary between 0.185 and 0.20 at a lift coefficient of 0.6, while the maximum lift-curve slope for the simulated wide-body configuration is about 0.14 at a lift coefficient of 0.45. These maximum values of lift-curve slope (C_{L_α}) occur approximately 0.02 to 0.03 in Mach number before the drag rise.

5. The pitching-moment coefficients at zero lift ($C_{m,o}$) are considerably more negative for the supercritical-wing configurations than for the simulated wide-body configuration. This is a reflection of both the higher camber and larger aspect ratios of the supercritical wings.

REFERENCES

1. Supercritical Wing Technology - A Progress Report on Flight Evaluations. NASA SP-301, 1972.

2. Advanced Subsonic Transport Technology Assessment. Astronautics and Aeronautics, Vol. 10, No. 8, Aug. 1972, pp. 26-55.

3. Schaefer, William T., Jr.: Characteristics of Major Active Wind Tunnels at the Langley Research Center. NASA TM X-1130, 1965.

4. Harris, Charles D.: Aerodynamic Characteristics of the 10-Percent-Thick NASA Supercritical Airfoil 33 Designed for a Normal-Force Coefficient of 0.7. NASA TM X-72711, 1975.

5. Harris, Charles D.: Aerodynamic Characteristics of 14-Percent-Thick NASA Supercritical Airfoil Designed for a Normal-Force Coefficient of 0.7. NASA TM X-72712, 1975.

6. Whitcomb, Richard T.: A Design Approach and Selected Wind-Tunnel Results at High Subsonic Speeds for Wing-Tip Mounted Winglets. NASA TN D-8260, 1976.

7. Braslow, Albert L.; and Knox, Eugene C.: Simplified Method for Determination of Critical Height of Distributed Roughness Particles for Boundary-Layer Transition at Mach Numbers From 0 to 5. NACA TN 4363, 1958.

8. Blackwell, James A., Jr.: Preliminary Study of Effects of Reynolds Number and Boundary-Layer Transition Location on Shock-Induced Separation. NASA TN D-5003, 1969.

9. Bauer, F.; Garabedian, P.; Korn, D.; and Jameson, A.: Supercritical Wing Sections II. Lecture Notes in Economics and Mathematical Systems, M. Beckmann and H. P. Lunzi, eds., Springer-Verlag, C. 1975.

TABLE I.- STREAMWI[redacted]OORDINATES FOR SUPERCRITICAL WING-1, $\Lambda_{c/4} = 27^0$

(a) $\frac{y}{b/2} = 0.096$ (Wing-fuselage juncture)

x/c	z/c	
	Upper surface	Lower surface
0	-.0017	-.0017
.002	.0118	-.0152
.005	.0183	-.0217
.010	.0258	-.0292
.020	.0348	-.0382
.030	.0403	-.0452
.040	.0448	-.0507
.050	.0483	-.0552
.060	.0513	-.0592
.070	.0540	-.0627
.080	.0563	-.0658
.090	.0583	-.0686
.100	.0600	-.0711
.110	.0614	-.0733
.120	.0626	-.0754
.130	.0636	-.0773
.140	.0645	-.0791
.150	.0653	-.0808
.160	.0660	-.0824
.170	.0666	-.0838
.180	.0671	-.0851
.190	.0675	-.0863
.200	.0678	-.0874
.210	.0680	-.0883
.220	.0682	-.0891
.230	.0682	-.0898
.240	.0682	-.0904
.250	.0681	-.0909
.260	.0680	-.0913
.270	.0678	-.0916
.280	.0675	-.0919
.290	.0672	-.0922
.300	.0669	-.0924
.310	.0665	-.0925
.320	.0660	-.0926
.330	.0655	-.0927
.340	.0650	-.0927
.350	.0644	-.0926
.360	.0637	-.0925
.370	.0630	-.0924
.380	.0623	-.0922
.390	.0615	-.0921
.400	.0606	-.0919
.410	.0597	-.0916
.420	.0588	-.0913
.430	.0578	-.0909
.440	.0568	-.0905
.450	.0557	-.0899
.460	.0546	-.0893
.470	.0535	-.0885
.480	.0523	-.0877
.490	.0511	-.0868
.500	.0498	-.0858
.510	.0485	-.0847
.520	.0472	-.0835
.530	.0459	-.0823
.540	.0445	-.0810
.550	.0430	-.0796
.560	.0416	-.0781
.570	.0401	-.0766
.580	.0385	-.0751
.590	.0370	-.0735
.600	.0354	-.0718
.610	.0337	-.0702
.620	.0321	-.0685
.630	.0304	-.0668
.640	.0286	-.0650
.650	.0269	-.0633
.660	.0251	-.0616
.670	.0233	-.0599
.680	.0215	-.0582
.690	.0197	-.0566
.700	.0178	-.0549
.710	.0160	-.0533
.720	.0141	-.0517
.730	.0122	-.0502

TABLE I.- STREAMWISE AIRFOIL COORDINATES FOR

SUPERCRITICAL WING-1, $\Lambda_{c/4} = 27^{0}$ - Continued

(a) $\frac{y}{b/2} = 0.096$ (Wing-fuselage juncture) - Concluded

x/c	z/c	
	Upper surface	Lower surface
.740	.0102	-.0488
.750	.0083	-.0474
.760	.0063	-.0461
.770	.0043	-.0448
.780	.0023	-.0437
.790	.0003	-.0426
.800	-.0017	-.0417
.810	-.0037	-.0408
.820	-.0057	-.0401
.830	-.0077	-.0394
.840	-.0097	-.0389
.850	-.0117	-.0385
.860	-.0137	-.0382
.870	-.0157	-.0380
.880	-.0177	-.0378
.890	-.0197	-.0379
.900	-.0217	-.0380
.910	-.0237	-.0383
.920	-.0257	-.0387
.930	-.0277	-.0392
.940	-.0297	-.0399
.950	-.0317	-.0408
.960	-.0337	-.0418
.970	-.0357	-.0430
.980	-.0377	-.0444
.990	-.0397	-.0460
1.000	-.0417	-.0477

c = 23.55 cm (9.27 in.)

$\varepsilon = 1.0^{0}$

ORIGINAL P
OF POOR Q

ORIGINAL PAGE IS
POOR QUALITY

TABLE I.- STREAMWISE AIRFOIL COORDINATES FOR SUPERCRITICAL WING-1, $\Lambda_{c/4} = 27^{\circ}$ - Continued

(b) $\frac{y}{b/2} = 0.383$ (Planform Break)

x/c	z/c	
	Upper surface	Lower surface
0	-.0044	-.0044
.002	.0066	-.0147
.005	.0126	-.0206
.010	.0184	-.0264
.020	.0256	-.0335
.030	.0306	-.0383
.040	.0344	-.0420
.050	.0376	-.0449
.060	.0403	-.0475
.070	.0426	-.0498
.080	.0448	-.0517
.090	.0467	-.0535
.100	.0485	-.0551
.110	.0402	-.0566
.120	.0517	-.0580
.130	.0530	-.0593
.140	.0543	-.0605
.150	.0555	-.0615
.160	.0567	-.0625
.170	.0578	-.0634
.180	.0588	-.064[illegible]
.190	.0597	-.0652
.200	.0606	-.0659
.210	.0615	-.0666
.220	.0623	-.0672
.230	.0630	-.0678
.240	.0637	-.0683
.250	.0644	-.0688
.260	.0649	-.0693
.270	.0655	-.0697
.280	.0660	-.0700
.290	.0665	-.0703
.300	.0669	-.0705
.310	.0573	-.0707
.320	.0676	-.0709
.330	.0680	-.0710
.340	.0682	-.0710
.350	.0685	-.0710

x/c	z/c	
	Upper surface	Lower surface
.360	.0687	-.0709
.370	.0689	-.0708
.380	.0690	-.0707
.390	.0690	-.0705
.400	.0691	-.0702
.410	.0691	-.0699
.420	.0691	-.0696
.430	.0691	-.0692
.440	.0691	-.0687
.450	.0690	.0683
.460	.0688	-.0677
.470	.0686	-.0670
.480	.0684	-.0663
.490	.0682	-.0655
.500	.0680	-.0646
.510	.0677	-.0637
.520	.0674	-.0626
.530	.0670	-.0614
.540	.0666	-.0601
.550	.0662	-.0587
.560	.0657	-.0572
.570	.0652	-.0557
.580	.0647	-.0540
.590	.0641	-.0522
.600	.0635	-.0503
.610	.0630	-.0484
.620	.0623	-.0464
.630	.0616	-.0443
.640	.0608	-.0422
.650	.0600	-.0400
.660	.0591	-.0379
.670	.0582	-.0357
.680	.0573	-.0334
.690	.0563	-.0311
.700	.0553	-.0288
.710	.0542	-.0265
[redacted]0	.0531	-.0242
.730	.0518	-.0219

CO[redacted]

TABLE I.- STREAMWISE AIRFOIL COORDINATES FOR SUPERCRITICAL WING-1, $\Lambda_{c/4} = 27^{0}$ - Continued

(b) $\frac{y}{b/2}$ = 0.383 (Planform Break) - Concluded

x/c	z/c	
	Upper surface	Lower surface
.740	.0506	-.0196
.750	.0493	-.0173
.760	.0479	-.0150
.770	.0465	-.0129
.780	.0450	-.0108
.790	.0434	-.0088
.800	.0417	-.0069
.810	.0400	-.0052
.820	.0383	-.0036
.830	.0365	-.0021
.840	.0346	-.0008
.850	.0327	.0003
.860	.0307	.0012
.870	.0287	.0018
.880	.0266	.0023
.890	.0243	.0026
.900	.0220	.0027
.910	.0197	.0025
.920	.0173	.0021
.930	.0148	.0014
.940	.0122	.0003
.950	.0096	-.0010
.960	.0069	-.0026
.970	.0041	-.0045
.980	.0012	-.0067
.990	-.0019	-.0093
1.000	-.0051	-.0121

c = 14.17 cm (5.58 in.)

$\varepsilon = -1.5^{0}$

[redacted]

TABLE I.- STREAMWISE AIRFOIL COORDINATES FOR

SUPERCRITICAL WING-1, $\Lambda_{c/4} = 27^{\circ}$ - Continued

(c) $\frac{y}{b/2} = 1.000$ (Tip)

x/c	z/c Upper surface	z/c Lower surface	x/c	z/c Upper surface	z/c Lower surface
0	-.0175	-.0175	.360	.0551	-.0648
.002	-.0077	-.0252	.370	.0555	-.0645
.005	-.0027	-.0305	.380	.0559	-.0641
.010	.0023	-.0354	.390	.0562	-.0637
.020	.0087	-.0412	.400	.0565	-.0632
.030	.0133	-.0449	.410	.0568	-.0627
.040	.0168	-.0478	.420	.0570	-.0622
.050	.0197	-.0501	.430	.0573	-.0616
.060	.0223	-.0521	.440	.0575	-.0610
.070	.0247	-.0538	.450	.0577	-.0603
.080	.0268	-.0552	.460	.0578	-.0595
.090	.0288	-.0565	.470	.0579	-.0587
.100	.0306	-.0577	.480	.0580	-.0578
.110	.0323	-.0587	.490	.0581	-.0569
.120	.0339	-.0597	.500	.0582	-.0559
.130	.0353	-.0606	.510	.0581	-.0548
.140	.0368	-.0613	.520	.0582	-.0537
.150	.0381	-.0620	.530	.0581	-.0524
.160	.0393	-.0626	.540	.0581	-.0511
.170	.0406	-.0632	.550	.0580	-.0496
.180	.0417	-.0637	.560	.0578	-.0482
.190	.0429	-.0641	.570	.0577	-.0466
.200	.0439	-.0645	.580	.0575	-.0449
.210	.0449	-.0648	.590	.0573	-.0432
.220	.0458	-.0652	.600	.0570	-.0413
.230	.0467	-.0654	.610	.0568	-.0395
.240	.0476	-.0656	.620	.0565	-.0376
.250	.0484	-.0658	.630	.0562	-.0355
.260	.0493	-.0659	.640	.0558	-.0334
.270	.0500	-.0660	.650	.0554	-.0313
.280	.0507	-.0660	.660	.0550	-.0292
.290	.0514	-.0660	.670	.0544	-.0270
.300	.0519	-.0660	.680	.0540	-.0248
.310	.0526	-.0659	.690	.0534	-.0226
.320	.0531	-.0658	.700	.0527	-.0203
.330	.0536	-.0656	.710	.0521	-.0181
.340	.0541	-.0654	.720	.0514	-.0158
.350	.0546	-.0651	.730	.0507	-.0135

[redacted]

TABLE I.- STREAMWISE AIRFOIL COORDINATES FOR SUPERCRITICAL WING-1, $\Lambda_{c/4} = 27^{o}$ - Concluded

(c) $\frac{y}{b/2}$ = 1.000 (Tip) - Concluded

ORIGINAL PAGE IS OF POOR QUALITY

x/c	z/c	
	Upper surface	Lower surface
.740	.0499	-.0113
.750	.0492	-.0090
.760	.0482	-.0067
.770	.0473	-.0046
.780	.0463	-.0024
.790	.0453	-.0005
.800	.0442	.0015
.810	.0431	.0034
.820	.0419	.0050
.830	.0405	.0067
.840	.0392	.0081
.850	.0378	.0095
.860	.0364	.0105
.870	.0348	.0115
.880	.0333	.0121
.890	.0315	.0126
.900	.0298	.0130
.910	.0281	.0130
.920	.0261	.0129
.930	.0242	.0134
.940	.0221	.0116
.950	.0200	.0106
.960	.0178	.0093
.970	.0155	.0077
.980	.0130	.0058
.990	.0103	.0036
1.000	.0075	.0011

c = 6.35 cm (3.50 in.)
$\varepsilon = -3.0^{o}$

TABLE II.- STREAMWISE AIRFOIL COORDINATES FOR

SUPERCRITICAL WING-2, $\Lambda_{c/4} = 27^{o}$

(a) $\frac{y}{b/2} = 0.096$ (Wing-fuselage juncture)

x/c	z/c	
	Upper surface	Lower surface
0	-.0017	-.0017
.002	.0096	-.0132
.005	.0158	-.0192
.010	.0226	-.0261
.020	.0313	-.0345
.030	.0364	-.0401
.040	.0405	-.0446
.050	.0435	-.0484
.060	.0462	-.0518
.070	.0484	-.0548
.080	.0503	-.0577
.090	.0520	-.0603
.100	.0534	-.0628
.110	.0546	-.0650
.120	.0556	-.0672
.130	.0565	-.0691
.140	.0572	-.0709
.150	.0579	-.0727
.160	.0585	-.0742
.170	.0590	-.0756
.180	.0595	-.0769
.190	.0597	-.0782
.200	.0599	-.0793
.210	.0600	-.0803
.220	.0600	-.0812
.230	.0600	-.0821
.240	.0600	-.0828
.250	.0599	-.0834
.260	.0597	-.0840
.270	.0595	-.0845
.280	.0593	-.0849
.290	.0589	-.0853
.300	.0586	-.0856
.310	.0583	-.0859
.320	.0578	-.0862
.330	.0574	-.0864
.340	.0569	-.0866
.350	.0563	-.0867
.360	.0557	-.0868
.370	.0551	-.0869
.380	.0544	-.0869
.390	.0537	-.0868
.400	.0529	-.0867
.410	.0522	-.0865
.420	.0514	-.0862
.430	.0505	-.0859
.440	.0497	-.0855
.450	.0488	-.0850
.460	.0478	-.0845
.470	.0469	-.0839
.480	.0459	-.0832
.490	.0448	-.0821
.500	.0438	-.0815
.510	.0426	-.0806
.520	.0415	-.0796
.530	.0404	-.0785
.540	.0391	-.0774
.550	.0379	-.0761
.560	.0366	-.0748
.570	.0353	-.0734
.580	.0340	-.0720
.590	.0326	-.0705
.600	.0313	-.0690
.610	.0298	-.0675
.620	.0284	-.0659
.630	.0270	-.0643
.640	.0255	-.0628
.650	.0240	-.0612
.660	.0226	-.0596
.670	.0209	-.0580
.680	.0193	-.0565
.690	.0176	-.0550
.700	.0160	-.0537
.710	.0144	-.0523
.720	.0126	-.0509
.730	.0109	-.0497

TABLE II.- STREAMWISE AIRFOIL COORDINATES FOR

SUPERCRITICAL WING-2, $\Lambda_{c/4} = 27^{\circ}$ - Continued

(a) $\frac{y}{b/2} = 0.096$ (Wing-fuselage juncture) - Concluded

x/c	z/c	
	Upper surface	Lower surface
.740	.0092	-.0485
.750	.0073	-.0473
.760	.0055	-.0462
.770	.0037	-.0451
.780	.0018	-.0441
.790	-.0001	-.0433
.800	-.0020	-.0424
.810	-.0040	-.0417
.820	-.0060	-.0410
.830	-.0080	-.0404
.840	-.0100	-.0400
.850	-.0120	-.0396
.860	-.0140	-.0393
.870	-.0158	-.0391
.880	-.0181	-.0390
.890	-.0201	-.0391
.900	-.0221	-.0392
.910	-.0241	-.0395
.920	-.0261	-.0399
.930	-.0280	-.0404
.940	-.0300	-.0410
.950	-.0320	-.0418
.960	-.0340	-.0427
.970	-.0360	-.0438
.980	-.0379	-.0450
.990	-.0399	-.0465
1.000	-.0418	-.0481

c = 23.55 cm (9.27 in.)
$\varepsilon = 1.0^{\circ}$

TABLE II.- STREAMWISE AIRFOIL COORDINATES FOR

SUPERCRITICAL WING-2, $\Lambda_{c/4} = 27^{0}$ - Continued

(b) $\frac{y}{b/2}$ = 0.383 (Planform Break)

x/c	z/c	
	Upper surface	Lower surface
0	-.0044	-.0044
.002	.0049	-.0131
.005	.0099	-.0181
.010	.0148	-.0230
.020	.0210	-.0290
.030	.0253	-.0329
.040	.0286	-.0360
.050	.0312	-.0386
.060	.0336	-.0408
.070	.0357	-.0427
.080	.0376	-.0444
.090	.0393	-.0459
.100	.0409	-.0473
.110	.0424	-.0487
.120	.0436	-.0499
.130	.0448	-.0510
.140	.0460	-.0520
.150	.0471	-.0529
.160	.0481	-.0538
.170	.0491	-.0546
.180	.0500	-.0554
.190	.0508	-.0561
.200	.0516	-.0567
.210	.0523	-.0573
.220	.0530	-.0579
.230	.0537	-.0584
.240	.0543	-.0588
.250	.0548	-.0593
.260	.0554	-.0597
.270	.0559	-.0600
.280	.0563	-.0603
.290	.0568	-.0605
.300	.0571	-.0607
.310	.0575	-.0609
.320	.0578	-.0611
.330	.0580	-.0612
.340	.0582	-.0612
.350	.0585	-.0612
.360	.0587	-.0611
.370	.0589	-.0610
.380	.0590	-.0609
.390	.0590	-.0608
.400	.0591	-.0606
.410	.0591	-.0603
.420	.0591	-.0601
.430	.0591	-.0597
.440	.0591	-.0593
.450	.0590	-.0590
.460	.0588	-.0584
.470	.0587	-.0578
.480	.0585	-.0572
.490	.0584	-.0565
.500	.0582	-.0558
.510	.0579	-.0549
.520	.0577	-.0541
.530	.0573	-.0531
.540	.0570	-.0520
.550	.0567	-.0508
.560	.0563	-.0496
.570	.0559	-.0482
.580	.0555	-.0468
.590	.0550	-.0454
.600	.0544	-.0438
.610	.0539	-.0422
.620	.0534	-.0405
.630	.0528	-.0387
.640	.0522	-.0369
.650	.0515	-.0351
.660	.0509	-.0332
.670	.0501	-.0314
.680	.0493	-.0294
.690	.0485	-.0275
.700	.0476	-.0255
.710	.0467	-.0235
.720	.0458	-.0215
.730	.0448	-.0195

TABLE II.- STREAMWISE AIRFOIL COORDINATES FOR SUPERCRITICAL WING-2, $\Lambda_{c/4} = 27^{0}$ - Continued

(b) $\frac{y}{b/2}$ = 0.383 (Planform Break) - Concluded

x/c	z/c	
	Upper surface	Lower surface
.740	.0438	-.0175
.750	.0427	-.0155
.760	.0415	-.0135
.770	.0404	-.0116
.780	.0391	-.0098
.790	.0378	-.0081
.800	.0365	-.0064
.810	.0351	-.0048
.820	.0336	-.0034
.830	.0320	-.0020
.840	.0304	-.0008
.850	.0289	.0003
.860	.0271	.0011
.870	.0253	.0017
.880	.0235	.0021
.890	.0215	.0025
.900	.0195	.0025
.910	.0174	.0023
.920	.0152	.0019
.930	.0130	.0011
.940	.0107	-.0001
.950	.0083	-.0012
.960	.0058	-.0027
.970	.0033	-.0046
.980	.0005	-.0067
.990	-.0025	-.0092
1.000	-.0056	-.0120

c = 14.17 cm (5.58 in.)

$\varepsilon = -1.5^{0}$

TABLE II.- STREAMWISE AIRFOIL COORDINATES FOR

SUPERCRITICAL WING-2, $\Lambda_{c/4} = 27^0$ - Continued

(c) $\frac{y}{b/2} = 0.900$ (Tip for SCW-2c)

x/c	z/c	
	Upper surface	Lower surface
0	-.0135	-.0135
.002	-.0052	-.0209
.005	-.0007	-.0253
.010	.0036	-.0295
.020	.0092	-.0344
.030	.01[illegible]1	-.0376
.040	.0162	-.0402
.050	.0188	-.0423
.060	.0211	-.0441
.070	.0231	-.0456
.080	.0250	-.0469
.090	.0267	-.0481
.100	.0283	-.0492
.110	.0299	-.0502
.120	.0312	-.0511
.130	.0325	-.0519
.140	.0339	-.0527
.150	.0349	-.0533
.160	.0360	-.0539
.170	.0370	-.0545
.180	.0380	-.0550
.190	.0390	-.0554
.200	.0399	-.0558
.210	.0407	-.0562
.220	.0415	-.0565
.230	.0423	-.0568
.240	.0431	-.0570
.250	.0438	-.0572
.260	.0445	-.0573
.270	.0451	-.0575
.280	.0456	-.0575
.290	.0462	-.0576
.300	.0467	-.0576
.310	.0472	-.0576
.320	.0477	-.0575
.330	.0480	-.0574
.340	.0484	-.0573
.350	.0488	-.0571
.360	.0492	-.0569
.370	.0495	-.0567
.380	.0498	-.0564
.390	.0501	-.0561
.400	.0503	-.0557
.410	.0505	-.0553
.420	.0507	-.0550
.430	.0508	-.0545
.440	.0510	-.0540
.450	.0511	-.0534
.460	.0512	-.0527
.470	.0513	-.0520
.480	.0513	-.0513
.490	.0514	-.0505
.500	.0514	-.0497
.510	.0513	-.0488
.520	.0513	-.0478
.530	.0512	-.0468
.540	.0511	-.0457
.550	.0510	-.0445
.560	.0508	-.0433
.570	.0507	-.0419
.580	.0505	-.0406
.590	.0502	-.0391
.600	.0500	-.0376
.610	.0497	-.0360
.620	.0494	-.0343
.630	.0491	-.0326
.640	.0487	-.0308
.650	.0483	-.0290
.660	.0480	-.0272
.670	.0475	-.0253
.680	.0470	-.0234
.690	.0465	-.0215
.700	.0459	-.0196
.710	.0453	-.0176
.720	.0447	-.0156
.730	.0440	-.0136

TABLE II.- STREAMWISE AIRFOIL COORDINATES FOR SUPERCRITICAL WING-2, $\Lambda_{c/4} = 27^{\circ}$ - Continued

(c) $\frac{y}{b/2} = 0.900$ (Tip for SCW-2c)- Concluded

x/c	z/c	
	Upper surface	Lower surface
.740	.0434	-.0117
.750	.0427	-.0098
.760	.0418	-.0077
.770	.0410	-.0059
.780	.0401	-.0040
.790	.0392	-.0023
.800	.0383	-.0005
.810	.0372	.0011
.820	.0362	.0026
.830	.0349	.0041
.840	.0337	.0054
.850	.032[illegible]	.0066
.860	.03[illegible]	.0076
.870	.0297	.0084
.880	.0282	.0090
.890	.0266	.0094
.900	.0250	.0096
.910	.0233	.0096
.920	.0215	.0093
.930	.0196	.0089
.940	.0177	.0080
.950	.0156	.0069
.960	.0135	.0056
.970	.0112	.0039
.980	.0087	.0020
.990	.0060	-.0003
1.000	.0031	-.0028

$c = 7.62$ cm (3.00 in.)
$\varepsilon = -2.6^{\circ}$

OP'GI
OF PO

TABLE II.- STREAMWISE AIRFOIL COORDINATES FOR

SUPERCRITICAL WING-2, $\Lambda_{c/4} = 27^{o}$ - Continued

(d) $\frac{y}{b/2} = 1.000$ (Tip)

x/c	z/c	
	Upper surface	Lower surface
0	-.0175	-.0175
.002	-.0095	-.0243
.005	-.0053	-.0284
.010	-.0012	-.0323
.020	.0041	-.0367
.030	.0078	-.0397
.040	.0108	-.0420
.050	.0134	-.0439
.060	.0157	-.0455
.070	.0177	-.0468
.080	.0195	-.0480
.090	.0213	-.0491
.100	.0229	-.0500
.110	.0245	-.0509
.120	.0258	-.0516
.130	.0272	-.0523
.140	.0286	-.0530
.150	.0296	-.0535
.160	.0308	-.0540
.170	.0318	-.0544
.180	.0329	-.0548
.190	.0339	-.0551
.200	.0349	-.0554
.210	.0357	-.0557
.220	.0366	-.0559
.230	.0374	-.0561
.240	.0382	-.0562
.250	.0390	-.0563
.260	.0397	-.0563
.270	.0404	-.0564
.280	.0410	-.0564
.290	.0417	-.0563
.300	.0422	-.0563
.310	.0428	-.0561
.320	.0433	-.0560
.330	.0437	-.0558
.340	.0442	-.0556
.350	.0446	-.0553
.360	.0451	-.0551
.370	.0455	-.0548
.380	.0459	-.0544
.390	.0462	-.0541
.400	.0465	-.0536
.410	.0468	-.0532
.420	.0470	-.0527
.430	.0473	-.0522
.440	.0475	-.0516
.450	.0478	-.0510
.460	.0479	-.0503
.470	.0481	-.0495
.480	.0482	-.0488
.490	.0483	-.0479
.500	.0484	-.0471
.510	.0484	-.0462
.520	.0485	-.0451
.530	.0485	-.0441
.540	.0486	-.0429
.550	.0485	-.0418
.560	.0485	-.0405
.570	.0484	-.0392
.580	.0484	-.0378
.590	.0482	-.0364
.600	.0481	-.0349
.610	.0479	-.0333
.620	.0477	-.0316
.630	.0475	-.0299
.640	.0472	-.0281
.650	.0470	-.0264
.660	.0467	-.0245
.670	.0464	-.0227
.680	.0460	-.0208
.690	.0456	-.0189
.700	.0452	-.0170
.710	.0448	-.0150
.720	.0443	-.0131
.730	.0437	-.0111

TABLE II.- STREAMWISE AIRFOIL COORDINATES FOR SUPERCRITICAL WING-2, $\Lambda_{c/4} = 27^{\circ}$ - Concluded

(d) $\frac{y}{b/2} = 1.000$ (Tip) - Concluded

x/c	z/c	
	Upper surface	Lower surface
.740	.0432	-.0092
.750	.0426	-.0072
.760	.0420	-.0052
.770	.0413	-.0034
.780	.0406	-.0015
.790	.0398	.0003
.800	.0391	.0020
.810	.0382	.0037
.820	.0372	.0052
.830	.0362	.0067
.840	.0351	.0081
.850	.0340	.0094
.860	.0328	.0104
.870	.0316	.0113
.880	.0302	.0119
.890	.0288	.0123
.900	.0273	.0127
.910	.0258	.0127
.920	.0241	.0126
.930	.0224	.0122
.940	.0207	.0114
.950	.0188	.0104
.960	.0168	.0091
.970	.0146	.0076
.980	.0123	.0057
.990	.0097	.0036
1.000	.0069	.0012

c = 6.35 cm (2.50 in.)
$\varepsilon = -3.0^{\circ}$

[redacted]

[redacted]

TABLE III.- STREAMWISE AIRFOIL COORDINATES FOR THE REPRESENTATIVE WIDE-BODY CONFIGURATION, $\Lambda_{c/4} = 35^{o}$

(a) $\frac{y}{b/2} = 0.136$

Upper surface		Lower surface	
x/c	z/c	x/c	z/c
.0001	.0037	0.0000	0.0000
.0003	.0048	.0008	-.0039
.0006	.0057	.0020	-.0074
.0008	.0066	.0032	-.0101
.0011	.0077	.0053	-.0134
.0015	.0085	.0078	-.0165
.0018	.0096	.0098	-.0188
.0024	.0109	.0139	-.0224
.0035	.0127	.0185	-.0255
.0041	.0136	.0249	-.0292
.0048	.0145	.0320	-.0326
.0061	.0162	.0370	-.0348
.0068	.0172	.0440	-.0376
.0096	.0201	.0491	-.0395
.0126	.0226	.0575	-.0423
.0147	.0243	.0627	-.0438
.0192	.0270	.0720	-.0467
.0218	.0284	.0816	-.0498
.0237	.0296	.0913	-.0527
.0259	.0304	.1024	-.0554
.0270	.0310	.1106	-.0577
.0291	.0316	.1198	-.0600
.0323	.0329	.1300	-.0625
.0348	.0340	.1358	-.0645
.0420	.0365	.1474	-.0665
.0447	.0376	.1563	-.0687
.0471	.0382	.1655	-.0702
.0516	.0388	.1770	-.0723
.0550	.0396	.1880	-.0741
.0586	.0404	.1975	-.0758
.0627	.0413	.2007	-.0760
.0670	.0421	.2086	-.0771
.0767	.0435	.2184	-.0785

TABLE III.- STREAMWISE AIRFOIL COORDINATES FOR THE REPRESENTATIVE WIDE-BODY CONFIGURATION, $\Lambda_{c/4} = 35^{\circ}$ - Continued

(a) $\frac{y}{b/2} = 0.136$ - Continued

Upper surface		Lower surface	
x/c	z/c	x/c	z/c
.0834	.0445	.2328	-.0803
.0921	.0452	.2429	-.0815
.1008	.0459	.2546	-.0829
.1063	.0463	.2708	-.0845
.1137	.0465	.2816	-.0862
.1247	.0467	.2940	-.0867
.1326	.0468	.3113	-.0876
.1413	.0468	.3283	-.0883
.1507	.0466	.3421	-.0886
.16[illegible]	.0463	.3630	-.088[illegible]
.1[illegible]	.0458	.3784	-.0883
.1820	.0453	.3946	-.0884
.1958	.0447	.4105	-.0880
.2040	.0443	.4228	-.0875
.2150	.0435	.4308	-.0872
.2244	.0429	.4397	-.0868
.2394	.0418	.4509	-.0862
.2485	.0411	.4650	-.0855
.2636	.0397	.4766	-.0849
.2706	.0390	.4872	-.0843
.2807	.0380	.4907	-.0840
.2985	.0361	.5107	-.0829
.3161	.0342	.5268	-.0820
.3362	.0321	.5434	-.0810
.3510	.0303	.5584	-.0801
.3613	.0292	.5765	-.0790
.3769	.0275	.5951	-.0778
.3901	.0260	.6099	-.0770
.4055	.0243	.6279	-.0758
.4189	.0228	.6456	-.0747
.4342	.0211	.6541	-.0742
.4474	.0196	.6685	-.0733
.4609	.0181	.6862	-.0721

TABLE III.- STREAMWISE AIRFOIL COORDINATES FOR THE REPRESENTATIVE WIDE-BODY CONFIGURATION, $\Lambda_{c/4} = 35^{\circ}$ - Concluded

(a) $\frac{y}{b/2} = 0.136$ - Concluded

Upper surface		Lower surface	
x/c	z/c	x/c	z/c
.4750	.0165	.7039	-.0710
.4891	.0149	.7205	-.0699
.5033	.0133	.7375	-.0689
.5137	.0122	.7543	-.0678
.5256	.0109	.7693	-.0669
.5396	.0093	.7786	-.0663
.5534	.0078	.7945	-.0654
.5654	.0065	.8090	-.0646
.5790	.0050	.8253	-.0636
.5907	.0037	.8400	-.0627
.6078	.0017	.8575	-.0616
.6220	.0001	.8718	-.0608
.6344	-.0014	.8836	-.0600
.6457	-.0028	.8939	-.0593
.6626	-.0048	.9070	-.0584
.6791	-.0068	.9213	-.0575
.6950	-.0087	.9343	-.0566
.7125	-.0108	.9457	-.0558
.7235	-.0120	.9609	-.0548
.7370	-.0136	.9725	-.0540
.7533	-.0155	.9804	-.0535
.7718	-.0177	.9883	-.0529
.7845	-.0192	.9968	-.0522
.7971	-.0207	1.0000	-.0519
.8084	-.0221		
.8222	-.0238		
.8345	-.0254		
.8455	-.0269		
.8582	-.0286		
.8765	-.0313		
.8905	-.0332		
.8956	-.0339		
.9082	-.0359		
.9201	-.0377		
.9332	-.0395		
.9461	-.0415		
.9532	-.0435		
.9717	-.0453		
.9831	-.0470		
.9937	-.0487		

c = 28.65 cm (11.28 in.)
$\varepsilon = 3.1^{\circ}$

TABLE III.- STREAMWISE AIRFOIL COORDINATES FOR THE REPRESENTATIVE WIDE-BODY CONFIGURATION, $\Lambda_{c/4} = 35^{o}$ - Continued.

(b) $\frac{y}{b/2}$ = 0.422 (Planform break) - Continued.

Upper surface		Lower surface	
x/c	z/c	x/c	z/c
.2560	.0526	.4311	-.0375
.2684	.0539	.4439	-.0373
.2909	.0548	.4612	-.0369
.3045	.0552	.4752	-.0365
.3150	.0555	.4905	-.0361
.3268	.0557	.5071	-.0354
.3441	.0560	.5247	-.0347
.3564	.0562	.5546	-.0333
.3753	.0564	.5804	-.0319
.3944	.0564	.5973	-.0309
.4188	.0560	.6215	-.0294
.4352	.0556	.6399	-.0283
.4489	.0552	.6610	-.0269
.4633	.0547	.6882	-.0249
.4807	.0541	.7109	-.0233
.5017	.0529	.7302	-.0219
.5166	.0520	.7471	-.0206
.5304	.0512	.7693	-.0188
.5493	.0498	.7903	-.0173
.5673	.0484	.8238	-.0148
.5904	.0466	.8520	-.0128
.6075	.0451	.8705	-.0114
.6232	.0436	.8859	-.0103
.6339	.0426	.9013	-.0092
.6482	.0412	.9143	-.0083
.6624	.0398	.9272	-.0074
.6813	.0378	.9434	-.0063

TABLE III.- STREAMWISE AIRFOIL COORDINATES FOR THE REPRESENTATIVE WIDE-BODY CONFIGURATION, $\Lambda_{c/4} = 35^{0}$ - Continued

(b) $\frac{y}{b/2} = 0.422$ (Planform break)

Upper surface		Lower surface	
x/c	z/c	x/c	z/c
		0.0000	0.0000
.0001	.0061	.0004	-.0003
.0010	.0076	.0044	-.0037
.0023	.0095	.0095	-.0050
.0045	.0118	.0195	-.0070
.0044	.0118	.0271	-.0083
.0081	.0151	.0391	-.0106
.0103	.0166	.0467	-.0119
.0173	.0207	.0575	-.0137
.0252	.0243	.0705	-.0157
.0297	.0260	.0814	-.0173
.0386	.0288	.0932	-.0188
.0469	.0308	.1071	-.0208
.0538	.0325	.1150	-.0217
.0617	.0340	.1301	-.0235
.0692	.0354	.1396	-.0248
.0792	.0369	.1573	-.0268
.0866	.0381	.1776	-.0286
.0932	.0391	.1886	-.0295
.1043	.0404	.2120	-.0310
.1145	.0418	.2249	-.0318
.1254	.0431	.2410	-.0329
.1346	.0440	.2589	-.0338
.1492	.0456	.2850	-.0351
.1660	.0473	.3037	-.0360
.1803	.0485	.3222	-.0365
.1924	.0495	.3430	-.0371
.2050	.0505	.3608	-.0374
.2174	.0513	.3777	-.0376
.2288	.0534	.3951	-.0377
.2411	.0519	.4124	-.0377

TABLE III.- STREAMWISE AIRFOIL COORDINATES FOR THE REPRESENTATIVE WIDE-BODY CONFIGURATION, $\Lambda_{c/4} = 35^{o}$ - Continued.

(b) $\frac{y}{b/2}$ = 0.422 (Planform break) - Concluded.

Upper surface		Lower surface	
x/c	z/c	x/c	z/c
.7044	.0354	.9576	-.0054
.7203	.0337	.9718	-.0045
.7354	.0319	.9806	-.0040
.7594	.0291	.9883	-.0036
.7809	.0265	1.0000	-.0037
.7984	.0245		
.8136	.0226		
.8342	.0200		
.8512	.0179		
.8669	.0159		
.8828	.0138		
.8998	.0116		
.9219	.0088		
.9363	.0068		
.9565	.0043		
.9692	.0027		
.9798	.0015		
.9899	.0000		

c = 18.01 cm (7.09 in.)

$\varepsilon = 0.31^{o}$

TABLE III.- STREAMWISE AIRFOIL COORDINATES FOR THE REPRESENTATIVE WIDE-BODY CONFIGURATION, $\Lambda_{c/4} = 35^{\circ}$ - Continued

(c) $\frac{y}{b/2} = 0.732$

Upper surface		Lower surface	
x/c	z/c	x/c	z/c
.0001	.0050	.0005	.0000
.0014	.0071	.0091	-.0038
.0040	.0100	.0165	-.0051
.0057	.0117	.0231	-.0064
.0078	.0136	.0339	-.0077
.0121	.0166	.0432	-.0091
.0217	.0219	.0548	-.0104
.0270	.0243	.0642	-.0114
.0363	.0272	.0746	-.0127
.0461	.0299	.0887	-.0141
.0592	.0328	.1065	-.0158
.0754	.0360	.1234	-.0172
.0853	.0377	.1439	-.0187
.1010	.0403	.1575	-.0197
.1135	.0420	.1735	-.0207
.1292	.0441	.2009	-.0220
.1561	.0473	.2204	-.0231
.1791	.0498	.2473	-.0238
.1986	.0518	.2757	-.0247
.2283	.0545	.2981	-.0251
.2443	.0558	.3109	-.0252
.2656	.0573	.3305	-.0252
.2821	.0582	.3644	-.0252
.3033	.0595	.3934	-.0248
.3258	.0605	.4118	-.0245
.3494	.0616	.4317	-.0238
.3715	.0623	.4584	-.0226
.3984	.0628	.4893	-.0209
.4228	.0630	.5213	-.0189
.4533	.0628	.5484	-.0168
.4745	.0624	.5764	-.0146
.4998	.0618	.6034	-.0123
.5226	.0610	.6286	-.0102

[redacted]

TABLE III.- STREAMWISE AIRFOIL COORDINATES FOR THE REPRESENTATIVE WIDE-BODY CONFIGURATION, $\Lambda_{c/4} = 35^{o}$ - Continued.

(c) $\frac{y}{b/2} = 0.732$ - Concluded.

Upper surface		Lower surface	
x/c	z/c	x/c	z/c
.5447	.0601	.6477	-.0084
.5682	.0590	.6707	-.0064
.5944	.0576	.7046	-.0032
.6201	.0562	.7337	-.0003
.6426	.0546	.7564	.0017
.6666	.0529	.7753	.0036
.6884	.0513	.7812	.0041
.7148	.0491	.8026	.0062
.7308	.0478	.8230	.0080
.7534	.0459	.8453	.0100
.7716	.0442	.8743	.0127
.7920	.0422	.8969	.0147
.8171	.0399	.9119	.0158
.8358	.0382	.9294	.0171
.8529	.0366	.9366	.0177
.8768	.0343	.9483	.0187
.8900	.0330	.9611	.0195
.9146	.0305	.9743	.0204
.9348	.0287	.9808	.0210
.9516	.0274	.9864	.0213
.9594	.0269	1.0000	.0227
.9635	.0269		
.9825	.0256		
.9972	.0237		

c = 12.40 cm (4.88 in.)
$\varepsilon = -1.2^{o}$

[redacted]

TABLE III.- STREAMWISE AIRFOIL COORDINATES FOR THE REPRESENTATIVE WIDE-BODY CONFIGURATION, $\Lambda_{c/4} = 35^{o}$

(d) $\frac{y}{b/2} = 1.000$

Upper surface		Lower surface	
x/c	z/c	x/c	z/c
.0002	-.0021	.0009	-.0064
.0042	.0054	.0123	-.0106
.0066	.0078	.0265	-.0130
.0126	.0118	.0383	-.0150
.0255	.0188	.0736	-.0179
.0391	.0236	.1012	-.0186
.0485	.0263	.1215	-.0205
.0727	.0328	.1327	-.0211
.0846	.0363	.1549	-.0217
.0964	.0398	.1774	-.0225
.1155	.0424	.2206	-.0222
.1494	.0474	.2571	-.0216
.1626	.0501	.2807	-.0211
.1866	.0529	.3079	-.0204
.2102	.0559	.3355	-.0188
.2339	.0588	.3638	-.0182
.2477	.0605	.3993	-.0154
.2600	.0617	.4263	-.0145
.2752	.0633	.4598	-.0113
.2957	.0653	.4953	-.0076
.3196	.0675	.5292	-.0040
.3468	.0697	.5558	-.0015
.3821	.0720	.5972	.0032
.4046	.0731	.6261	.0071
.4317	.0741	.6619	.0115
.4641	.0750	.6907	.0155
.4913	.0739	.7192	.0189
.5172	.0756	.7443	.0216
.5417	.0757	.7652	.0242
.5723	.0756	.7827	.0268
.5970	.0753	.7965	.0287
.6308	.0749	.8209	.0322

TABLE III.- STREAMWISE AIRFOIL COORDINATES FOR THE REPRESENTATIVE WIDE-BODY CONFIGURATION, $\Lambda_{c/4} = 35^{o}$ - Continued.

(d) $\frac{y}{b/2} = 1.000$ - Concluded.

Upper surface		Lower surface	
x/c	z/c	x/c	z/c
.6617	.0738	.8390	.0349
.6843	.0733	.8640	.0383
.7090	.0719	.8902	.0418
.7494	.0699	.9122	.0449
.7788	.0687	.9421	.0483
.8029	.0673	.9611	.0506
.8327	.0658	.9826	.0528
.8564	.0643	.9902	.0539
.8919	.0622	.9973	.0540
.9181	.0606	.9983	.0548
.9418	.0595		
.9664	.0588		
.9876	.0572		

c = 7.57 cm (2.98 in.)
$\varepsilon = -3.6^{o}$

TABLE IV - CONFIGURATION SCHEDULE

CONFIG.	$\Lambda_{c/4}$	$\Lambda_{c/2}$	i_w, deg	Γ, deg	AR	WING SPAN, cm	WING SPAN, in.	λ
SCW-1a*	27°	25°	0	5	11.954	151.821	59.772	0.33
SCW-1a	27°	25°	-1	5	11.954	151.821	59.772	0.33
SCW-1b	30°	28°	-1	5	11.362	149.103	58.702	0.33
SCW-2a	27°	25°	-1	5	11.954	151.821	59.772	0.33
SCW-2b	30°	28°	-1	5	11.362	149.103	58.702	0.33
SCW-2c	27°	25°	-1	5	10.246	136.639	53.795	0.40
WIDE-BODY	35°	32°	0	5.5	6.998	116.119	45.716	0.30

TABLE V - PERFORMANCE PARAMETERS

CONFIG.	AR	$\Lambda_{c/4}$	C_L	M_{DR}	L/D @ M_{DR}	$\frac{M_{DR}(L/D)}{sfc}$	% INCREASE $M_{DR}(L/D)/sfc$
SCW-1a	11.954	27°	0.60	0.783	20.5	24.66	20.6
SCW-1b	11.362	30°	.60	.802	20.5	24.95	22.0
SCW-2a	11.954	27°	.60	.802	21.3	25.92	26.8
SCW-2b	11.362	30°	.60	.811	21.2	25.97	27.0
SCW-2c	10.246	27°	.60	.791	20.5	24.80	21.3
SCW-2c	10.246	27°	.55	.800	19.9	24.19	18.3
WIDE-BODY	6.998	35°	.45	.835	16.45	20.45	0.0

TABLE VI - STRUCTURAL PARAMETERS

CONFIG	$\Lambda_{c/4}$	AR	WING TRAPEZOIDAL PLANFORM AREA m^2	ft^2	WING (t/c) @ ROOT	BREAK	TIP	$\frac{(SS)_r}{t_r}$	$\frac{(SS)_b}{t_b}$
SCW-1a	27^o	11.954	0.193	2.075	0.16	0.14	0.12	20.18	26.12
SCW-2a	27^c	11.954	0 193	2.075	.144	.12	.10	22.42	30.47
SCW-2c	27^o	10.246	0.182	1.961	.144	.12	.106	19.94	25.53
WIDE-BODY	35^o	6.998	0.193	2.075	.124	.93	.088	17.06	23.60

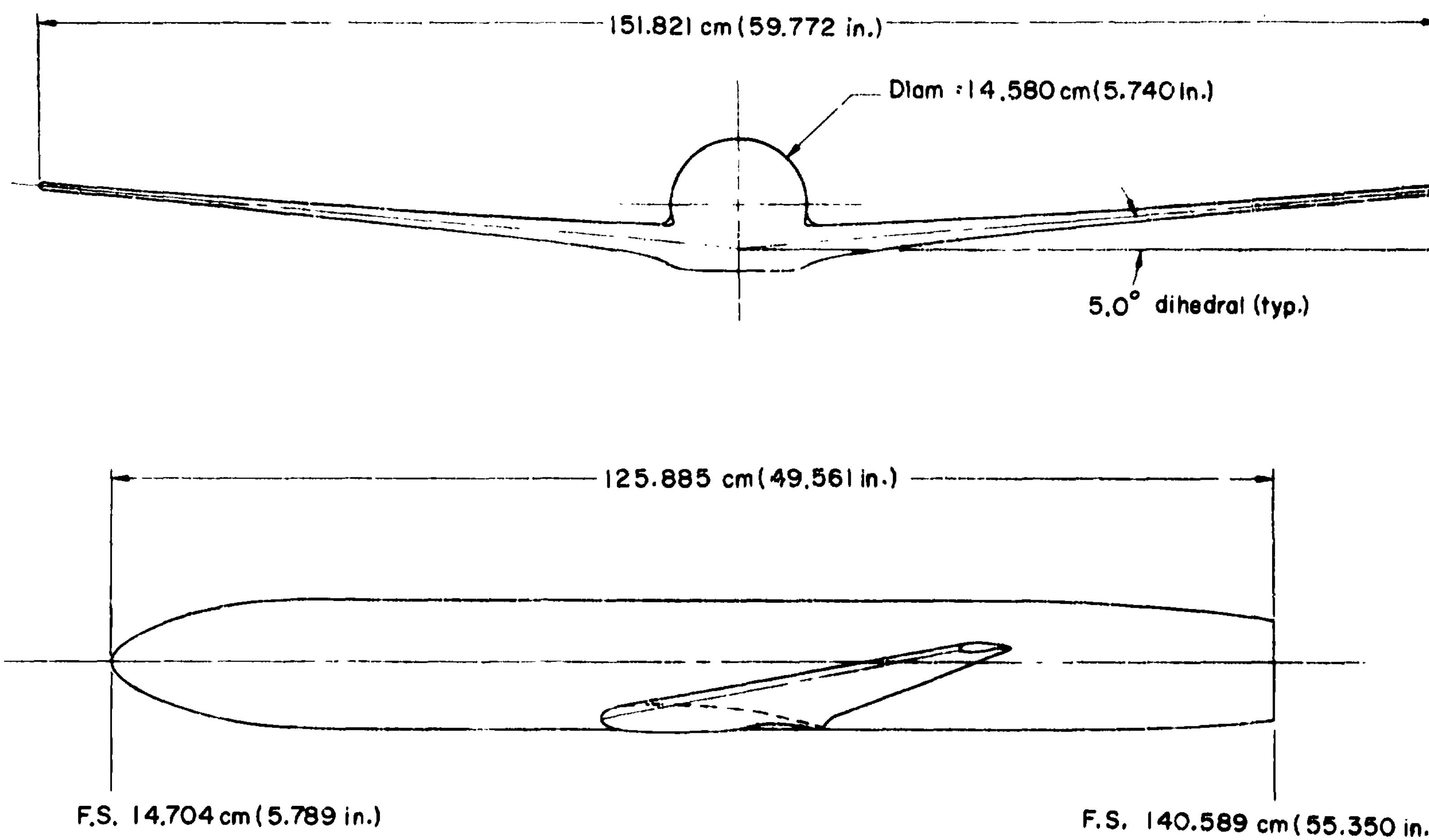

(a) Front and side ..ws of supercritical-wing configuration. AR=11.954.

Figure 1. - Model details. Linear dimensions are in centimeters (inches).

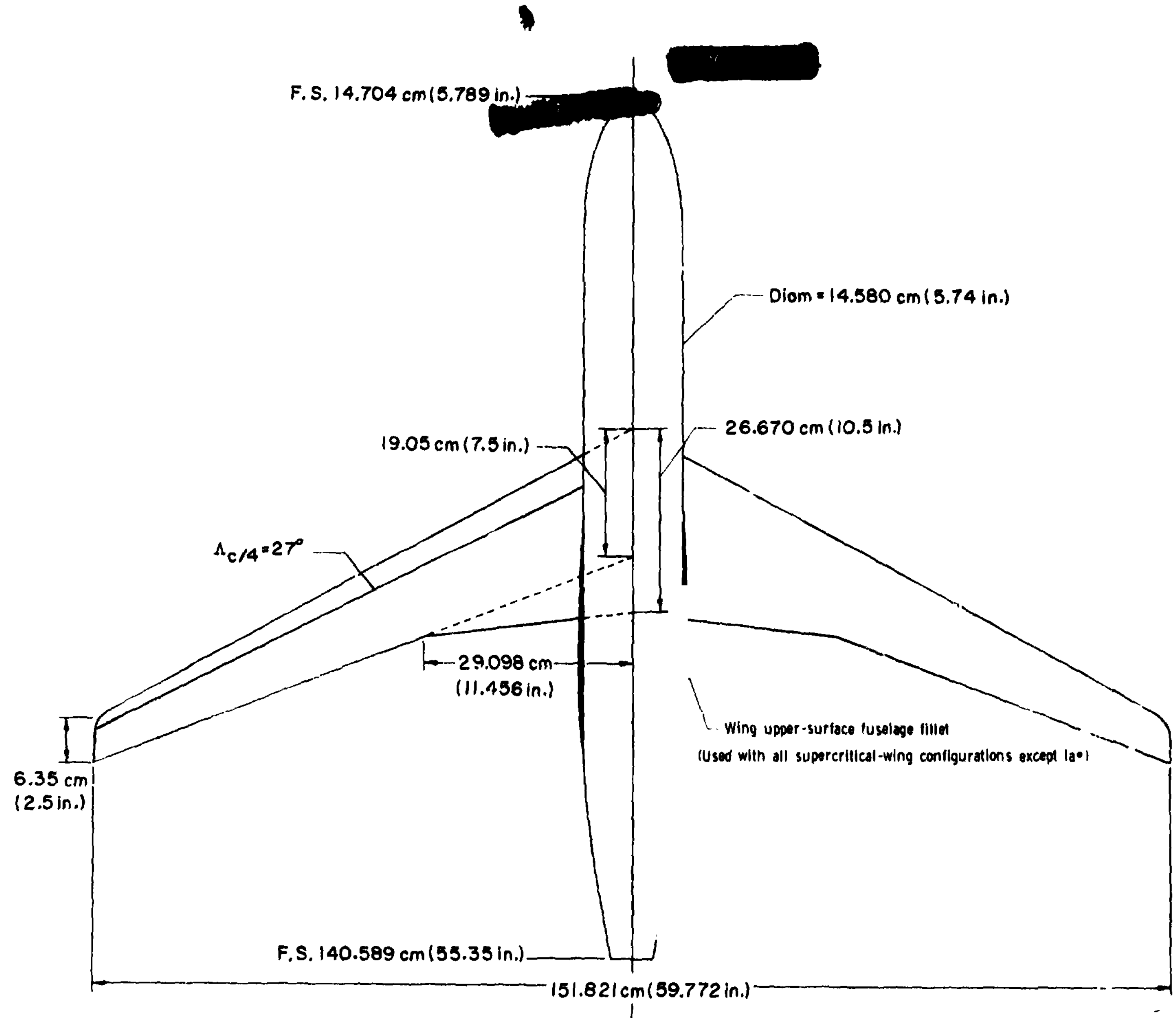

(b) Planform arrangement of supercritical-wing configuration. AR=11.954

Figure 1. - Continued.

[redacted]

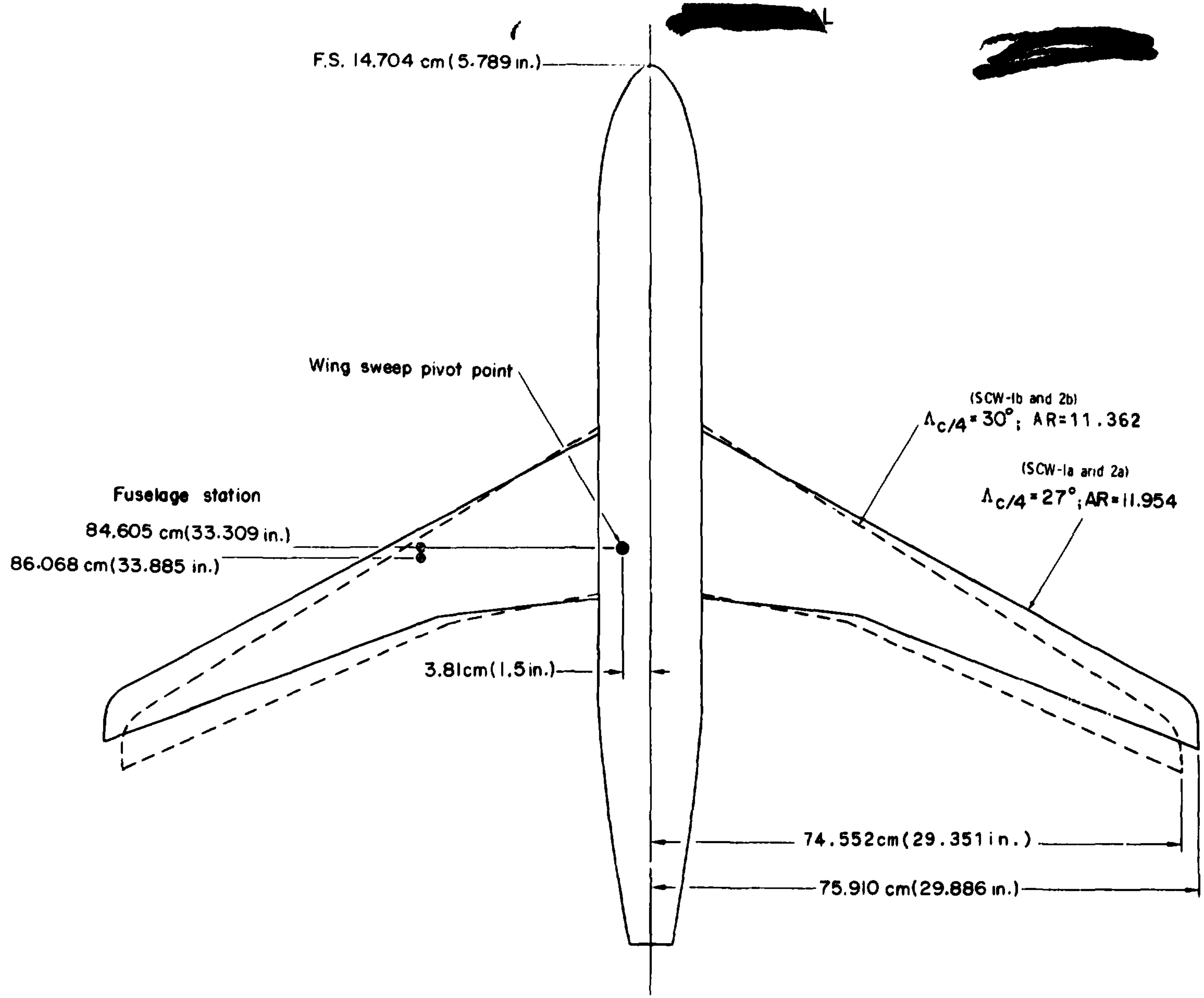

(c) Comparison of supercritical-wing planforms at quarter-chord sweep angles of 27° and 30°.

Figure 1. - Continued.

[redacted]

ORIGINAL PAGE IS
OF POOR QUALITY

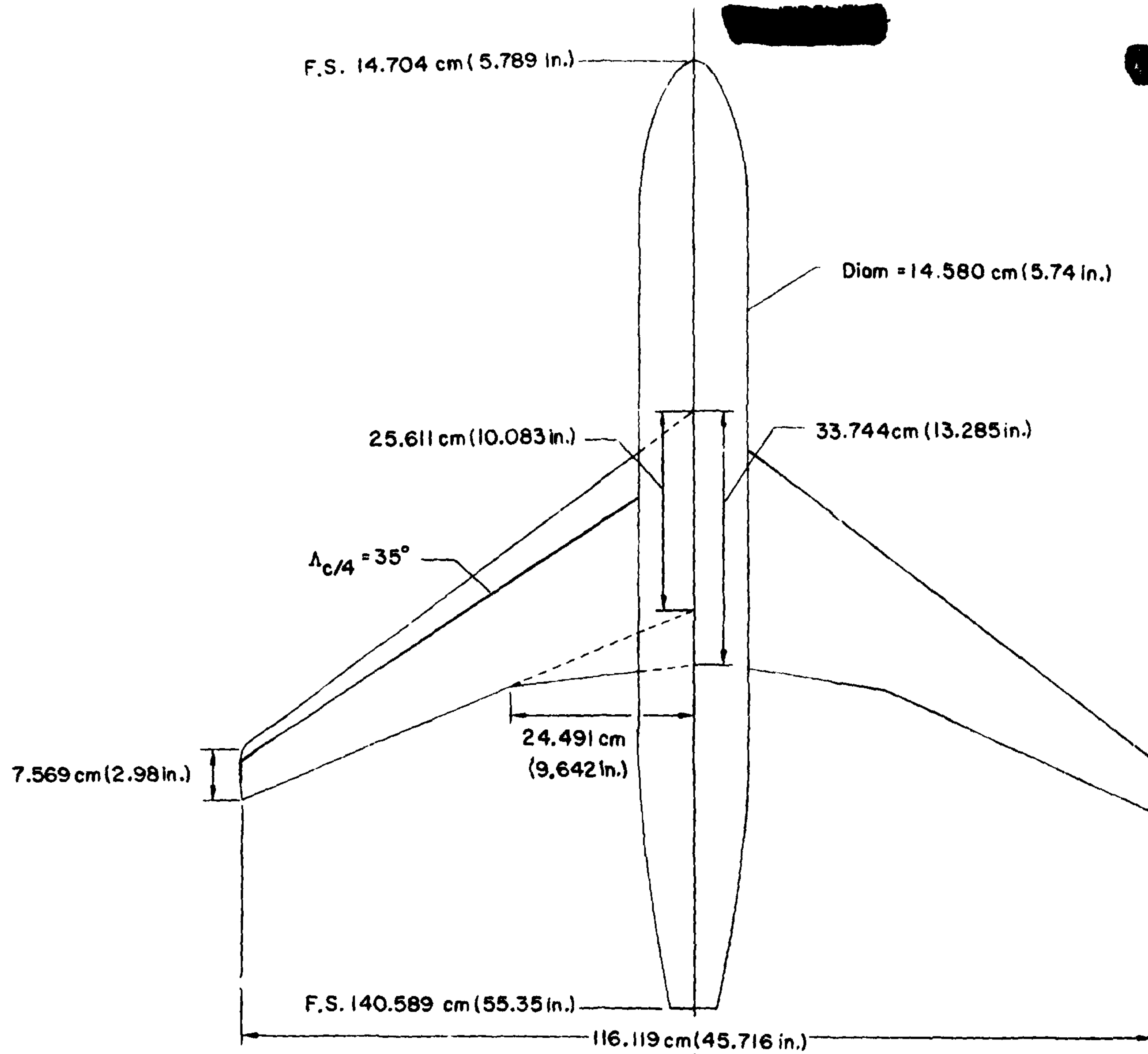

(d) Planform arrangement of the simulated current wide-body configuration.

Figure 1. - Continued.

[redacted]

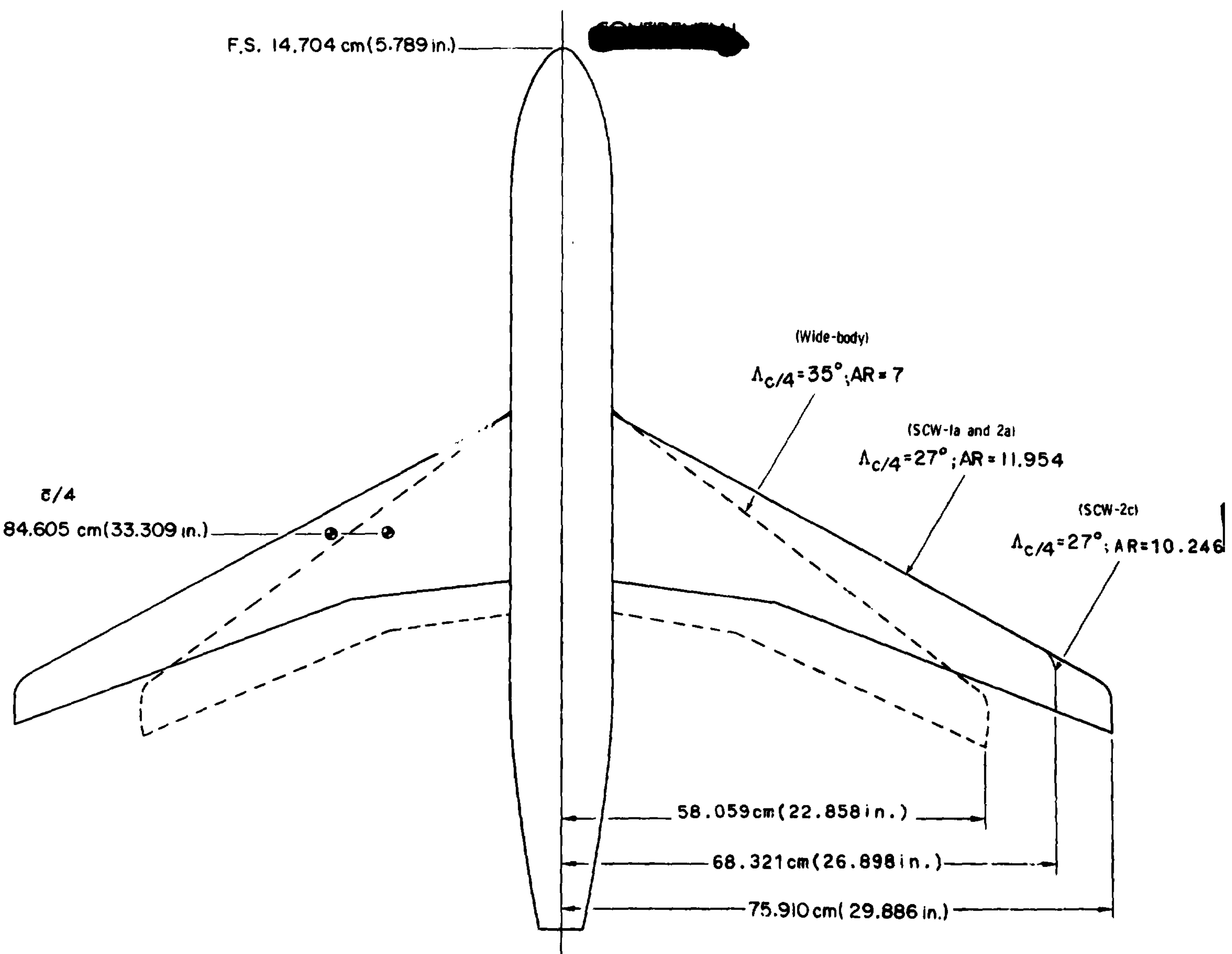

(e) Comparison of supercritical-wing planforms with the planform of the simulated wide-body configuration.

Figure 1. - Continued.

[redacted]

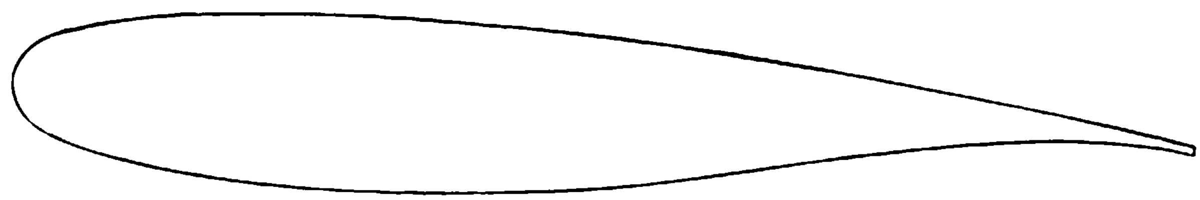

Wing-fuselage juncture; t/c = 0.144

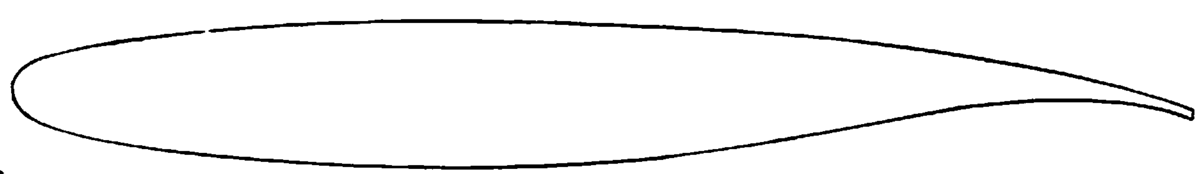

Planform break; t/c = 0.12

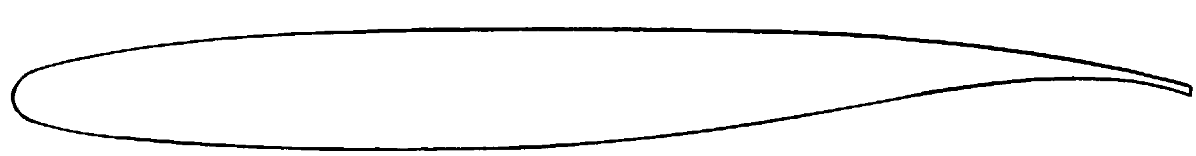

Tip; t/c = 0.10

(f) Streamwise airfoils for supercritical wing - 2. Quarter-chord sweep=27°

Figure 1. - Concluded.

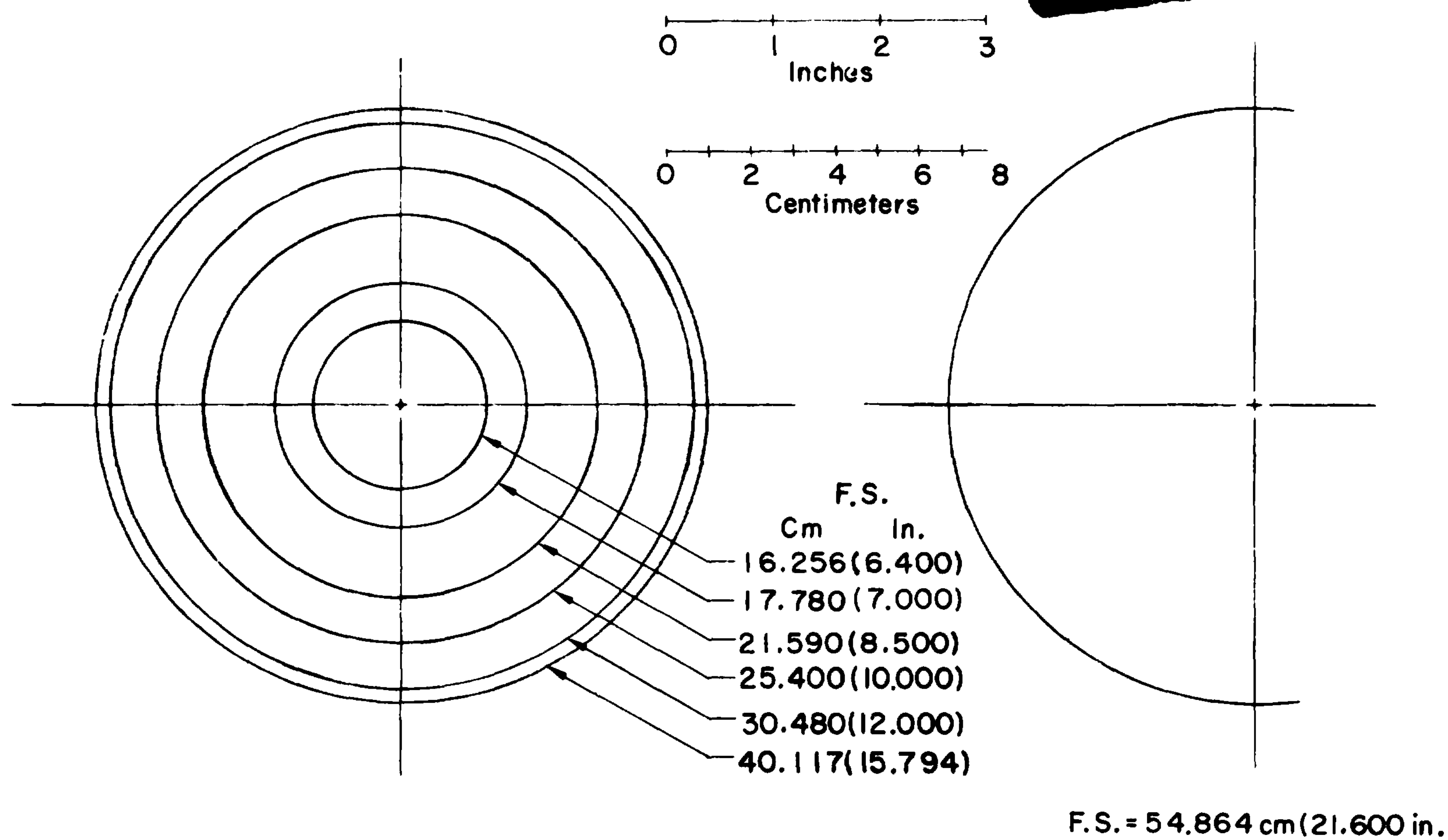

Figure 2. - Fuselage cross sections with supercritical wing - 1.

[redacted] [redacted]

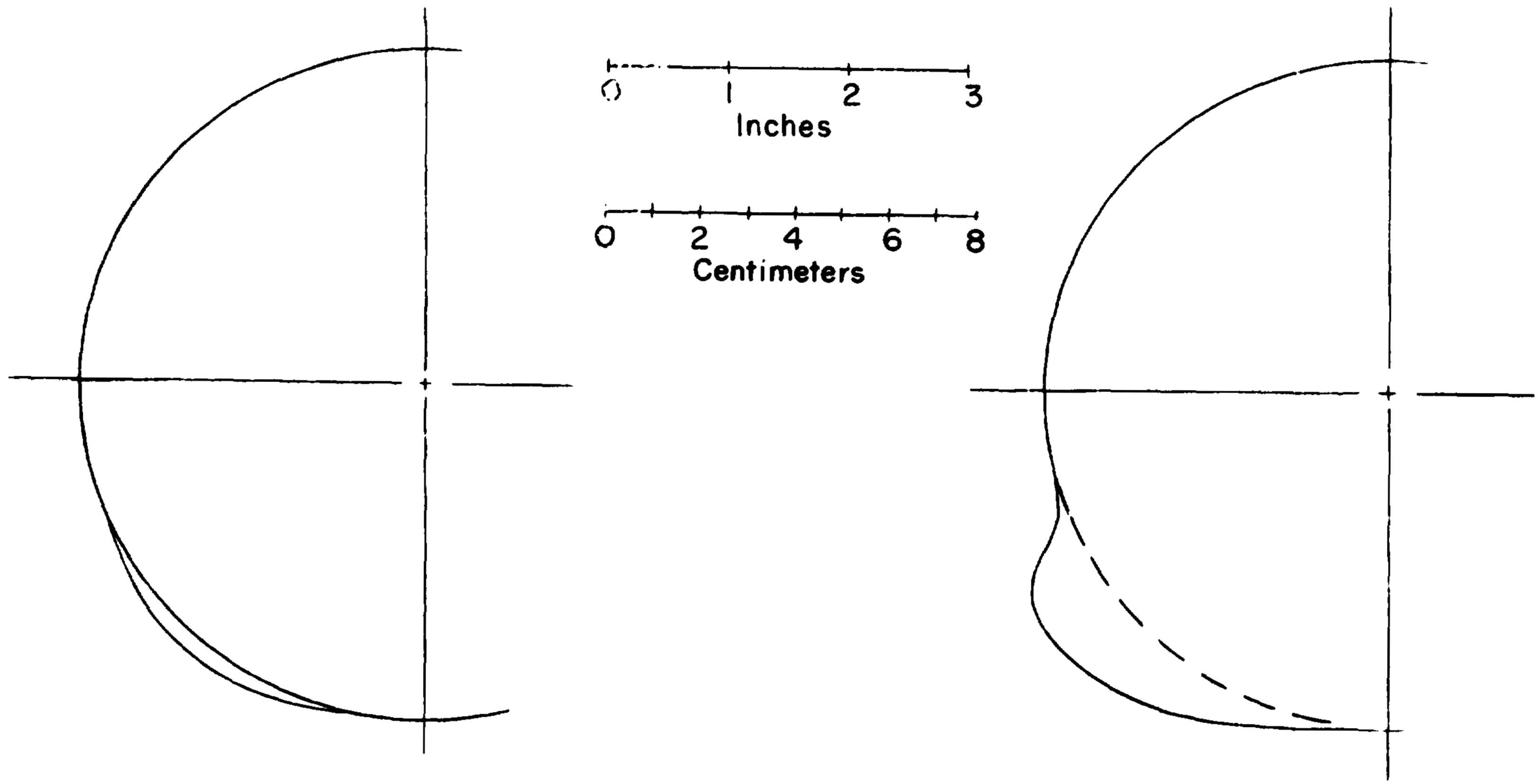

F.S. = 61.976 cm(24.400 in.)

F.S. = 67.056 cm(26.400in.)

Figure 2. - Continued.

CONFIDE[redacted]

[redacted]

[redacted]

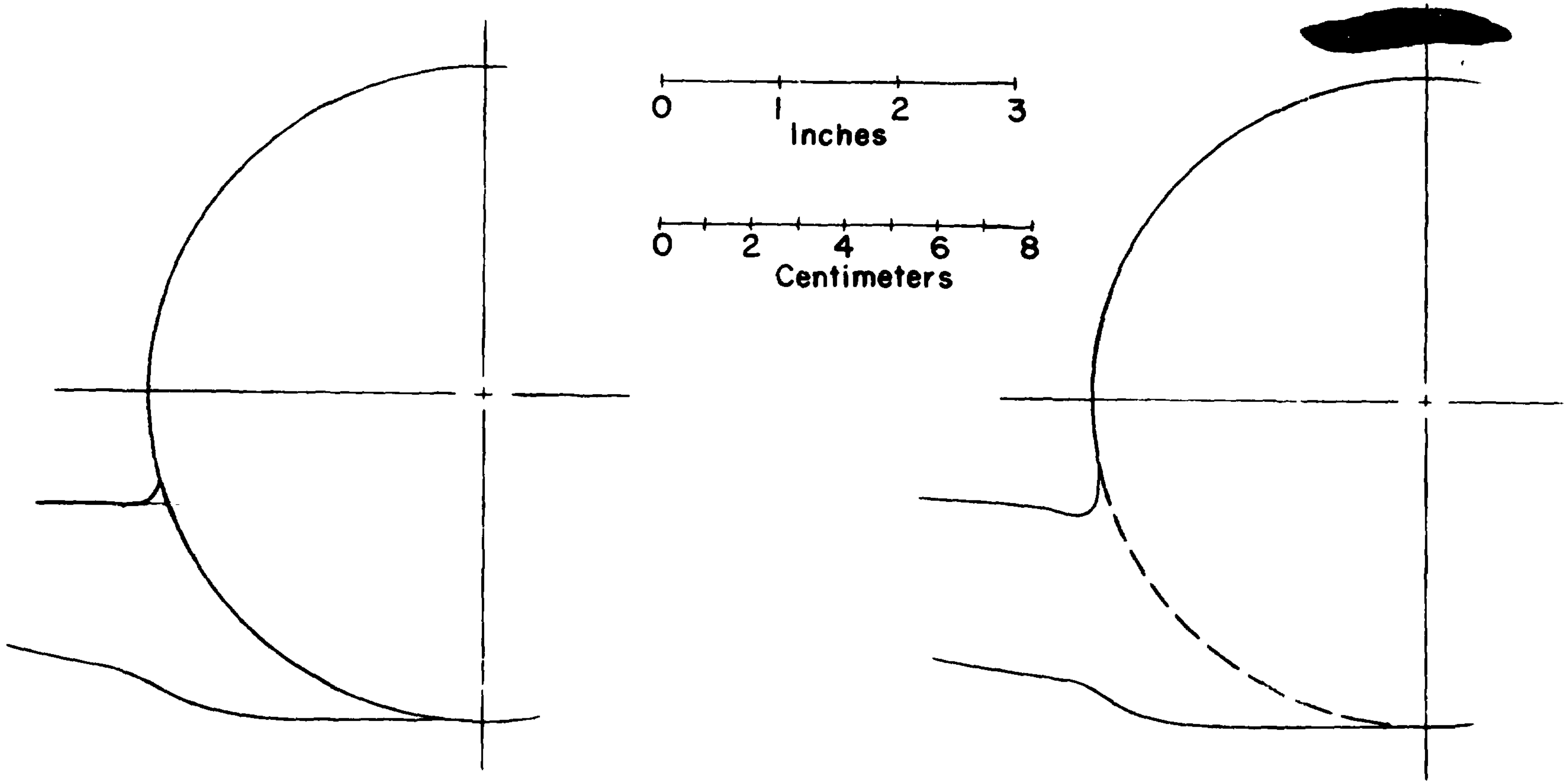

F.S. = 72.136 cm (28.400 in.)

F.S. = 77.216 cm (30.400 in.)

Figure 2. - Continued.

[redacted]

[redacted]

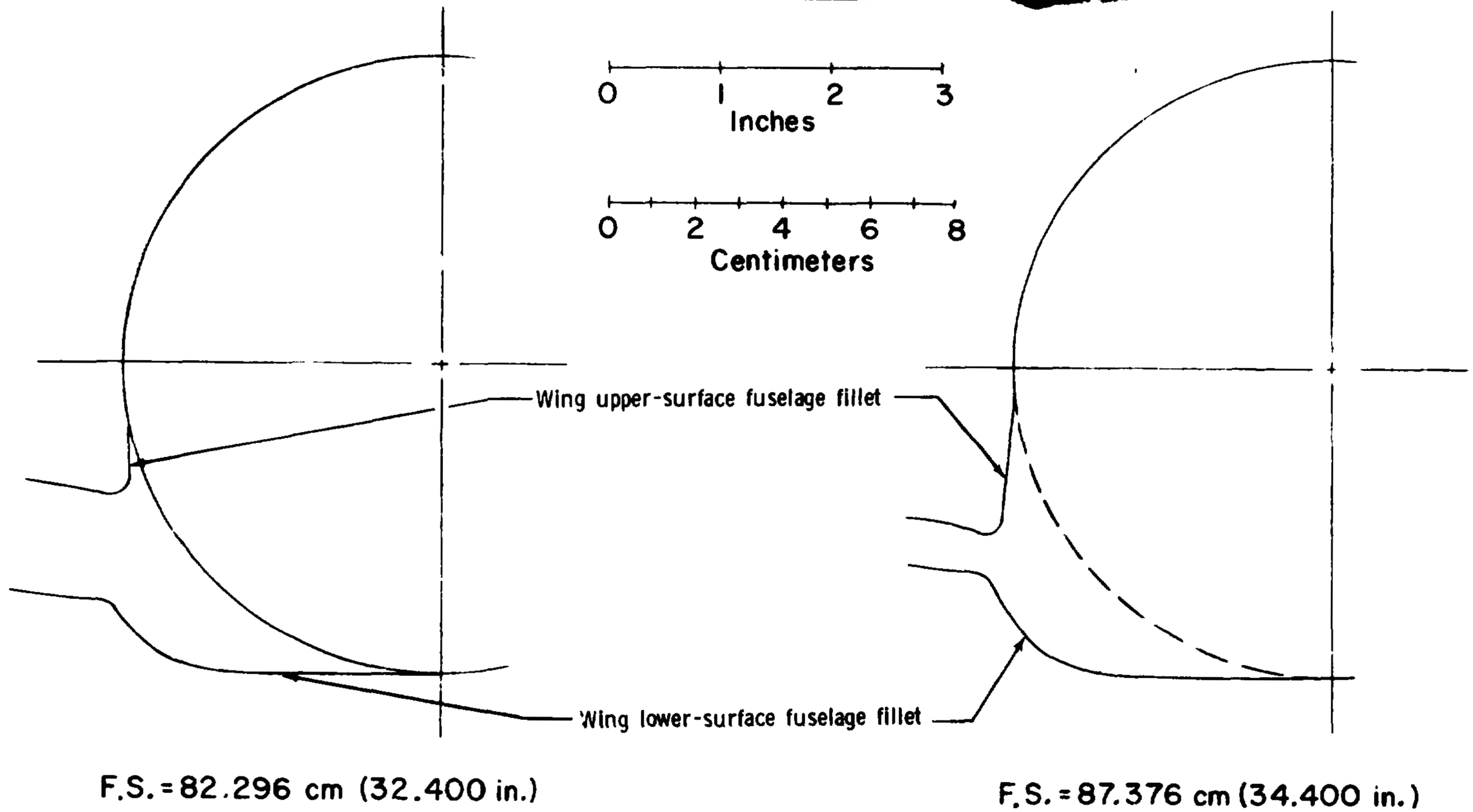

Figure 2. - Continued.

[redacted]

[redacted] [redacted]

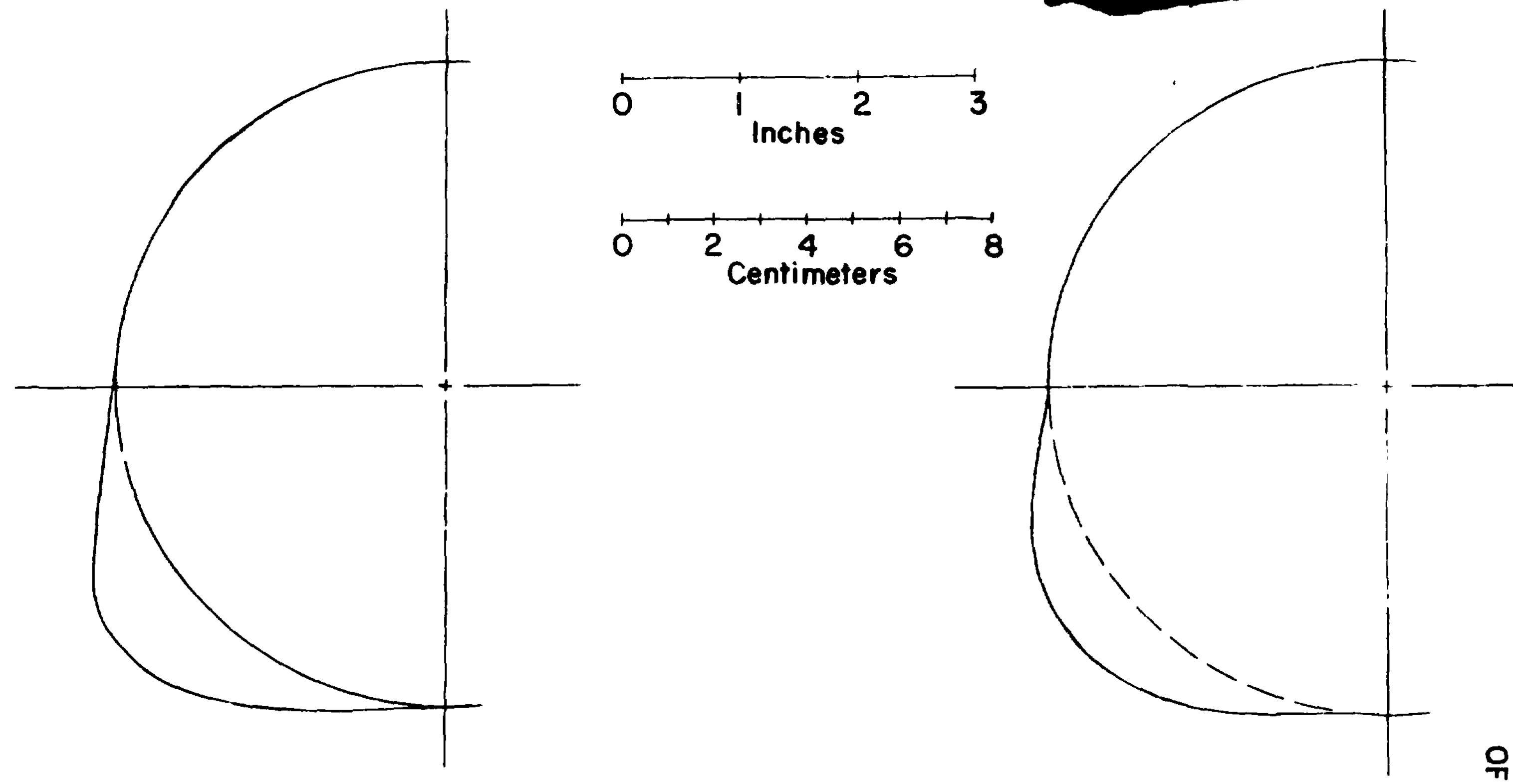

F.S. = 92.456 cm (36.400 in.)

F.S. = 97.536 cm (36.400 in.)

Figure 2. - Continued.

[redacted] [redacted]

[redacted] [redacted]

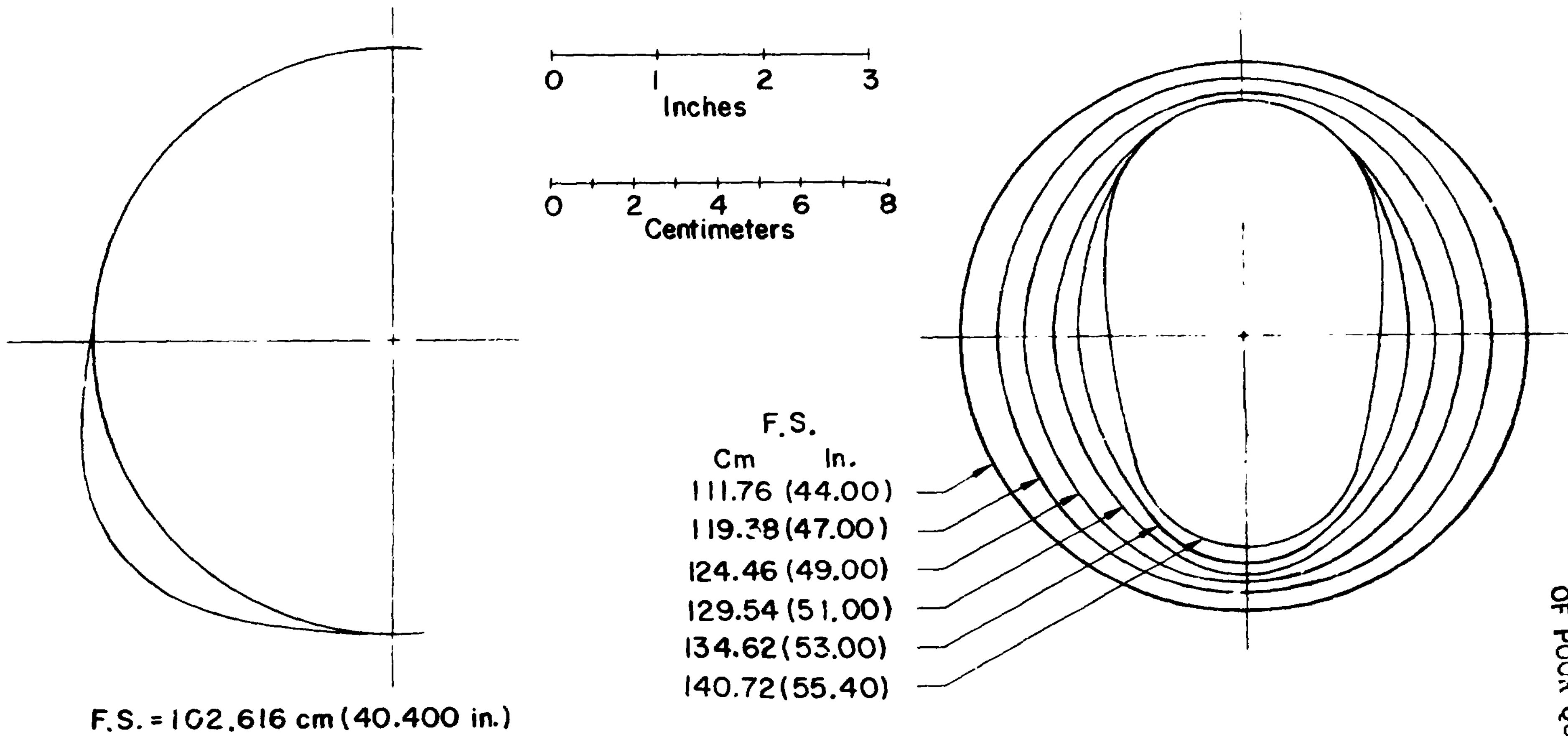

Figure 2. - Concluded.

[redacted] [redacted]

ORIGINAL PAGE IS
OF POOR QUALITY

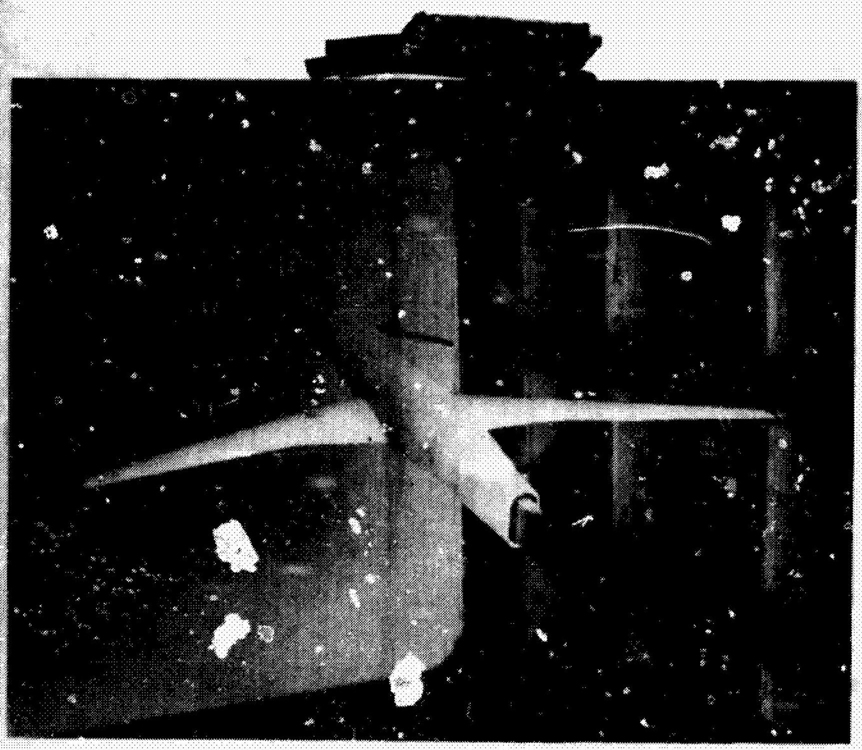

NASA

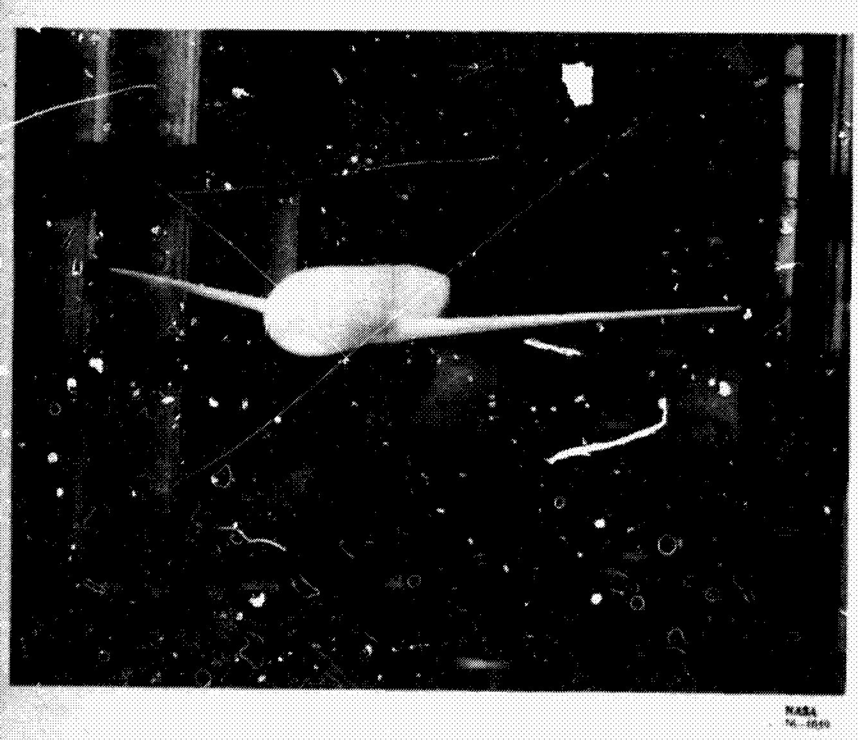

NASA

(a) Supercritical-wing configuration - Ib.

Figure 3. - Model photographs.

(b) Simulated wide-body configuration.

Figure 3. - Concluded

[redacted] [redacted]

ORIGINAL PAGE IS OF POOR QUALITY

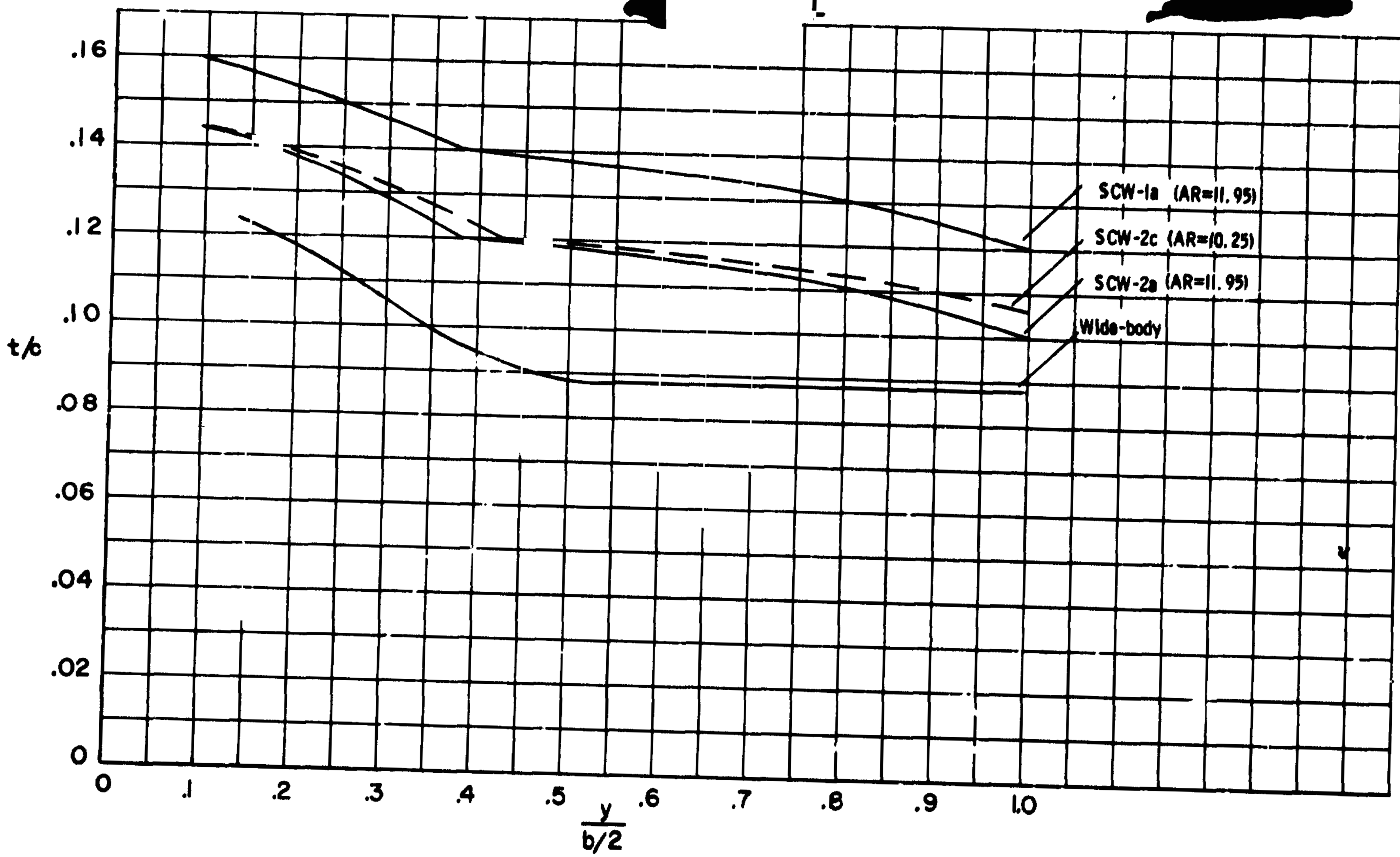

(a) Thickness distribi 'ion.

Figure 4. - Spanwise variation of wing maximum [redacted] nd local section incidence angle.

[redacted]

[redacted]

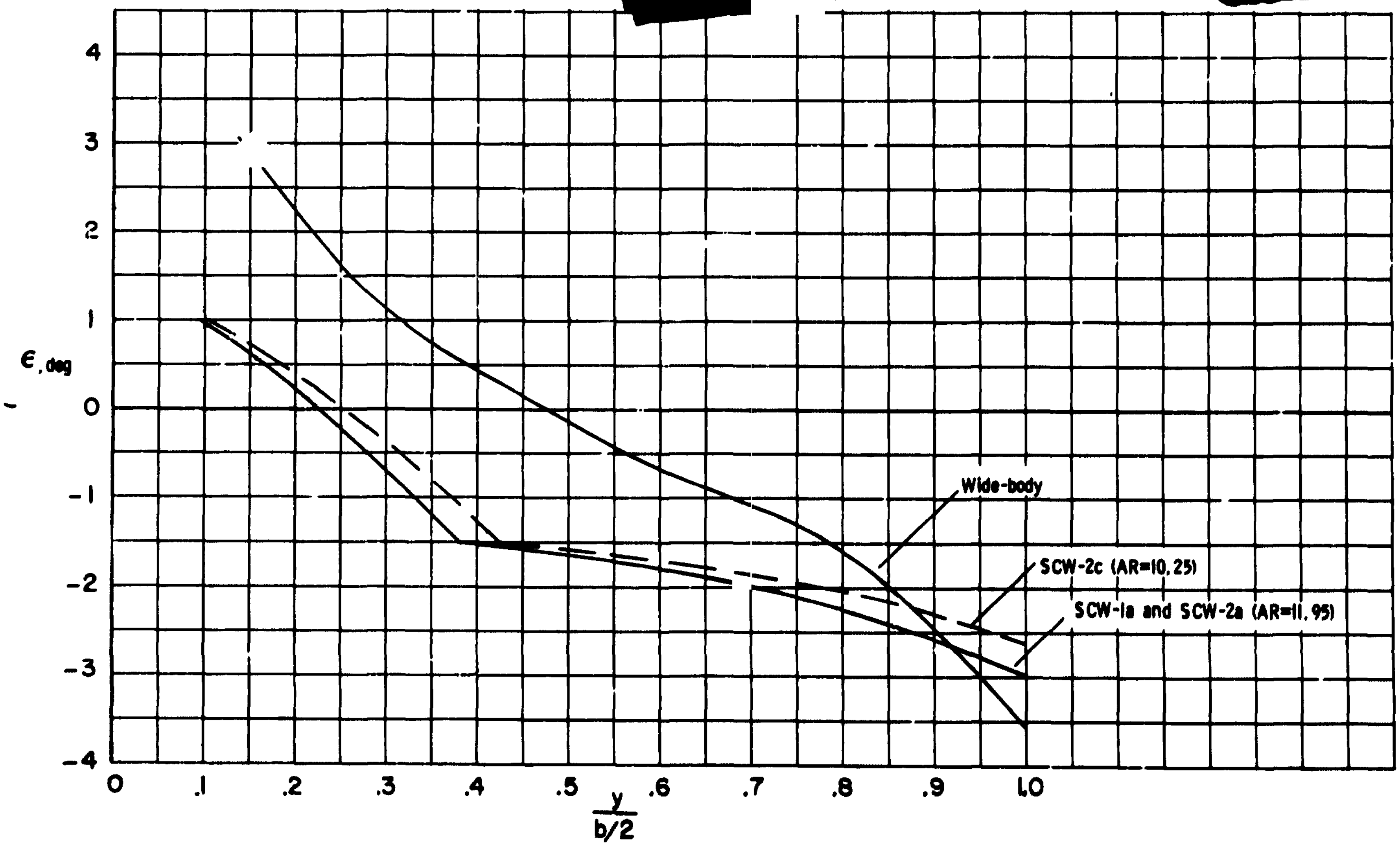

(b) Wing section incidence angle(streamwise).

Figure 4. - [redacted]

[redacted]

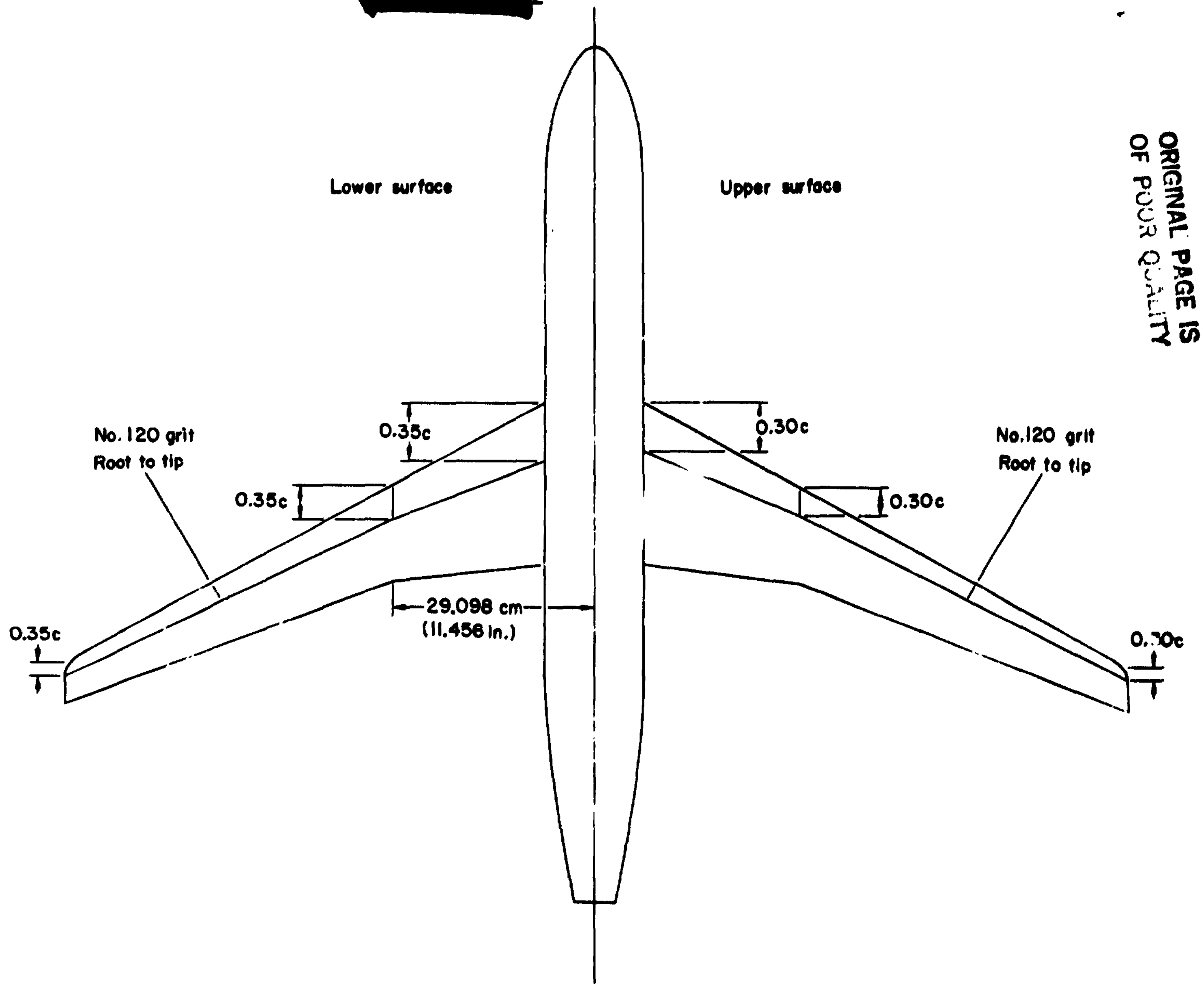

(a) Supercritical-wing configuration Ia*.

Figure 5. - Wing boundary-layer trip arrangements for the aft-chord locations.

[redacted]

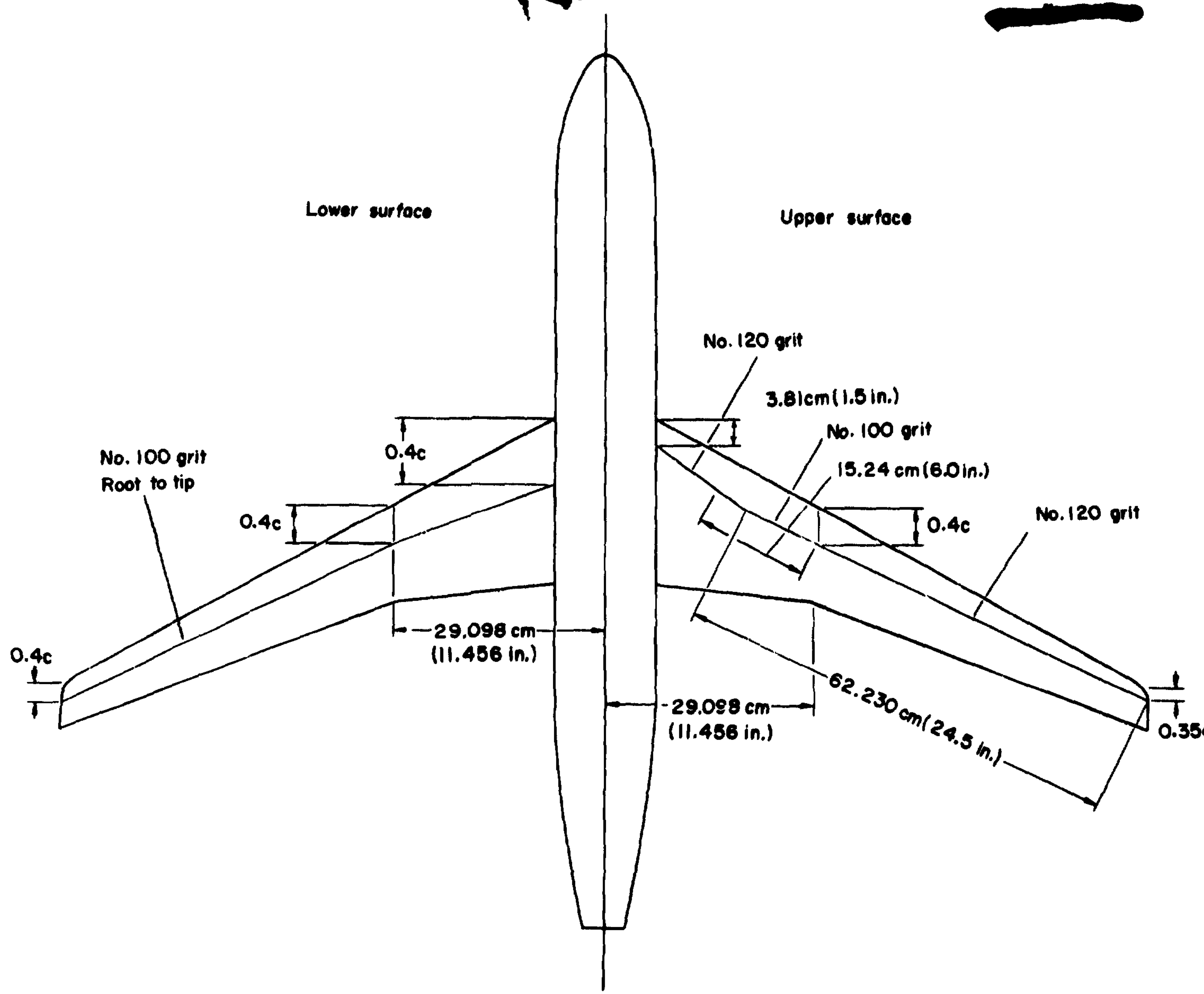

(b) Supercritical-wing configurations Ia and Ib.

Figure 5. - Continued.

[redacted]

CONFIDENTIAL

[redacted]

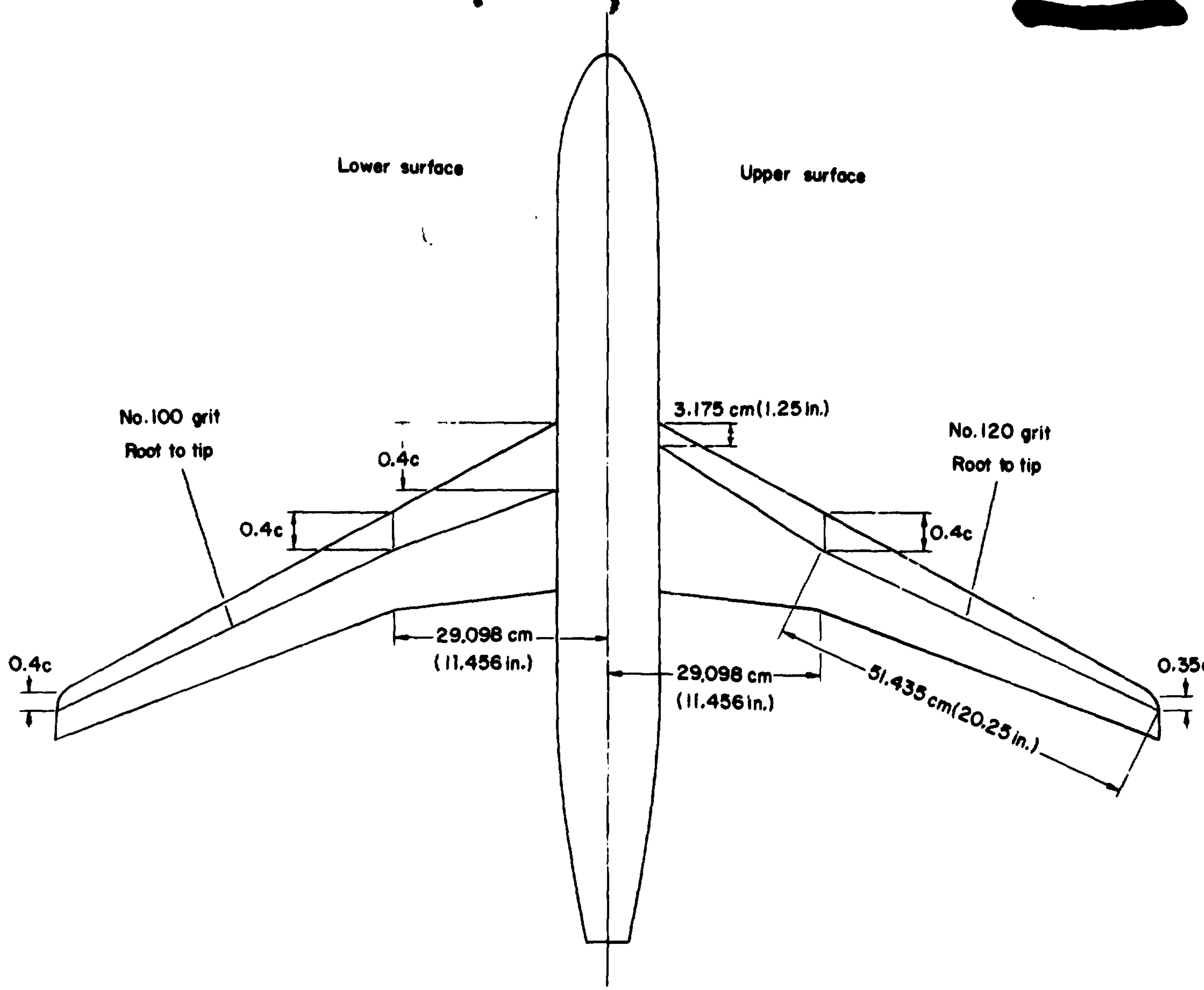

(c) Supercritical-wing configurations 2a and 2b.

Figure 5. - Continued.

[redacted]

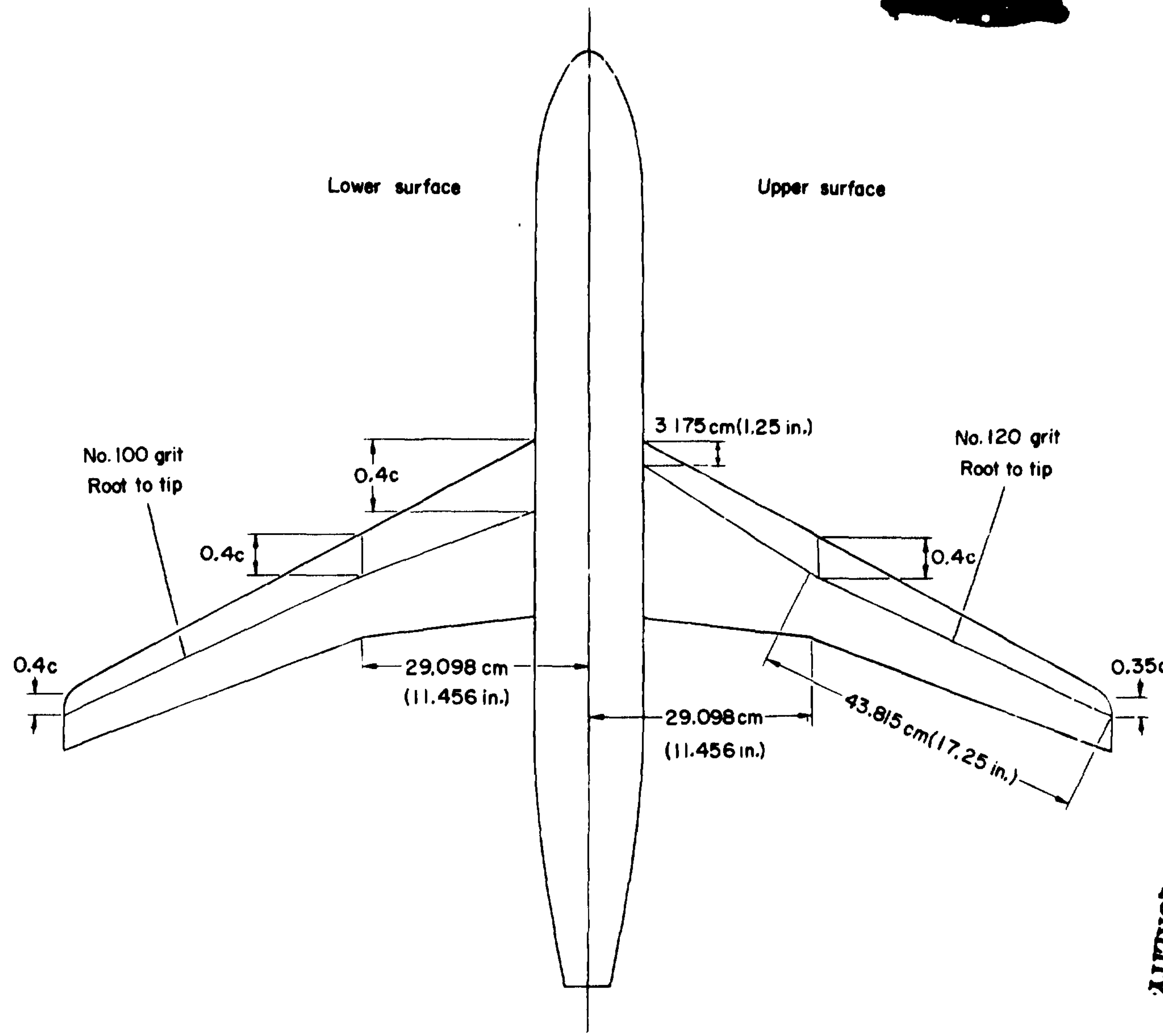

(d) Supercritical-wing configuration 2c.

Figure 5. - Continued.

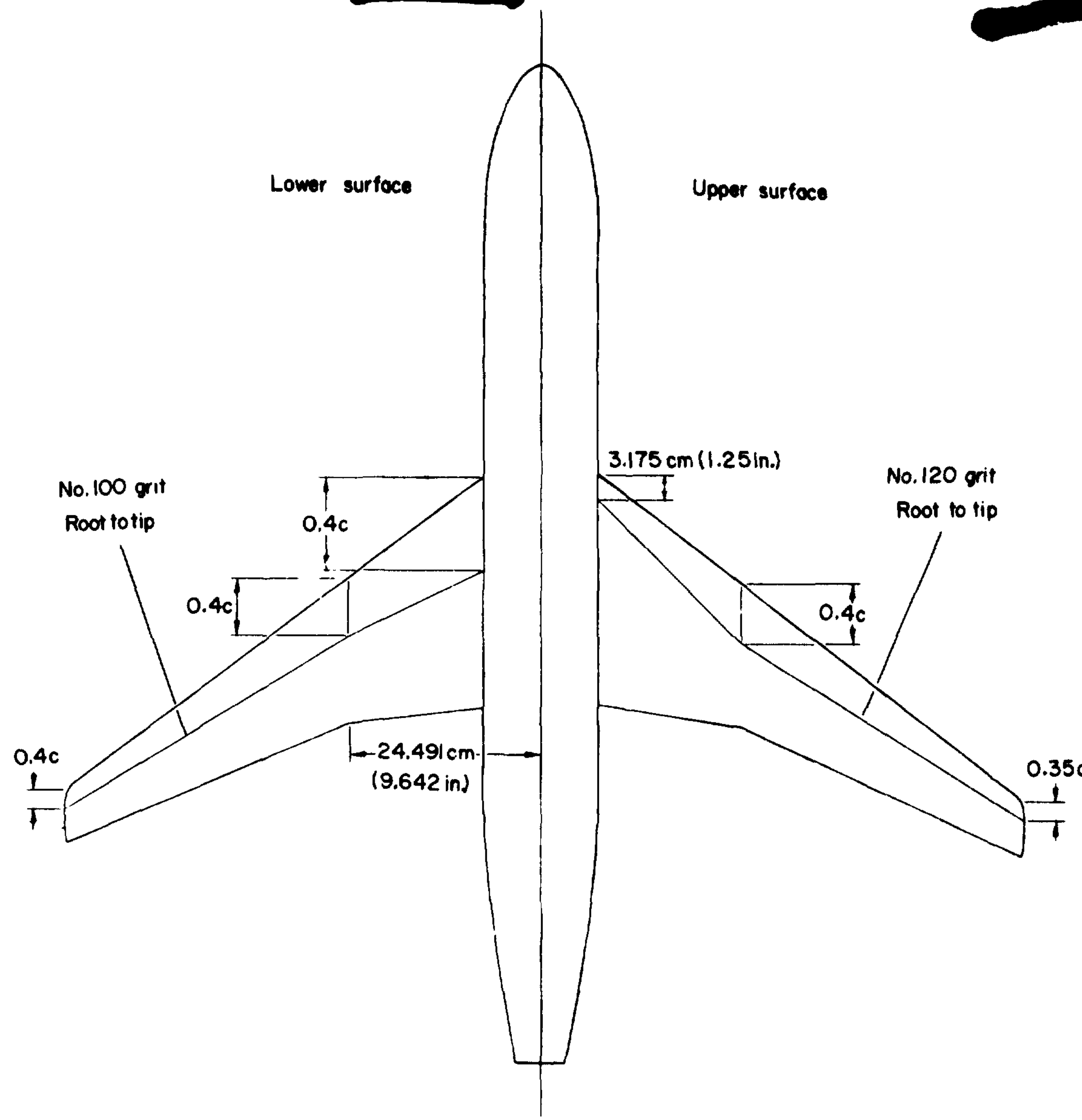

(e) Simulated wide-body configuration.

Figure 5. - Concluded.

ORIGINAL PAGE IS
OF POOR QUALITY

[redacted]

Wing U. S. grit aft

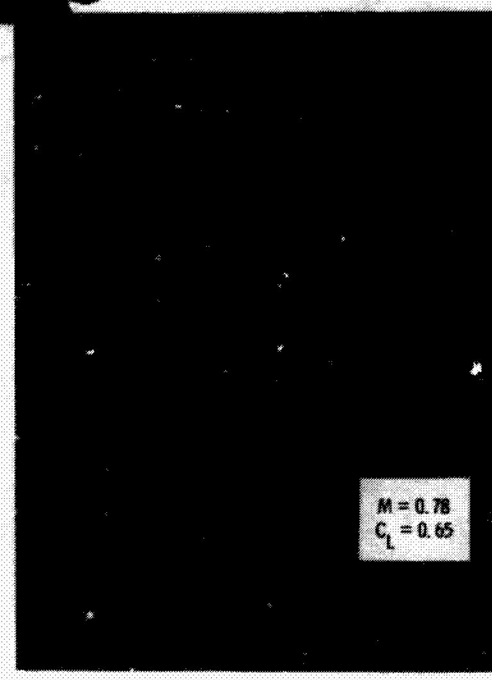

Wing U. S. grit forward ($x_T/c = 0.05$)

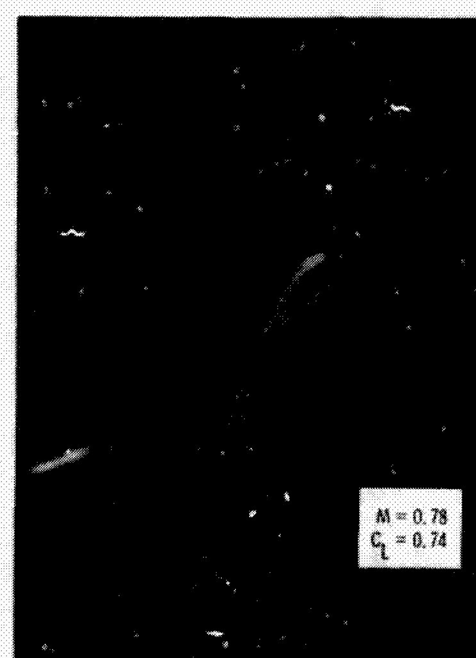

(a) Supercritical-wing configuration Ia*.

[redacted] Figure 6. - Wing upper-surface oil-flow photographs.

[redacted]

ORIGINAL PAGE IS
OF POOR QUALITY

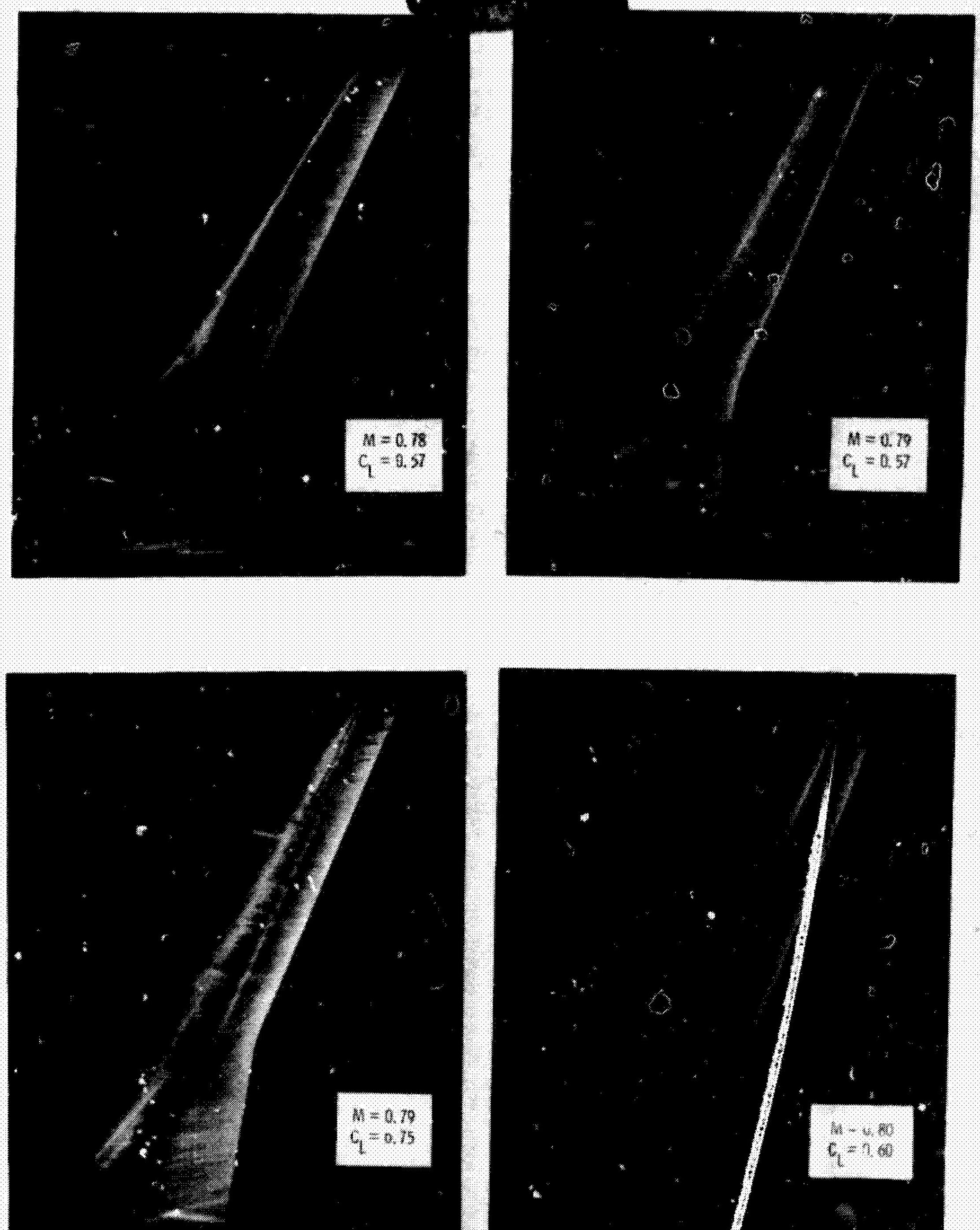

(b) Supercritical-wing configuration Ib. Wing U.S. gr. aft.

Figure 6. - Continued.

ORIGINAL PAGE IS
OF POOR QUALITY

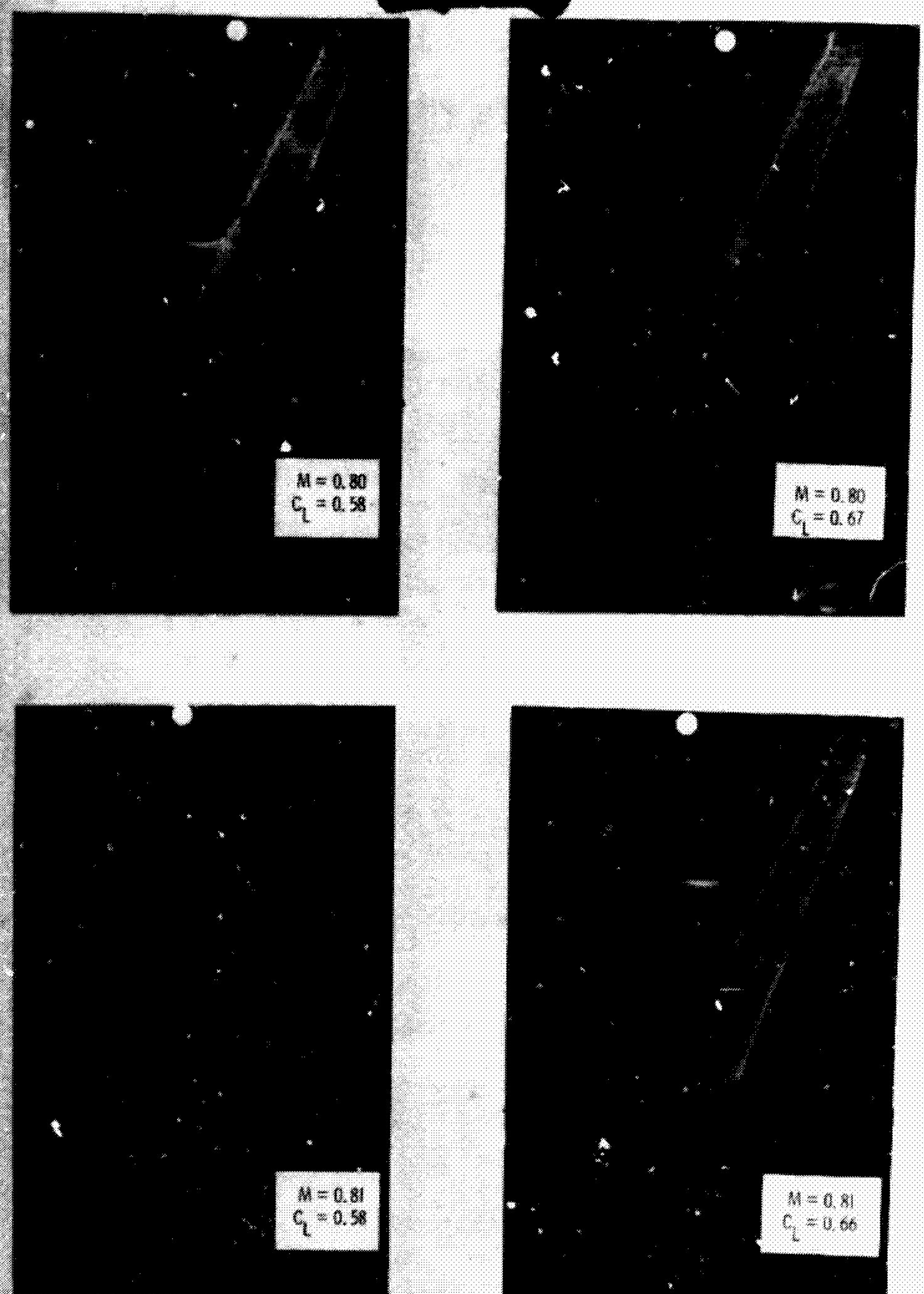

(c) Supercritical-wing configuration 2a, Wing U. S. grit aft.

Figure 6. - Continued.

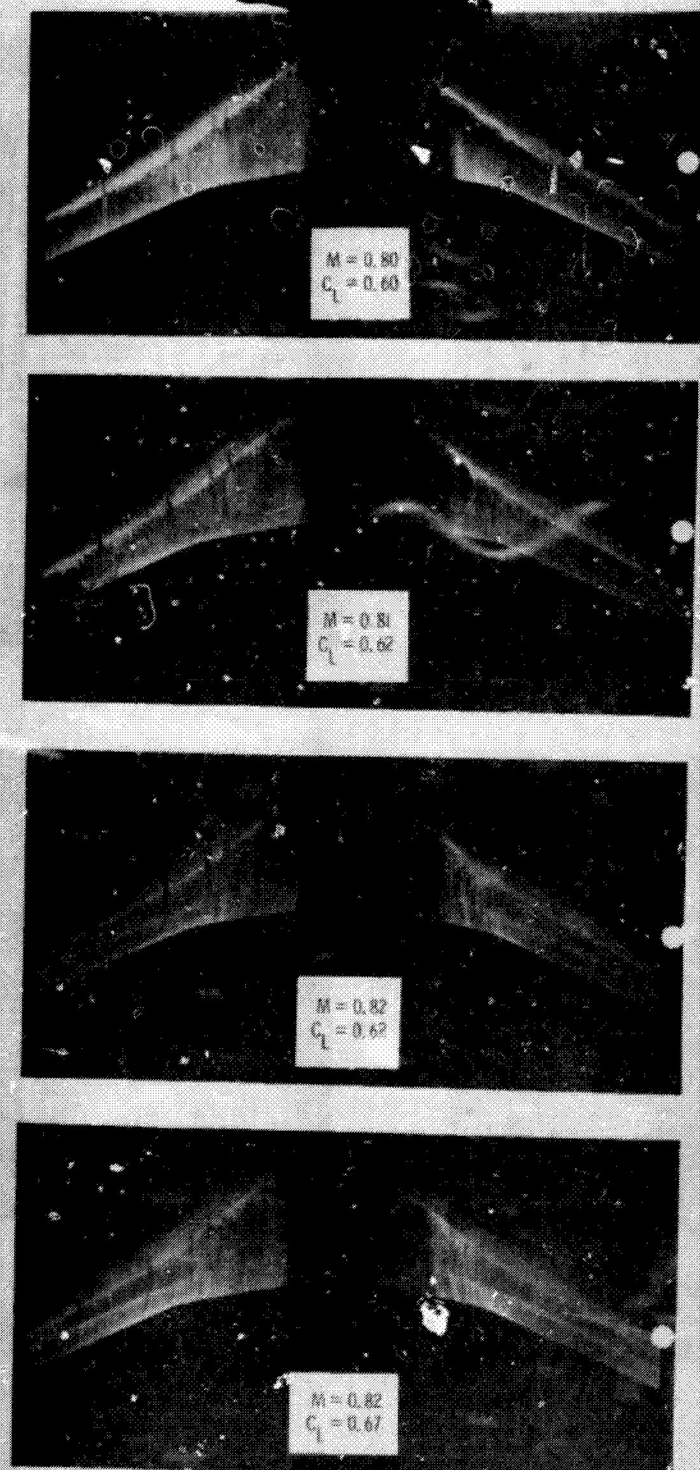

(Note: Wing tips not shown.)

(d) Supercritical-wing configuration 2b, Wing U.S. grit aft.

Figure 6. - Continued.

[redacted]

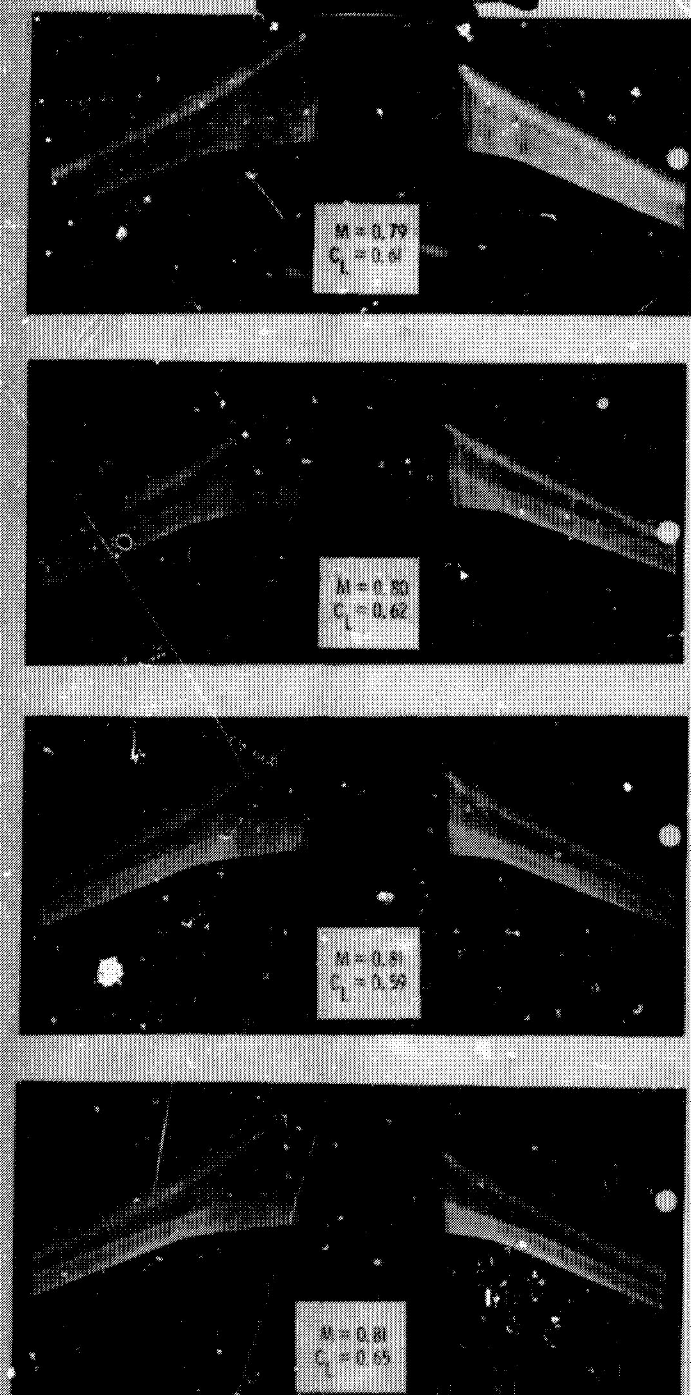

(Note: Wing tips not shown.)

(e) Supercritical-wing configuration 2c. Wing U.S. grit aft.

Figure 6. - Continued.

[redacted]NTIAL

[redacted]

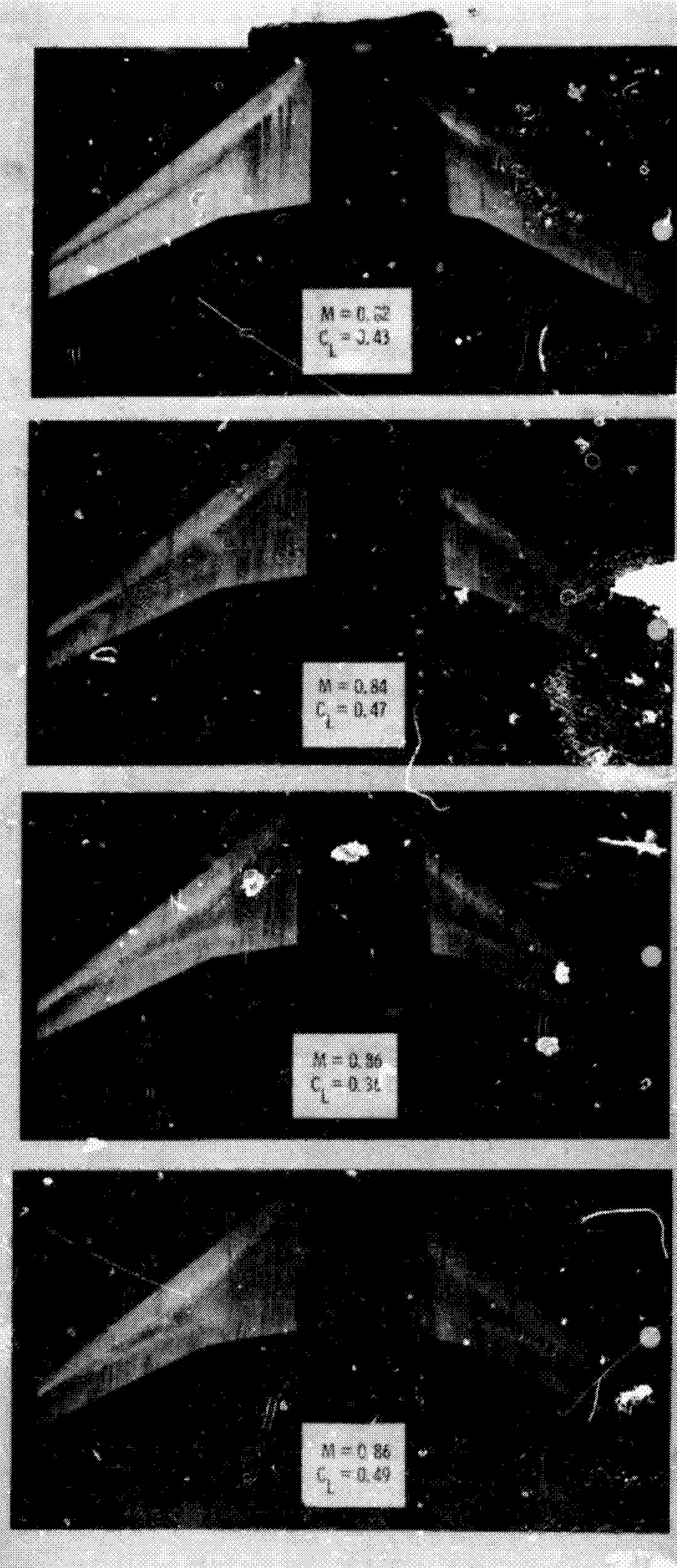

(f) Simulated wide-body configuration, Wing U. S. grit aft.

[redacted]ure 6. - Concluded.

ORIGINAL PAGE IS
OF POOR QUALITY

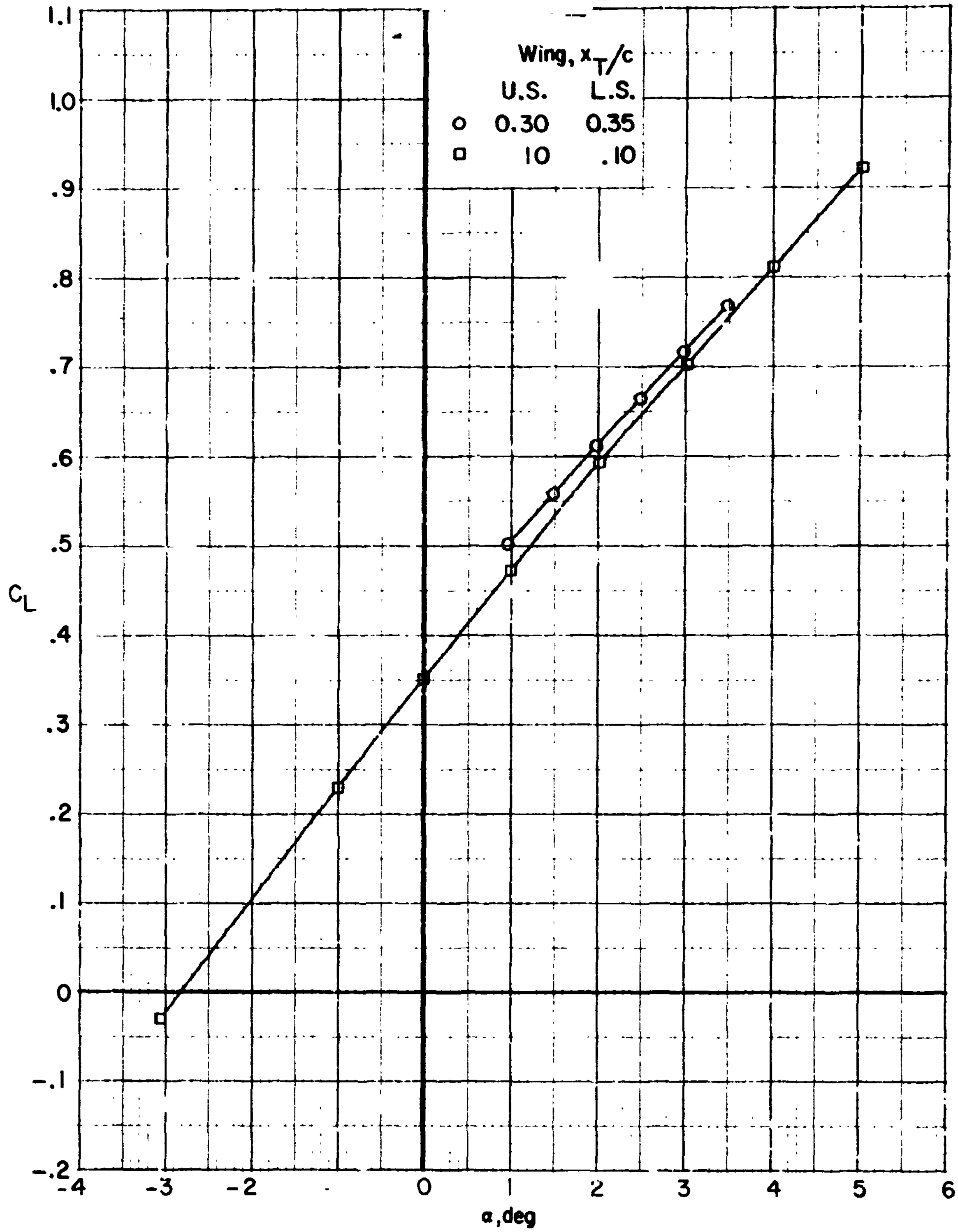

(c) M = 0.60.

Figure 7.- Longitudinal aerodynamic characteristics for supercritical wing configuration Ia* (SCW-Ia*). (*Results are from initial series of tests for this configuration.) c.g. (F.S.) = 84.605 cm (33.309 in.); $\Lambda_{c/4} = 27°$.

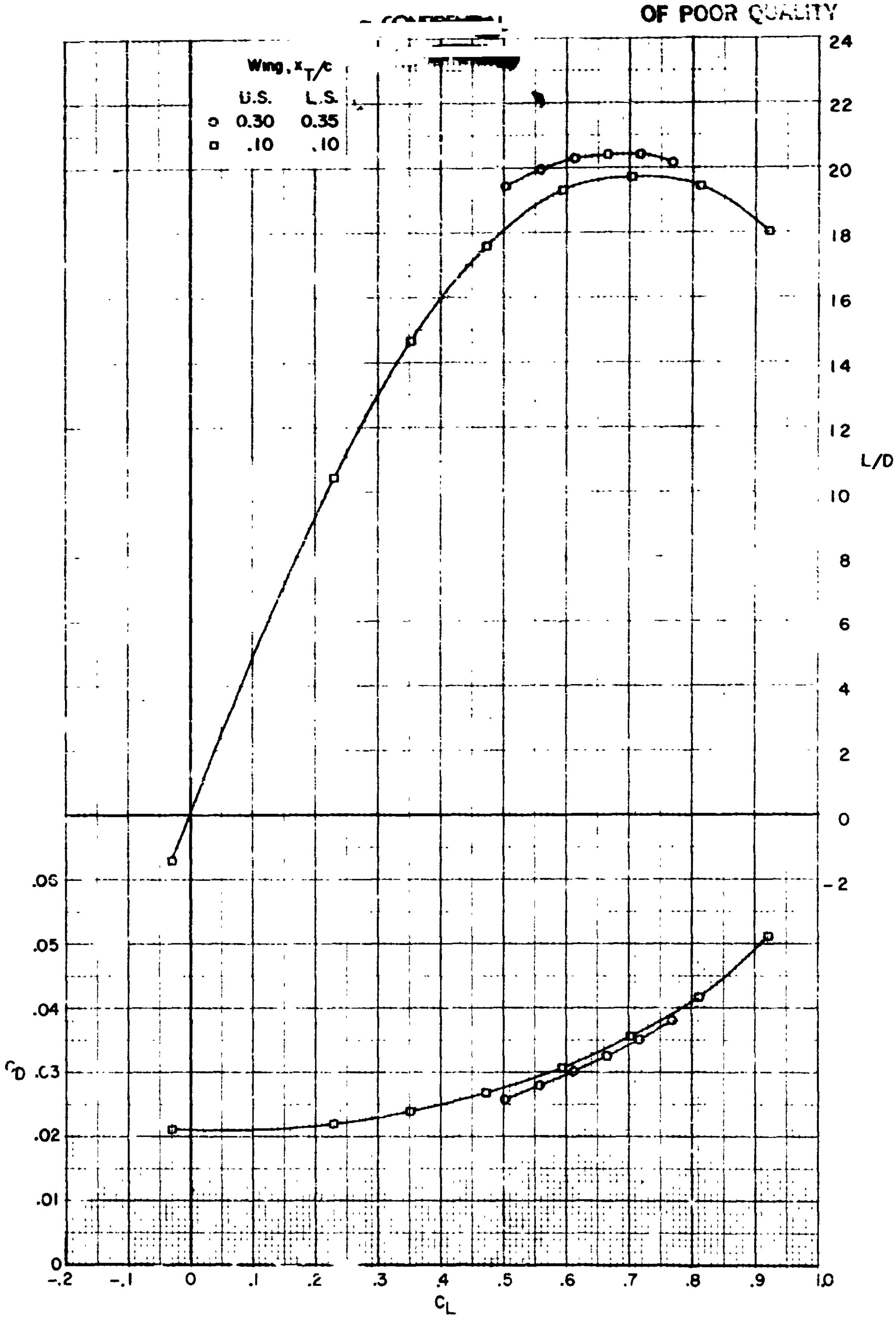

(a) M = 0.60. Continued.

Figure 7.- Continued.

[redacted]

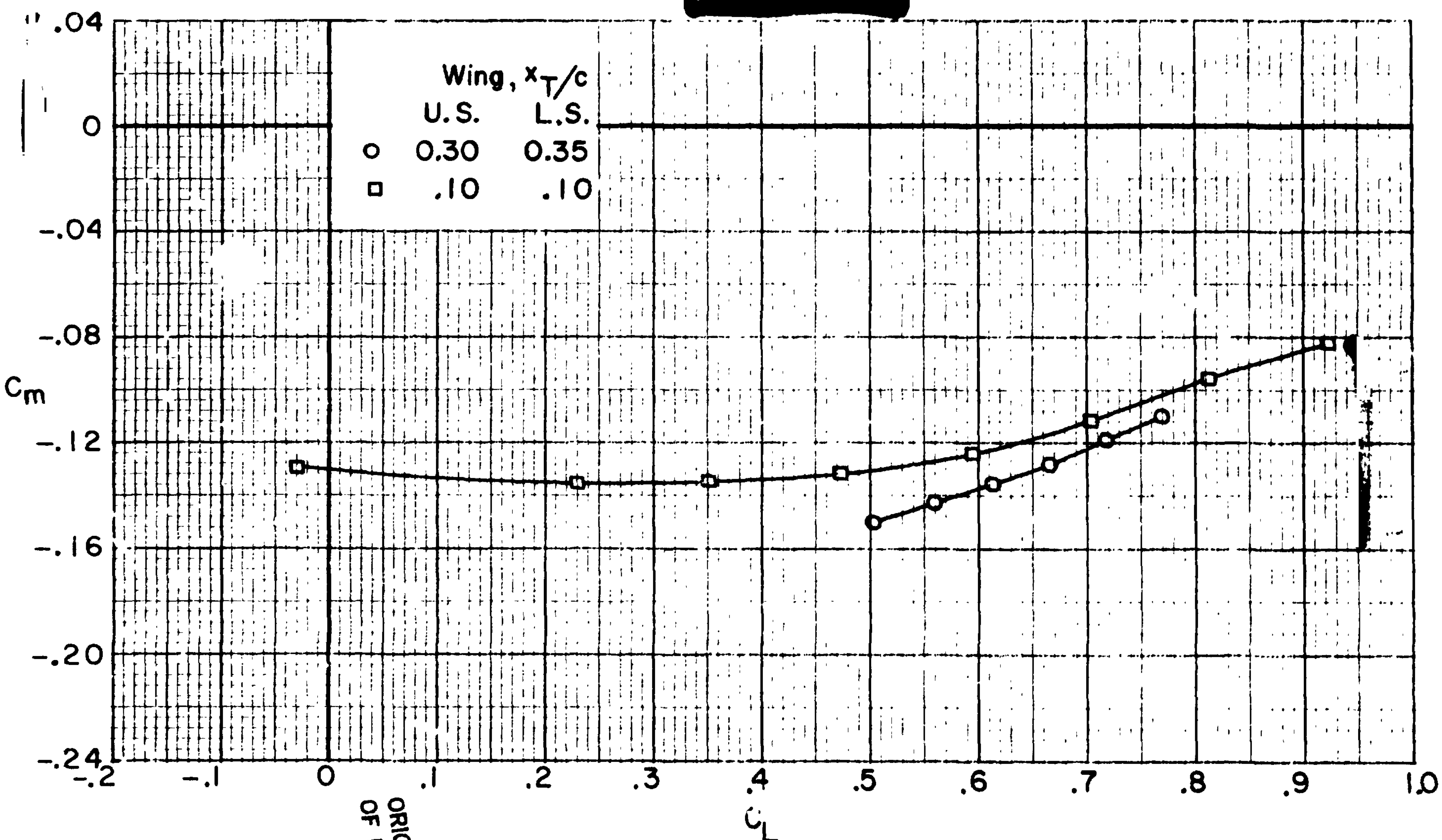

ORIGINAL PAGE IS OF POOR QUALITY

(a) M = 0.60. Concluded.

Figure 7.- Continued.

[redacted]

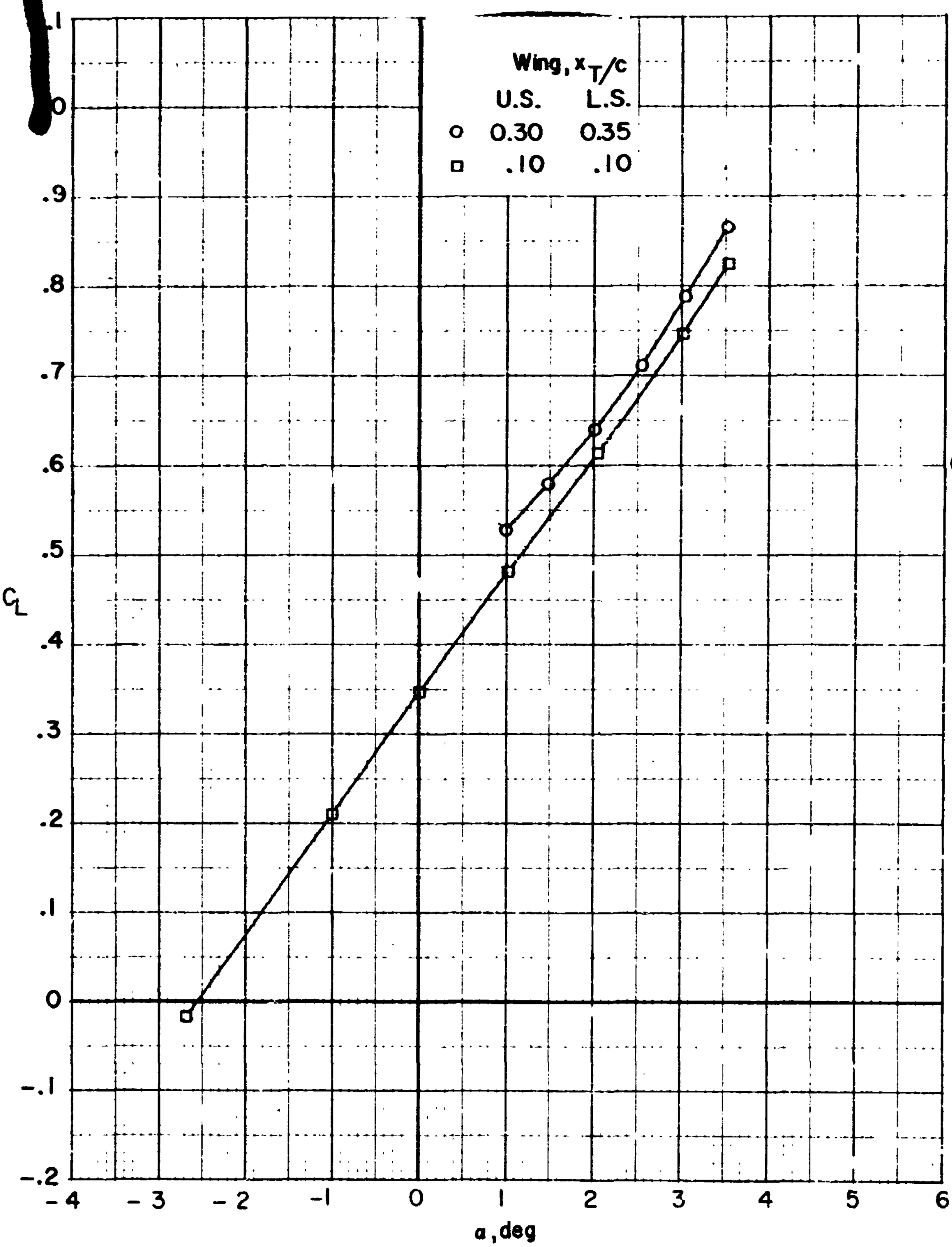

(b) M = 0.70.

Figure 7.- Continued.

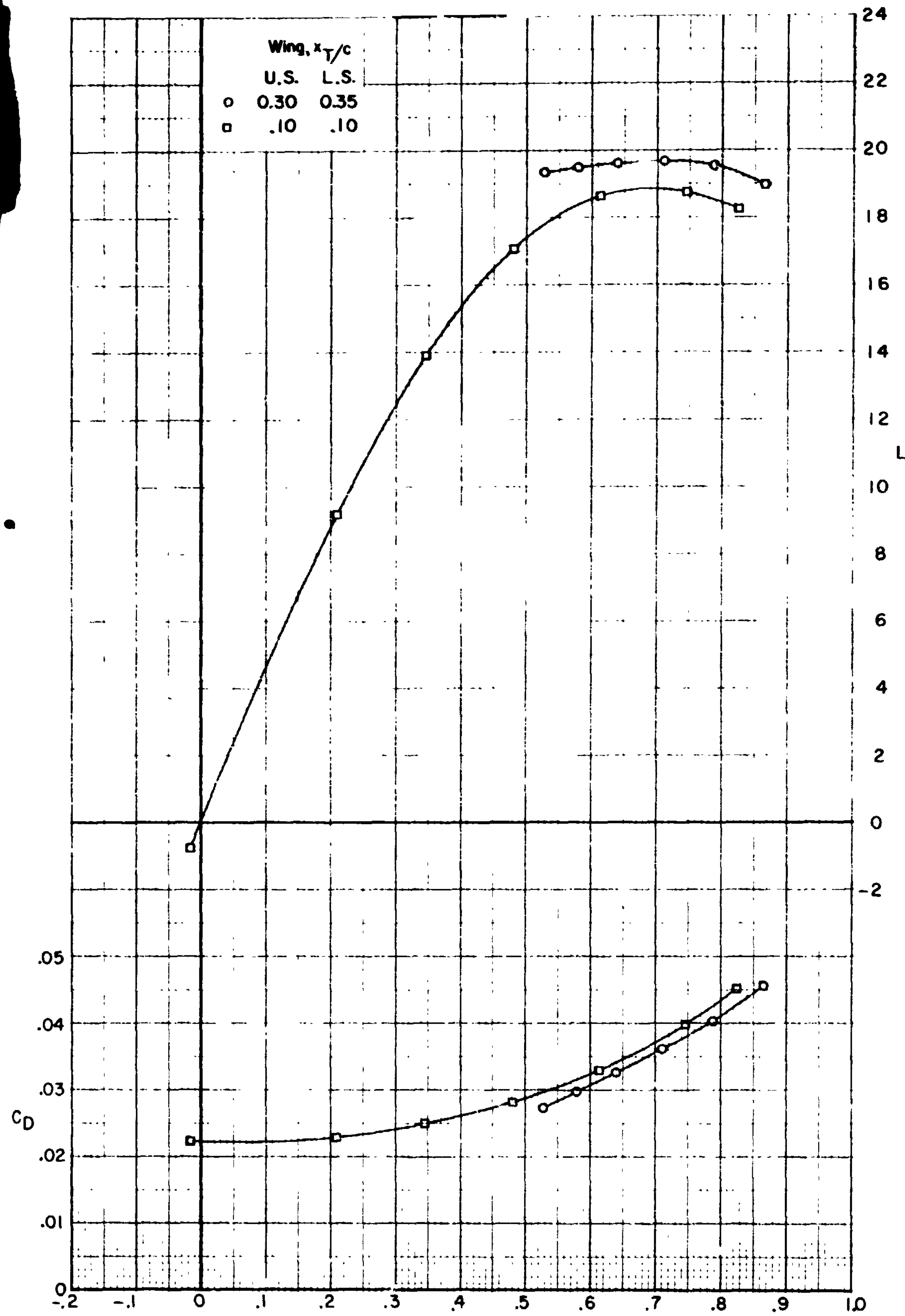

(b) M = 0.70. Continued.

Figure 7.- Continued.

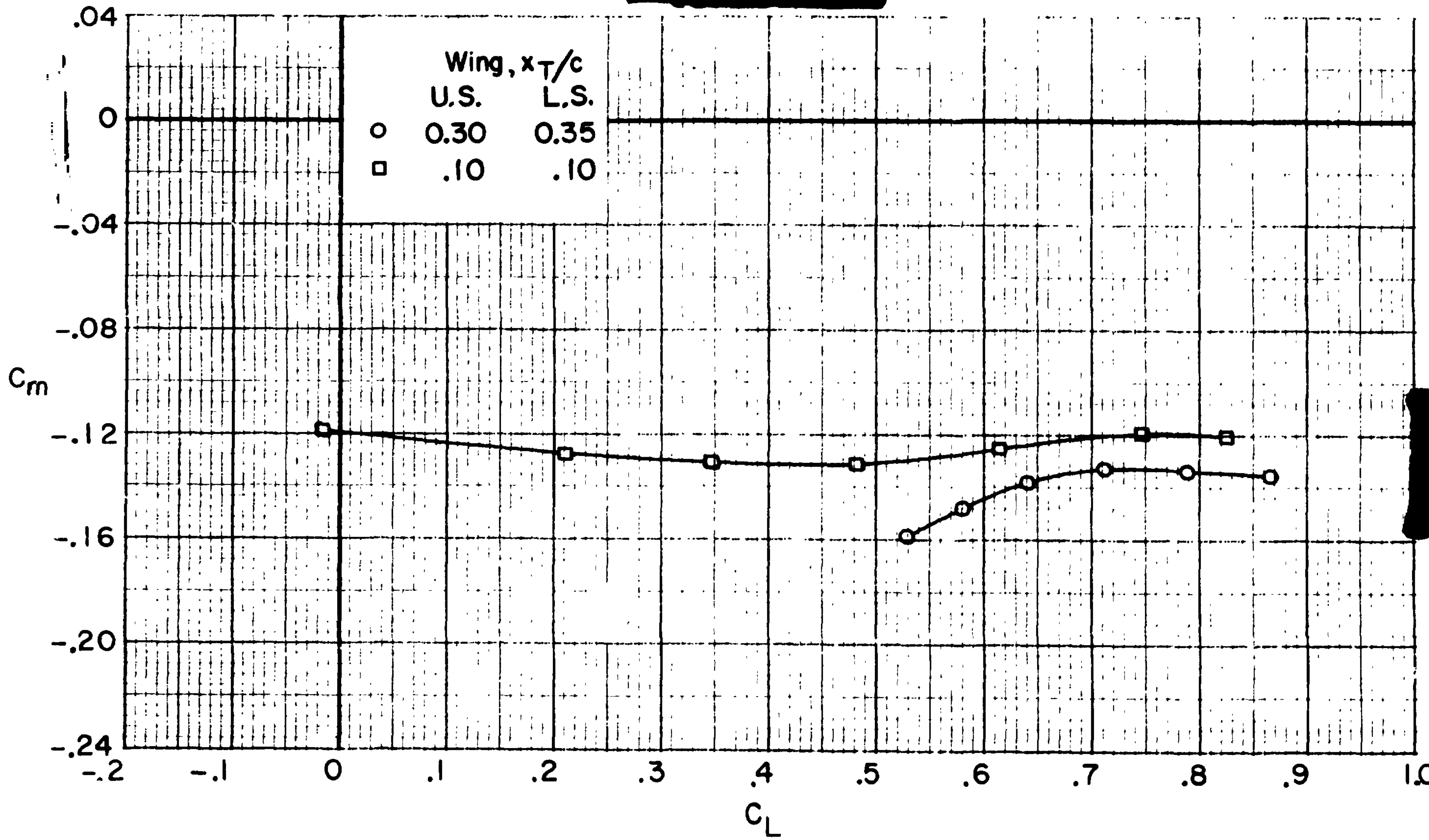

(b) M = 0.70. Concluded.

Figure 7.- Continued.

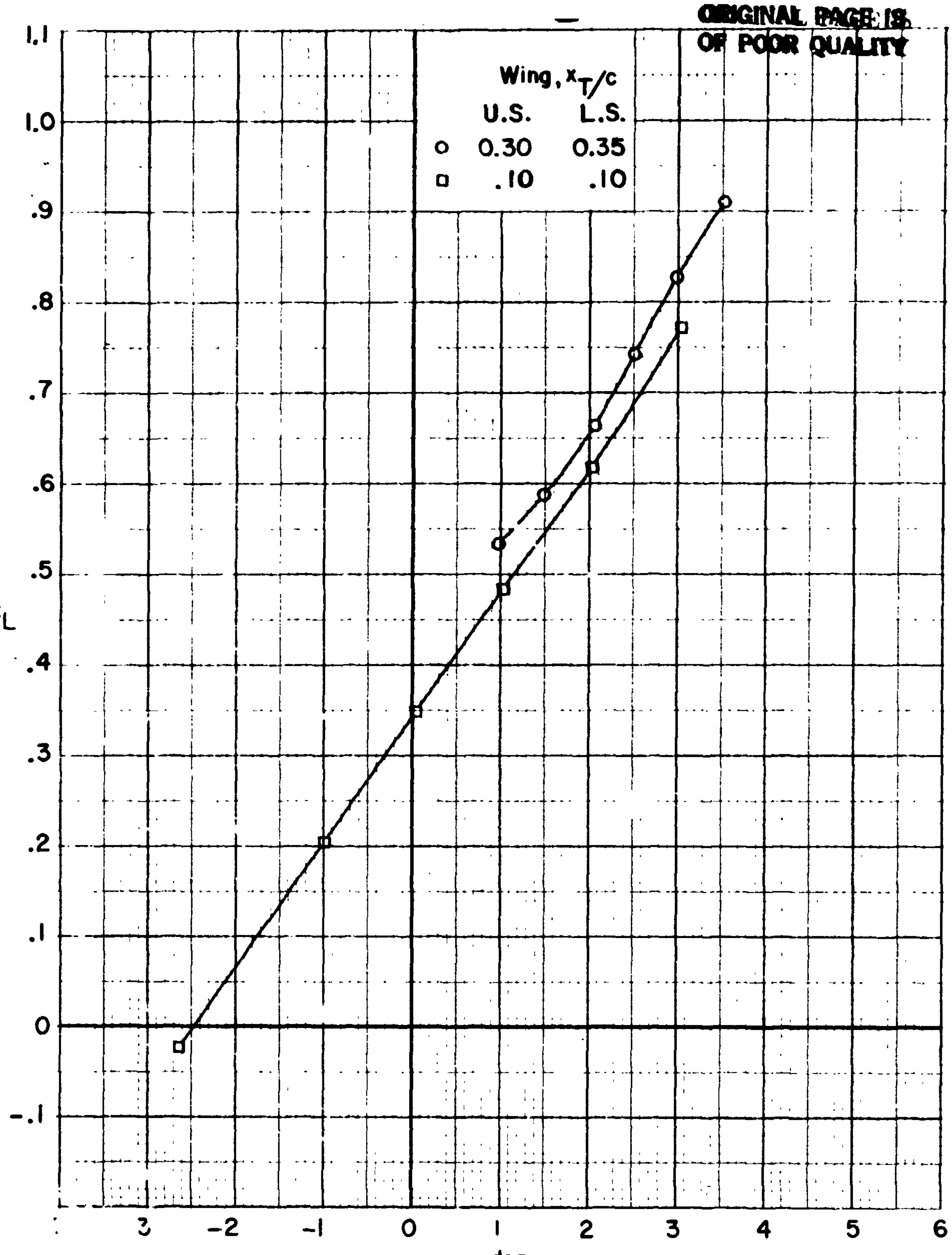

(c) M = 0.72.

Figure 7.- Continued.

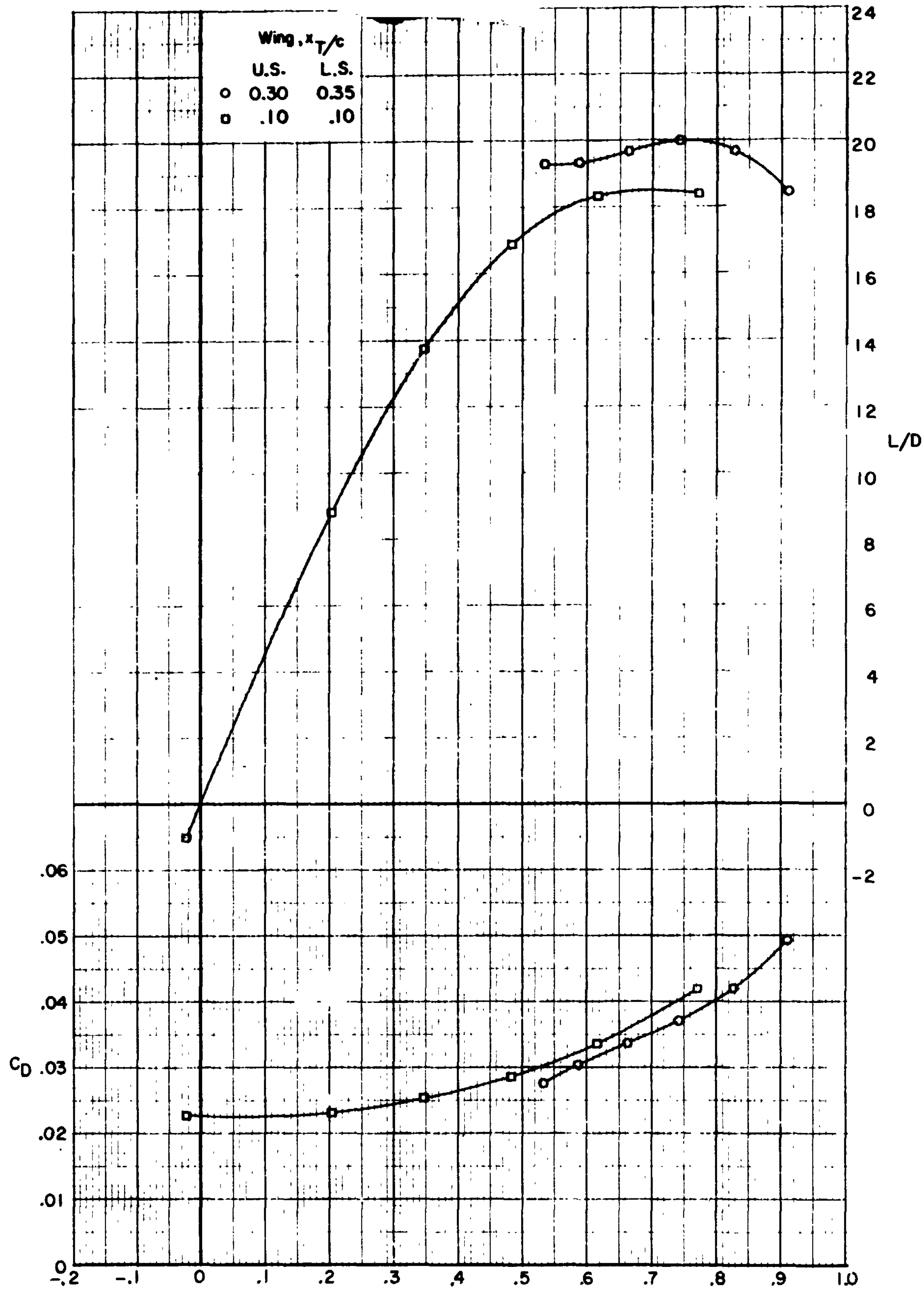

(c) M = 0.72. Continued.

Figure 7.- Continued.

[redacted]

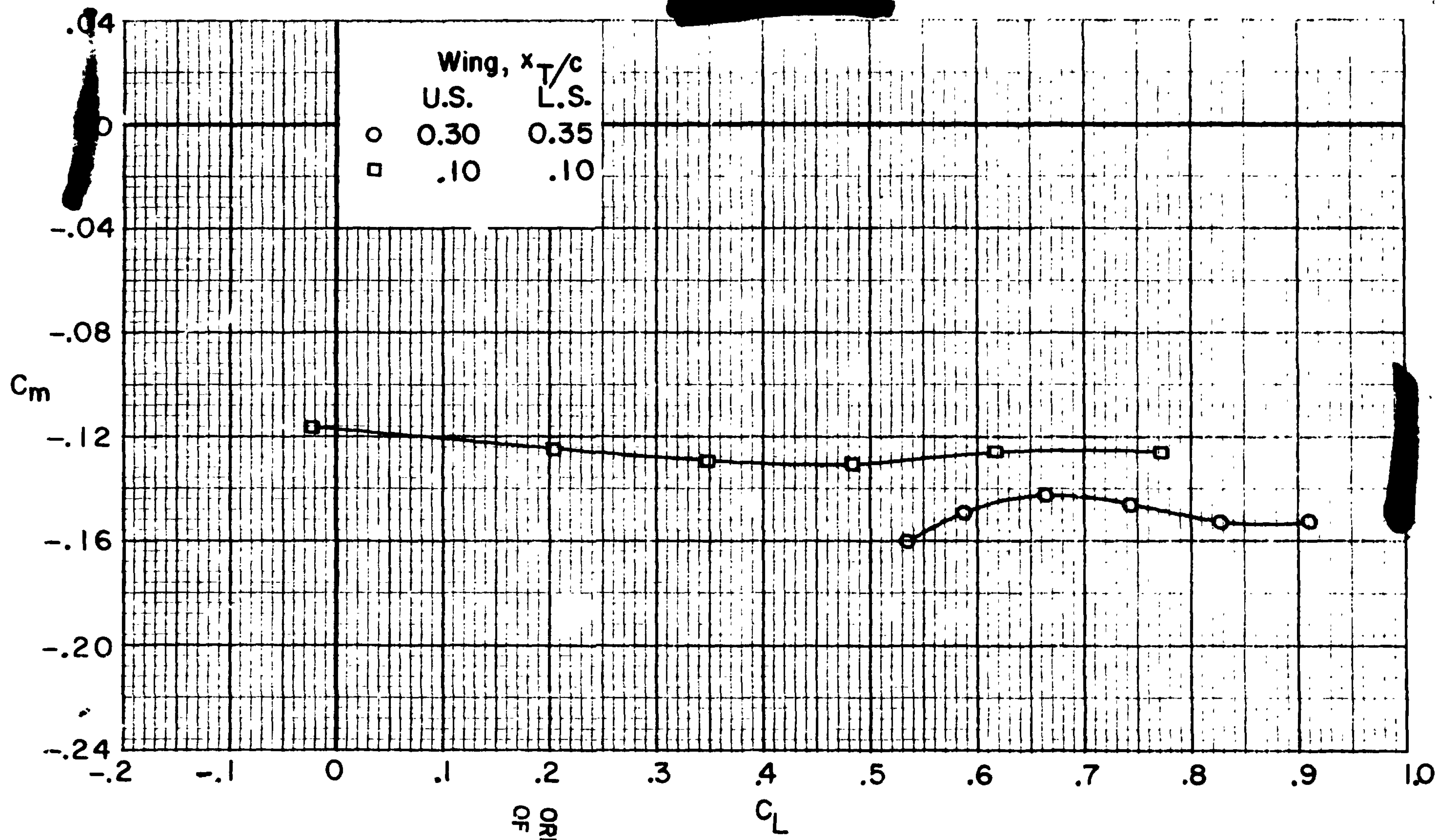

ORIGINAL PAGE IS OF POOR QUALITY

(c) M = 0.72. Concluded.

Figure 7.- Continued.

[redacted]

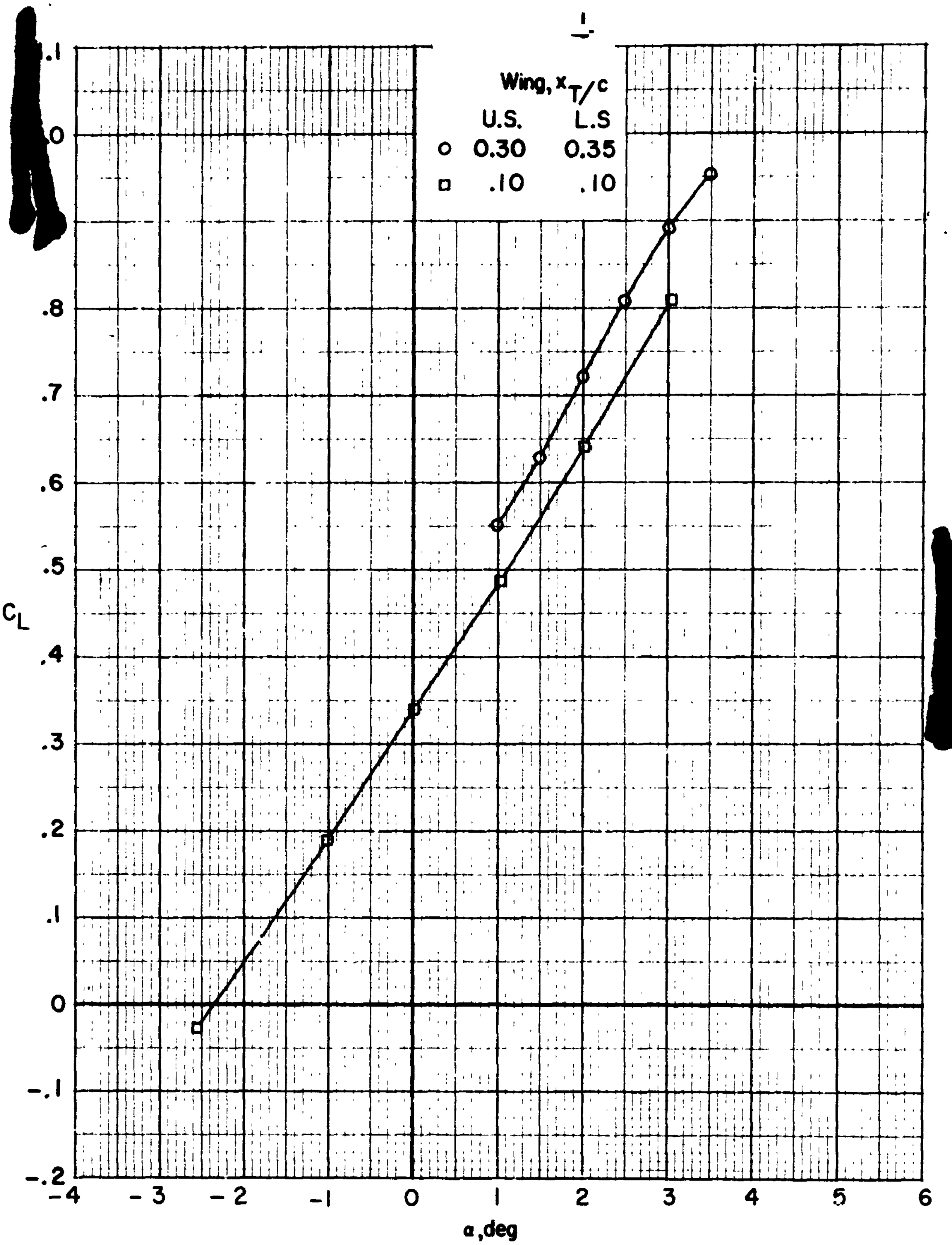

(d) M = 0.75.

Figure 7.- Continued.

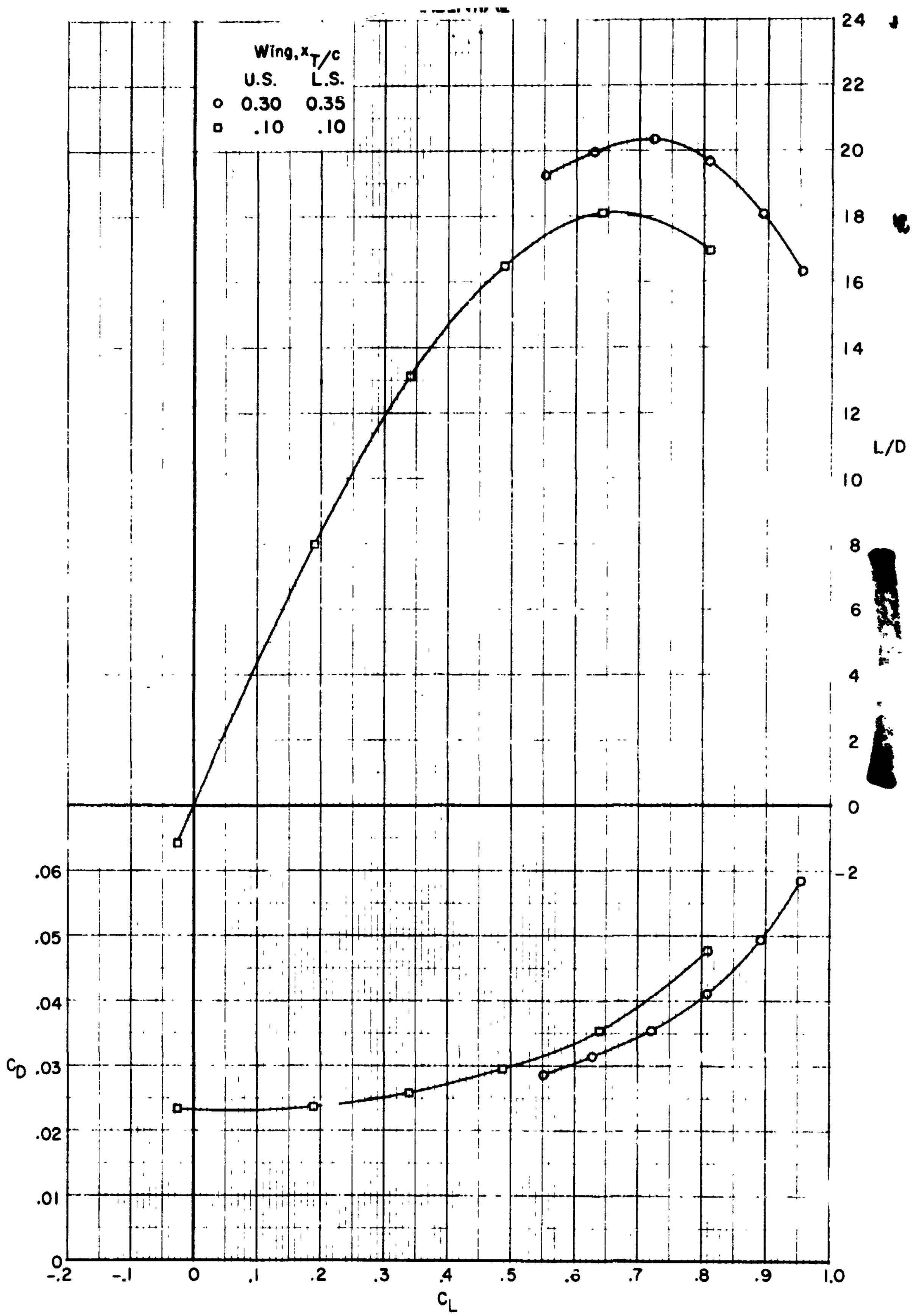

(d) M = 0.75. Continued.

Figure 7.- Continued.

[redacted]

[redacted]

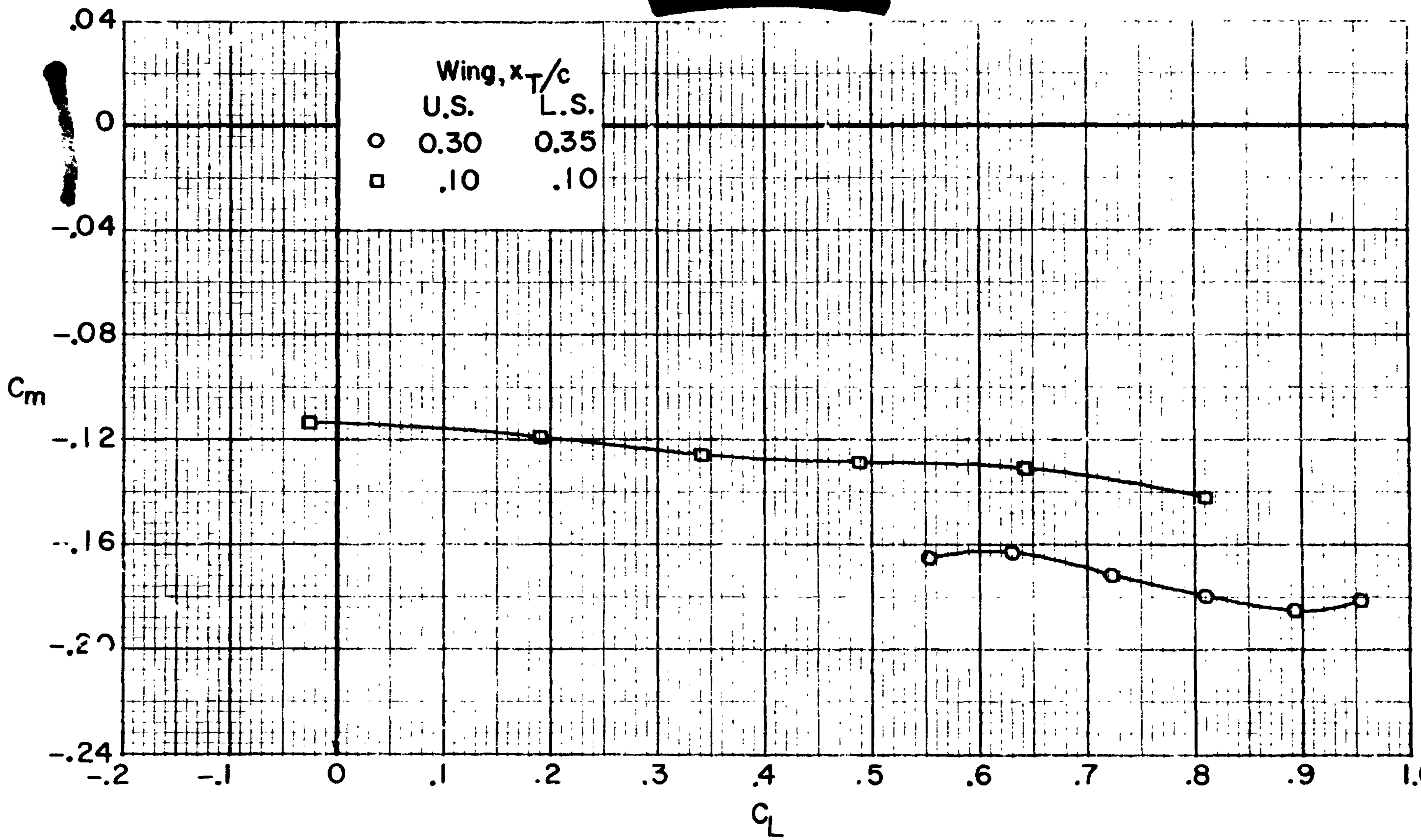

(d) M = 0.75. Concluded.

Figure 7.- Continued.

[redacted]

[redacted]

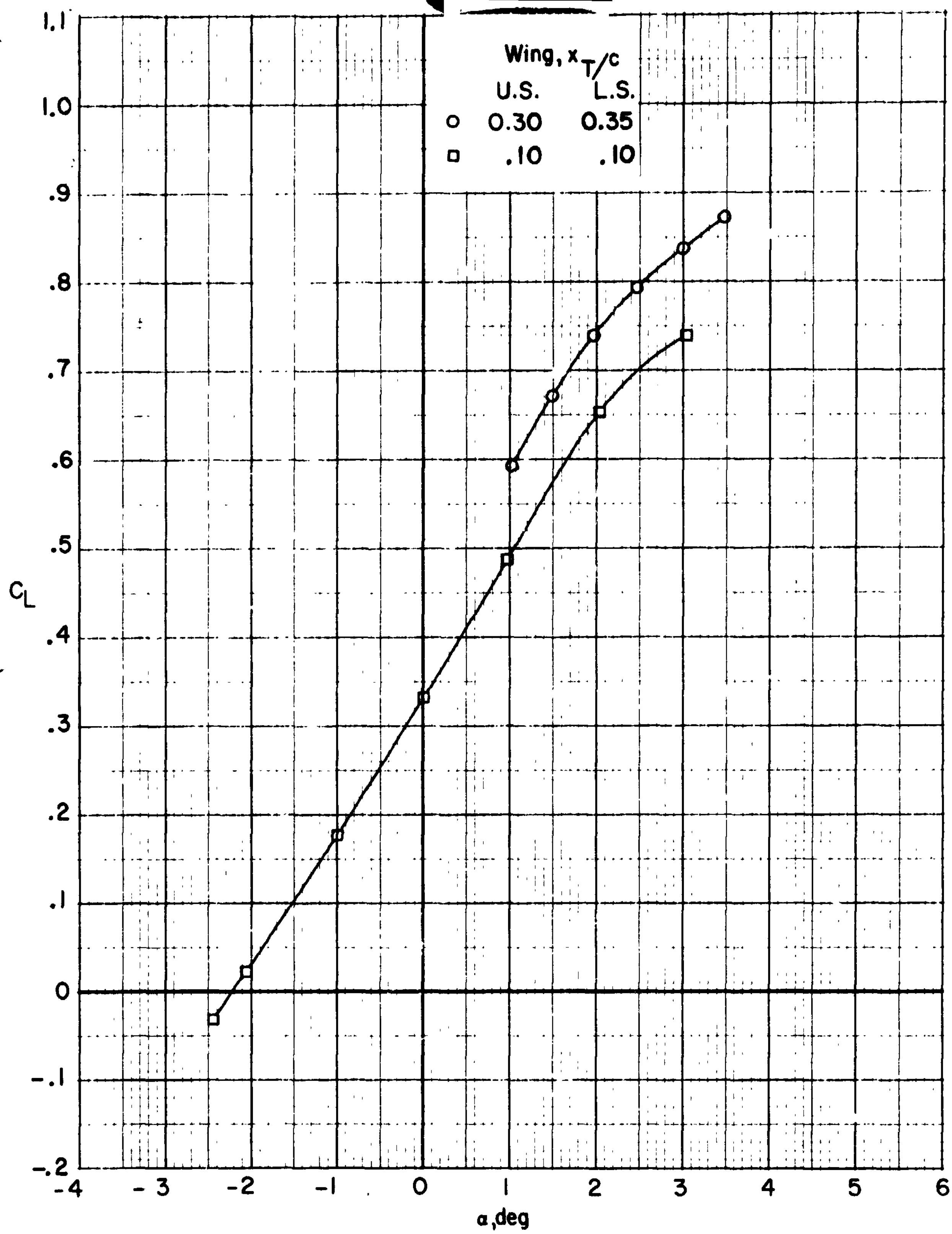

(e) M = 0.78.

Figure 7.- Continued.

...AGE IS
OF POOR QUALITY

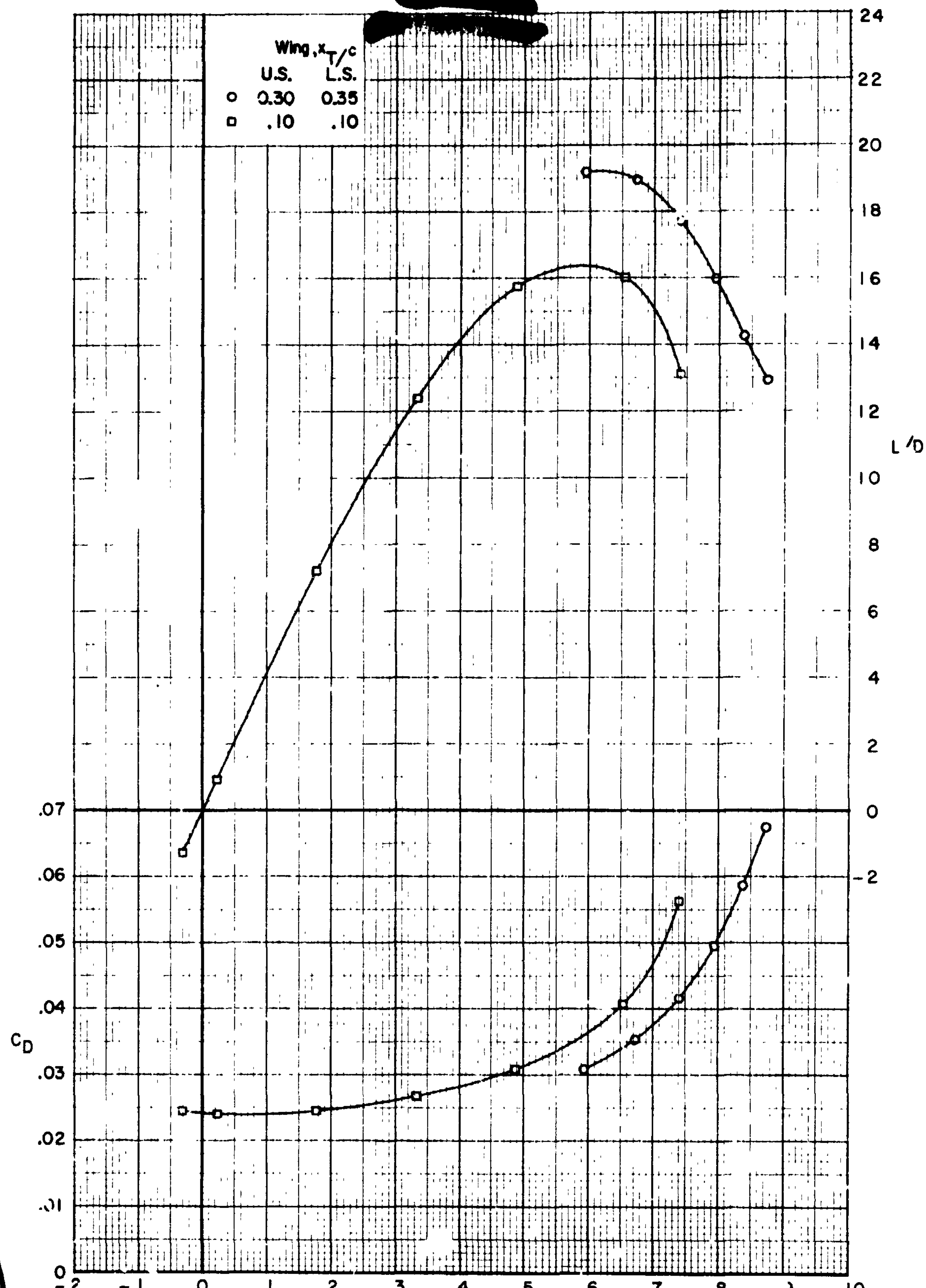

[redacted]

(e) M = 0.78. Continued.

Figure 7.- Continued.

[redacted]

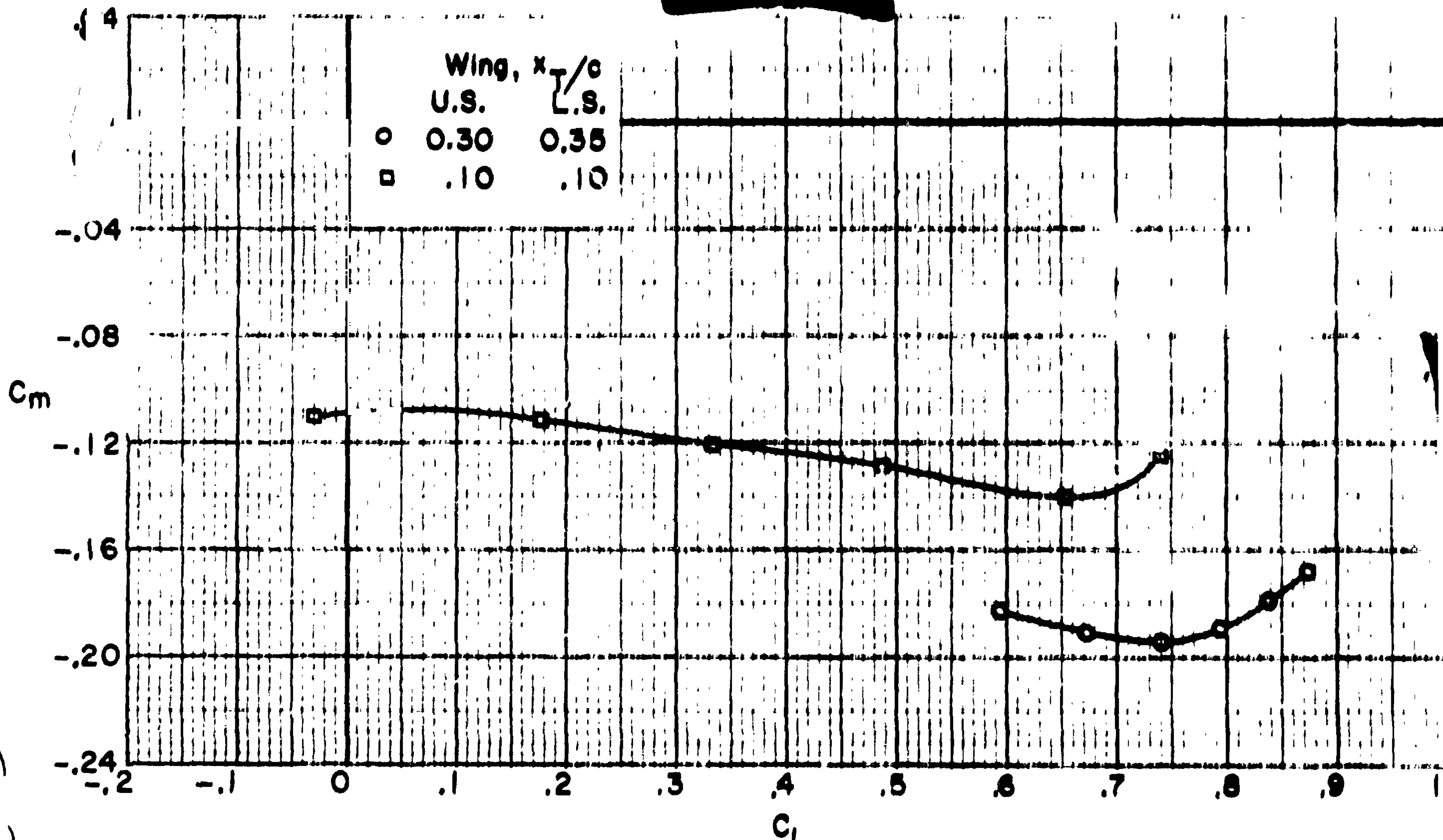

ORIGINAL PAGE IS OF POOR QUALITY

(e) M = 0.78. Concluded.

Figure 7.- Continued.

[redacted]

C-2

[redacted]

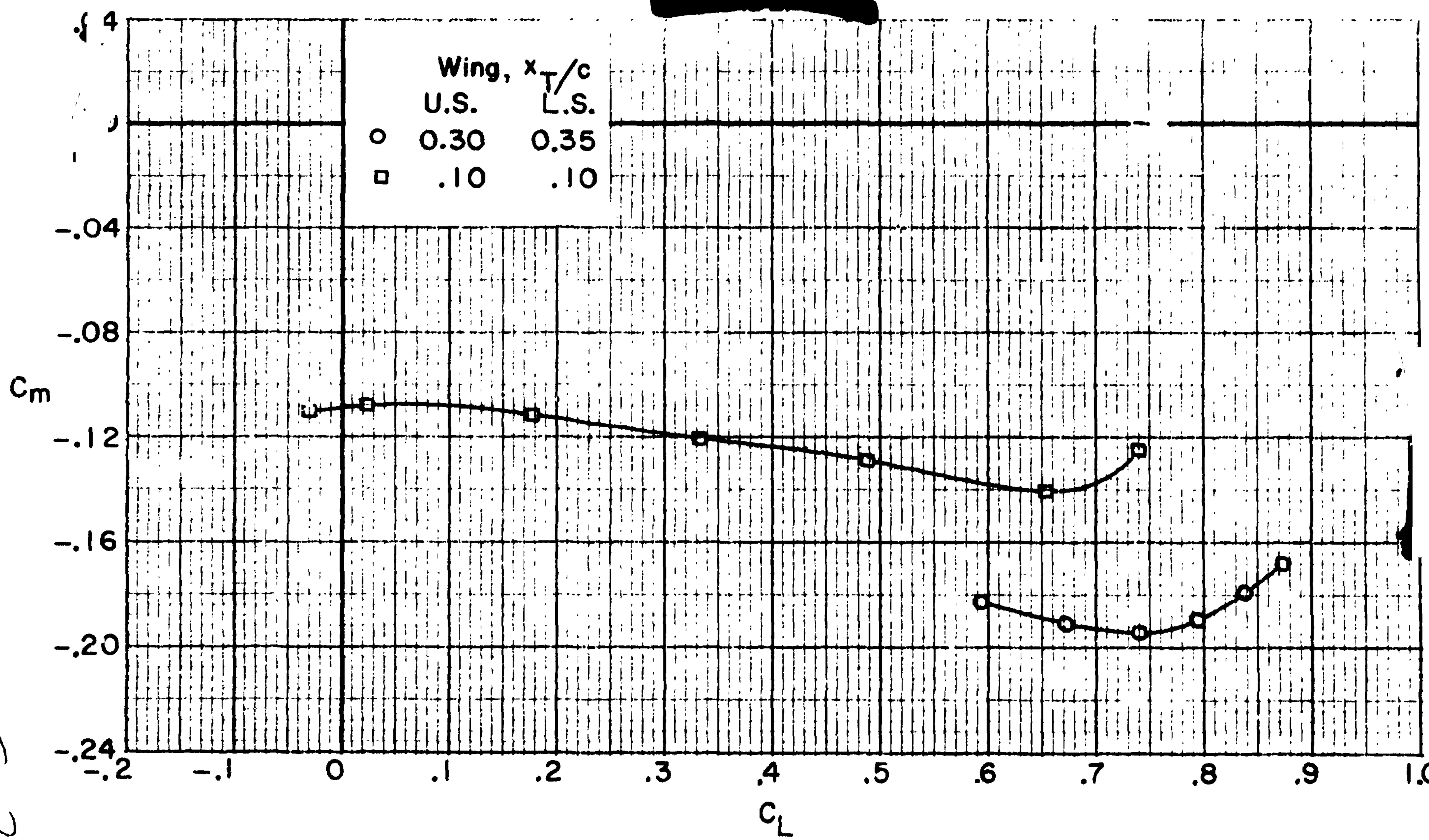

ORIGINAL PAGE IS OF POOR QUALITY

(e) M = 0.78. Concluded.

Figure 7.- Continued.

[redacted]

C-2

[redacted]

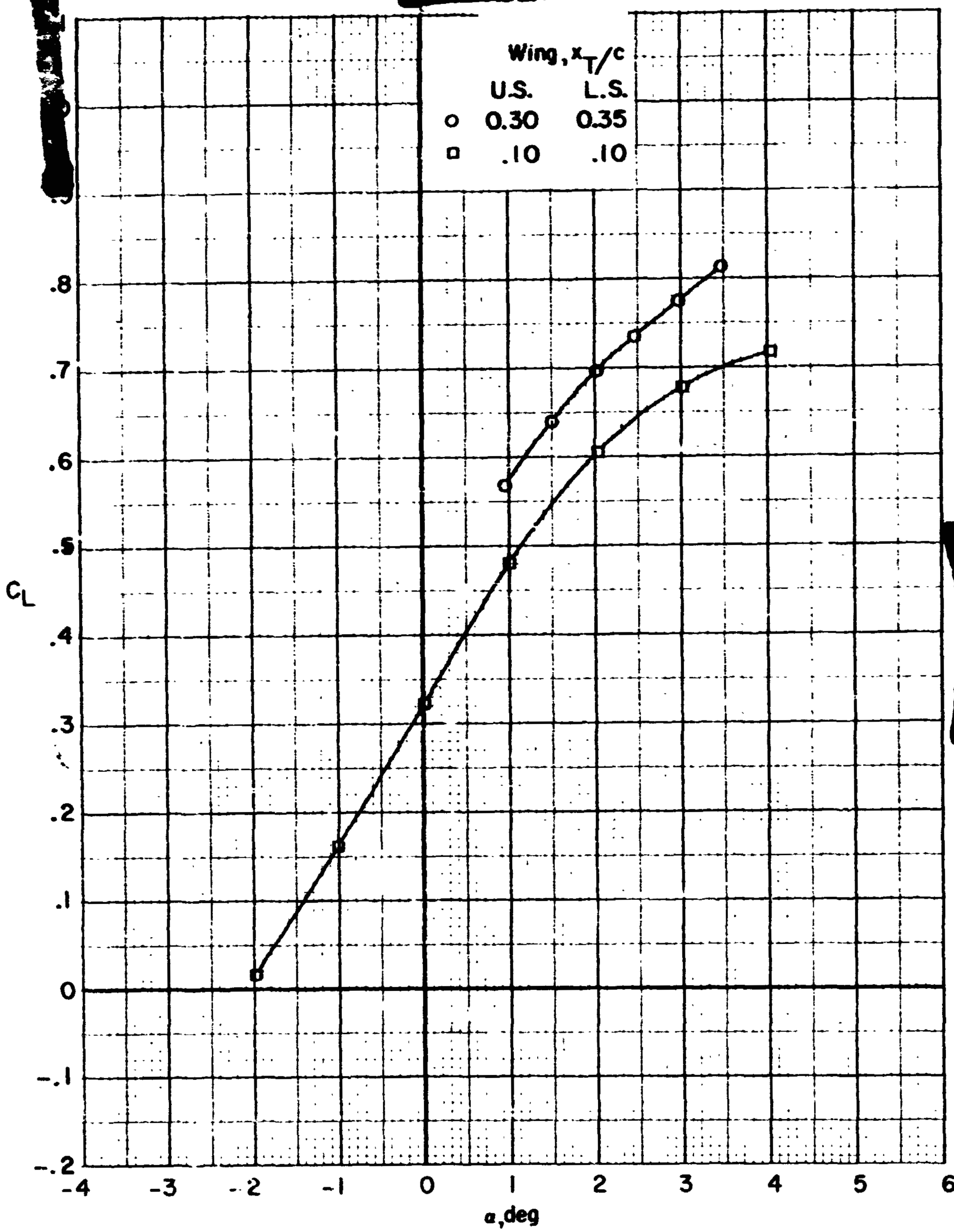

(f) M = 0.80.

Figure 7.- Continued.

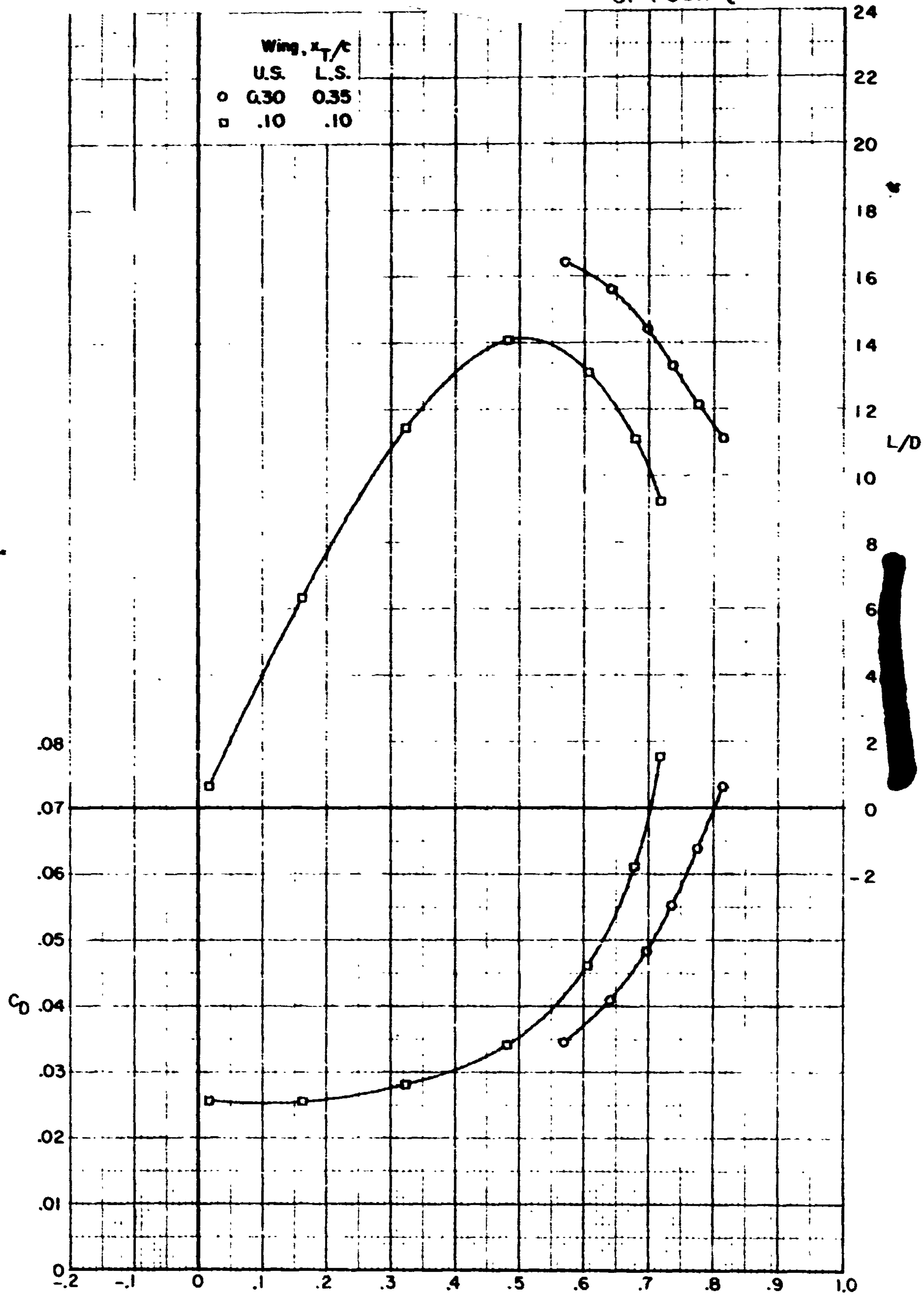

(f) M = 0.80. Continued.

Figure 7.- Continued.

[redacted]

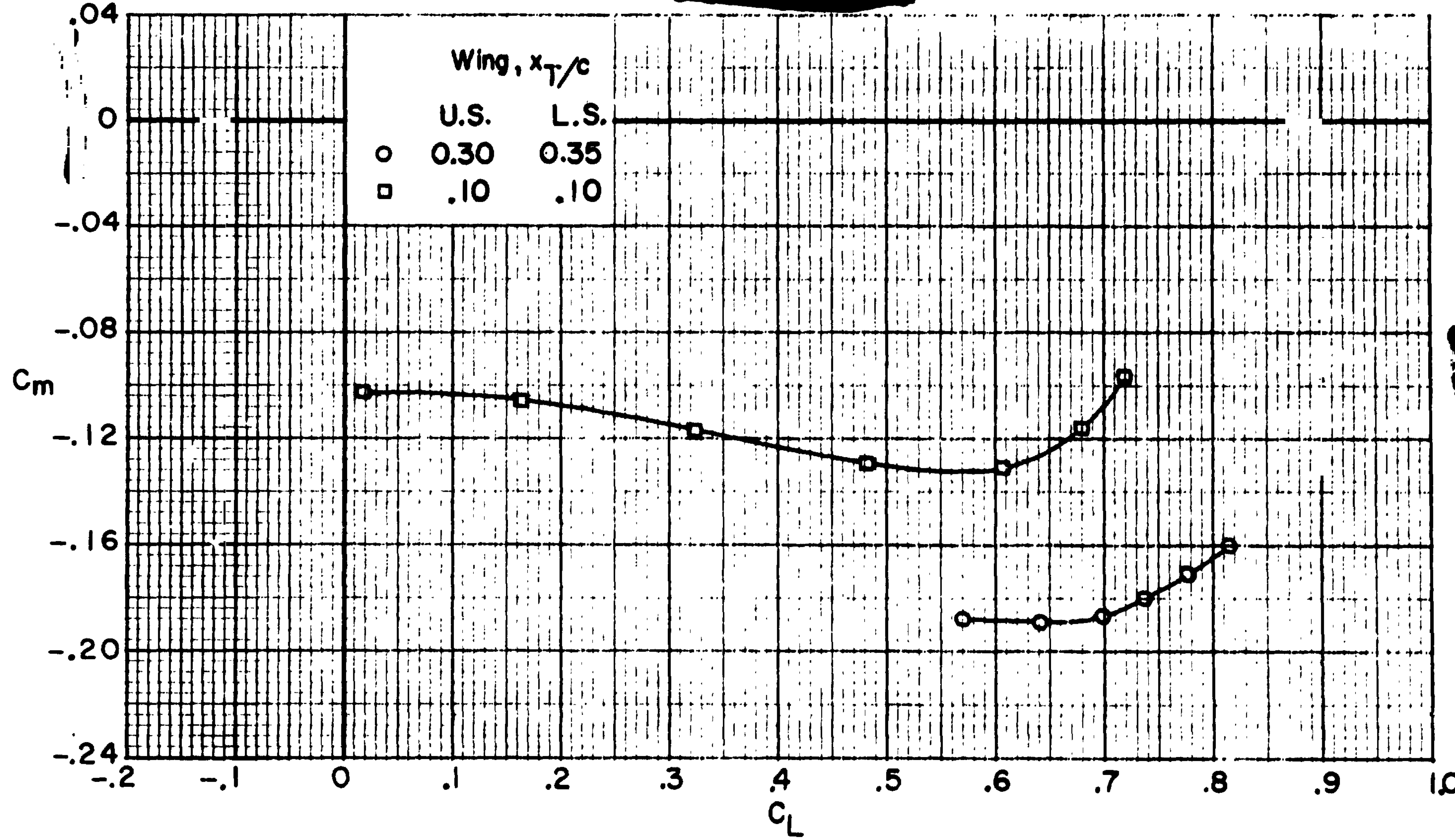

(f) M = 0.80. Concluded.

Figure 7.- Concluded.

[redacted]

[redacted]

ORIGINAL PAGE IS
OF POOR QUALITY

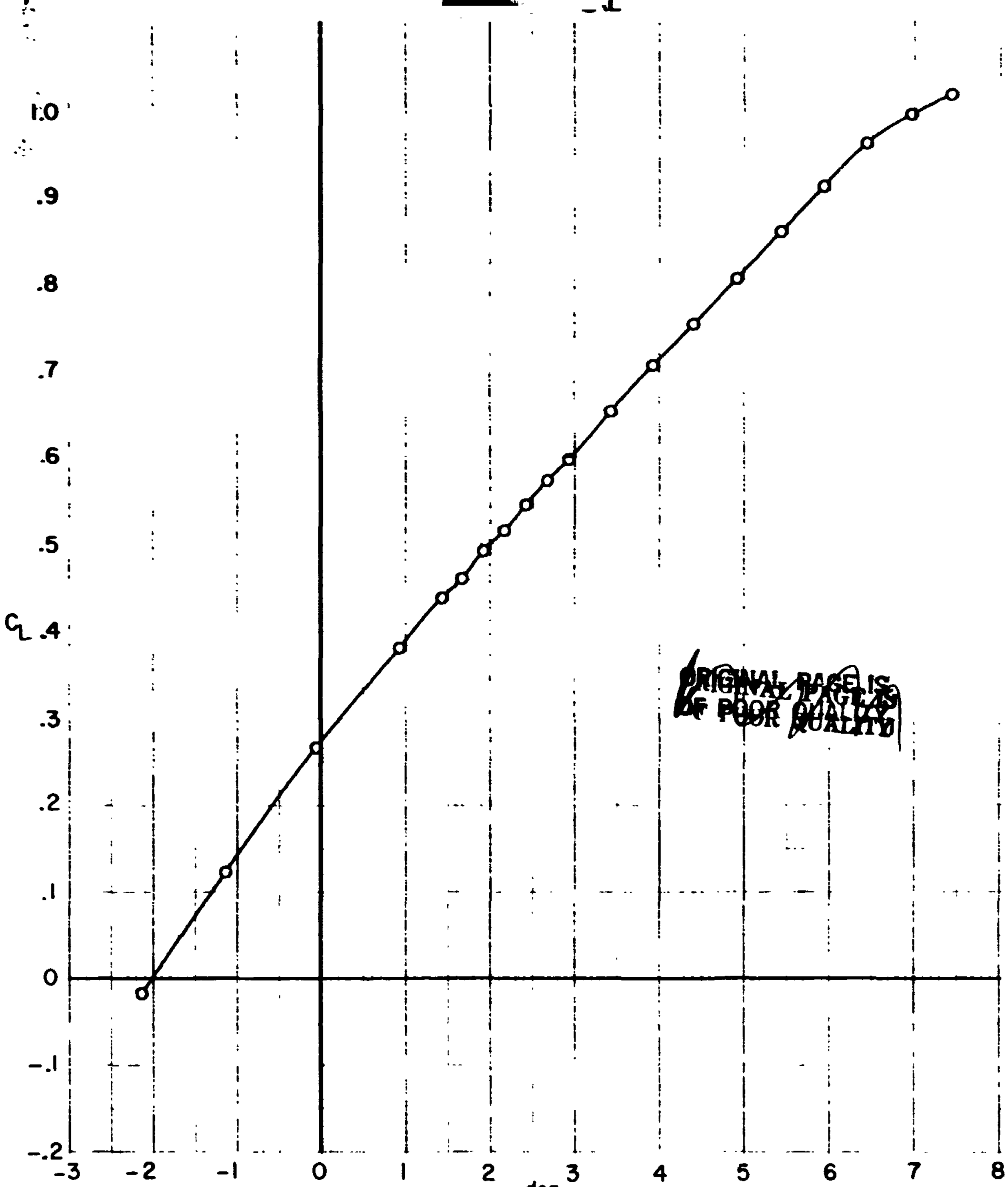

(a) M = 0.60.

Figure 8.- Longitudinal aerodynamic characteristics for supercritical wing configuration Ia (SCW-Ia) with wing upper surface grit aft (fig. 5). (Results are from final series of tests for this configuration.) c.g. (F.S.) = 84.605 cm (33.309 in.); $\Lambda_{c/4}$ = 27°.

[redacted]

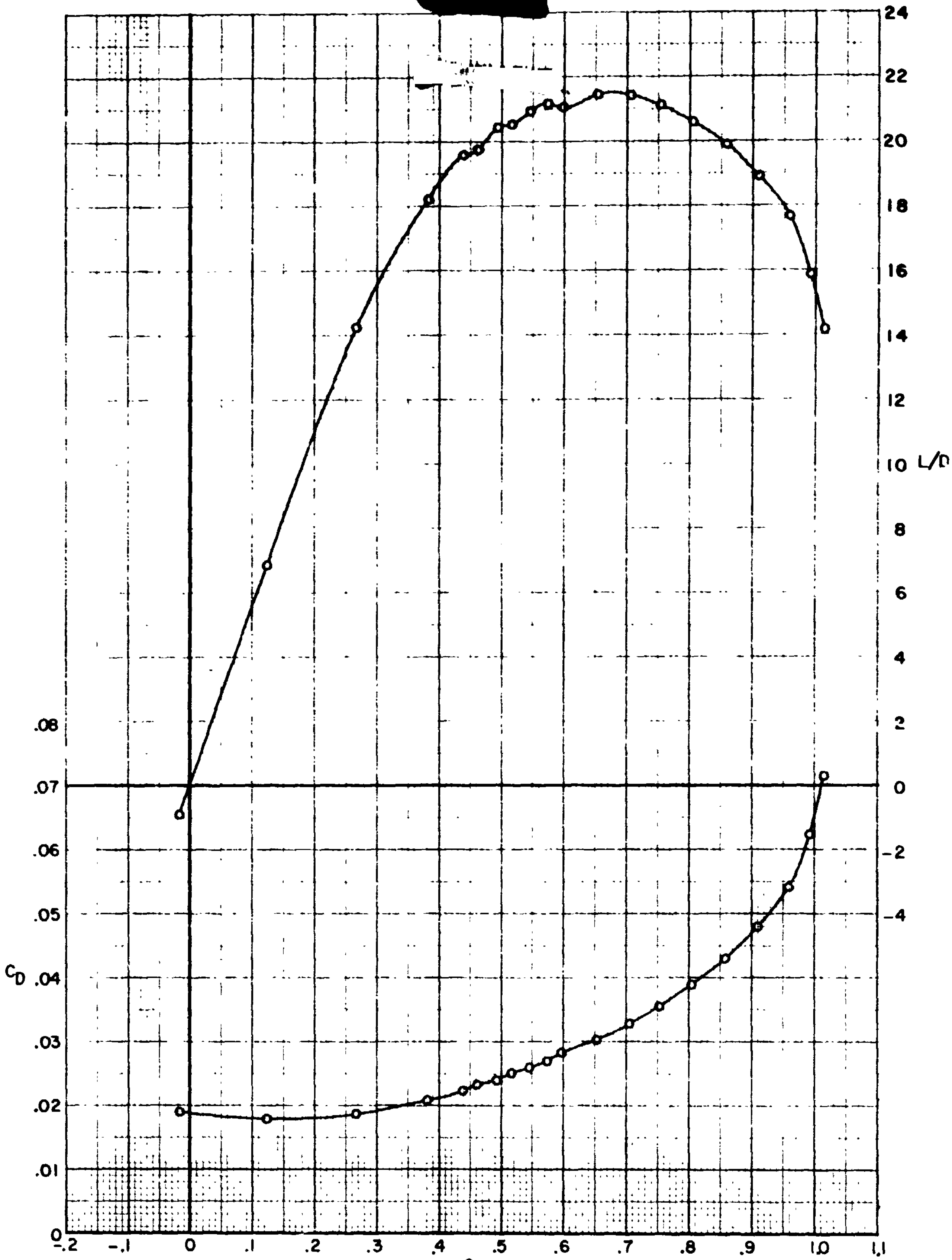

(a) M = 0.60. Continued.

Figure 8.- Continued.

[redacted]

[redacted]

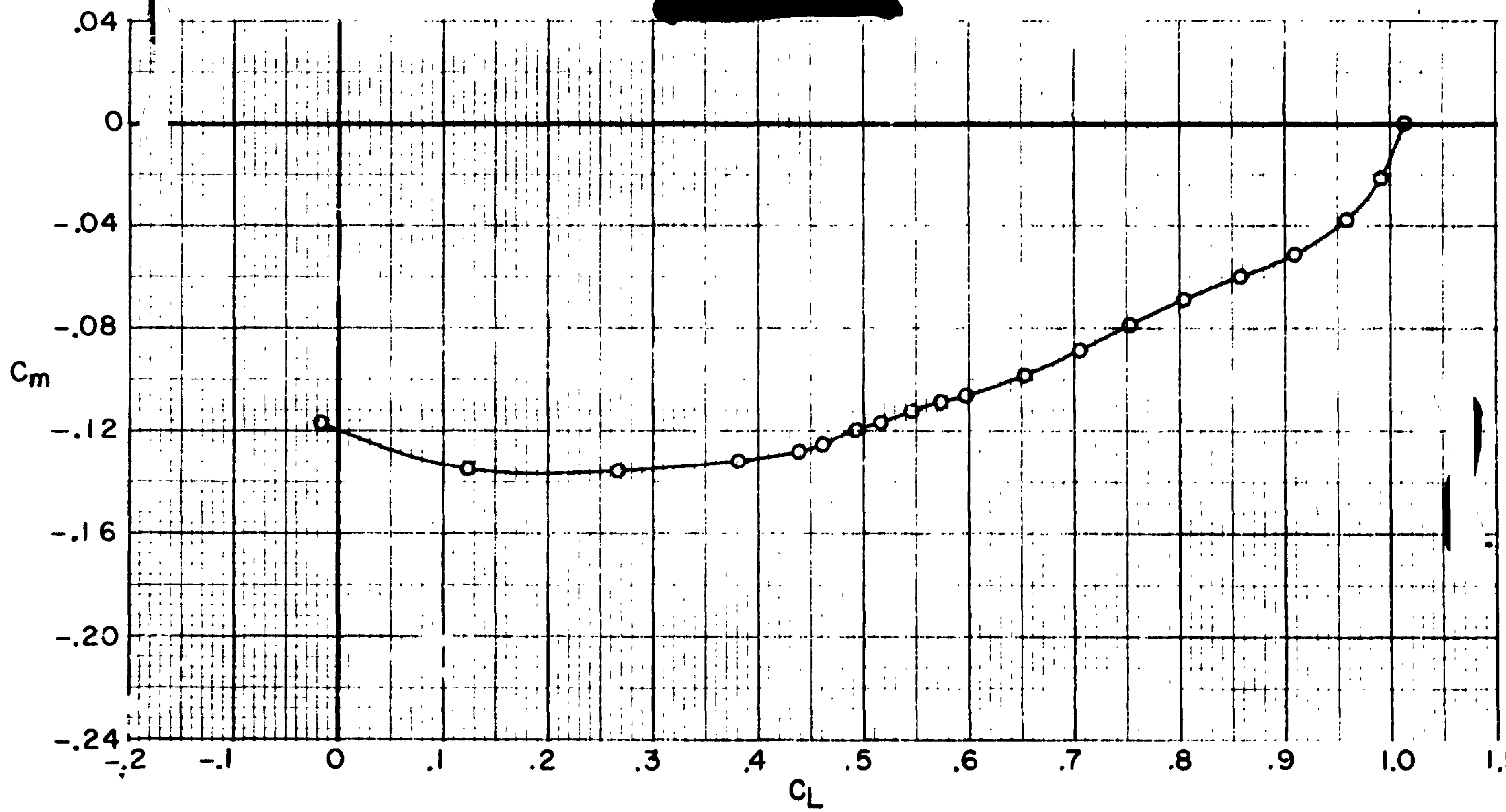

(a) M = 0.60. Concluded.

Figure 8. - Continued.

[redacted]

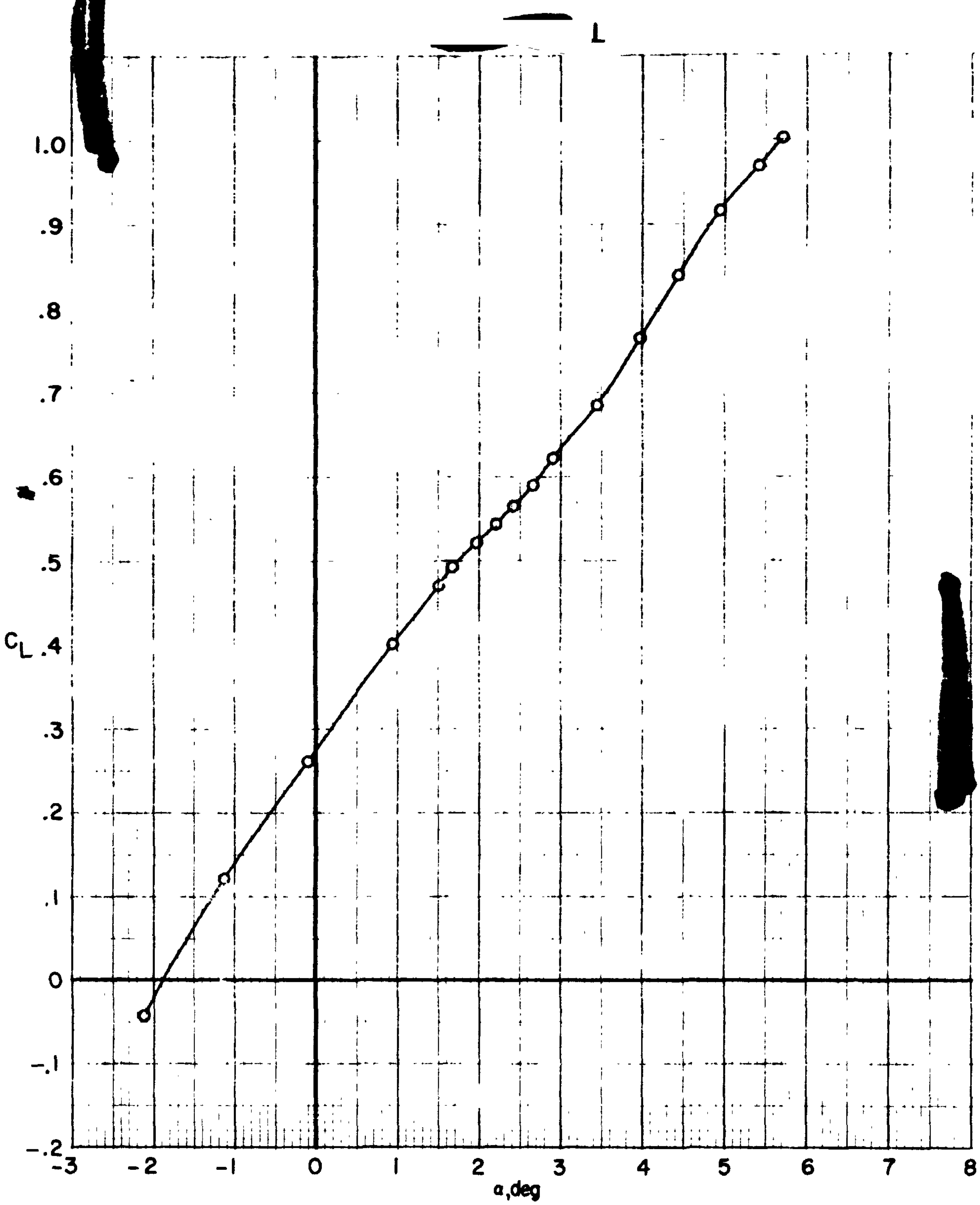

(b) M = 0.70.

Figure 8.- Continued.

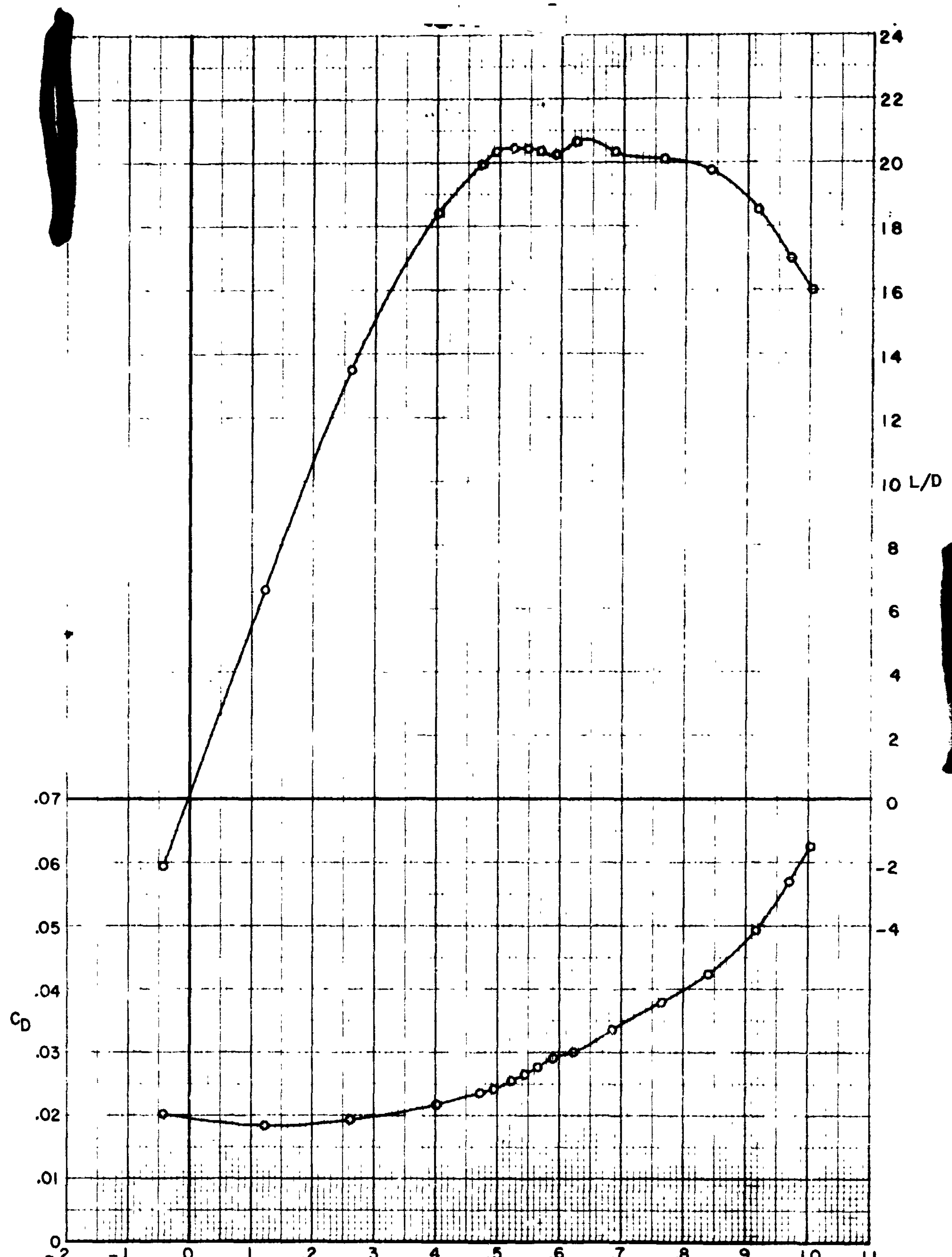

(b) M = 0.70. Continued.

Figure 8.- Continued.

[redacted]

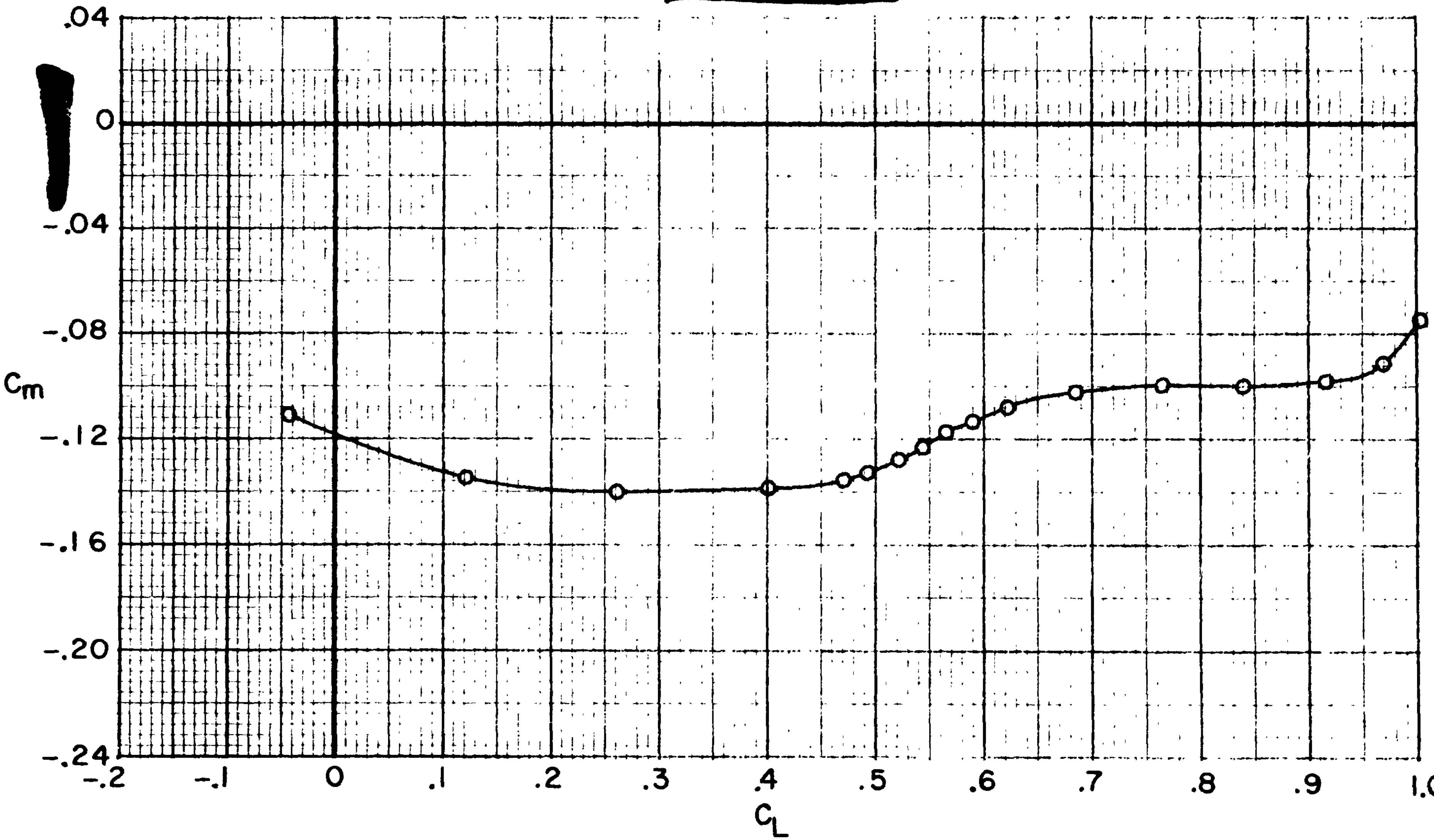

(b) M = 0.70. Concluded.

Figure 8.- Continued.

[redacted]

ORIGINAL PAGE IS
OF POOR QUALITY

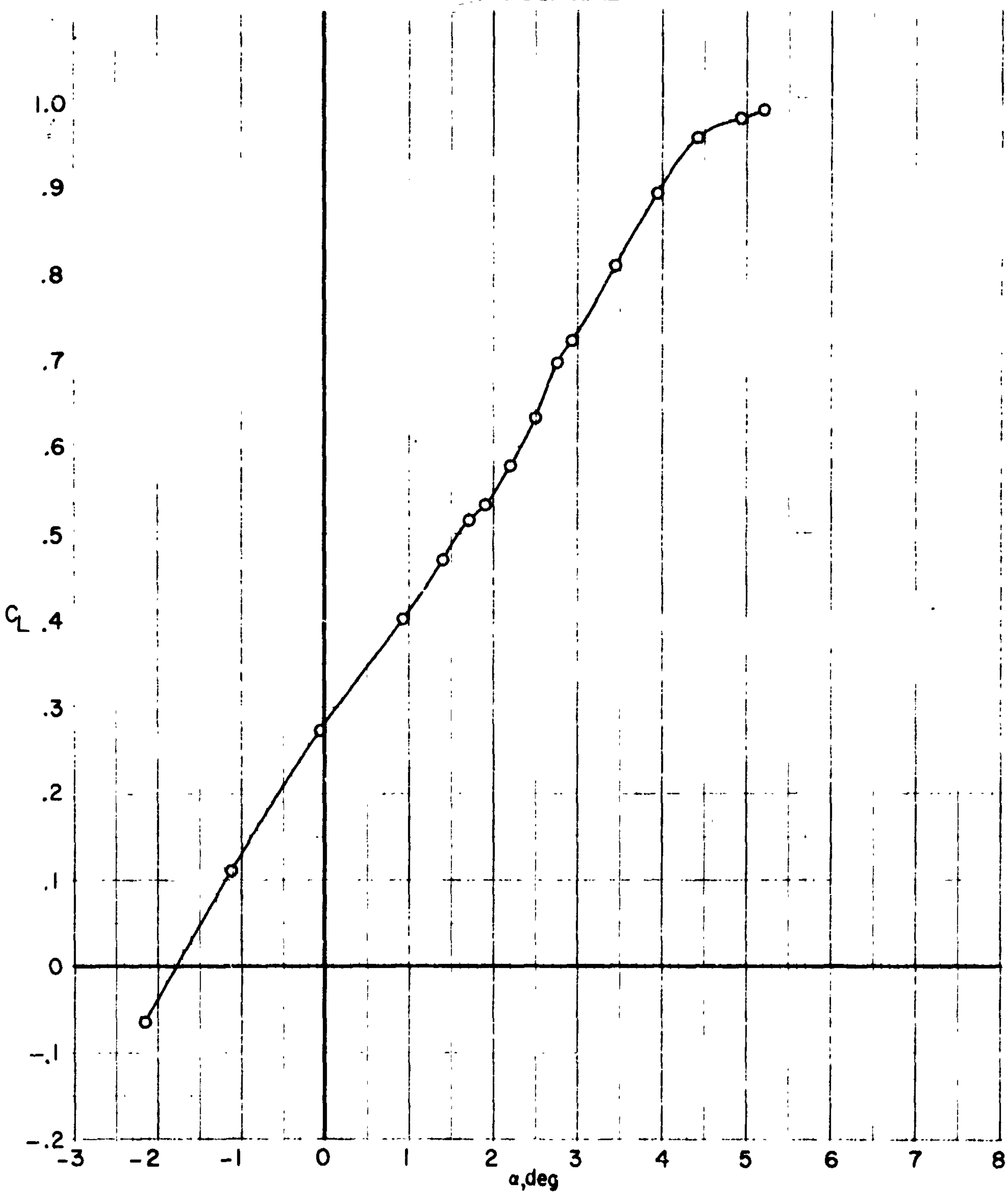

(c) M = 0.75.

Figure 8. - Continued.

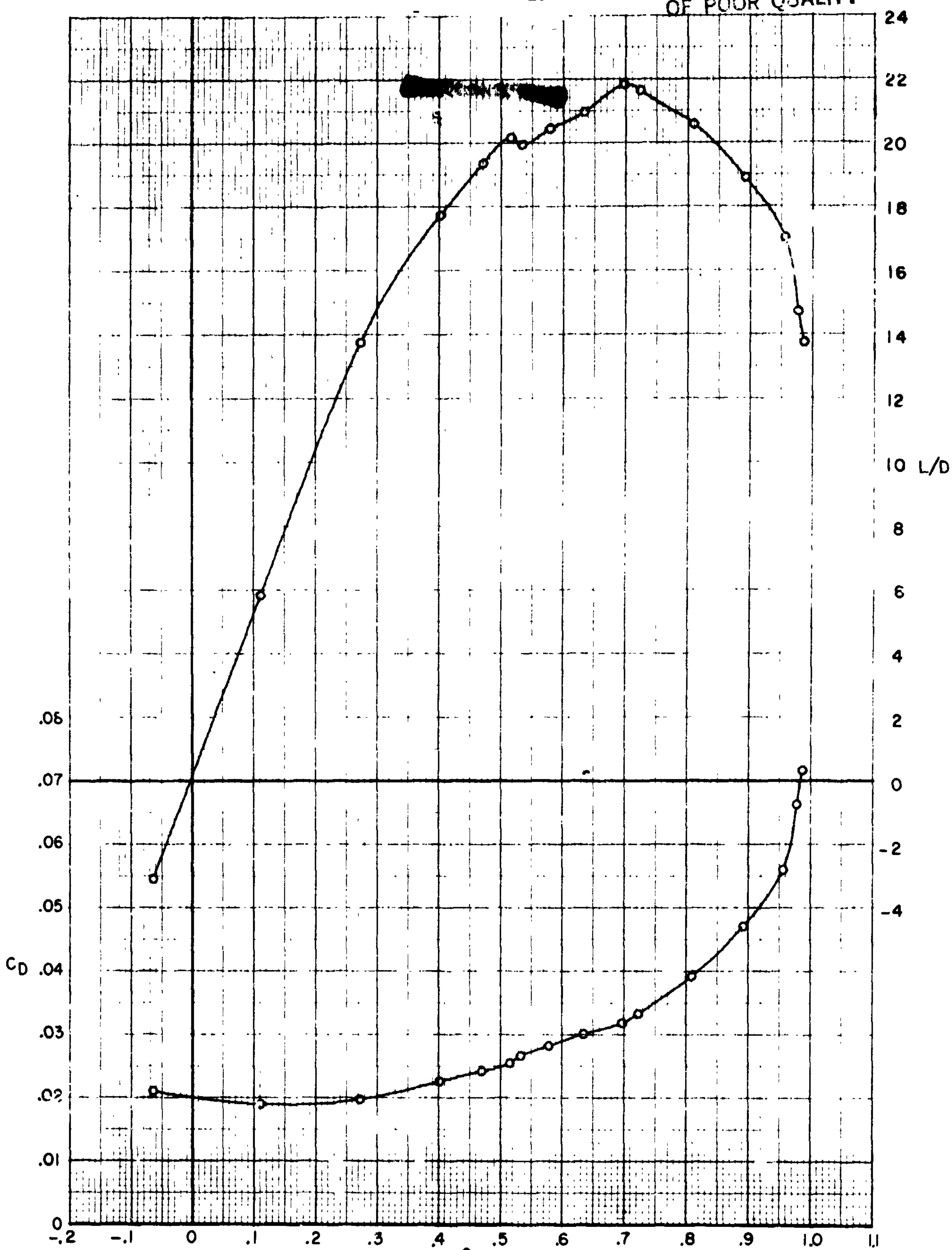

[redacted]

(c) M = 0.75. Continued.

Figure 8.- Continued.

[redacted]

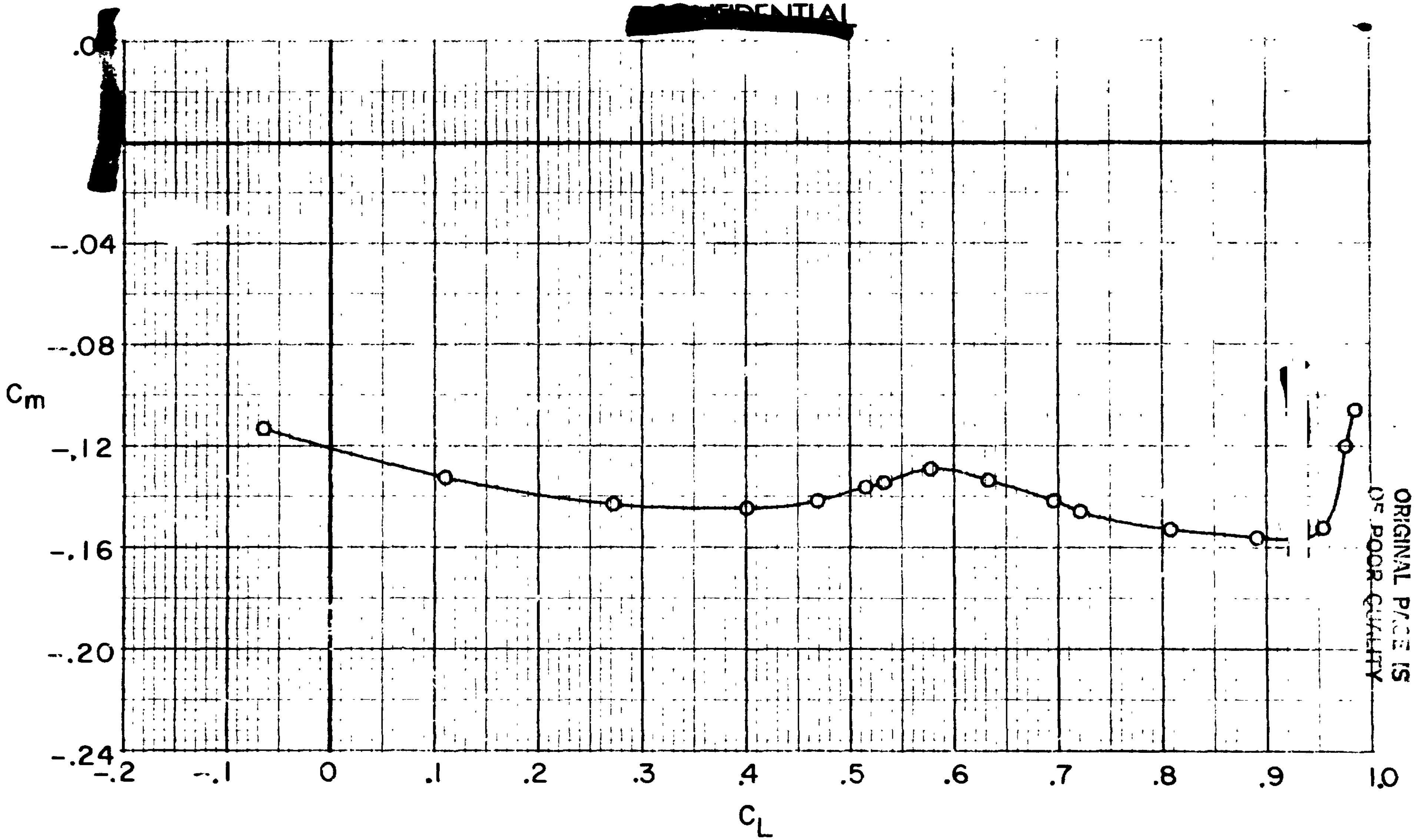

(c) M = 0.75. Concluded.

Figure 8. - Continued.

[redacted]

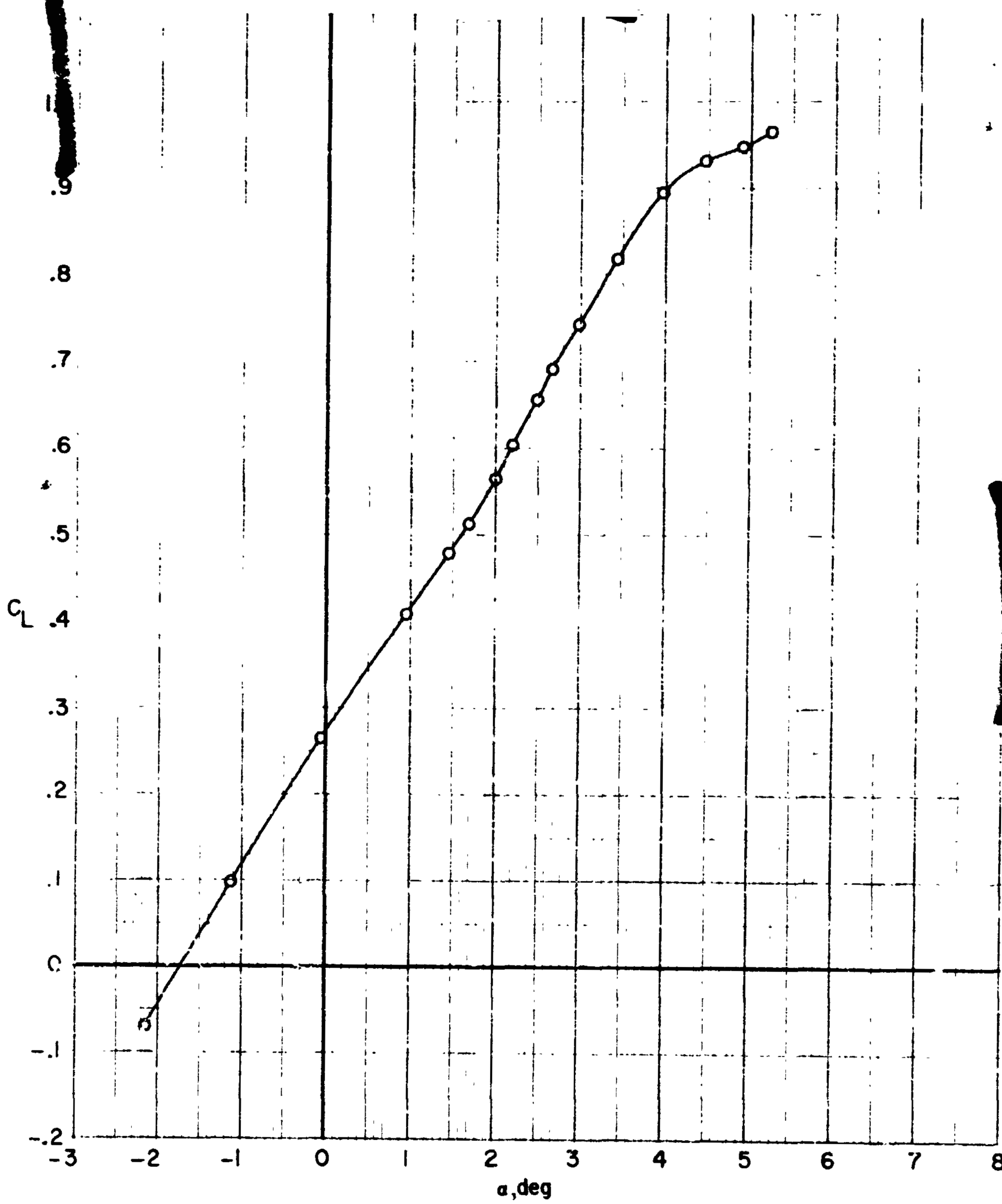

(d) M = 0.76.

Figure 8. - Continued.

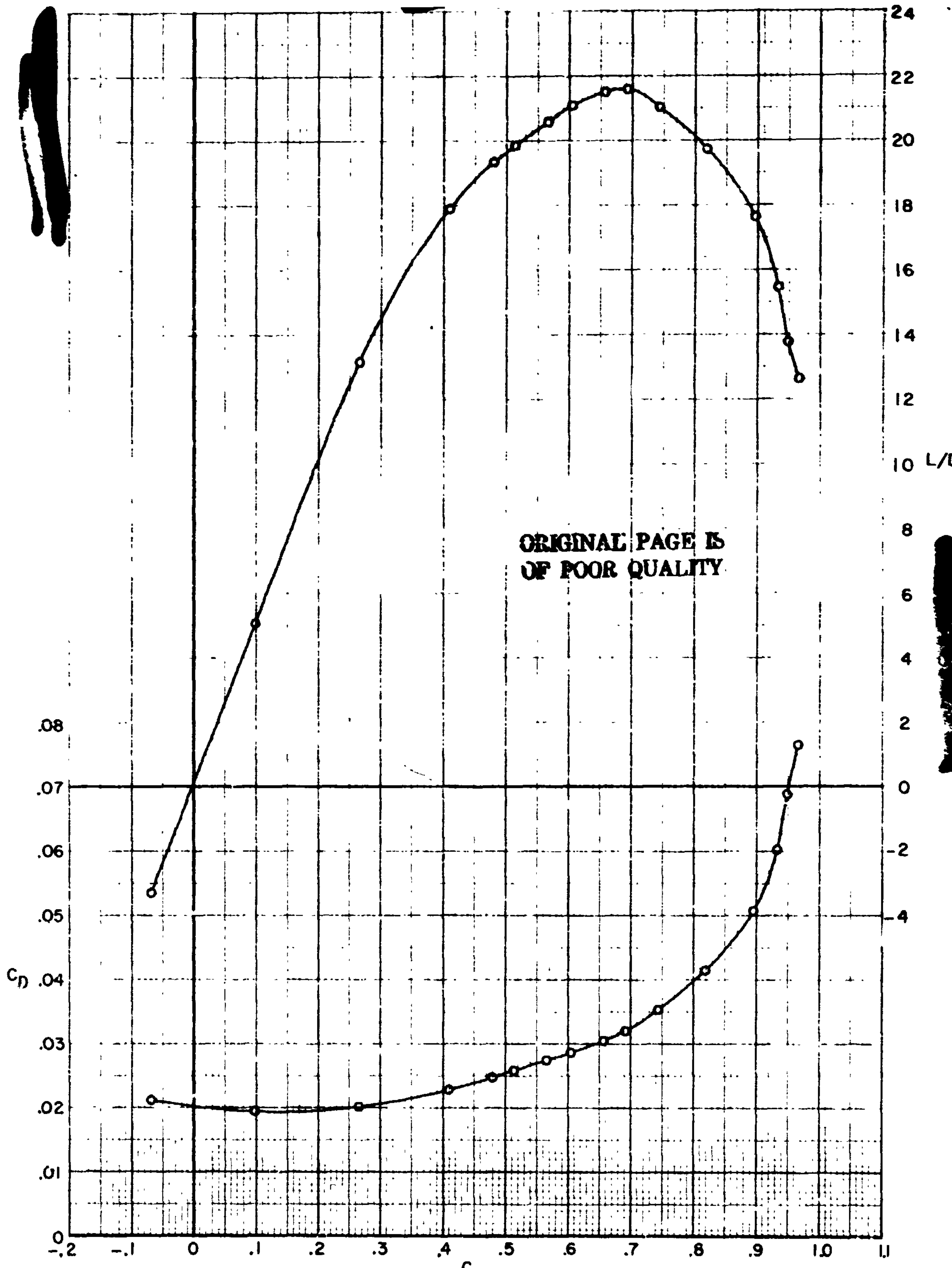

(d) M = 0.76. Continued.

Figure 8.- Continued.

[redacted]

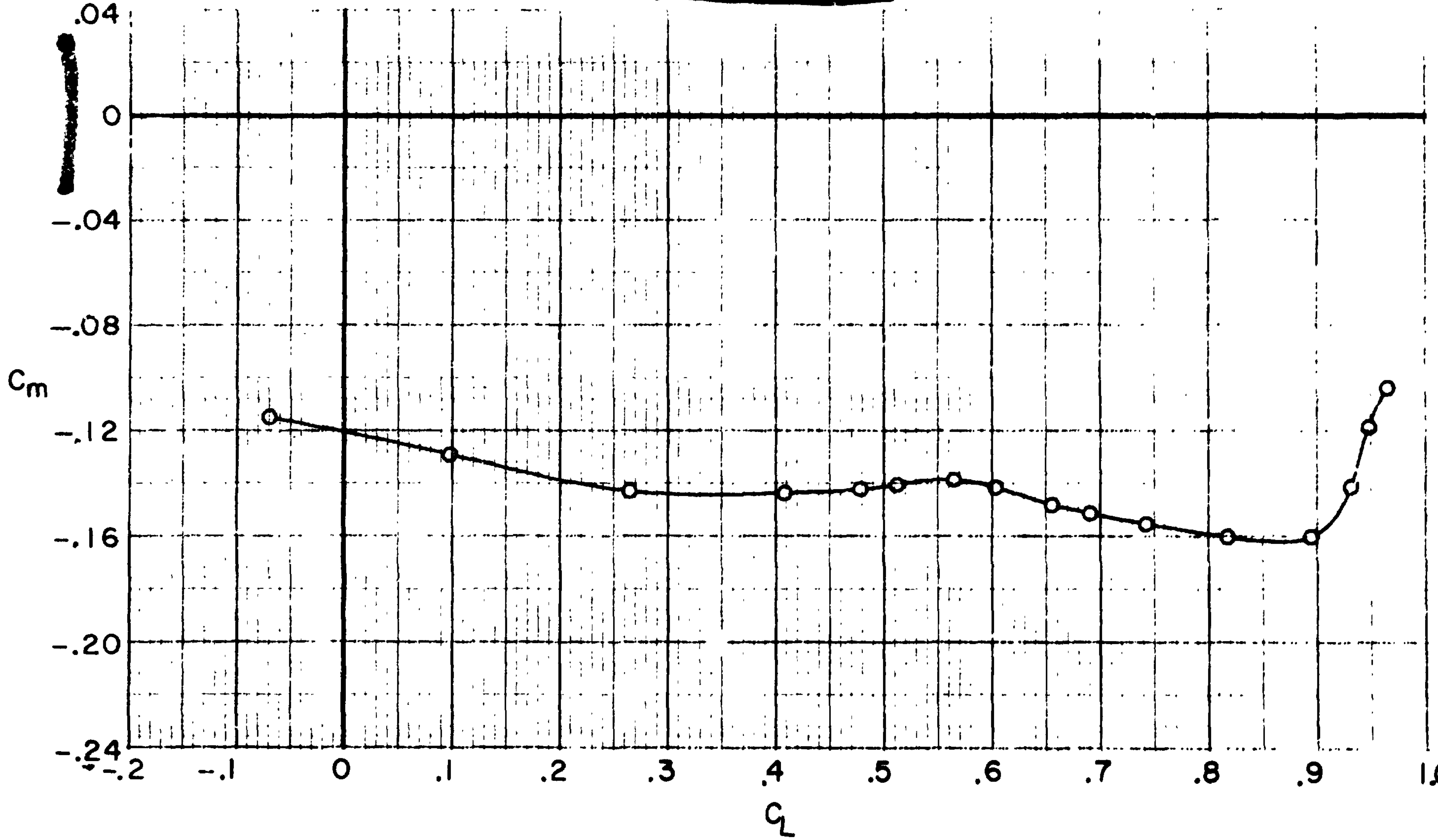

(d) M = 0.76. Concluded.

Figure 8.- Continued.

[redacted]

[redacted]

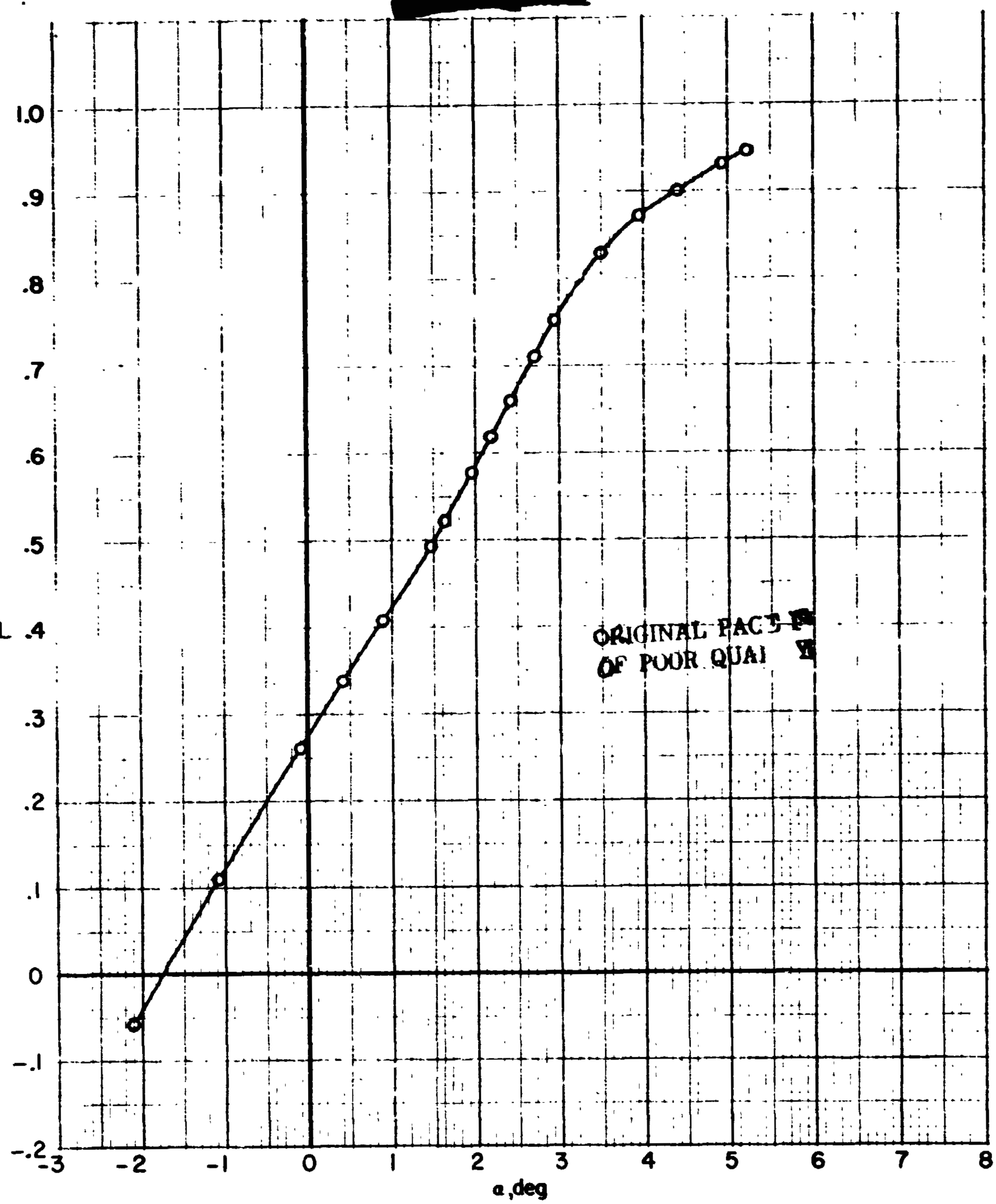

(e) M = 0.77.

Figure 8.- Continued.

[redacted]

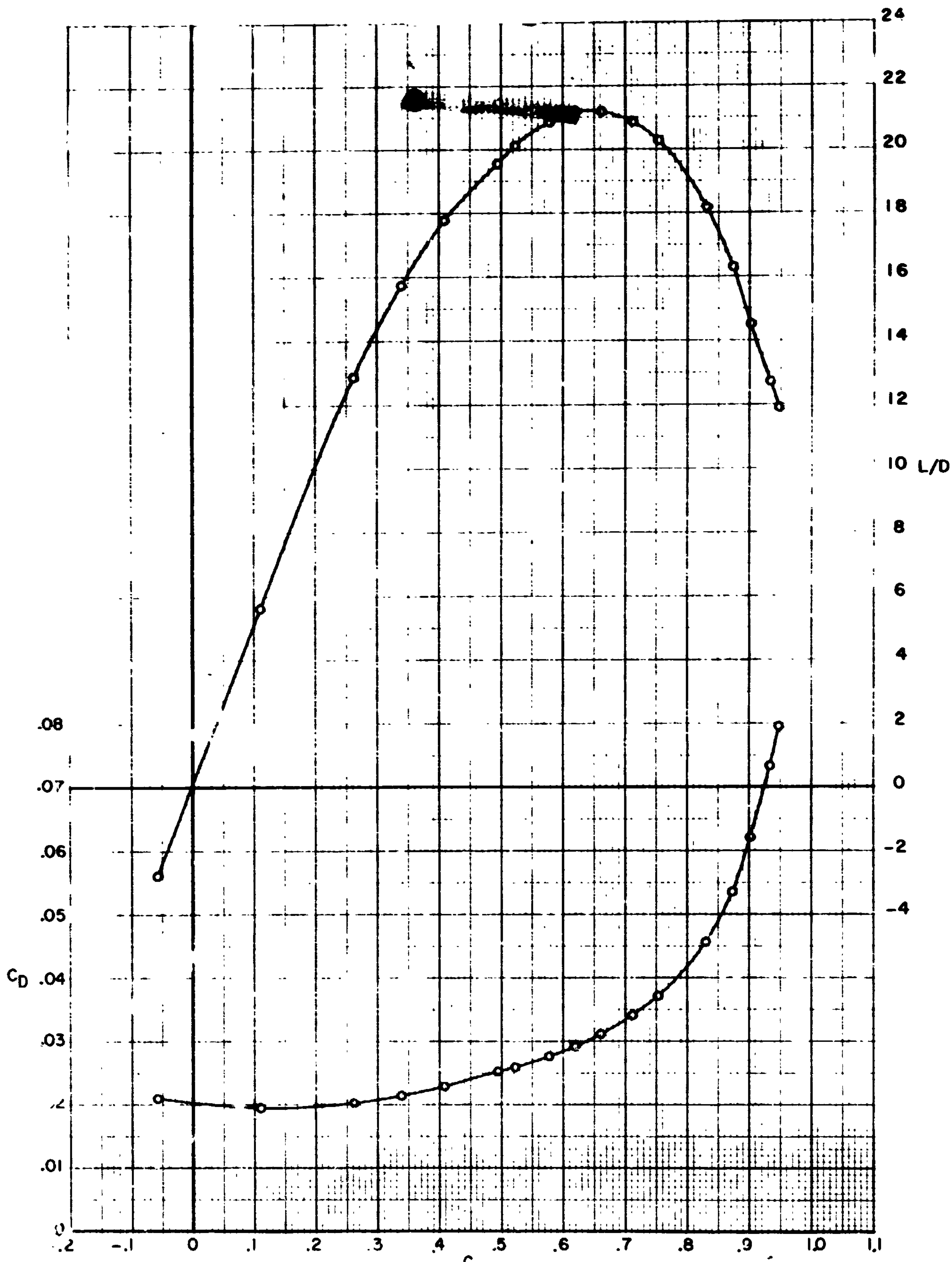

(e) M = 0.77. Continued.

Figure 8. - Continued.

ORIGINAL PAGE IS
OF POOR QUALITY

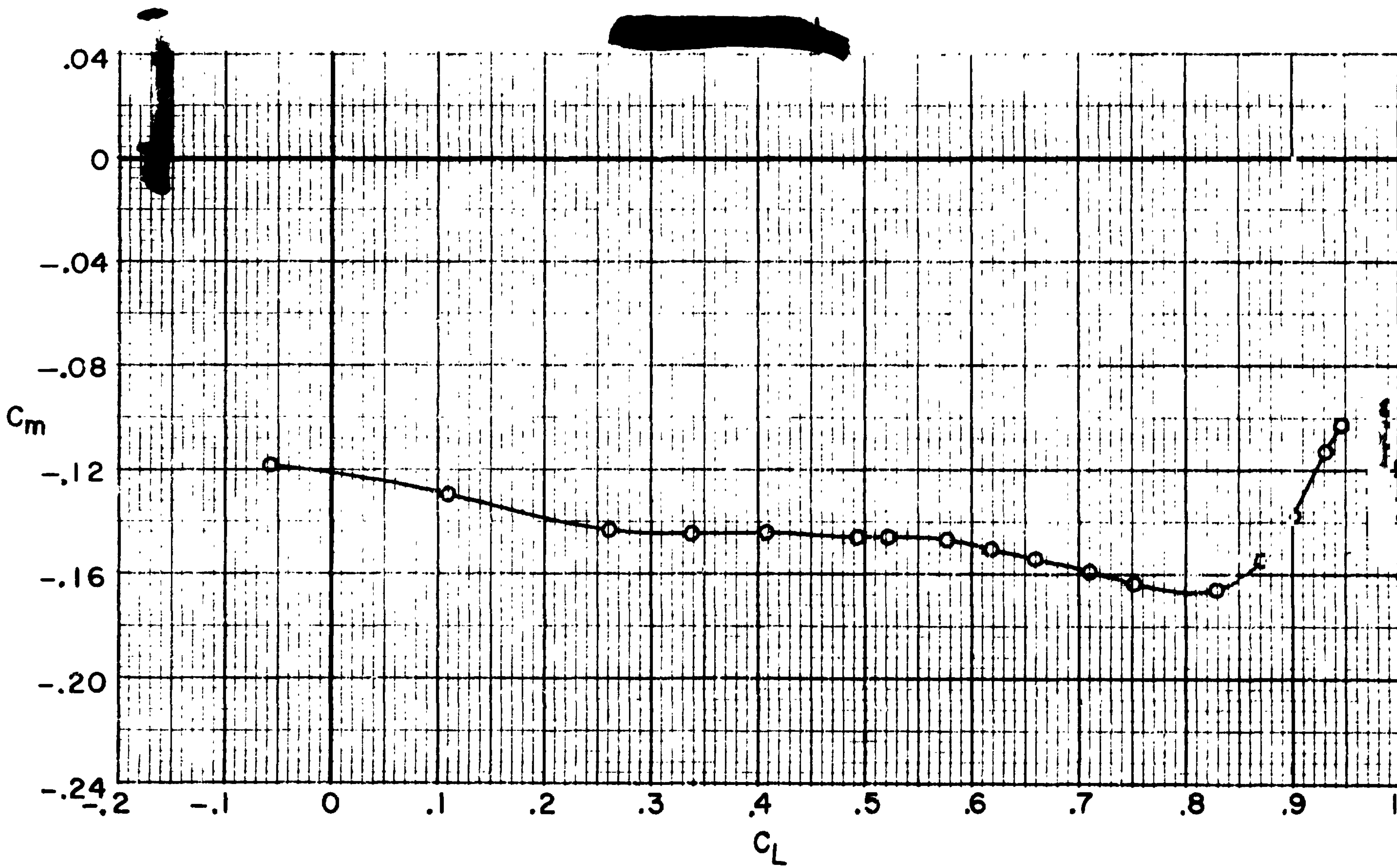

(e) M = 0.77. Concluded.

Figure 8.- Continued.

[redacted]

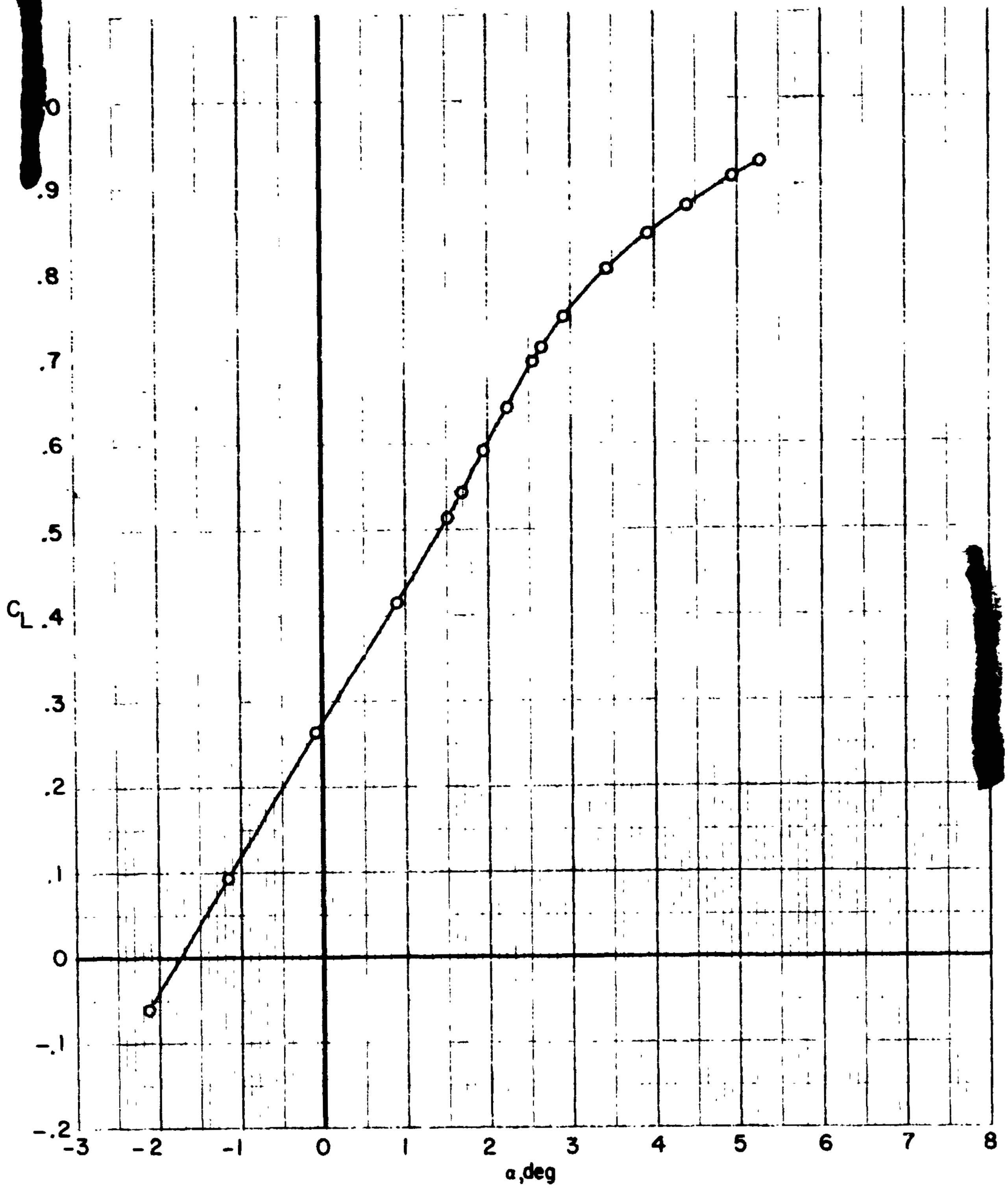

(f) M = 0.78.

Figure 8. - Continued.

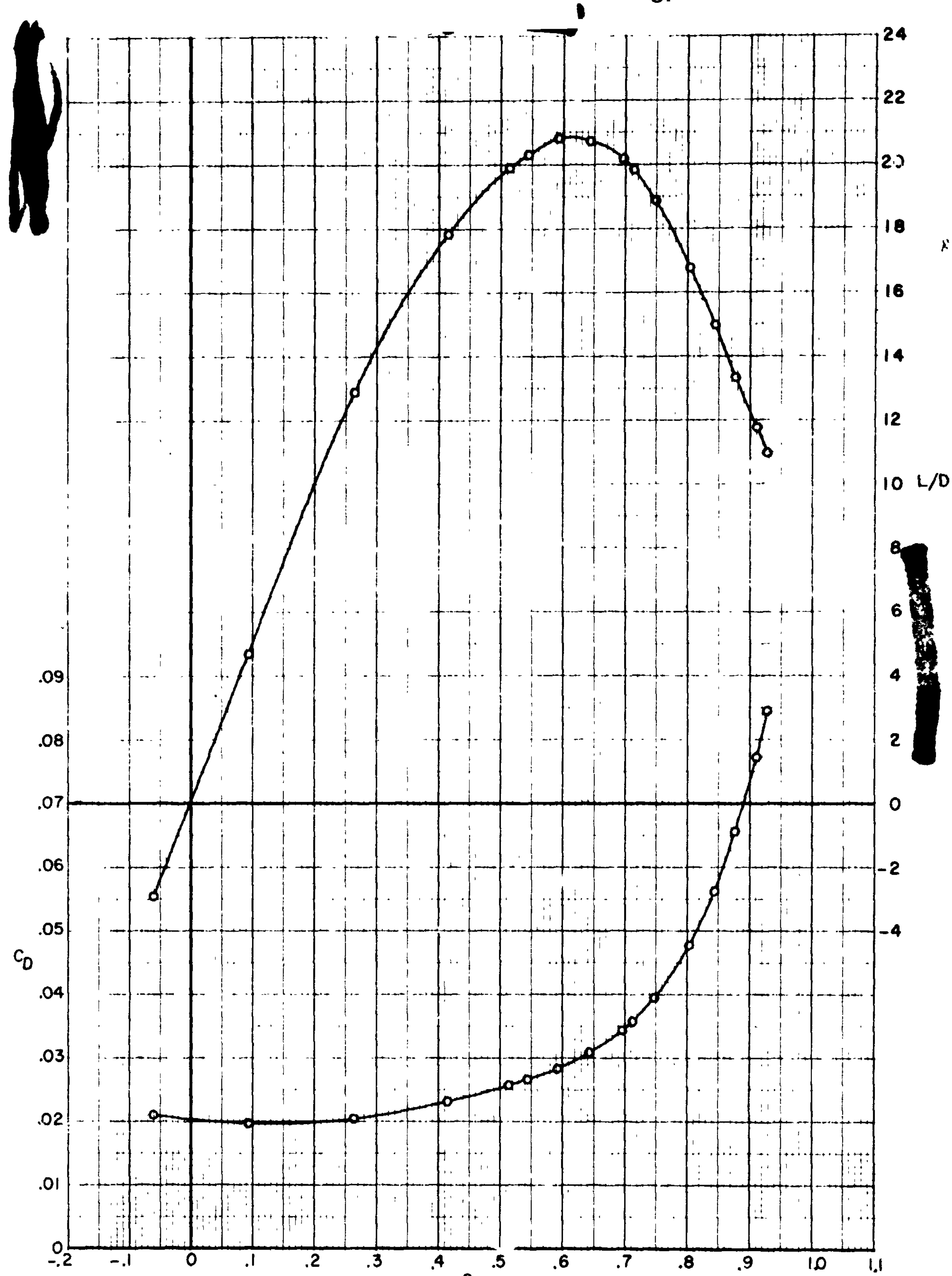

(f) M = 0.78. Continued.

Figure 8. - Continued.

[redacted]

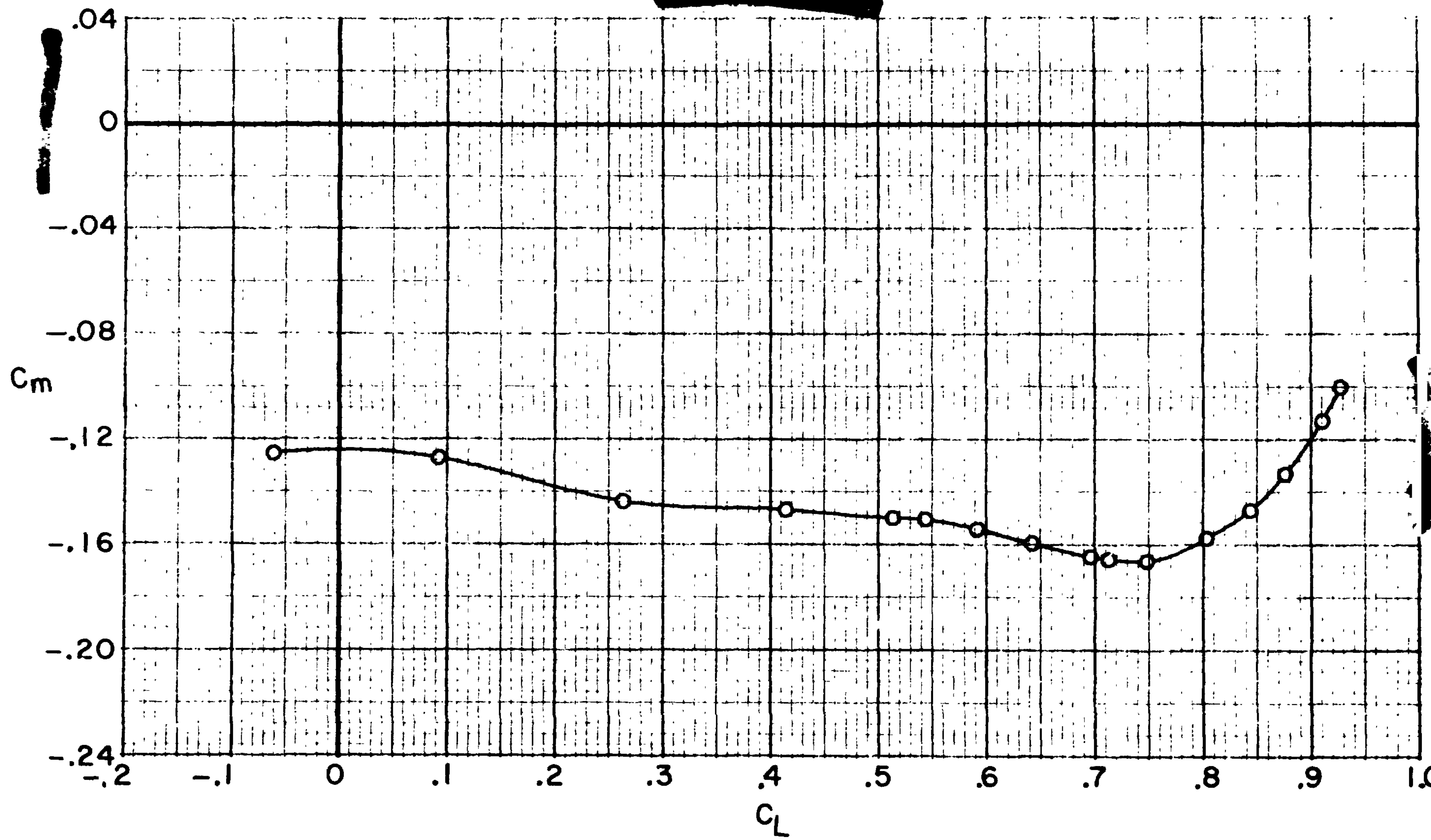

(f) M = 0.78. Concluded.

Figure 8.- Continued.

[redacted]

[redacted]

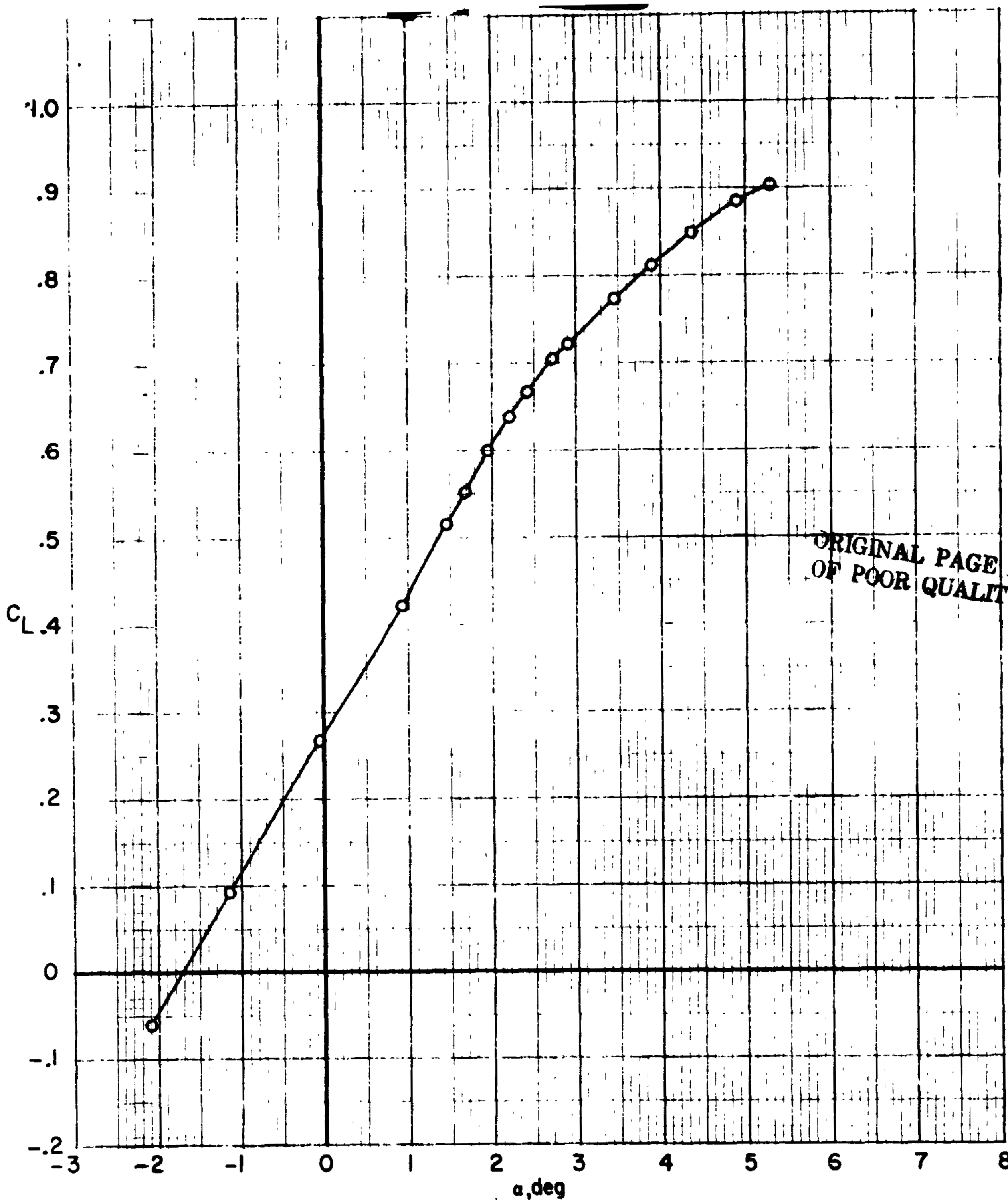

(g) M = 0.79.

Figure 8.- Continued.

ORIGINAL PAGE IS
OF POOR QUALITY

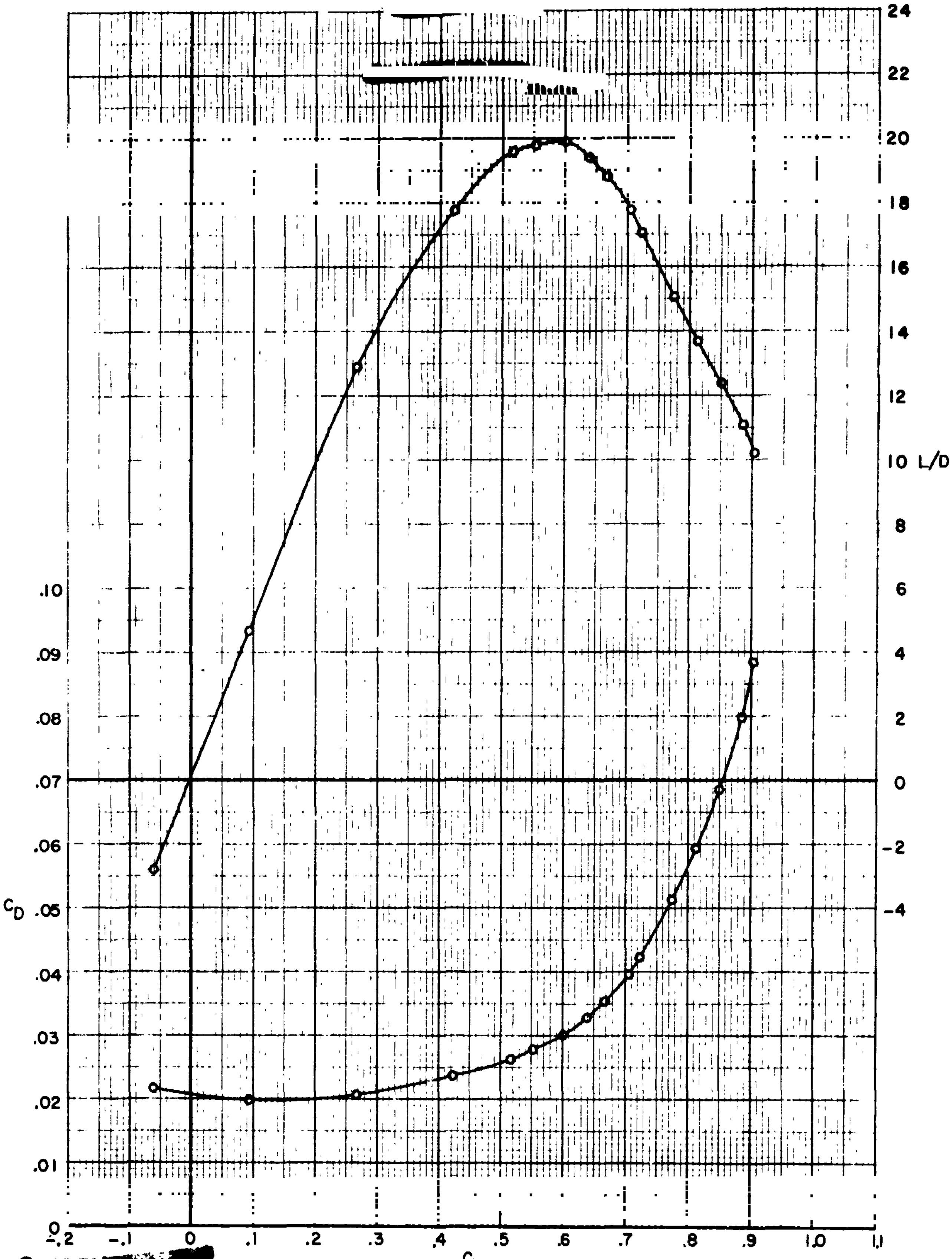

(g) M = 0.79. Continued.

Figure 8. - Continued.

[redacted]

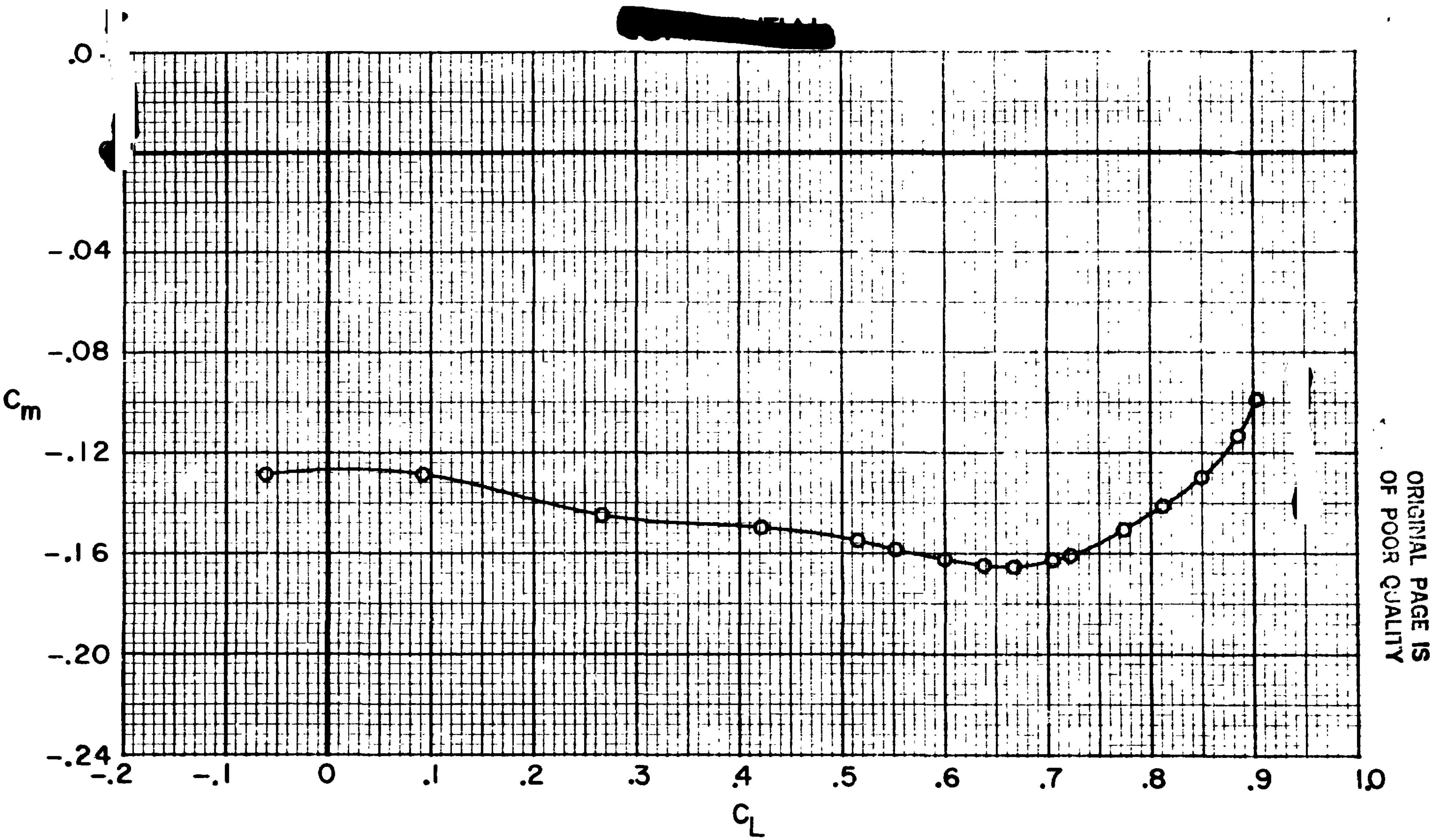

(g) M = 0.79. Concluded.

Figure 8. - Continued.

[redacted]

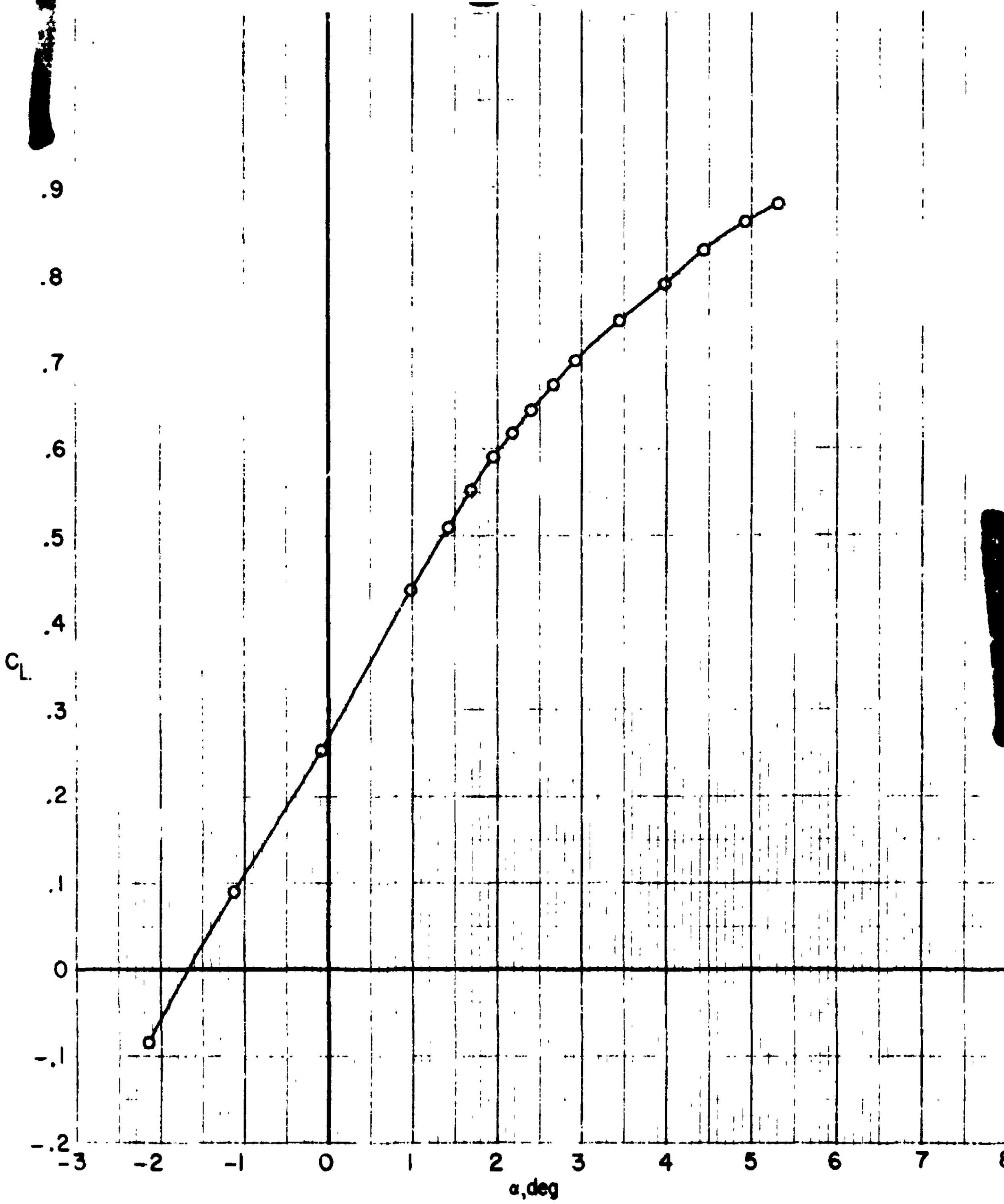

(h) M = 0.80.

Figure 8.- Continued.

[redacted]

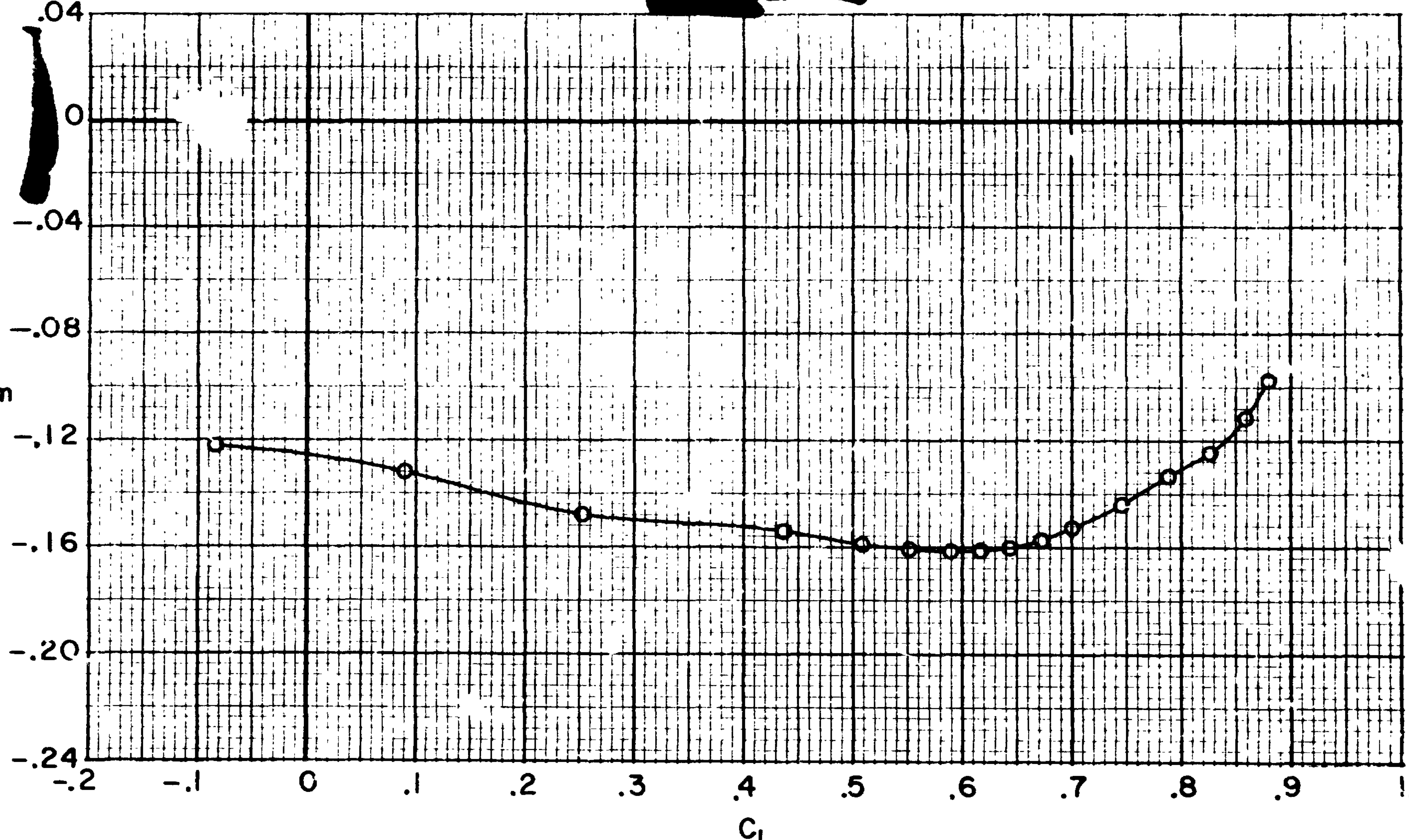

(h) M = 0.80. Concluded.

Figure 8. - Continued.

[redacted]

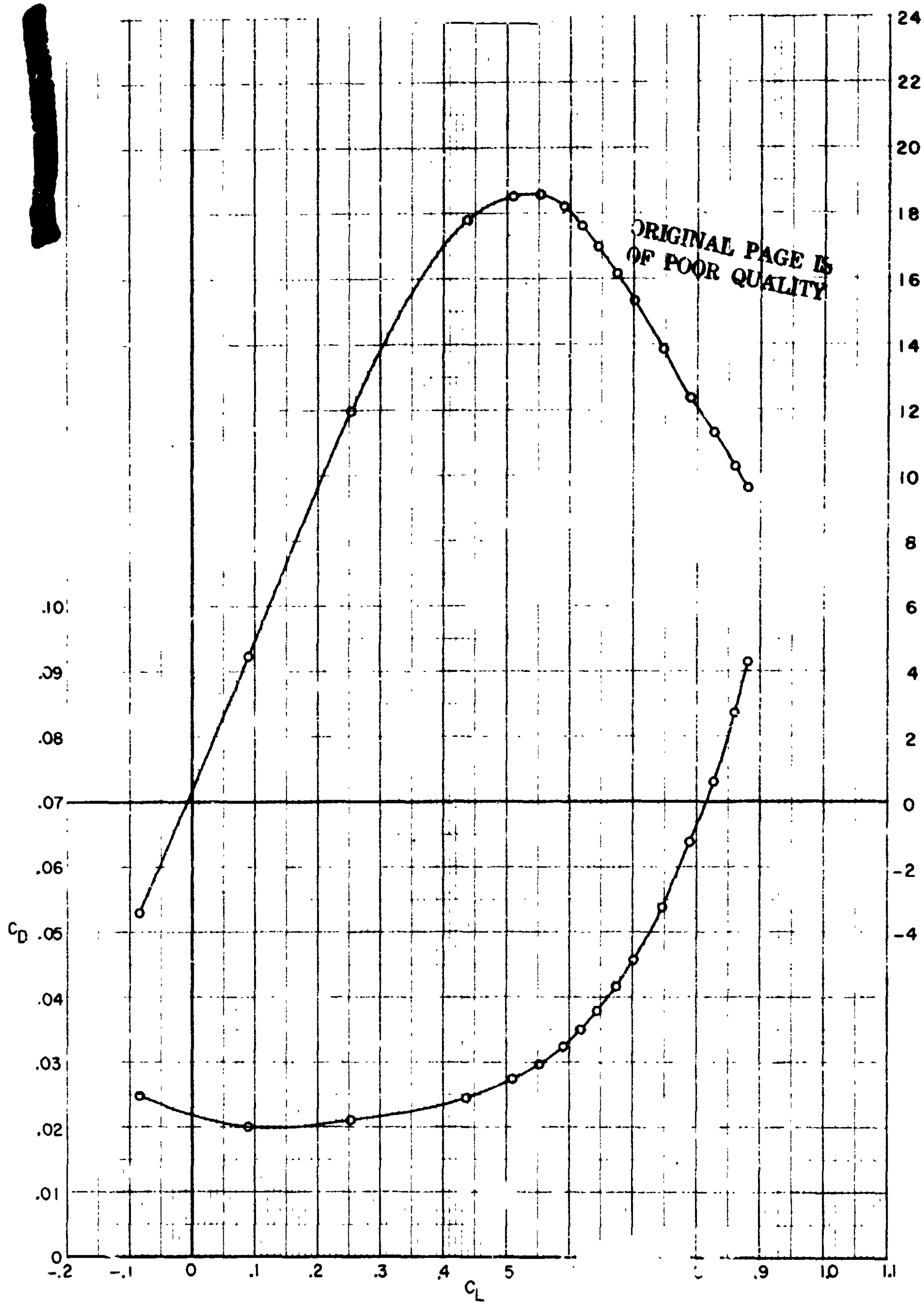

(h) M'= 0.80. Co...

Figure 8.- Continued.

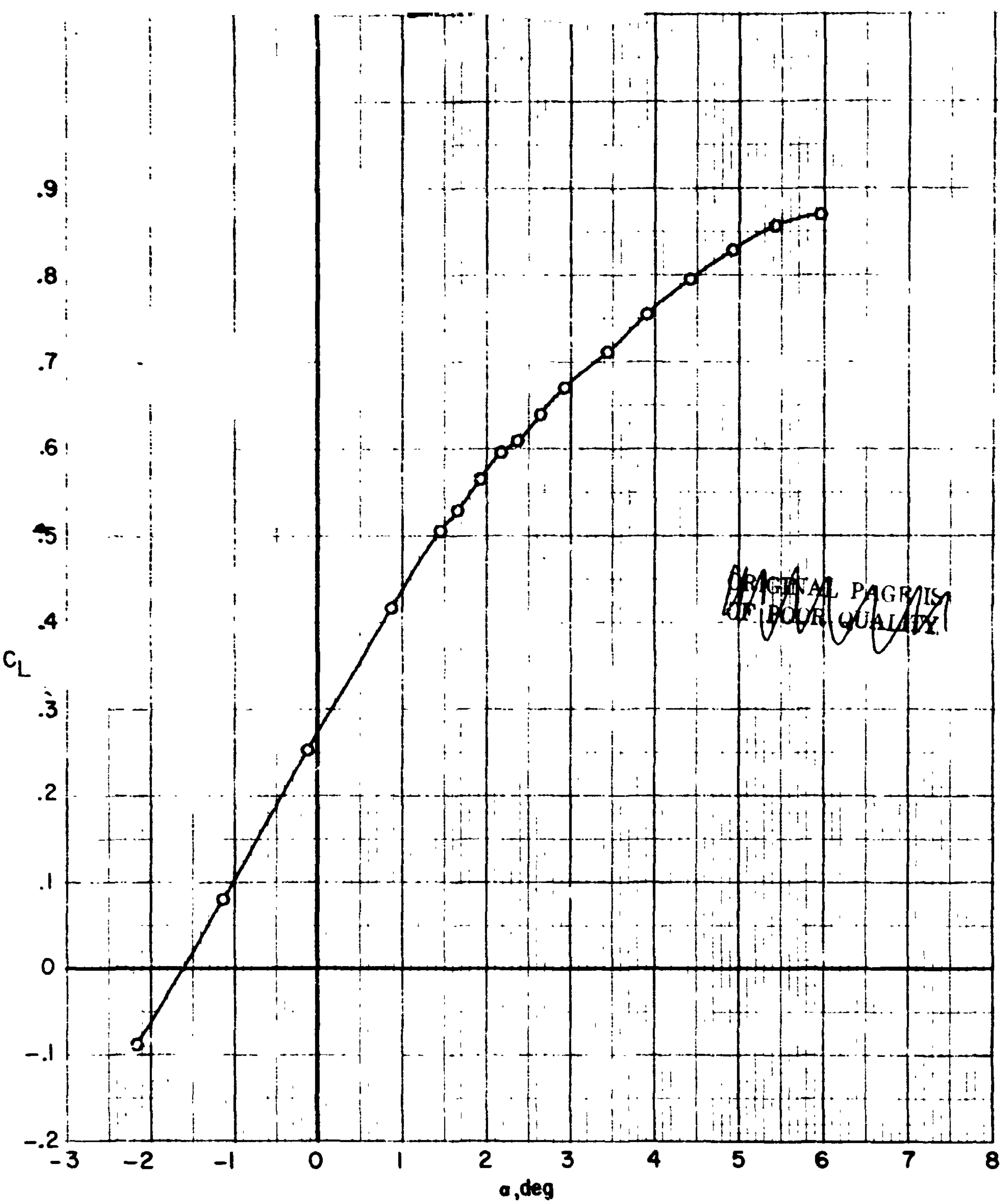

(i) M = 0.81.

Figure 8. - Continued.

[redacted]

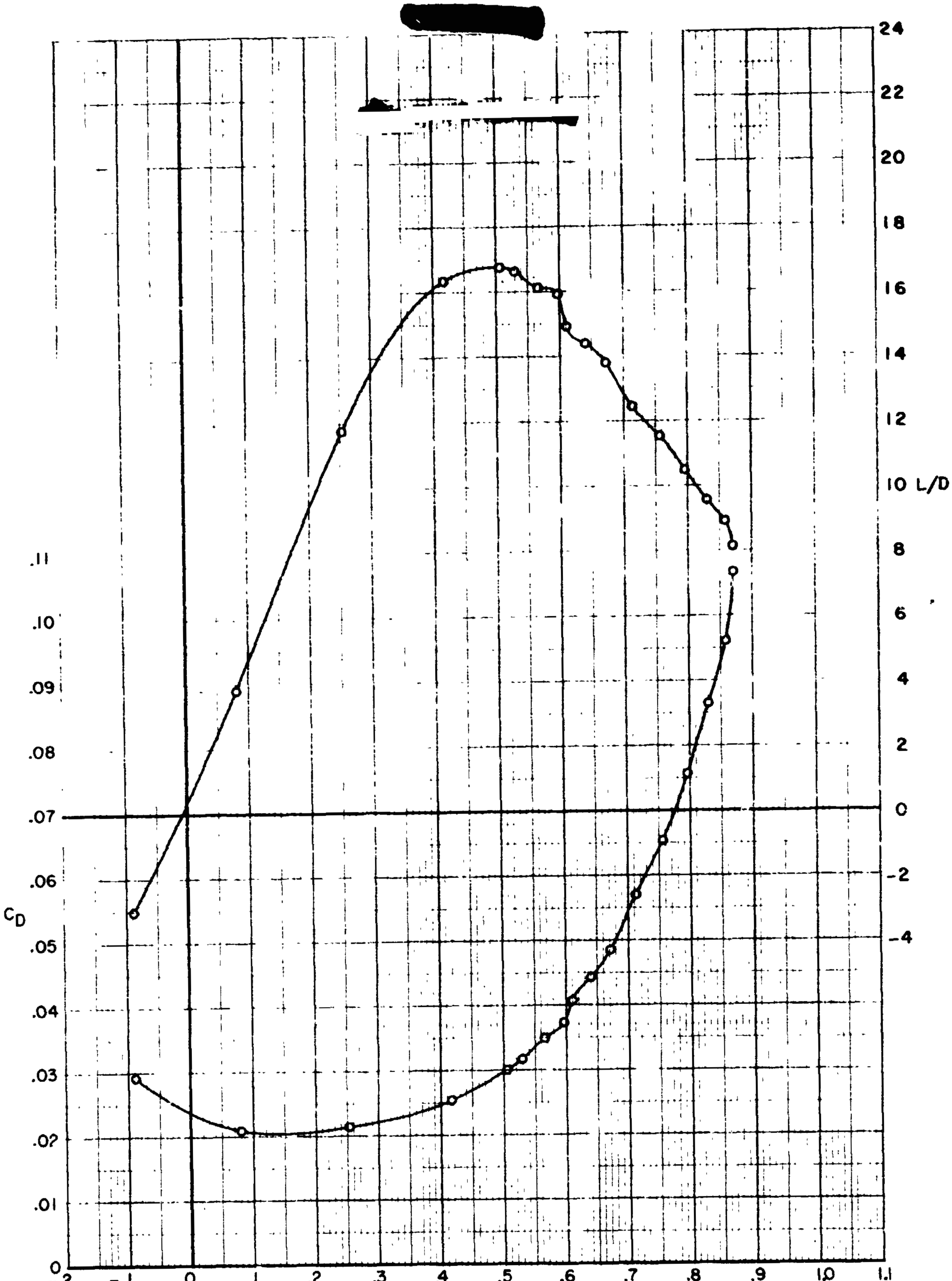

[redacted]

(i) M = 0.81. Continued.

Figure 8. - Continued.

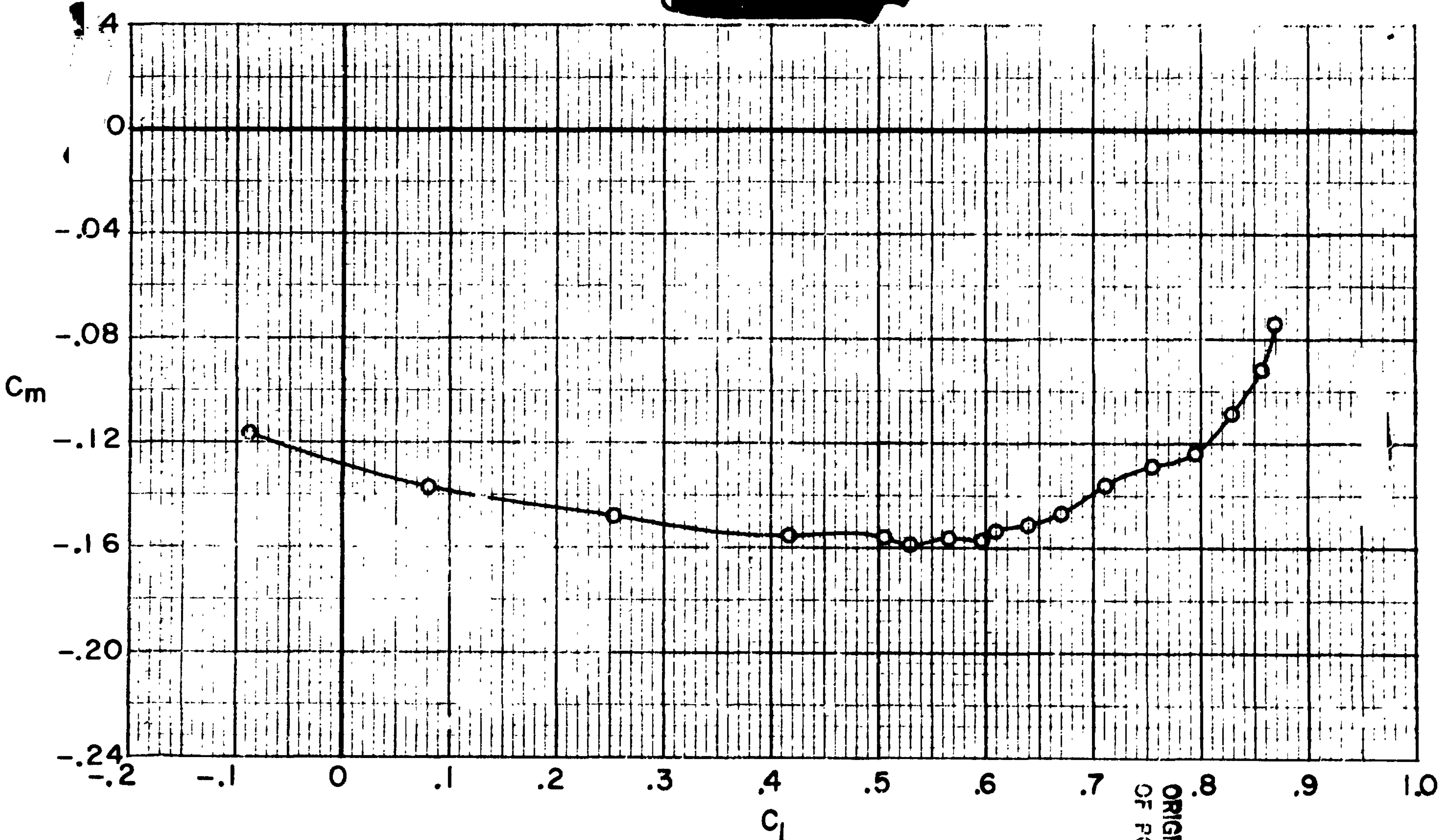

(l) M = 0.81. Concluded.

Figure 8. - Concluded.

ORIGINAL PAGE IS
OF POOR QUALITY

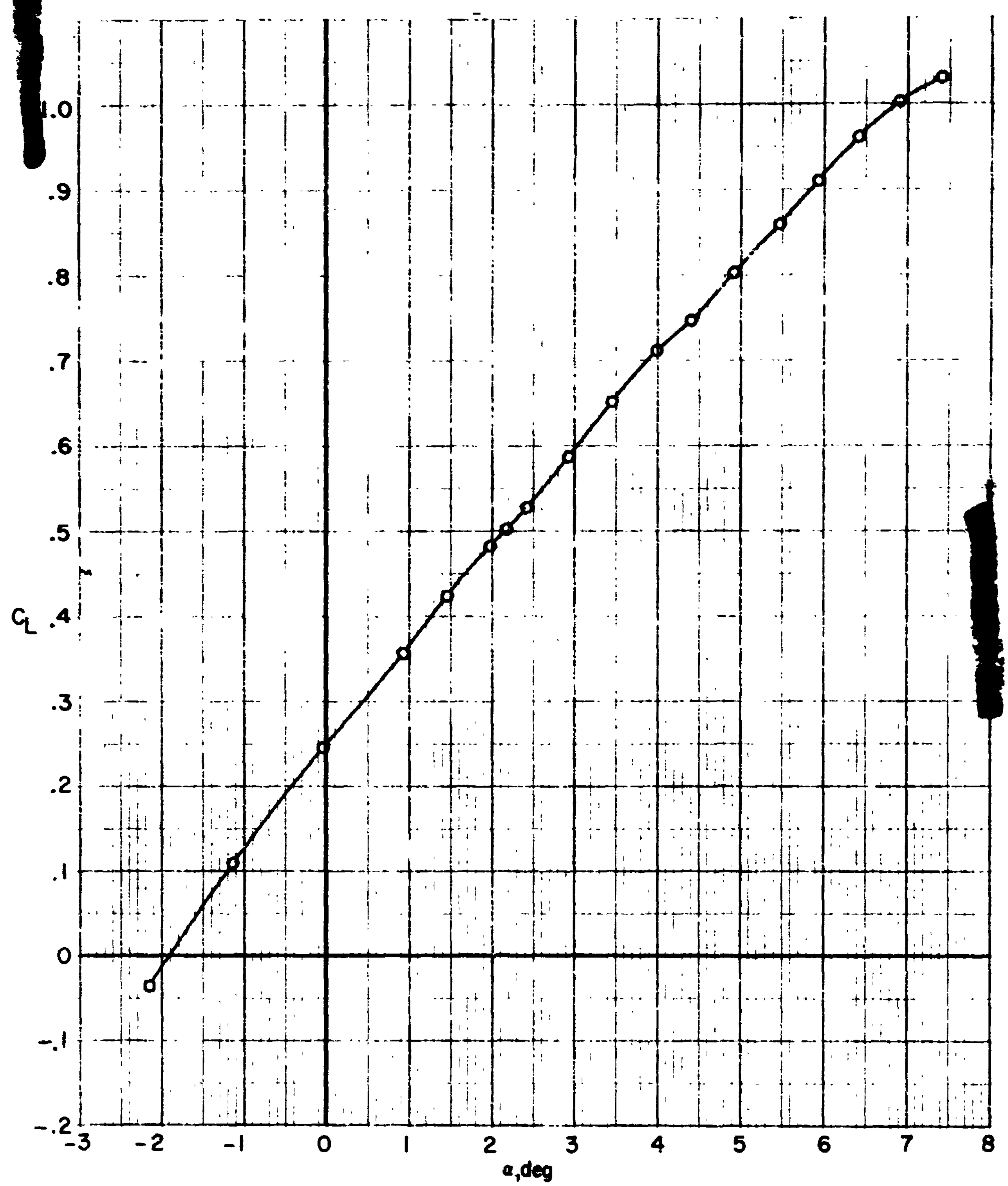

(a) M = 0.60.

Figure 9.- Longitudinal aerodynamic characteristics for supercritical wing configuration Ia (SCW-Ia) with wing upper surface grit forward ($x_T/C = 0.05$). (Results are from final series of tests for this configuration.) c.g. (F.S.) = 84.605 cm (33.309 in.); $\Lambda_{c/4} = 27°$.

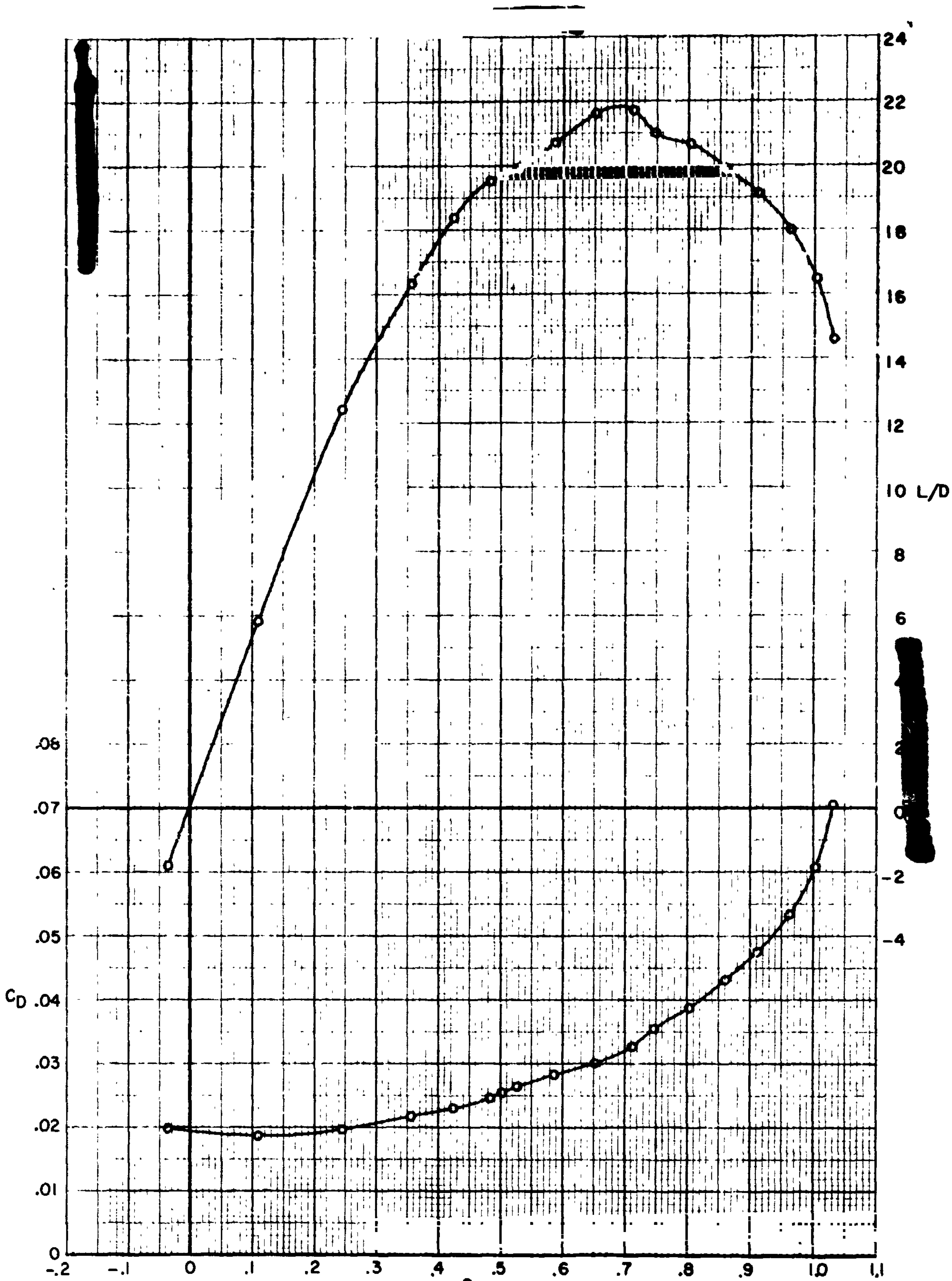

(a) M = 0.60. Continued.

Figure 9.- Continued. [redacted]

ORIGINAL PAGE IS
OF POOR QUALITY

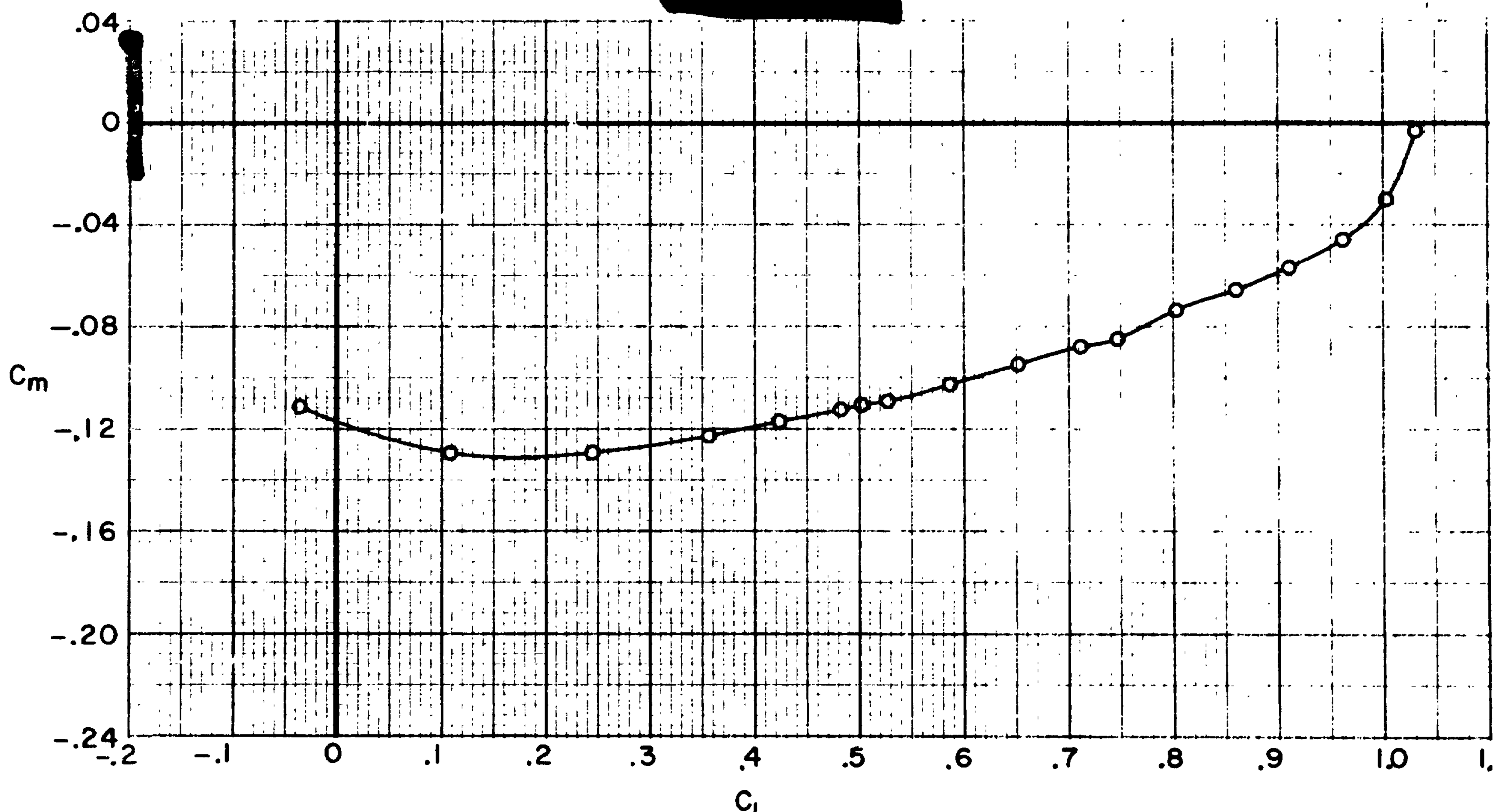

(a) M = 0.60. Concluded.

Figure 9.- Continued.

ORIGINAL PAGE IS
OF POOR QUALITY

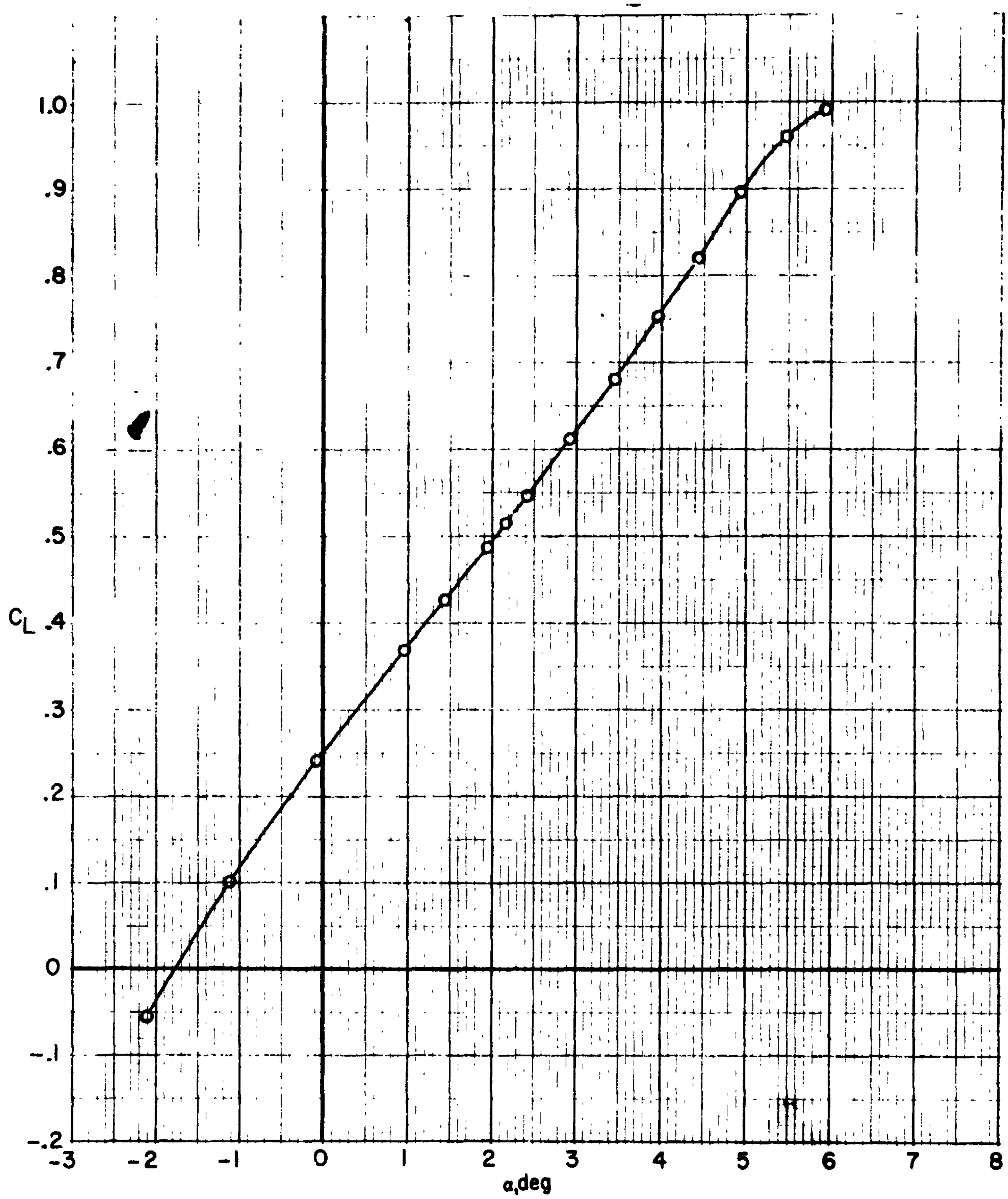

(b) M = 0.70.

Figure 9.- Continued.

ORIG[illegible] OF P[illegible]

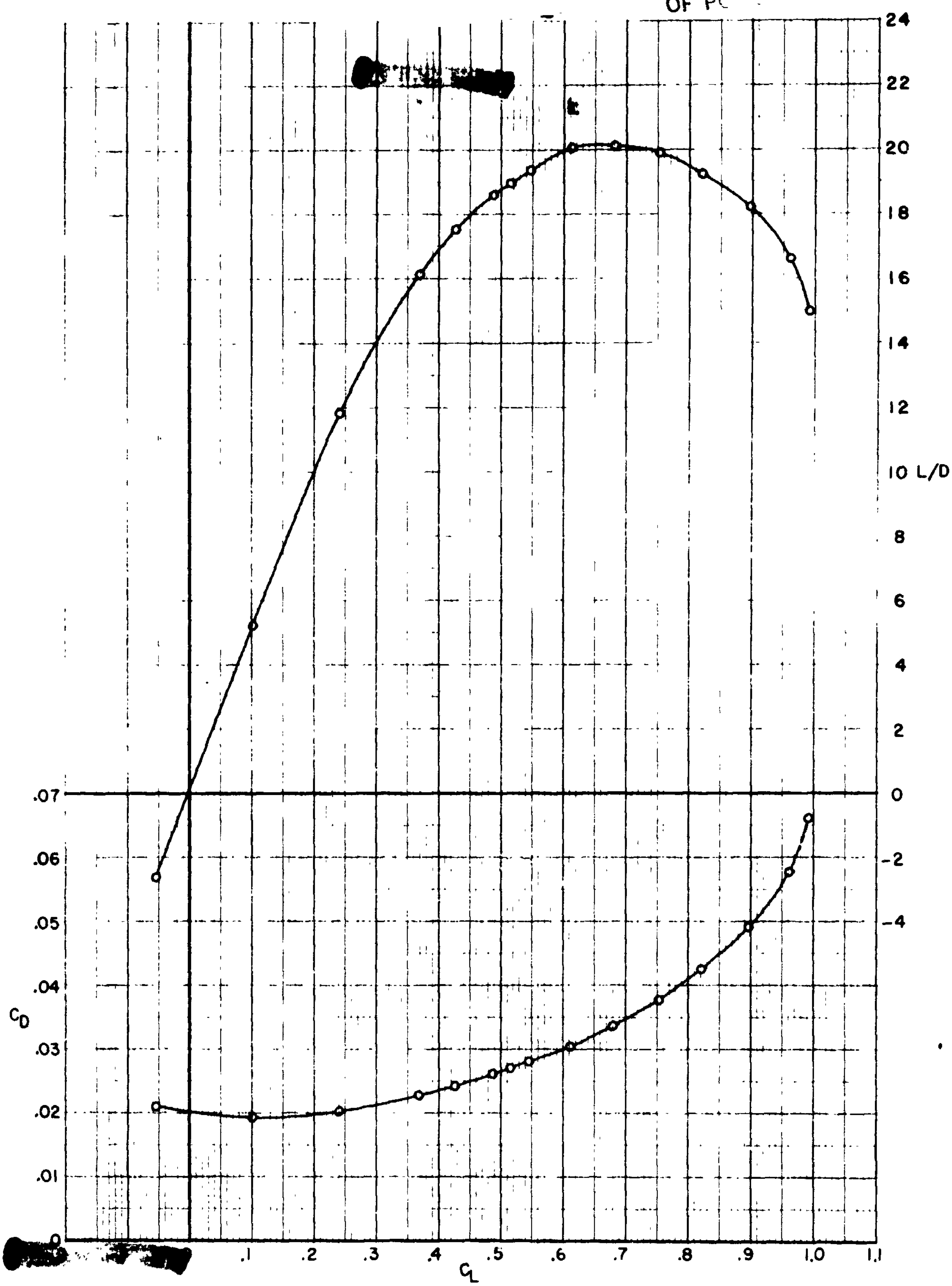

(b) M = 0.70. Continued.

Figure 9.- Continued.

[redacted]

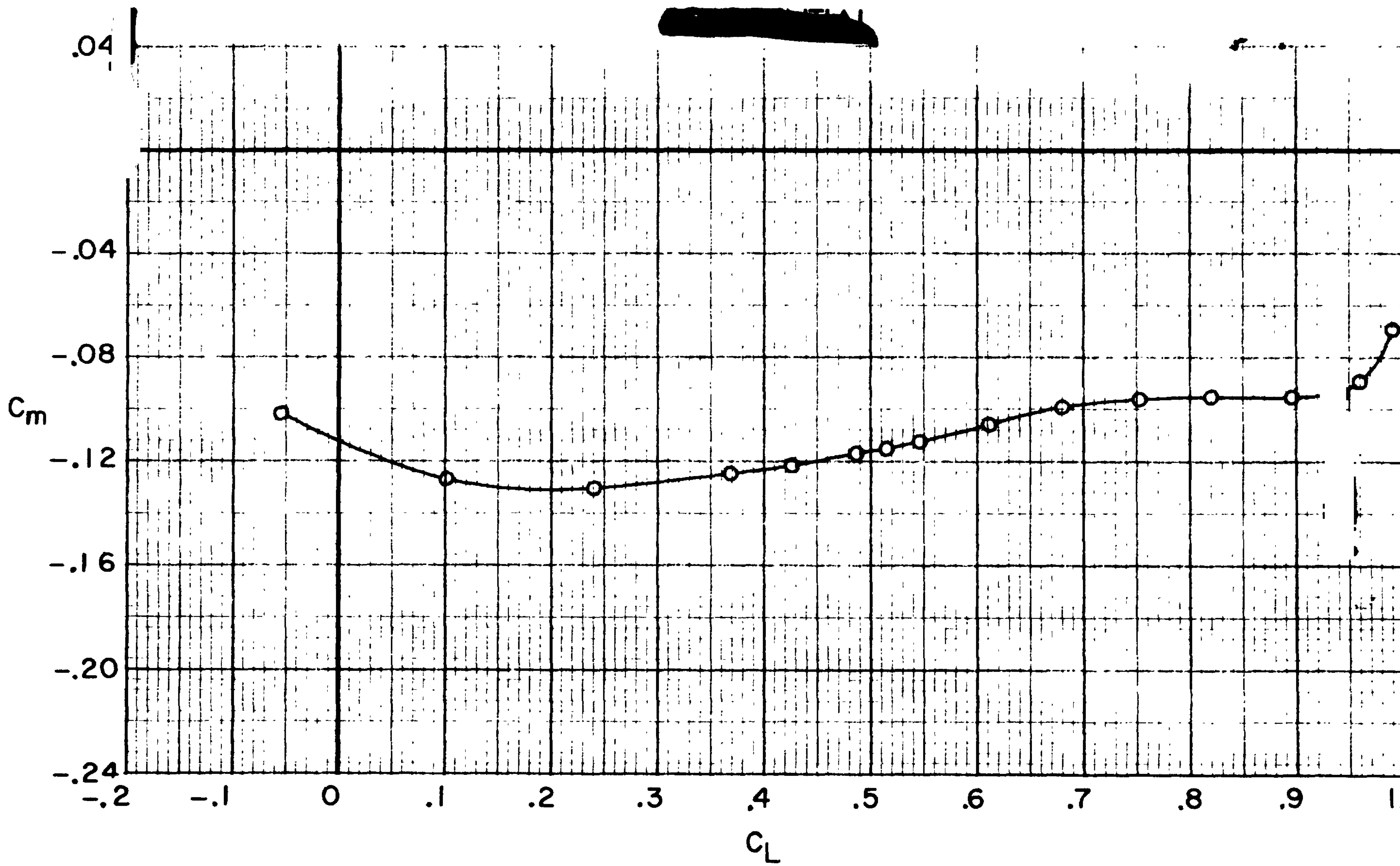

(b) M = 0.70. Concluded.

Figure 9.- Continued.

[redacted]

(c) M = 0.75.

Figure 9.- Continued.

ORIGINAL PAGE IS
OF POOR QUALITY

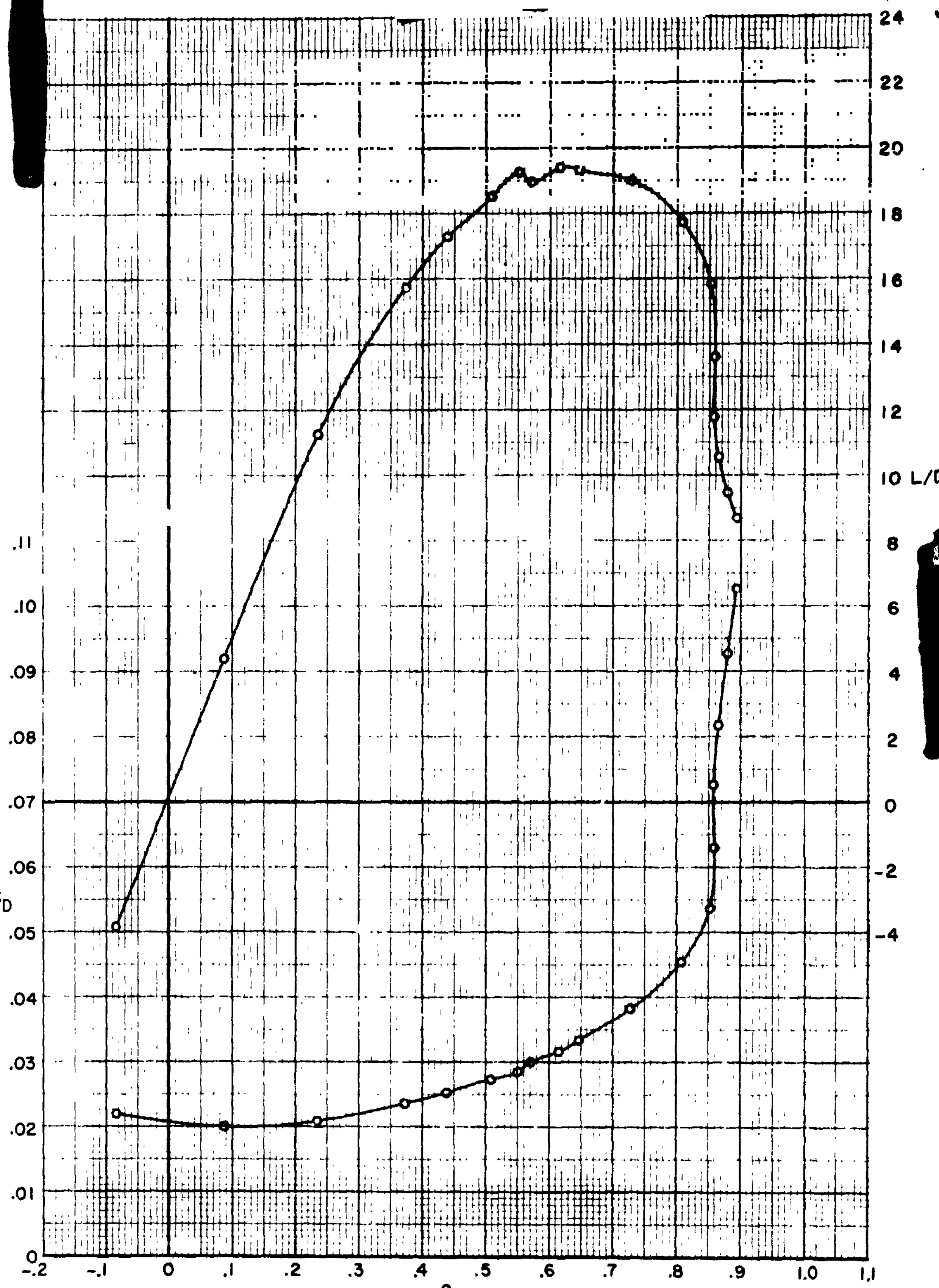

(c) M = 0.75. Continued.

Figure 9.- Continued.

[redacted]

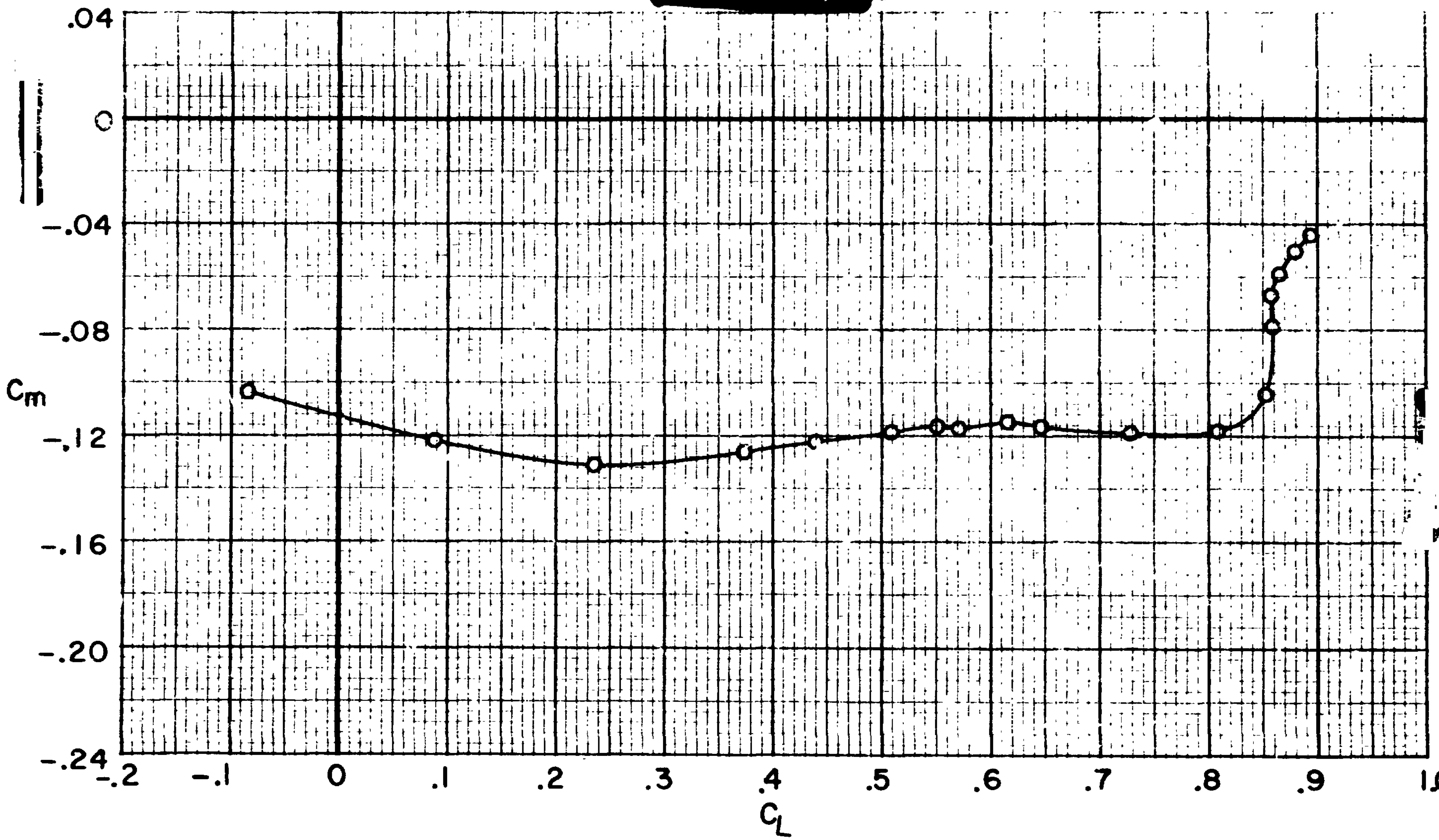

(c) M = 0.75. Concluded.

Figure 9.- Concluded.

[redacted]

ORIGINAL PAGE IS
OF POOR QUALITY

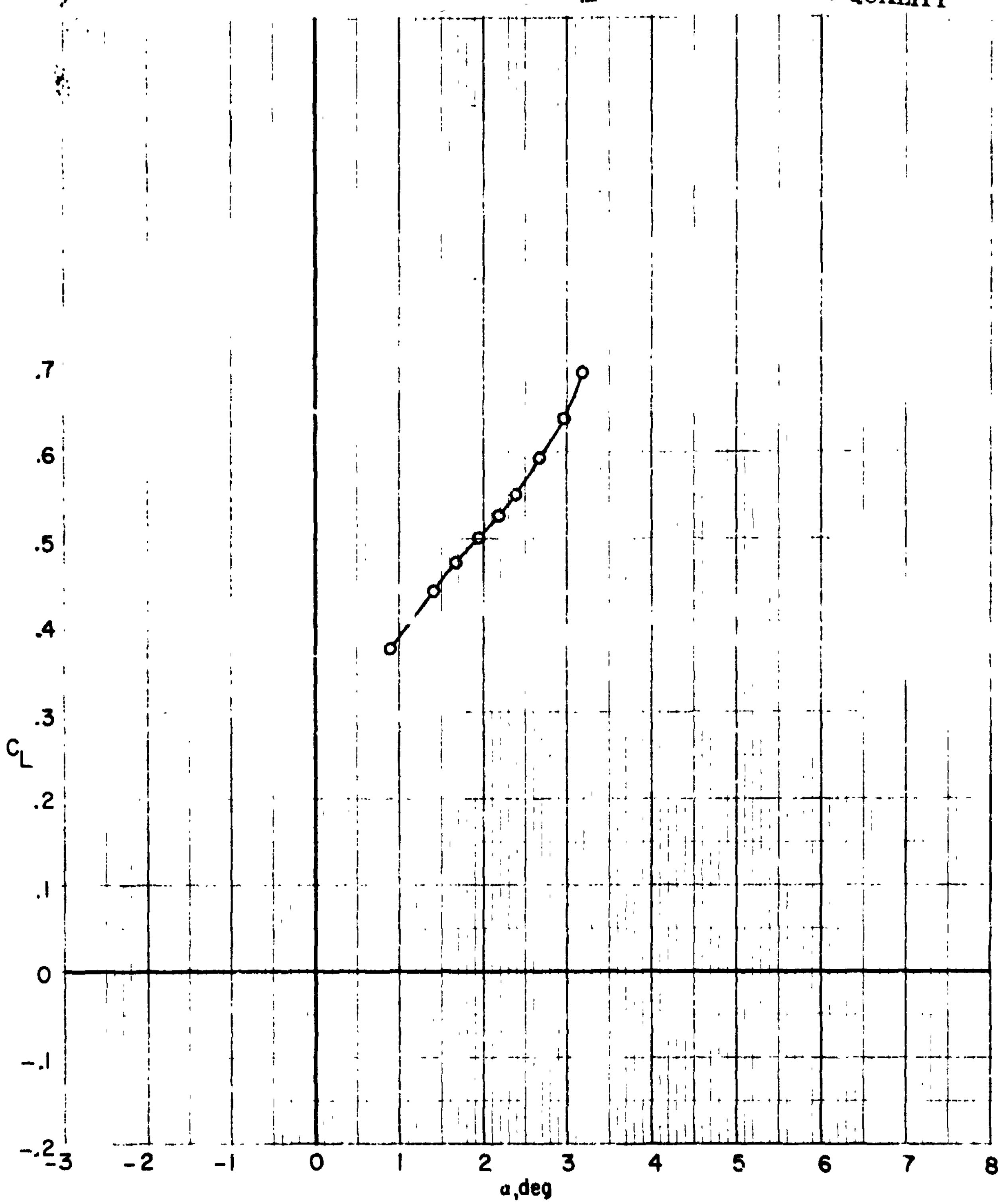

(a) M = 0.75.

Figure 10. - Longitudinal aerodynamic characteristics for supercritical wing configuration Ib (SCW-Ib) with wing upper surface grit aft (fig. 5). $\Lambda_{c/4} = 30°$.

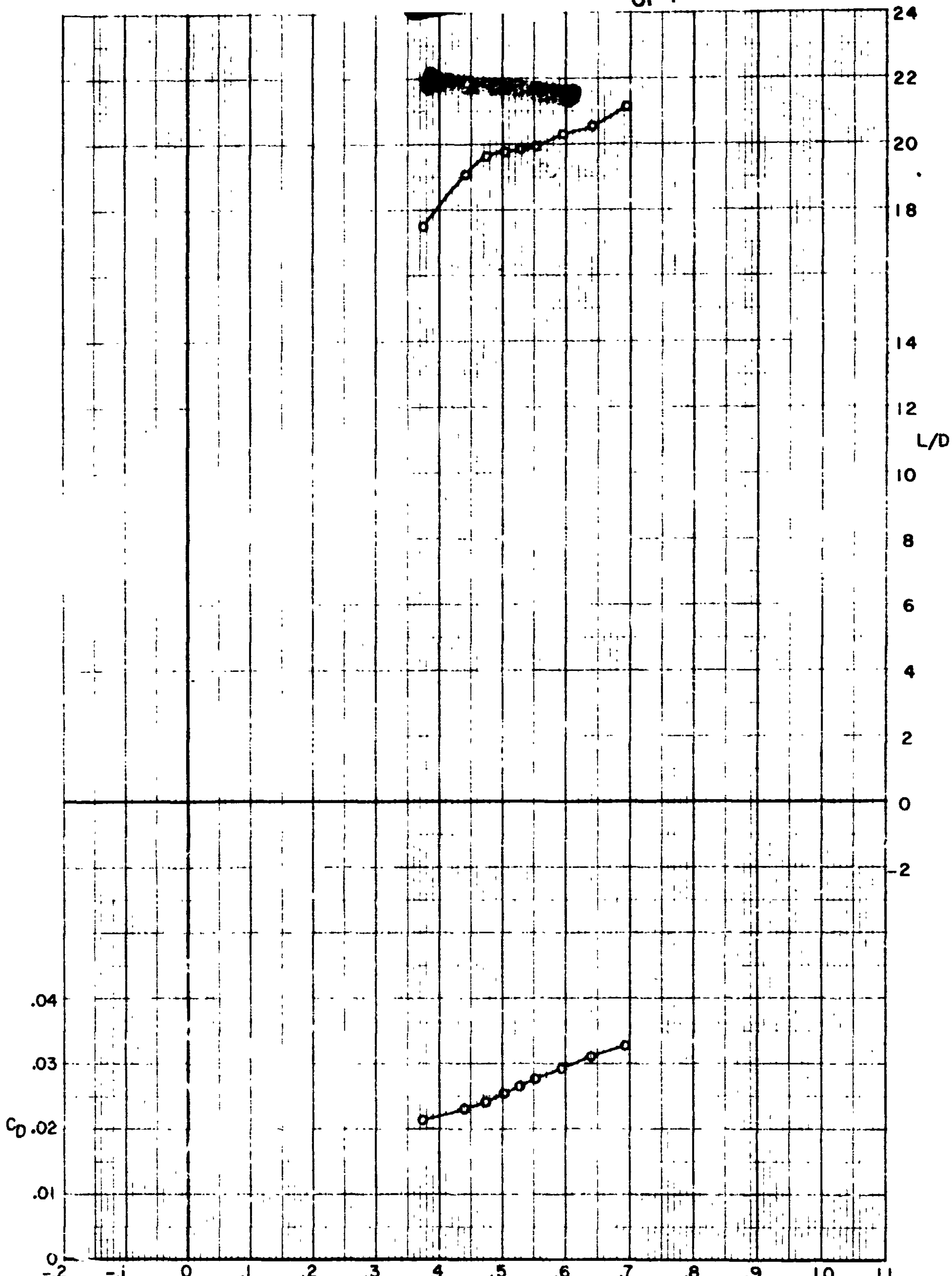

(a) M = 0.75. Continued.

Figure 10. - Continued.

ORIGINAL PAGE IS
OF POOR QUALITY

[redacted]

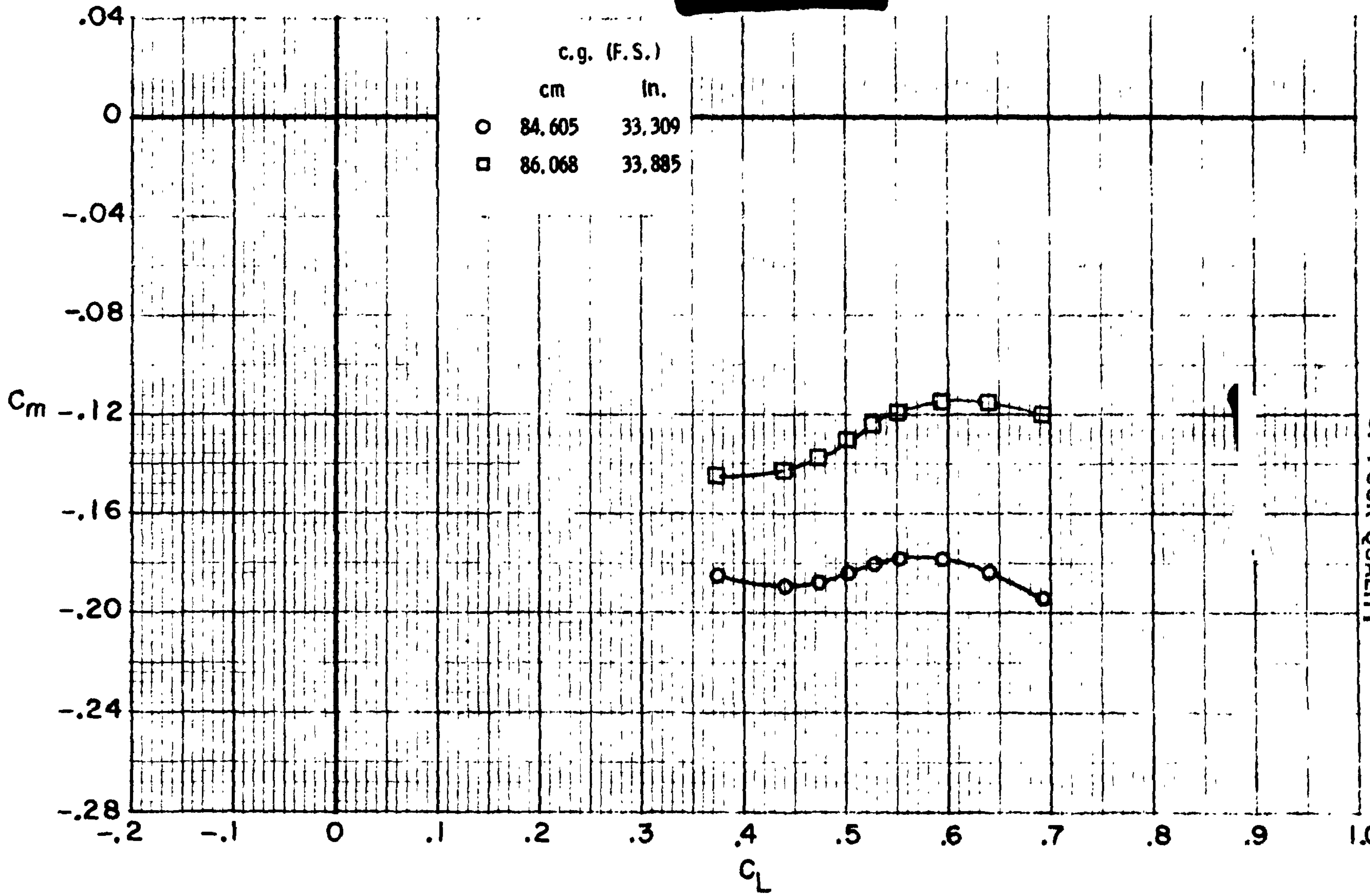

(a) M = 0.75. Concluded.

Figure 10.- Continued.

[redacted]

ORIGINAL PAGE IS
OF POOR QUALITY

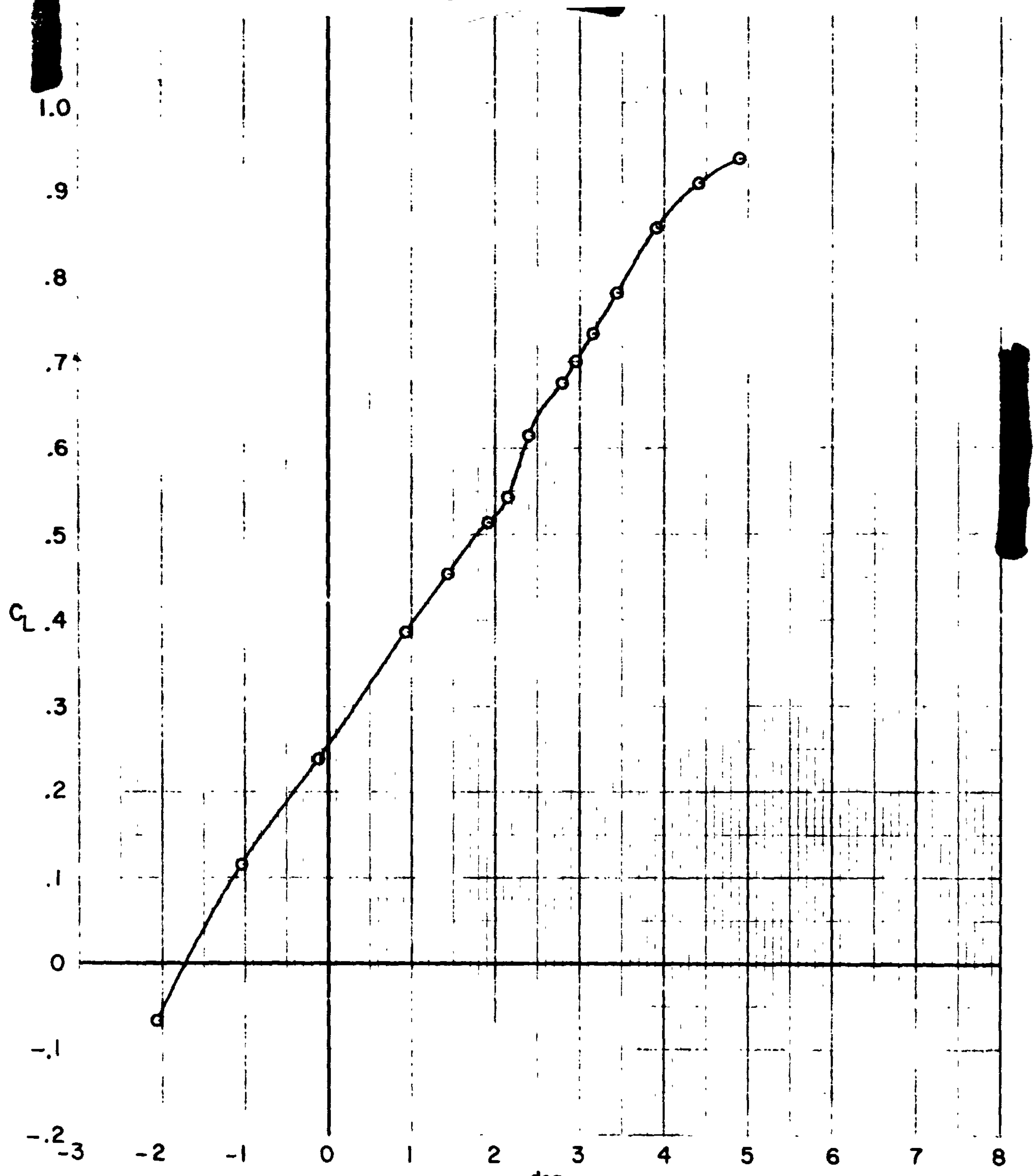

(b) M = 0.77.

Figure 10. - Continued.

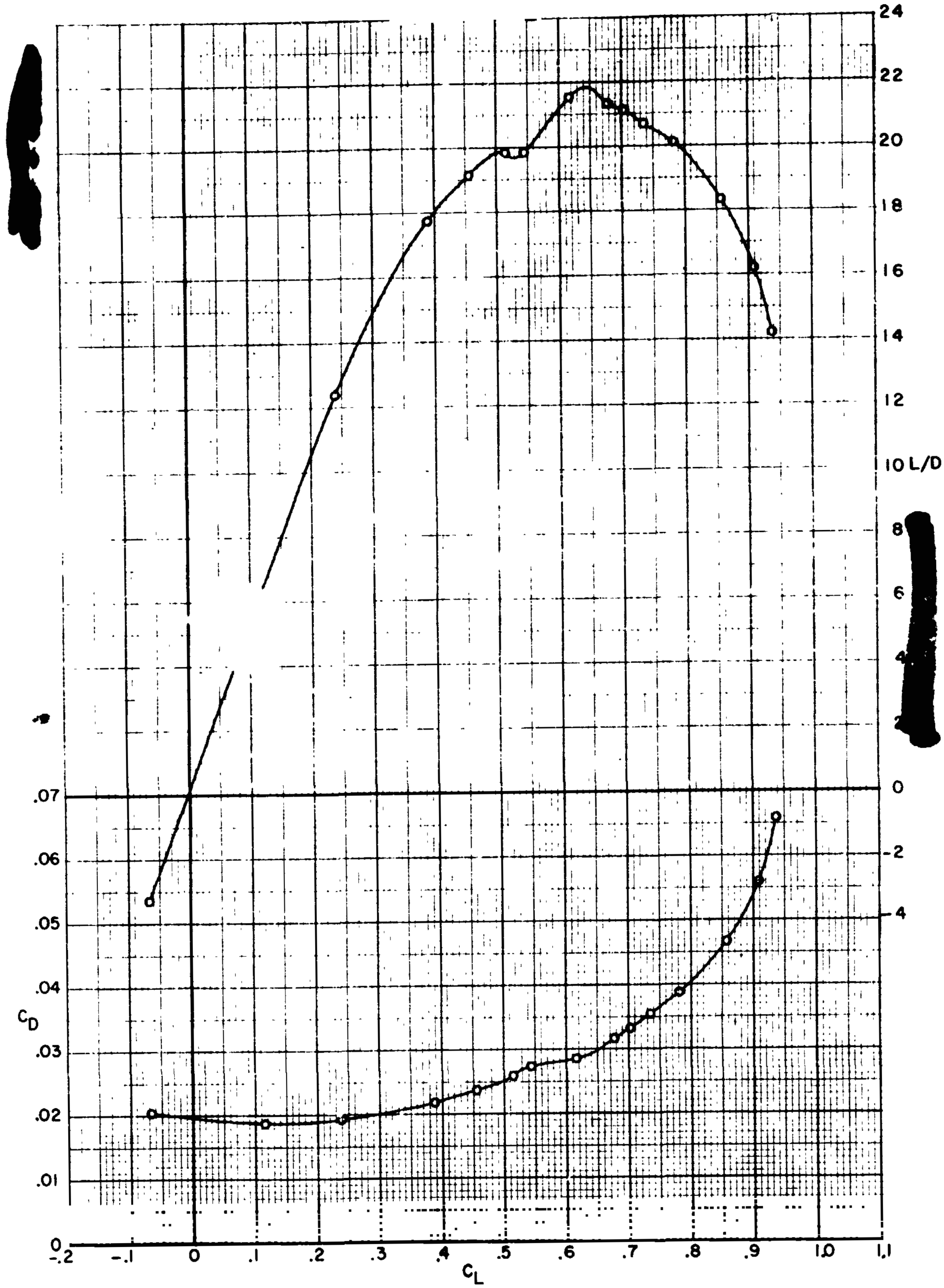

(b) M = 0.77. Continued.

Figure 10. - Continued.

ORIGINAL PAGE IS
OF POOR QUALITY

[redacted]

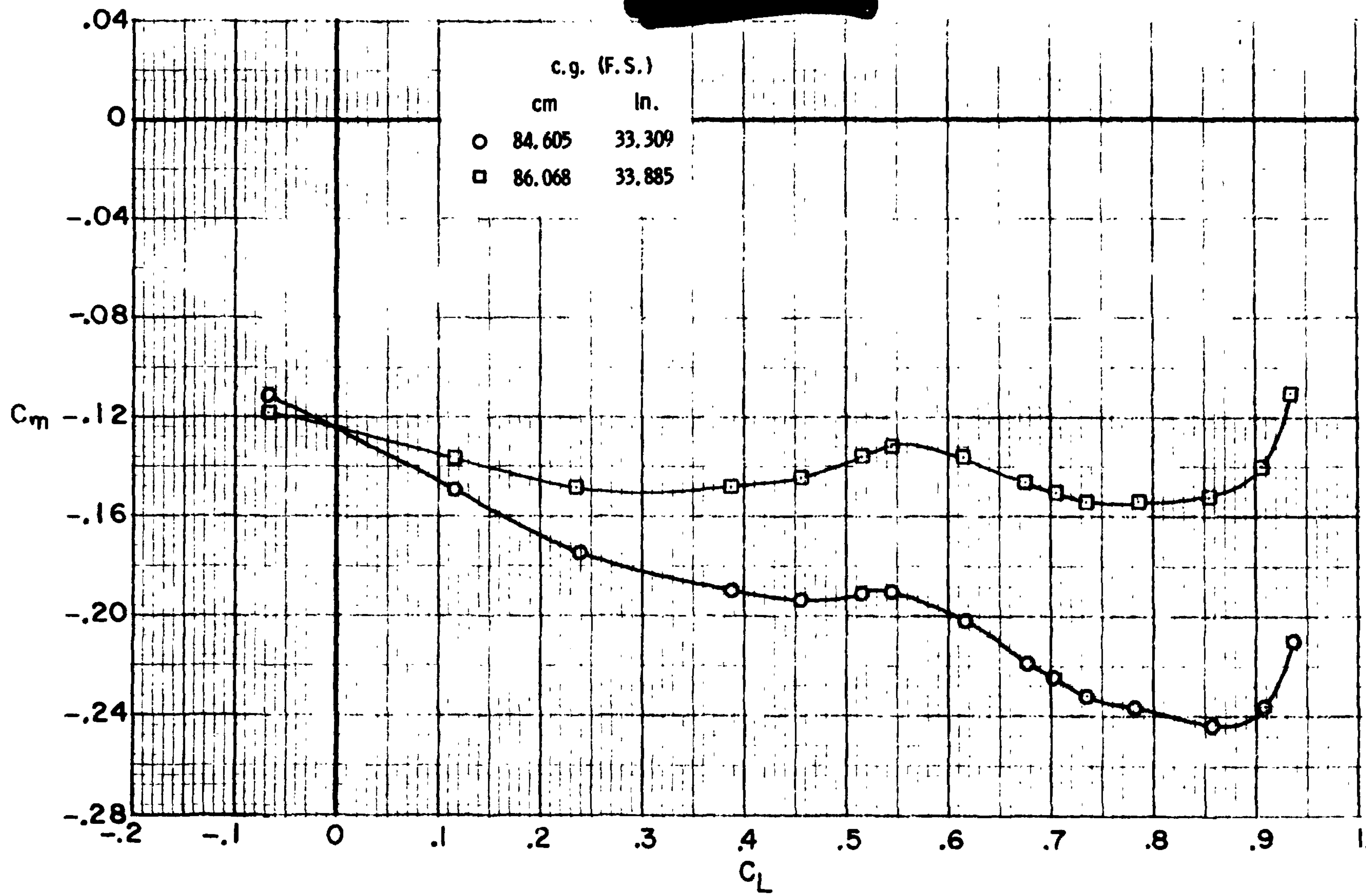

(b) M = 0.77. Concluded.

Figure 10. - Continued.

[redacted]

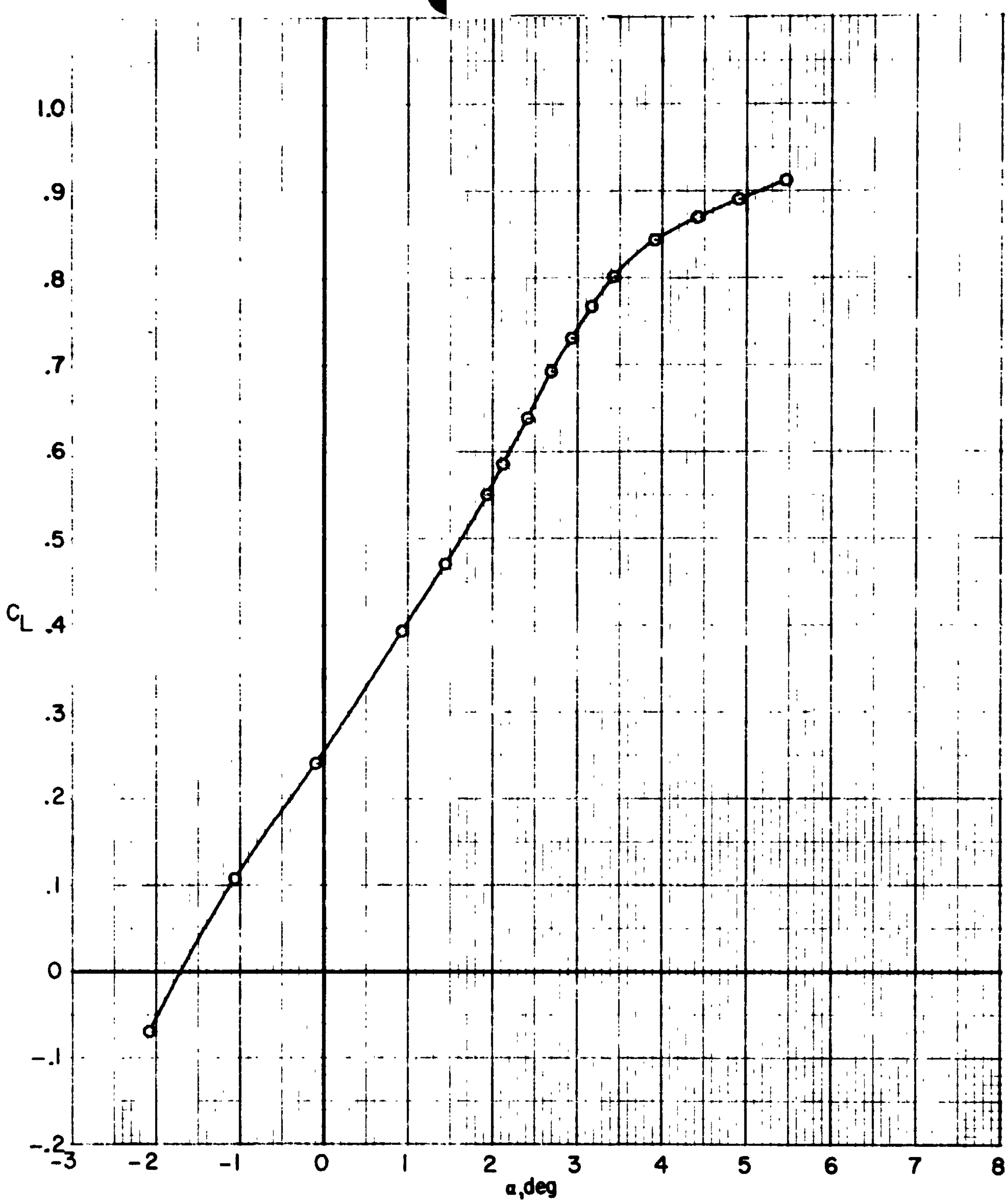

(c) M = 0.79.

Figure 10.- Continued.

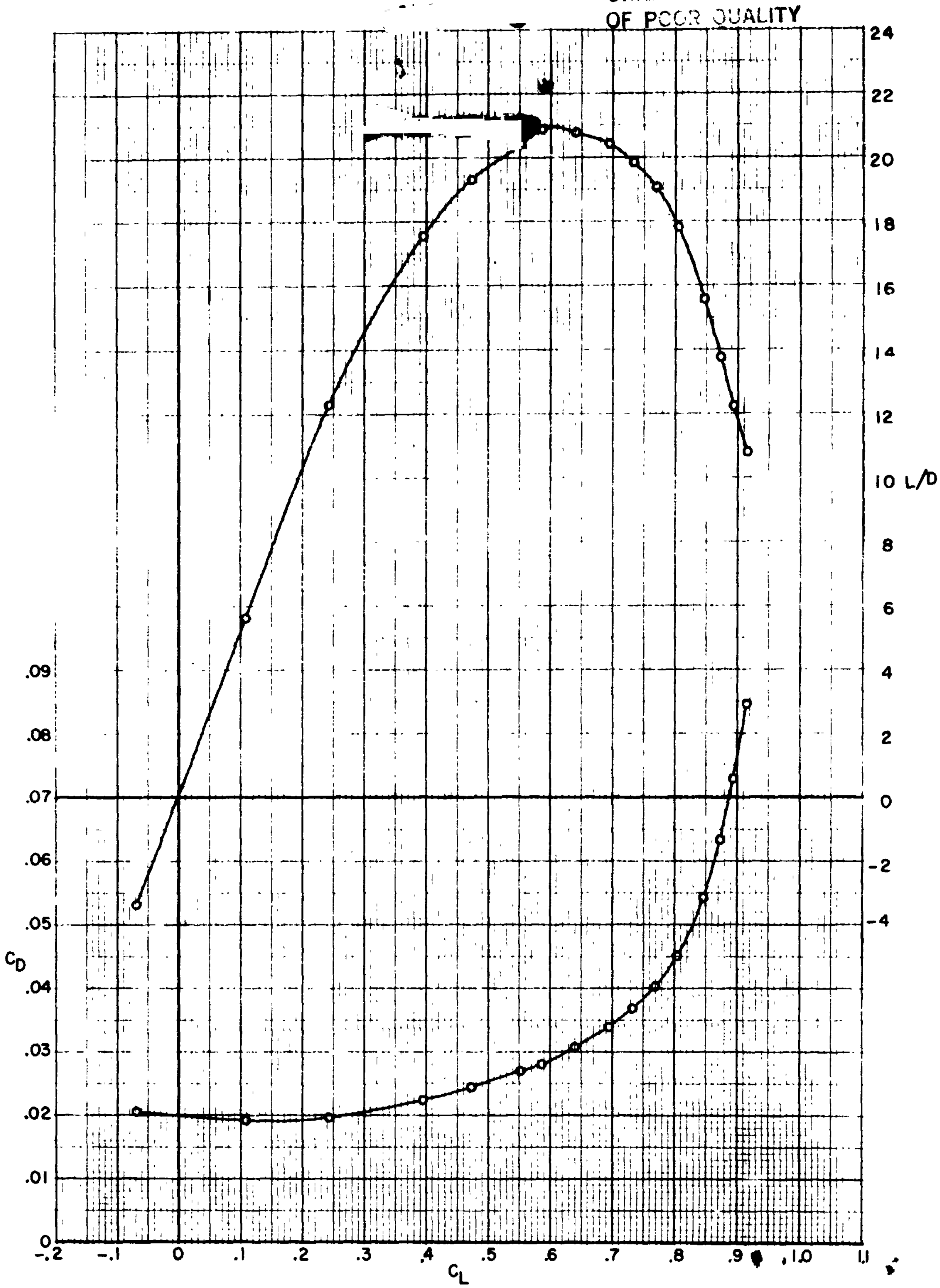

(c) M = 0.79. Continued.

Figure 10.- Continued.

[redacted]

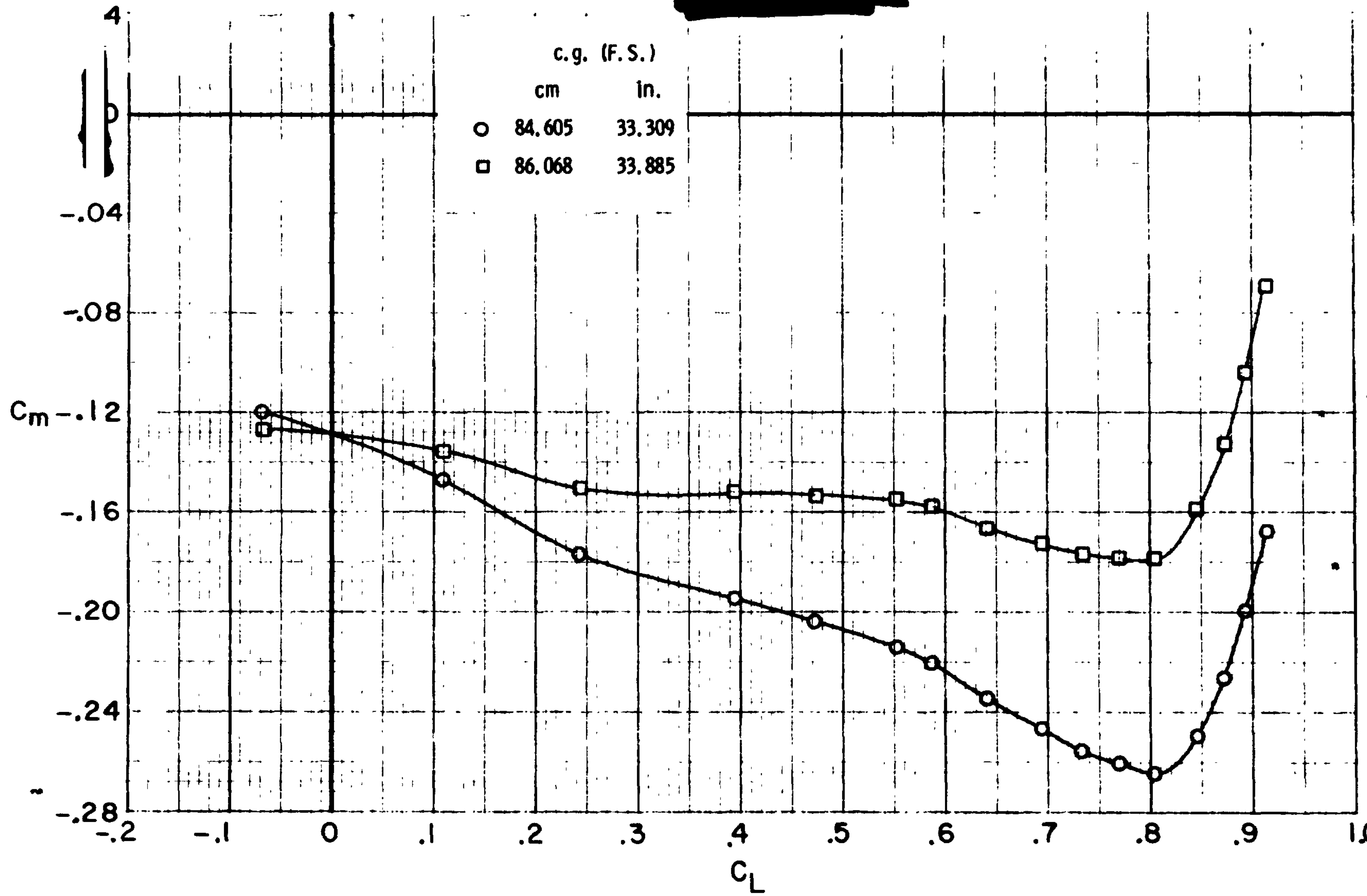

(c) M = 0.79. Concluded.

Figure 10. - Continued.

[redacted]

ORIGINAL PAGE IS
OF PO[illegible]

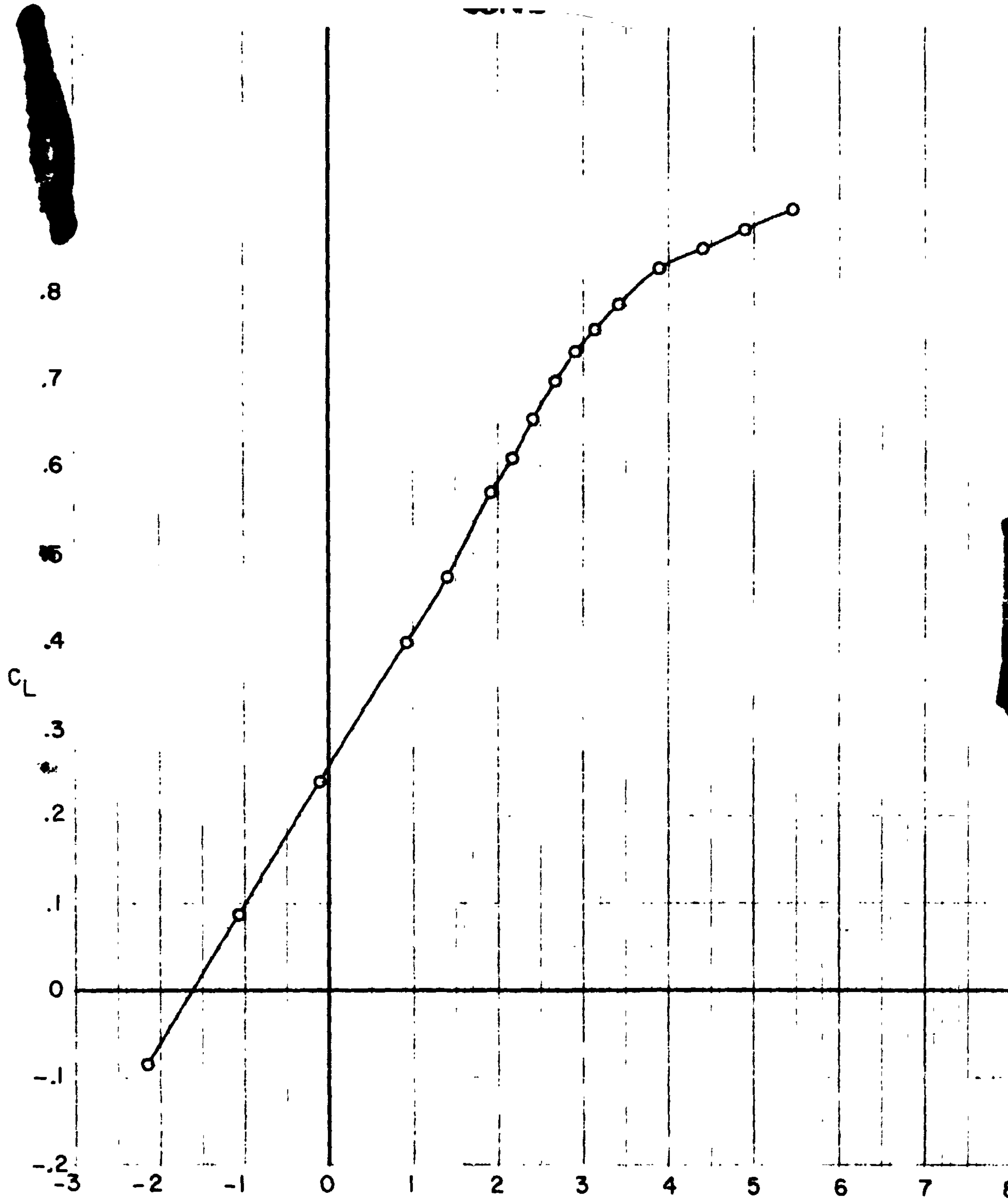

(d) M = 0.80.

Figure 10.- Continued.

(d) M = 0.80. Continued.

Figure 10. - Continued.

ORIGINAL PAGE IS
OF POOR QUALITY

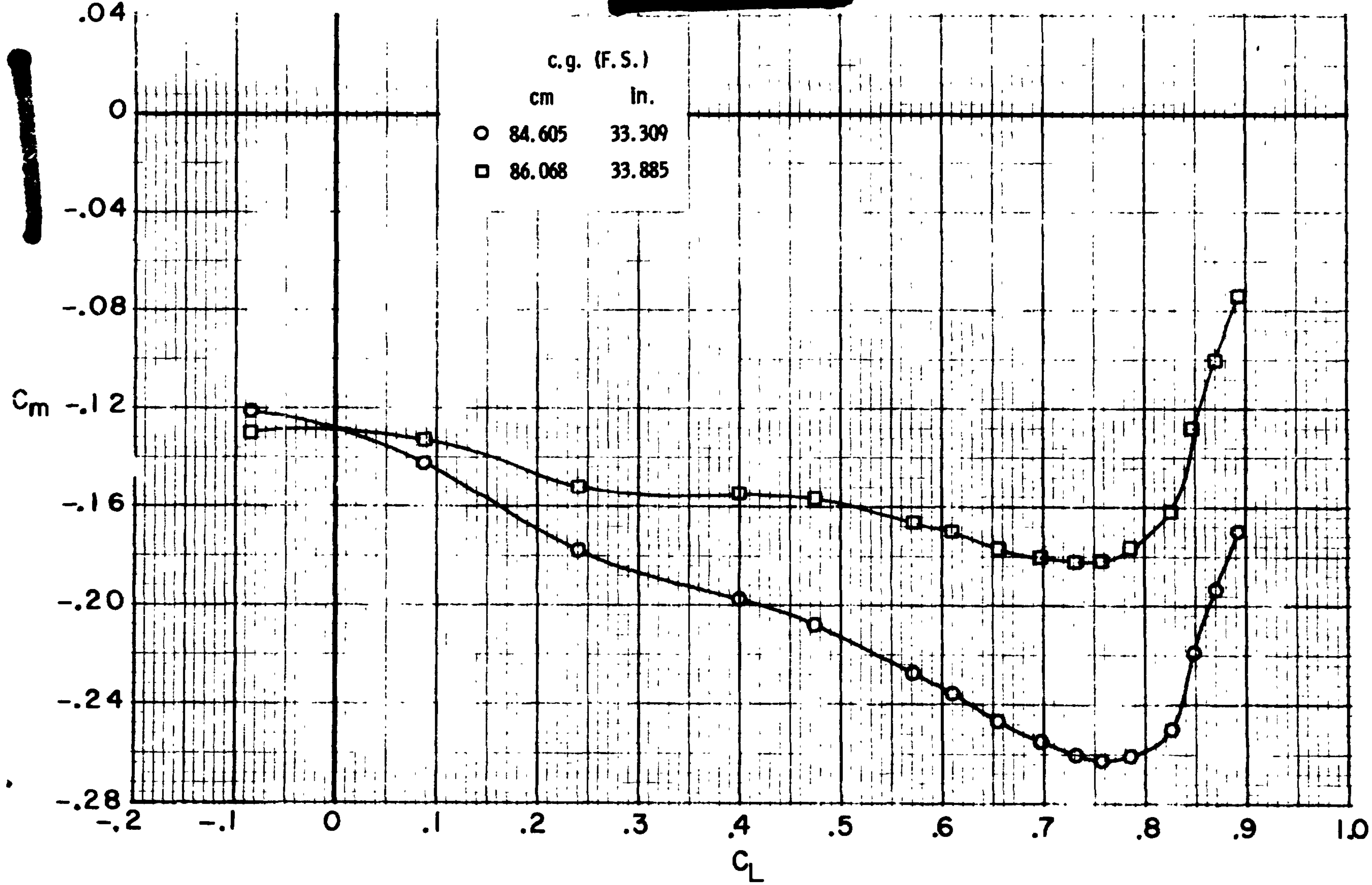

(d) M = 0.80. Concluded.

Figure 10.- Continued.

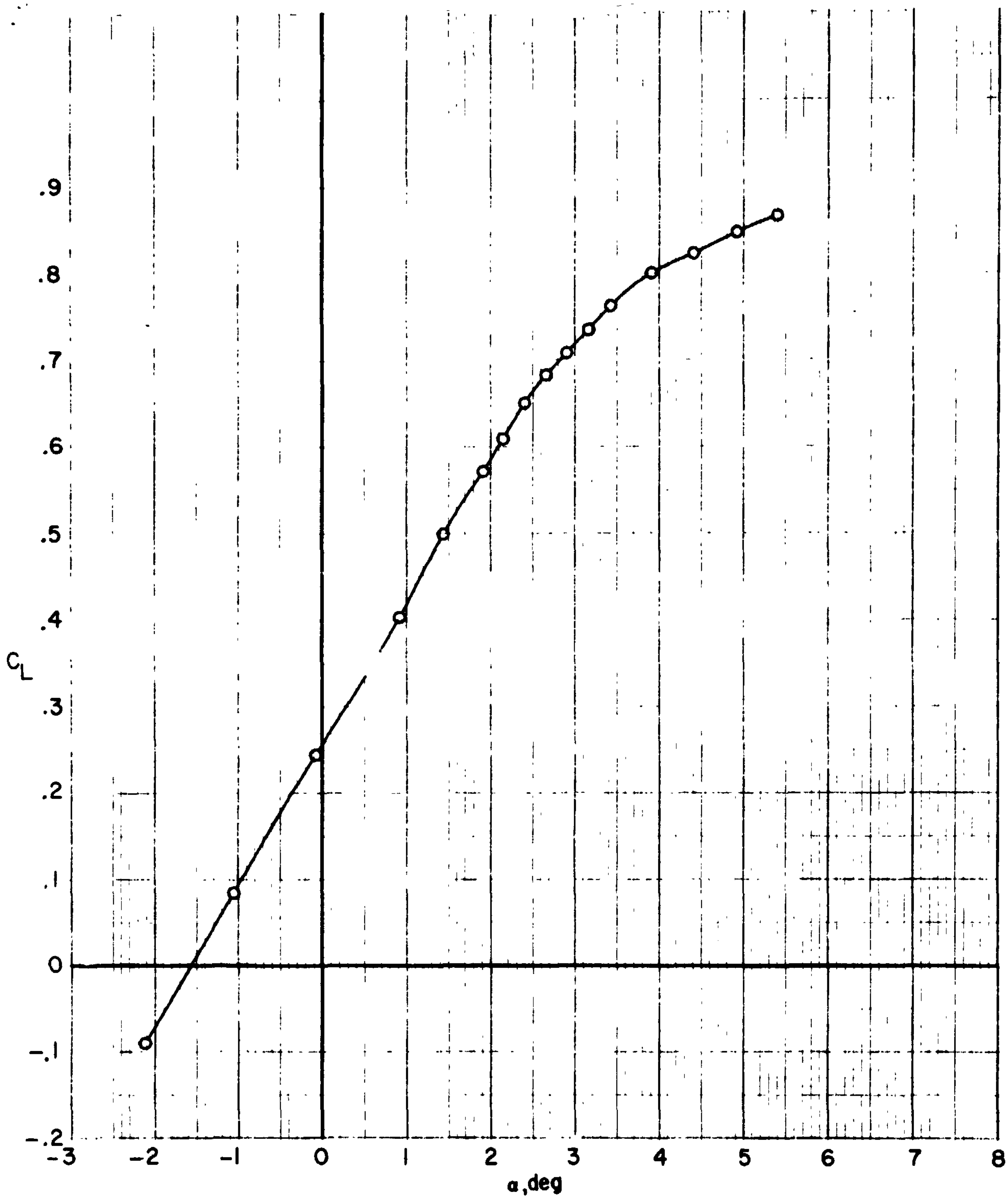

(e) M = 0.81.

Figure 10.- Continued.

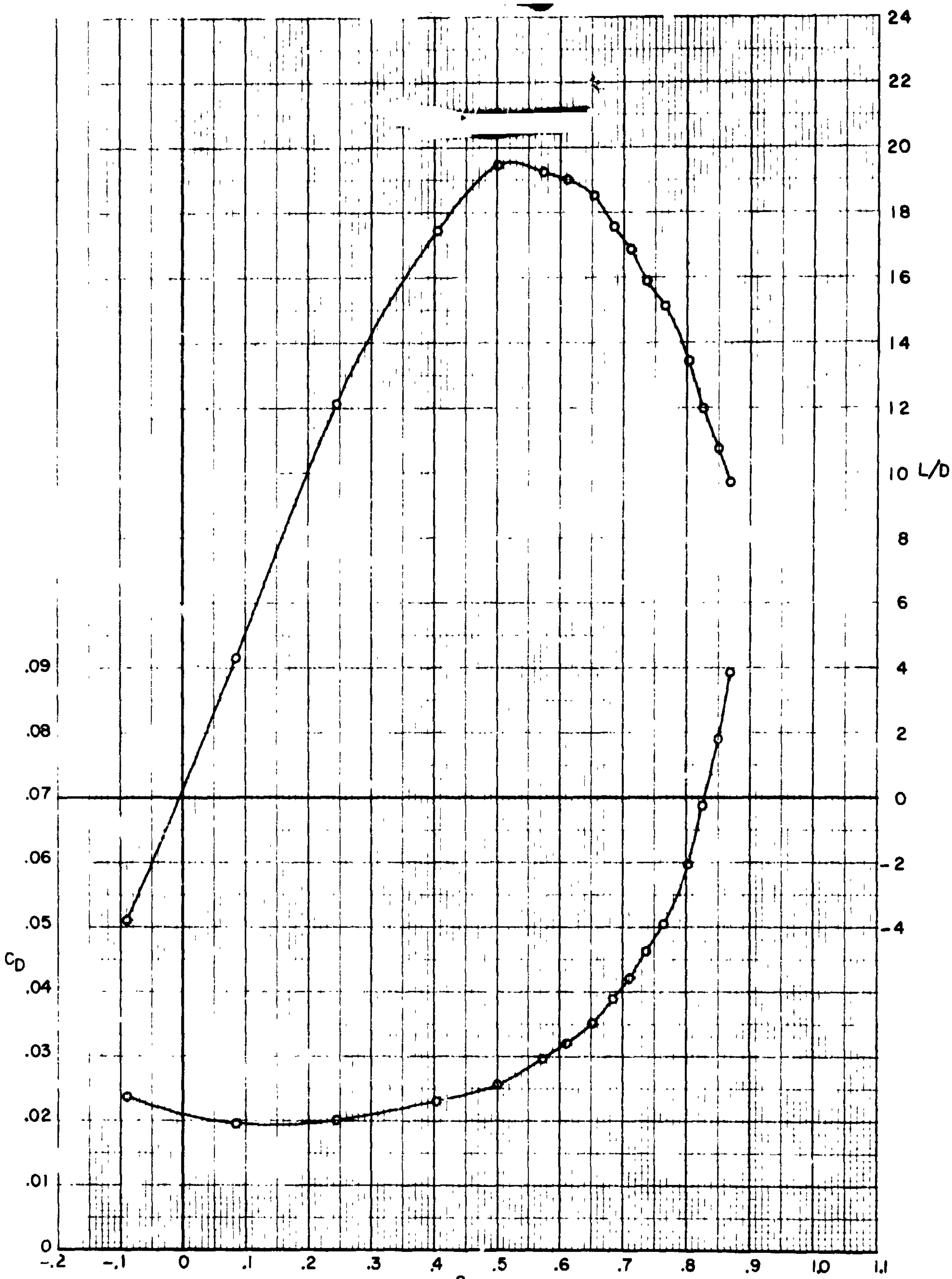

[redacted]

(e) M = 0.81. Continued.

Figure 10.- Continued

ORIGINAL PAGE IS
OF POOR QUALITY

[redacted]

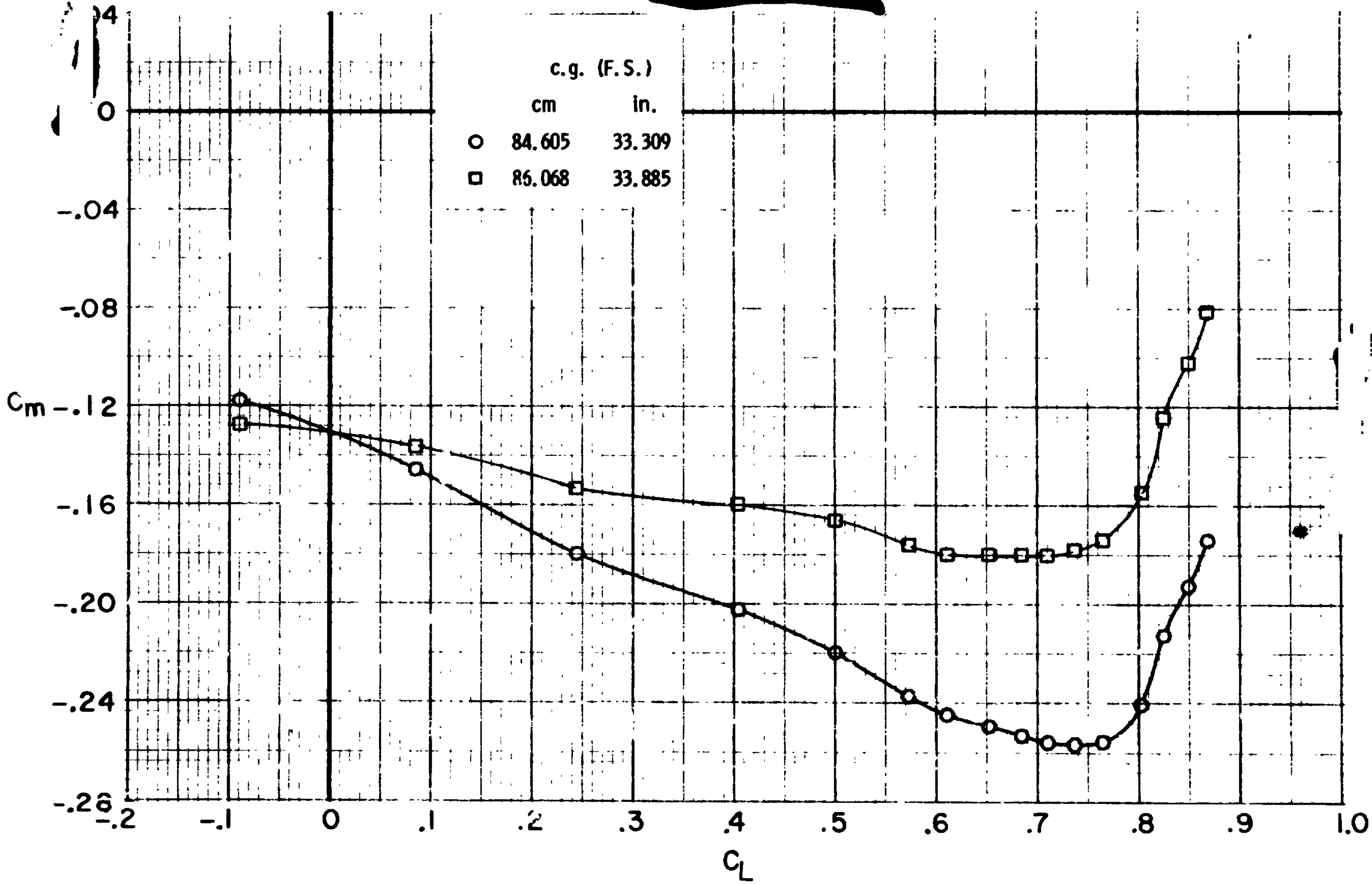

(e) M = 0.81. Concluded.

Figure 10.- Continued.

[redacted]

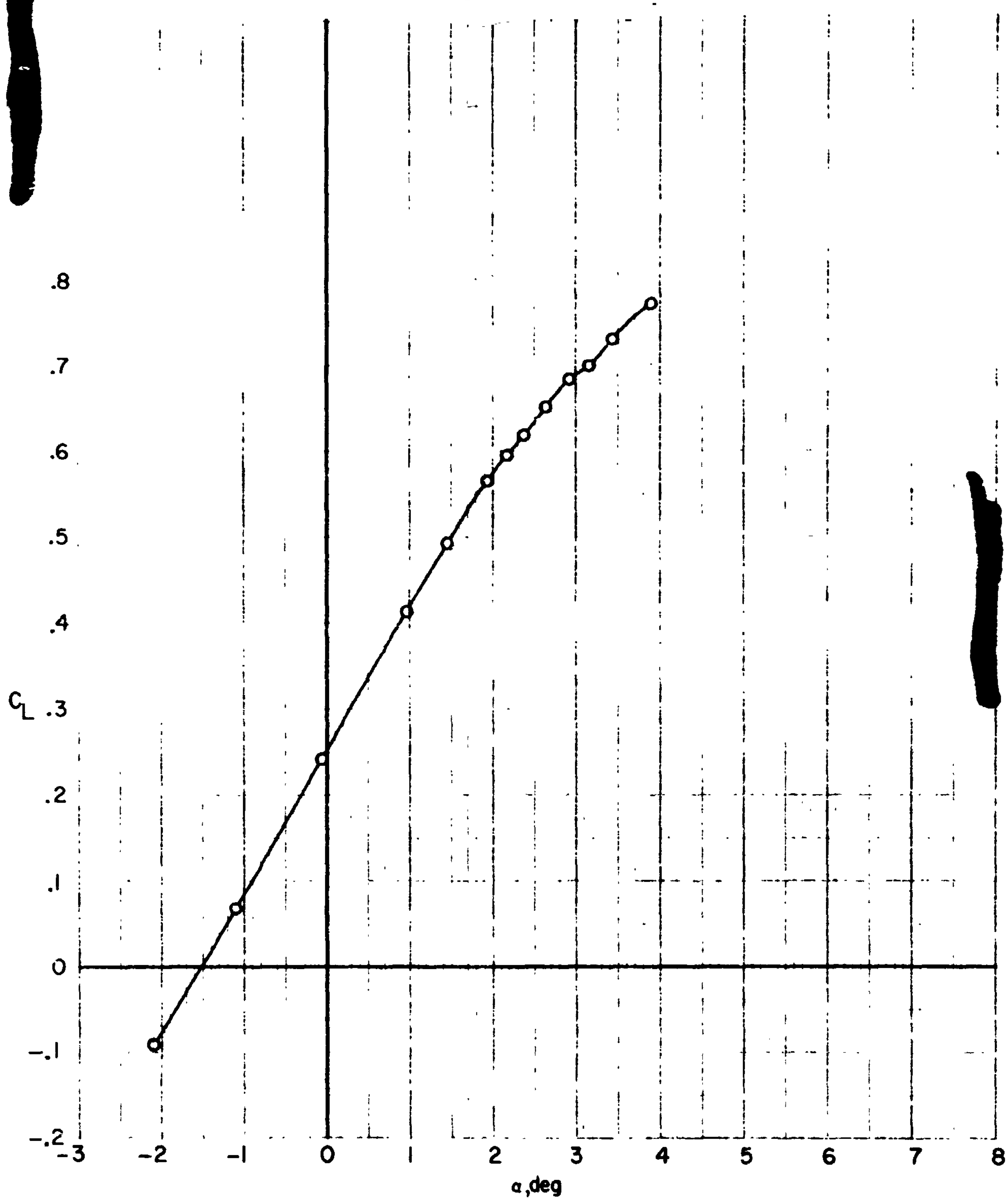

(f) M = 0.82.

Figure 10. - Continued.

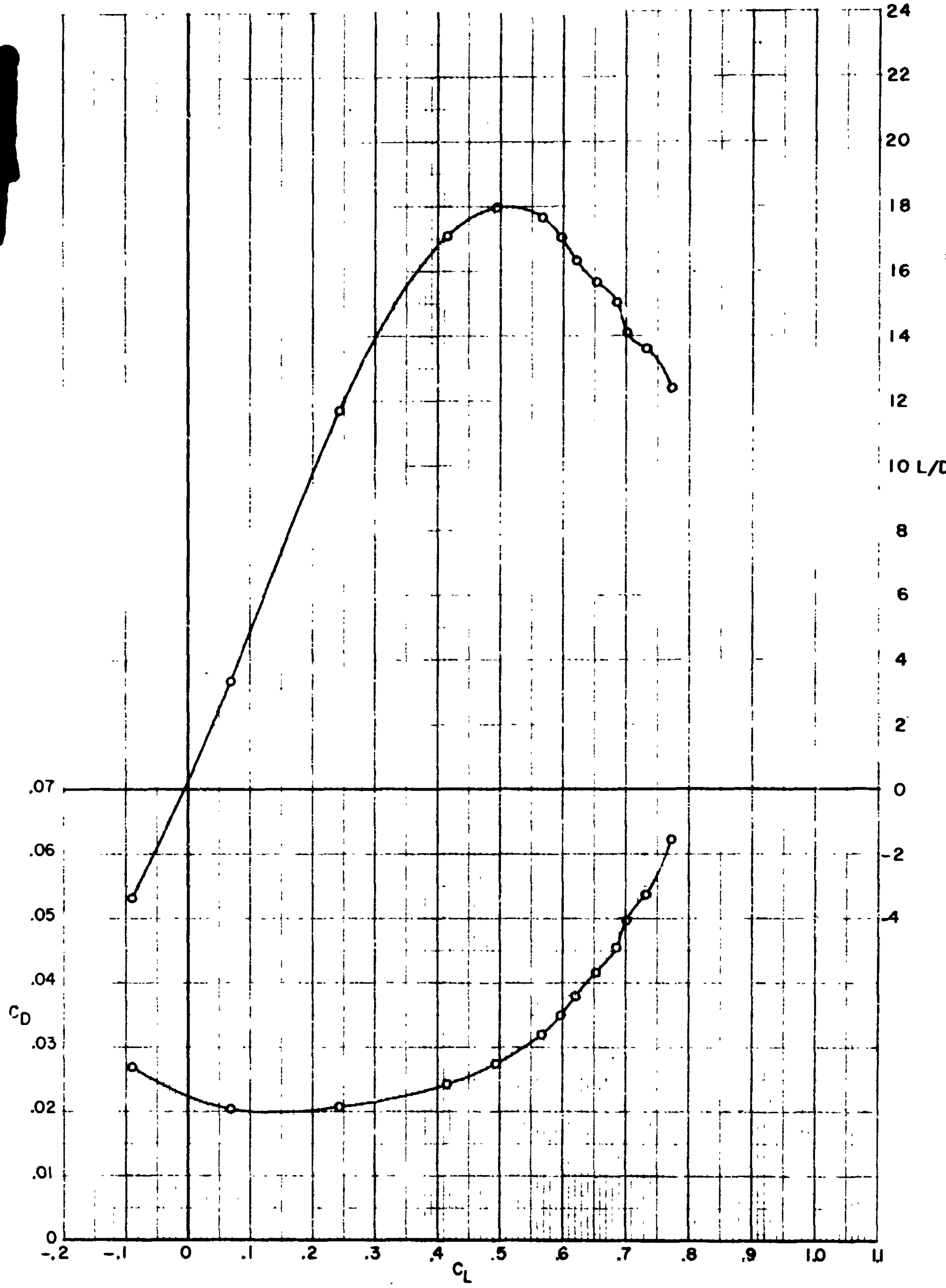

(f) M = 0.82. Continued.

Figure 10. - Continued.

[redacted]

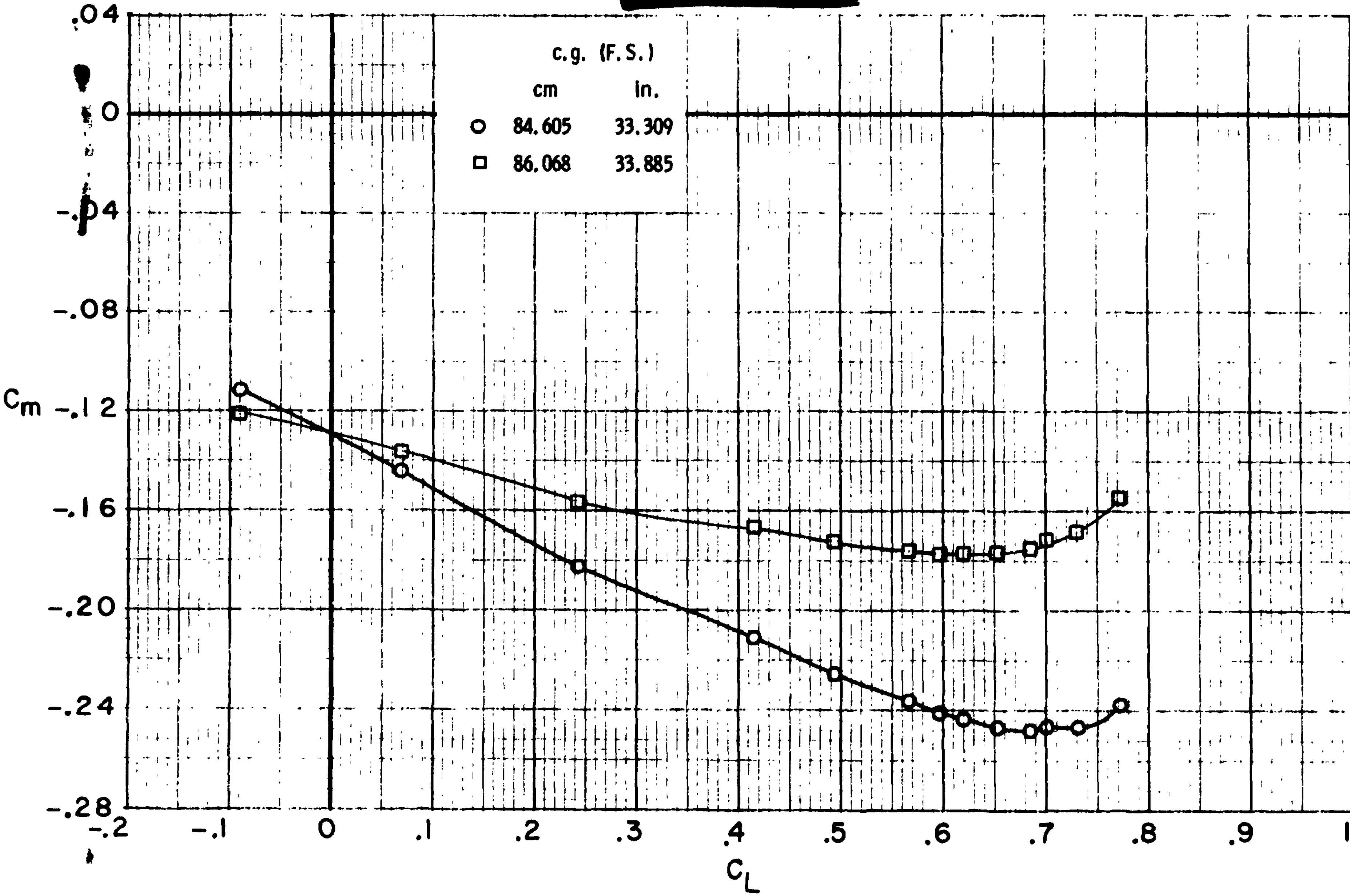

(f) M = 0.82. Concluded.

Figure 1^ - Concluded.

[redacted]

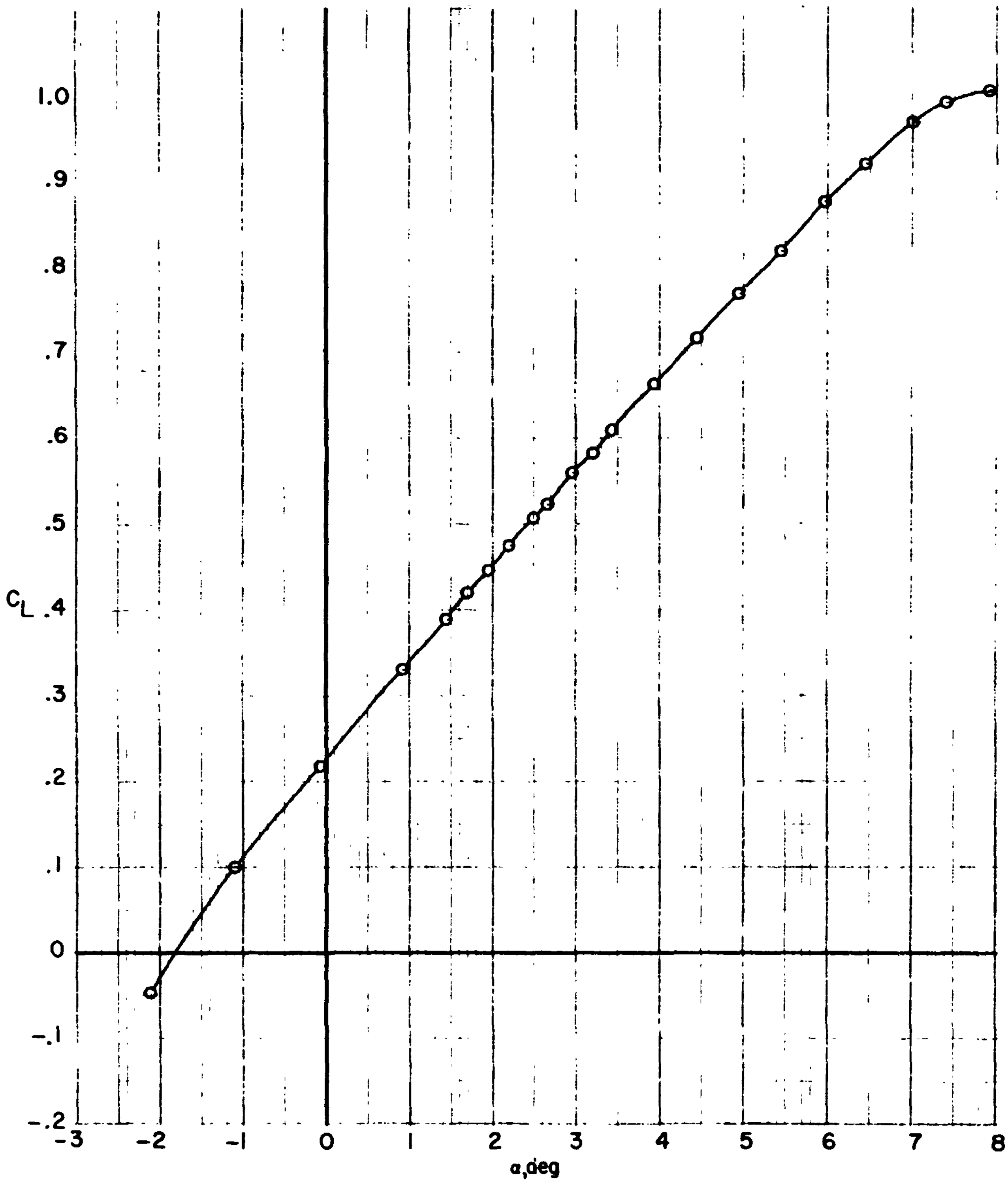

(a) M = 0.60.

Figure 11.- Longitudinal aerodynamic characteristics for supercritical wing configuration Ib (SCW-Ib) with wing uppersurface grit forward ($x_T/C = 0.05$). $\Lambda_{c/4} = 30°$.

ORIGINAL PAGE IS
OF POOR QUALITY

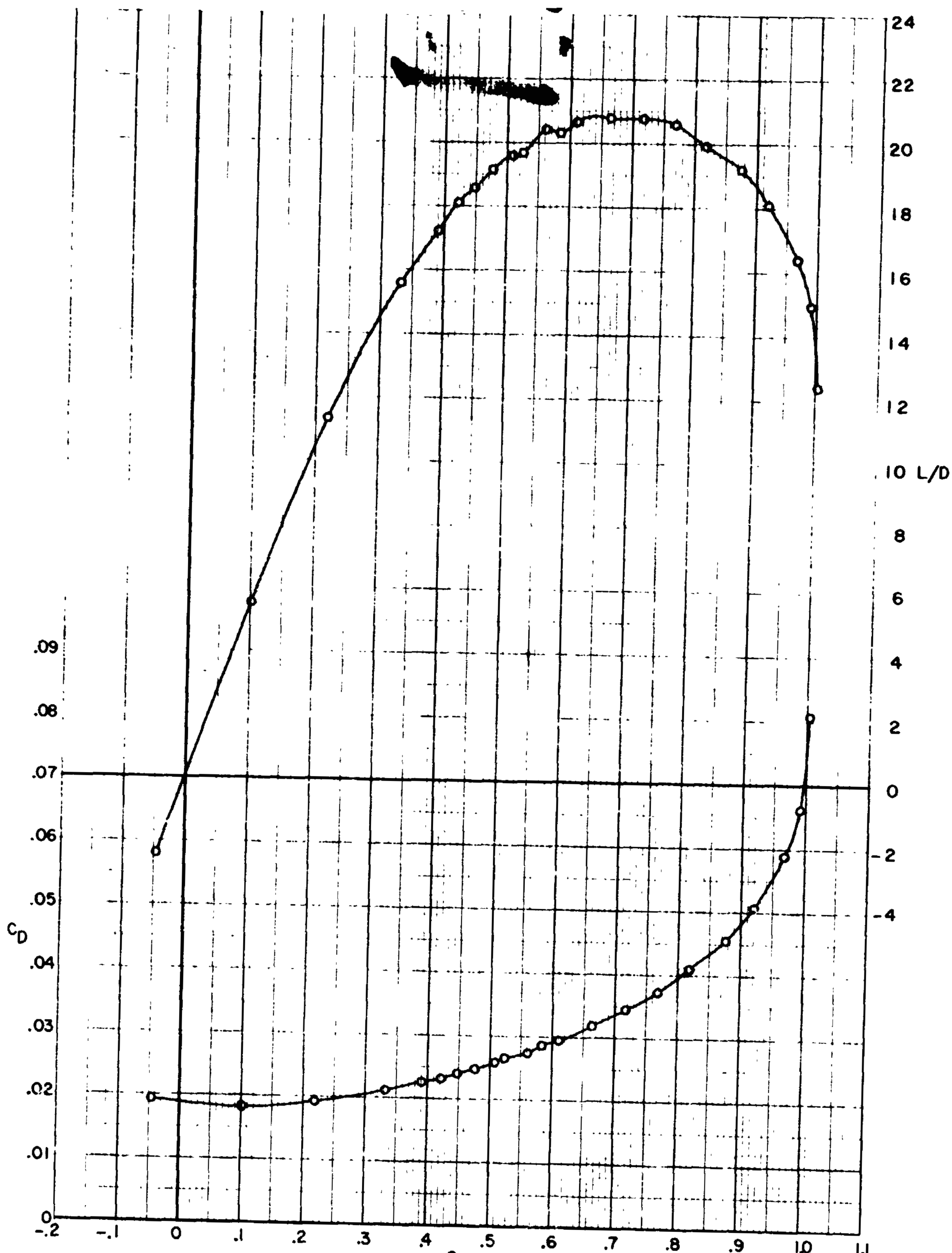

[redacted]

(a) M = 0.60. Continued.

Figure 11. - Continued.

ORIGINAL PAGE IS
OF POOR QUALITY

[redacted]

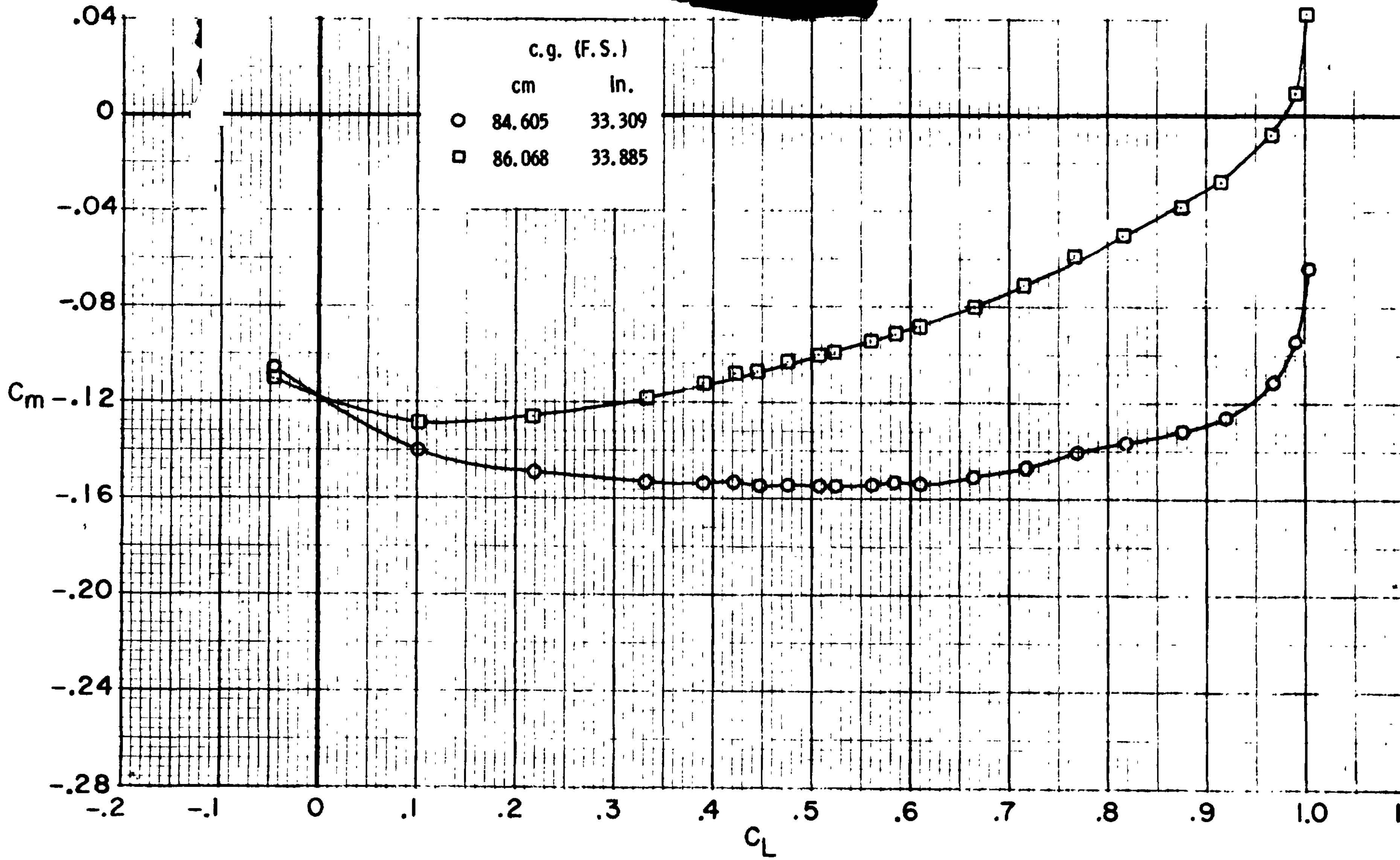

(a) M = 0.60. Concluded.

Figure 11.- Continued.

[redacted]

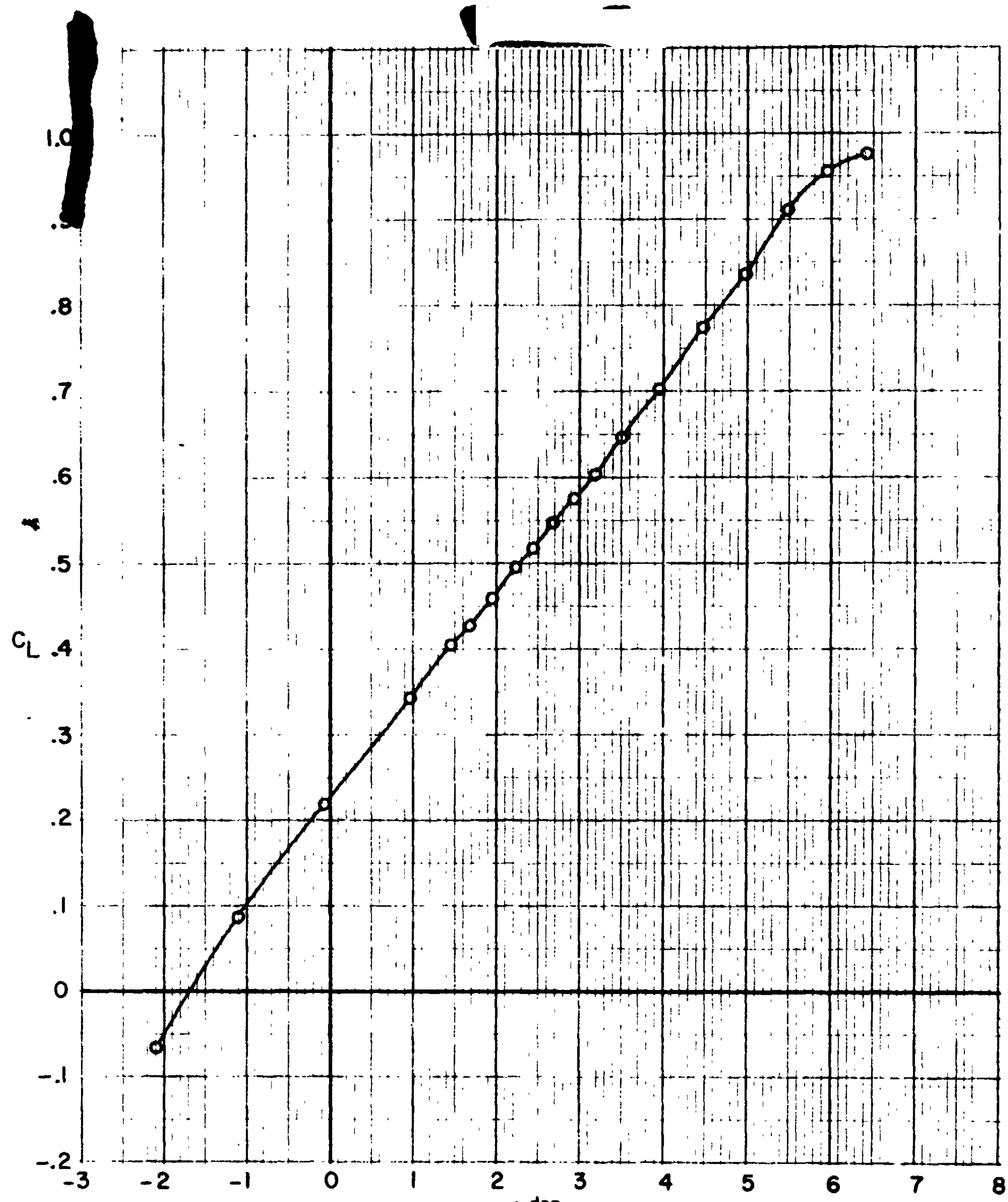

(b) M = 0.70.

Figure 11.- Continued.

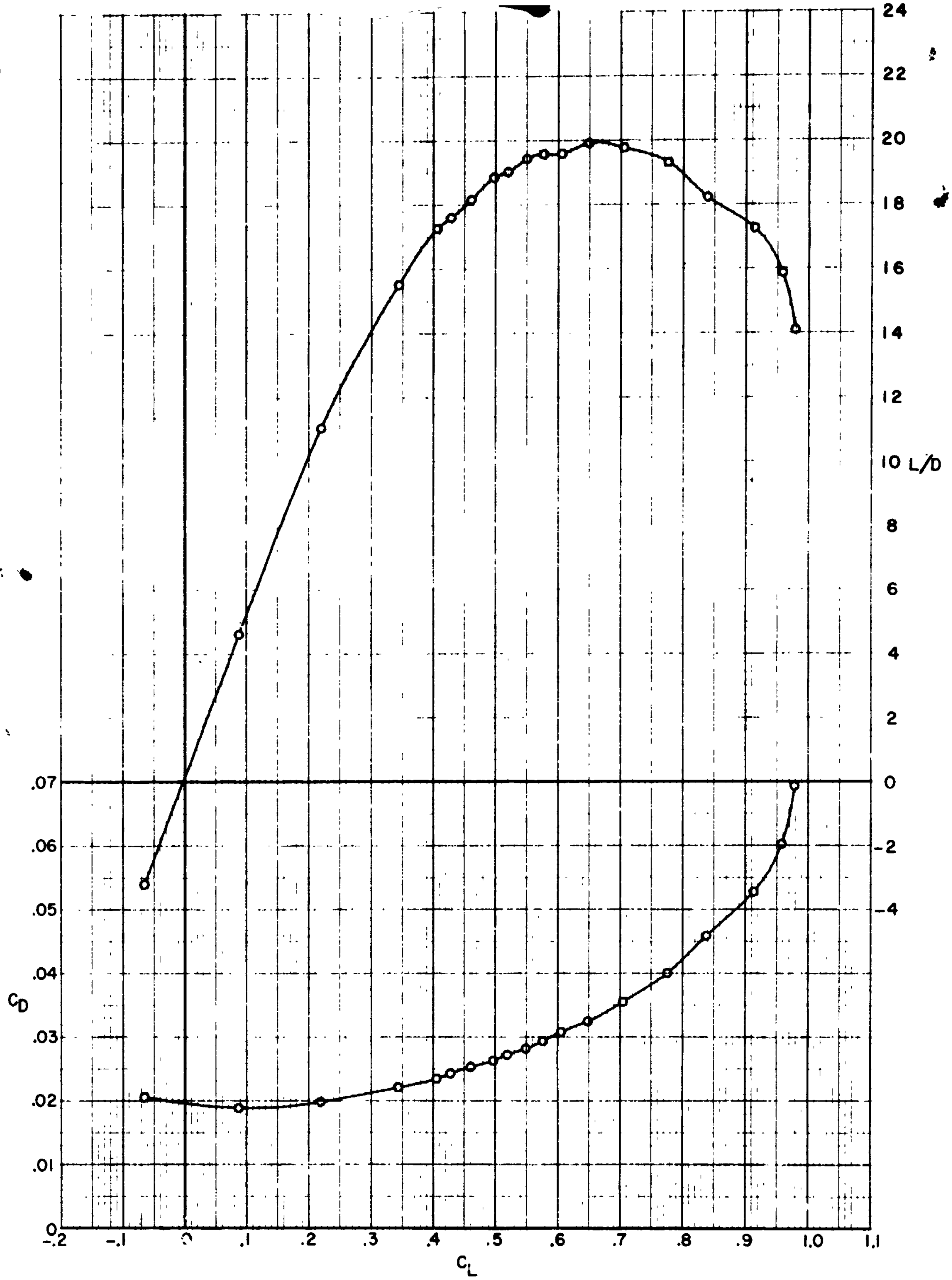

(b) M = 0.70. Continued.

Figure 11. - Continued.

[redacted]

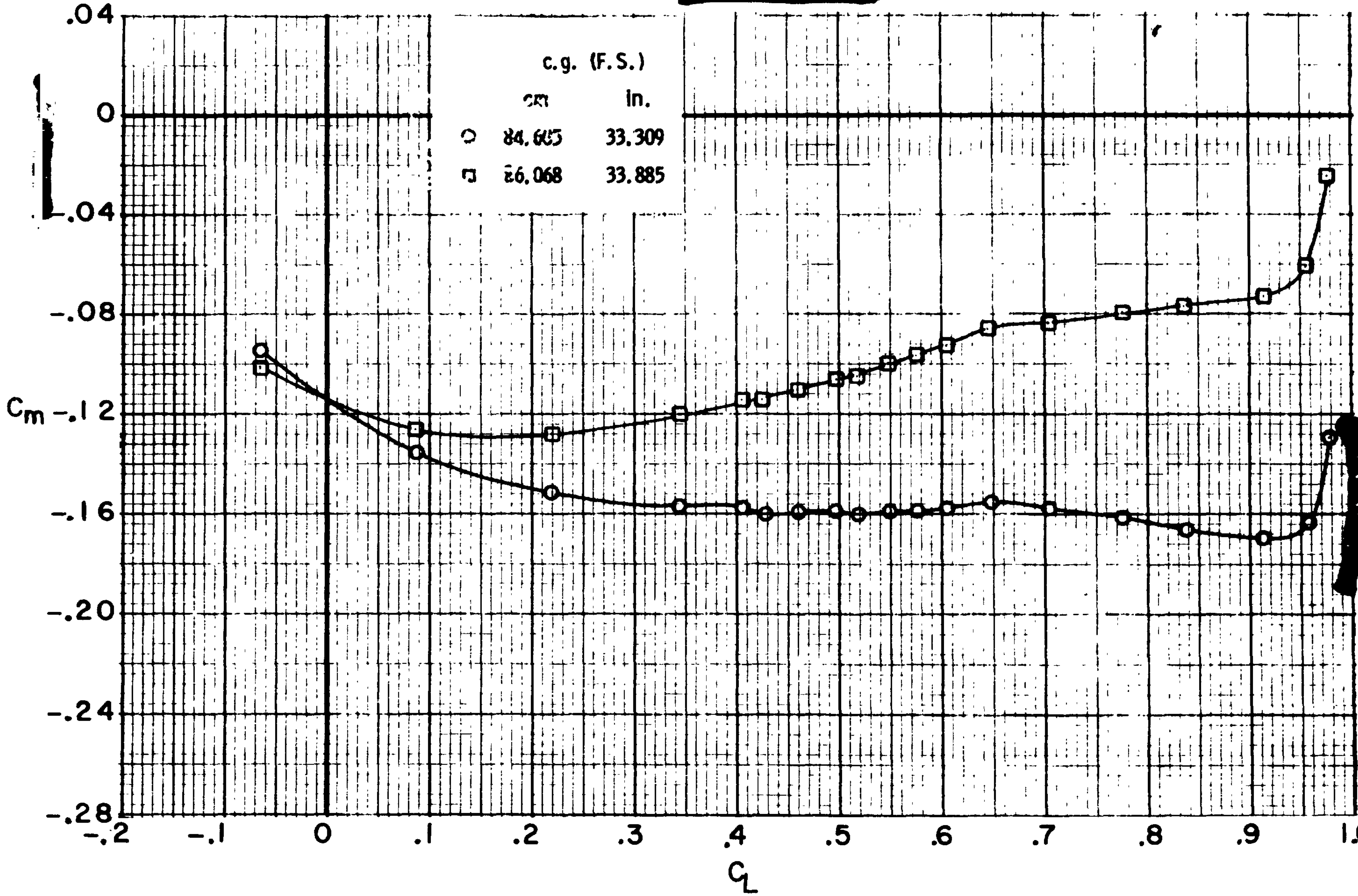

(b) M = 0.70. Concluded.

Figure 11. - Continued.

[redacted]

ORIGINAL PAGE IS
OF POOR QUALITY

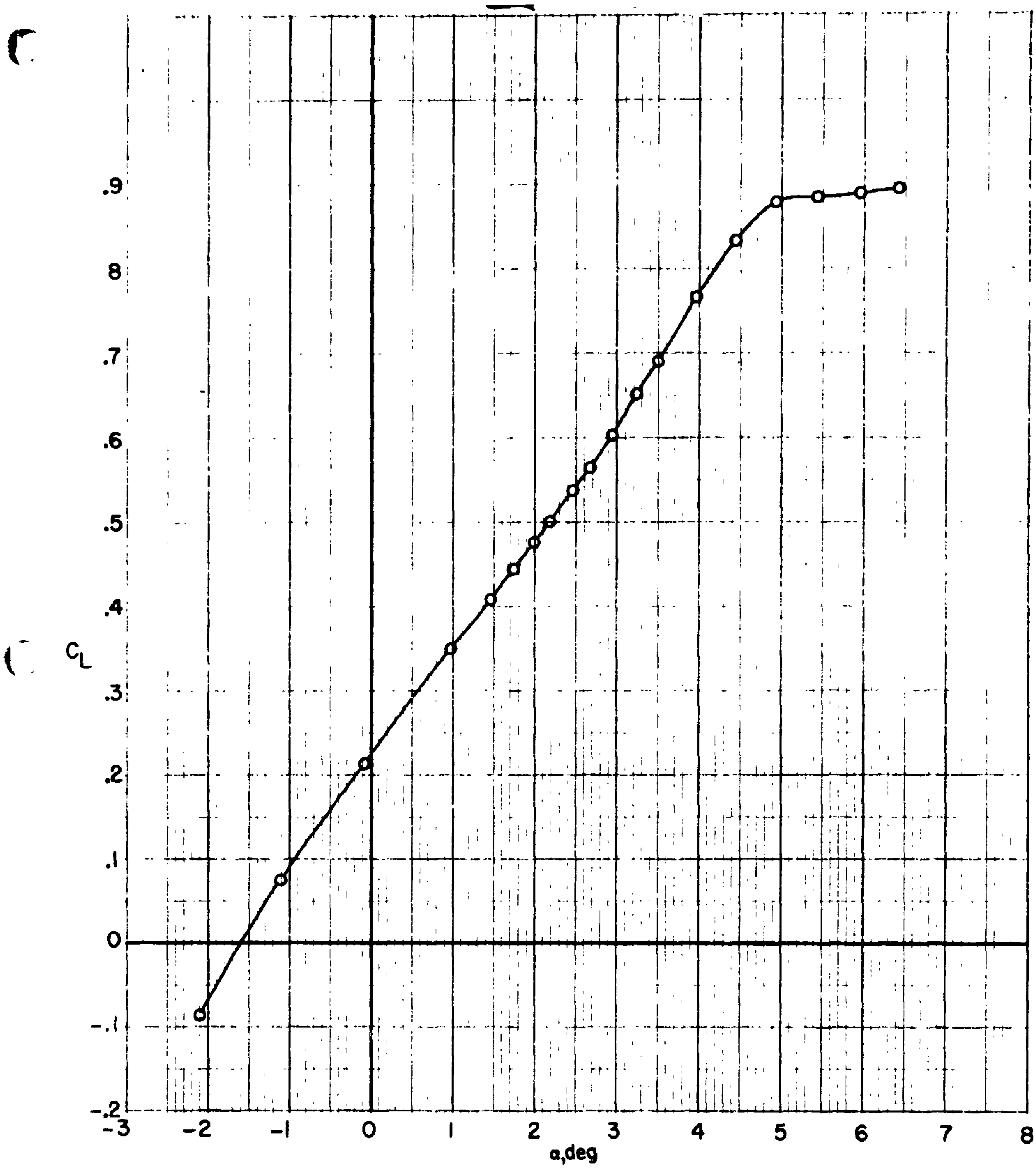

(c) M = 0.75.

Figure 11.- Continued.

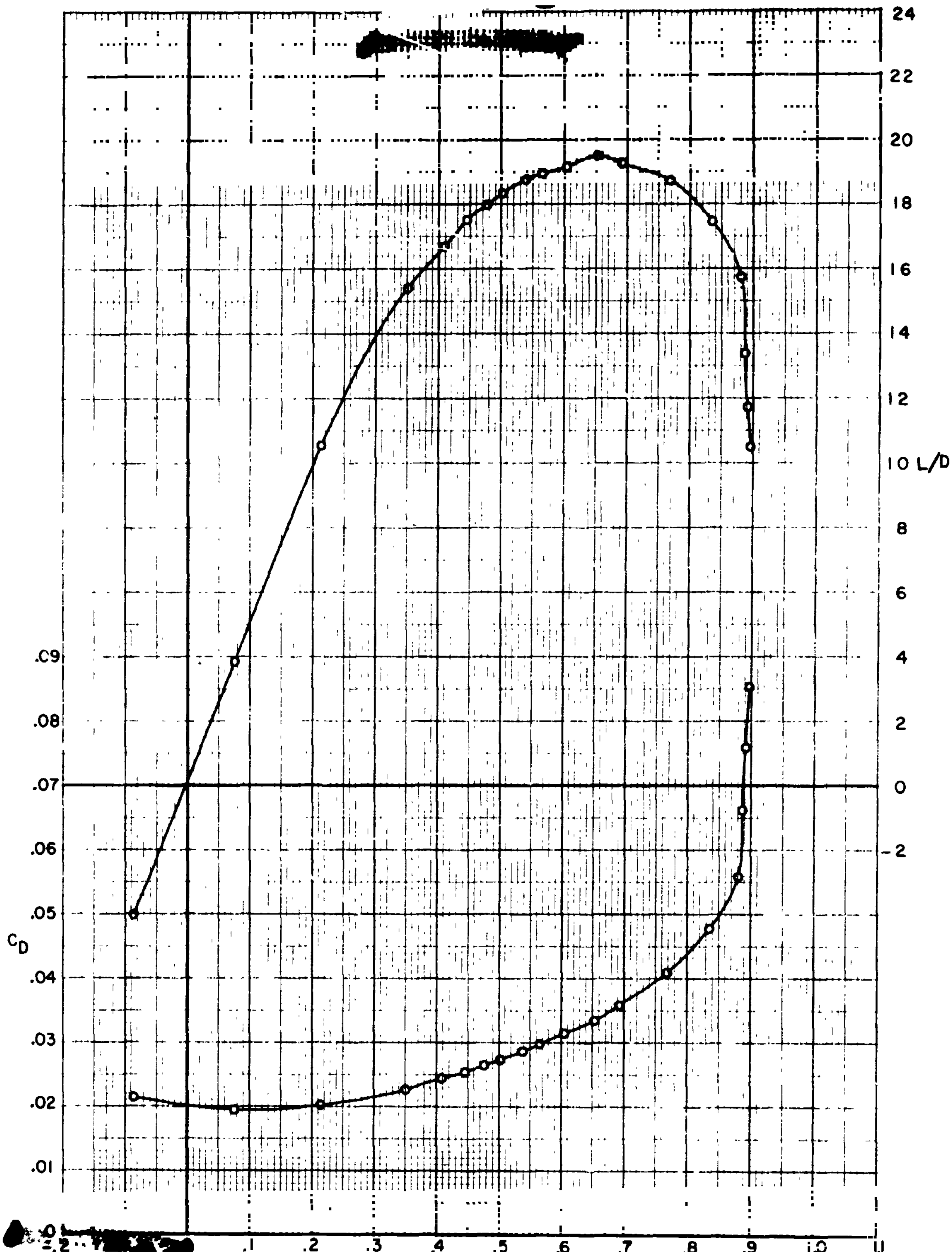

(c) M = 0.75. Continued.

Figure 11.- Continued.

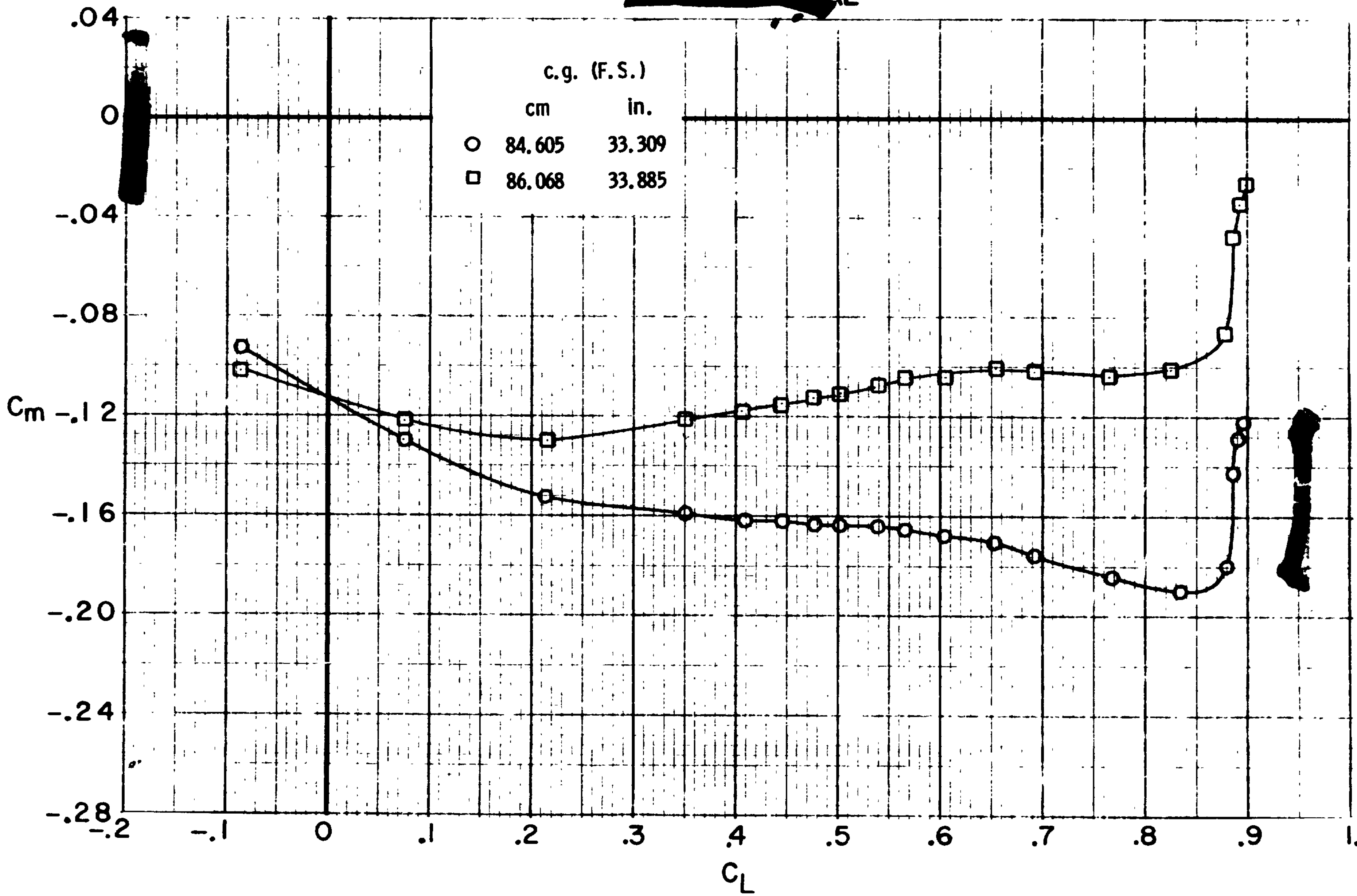

(c) M = 0.75. Concluded.

Figure II. - Continued.

[redacted]

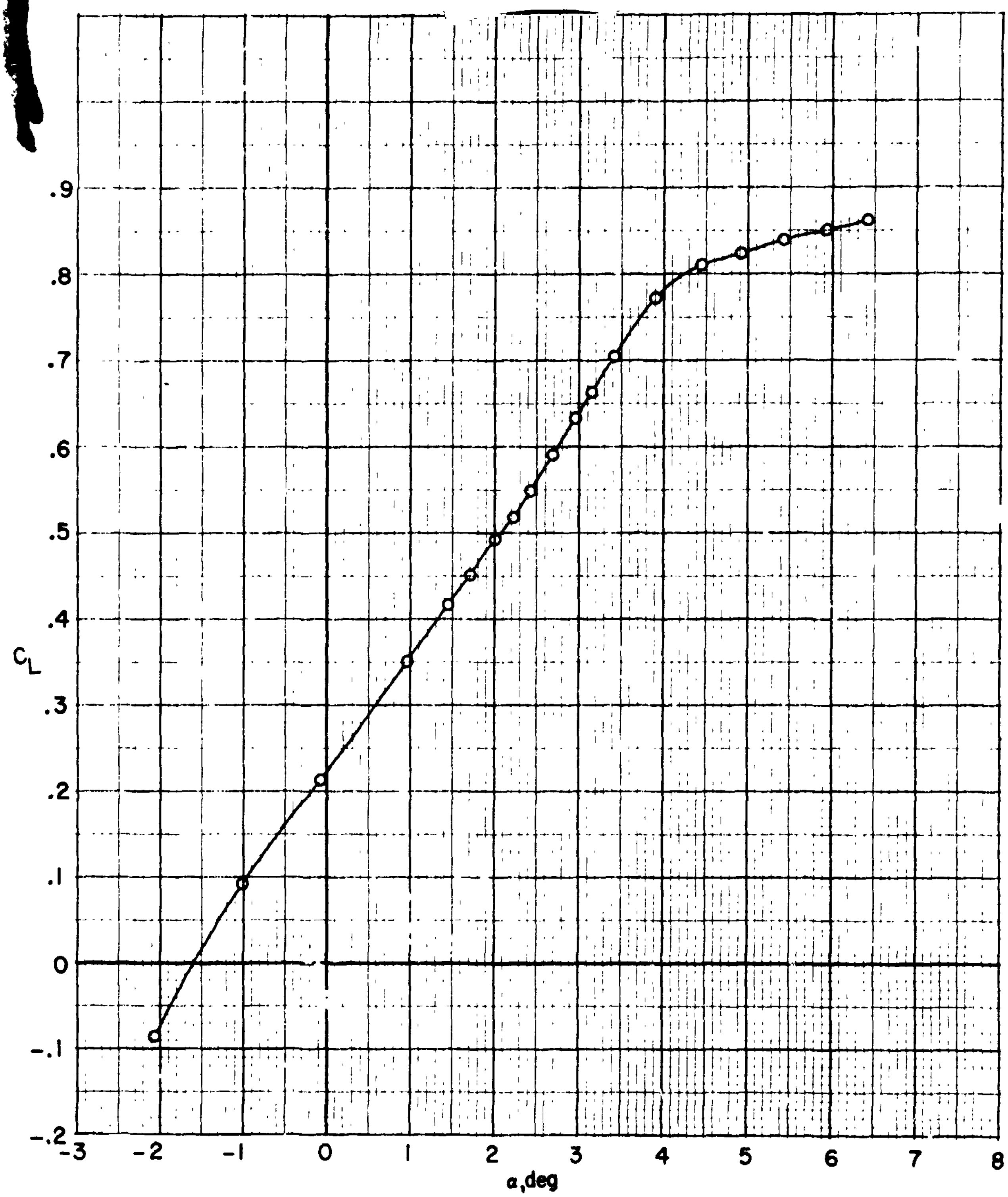

(d) M = 0.77.

Figure 11.- Continued.

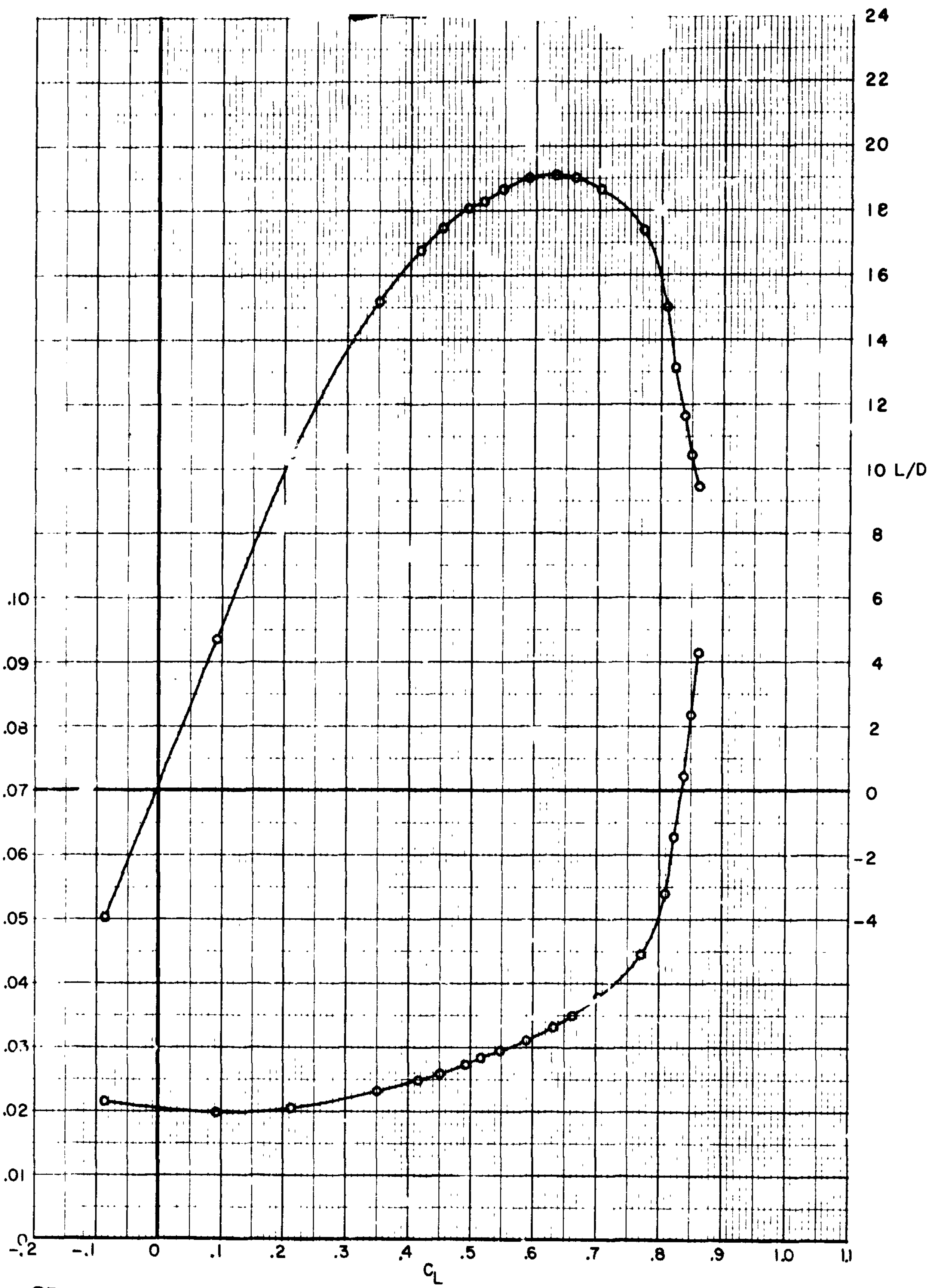

ORIGINAL PAGE IS OF POOR QUALITY

(d) M = 0.77. Continued.

Figure 11.- Continued.

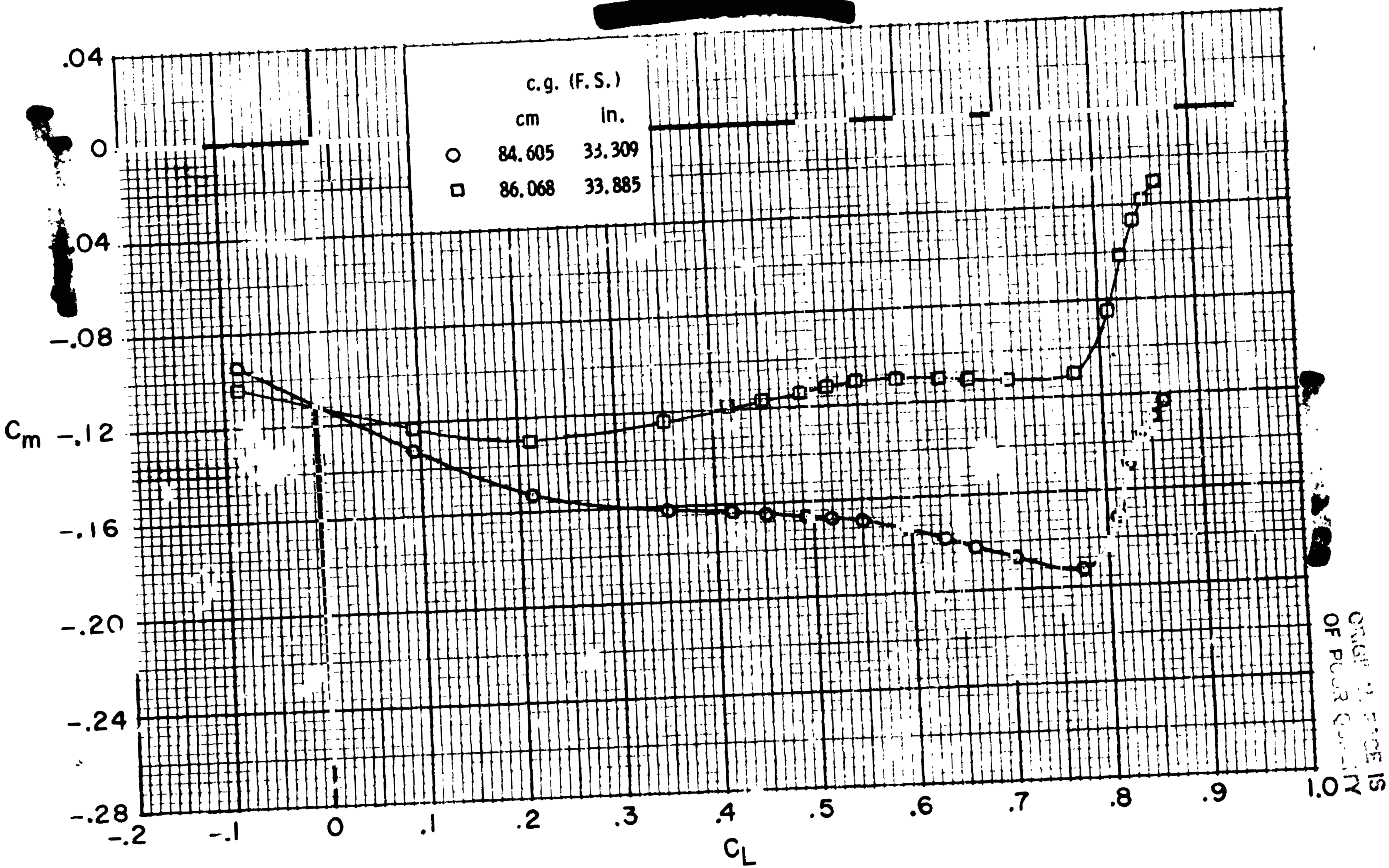

(d) M = 0.77. Concluded.

Figure 11.- Concluded.

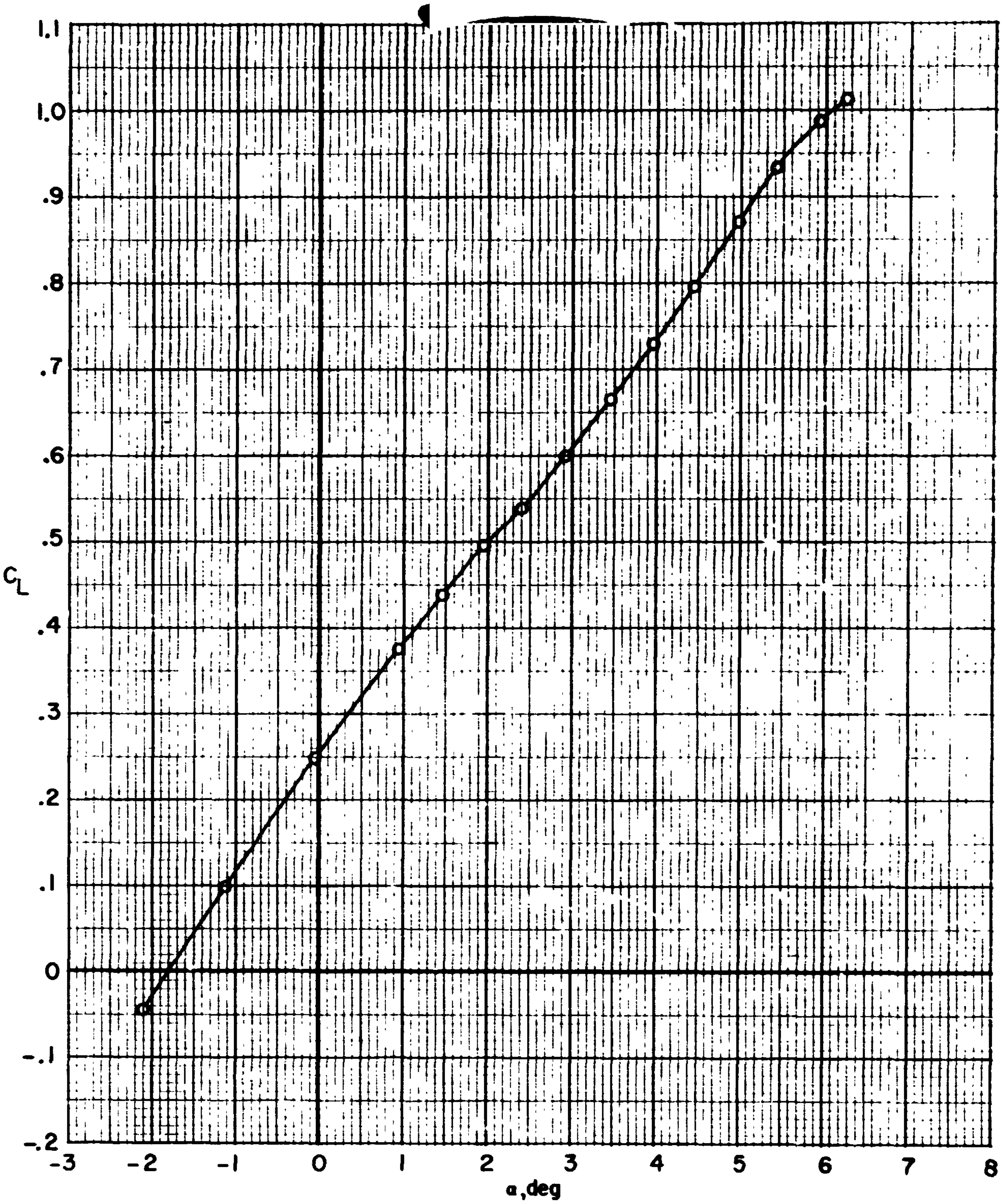

(a) M = 0.70.

Figure 12. - Longitudinal aerodynamic characteristics for supercritical wing configuration 2a (SCW-2a) with wing upper surface grit aft (fig. 5). c.g. (F.S.) = 84.605 cm (33.309 in.); $\Lambda_{c/4} = 27°$

[redacted]

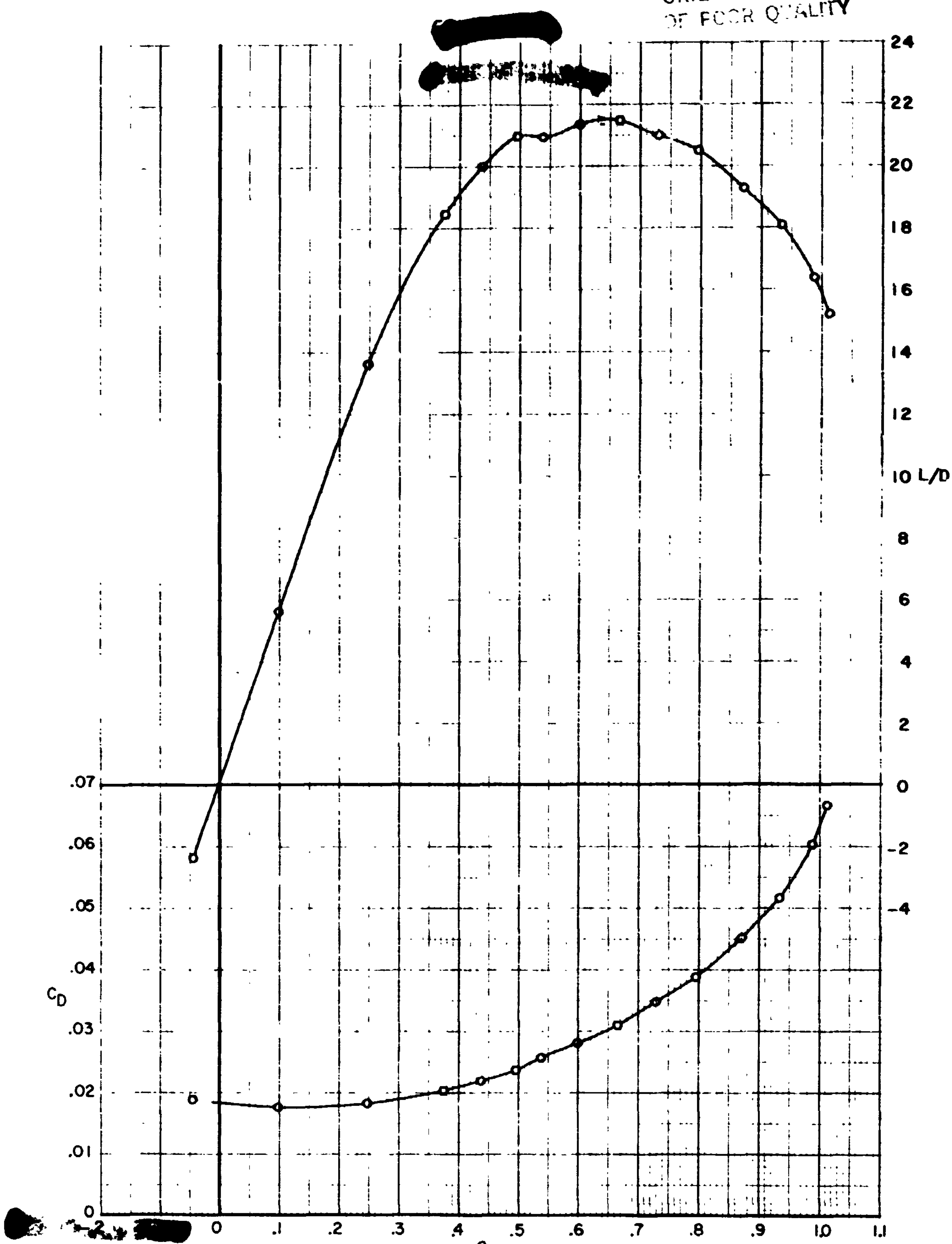

(a) M = 0.70. Continued.

Figure 12.- Continued.

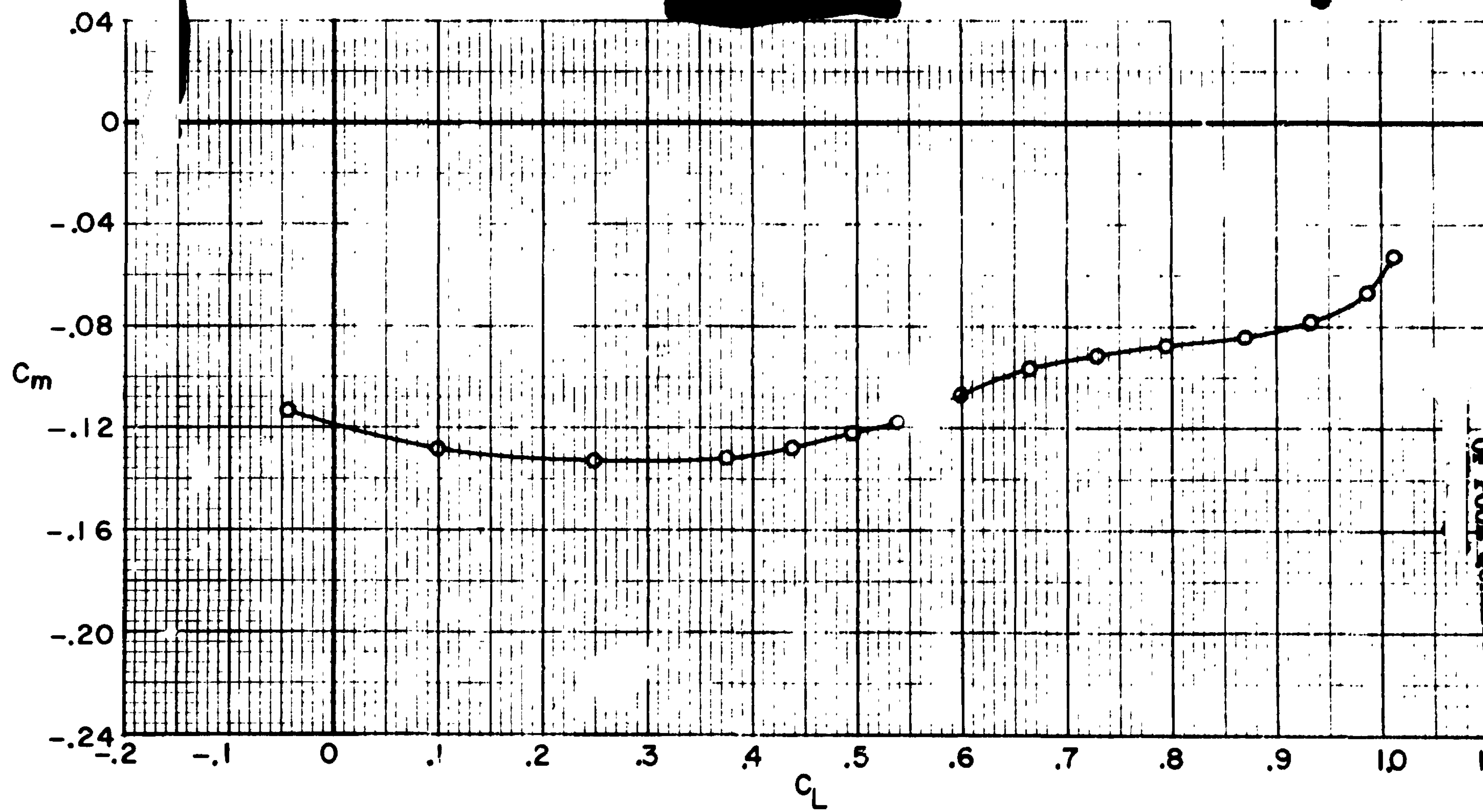

(a) M = 0.70. Concluded.

Figure 12.- Continued.

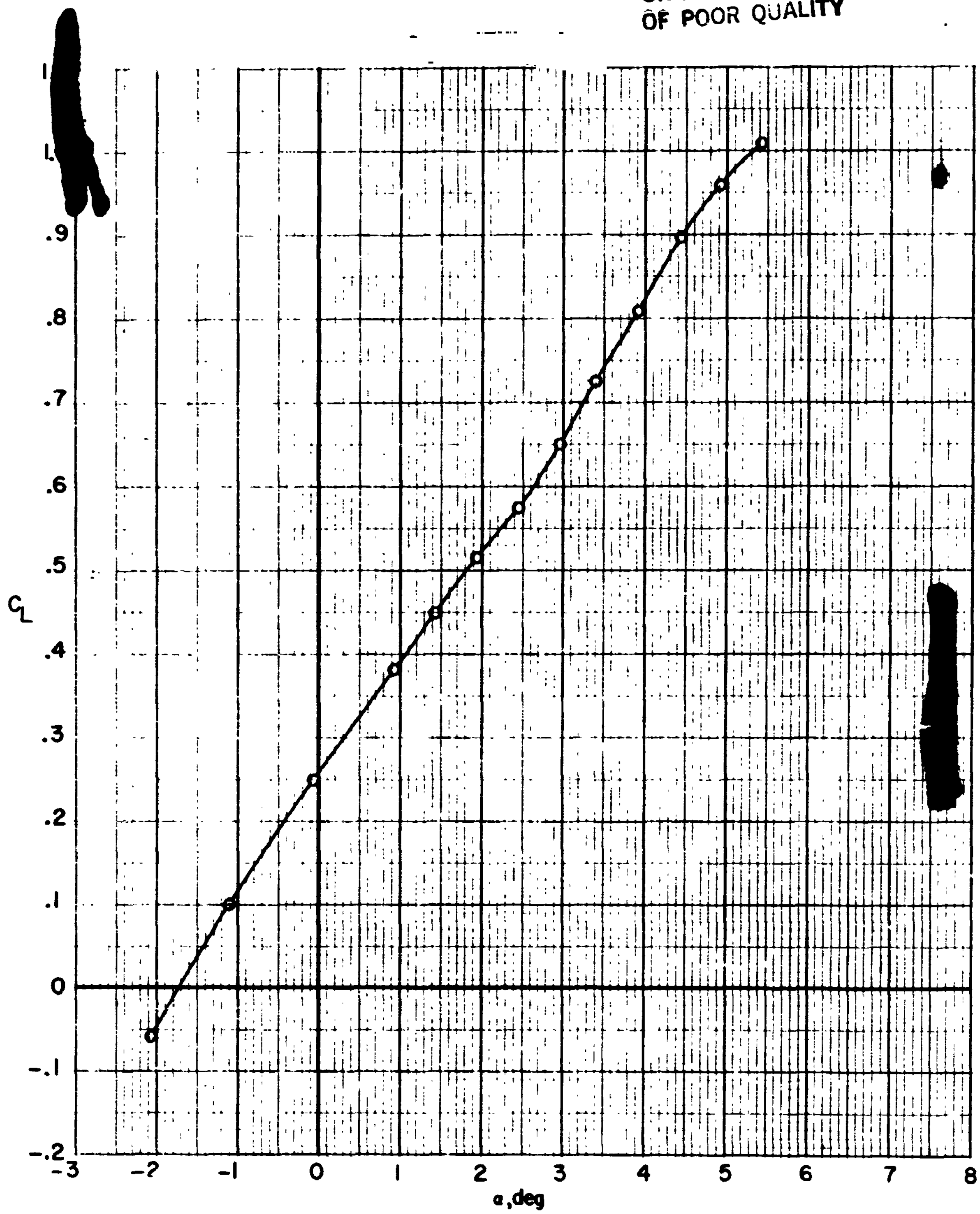

(b) M = 0.75.

Figure 12. - Continued.

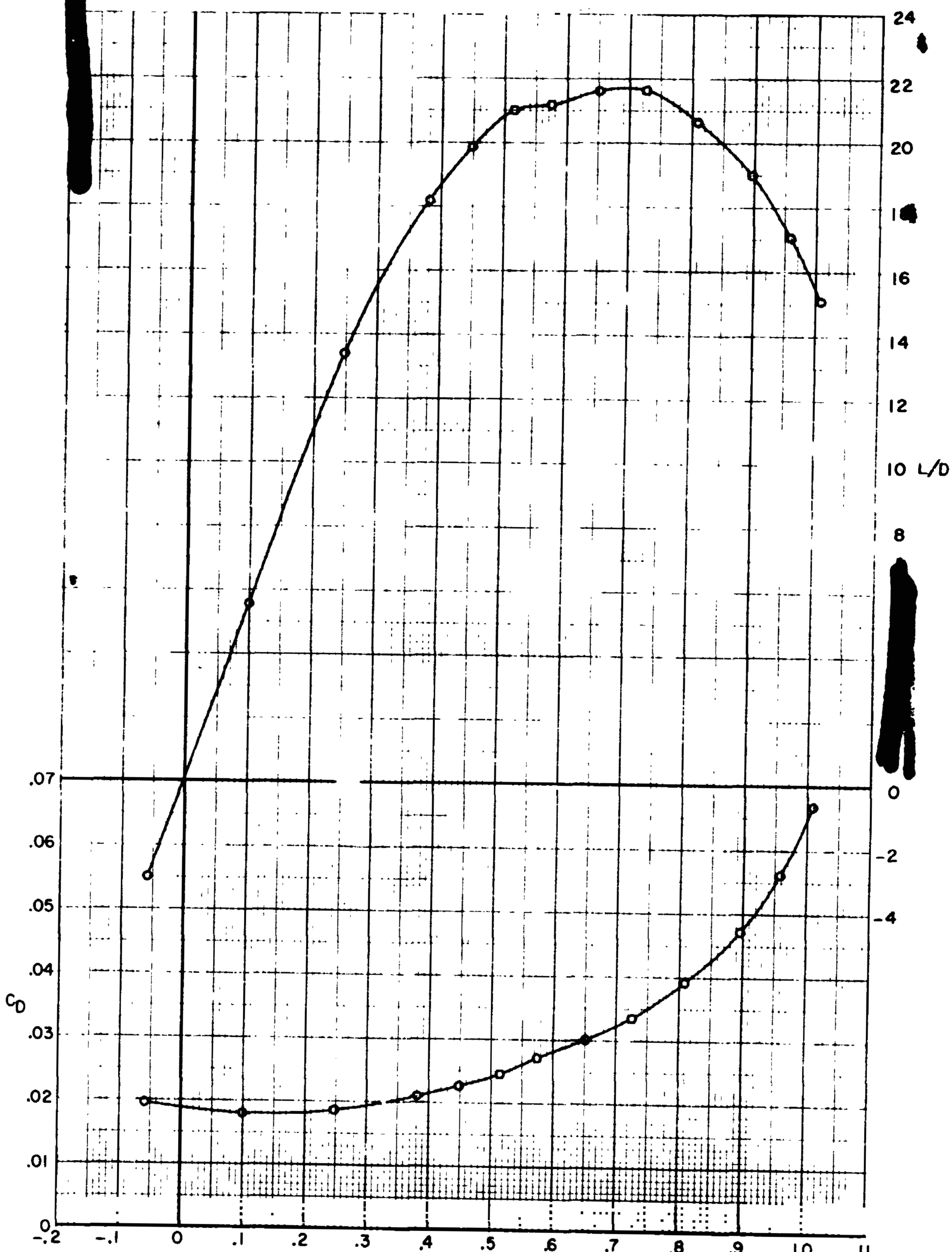

(b) M = 0.75. Continued.

Figure 12. - Continued.

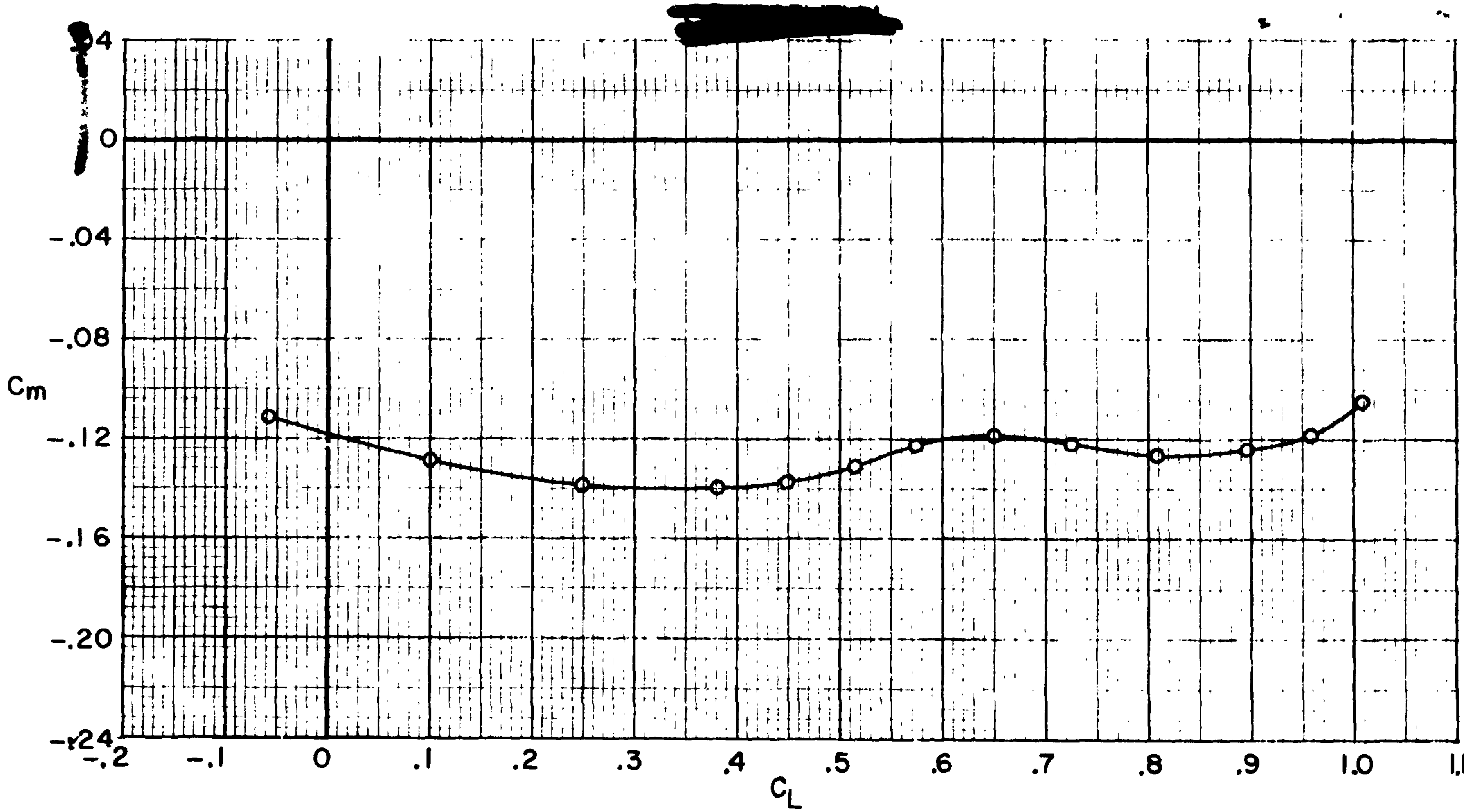

(b) M = 0.75. Concluded.

Figure 12.- Continued.

[redacted]

[redacted]

ORIGINAL PAGE IS
OF POOR QUALITY

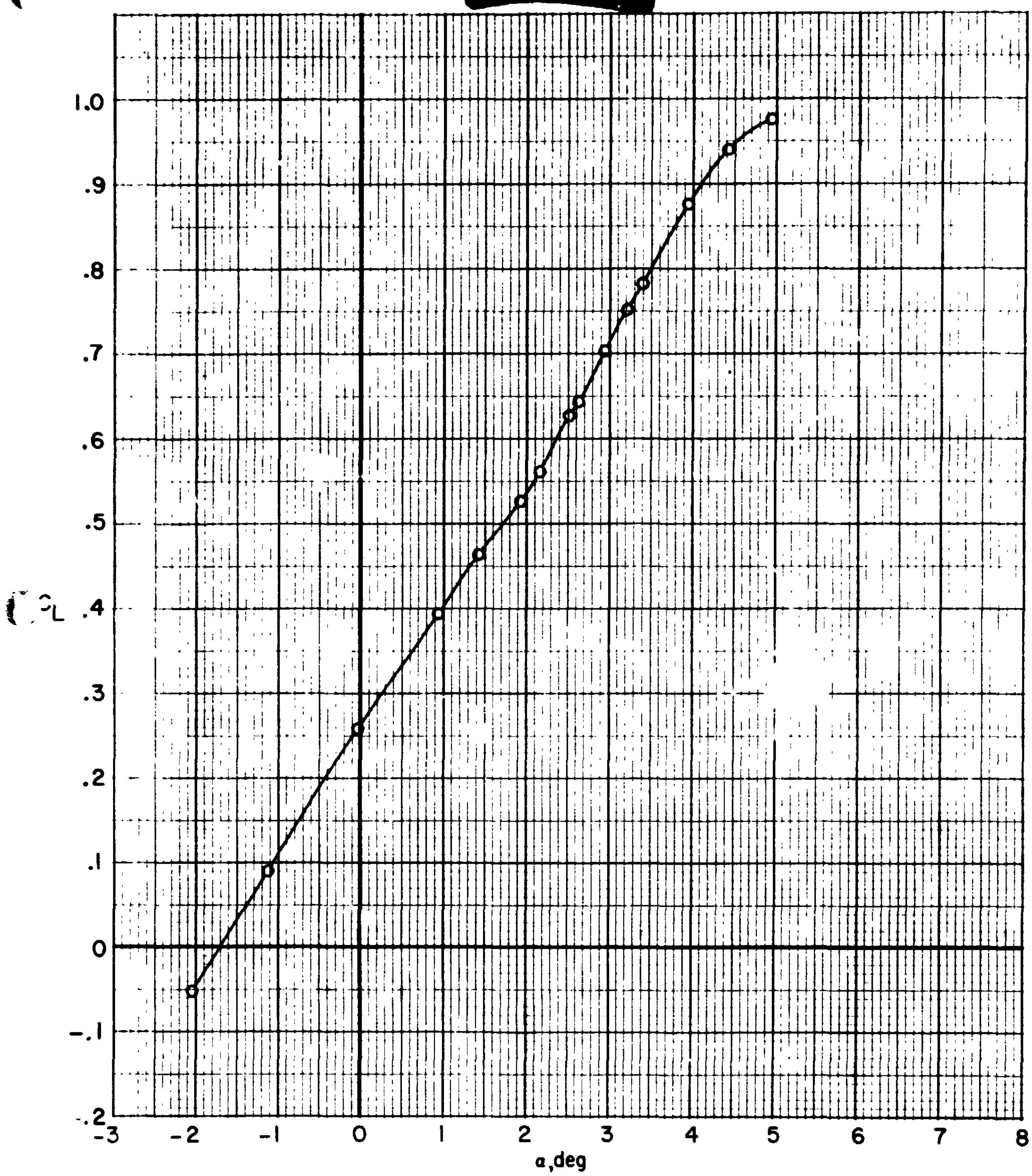

(c) M = 0.77.

Figure 12.- Continued.

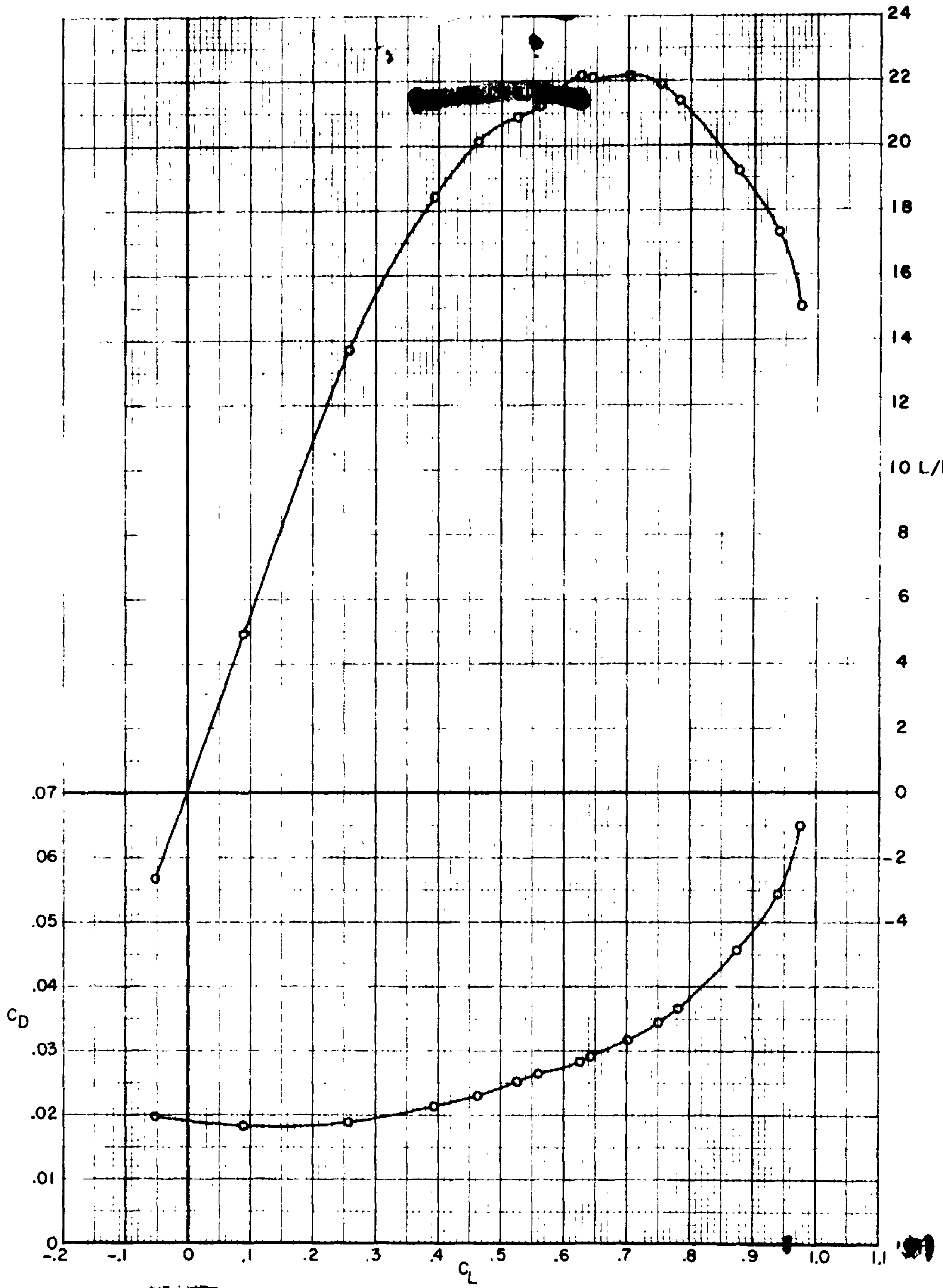

[redacted]

(c) M = 0.77. Continued.

Figure 12. - Continued.

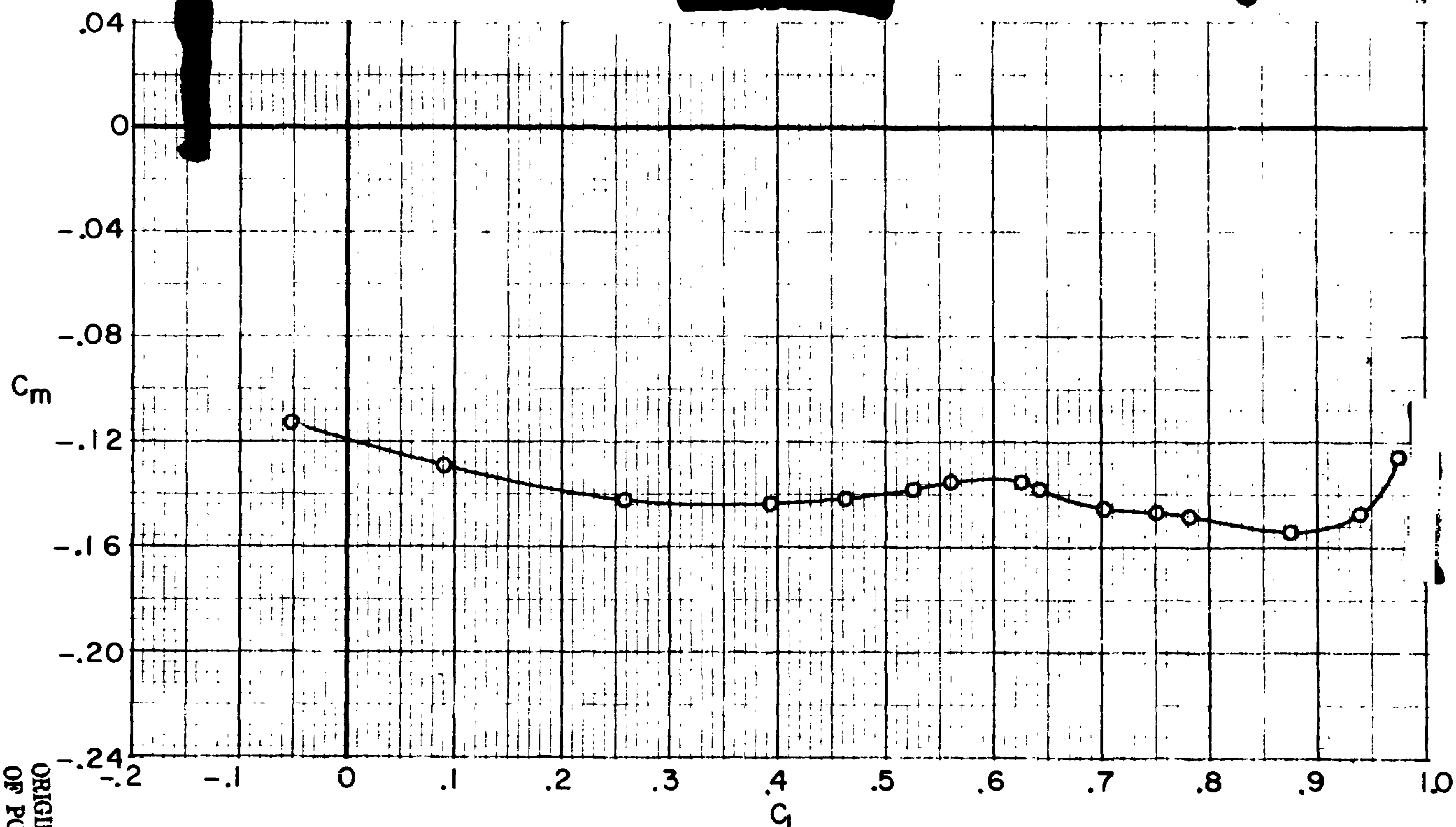

(c) M = 0.77. Concluded.

Figure 12. - Continued.

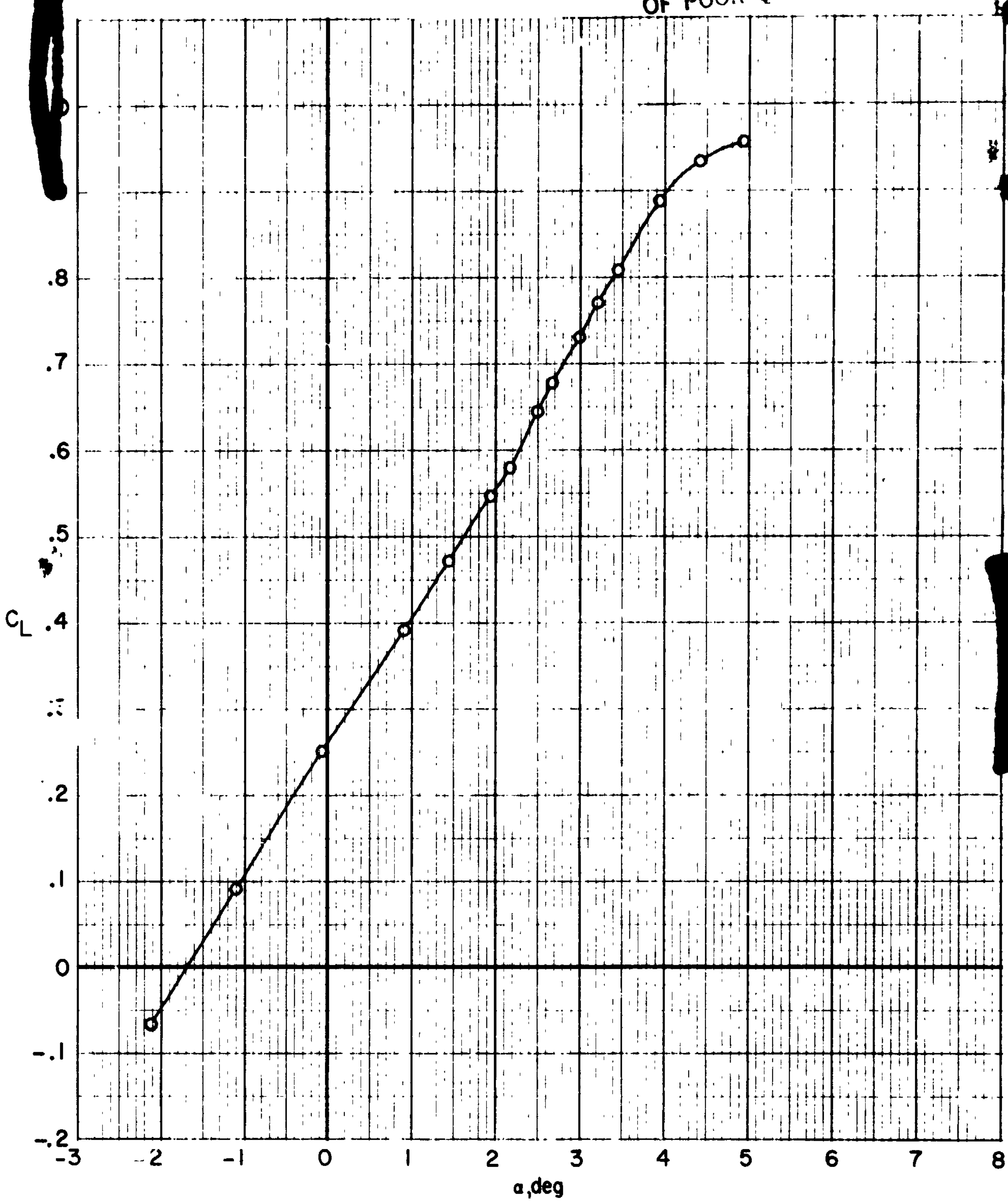

(d) M = 0.78.

Figure 12.- Continued.

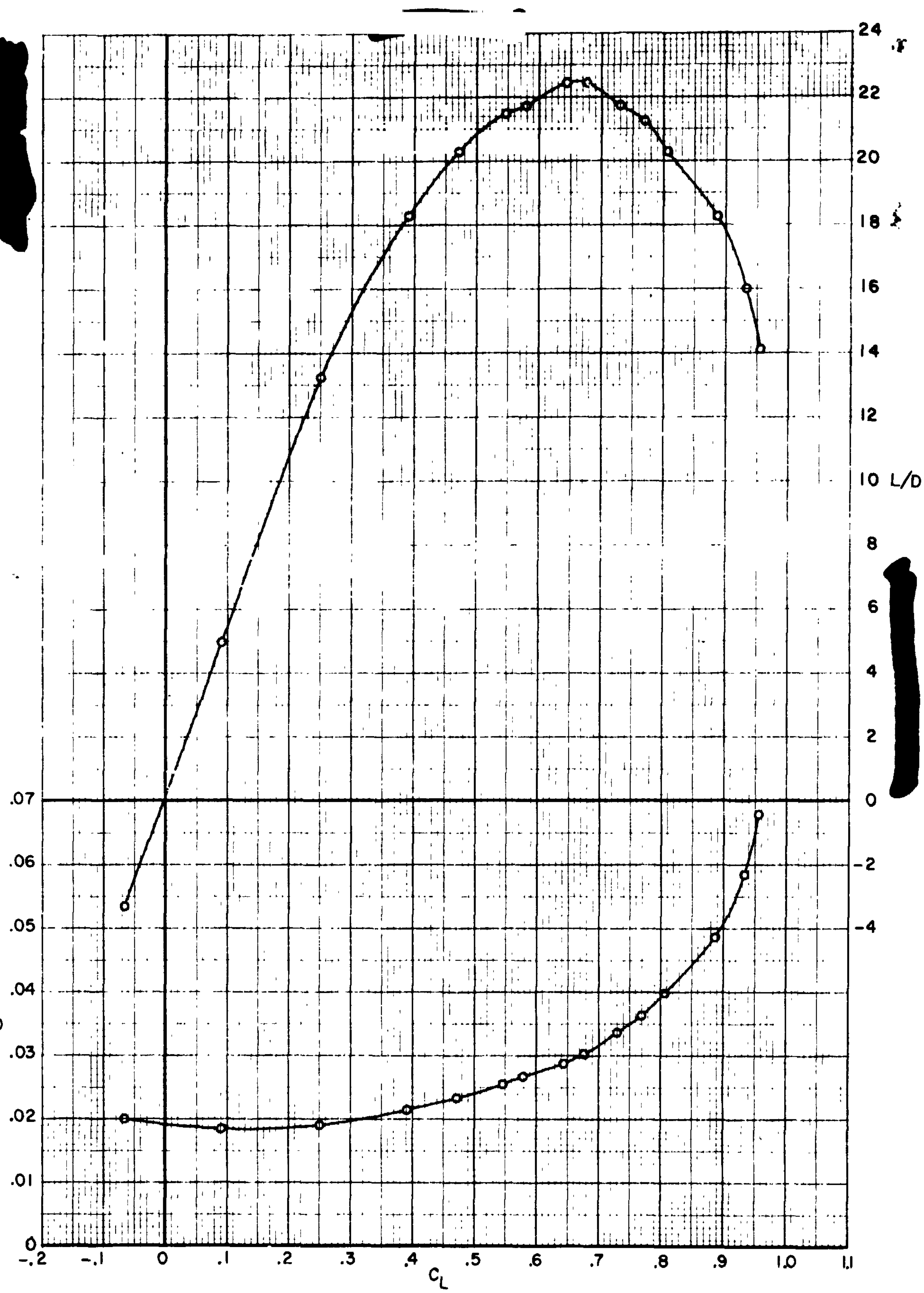

(d) M = 0.78. Continued.

Figure 12. - Continued.

[redacted]

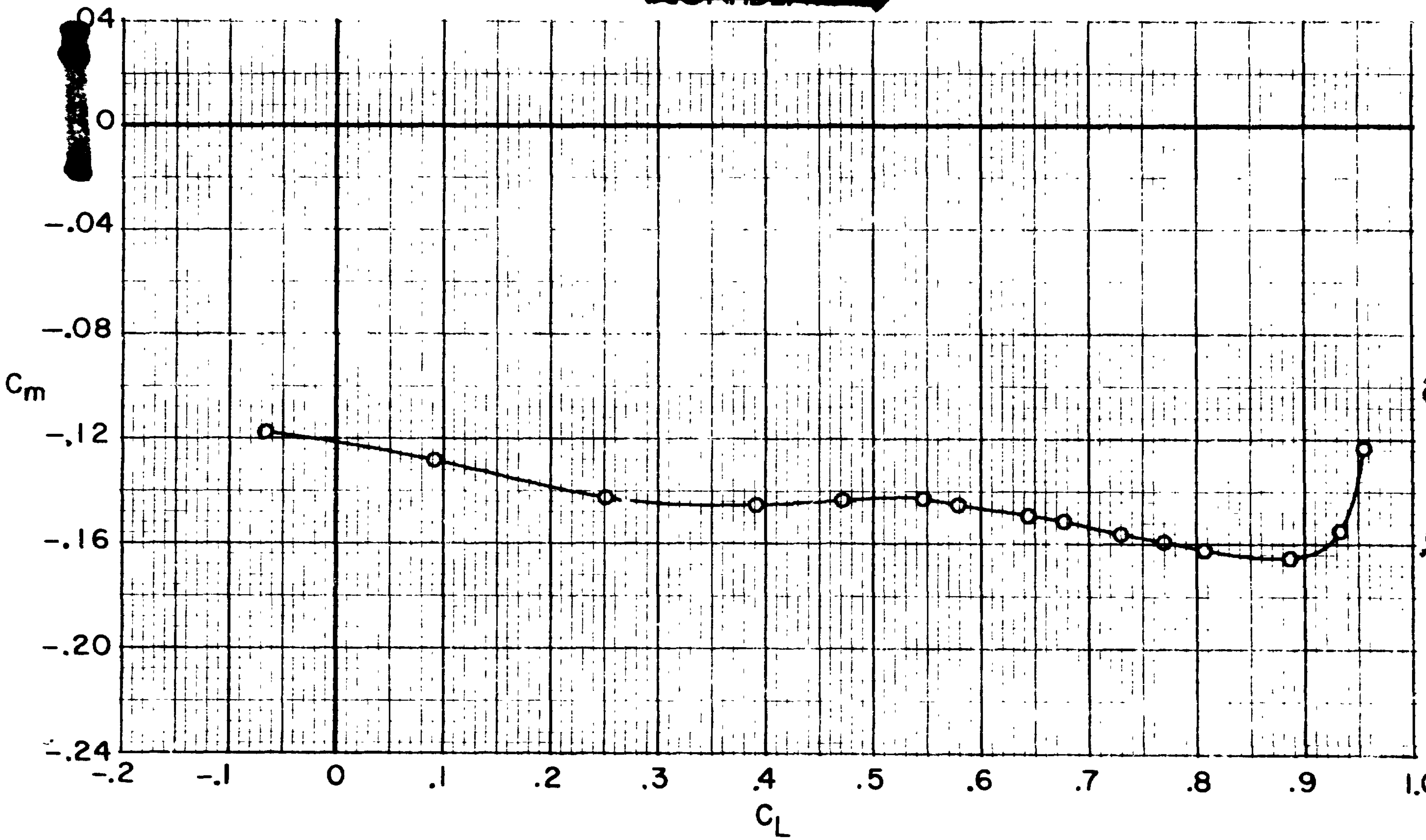

(d) M = 0.78. Concluded.

Figure 12. - Continued.

[redacted]

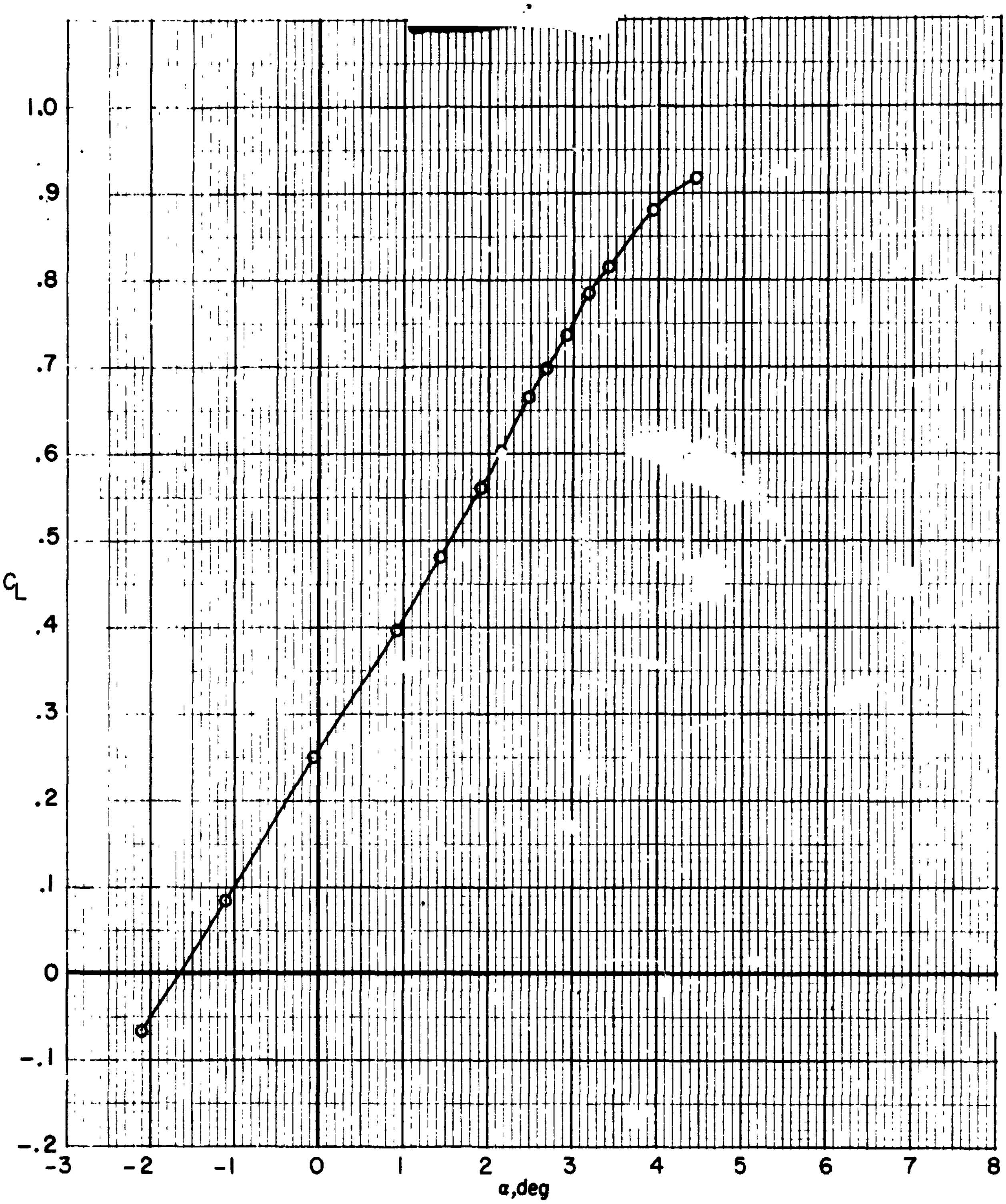

(e) M = 0.79.

Figure 12.- Continued.

OR [illegible] PAGE IS
OF [illegible]

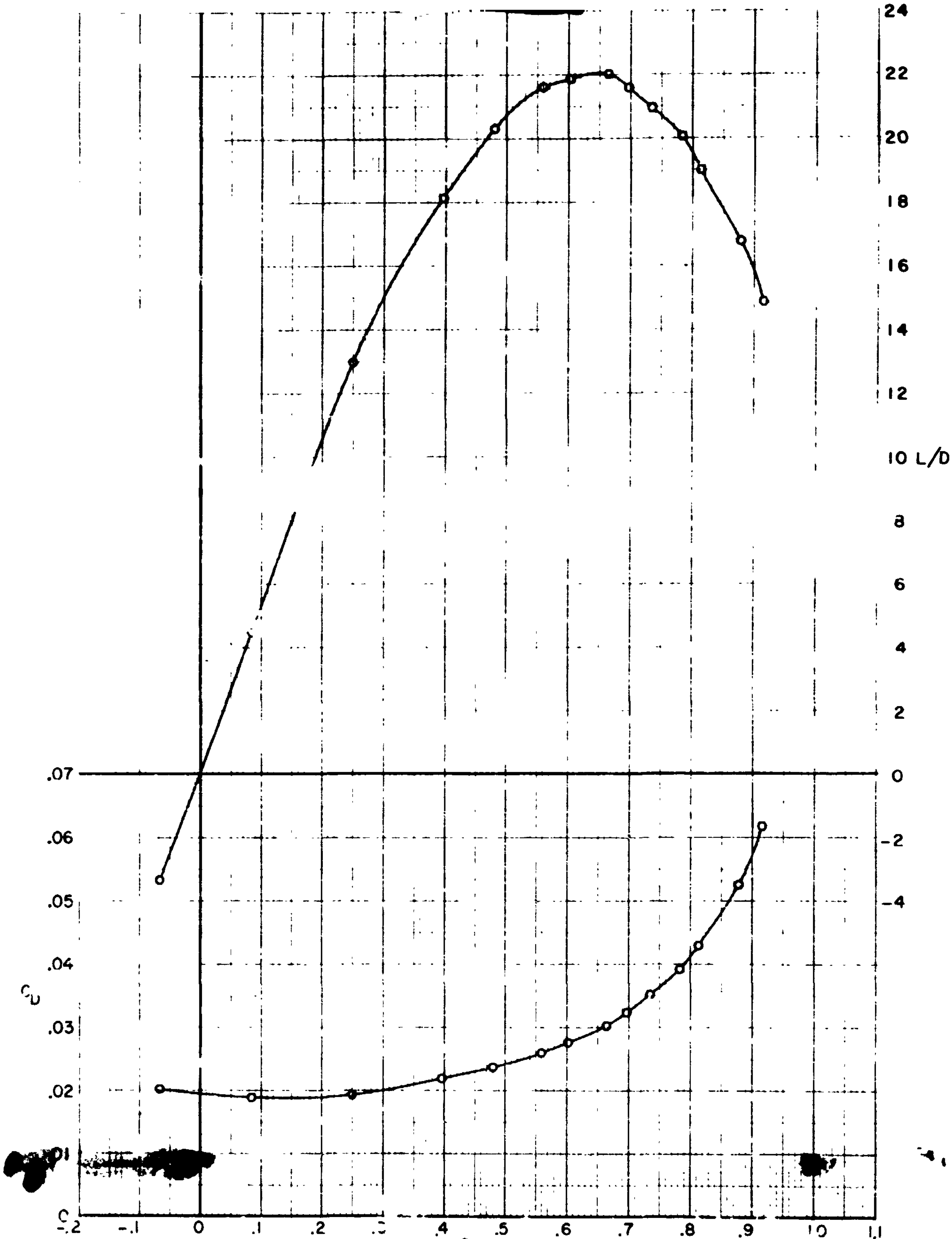

(e) [illegible] .79. Continued.

[illegible]gure 12.- Continued.

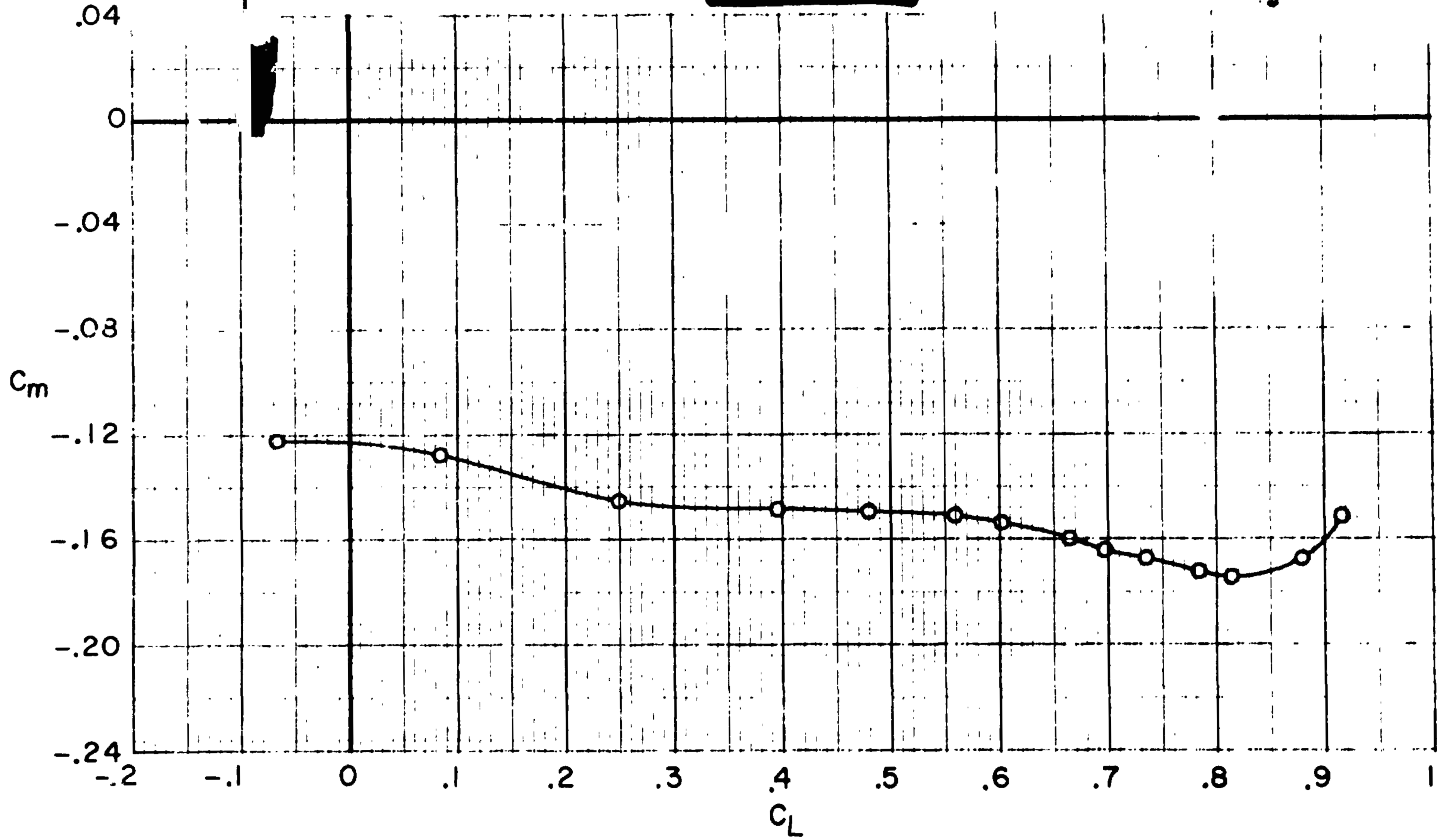

(e) M = 0.79. Concluded.

Figure 12. - Continued.

[redacted]

[redacted]

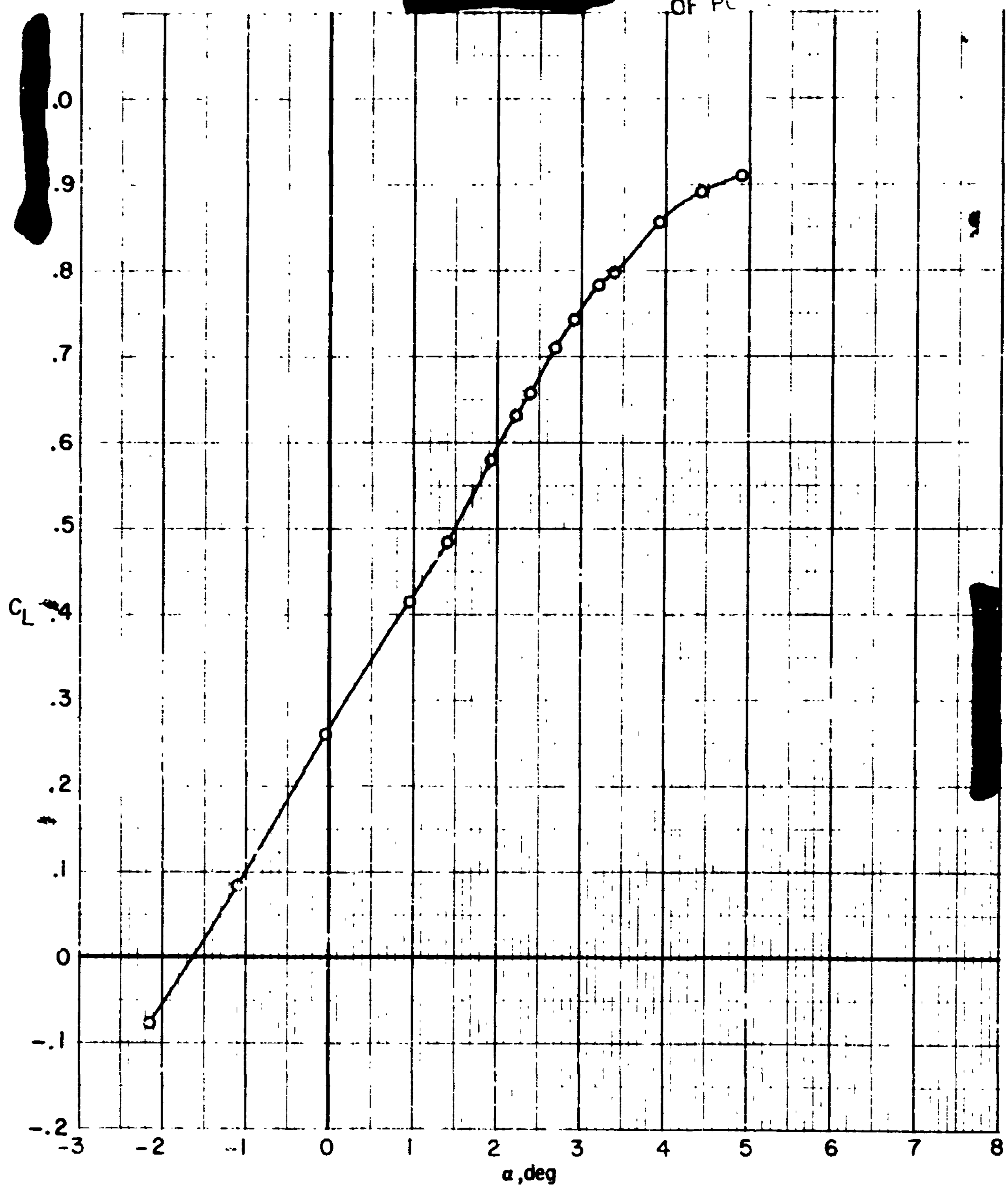

[redacted]

(c) M = 0.80.

Figure 12.- Continued.

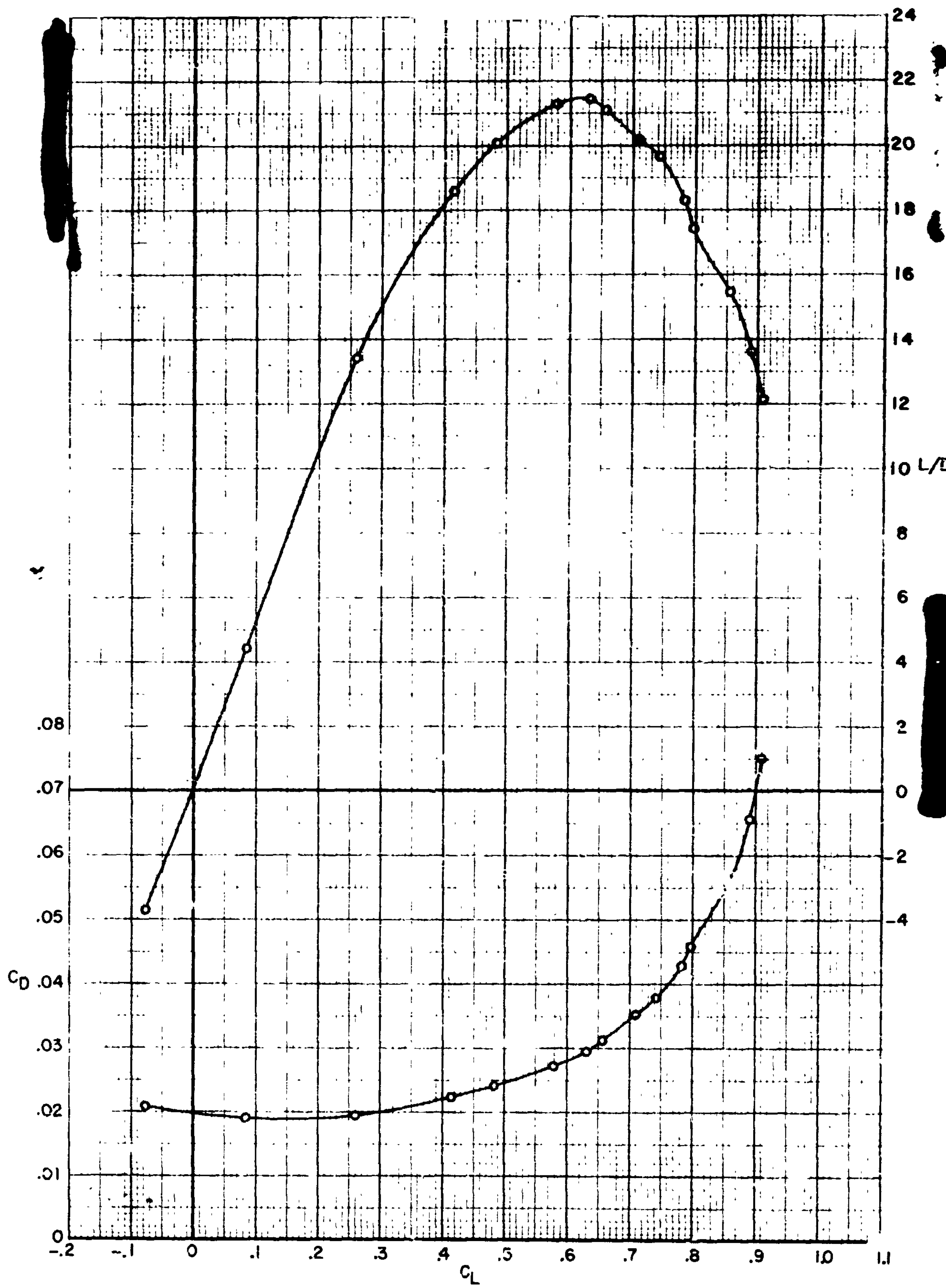

(f) M = 0.80. Continued.

Figure 12. - Continued.

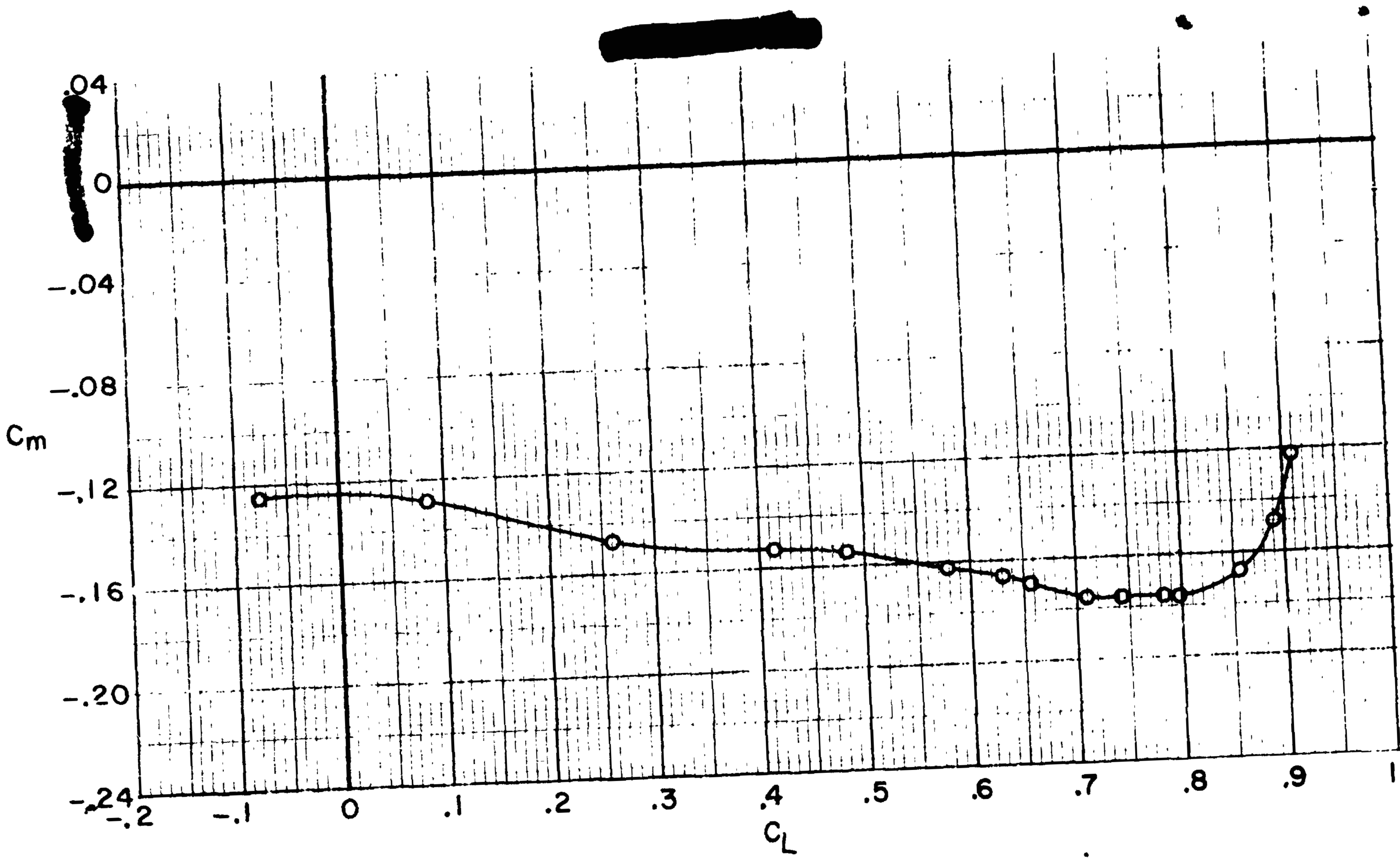

(f) M = 0.80. Concluded.

Figure 12.- Continued.

[redacted]

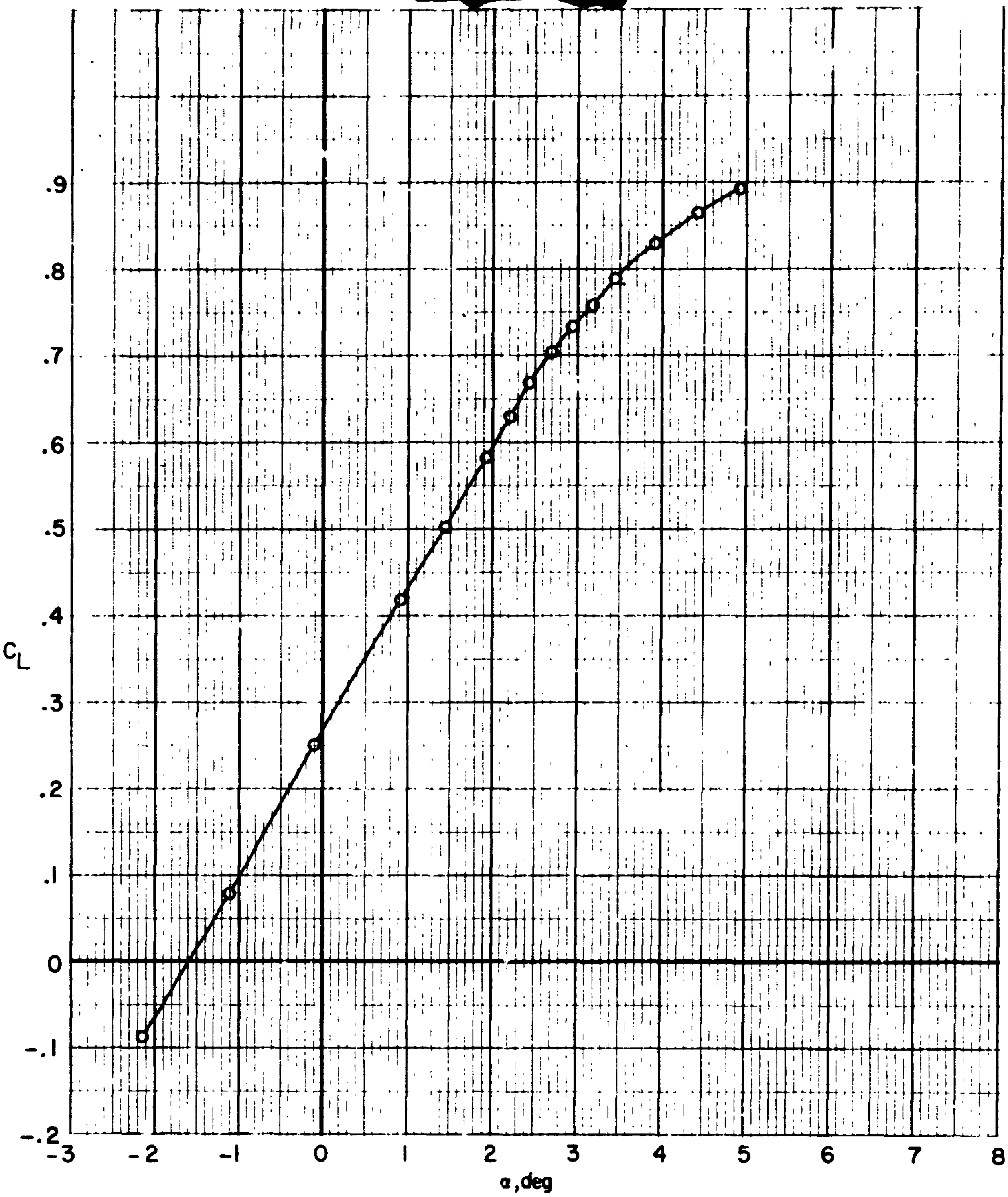

(g) M = 0.81.

Figure 12.- Continued.

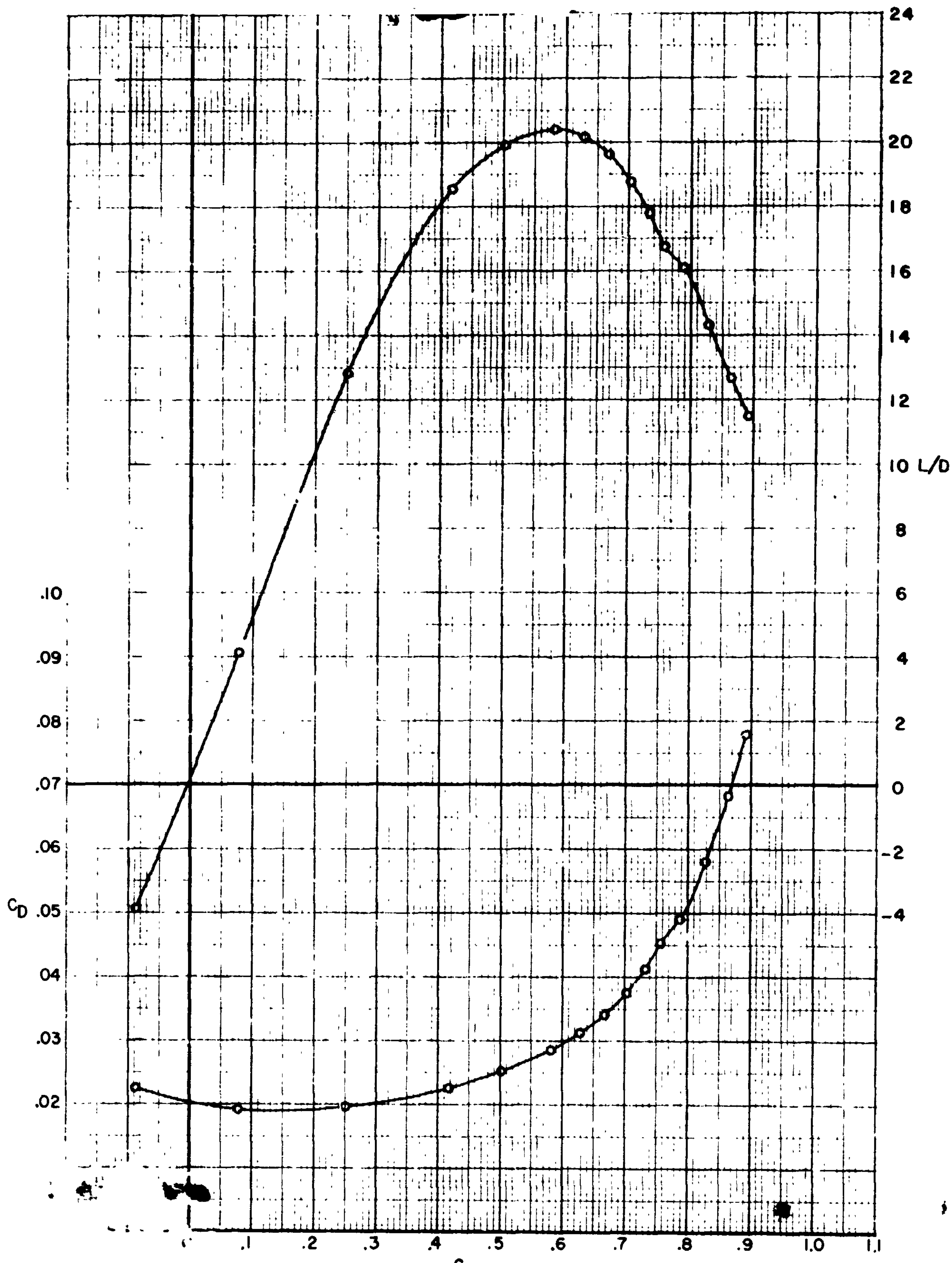

(g) M = 0.81. Continued.

Figure 12.- Continued.

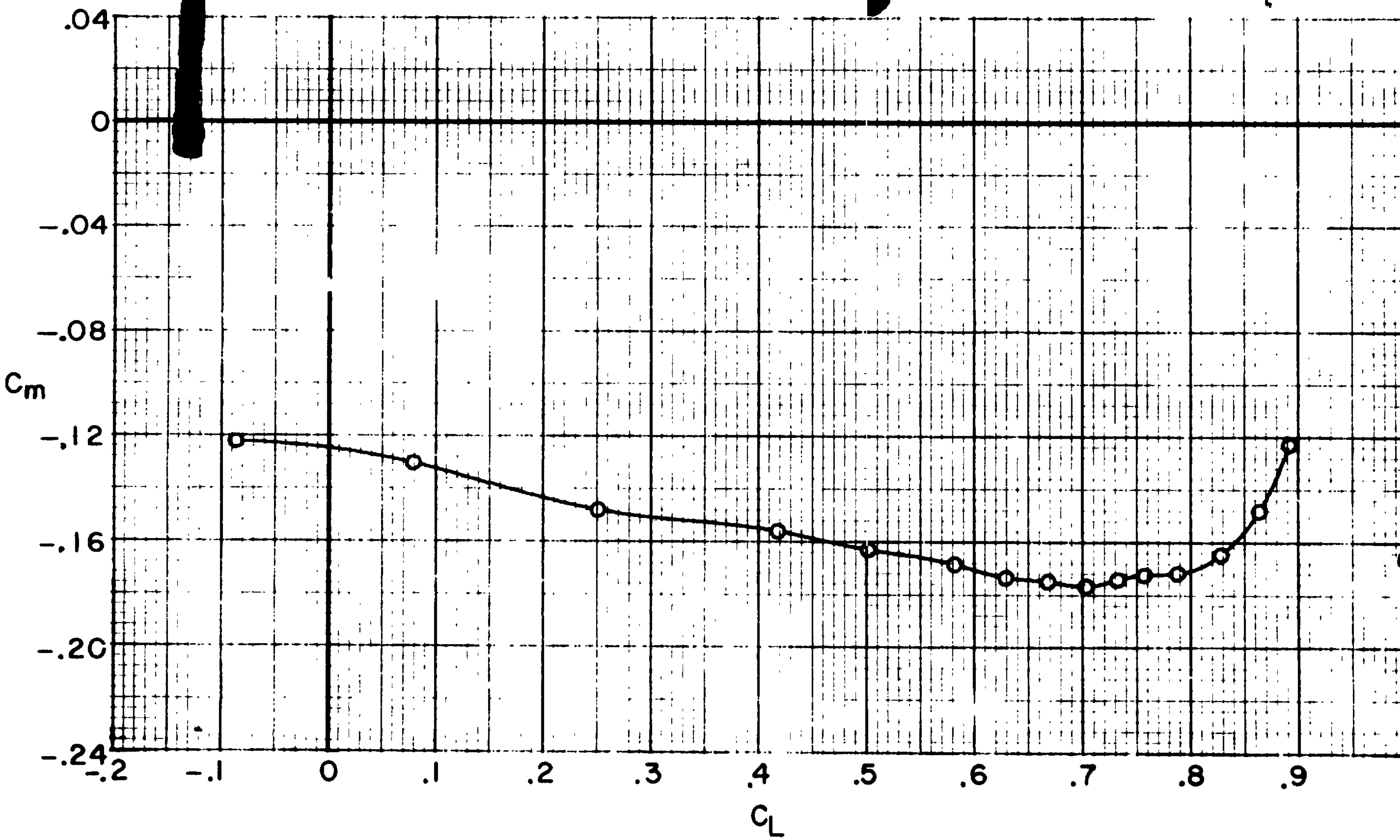

(g) M = 0.81. Concluded.

Figure 12. - Continued.

[redacted]

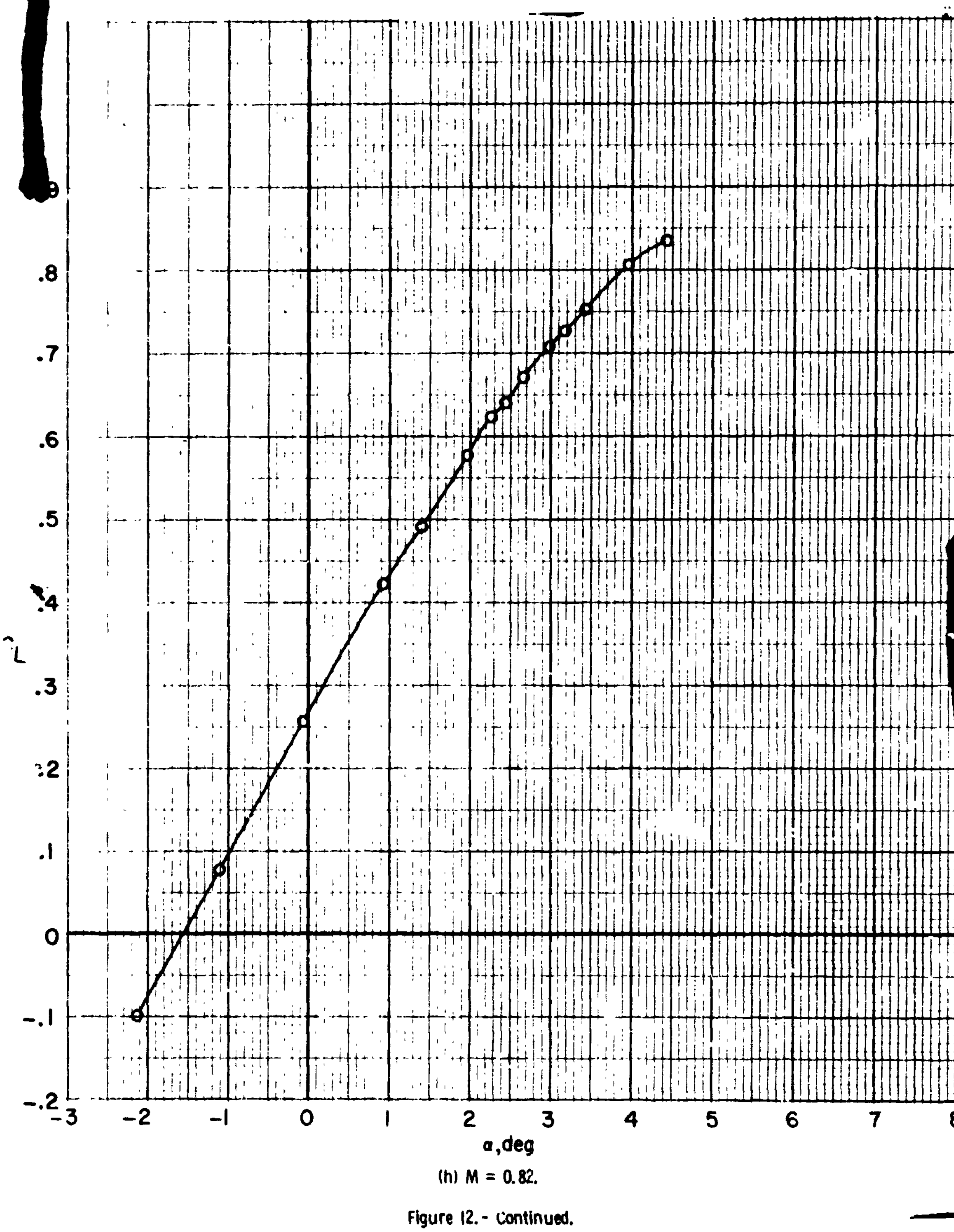

(h) M = 0.82.

Figure 12.- Continued.

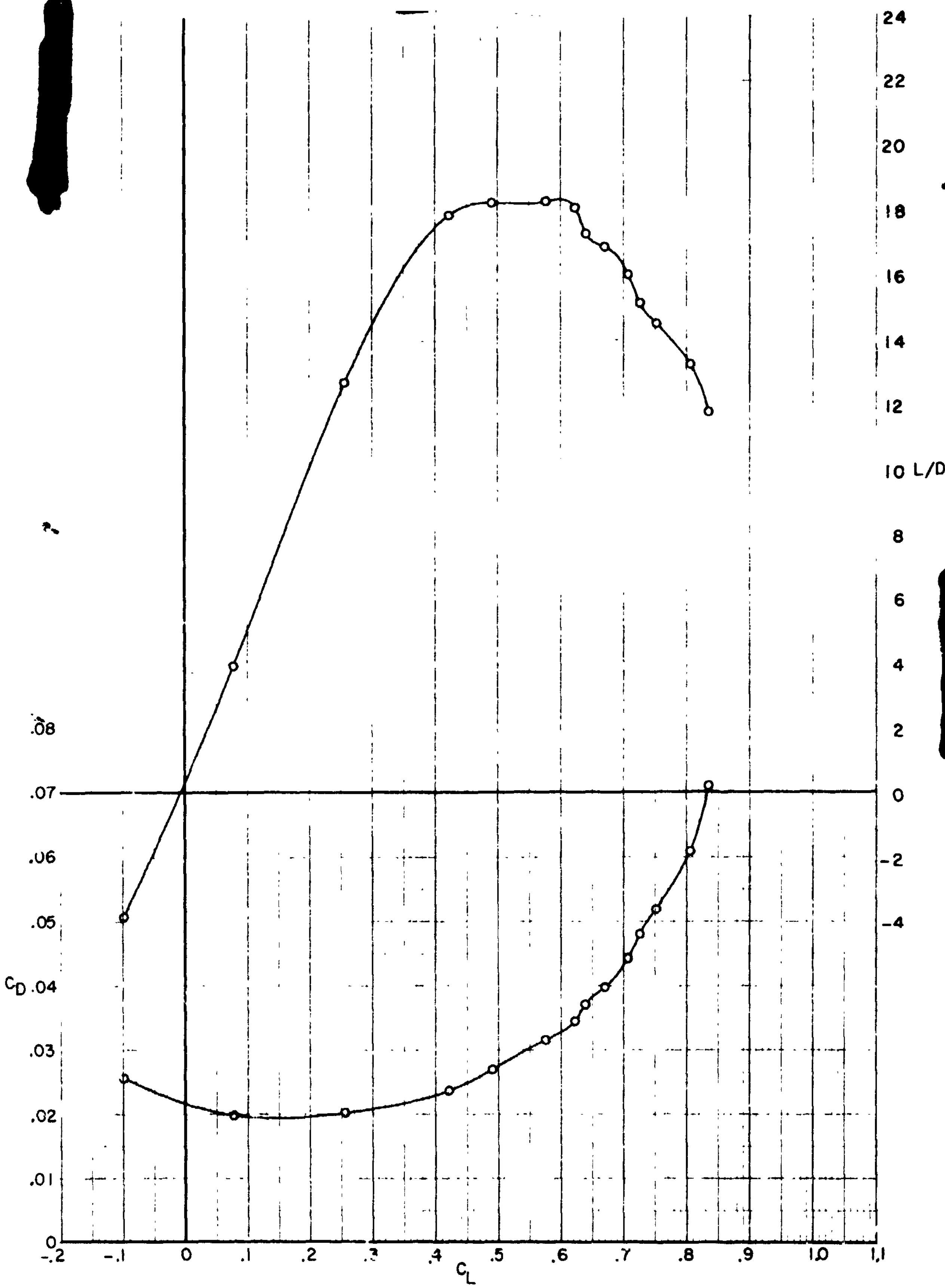

(h) M = 0.82. Continued

Figure 12. - Continued.

[redacted]

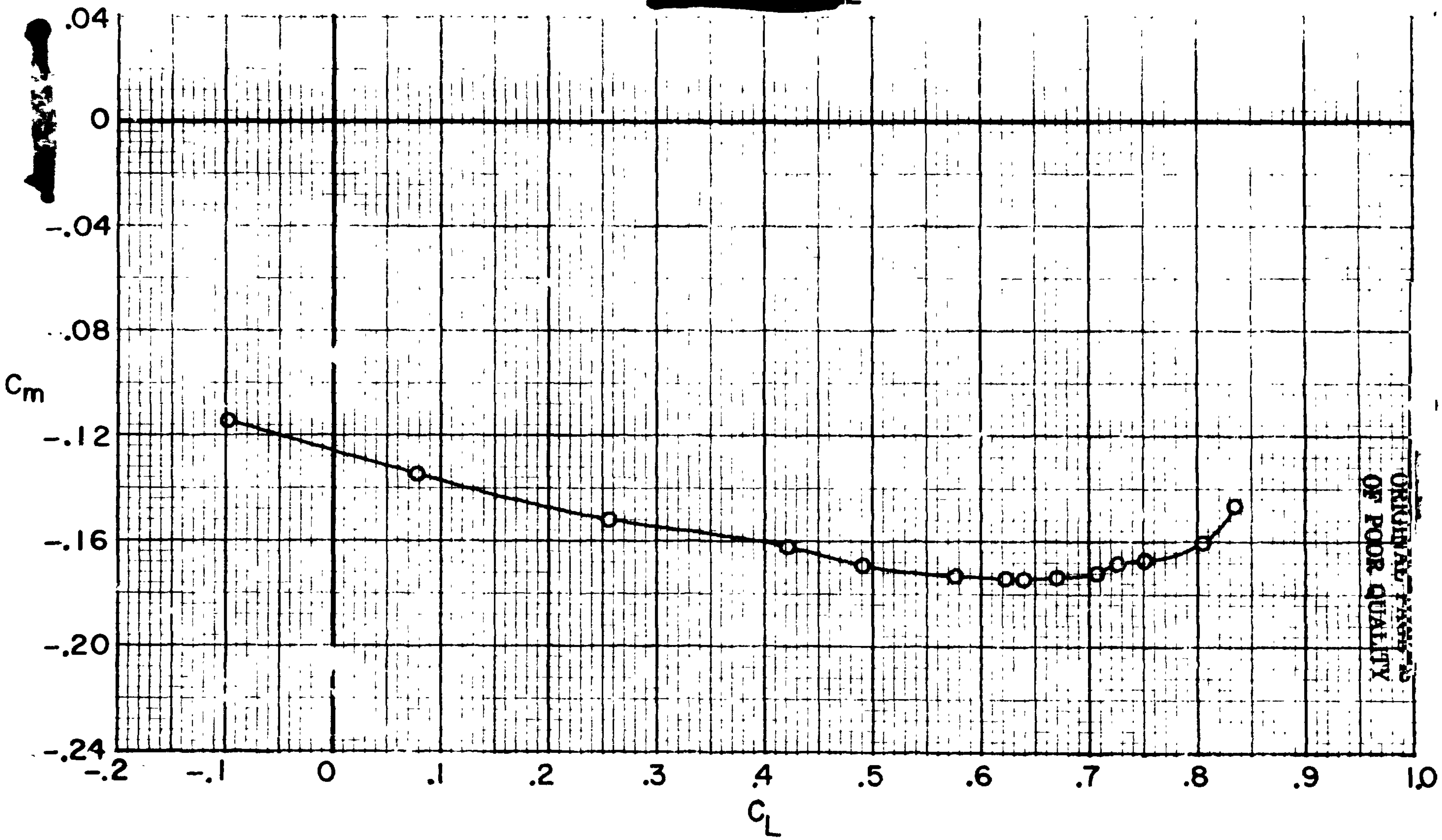

(h) M = 0.82. Concluded.

Figure 12. - Concluded.

[redacted]

[redacted]

[redacted]

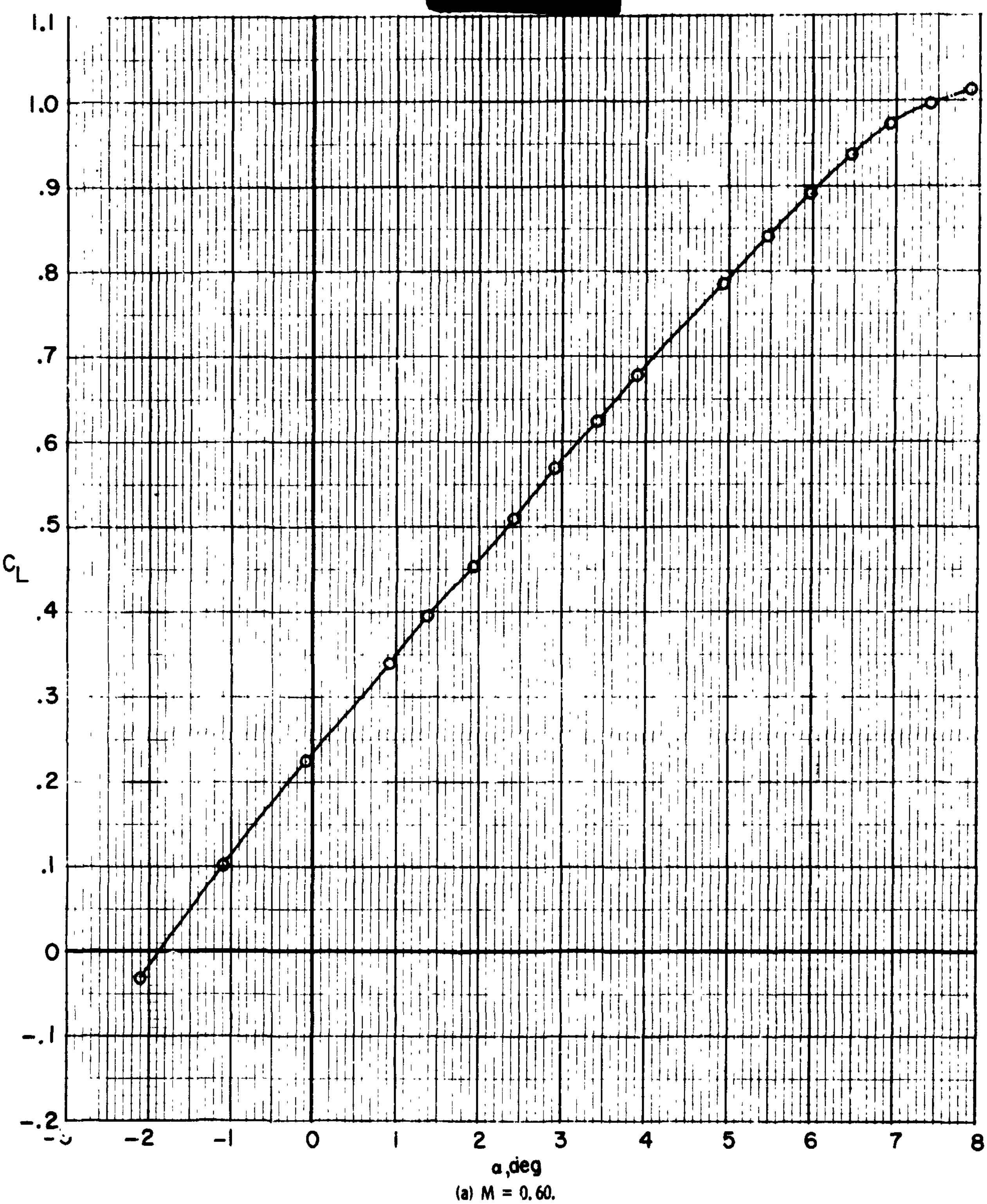

(a) M = 0.60.

Figure 13.- Longitudinal aerodynamic characteristics for supercritical wing configuration 2a (SCW-2a) with wing upper surface grit forward (x_T/c = 0.05). c.g. (F.S.) = [illegible]4.605 cm (33.309 in.); $\Lambda_{c/4}$ = 27°.

[redacted]

ORIGINAL PAGE IS
OF POOR QUALITY

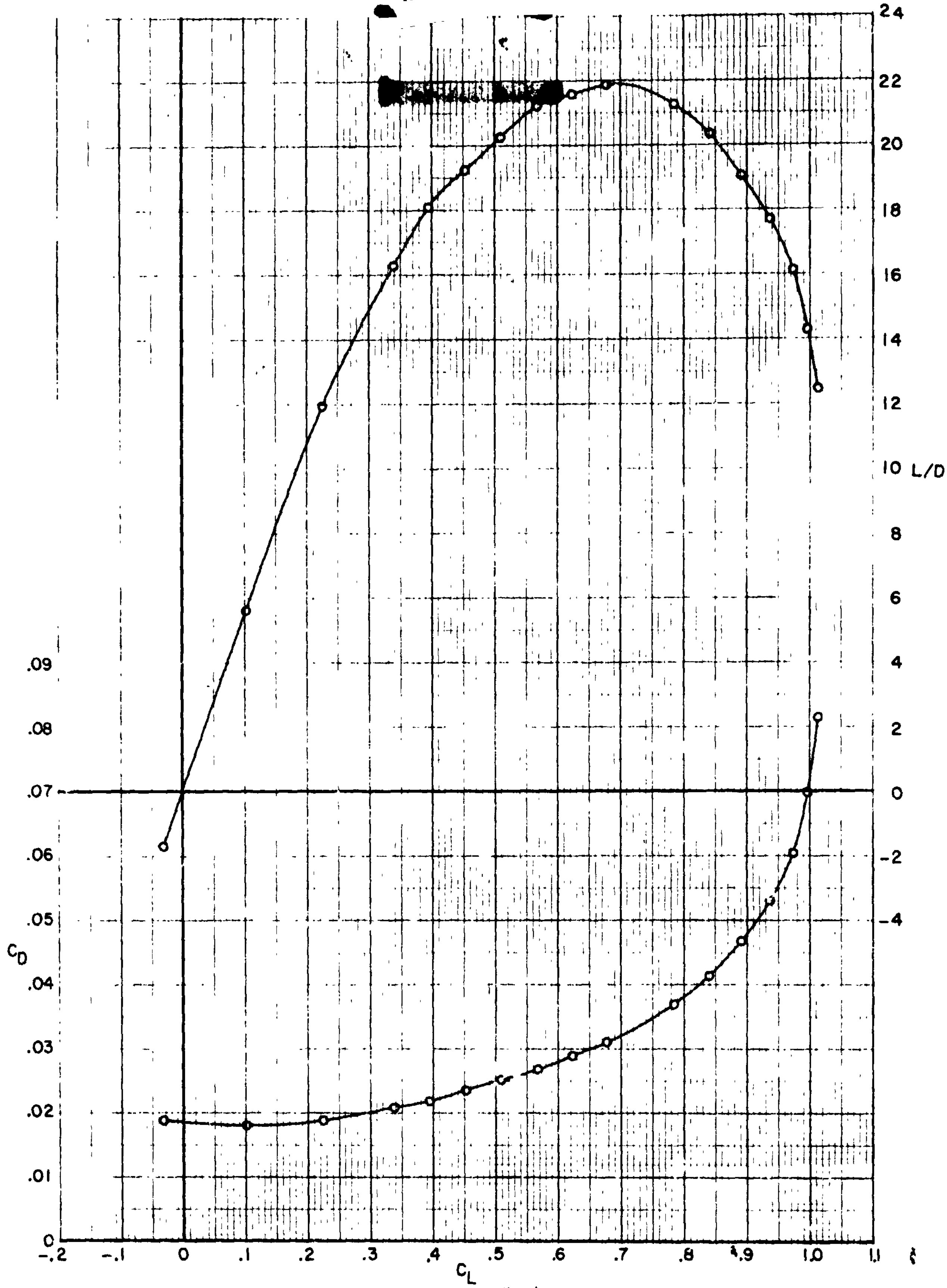

(a) M = 0.60. Continued.

Figure 13.- Continued.

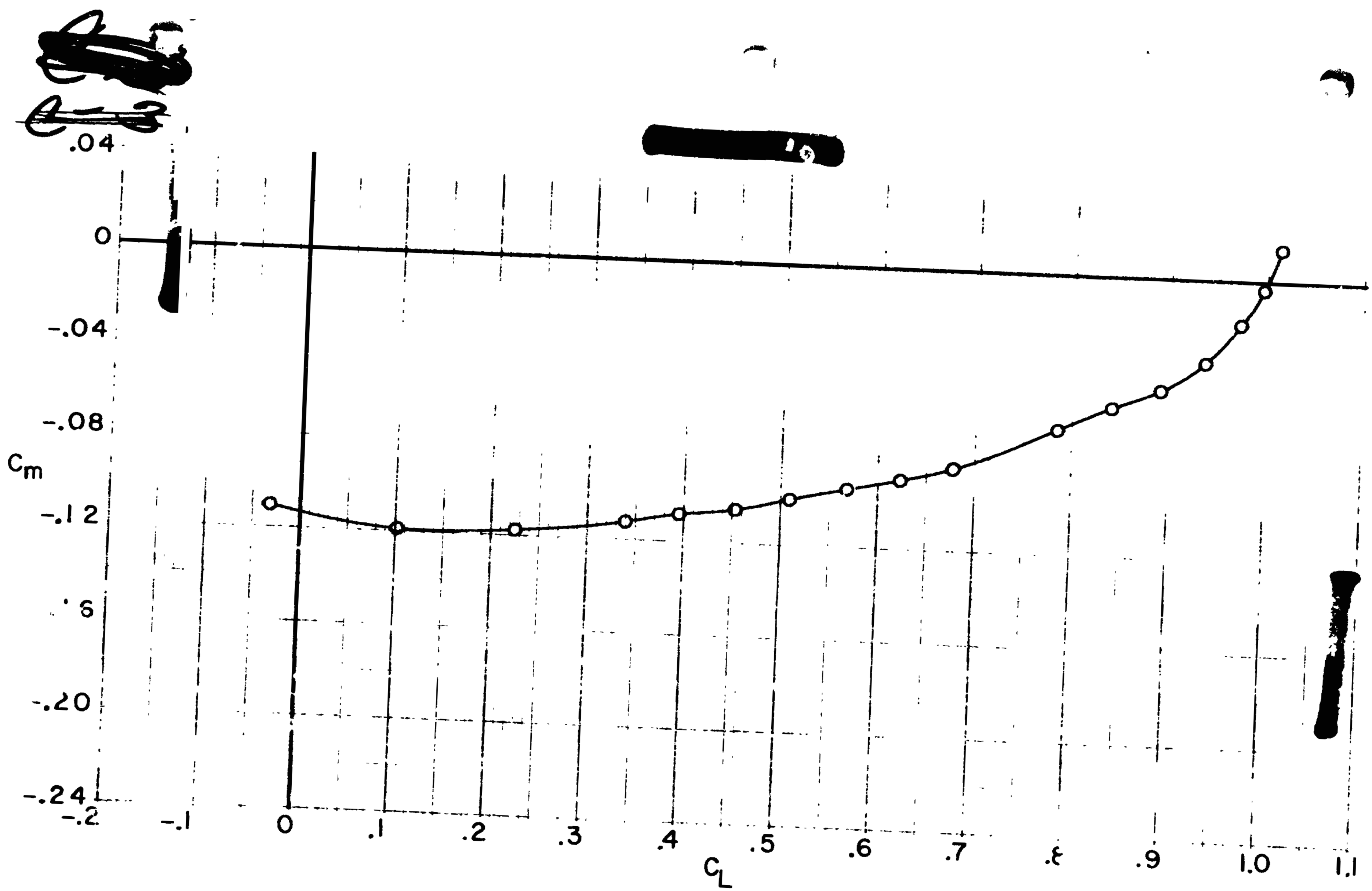

(a) M = 0.60. Concluded.

Figure 13. - Continued.

[redacted]

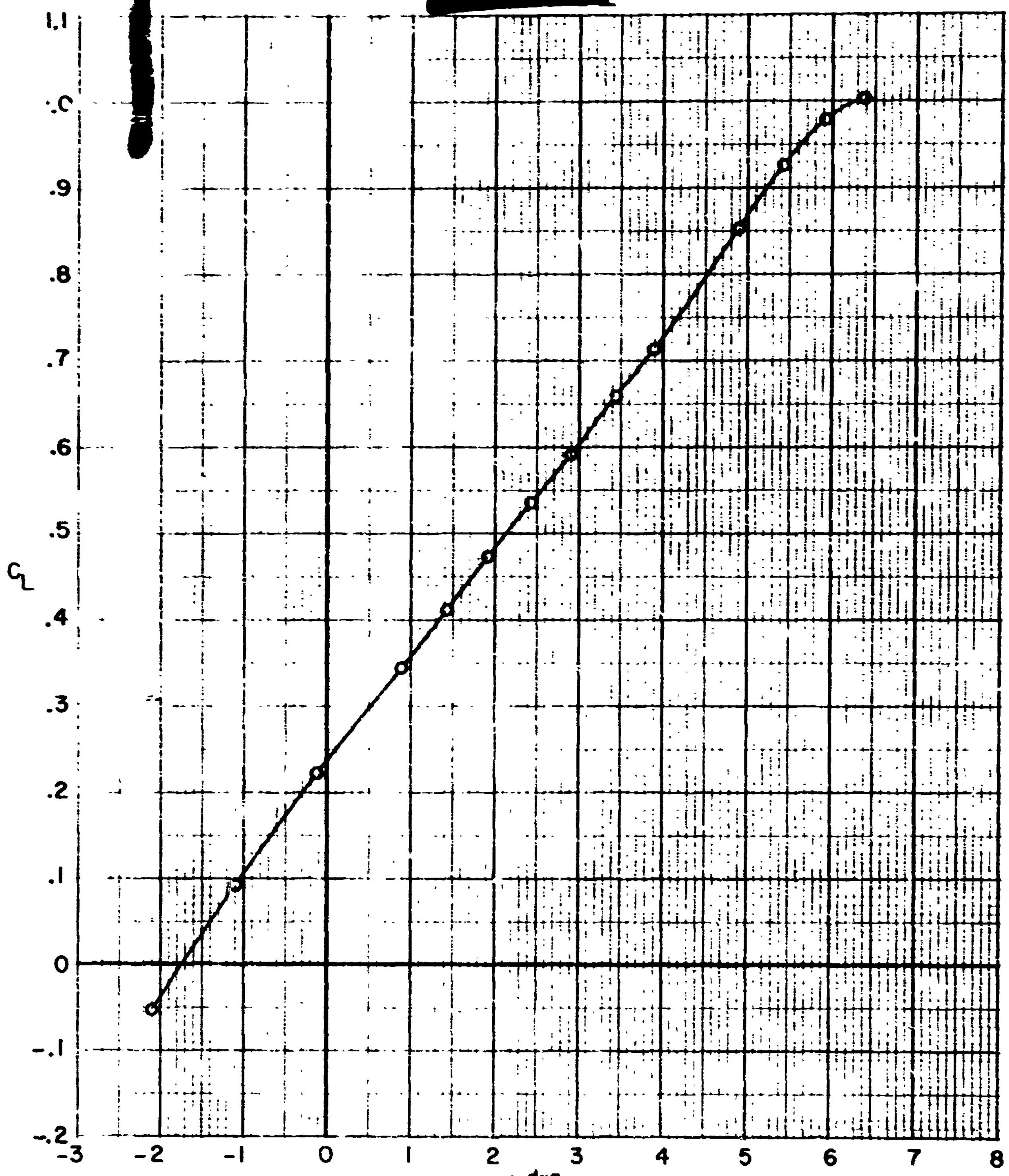

(b) M = 0.70.

Figure 13.- Continued.

C-3

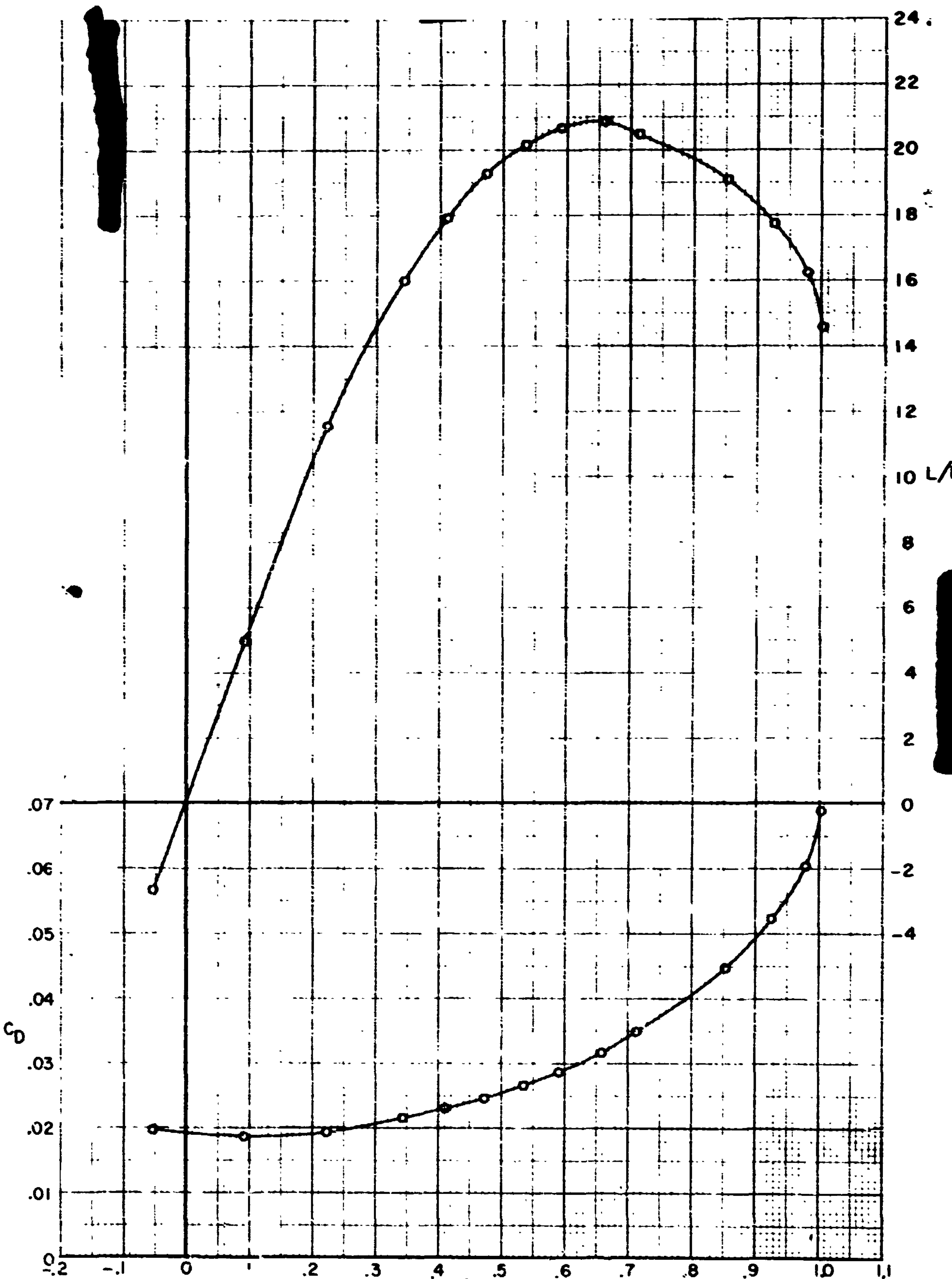

(b) M = 0.70. Continued.

Figure 15.- Continued.

[redacted]

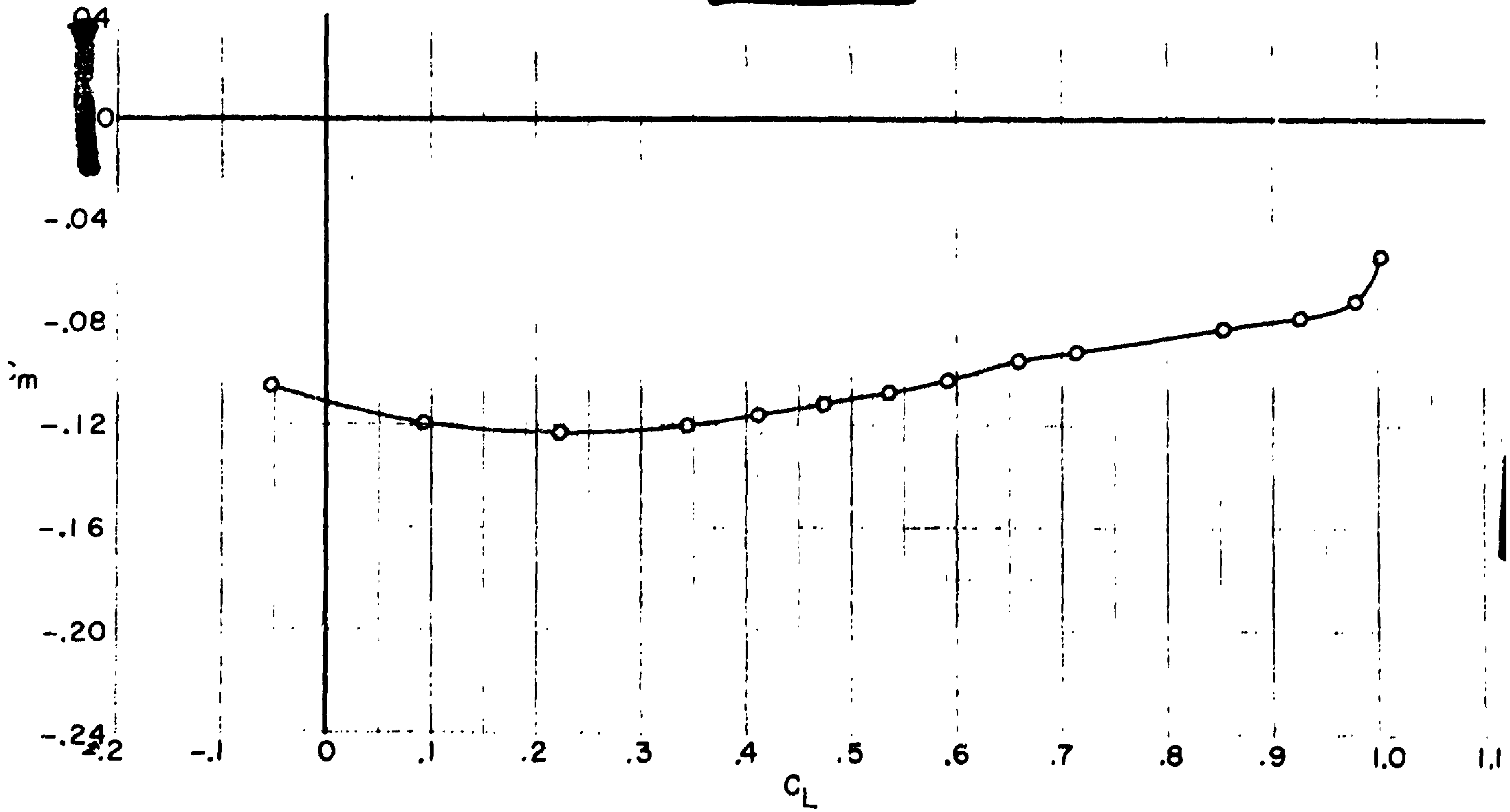

(b) M = 0.70. Concluded.

Figure 13. - Continued.

[redacted]

ORIGINAL PAGE IS
OF POOR QUALITY

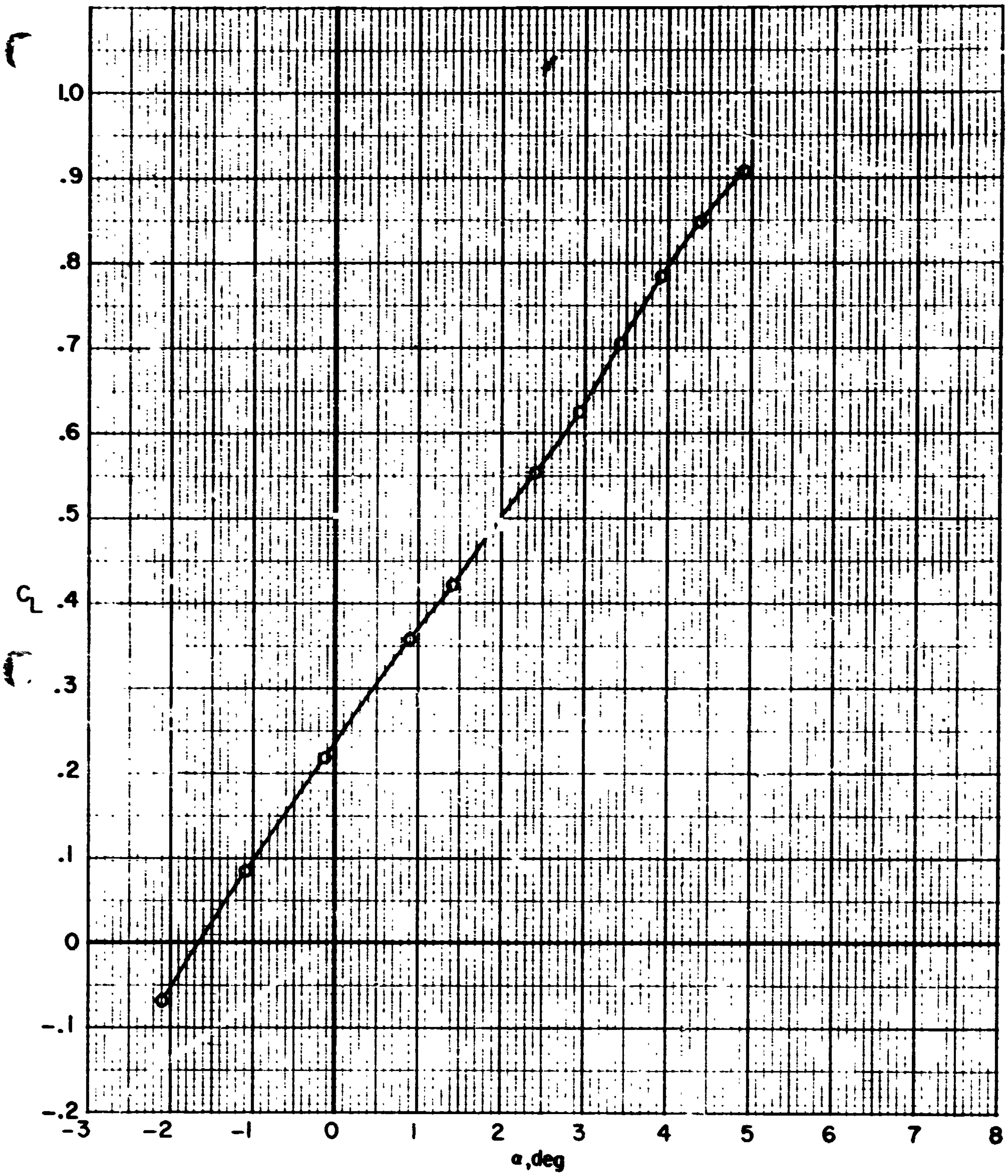

(c) M = 0.75.

Figure 13. - Continued.

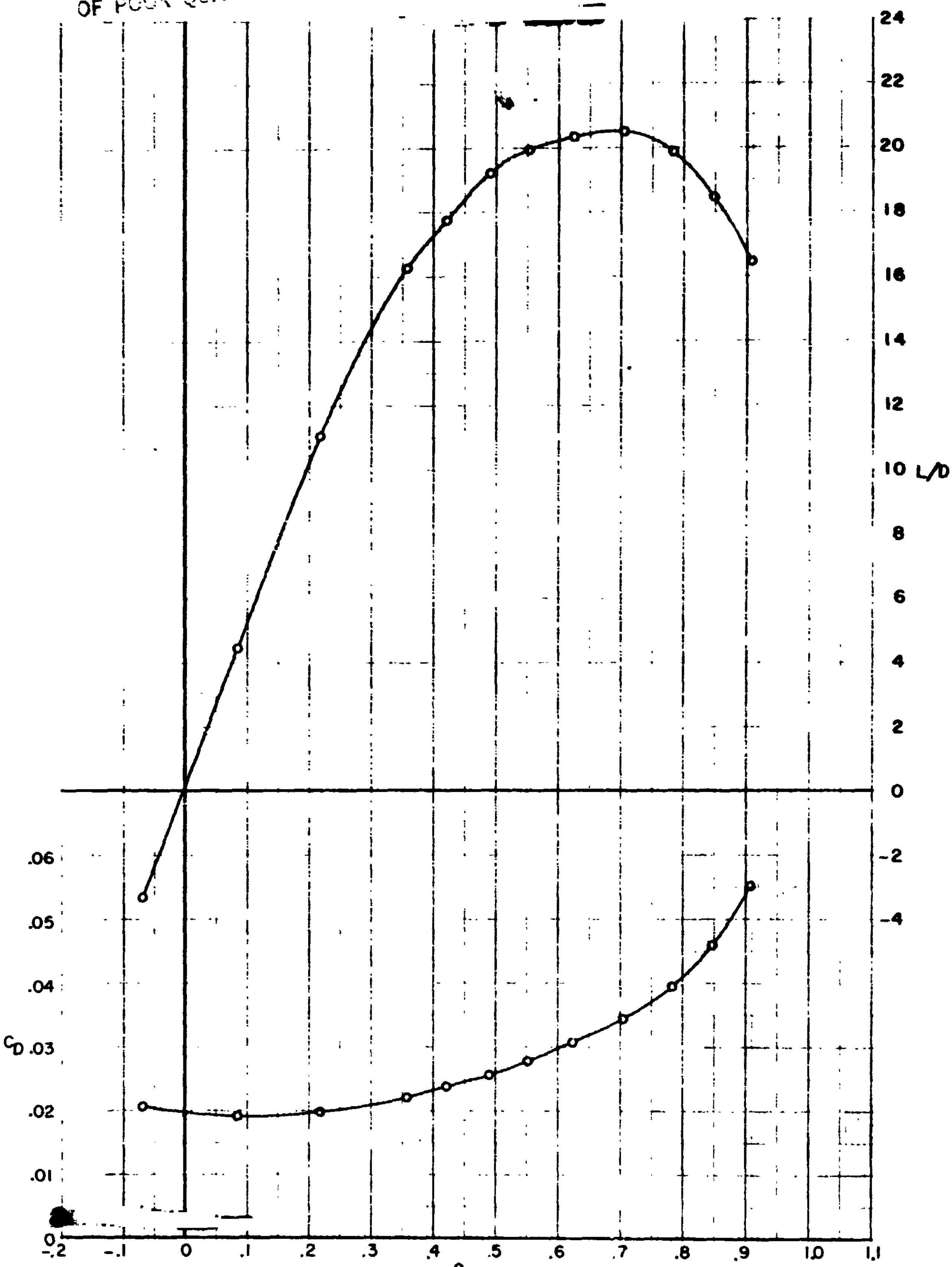

(c) M = 0.75. Continued.

Figure 13. - Continued.

[redacted]

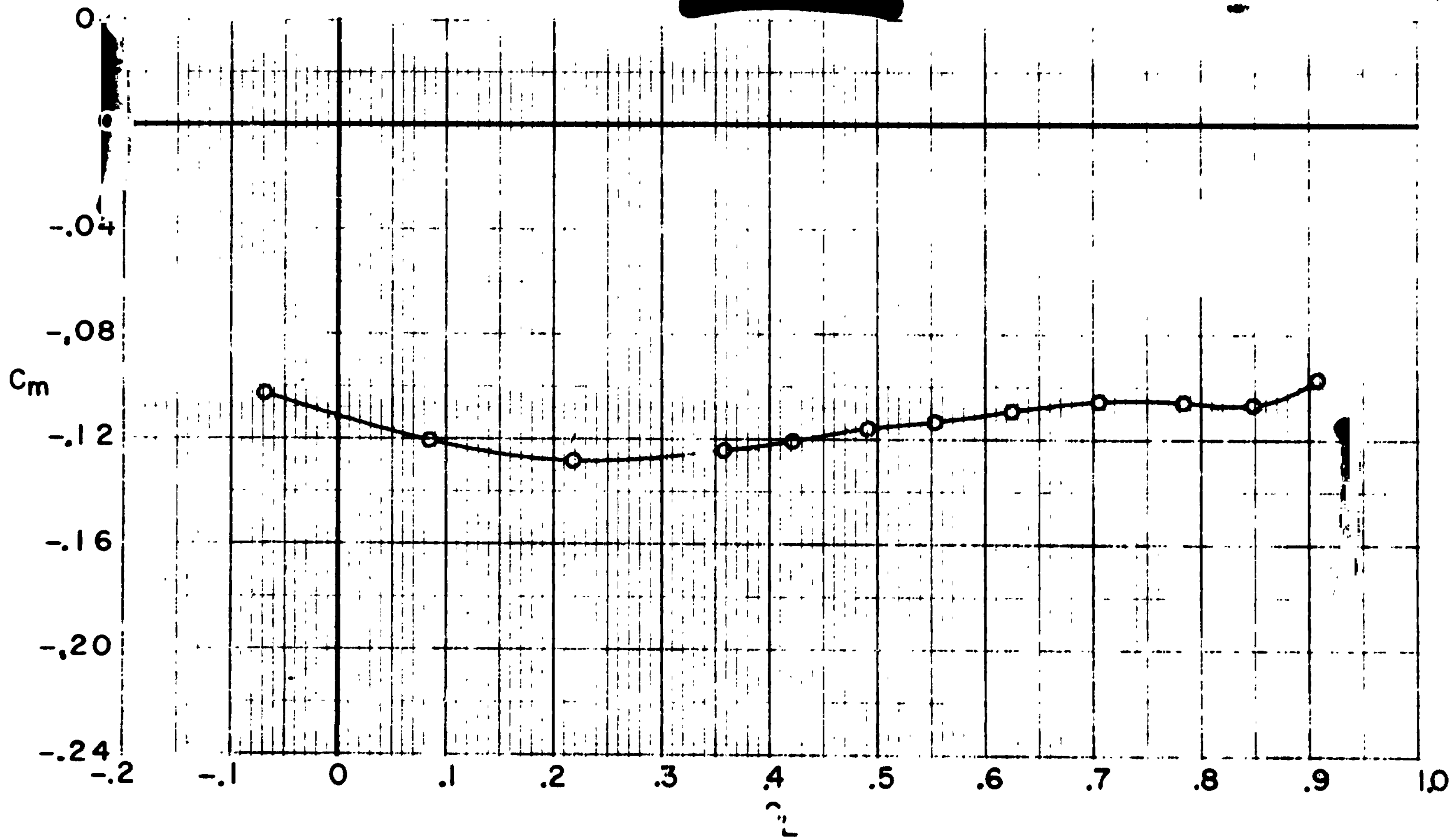

(c) M = 0.75. Concluded.

Figure 13.- Continued.

[redacted]

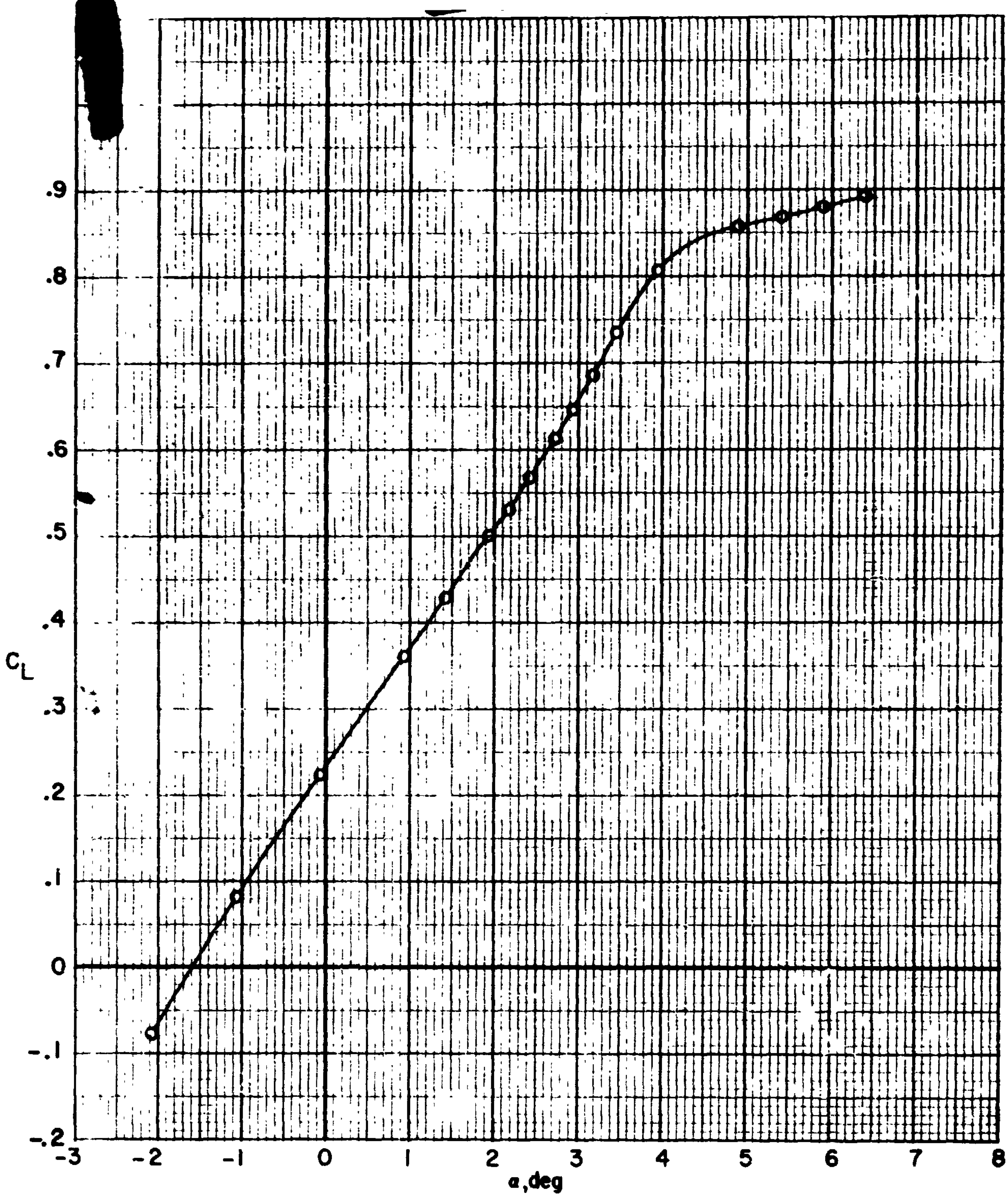

(d) M = 0.77.

Figure 13.- Continued.

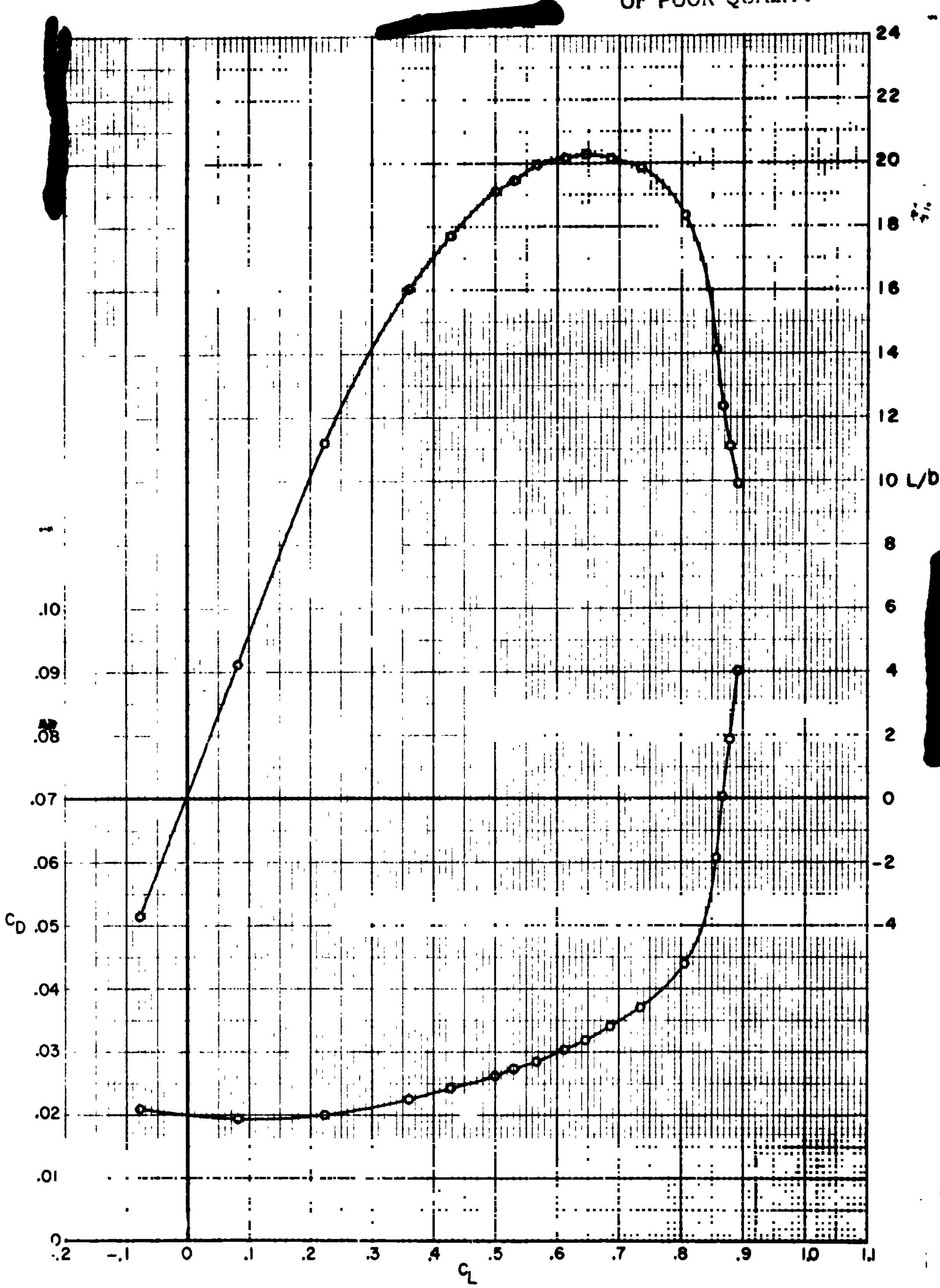

(d) M = 0.77. Continued.

Figure 13.- Continued.

[redacted]

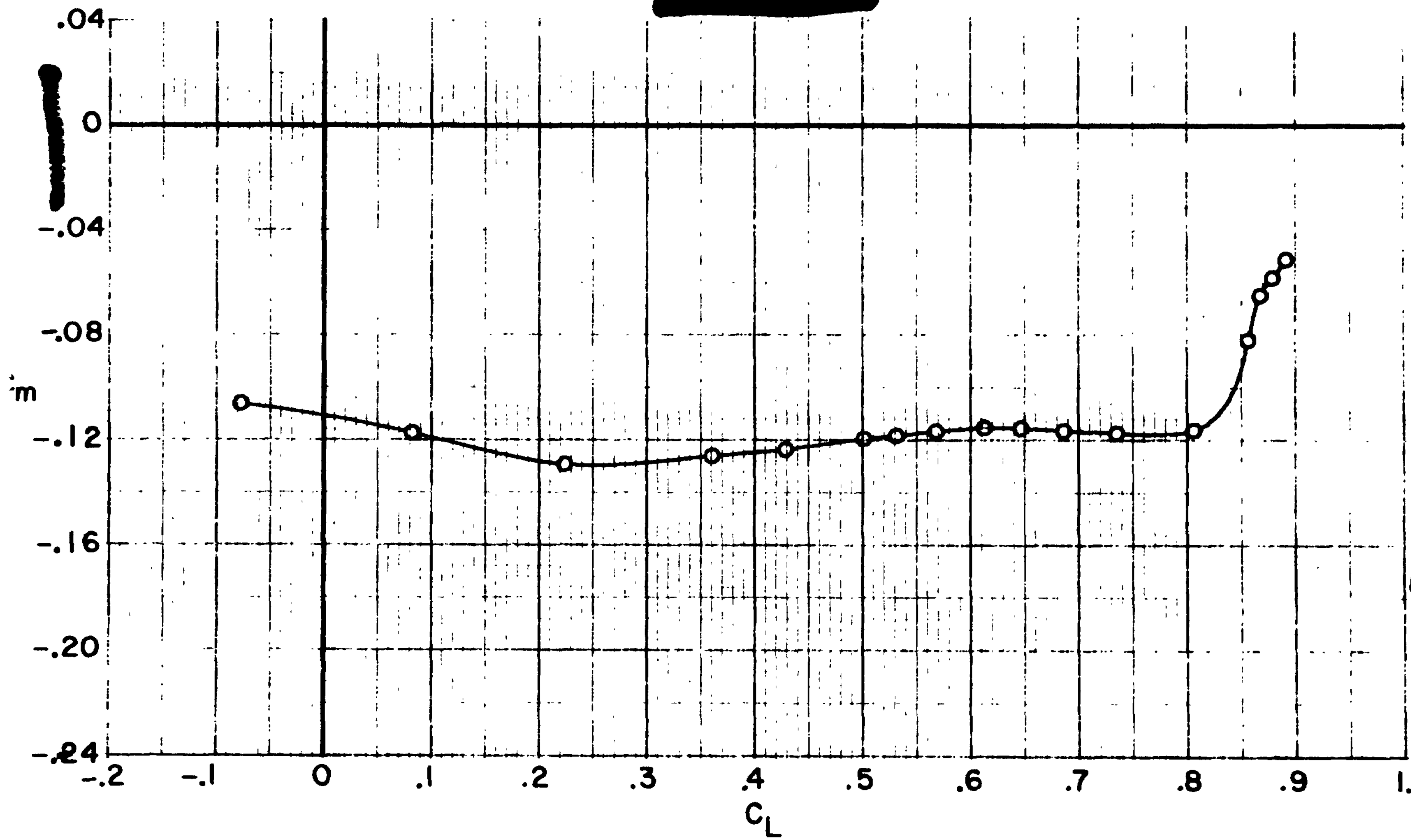

(d) M = 0.77. Concluded.

Figure 13.- Continued.

[redacted]

ORIGINAL PAGE IS
OF POOR QUALITY

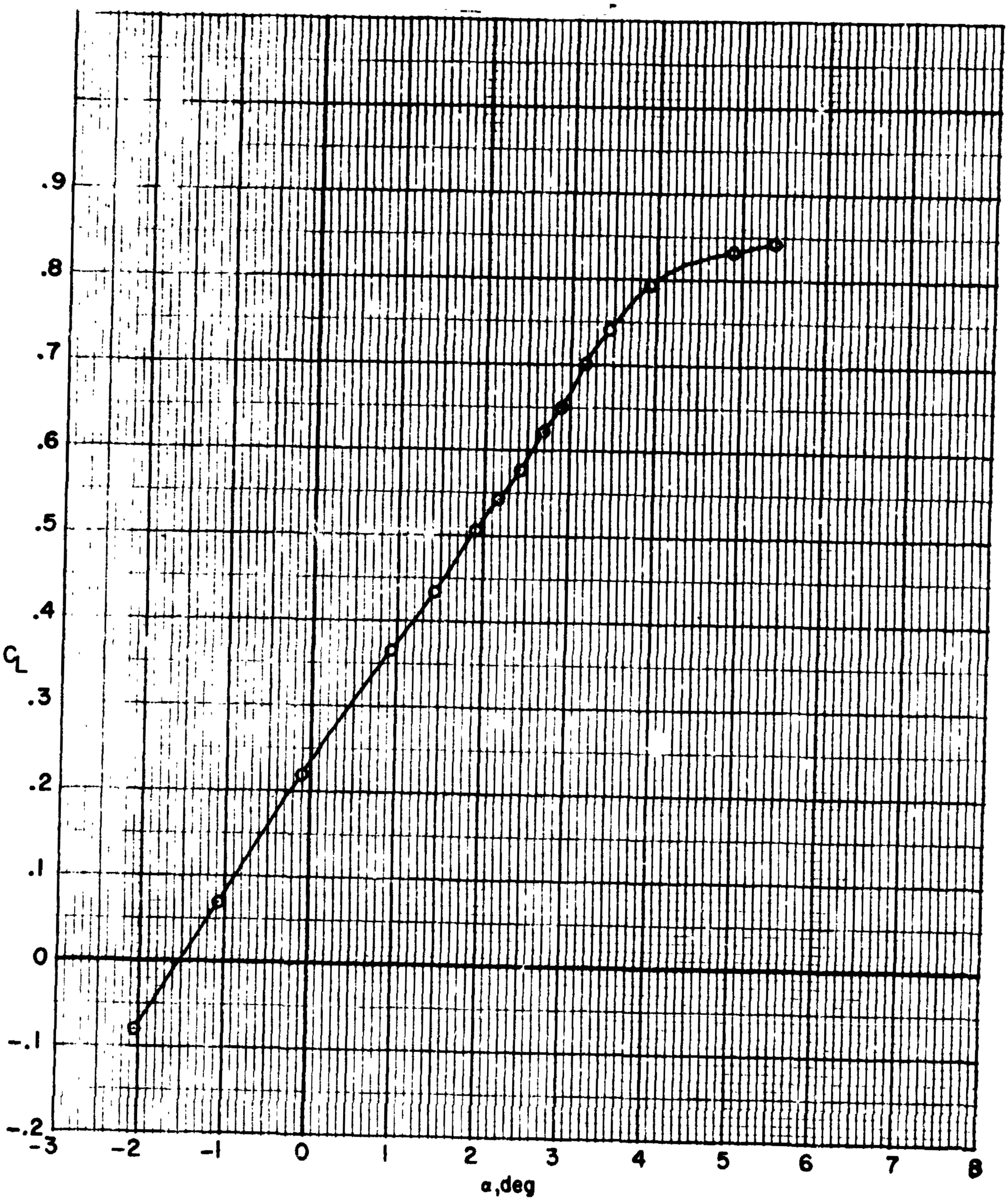

(e) M = 0.78.

Figure 13. - Continued.

[redacted]

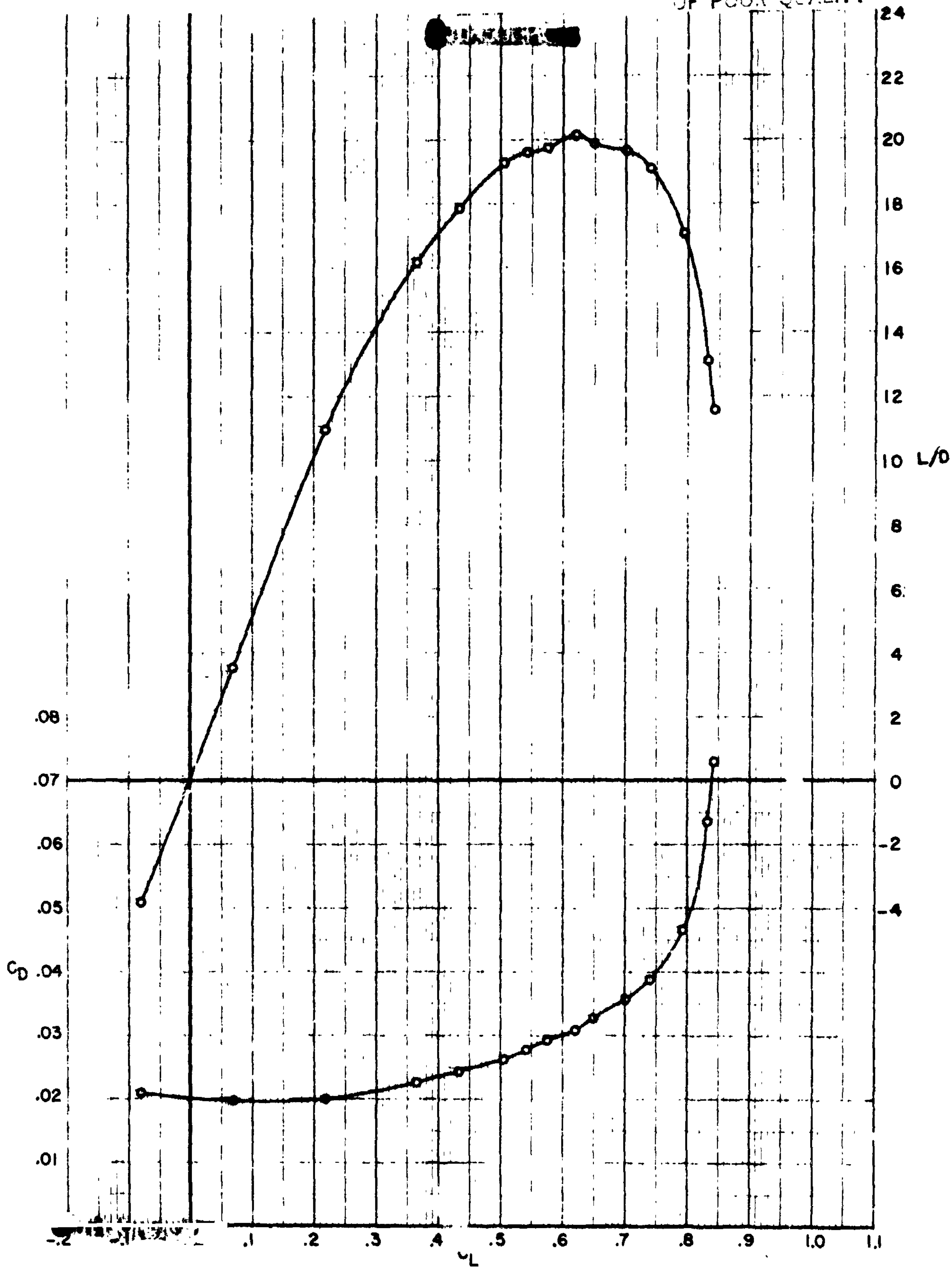

(e) M = 0.78. Continued.

Figure 13. - Continued.

[redacted]

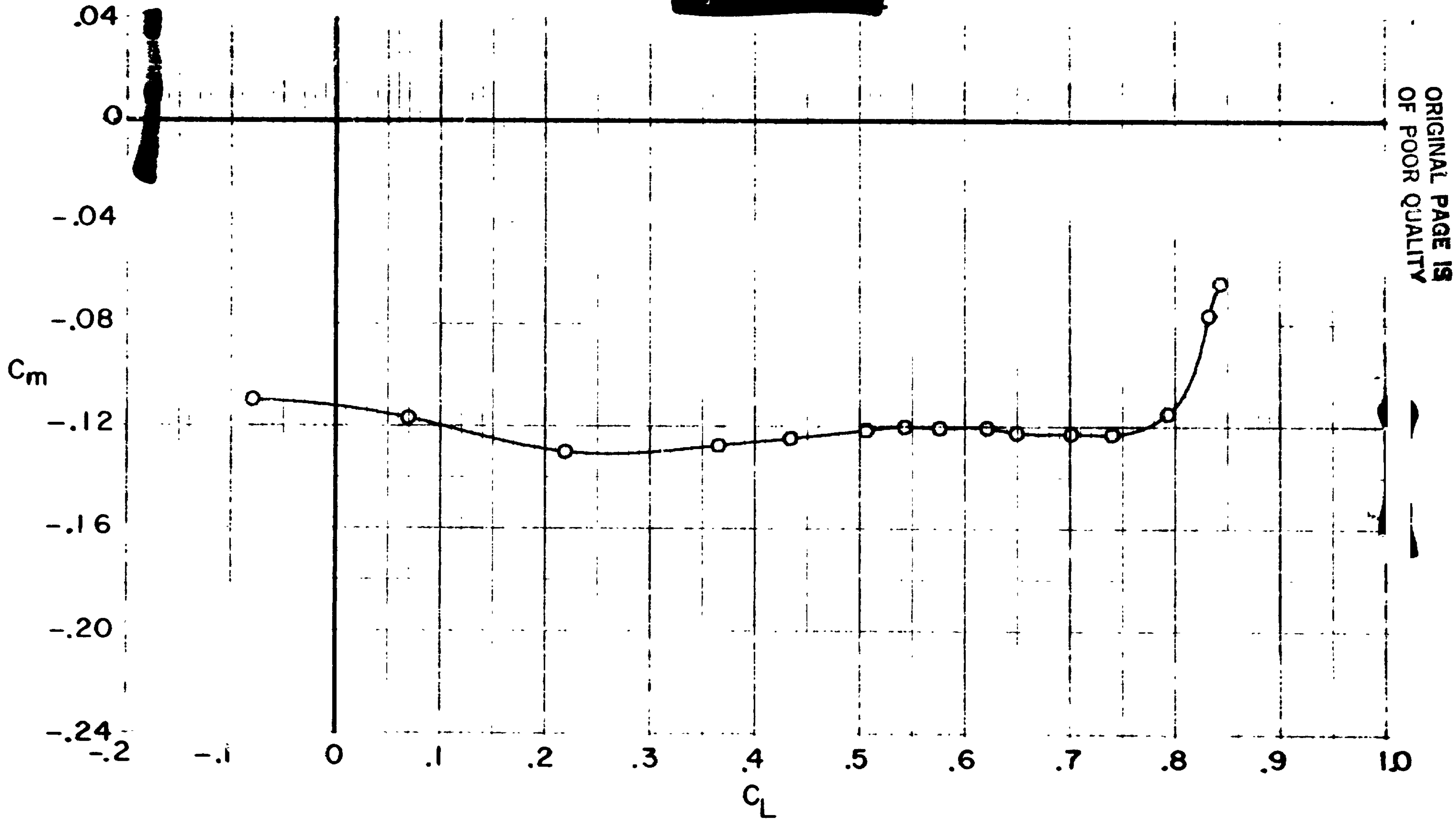

(e) M = 0.78. Concluded.

Figure 13.- Concluded.

[redacted]

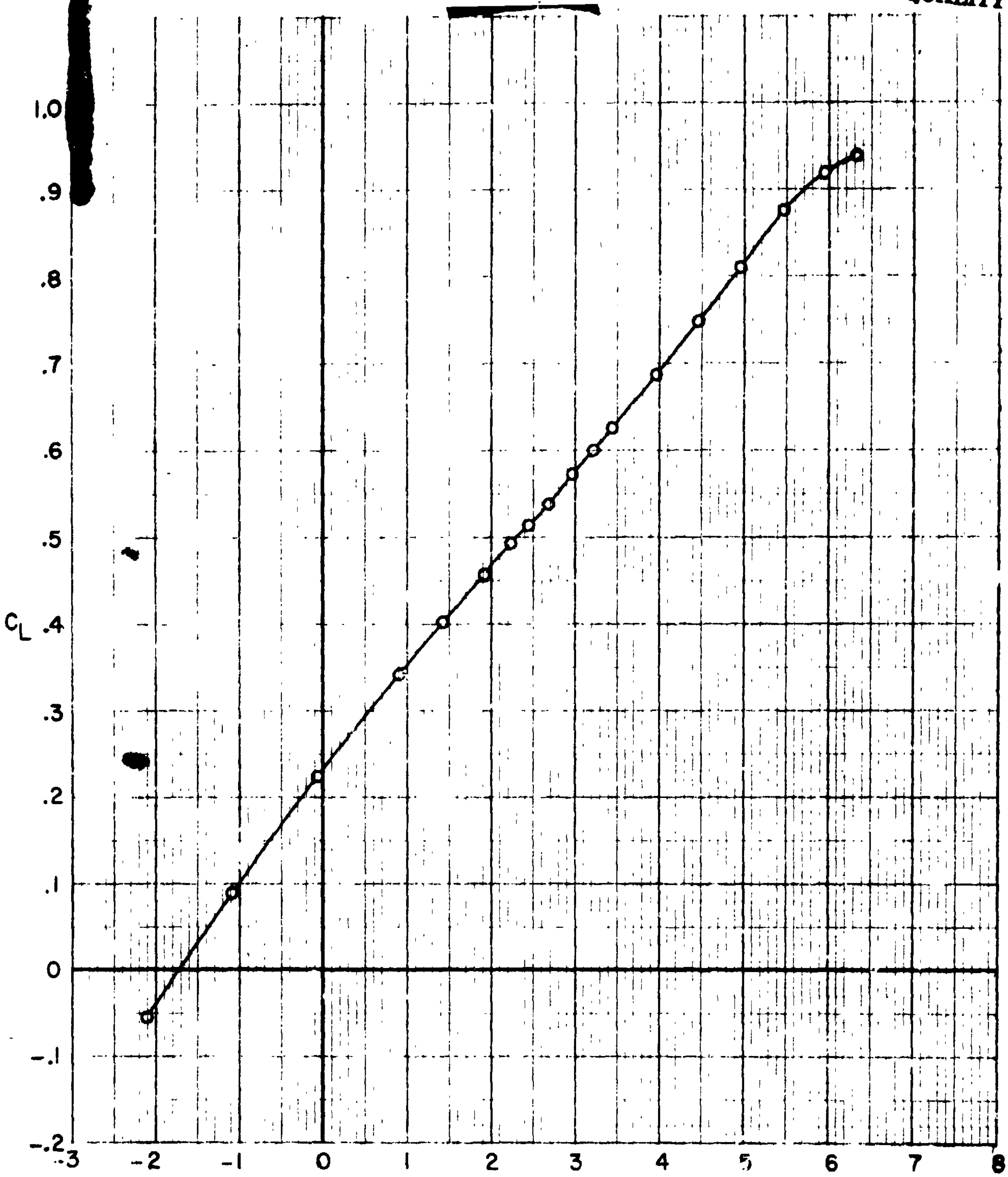

(a) M = 0.70.

Figure 14.- Longitudinal aerodynamic characteristics for supercritical wing configuration 2b (SCW-2b) with wing upper surface ·rit aft (fig. 5). $\Lambda_{c/4} = 30°$.

[redacted]

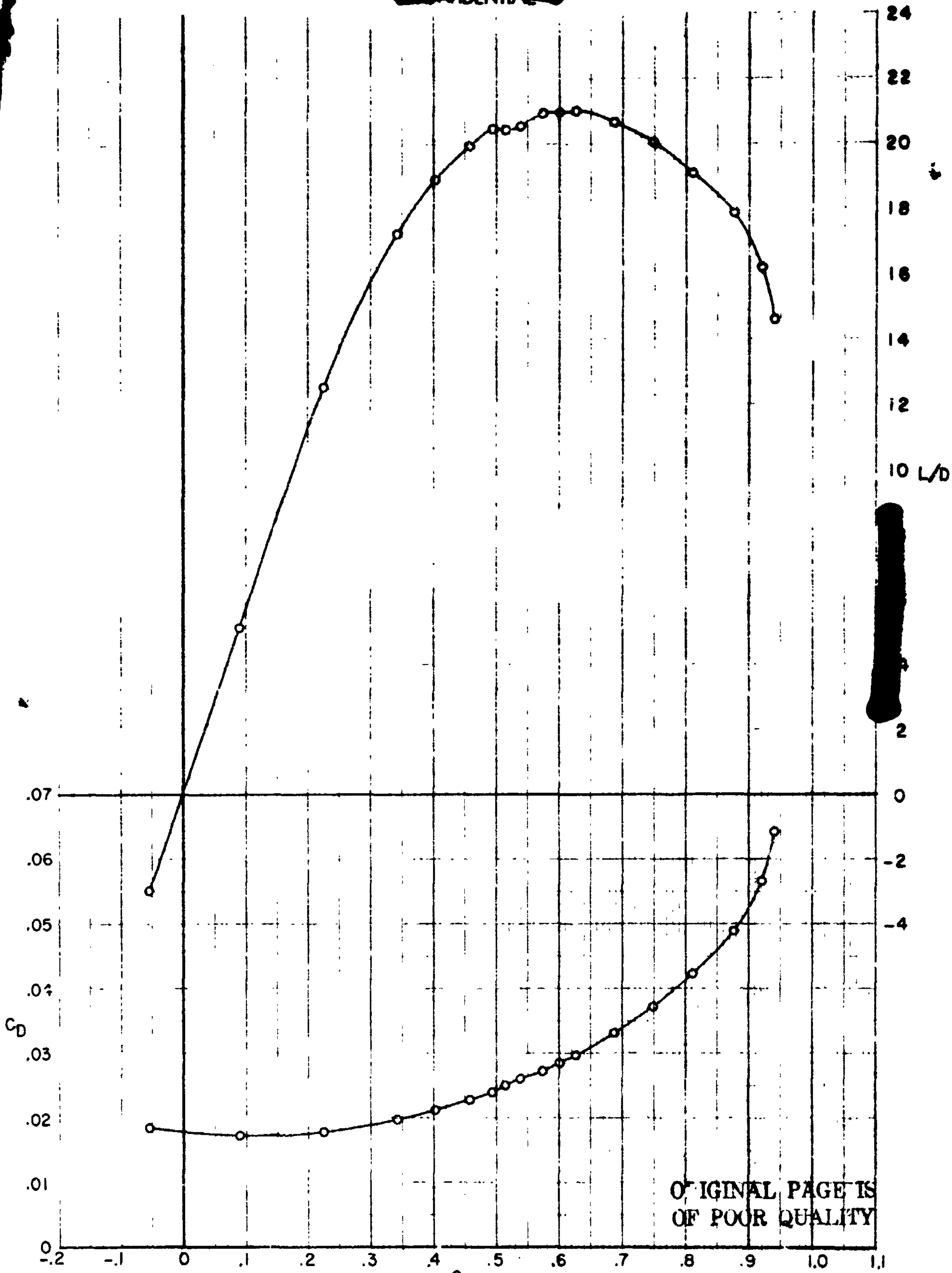

ORIGINAL PAGE IS
OF POOR QUALITY

(a) M = 0.70. Continued.

Figure 14.- Continued.

[redacted]

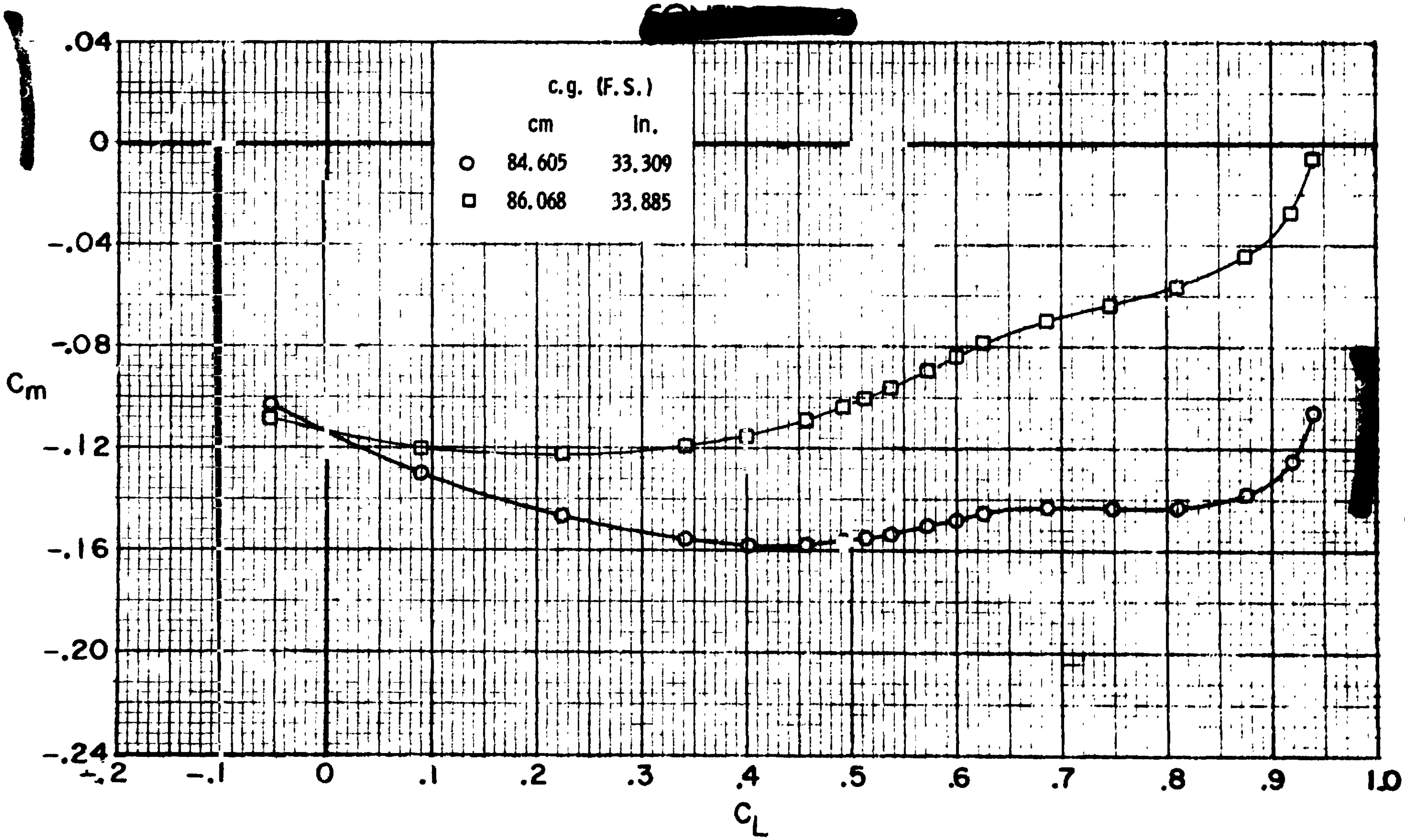

(a) M = 0.70. Concluded.

Figure 14. - Continued.

[redacted]

[redacted]

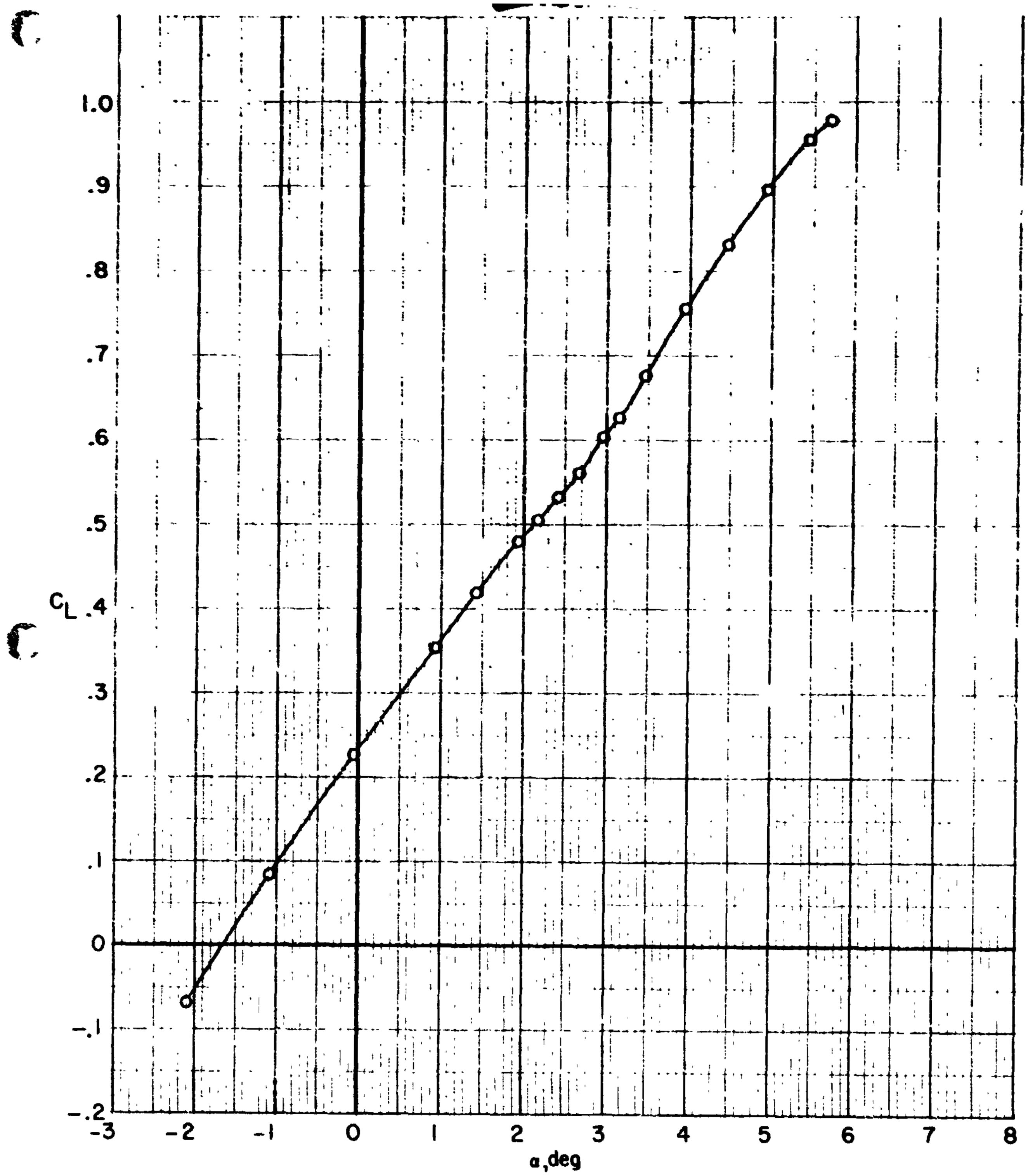

(b) M = 0.75.

Figure 14.- Continued.

[redacted]

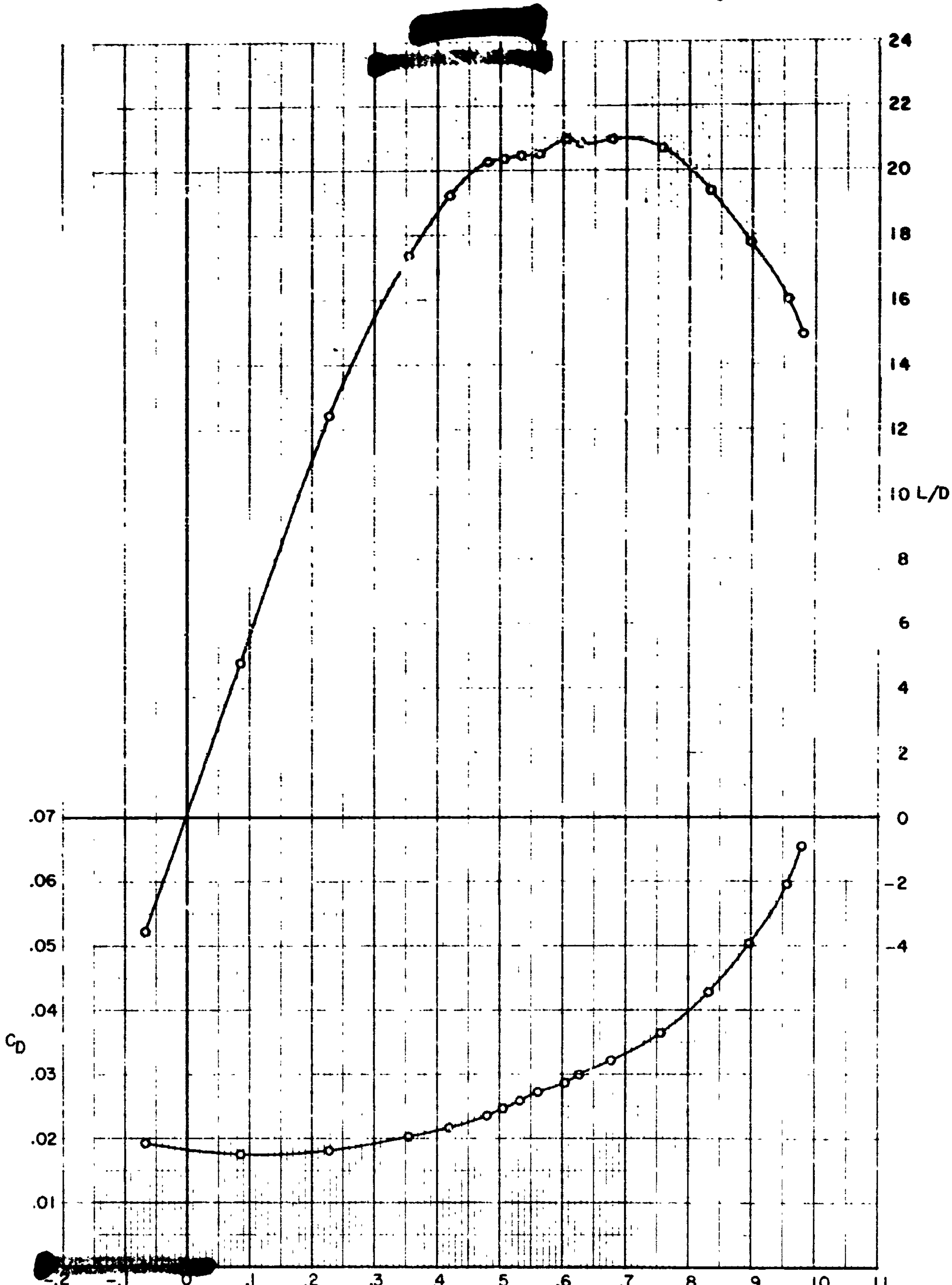

(b) M = 0.75. Continued.

Figure 14.- Continued.

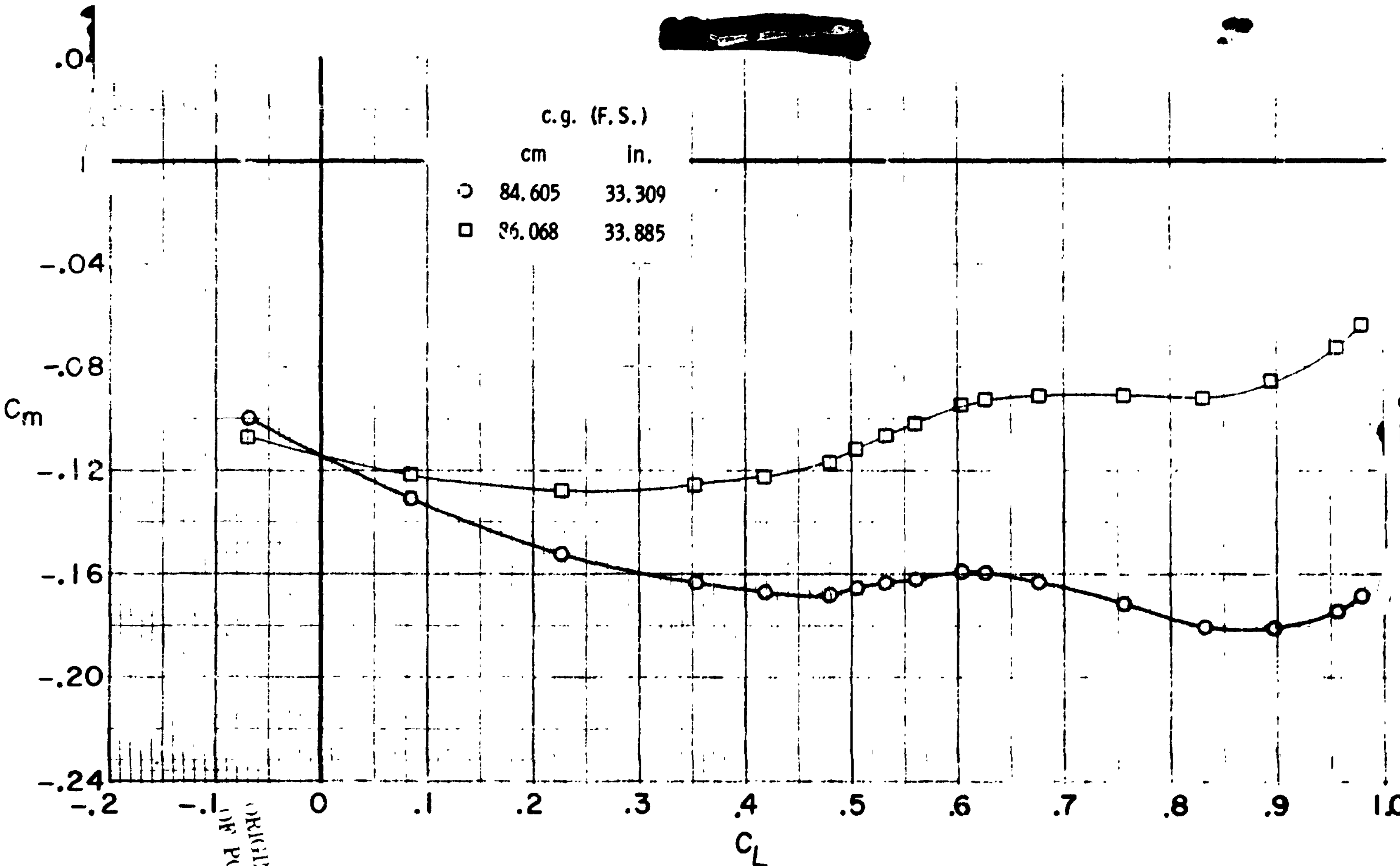

(b) M = 0.75. Concluded.

Figure 14. - Continued.

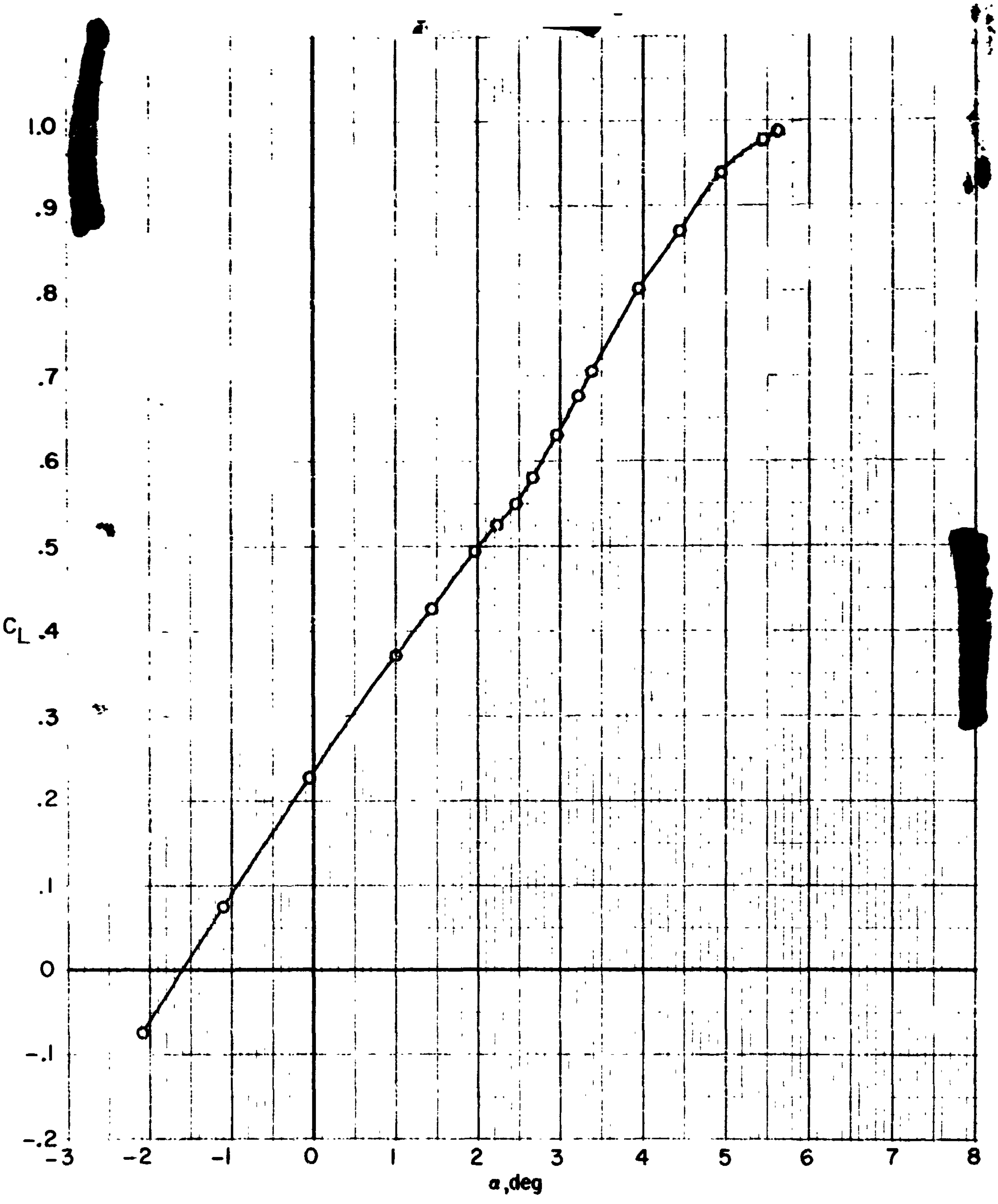

(c) M = 0.77.

Figure 14. - Continued.

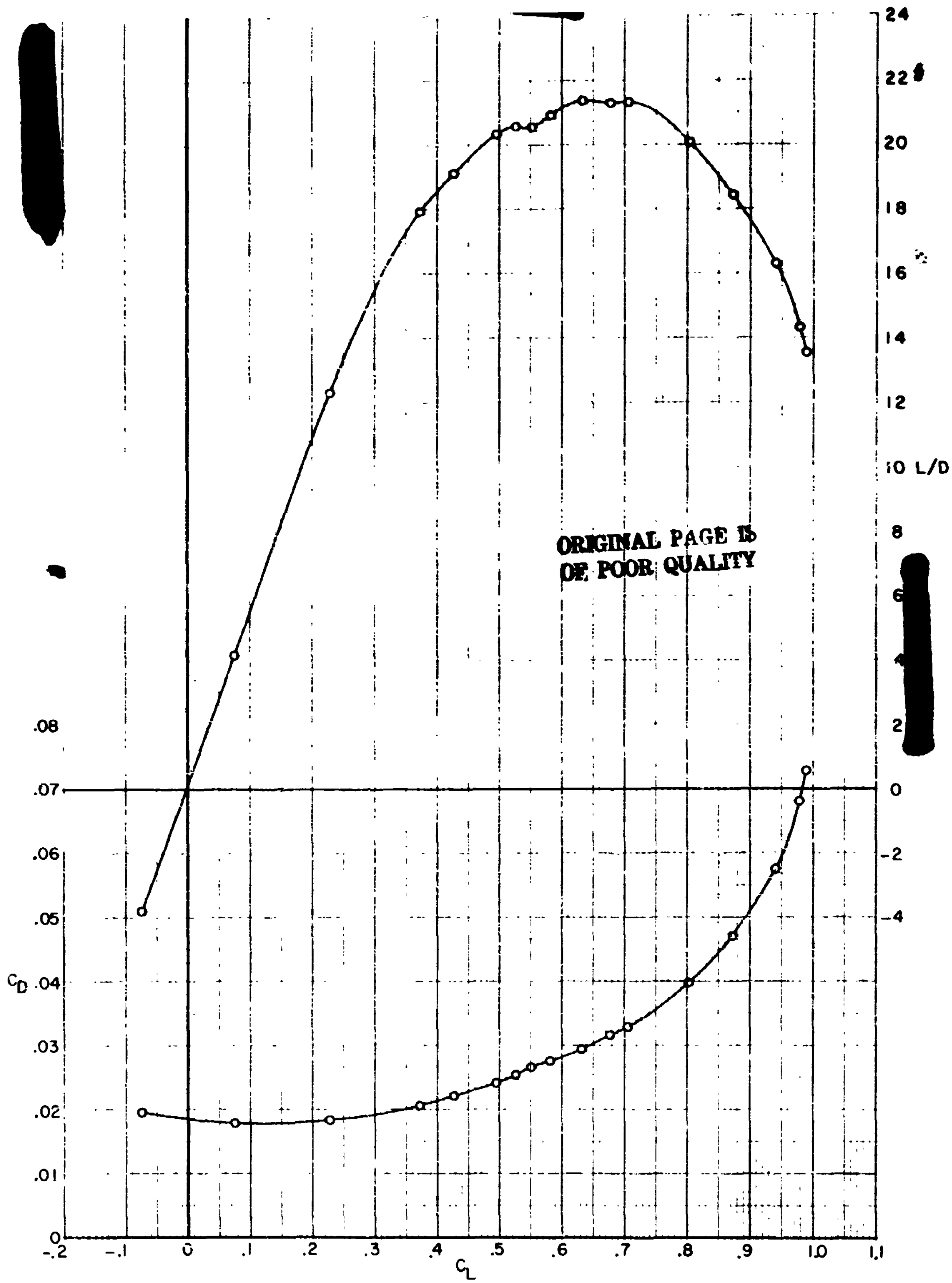

(c) M = 0.77. Continued.

Figure 14. - Continued.

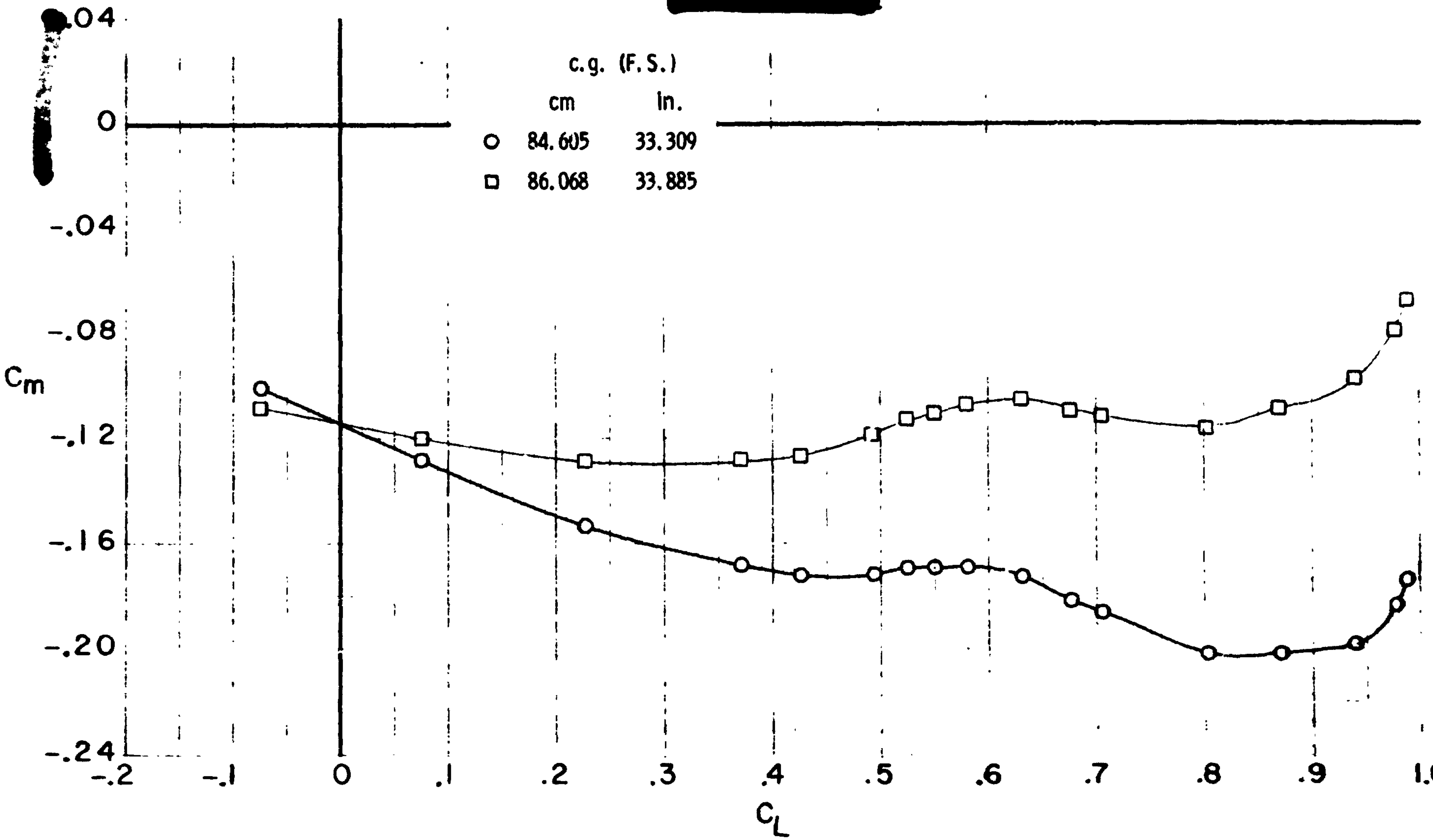

(c) M = 0.77. Concluded.

Figure 14. - Continued.

ORIGINAL PAGE IS
OF POOR QUALITY

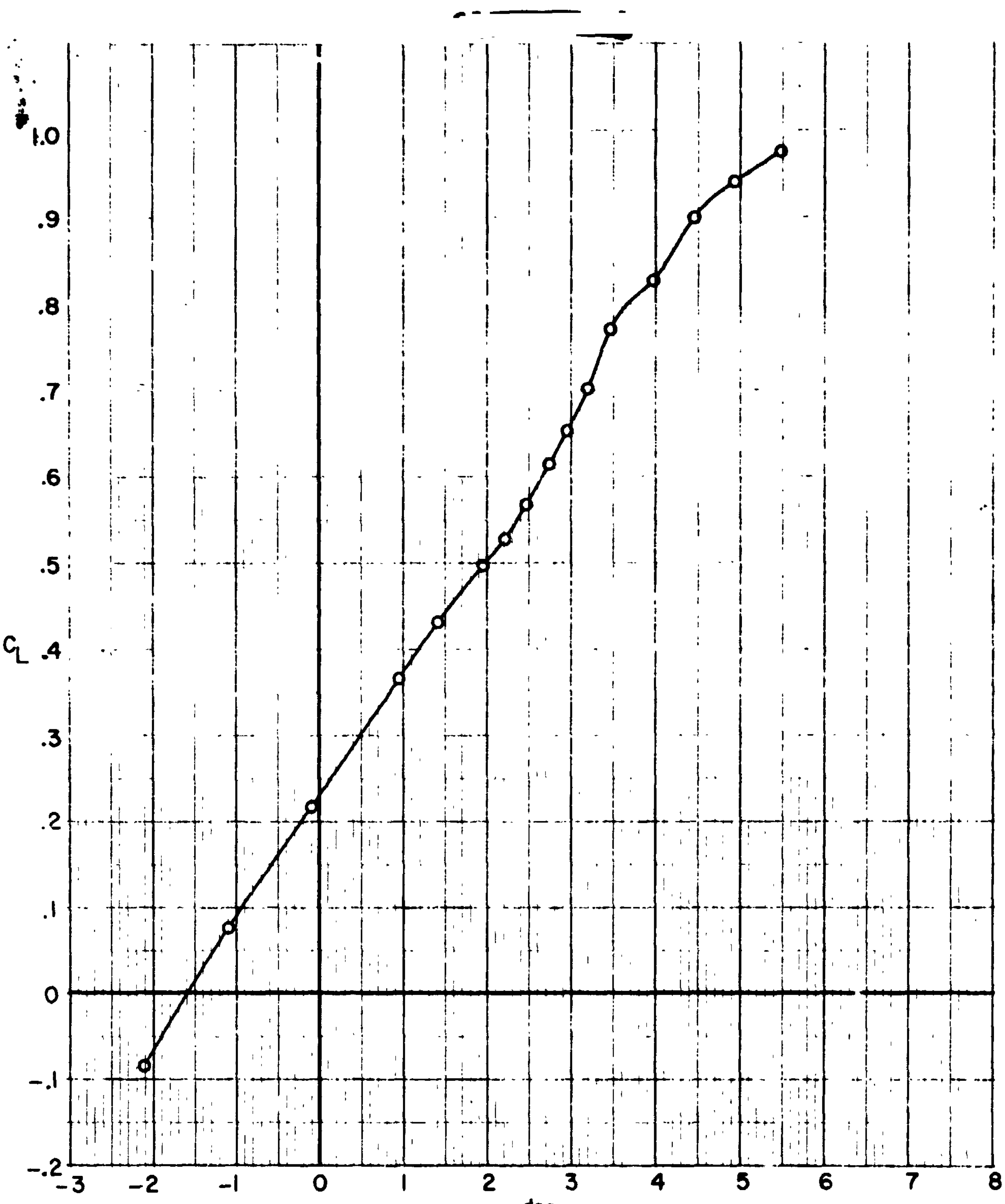

(d) M = 0.78.

Figure 14. - Continued.

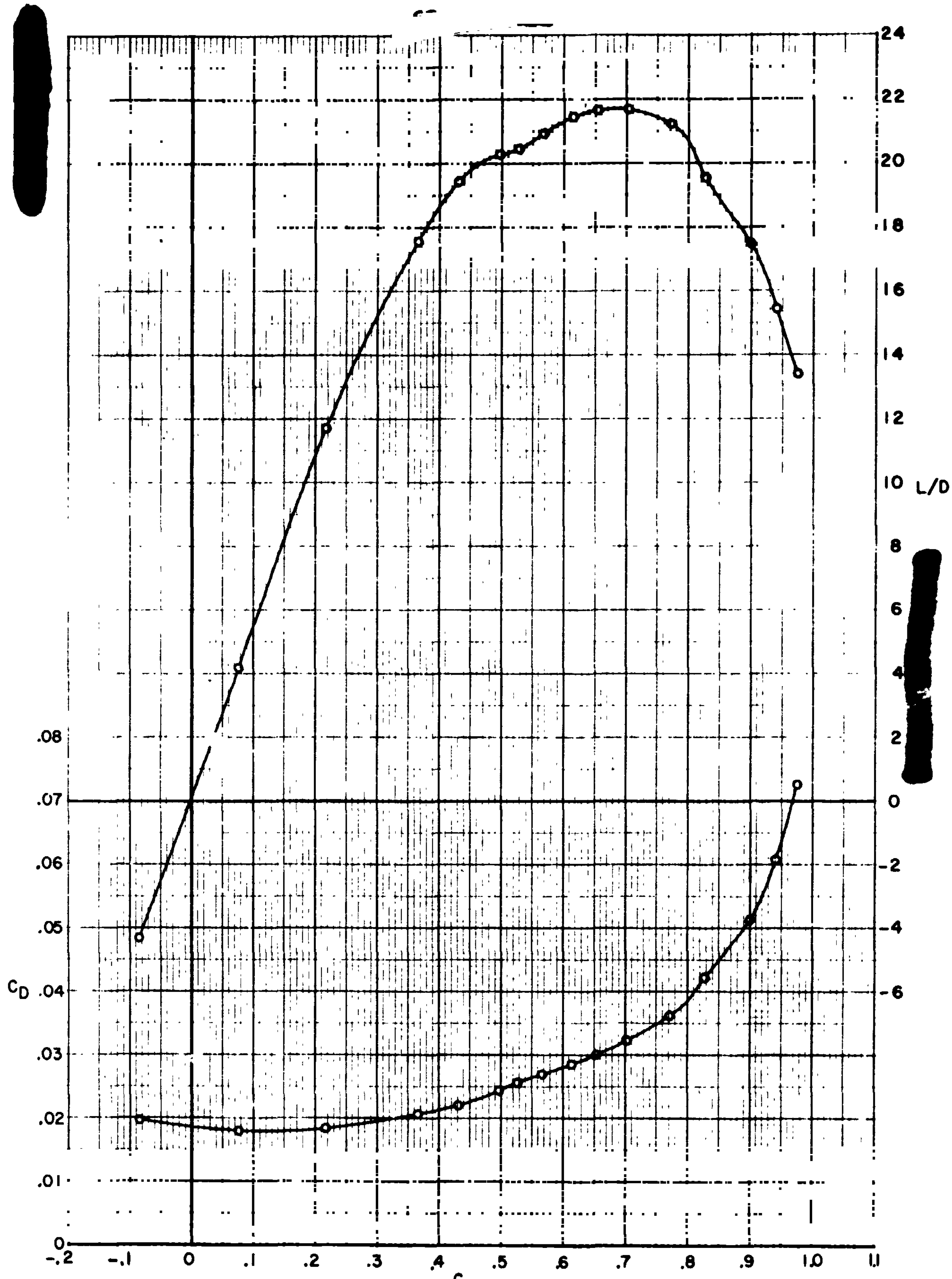

(d) M = 0.78. Continued.

Figure 14.- Continued.

[redacted]

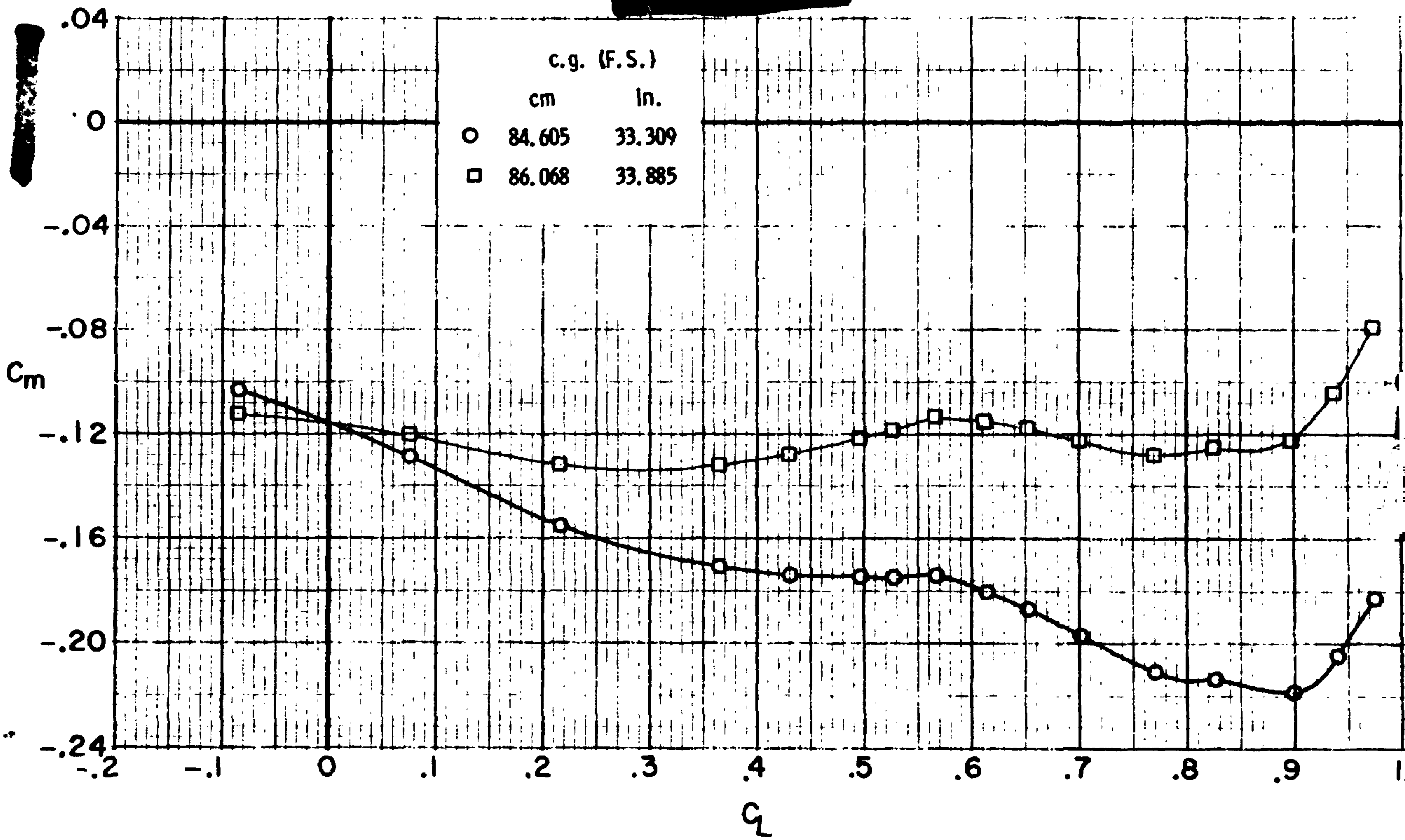

ORIGINAL PAGE IS OF POOR QUALITY

(d) M = 0.78. Concluded.

Figure 14. - Continued.

[redacted]

M= 0.79

[redacted]

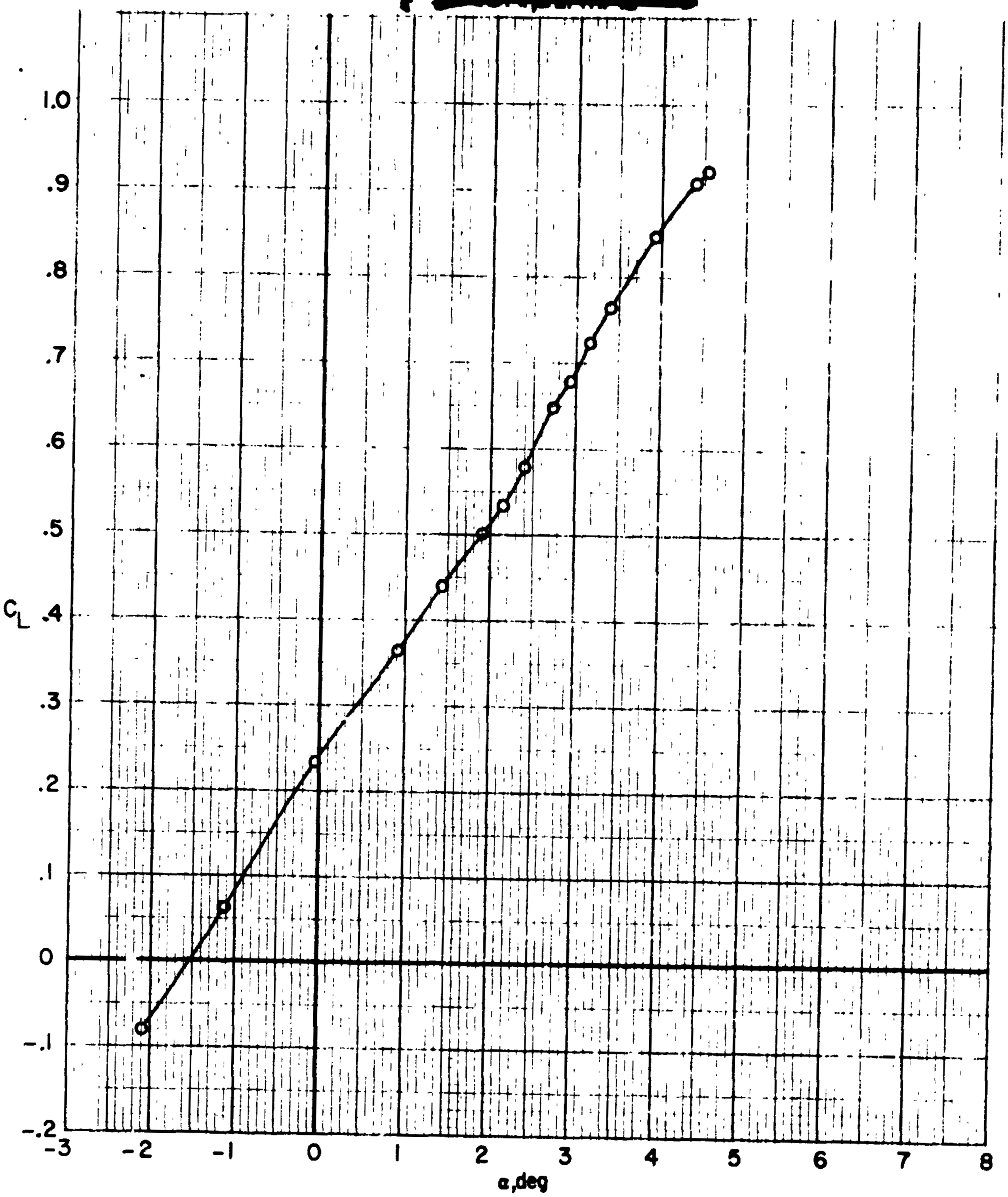

(e) $M = 0.79$.

Figure 14.- Continued.

ORIGINAL PAGE IS
OF POOR QUALITY

[redacted]

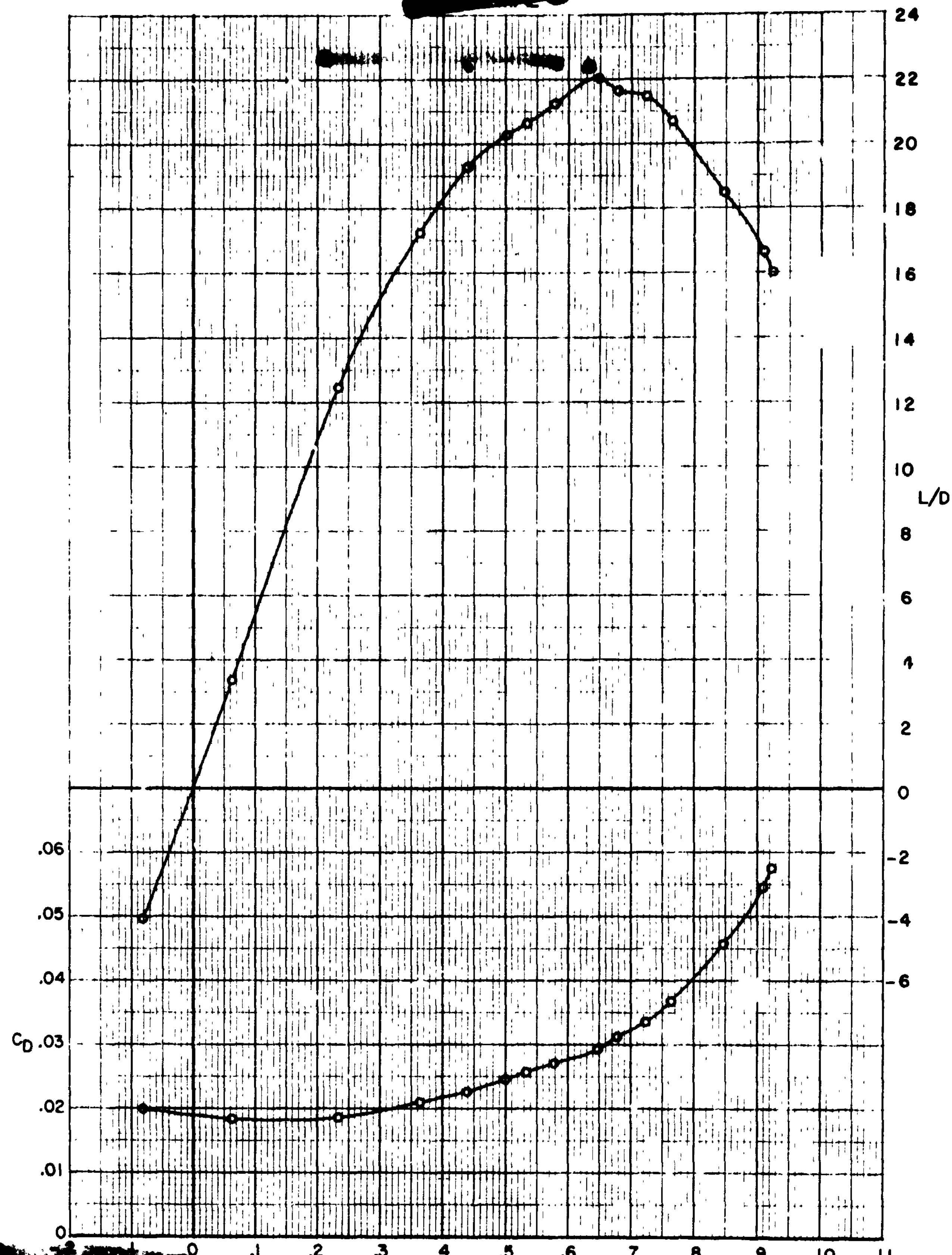

[redacted]

(e) M = 0.79. Continued.

Figure 14. - Continued.

[redacted]

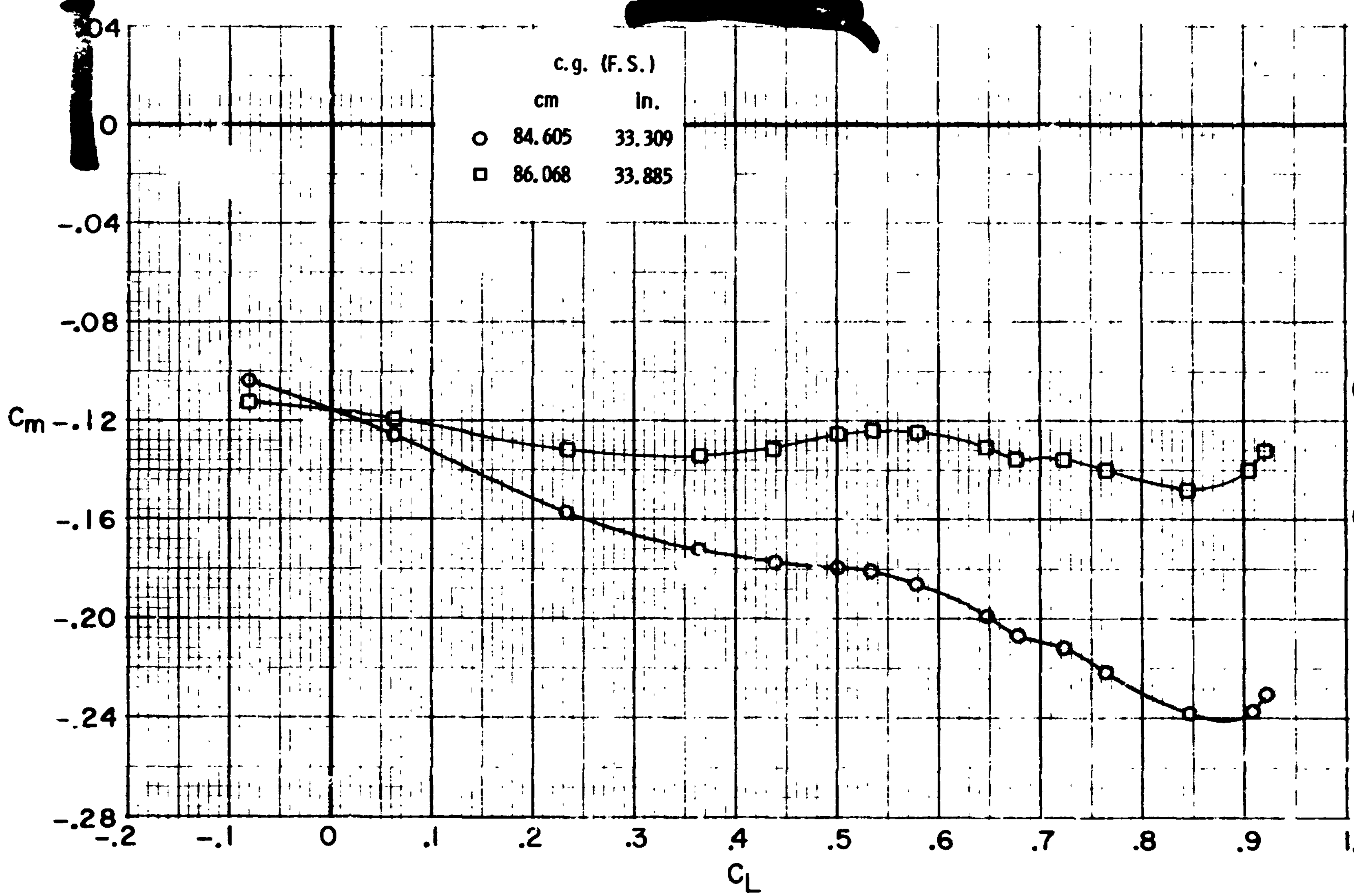

(e) M = 0.79. Concluded.

Figure 14.- Continued.

[redacted]

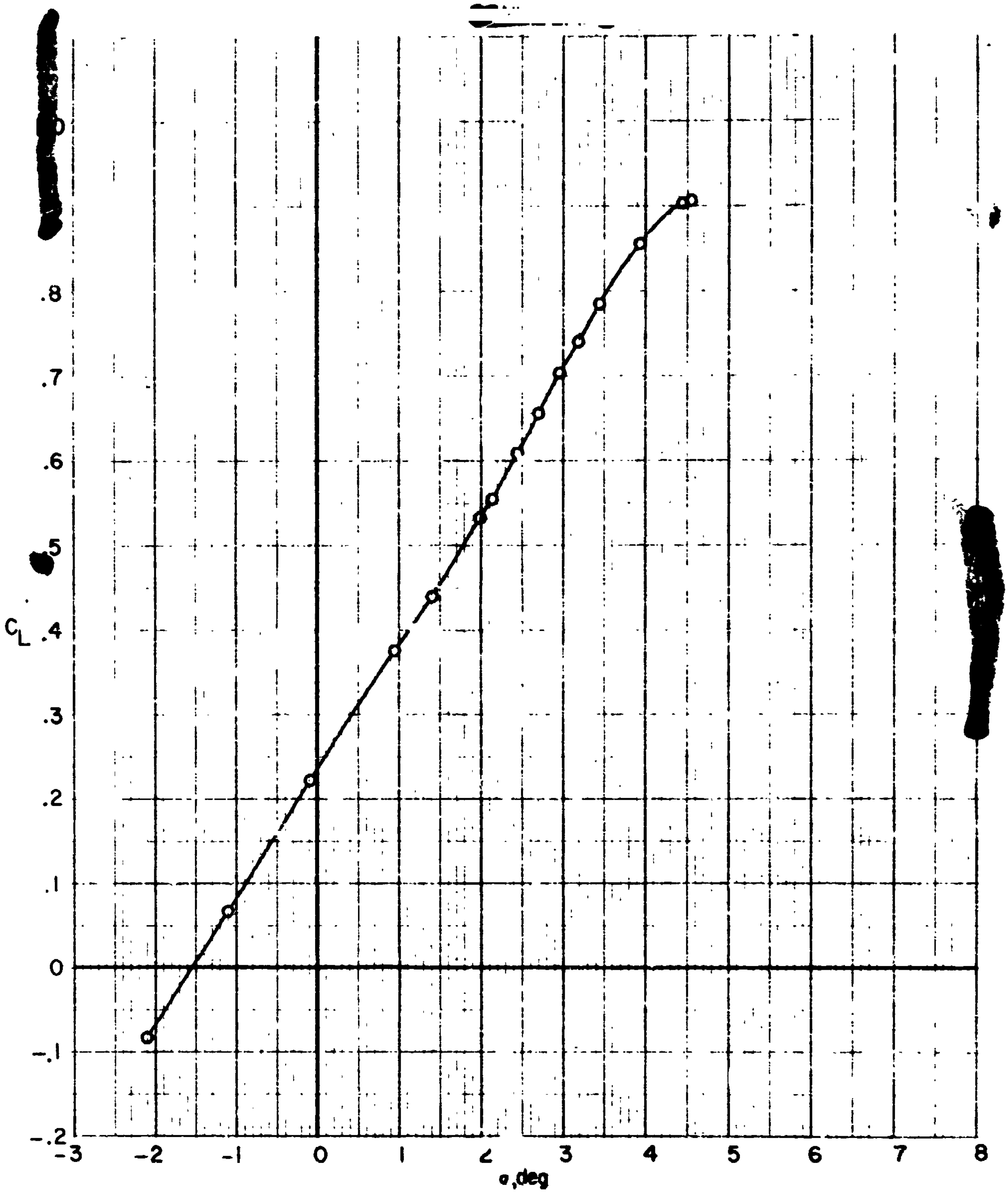

(f) M = 0.80.

Figure 14.- Contd.

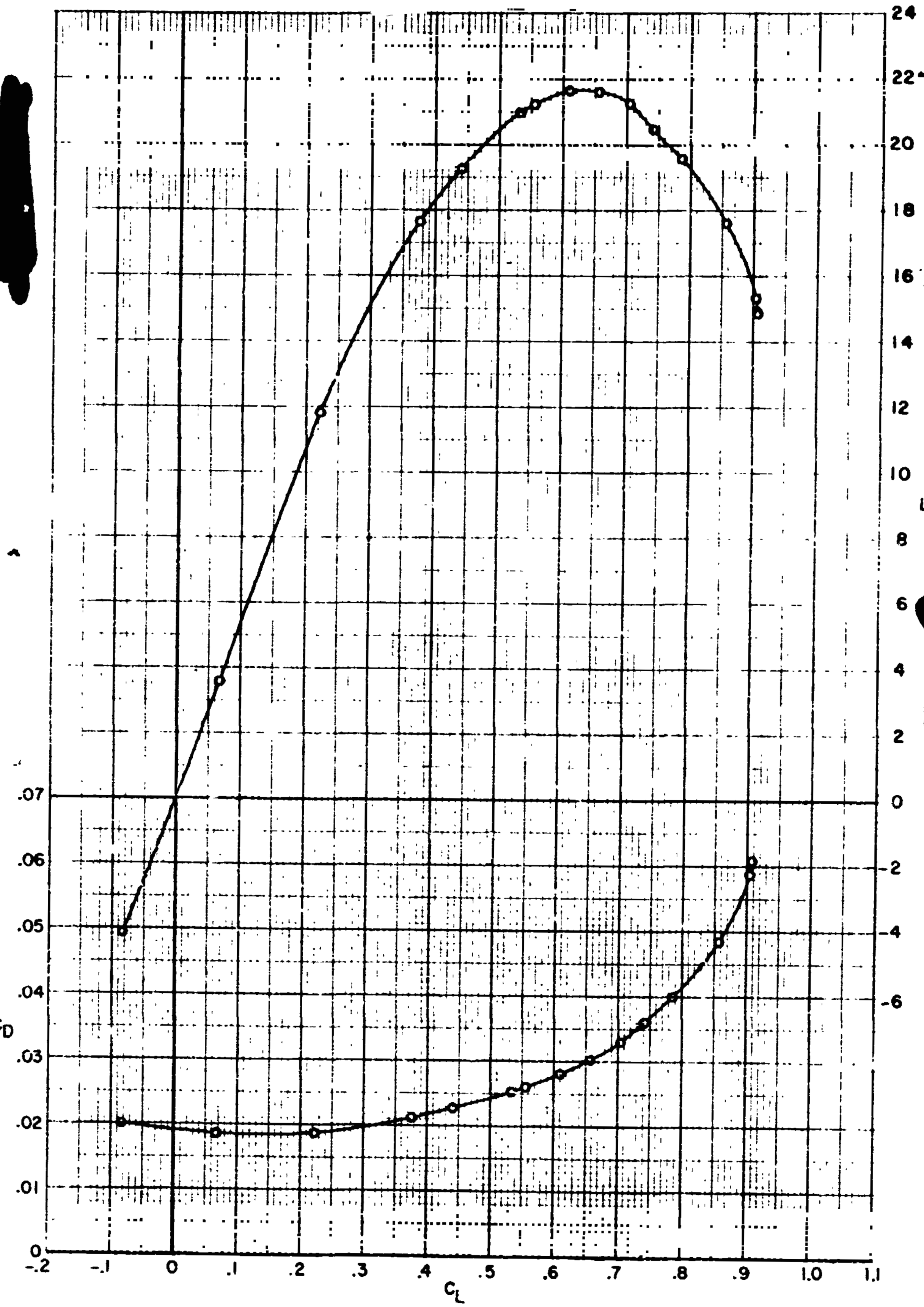

(f) M = 0.80. Continued.

Figure 14. - Continued.

[redacted]

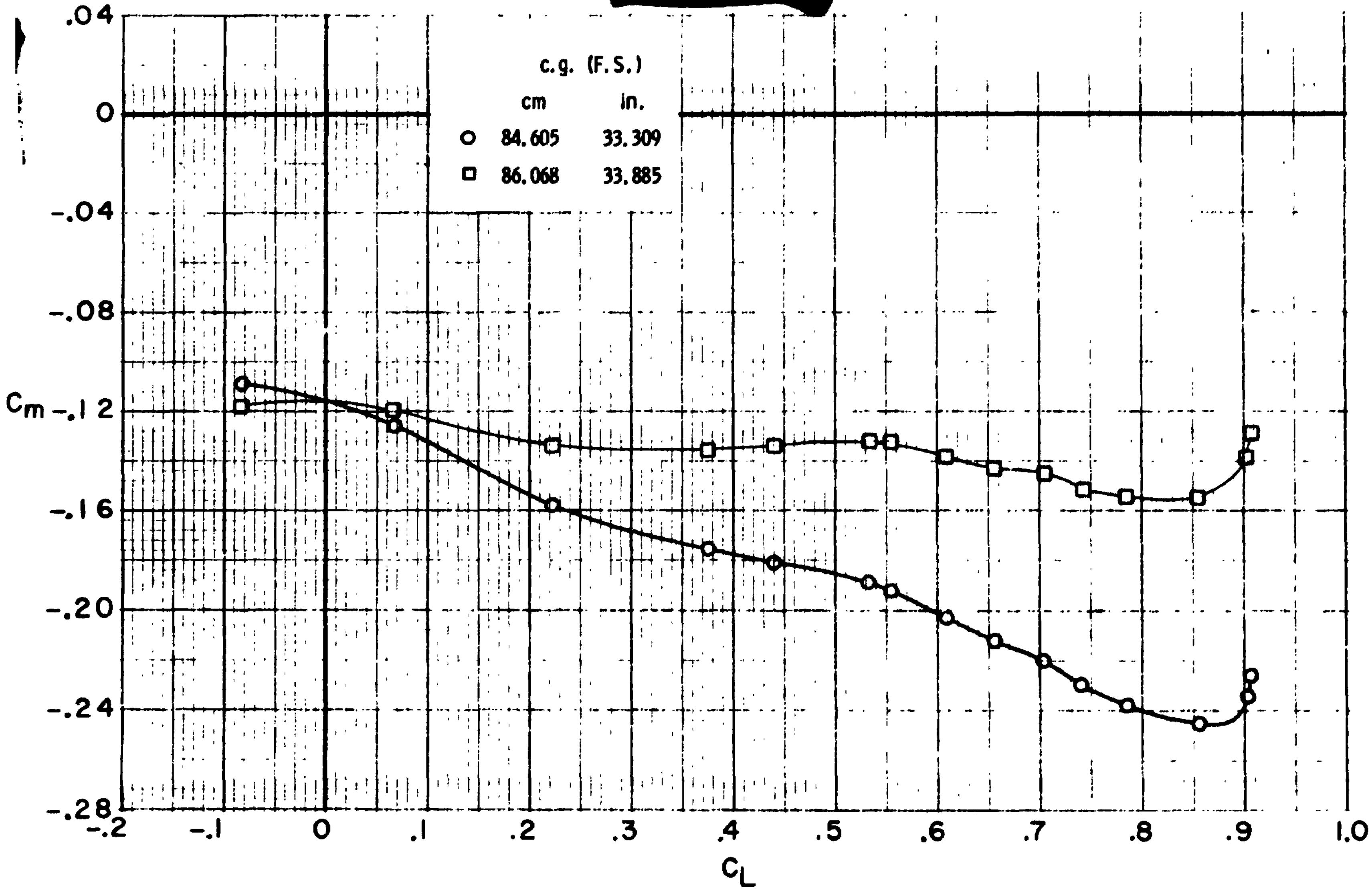

(f) M = 0.80. Concluded.

Figure 14. - Continued.

[redacted]

ORIGINAL PAGE IS
OF POOR QUALITY

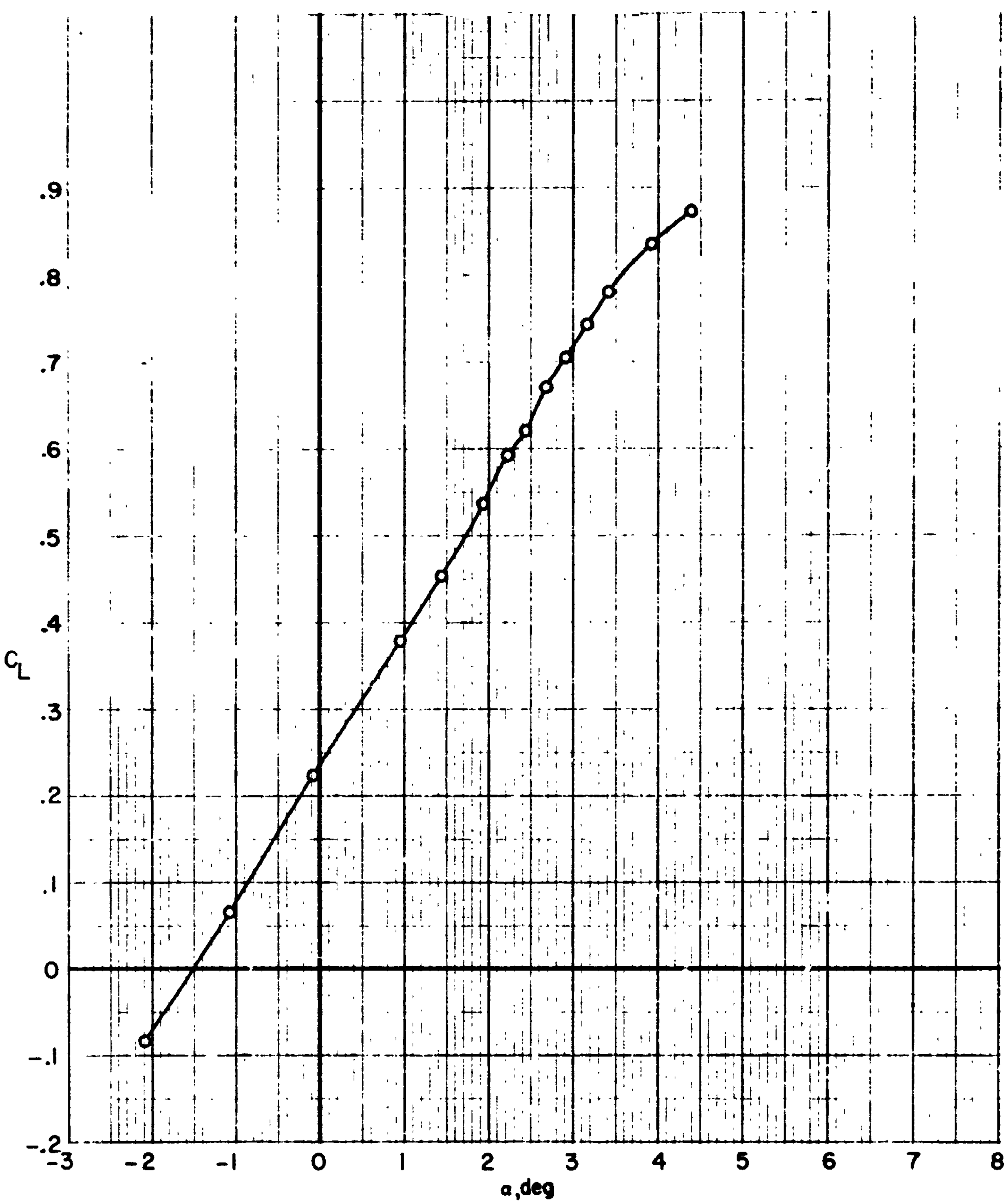

(g) M = 0.81.

Figure 14.- Continued.

[redacted]

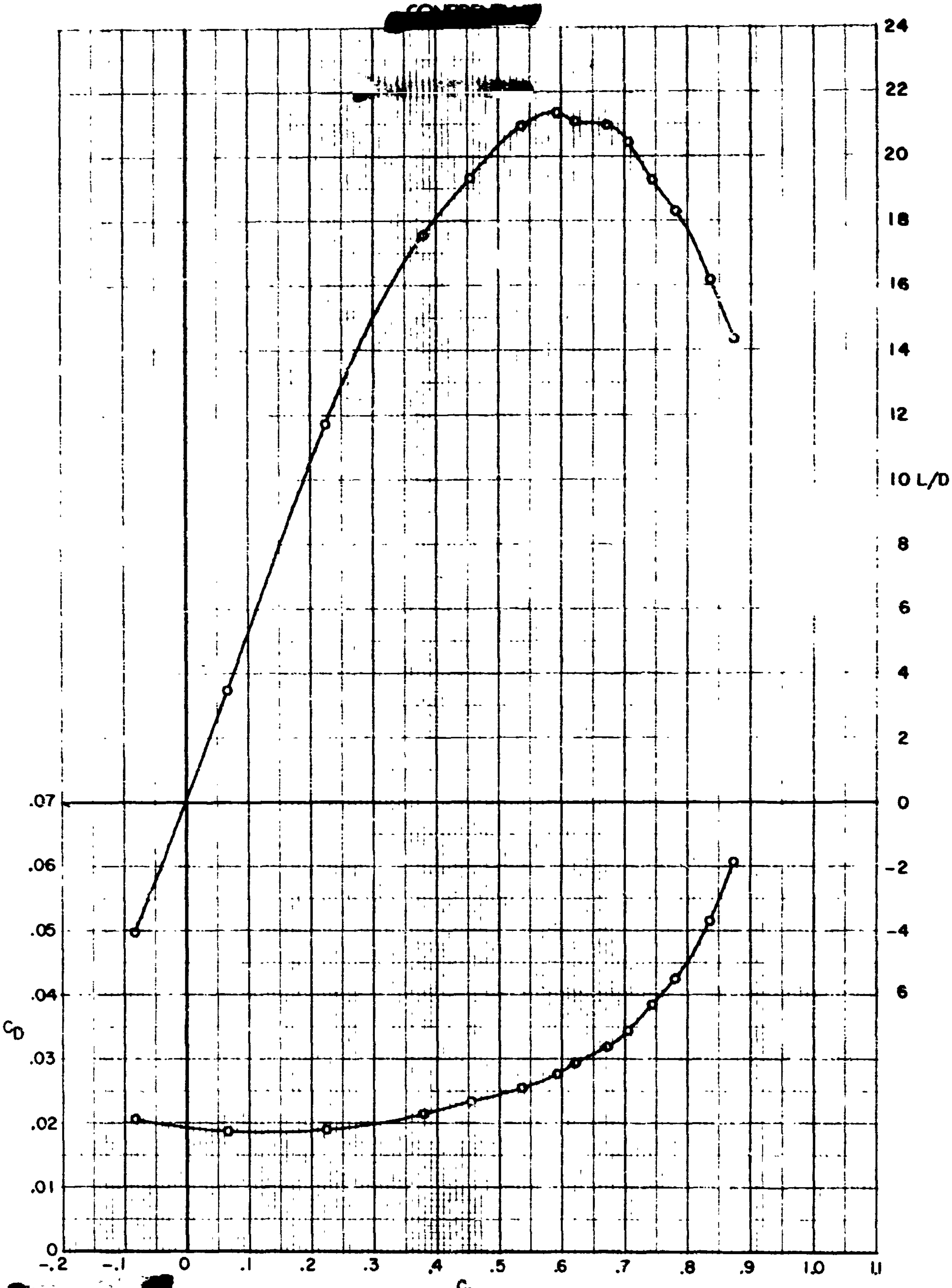

(g) M = 0.81. Continued.

Figure 14. - Continued.

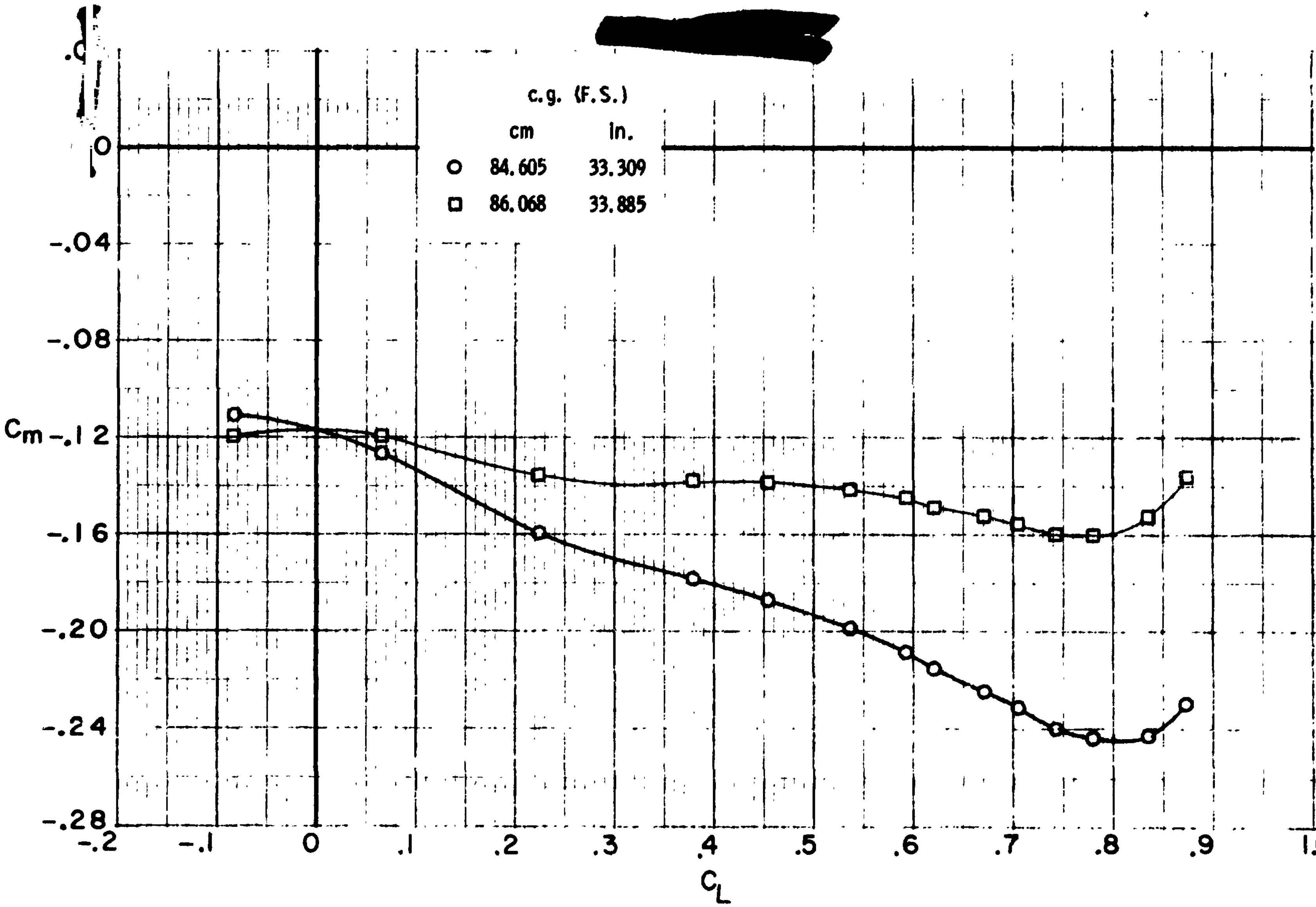

(g) M = 0.81. Concluded.

Figure 14.- Continued.

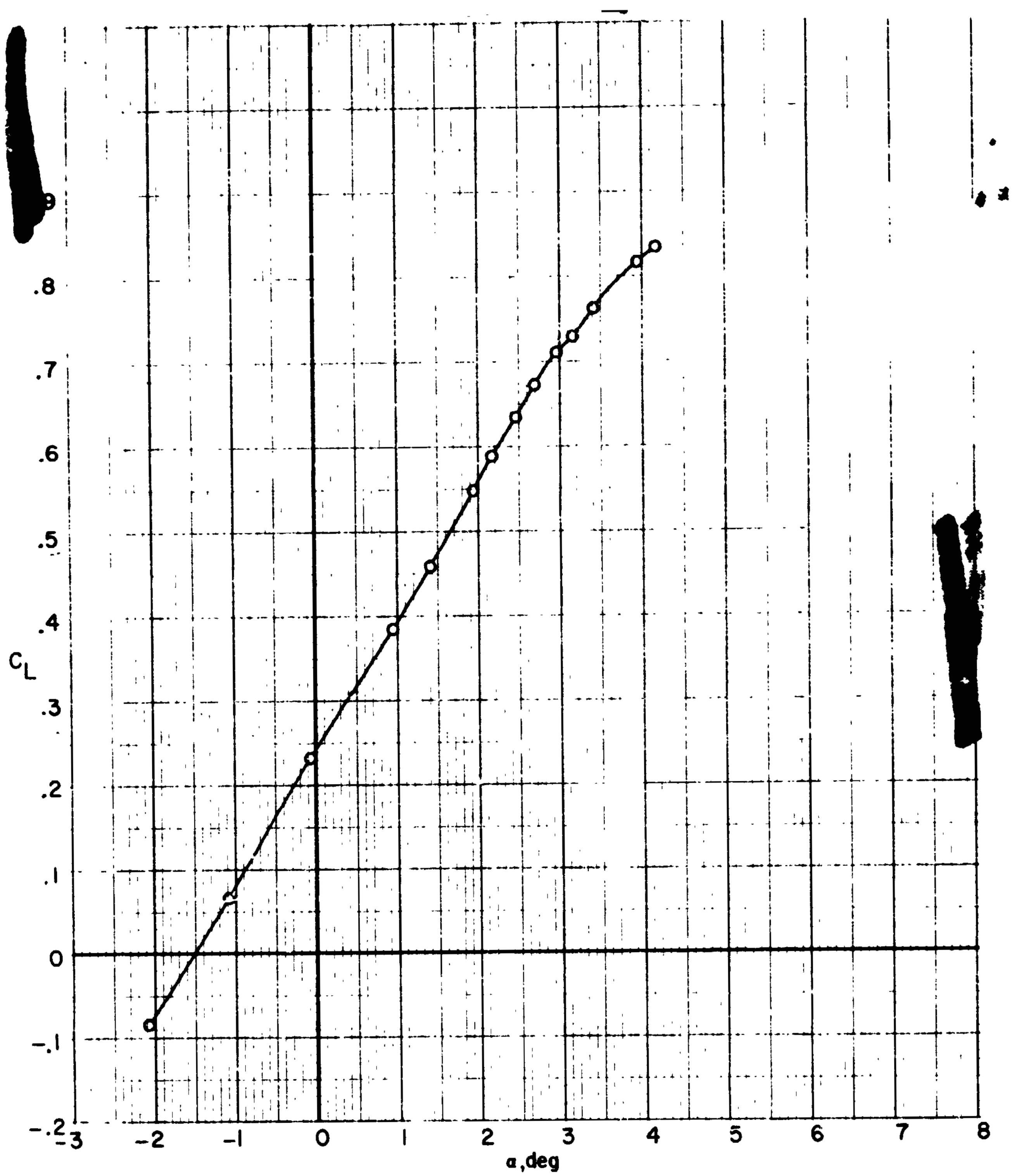

(h) $M = 0.82$.

Figure 14.- Continued.

ORIGINAL PAGE IS
OF POOR QUALITY

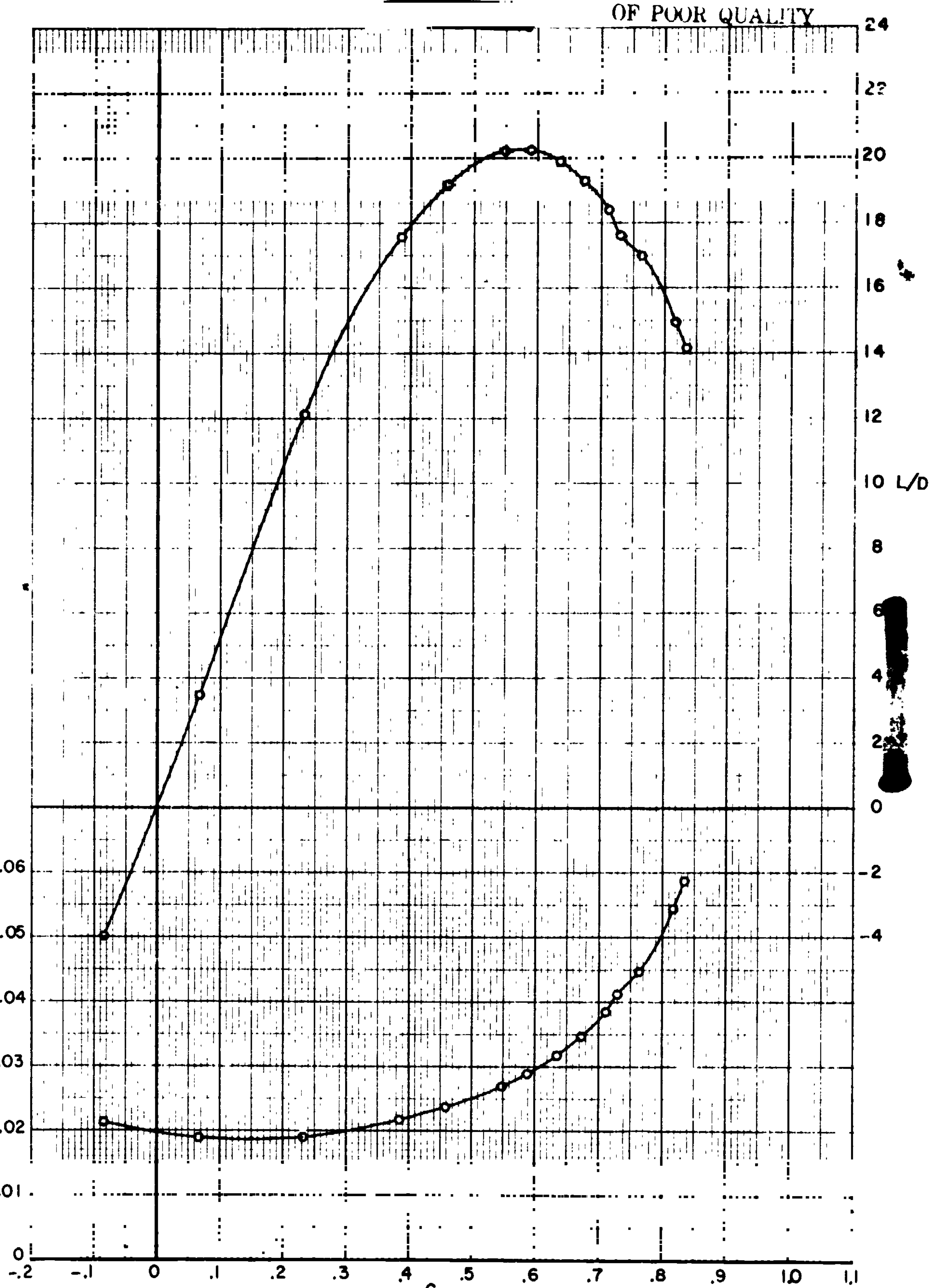

(h) M = 0.82. Continued.

Figure 14.- Continued.

[redacted]

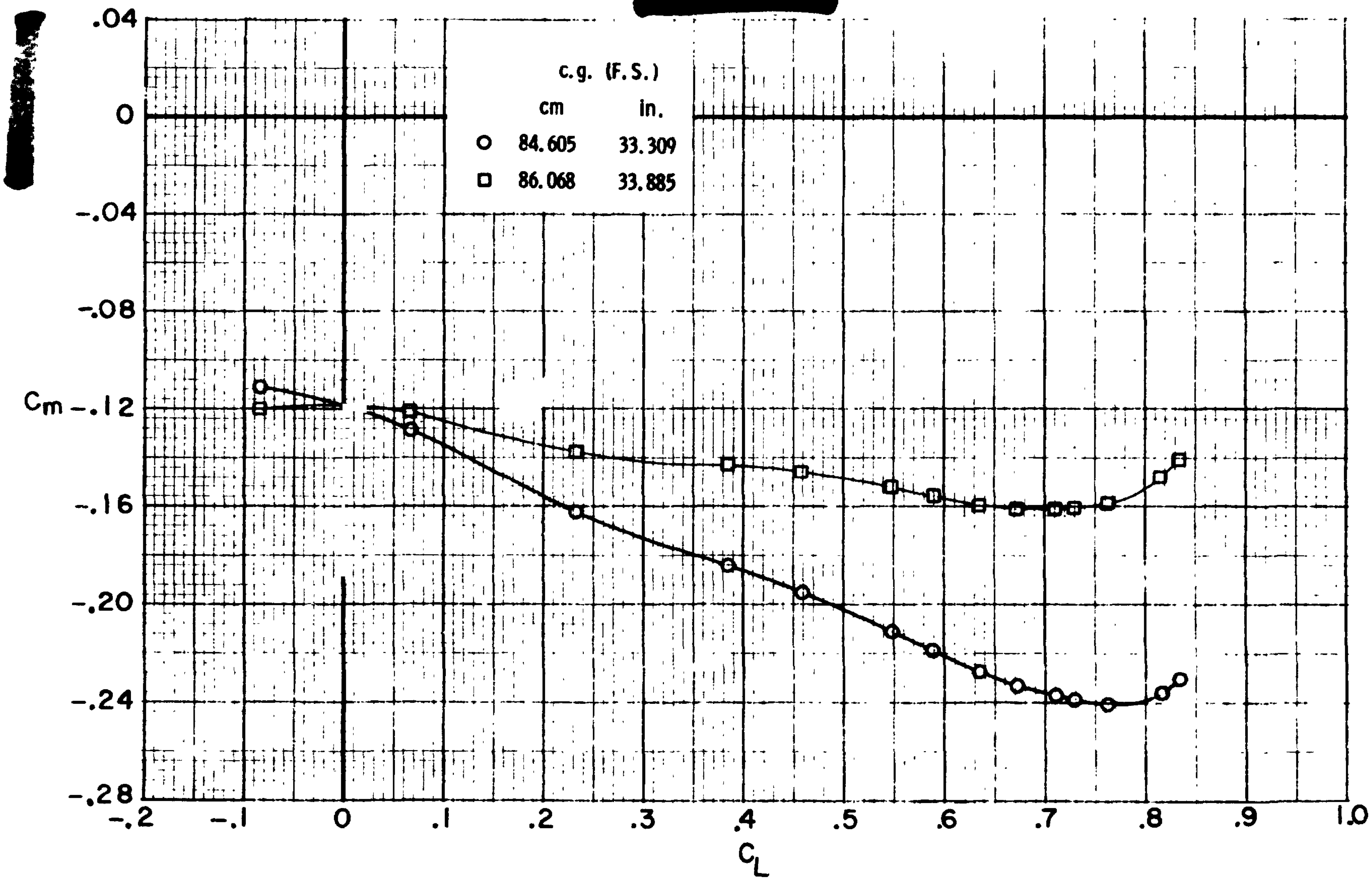

(h) M = 0.82. Concluded.

Figure 14. - Continued.

[redacted]

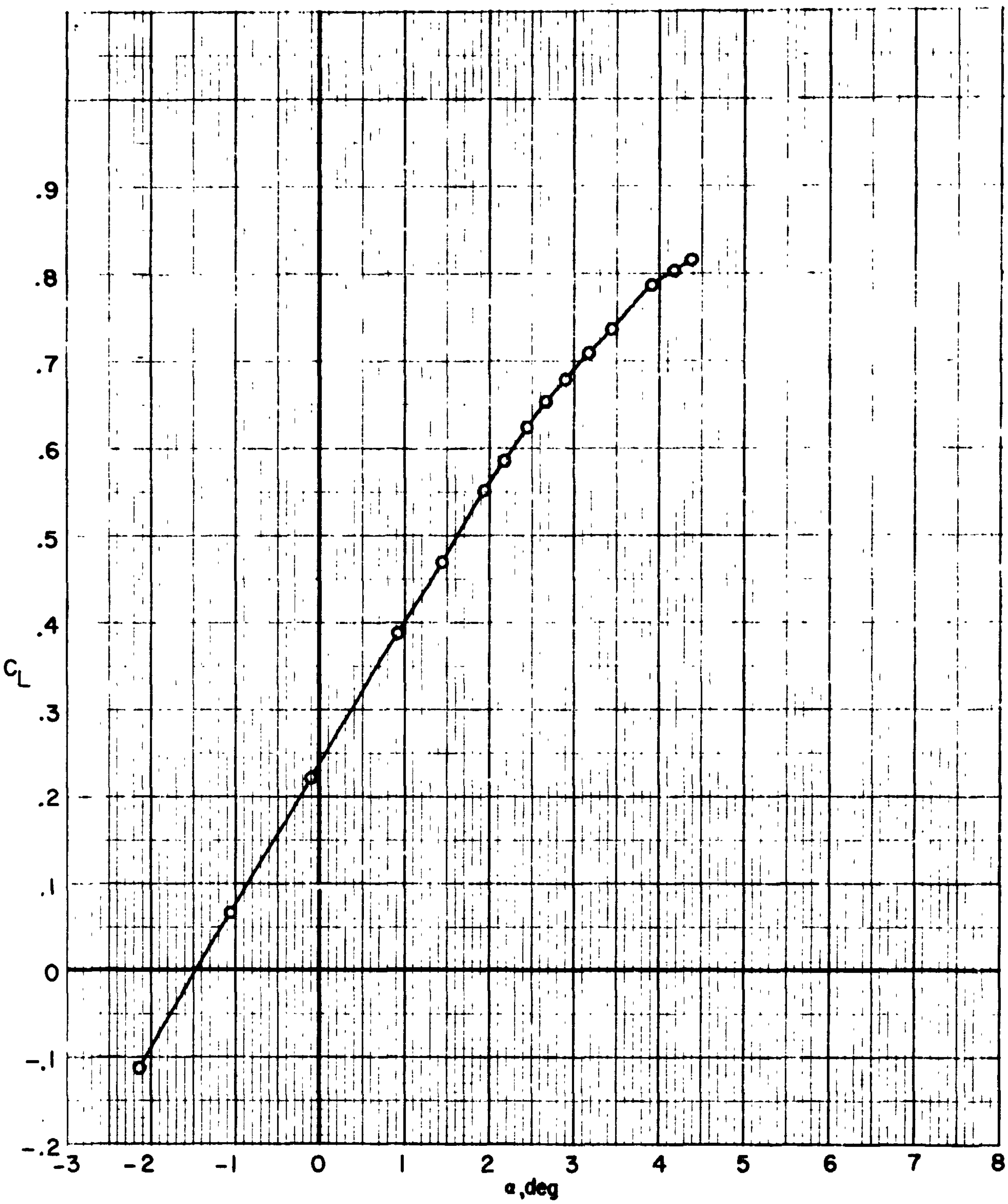

(l) M = 0.83.

Figure 14.- Continued.

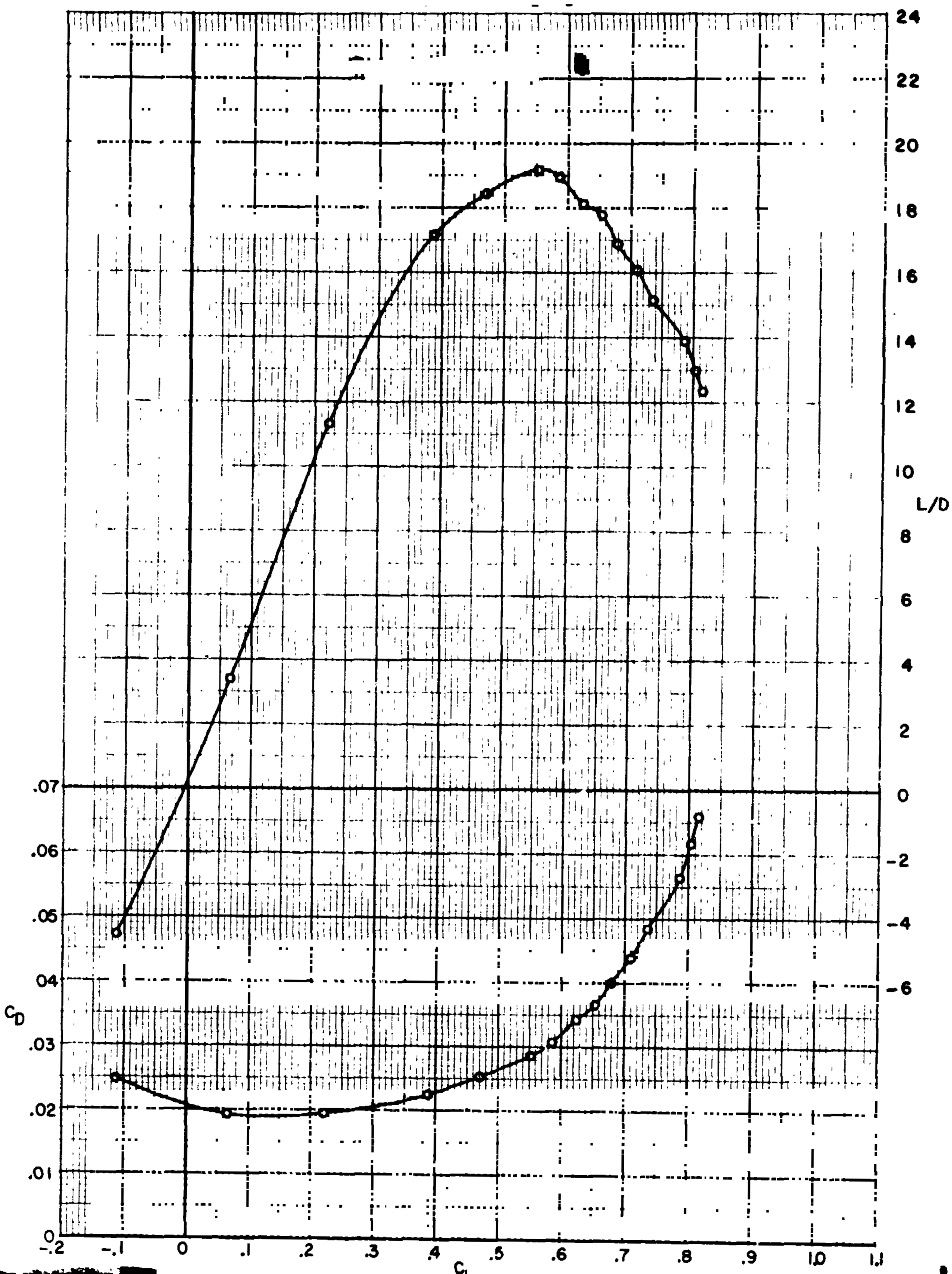

(l) M = 0.83. Continued.

Figure 14. - Continued.

[redacted]

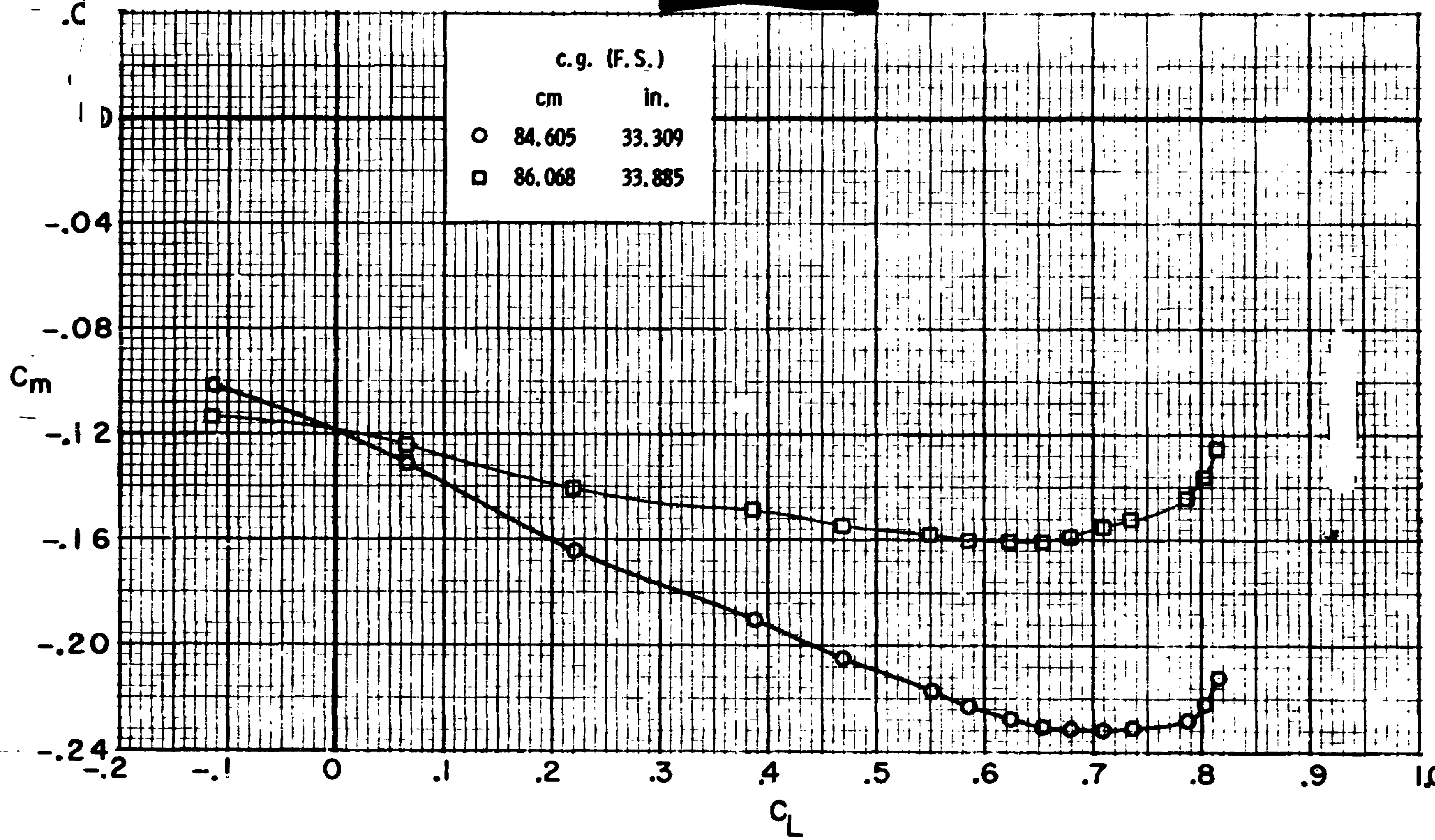

ORIGINAL PAGE IS
OF POOR QUALITY

(i) M = 0.83. Concluded.

Figure 14. - Concluded.

[redacted]

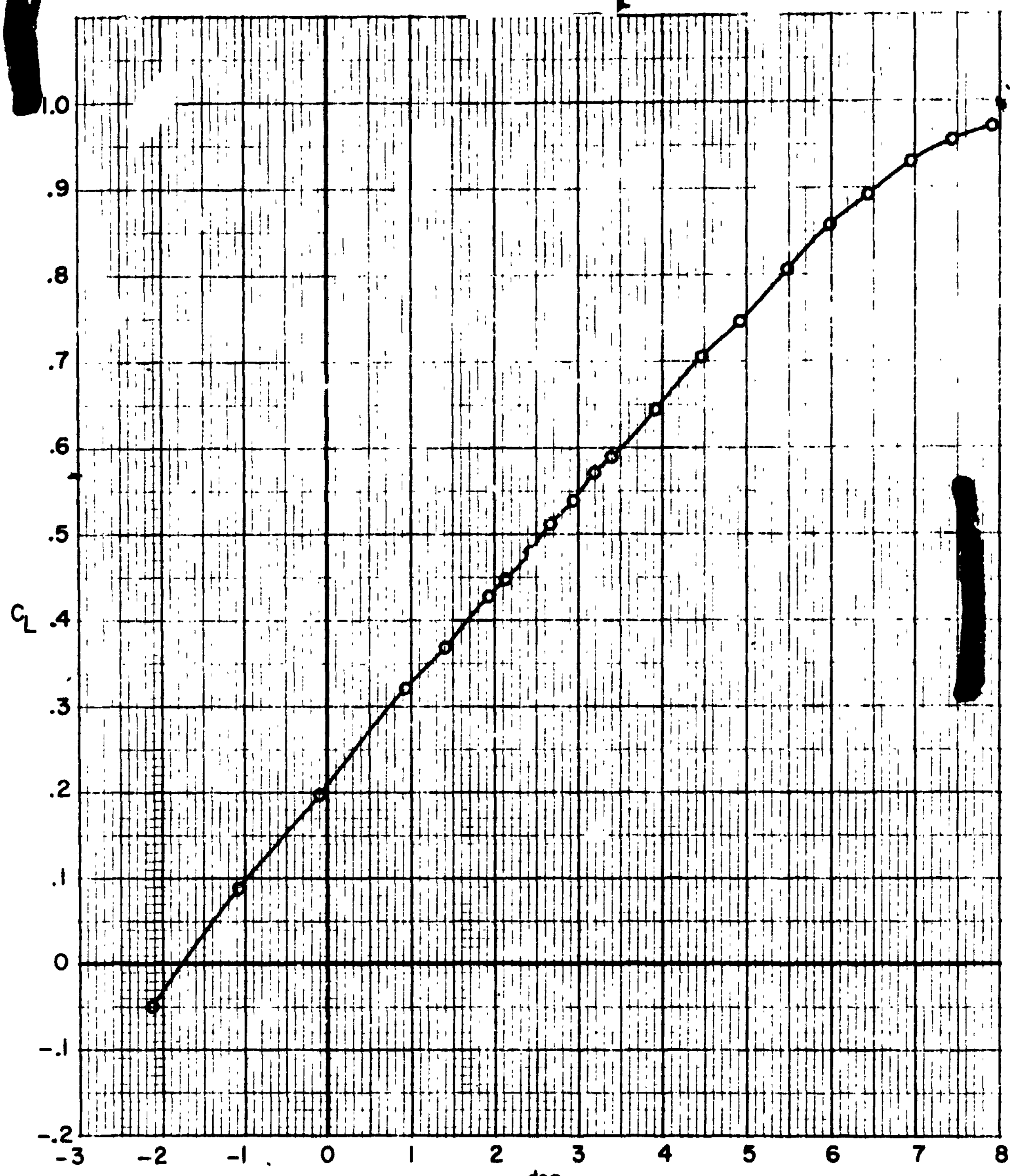

(a) M = 0.60.

Figure 15.- Longitudinal aerodynamic characteristics for supercritical wing configuration 2b (SCW-2b) with wing upper surface grit forward ($x_T/c = 0.05$). $\Lambda_{c/4} = 30°$.

ORIGINAL PAGE IS OF POOR QUALITY

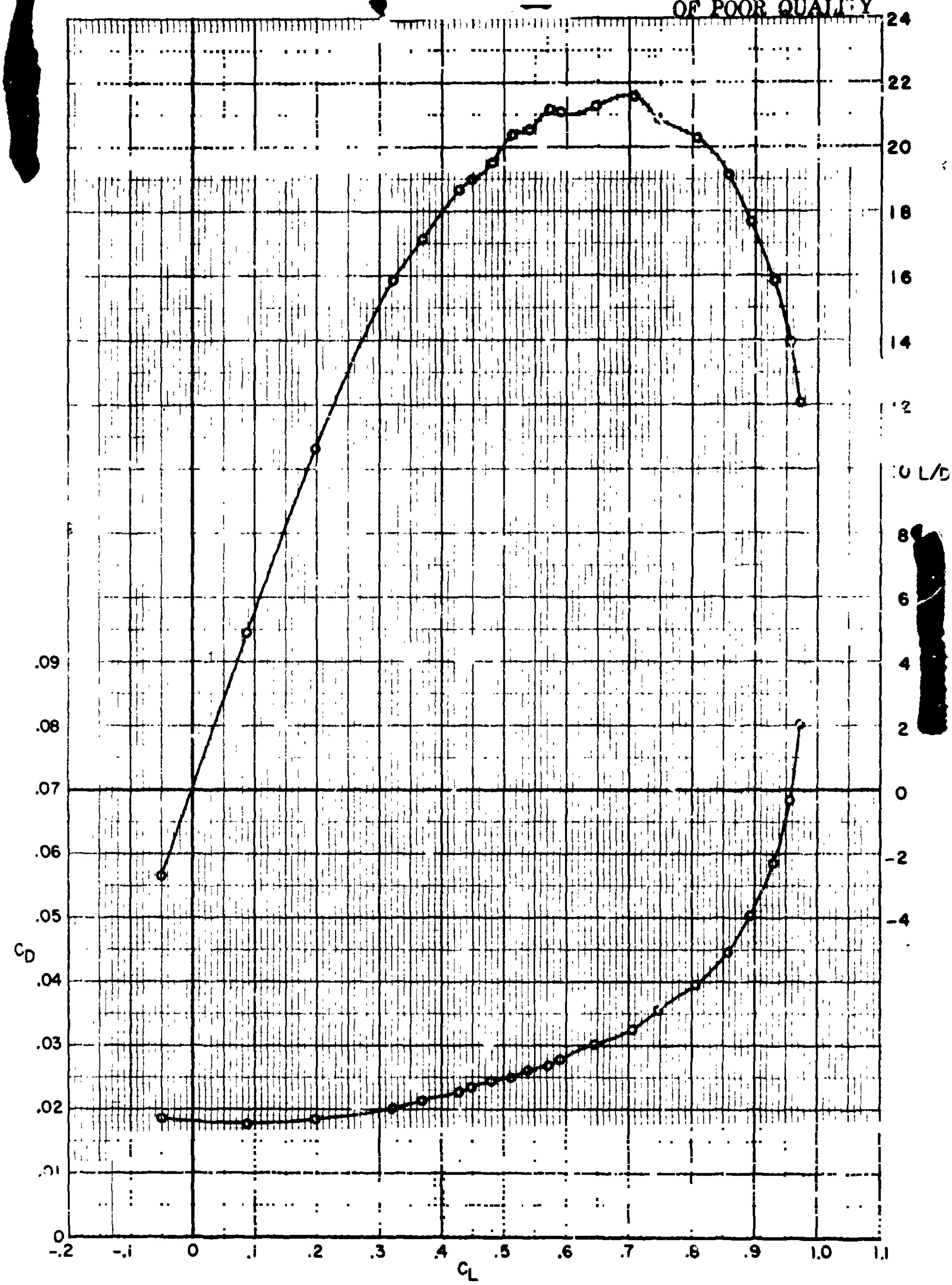

(a) M = 0.60, Continued.

Figure 15.- Continued.

[redacted]

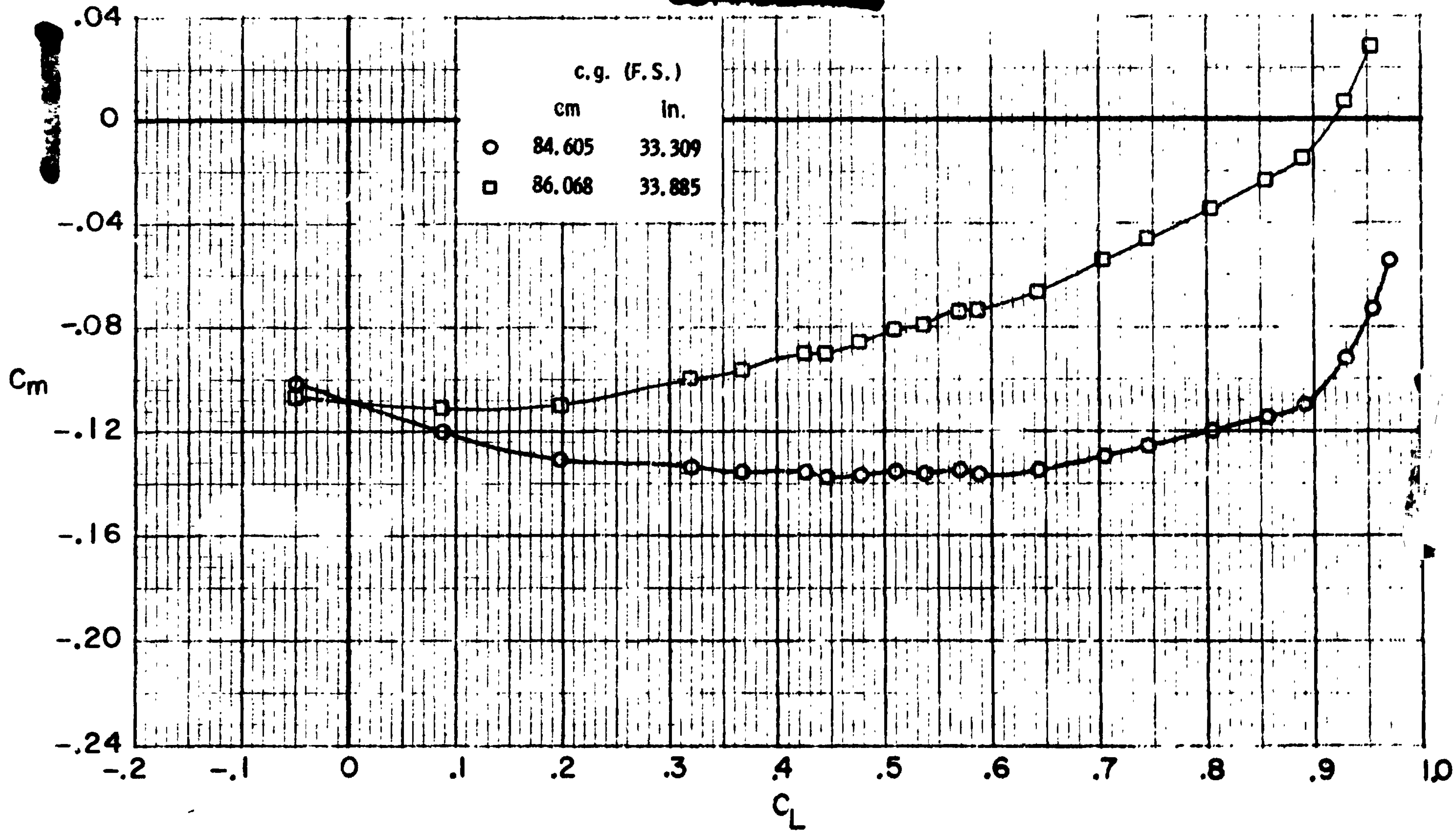

(a) M = 0.60. Concluded.

Figure 15.- Continued.

[redacted]

ORIGINAL PAGE IS
OF POOR QUALITY

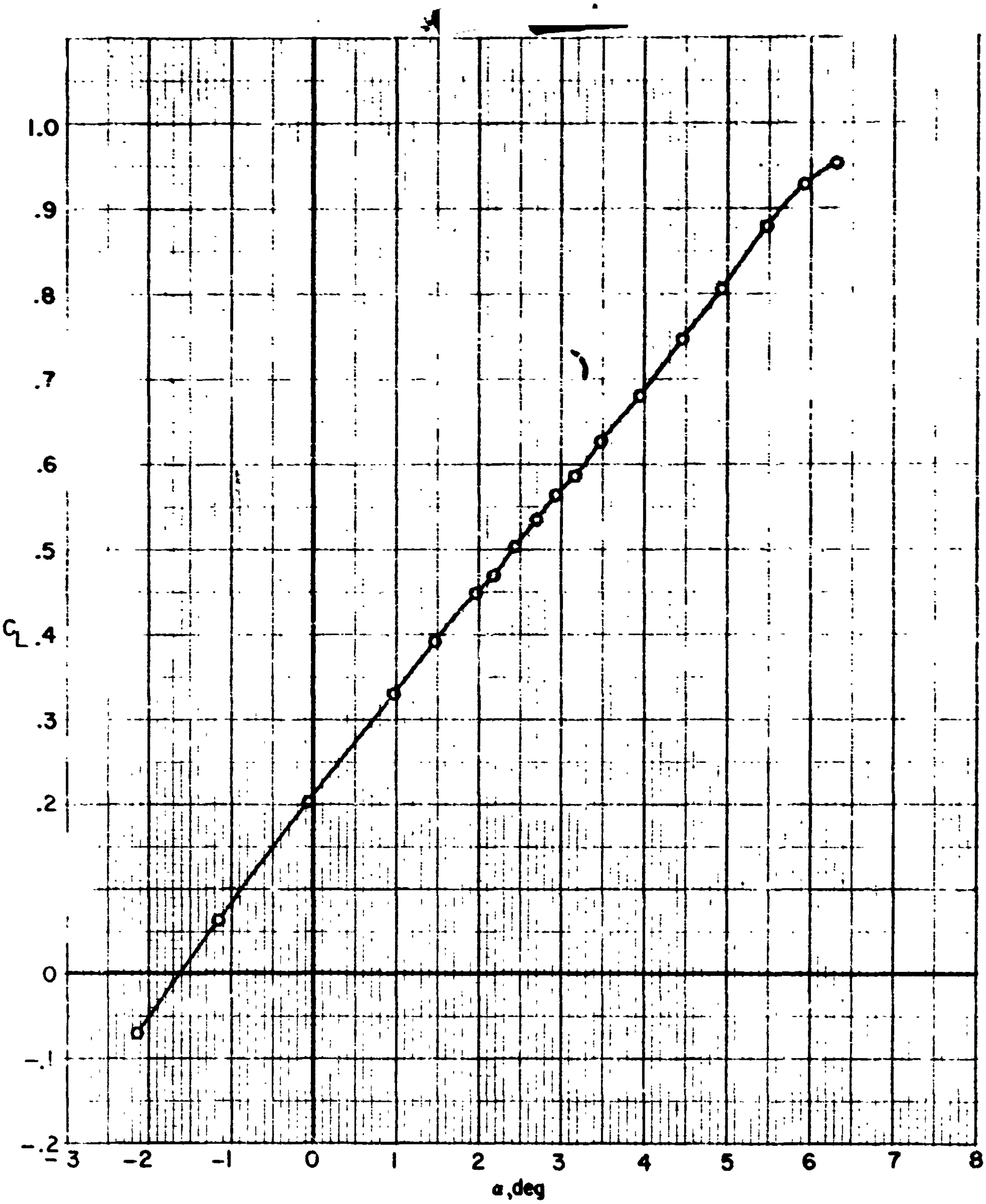

(b) M = 0.70.

Figure 15. - Continued.

ORIGINAL PAGE IS
OF POOR QUALITY

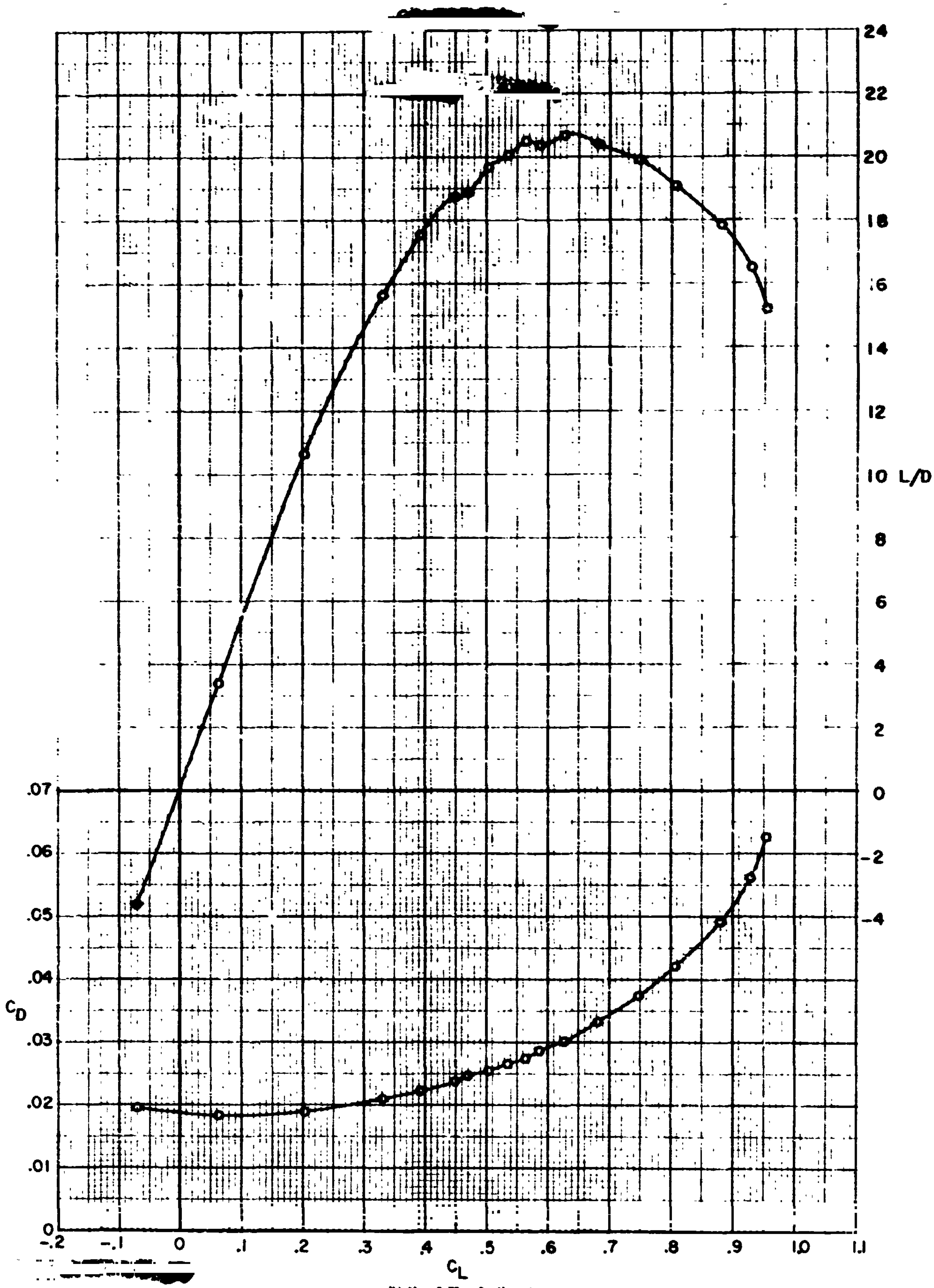

(b) M = 0.70. Continued.

Figure 15. - Continued.

[redacted]

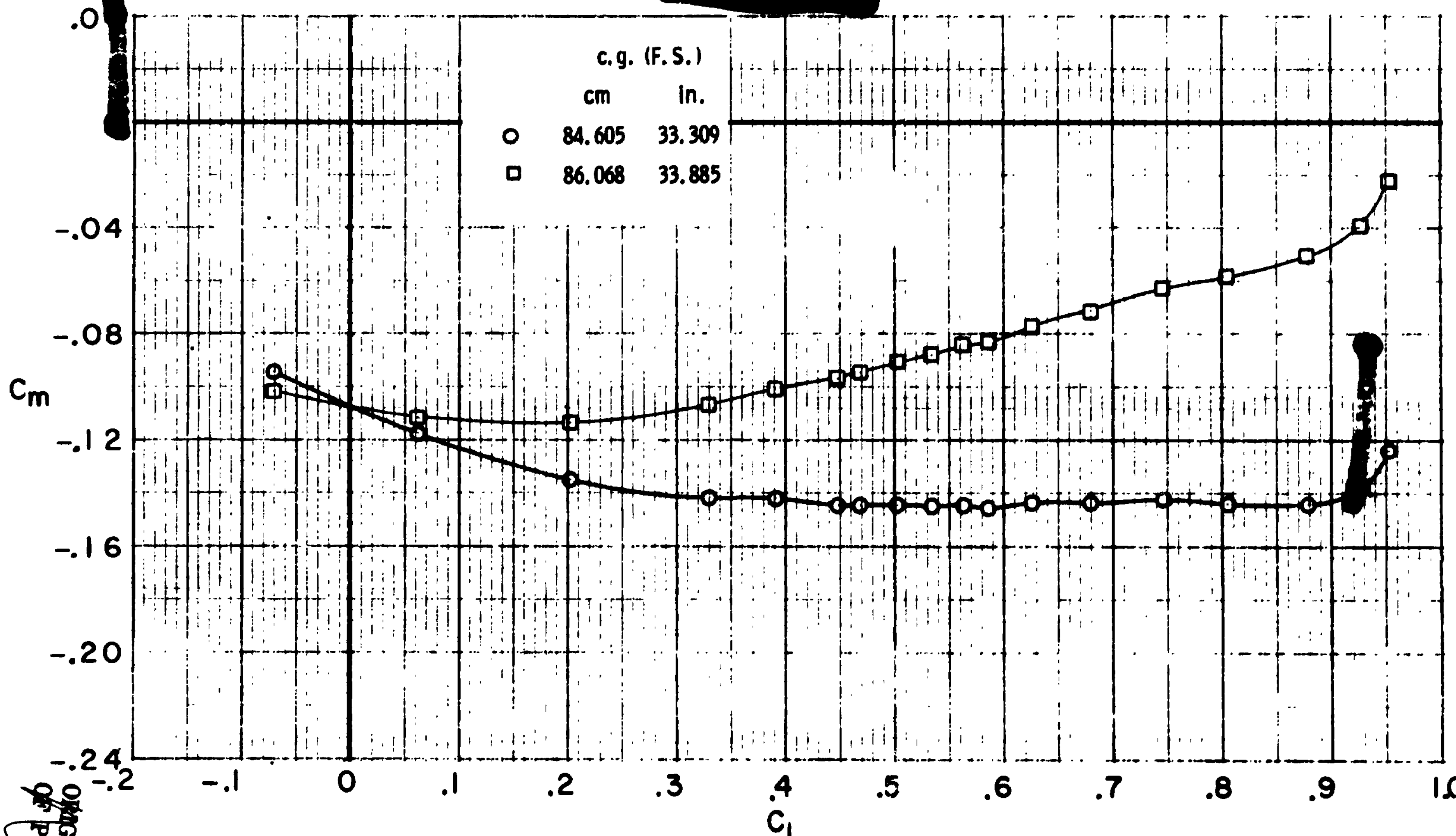

(b) M = 0.70. Concluded.

Figure 15.- Continued.

[redacted]

ORIGINAL PAGE IS
OF POOR QUALITY

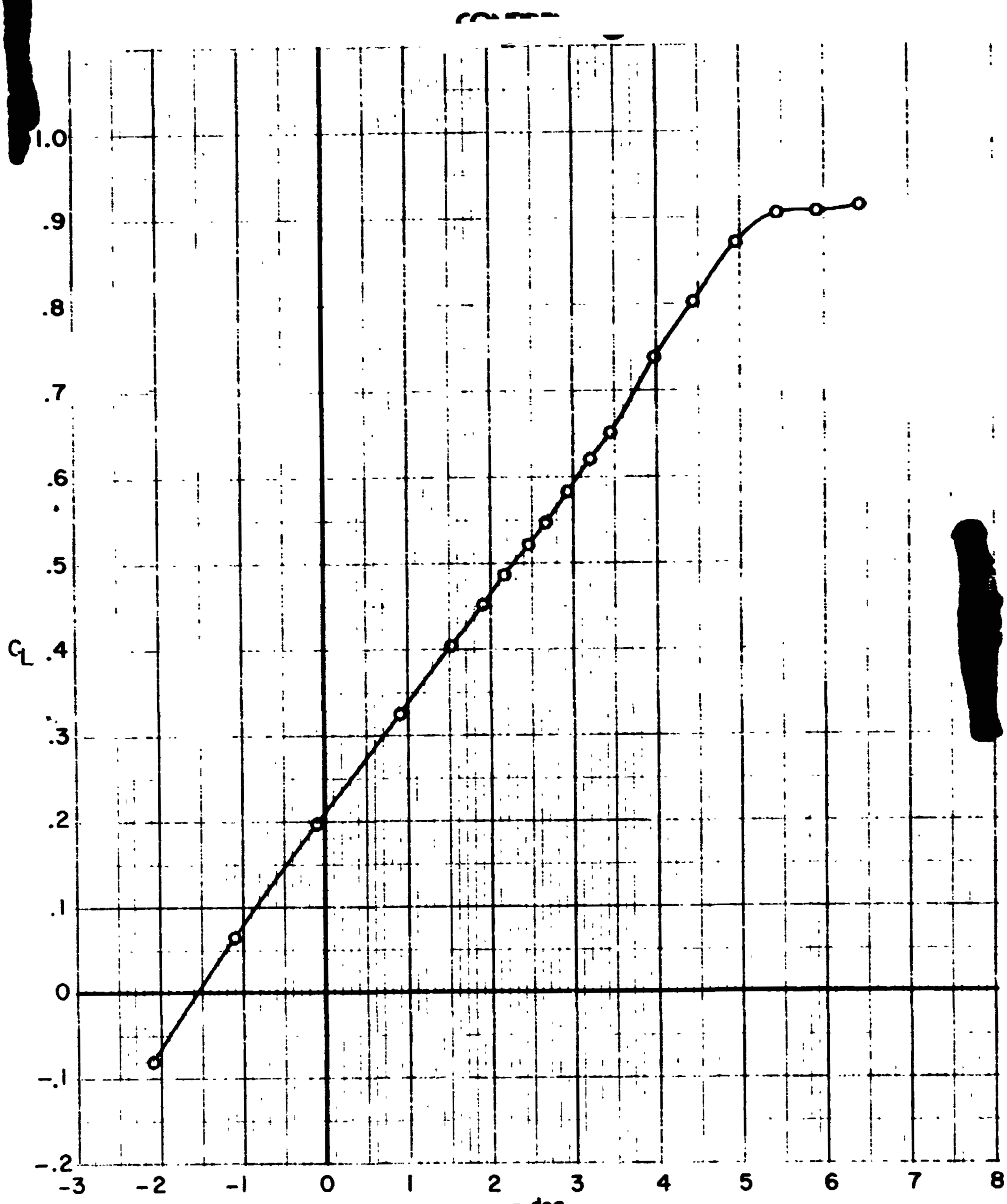

(c) M = 0.75.

Figure 15 - Continued.

[redacted]

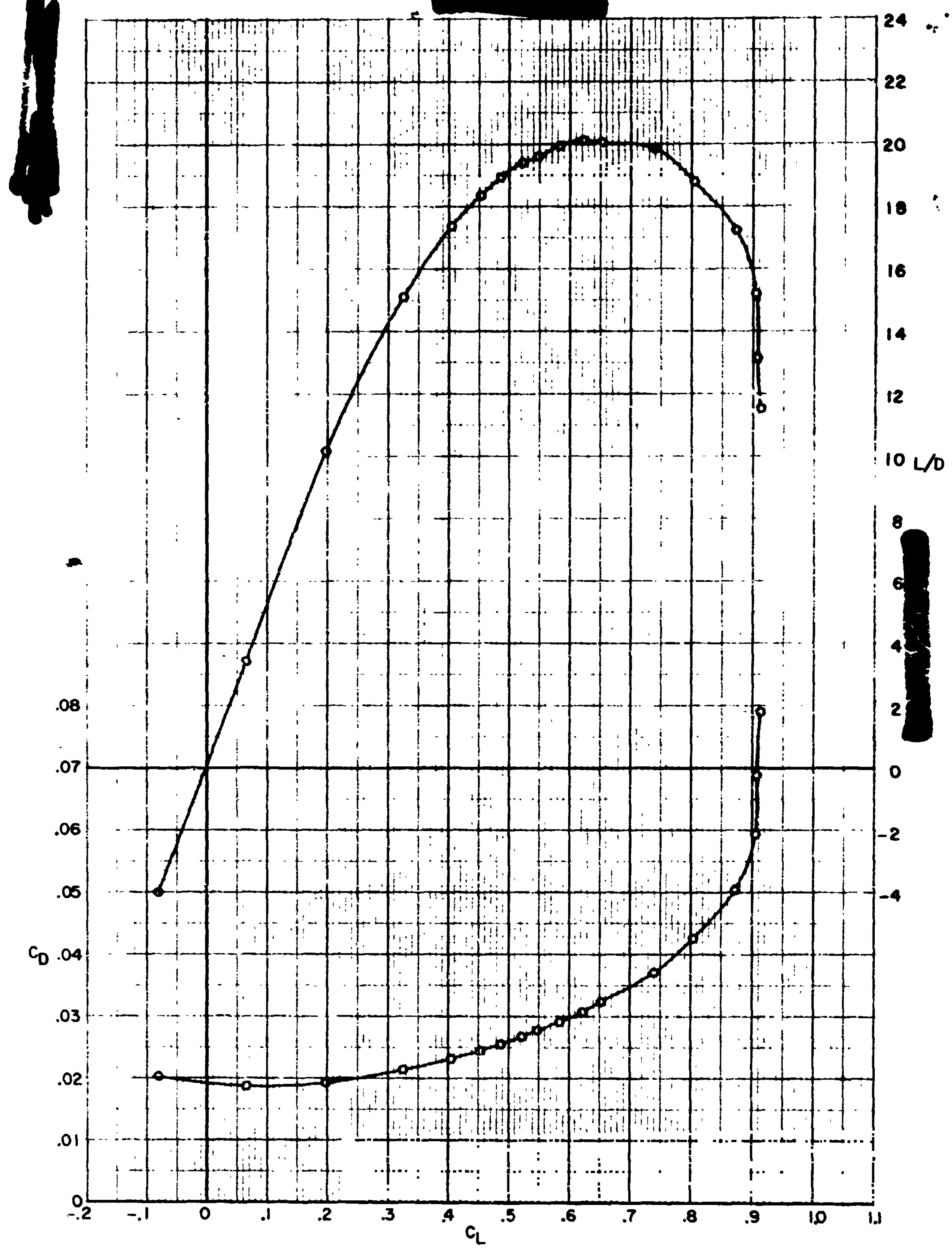

(c) M = 0.75. Continued.

Figure 15.- Continued.

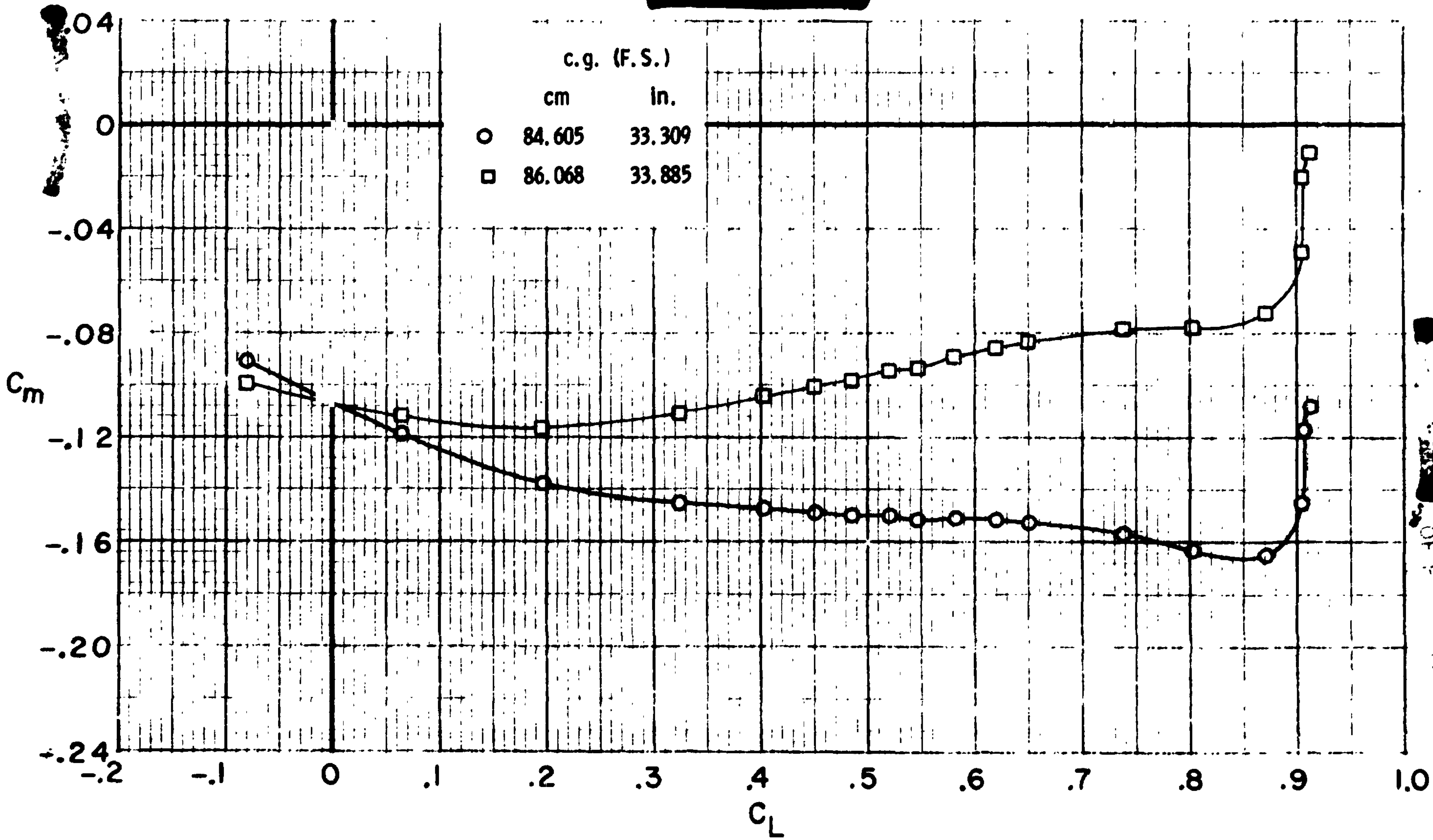

(c) M = 0.75. Concluded.

Figure 15.- Continued.

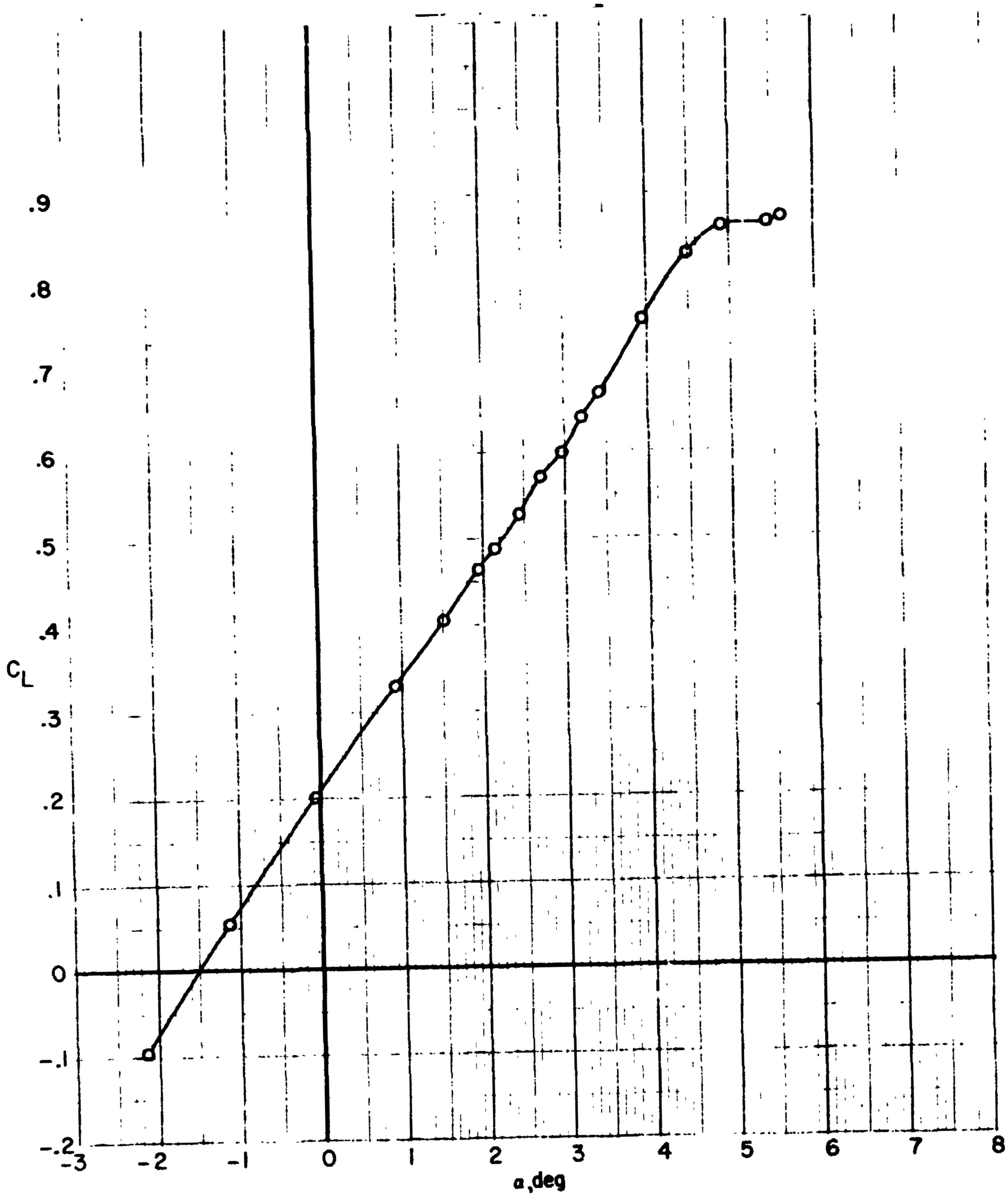

(d) M = 0.77.

Figure 15.- Continued.

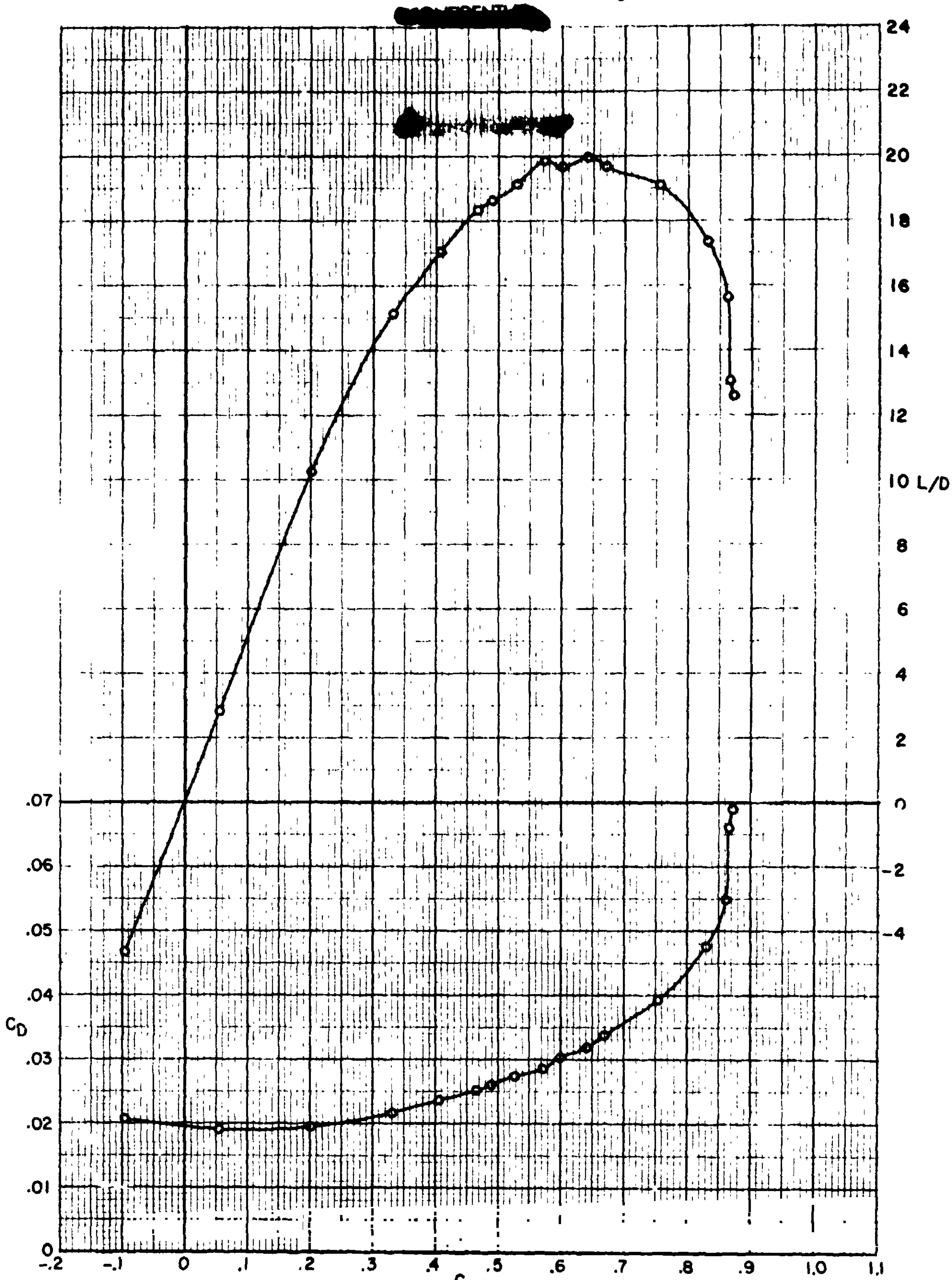

(d) M = 0.77. Continued.

Figure 15. - Continued.

[redacted]

[redacted]

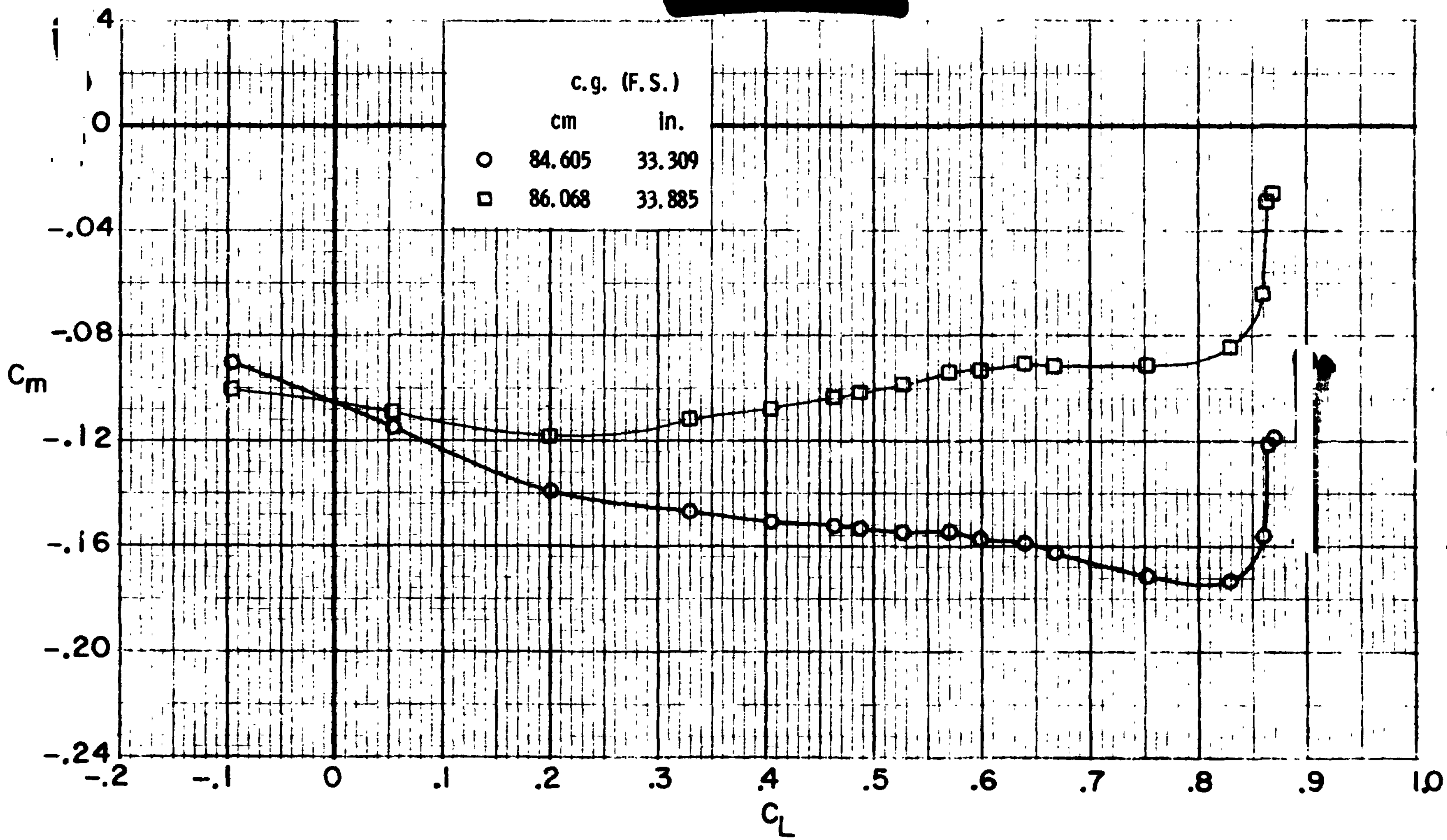

ORIGINAL PAGE IS
OF POOR QUALITY

(d) M = 0.77. Concluded.

Figure 15.- Continued.

[redacted]

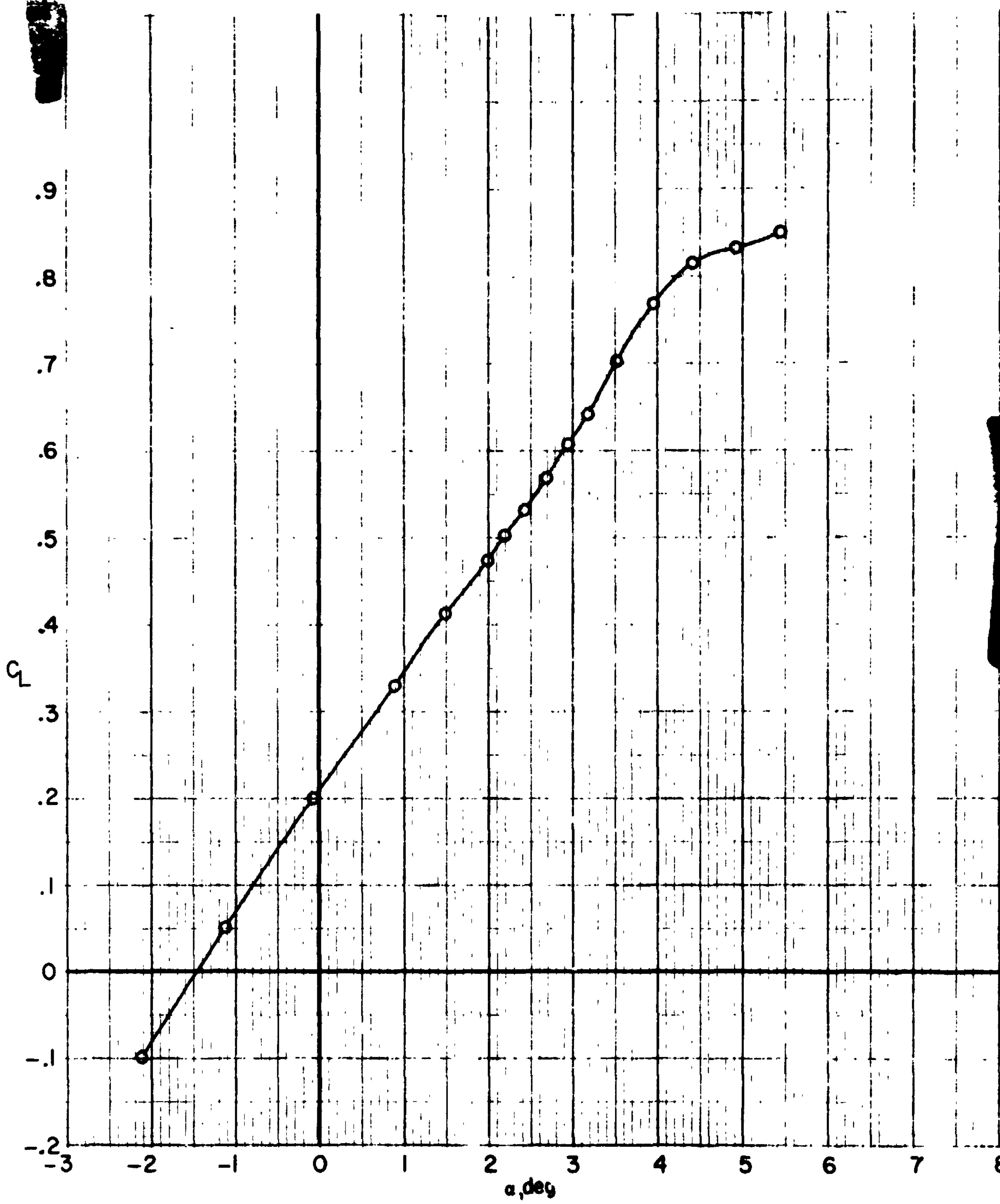

(e) M = 0.78.

Figure 15. - Continued.

[redacted]

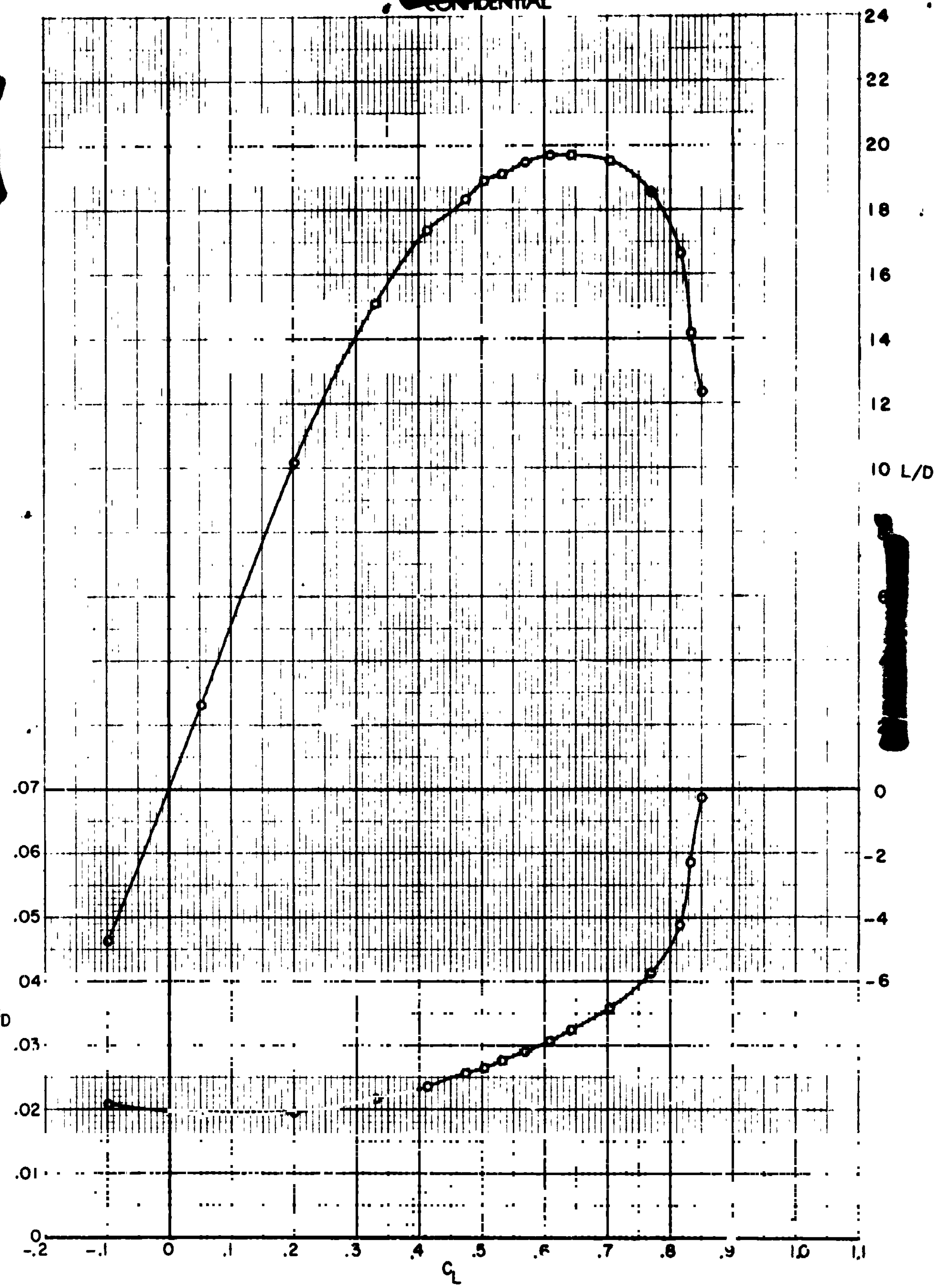

(e) M = 0.78. Continued.

Figure 15.- Continued.

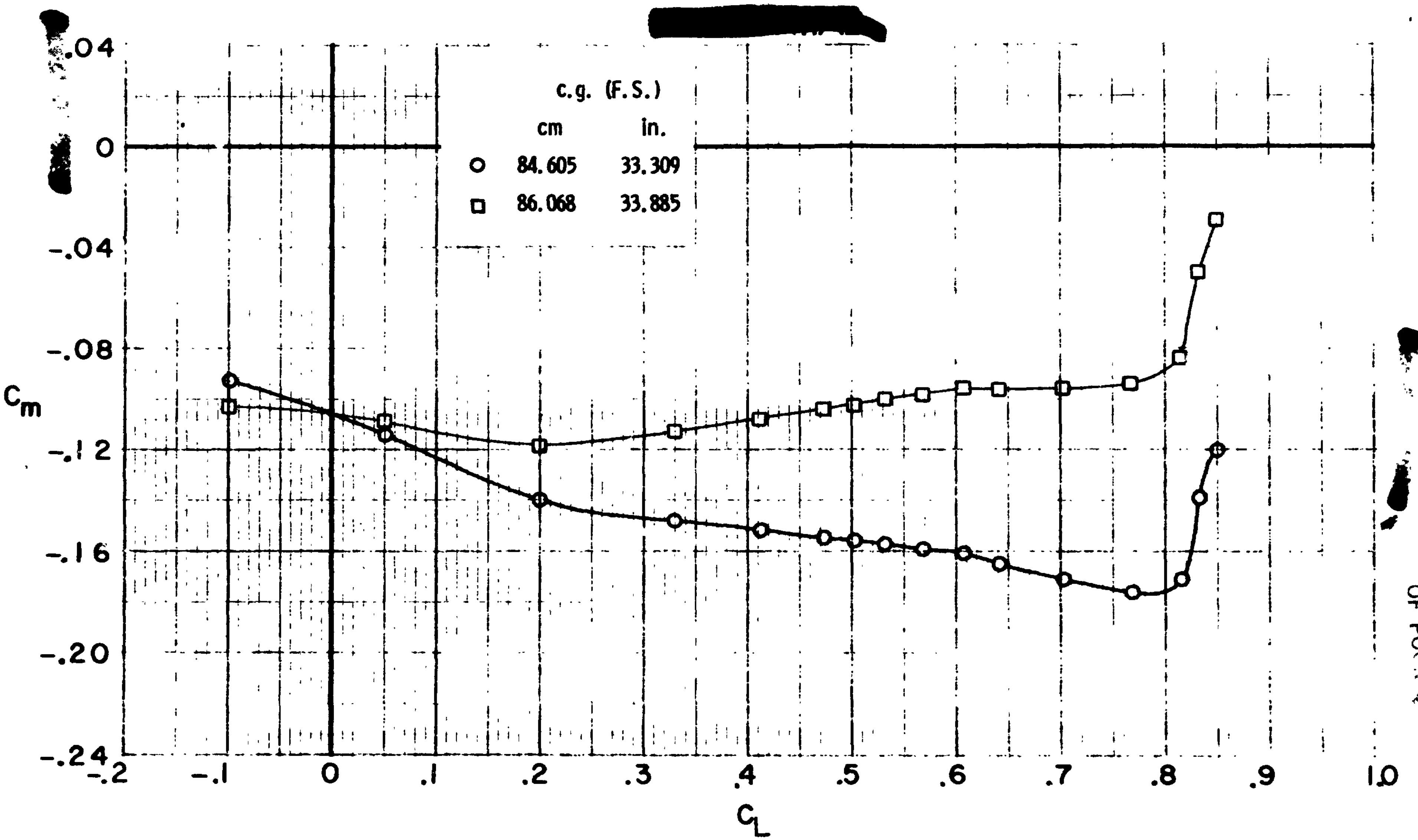

(e) M = 0.78. Concluded.

Figure 15. - Concluded.

[redacted]

Test 144 - 25 M = 0.60

ORIGINAL PAGE IS
OF POOR QUALITY

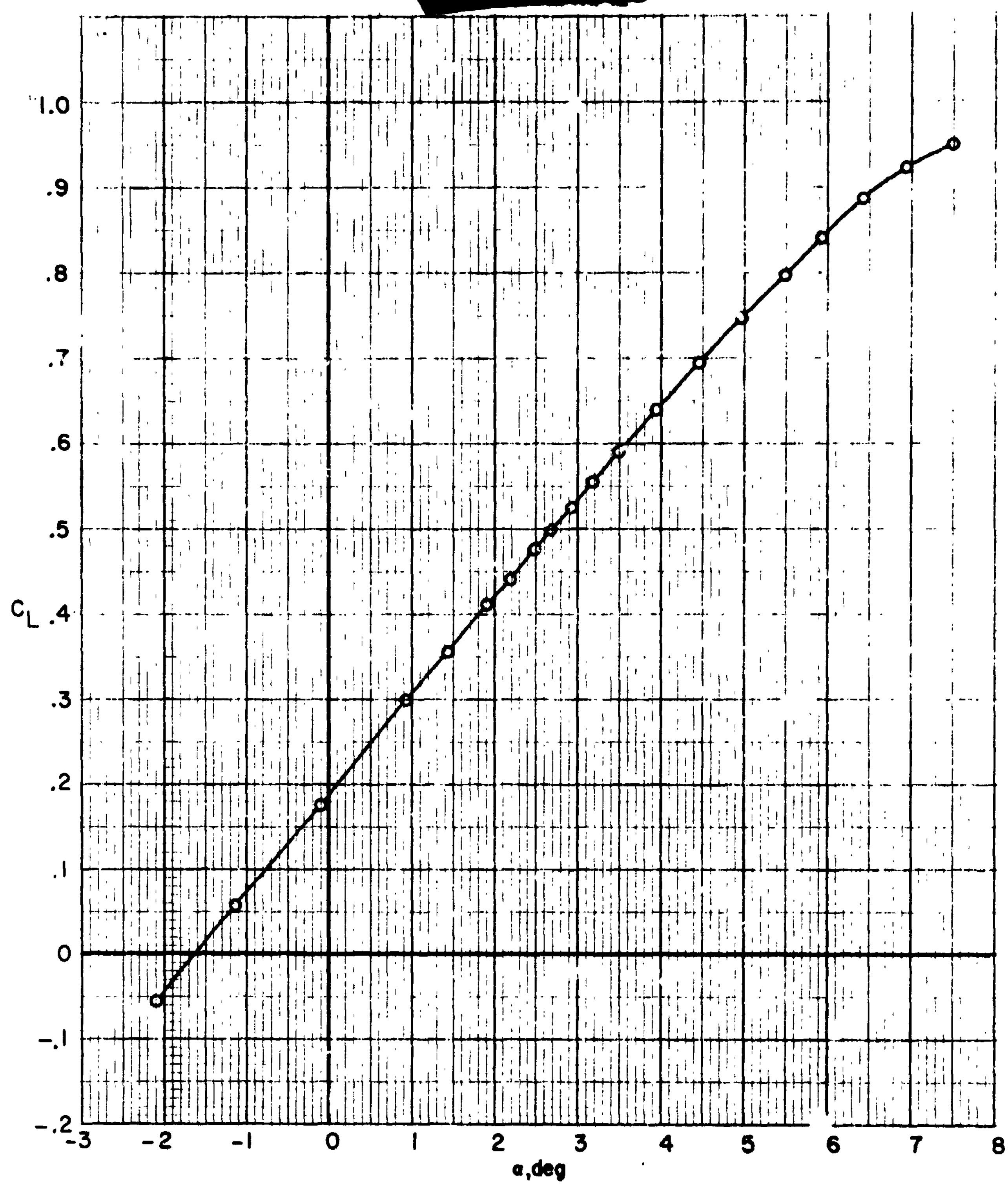

(a) M = 0.60.

Figure 16.- Longitudinal aerodynamic characteristics for supercritical wing configuration 2b (SCW-2b) with wing upper surface and lower surface grit forward (x_T/c = 0.05). $\Lambda_{c/4} = 30°$.

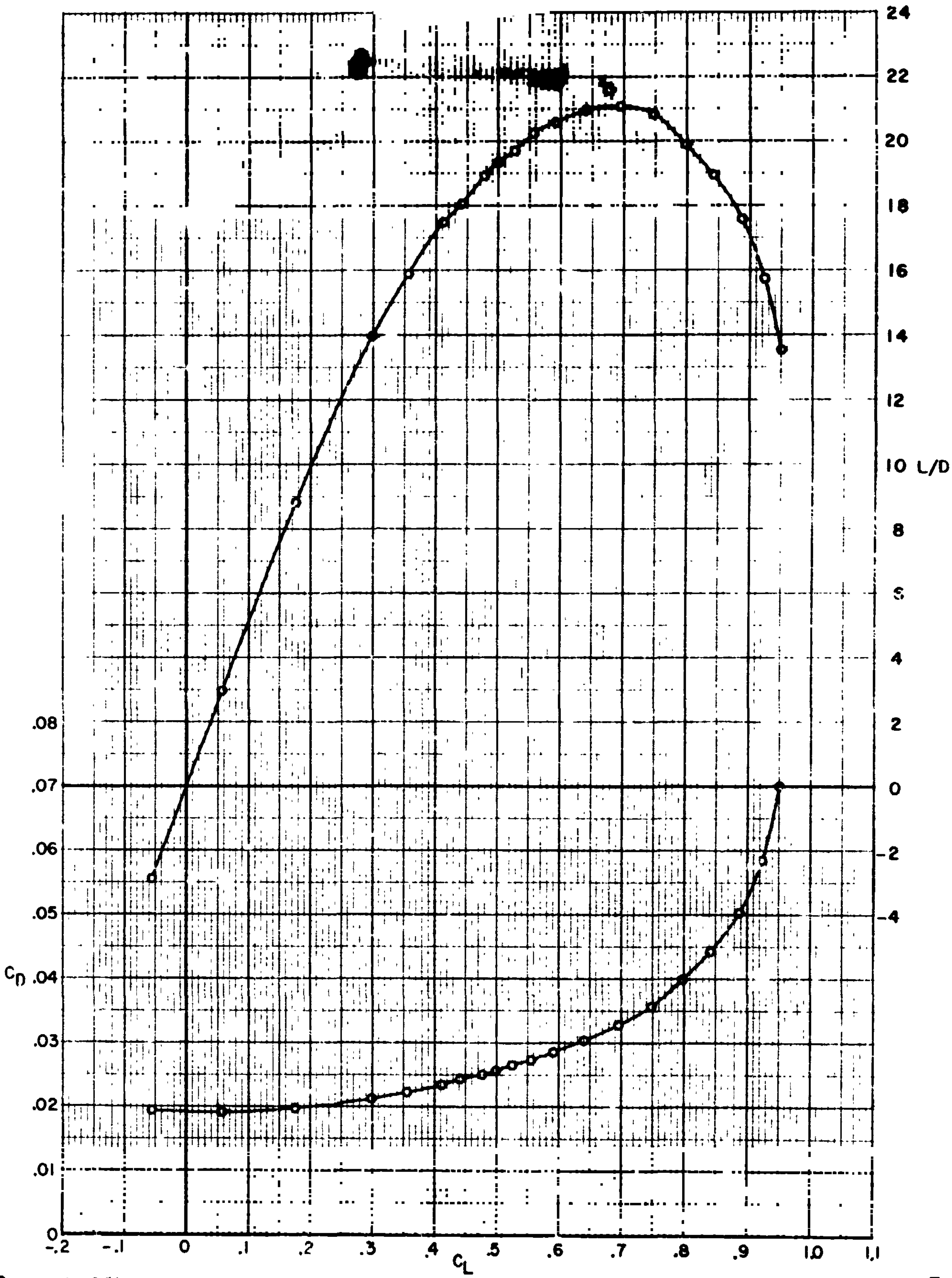

(a) M = 0.60. Continued.

Figure 16. - Continued.

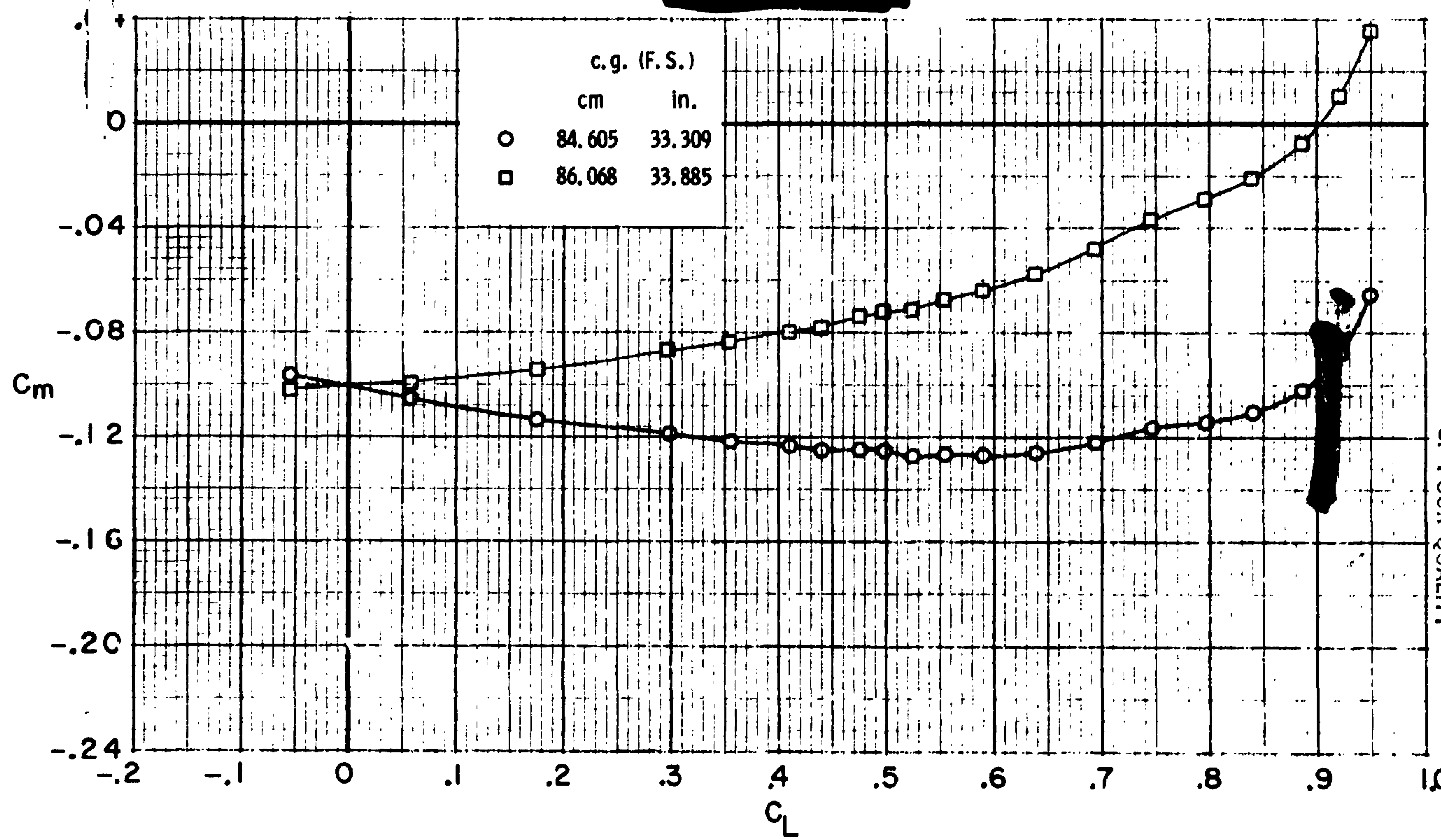

ORIGINAL PAGE IS OF POOR QUALITY

(a) M = 0.60. Concluded.

Figure 16.- Continued.

.44 - 24
3L + 15

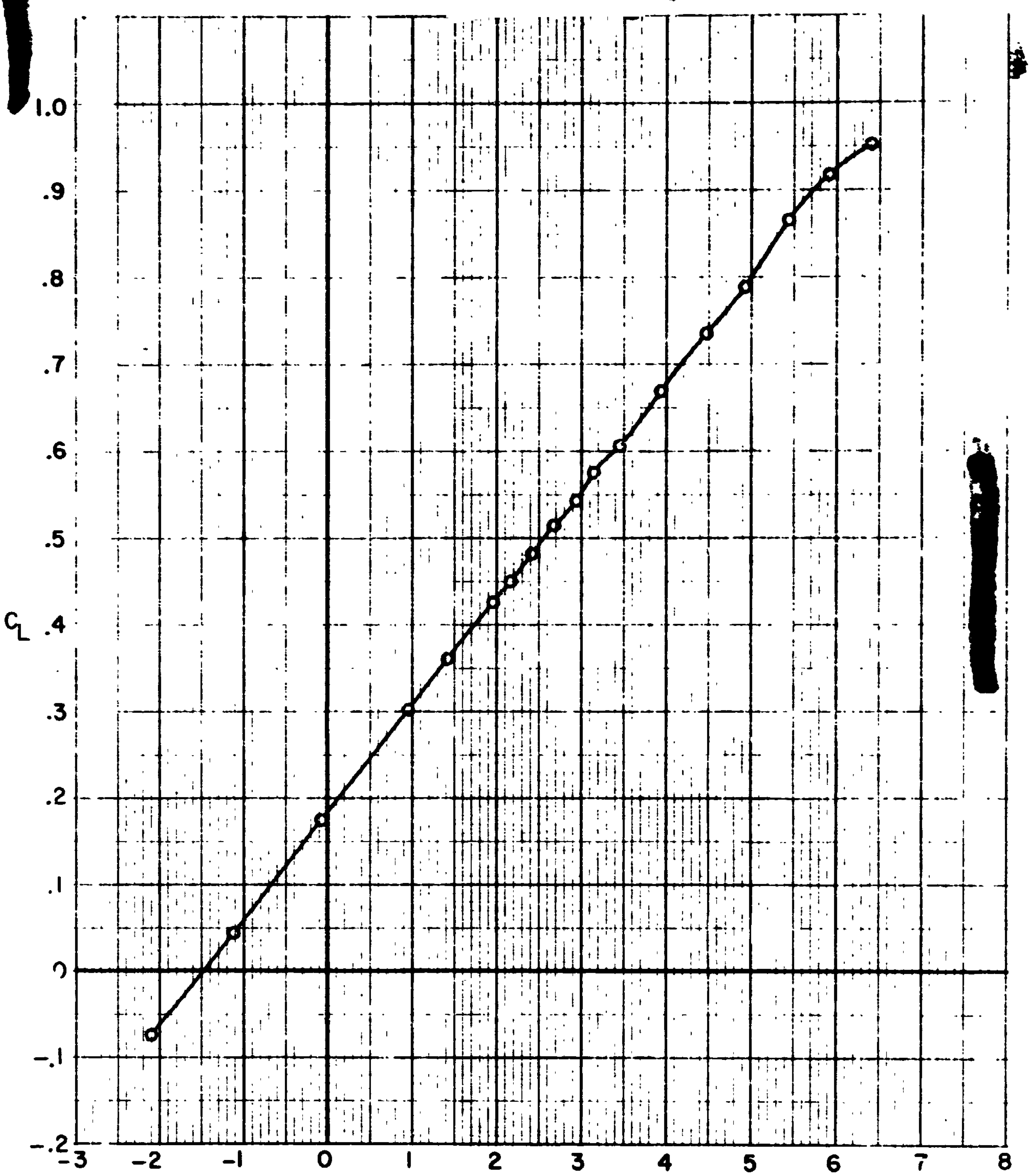

(b) M = 0.70.

Figure 16. - Continued.

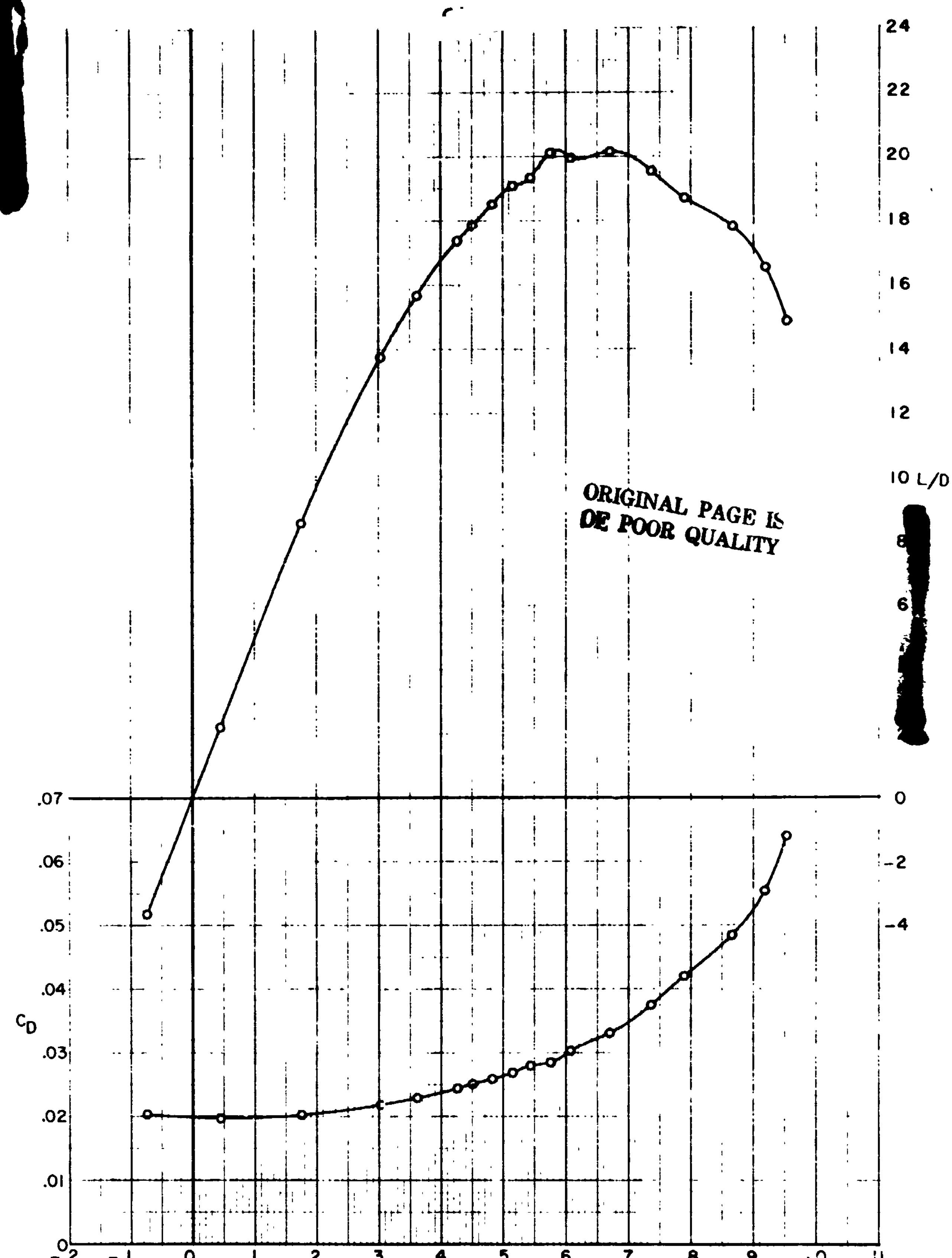

(b) M = 0.70. Continued.

Figure 16.- Continued.

[redacted]

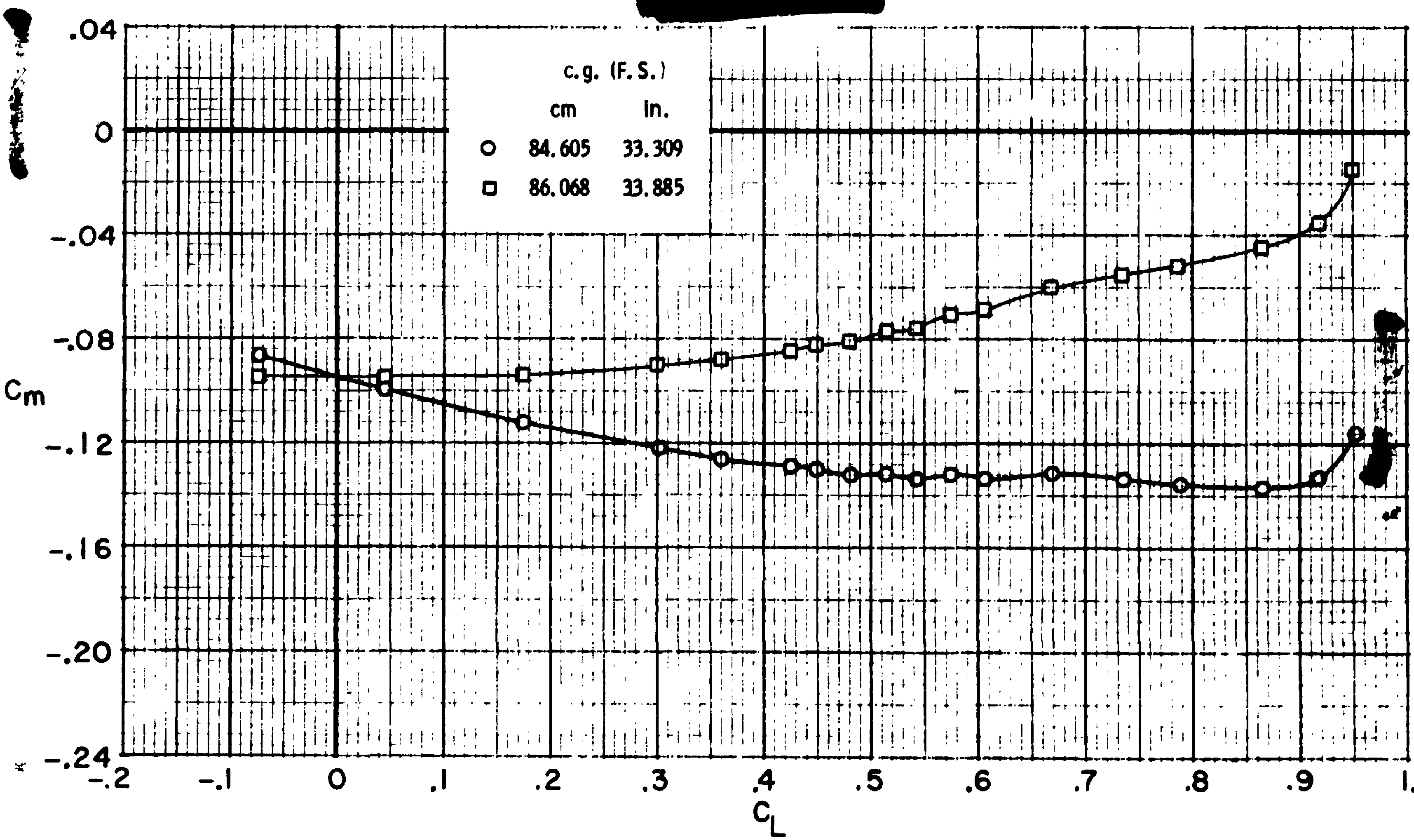

(b) M = 0.70. Concluded.

Figure 16. - Concluded.

[redacted]

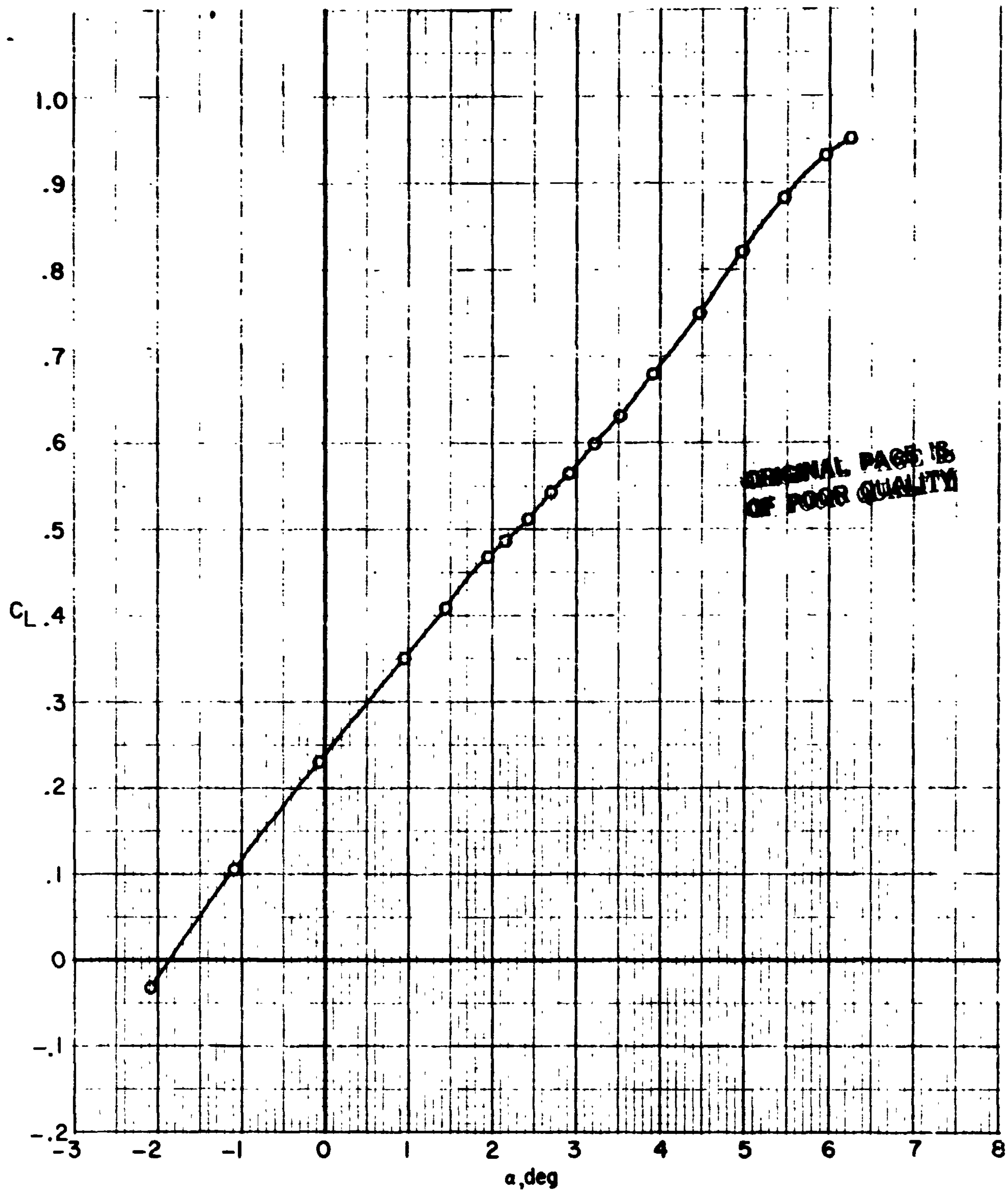

(a) M = 0.70.

Figure 17.- Longitudinal aerodynamic characteristics for supercritical wing configuration 2c (SCW-2c) with wing upper surface grit aft (fig. 5). $\Lambda_{c/4} = 27°$.

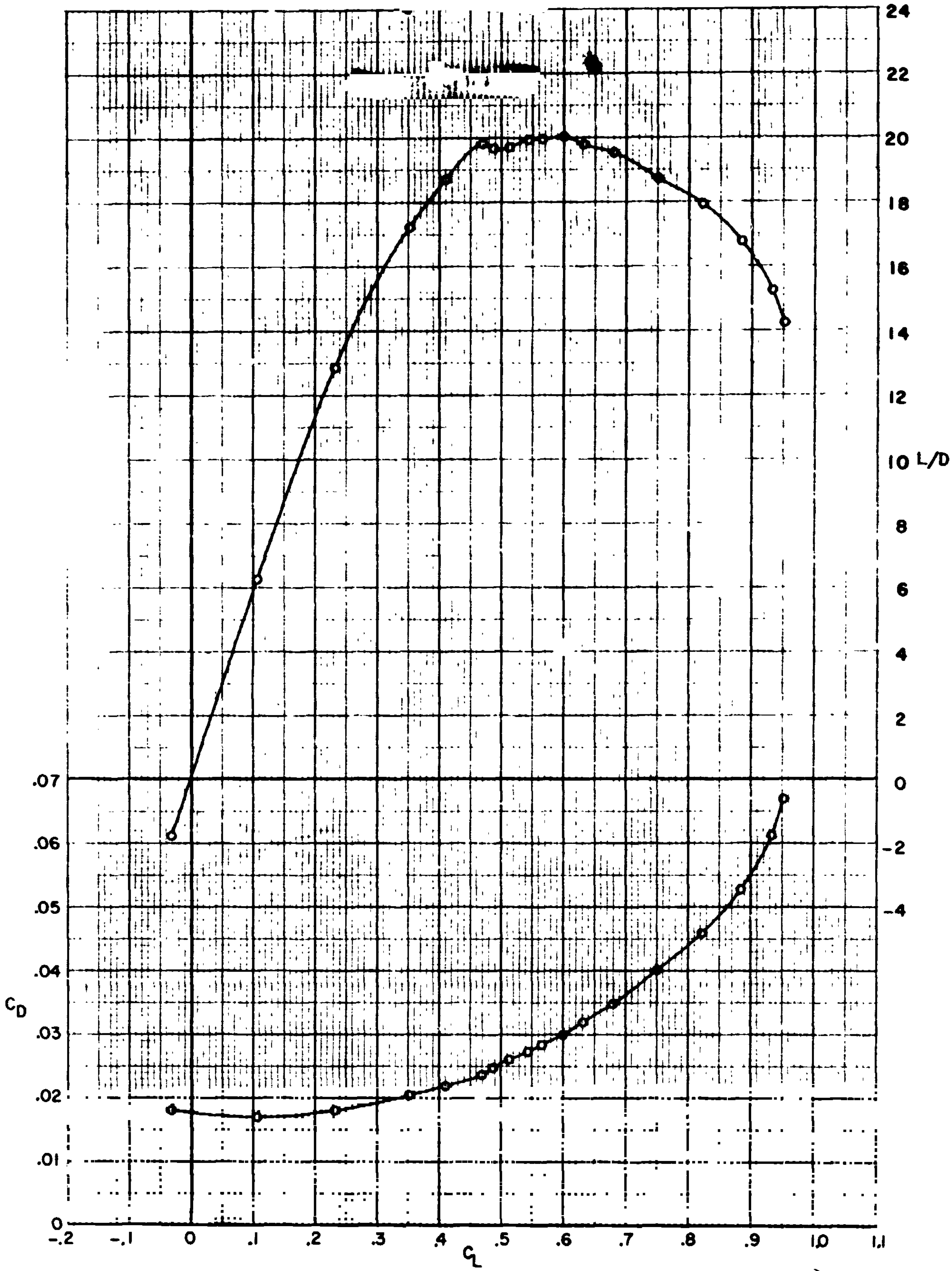

(a) M = 0.70. Continued.

Figure 17.- Continued.

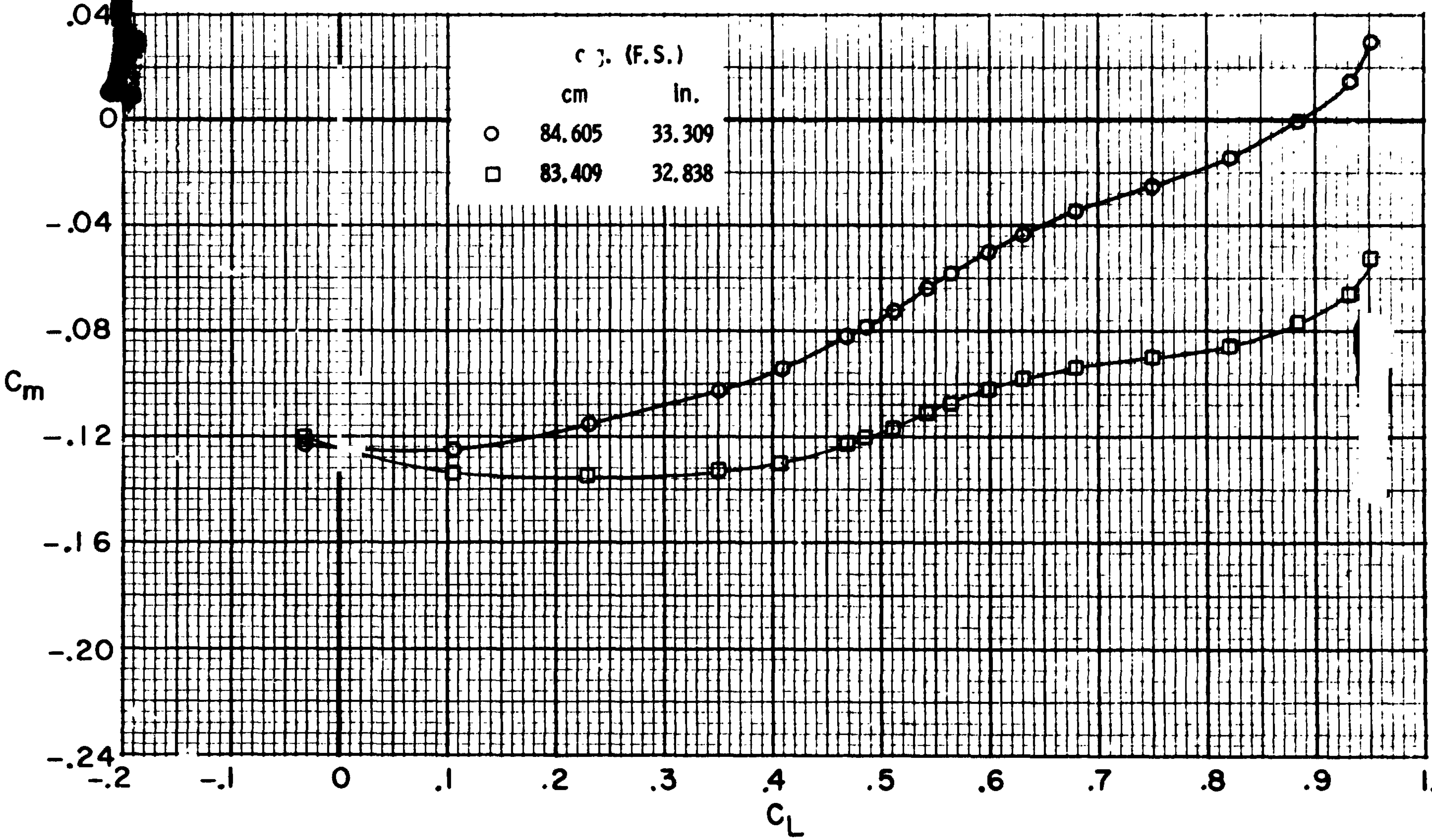

(a) M = 0.70. Concluded.

Figure 17. - Continued.

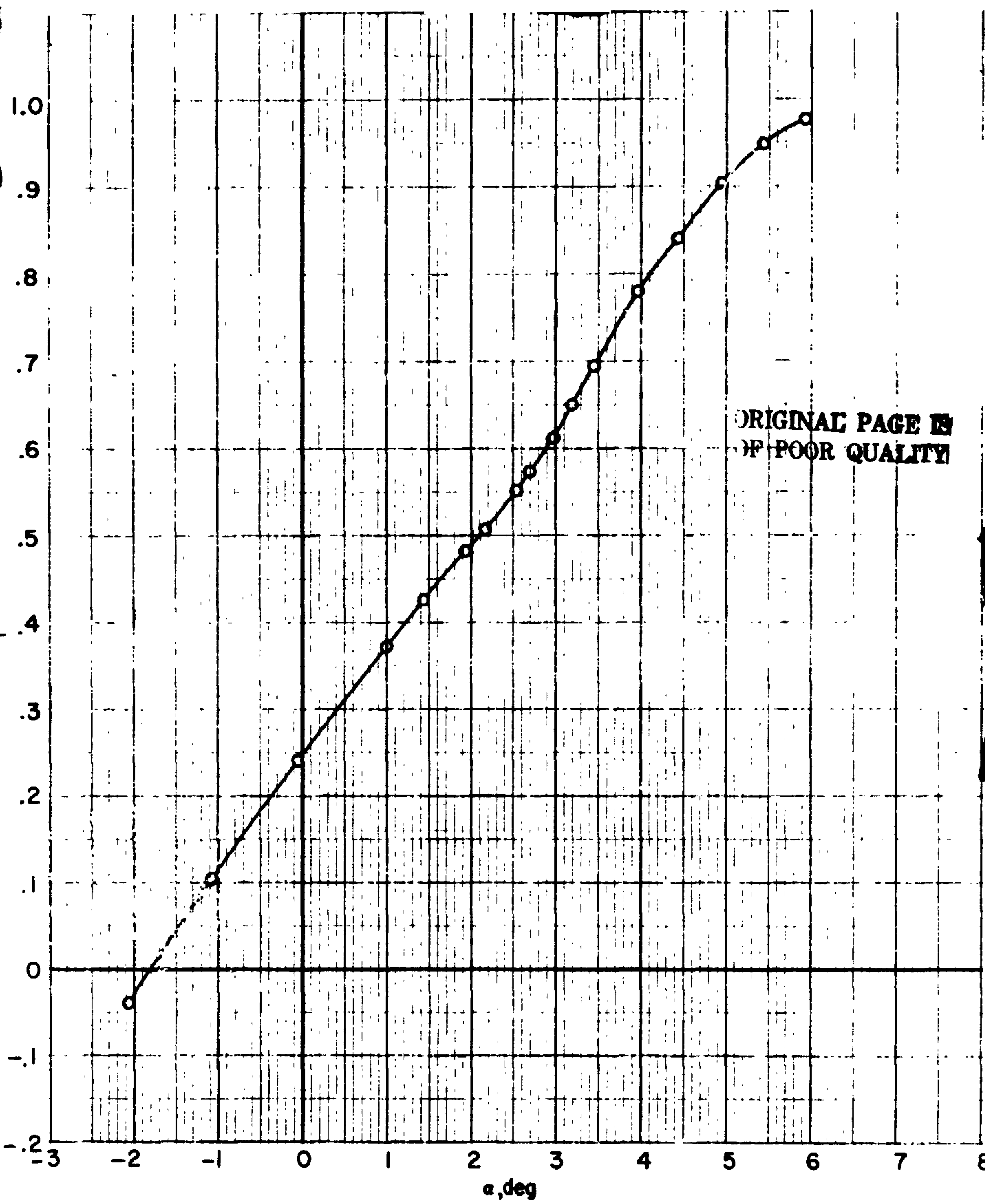

(b) M = 0.75.

Figure 17.- Continued.

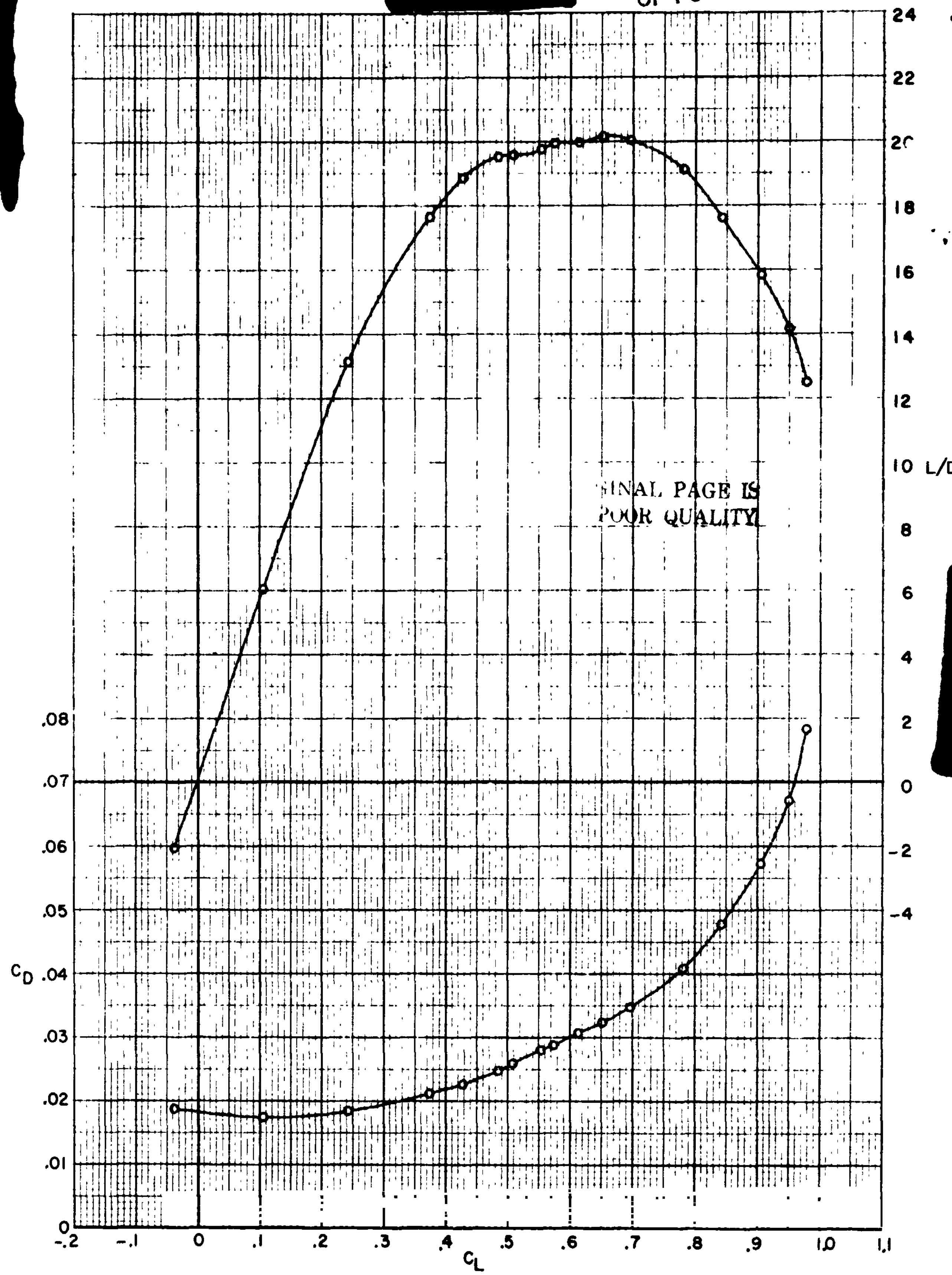

(b) M = 0.75. Continued.

Figure 17.- Continued.

[redacted]

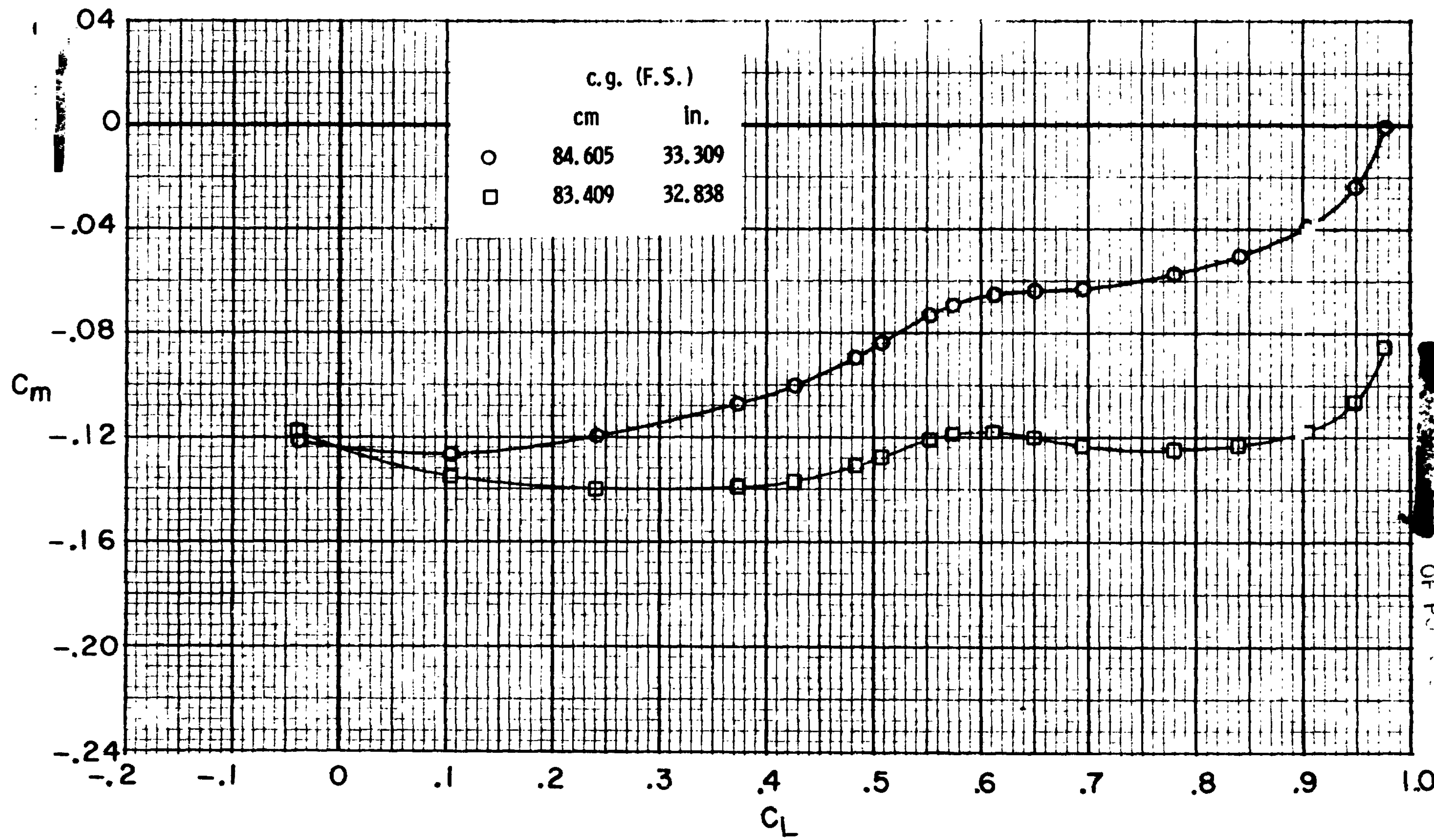

(b) M = 0.75. Concluded.

Figure 17. - Continued.

[redacted]

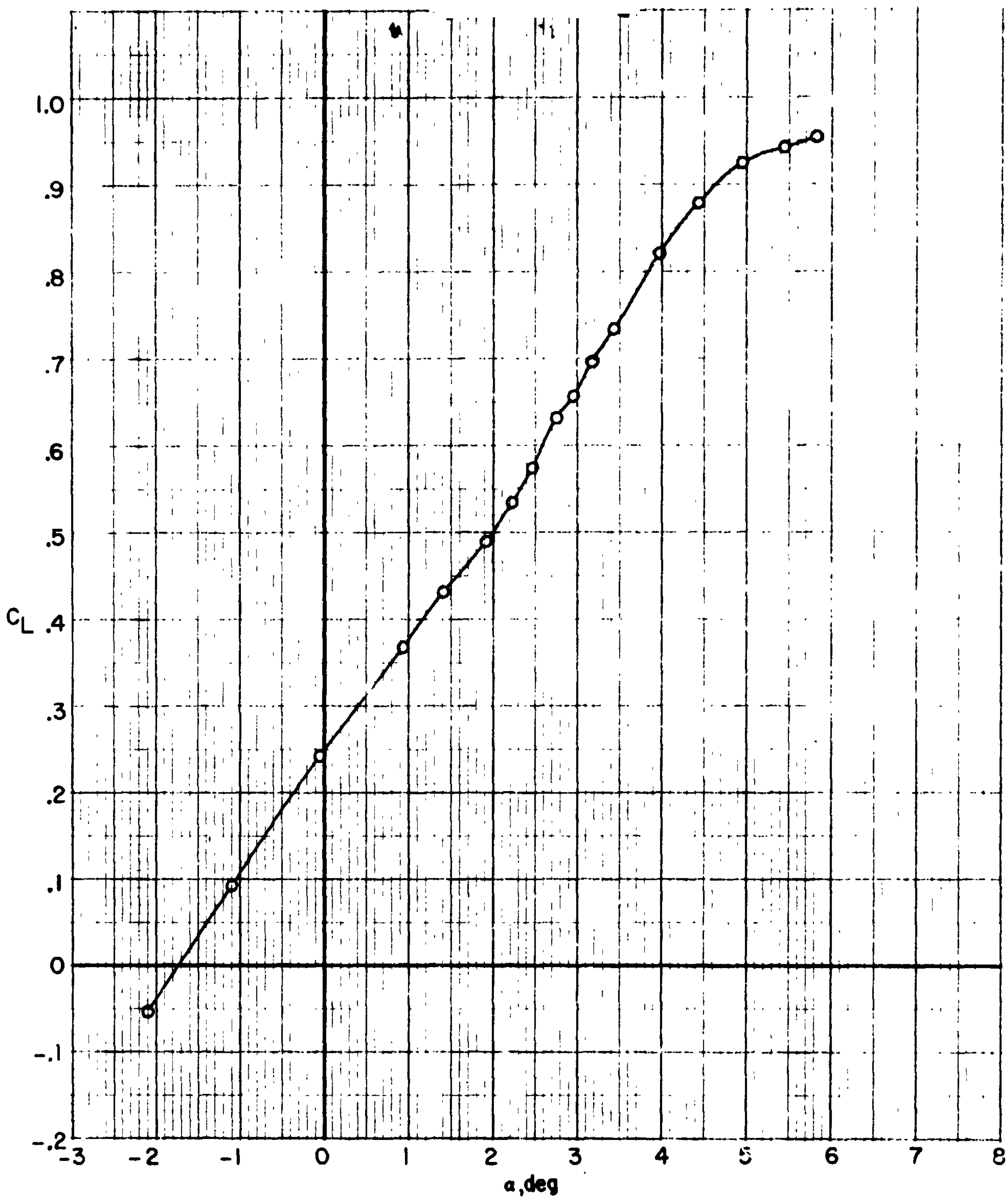

(c) M = 0.77.

Figure 17. - Continued.

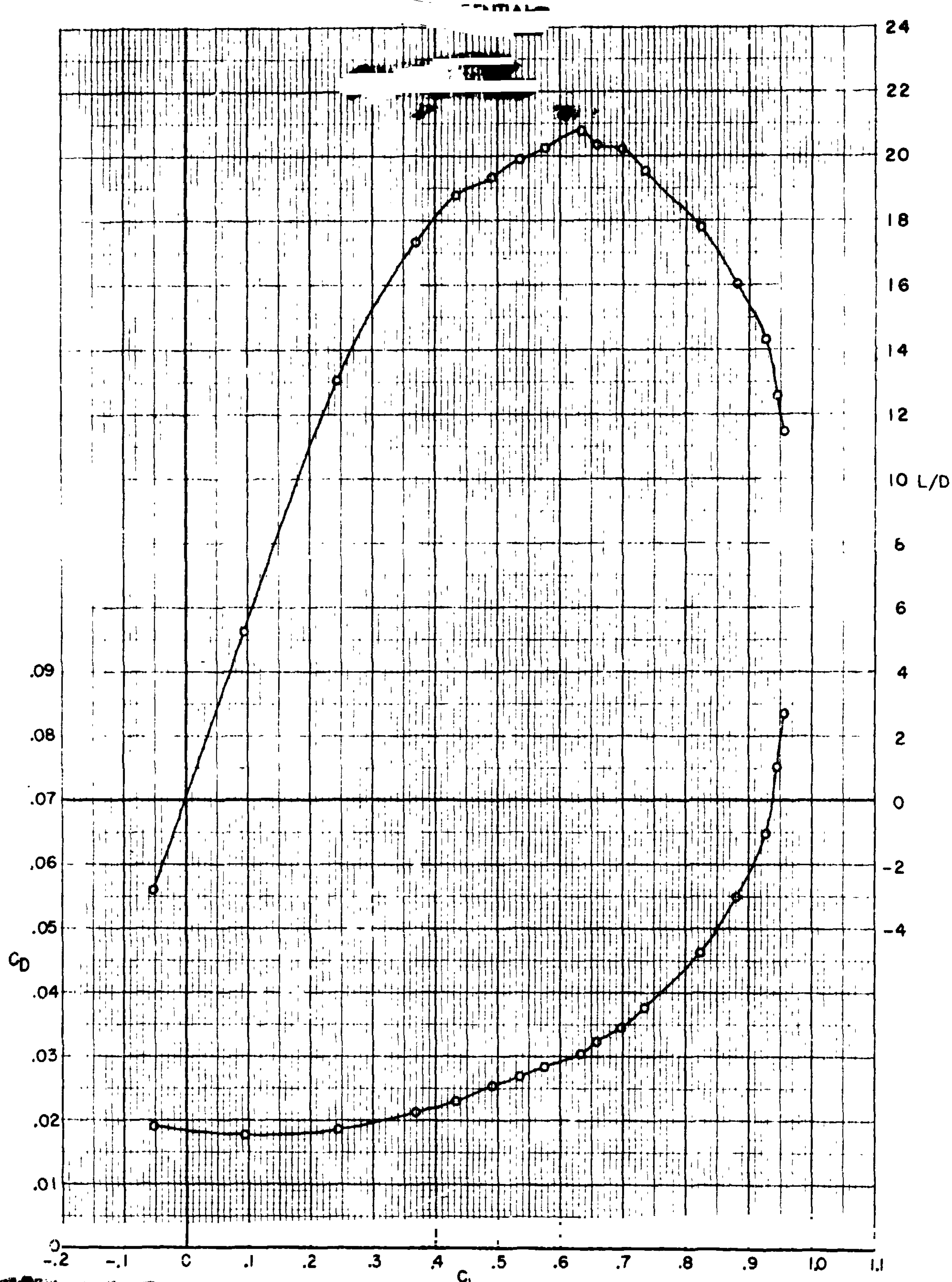

(c) M = 0.77. Continued.

Figure 17.- Continued.

[redacted]

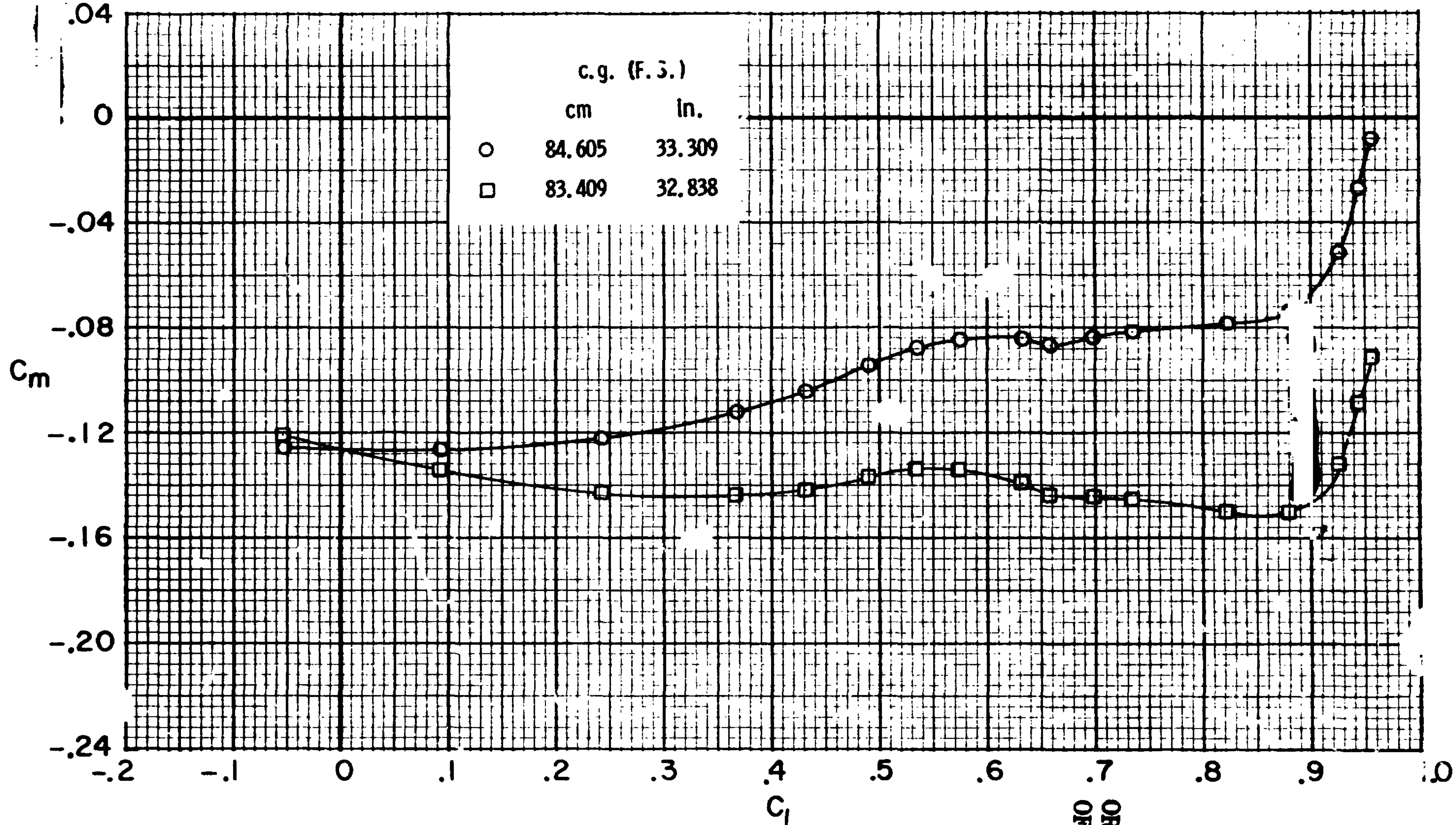

(c) M = 0.77. Concluded.

Figure 17.- Continued.

ORIGINAL PAGE IS
OF POOR QUALITY

[redacted]

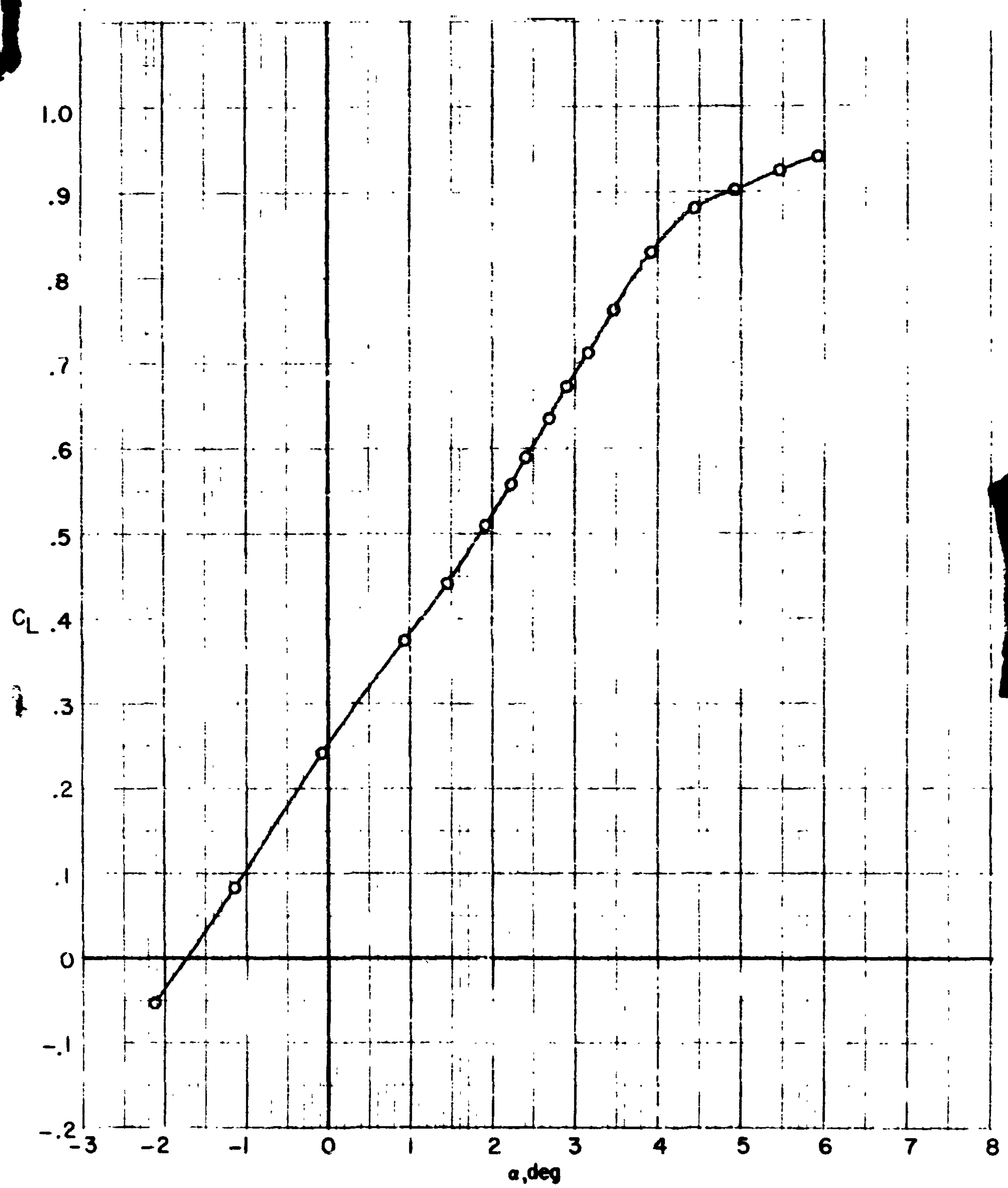

(d) M = ^ 78.

Figure I7 - Continued.

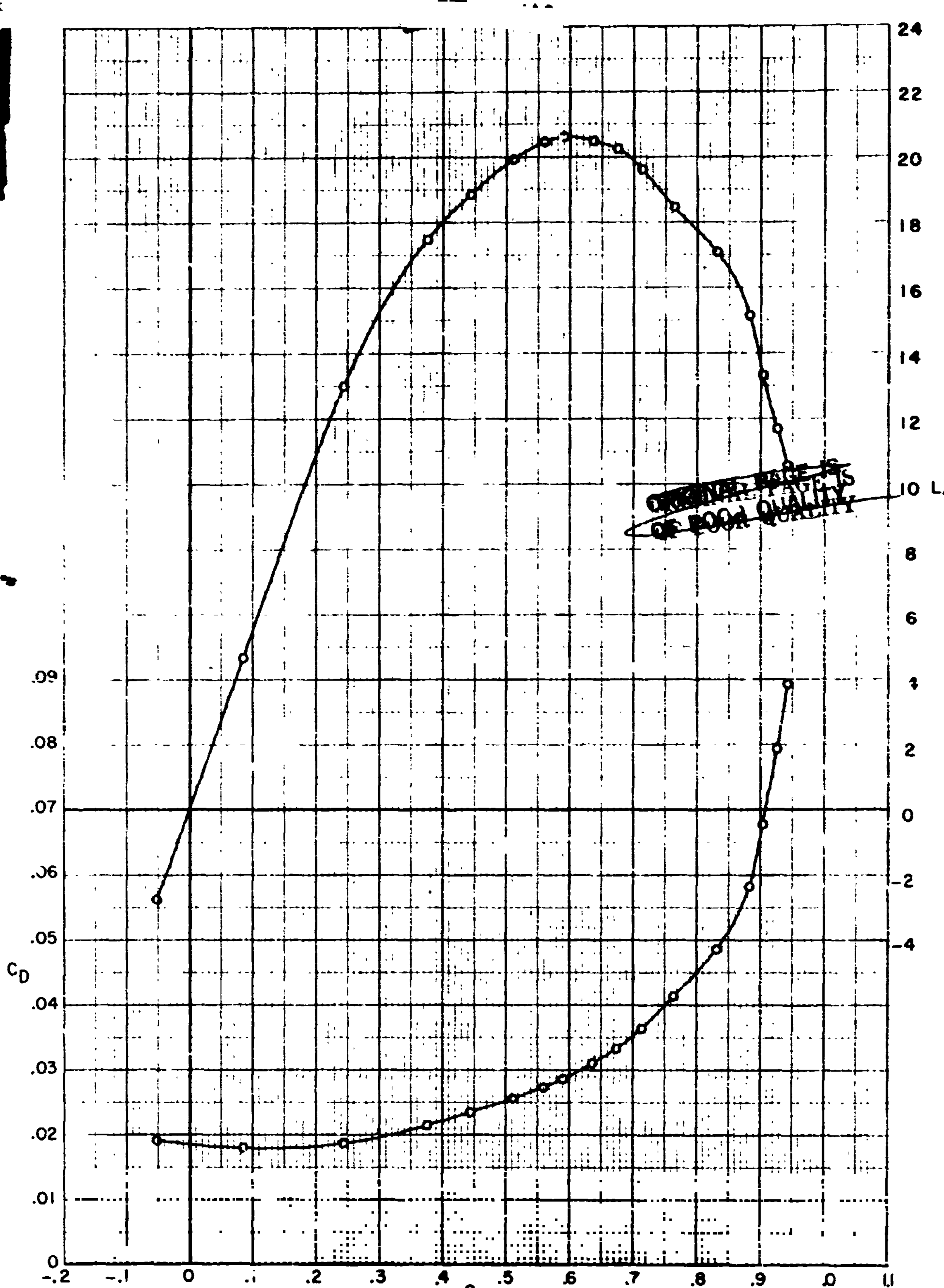

(d) M = 0.78. Continued.

Figure 17. - Continued.

[redacted]

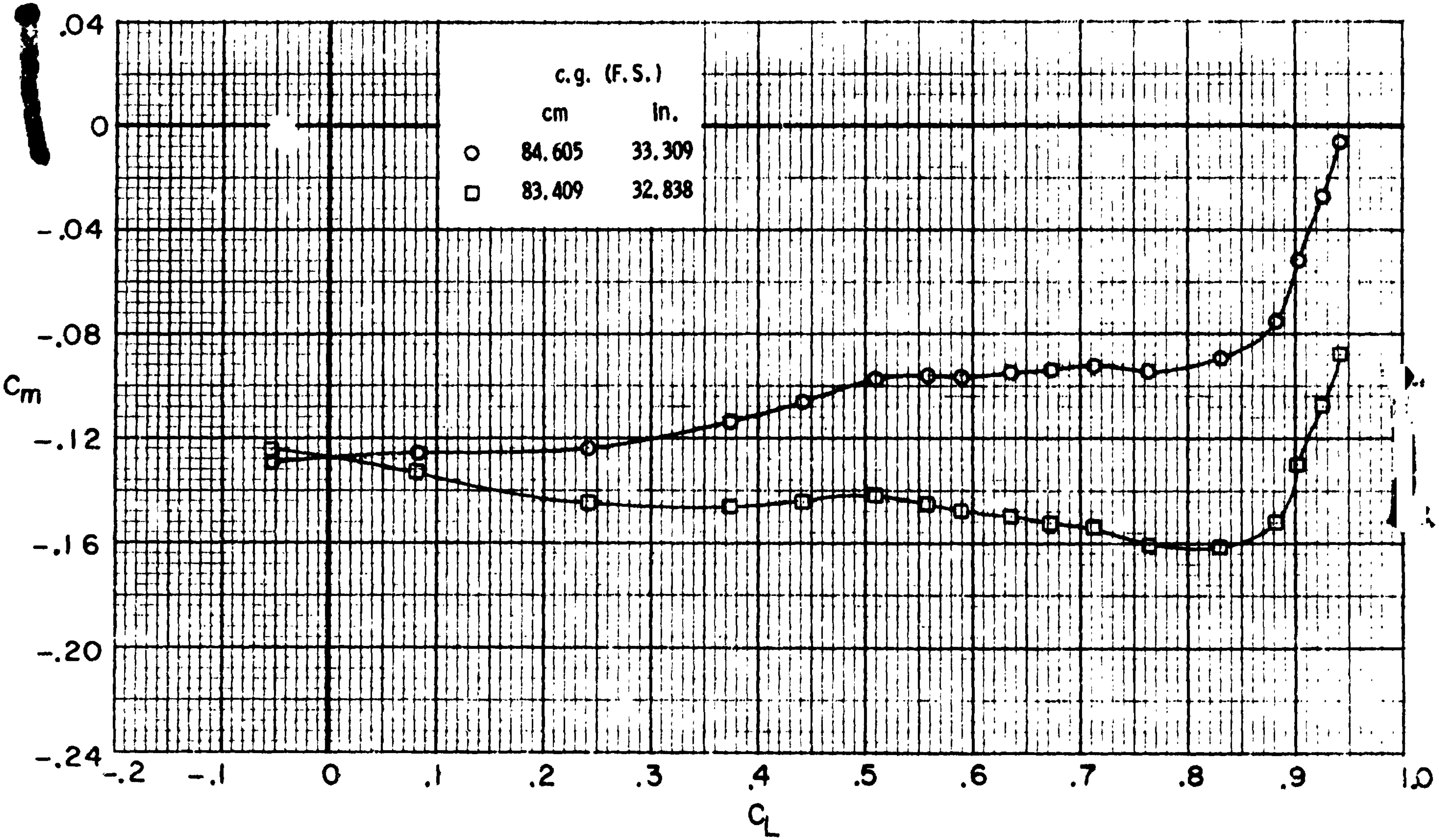

(d) M = 0.78. Concluded.

Figure 17.- Continued.

[redacted]

ORIGINAL PAGE IS
OF POOR QUALITY

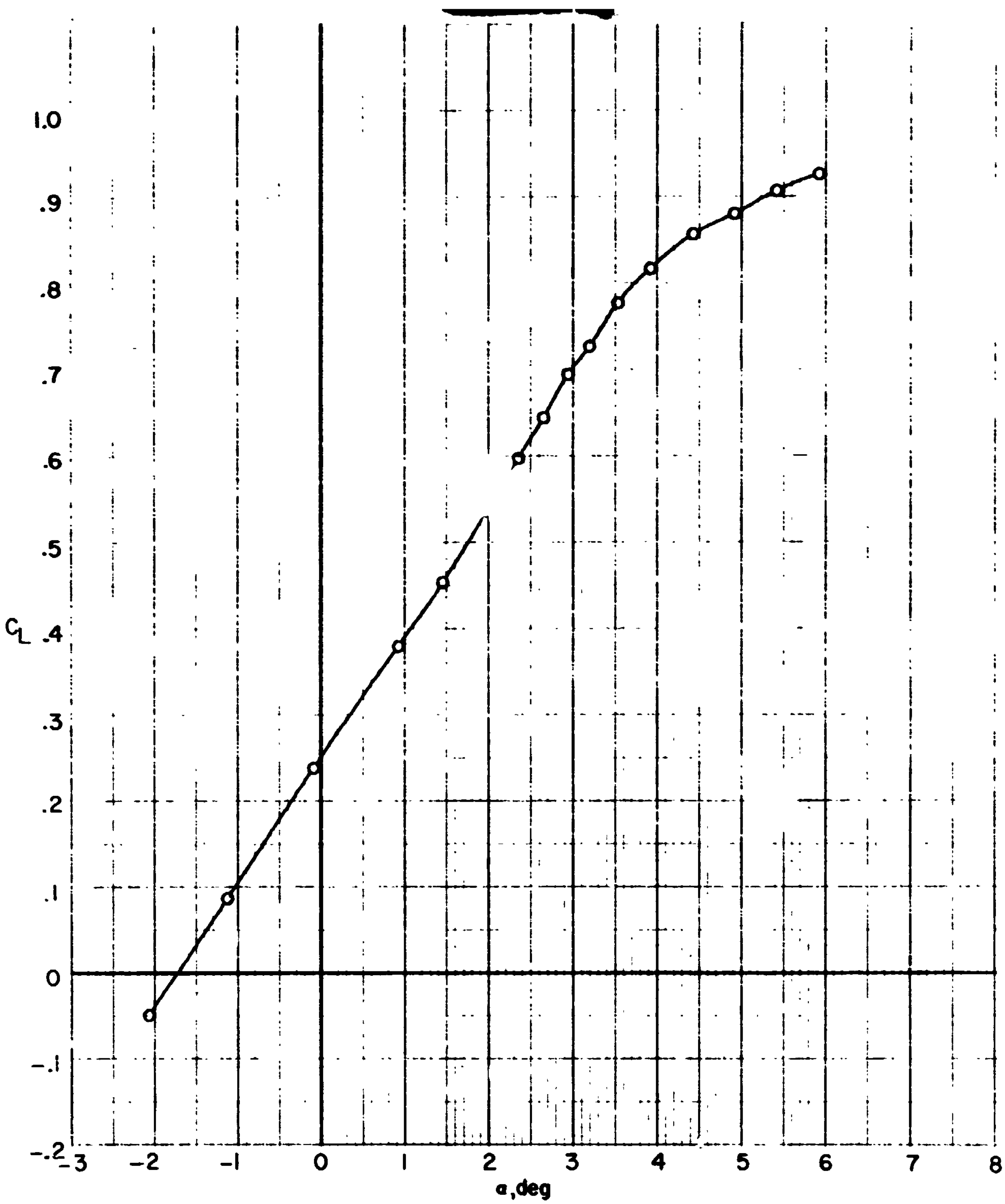

(e) M = 0.79.

Figure 17. - Continued.

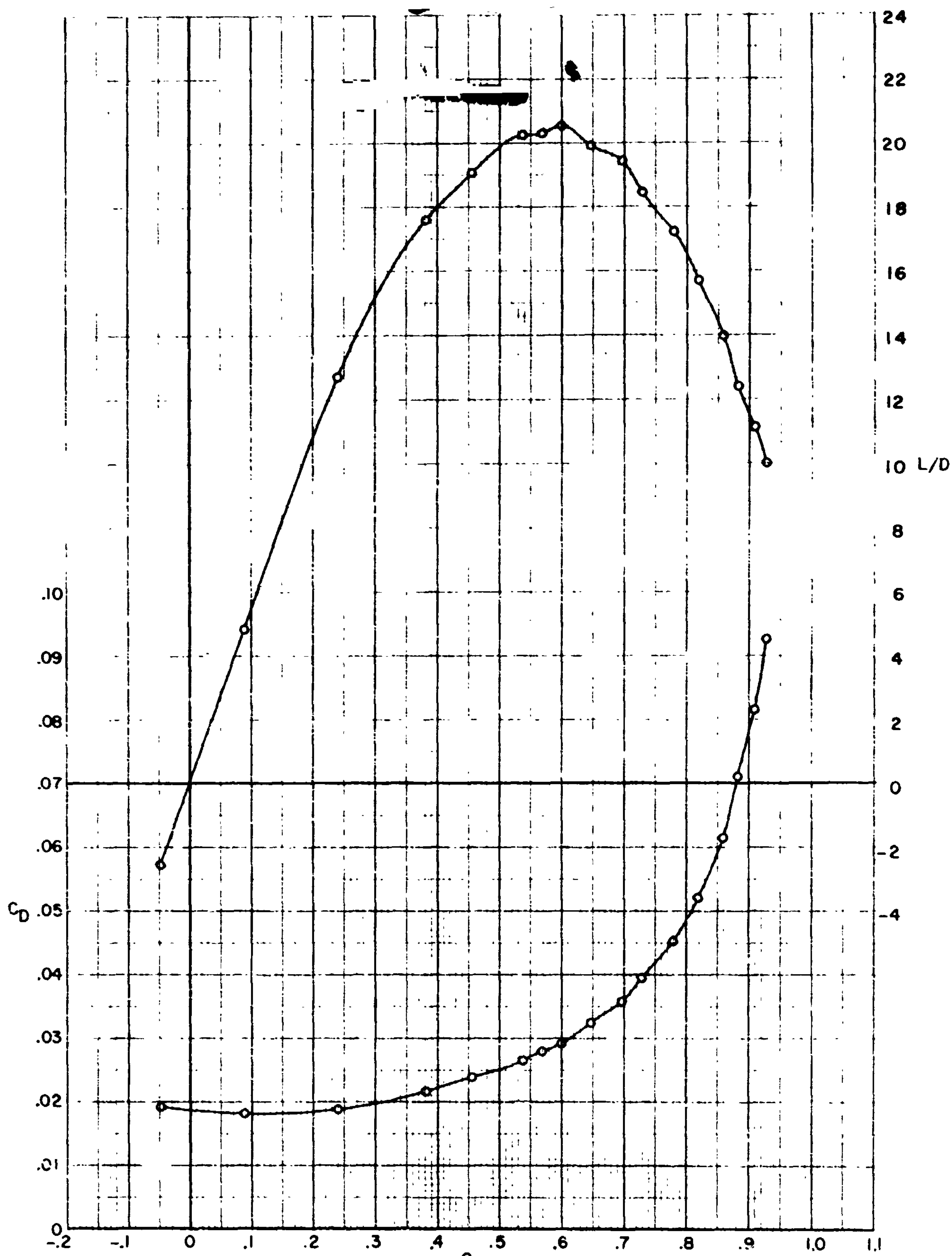

(e) M = 0.79. Continued.

Figure 17. - Continued.

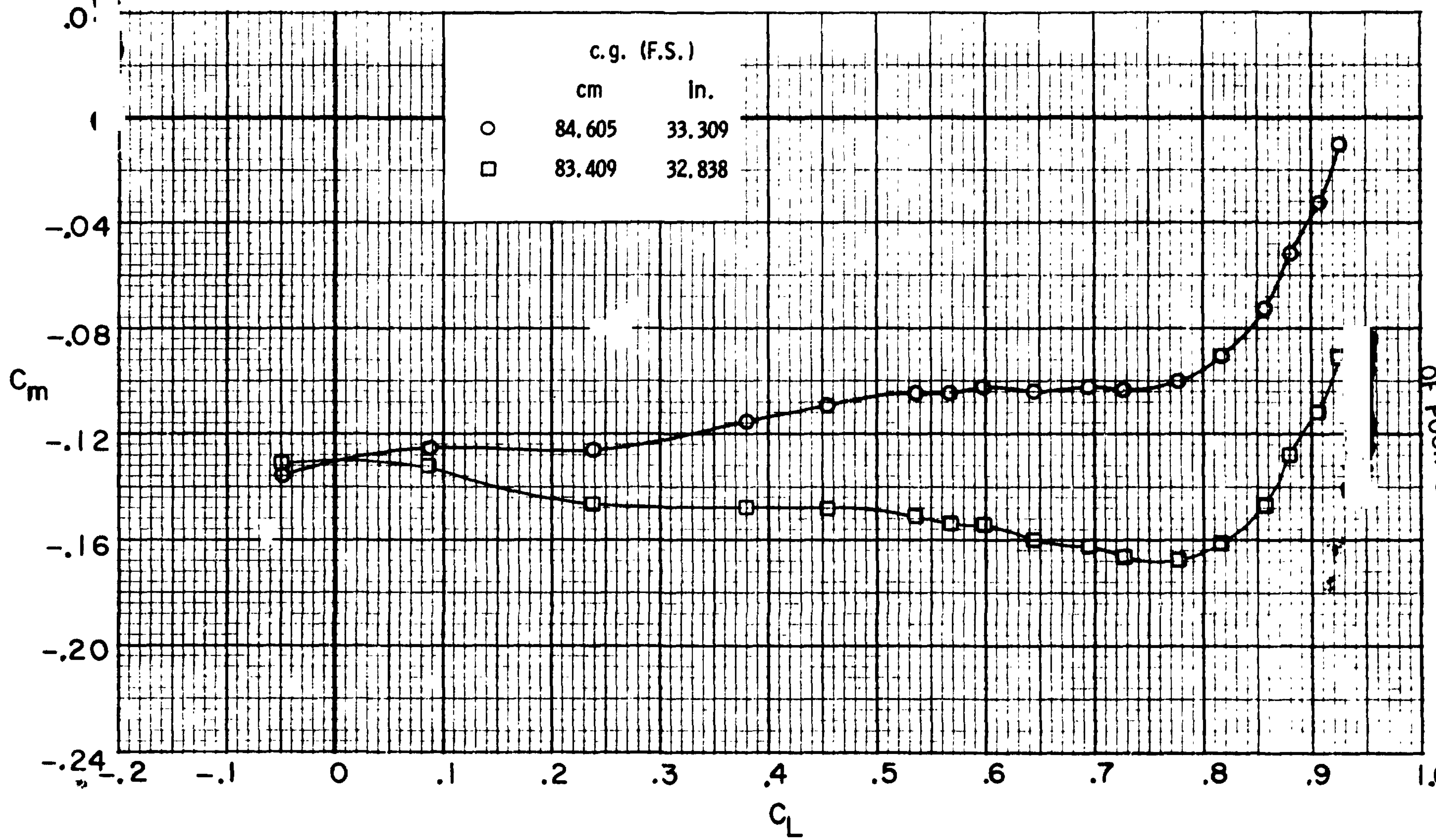

(e) M = 0.79. Concluded.

Figure 17. - Continued.

ORIGINAL PAGE IS
OF POOR QUALITY

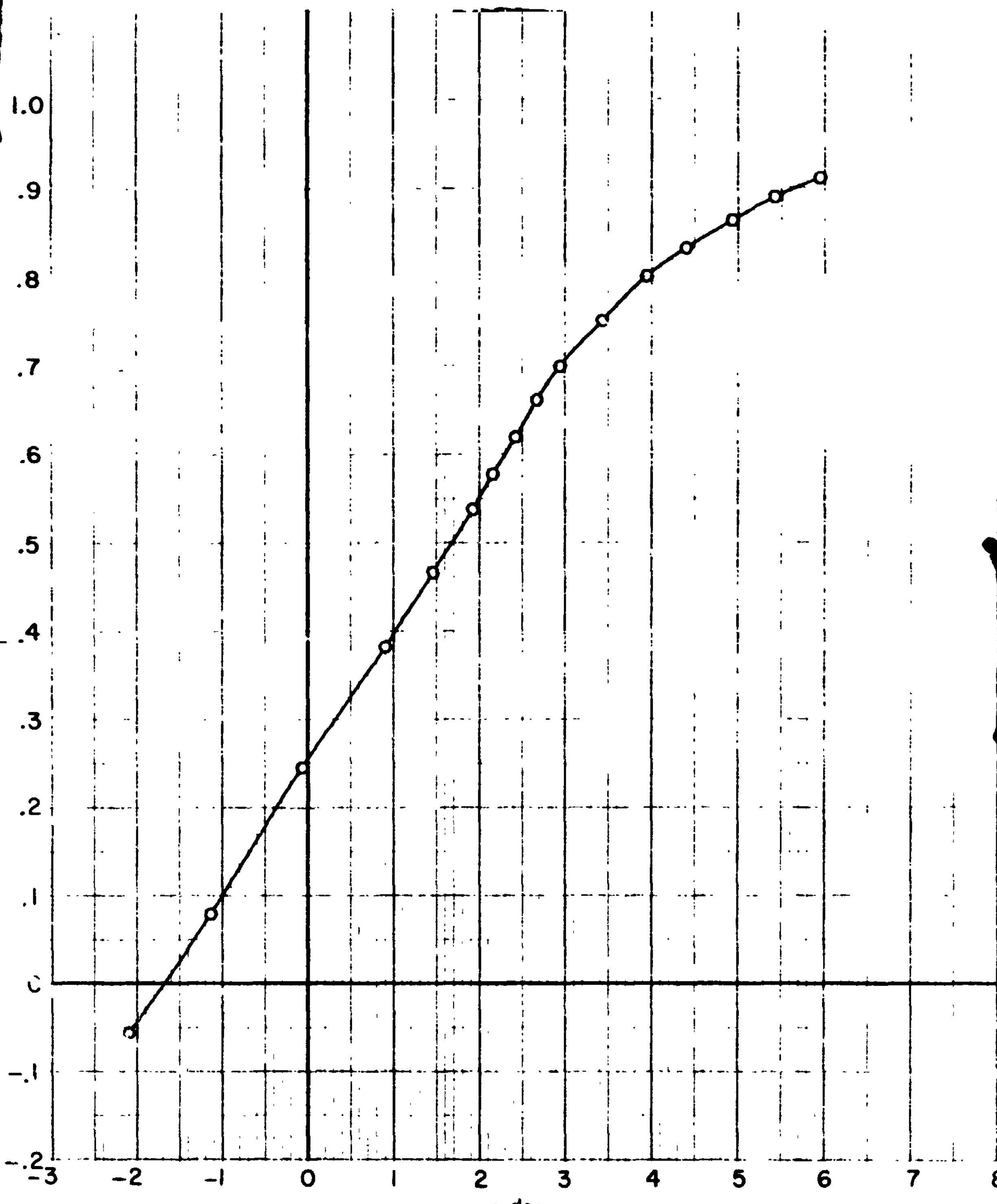

(f) M = 0.80.

Figure 17.- Continued.

[redacted]

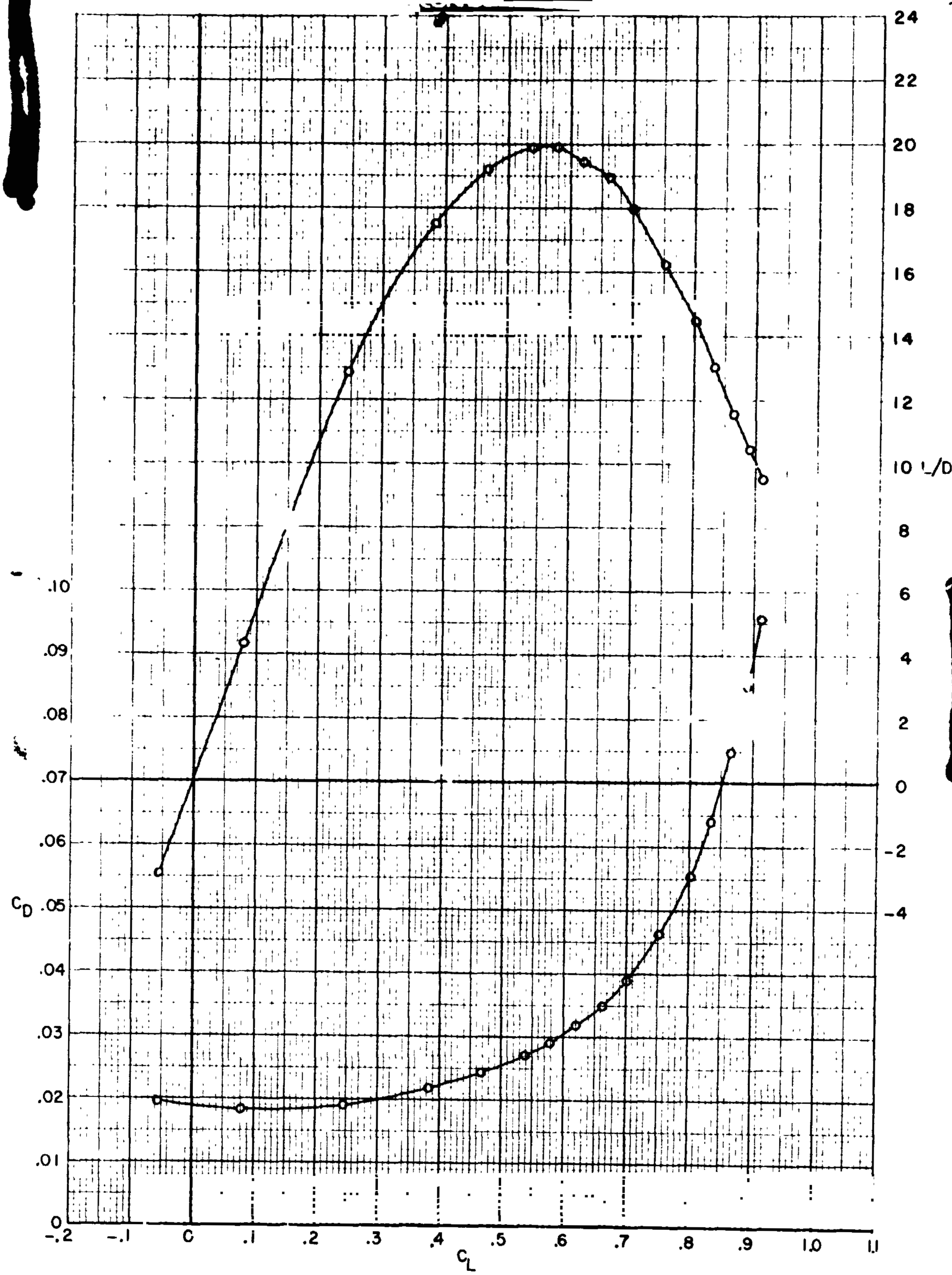

(f) M = 0.80. Continued.

Figure 17.- Continued.

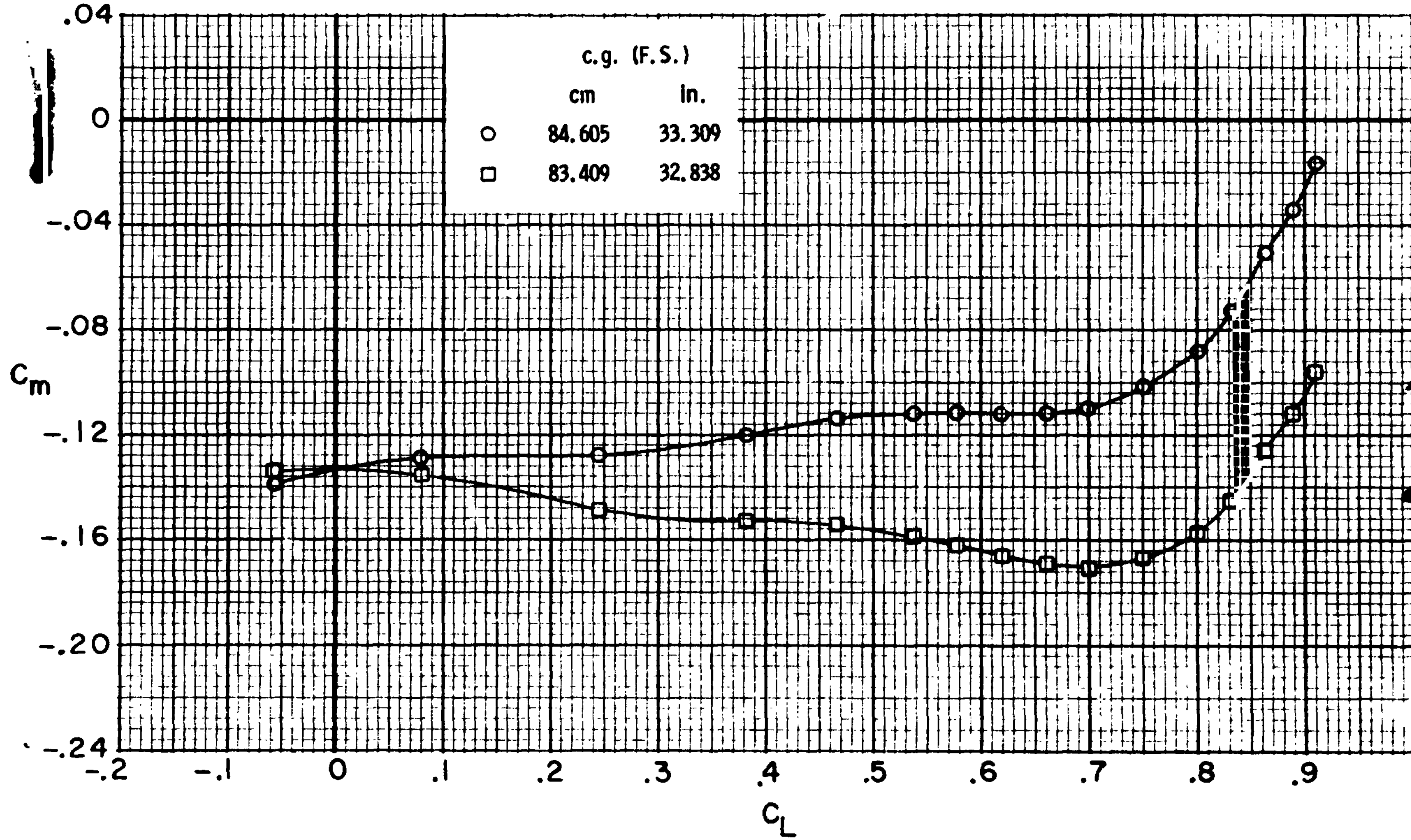

(f) M = 0.80. Concluded.

Figure 17.- Continued.

[redacted]

ORIGINAL PAGE IS
OF POOR QUALITY

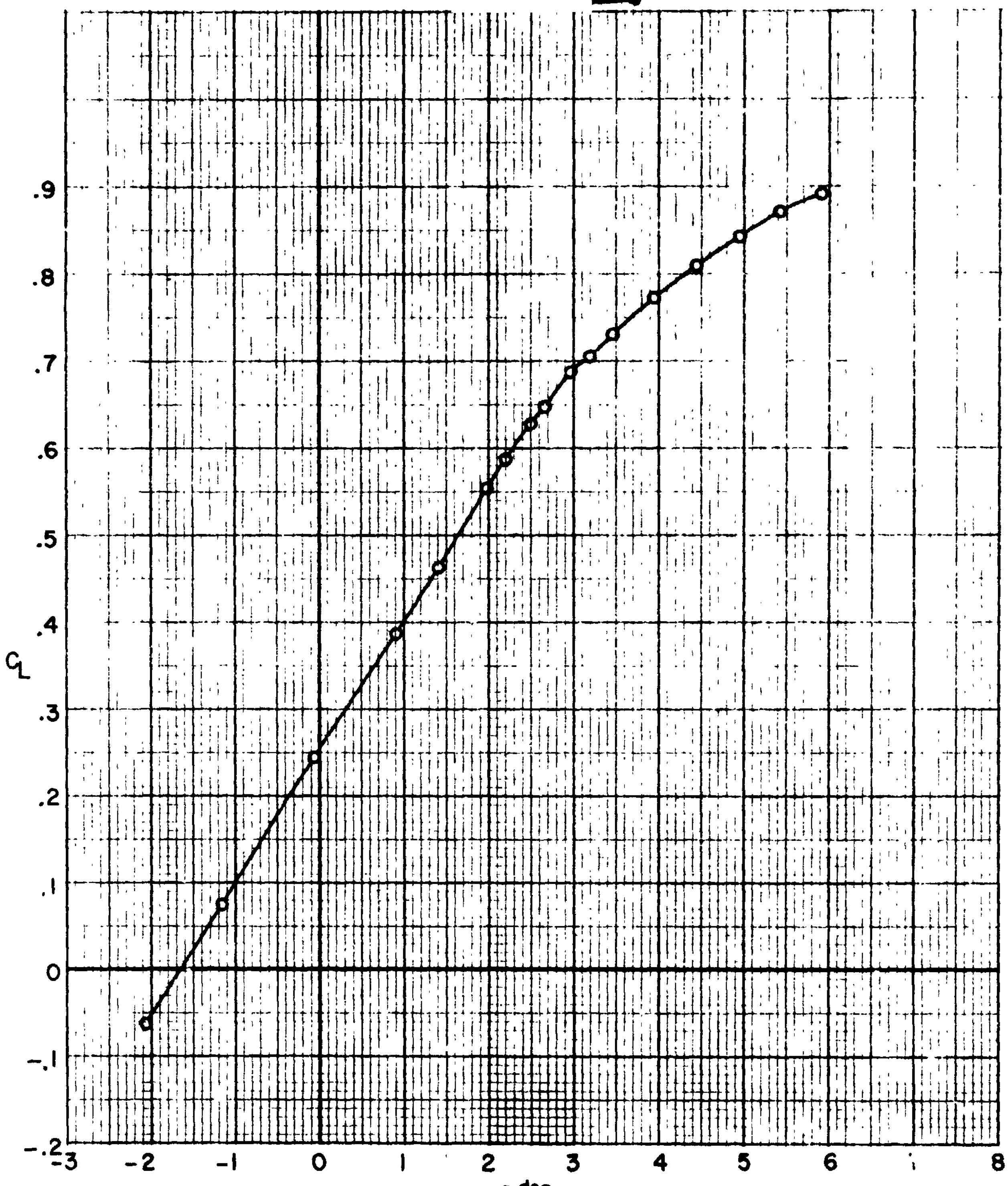

(g) M = 0.81.

Figure 17.- Continued.

[redacted]

ORIGINAL P
OF POOR Q

[redacted]

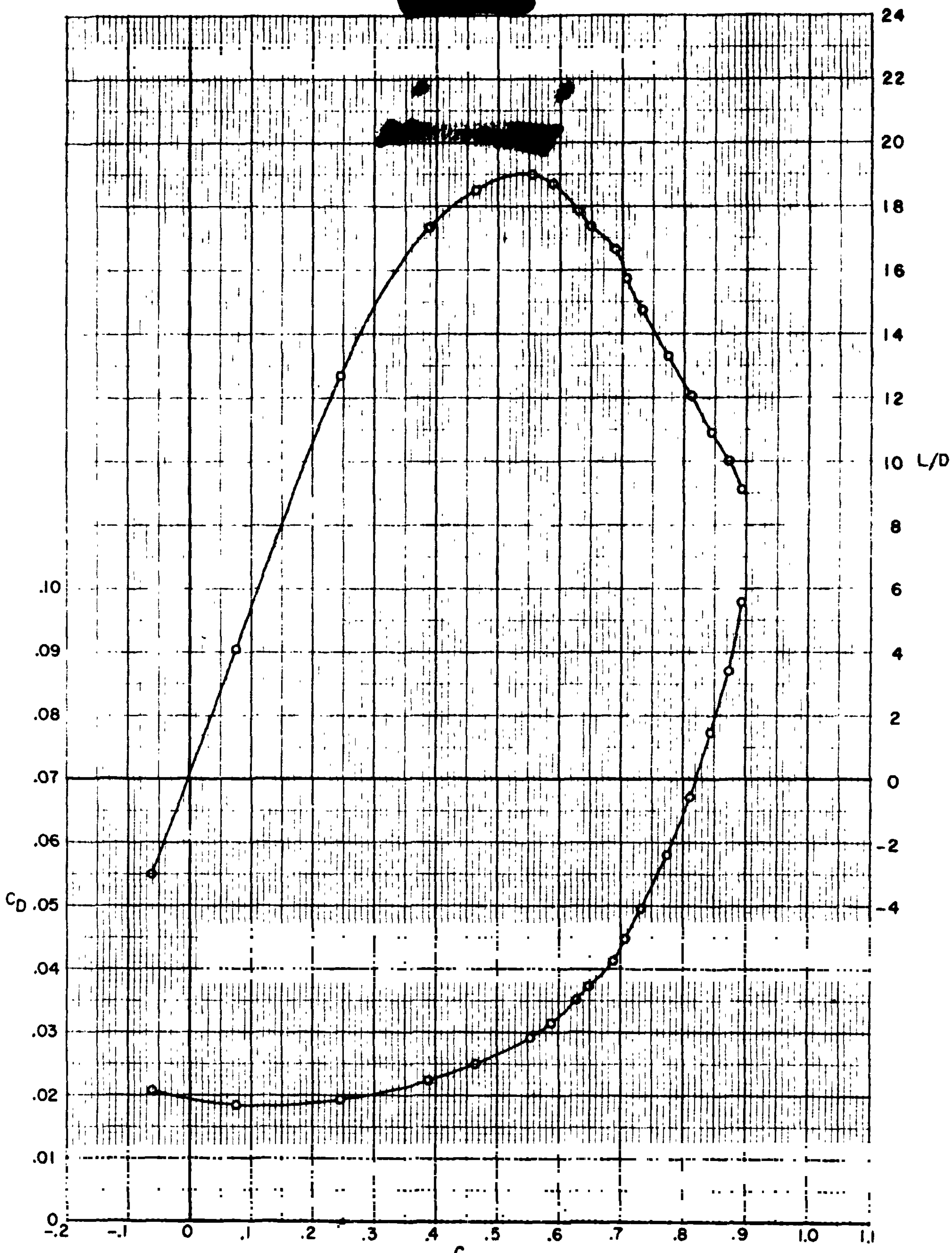

(g) M = 0.81. Continued.

Figure 17.- Continued.

[redacted]

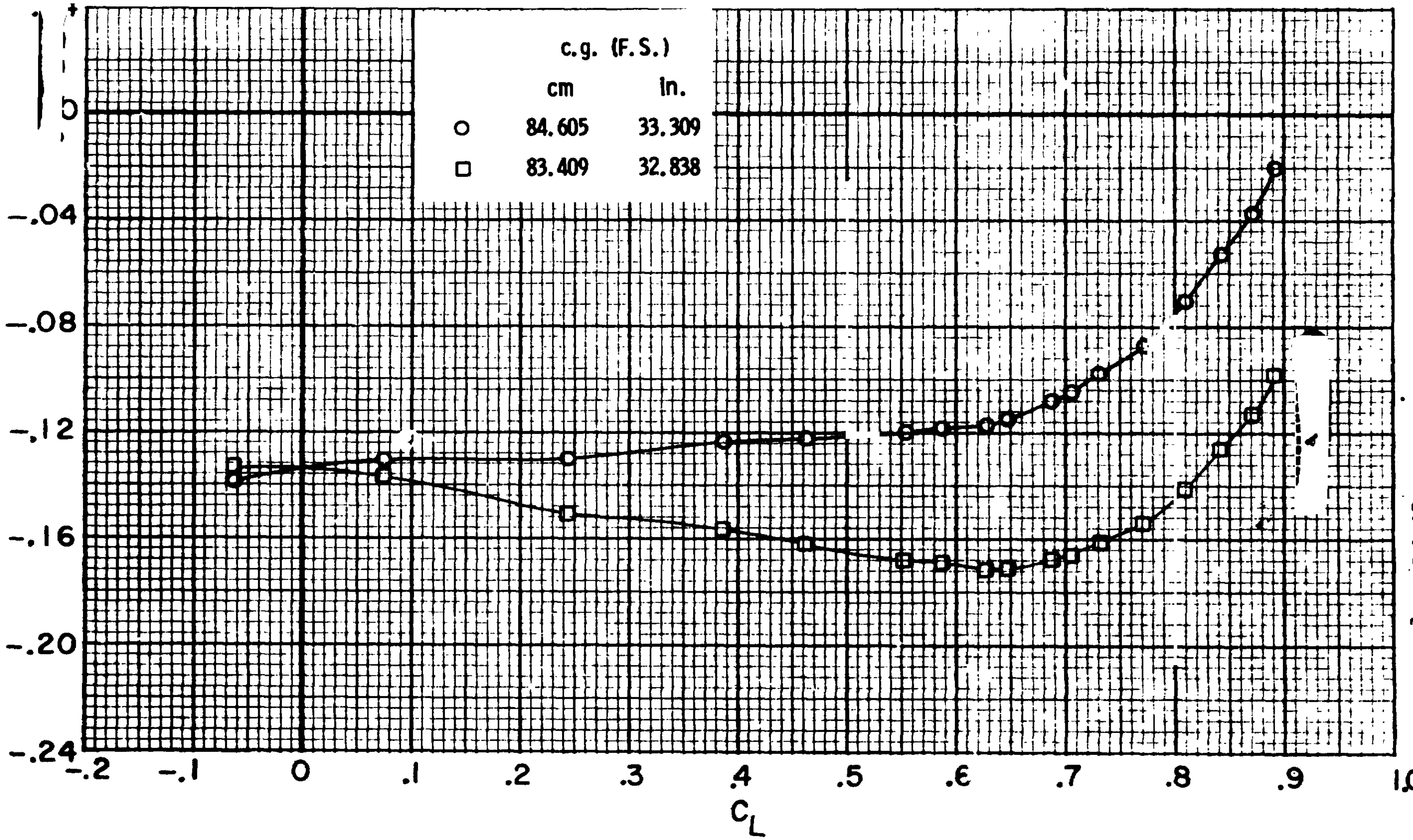

(g) M = 0.81. Concluded.

Figure 17.- Concluded.

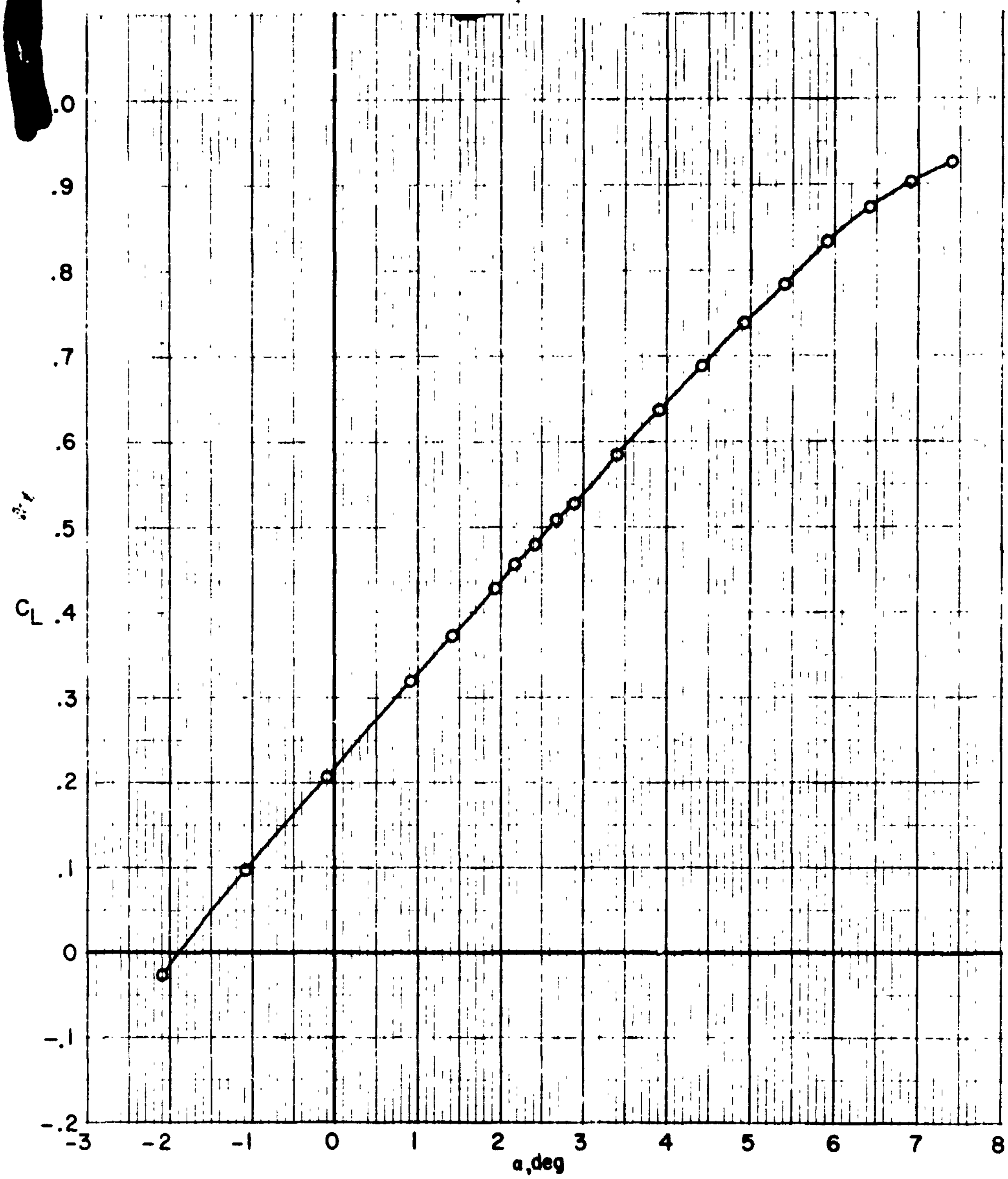

(a) M = 0.60.

Figure 18. - Longitudinal aerodynamic characteristics for supercritical wing configuration 2c (SCW-2c) with wing upper surface grit forward (x_T/c = 0.05). $\Lambda_{c/4}$ = 27°.

ORIGINAL PAGE IS
OF POOR QUALITY

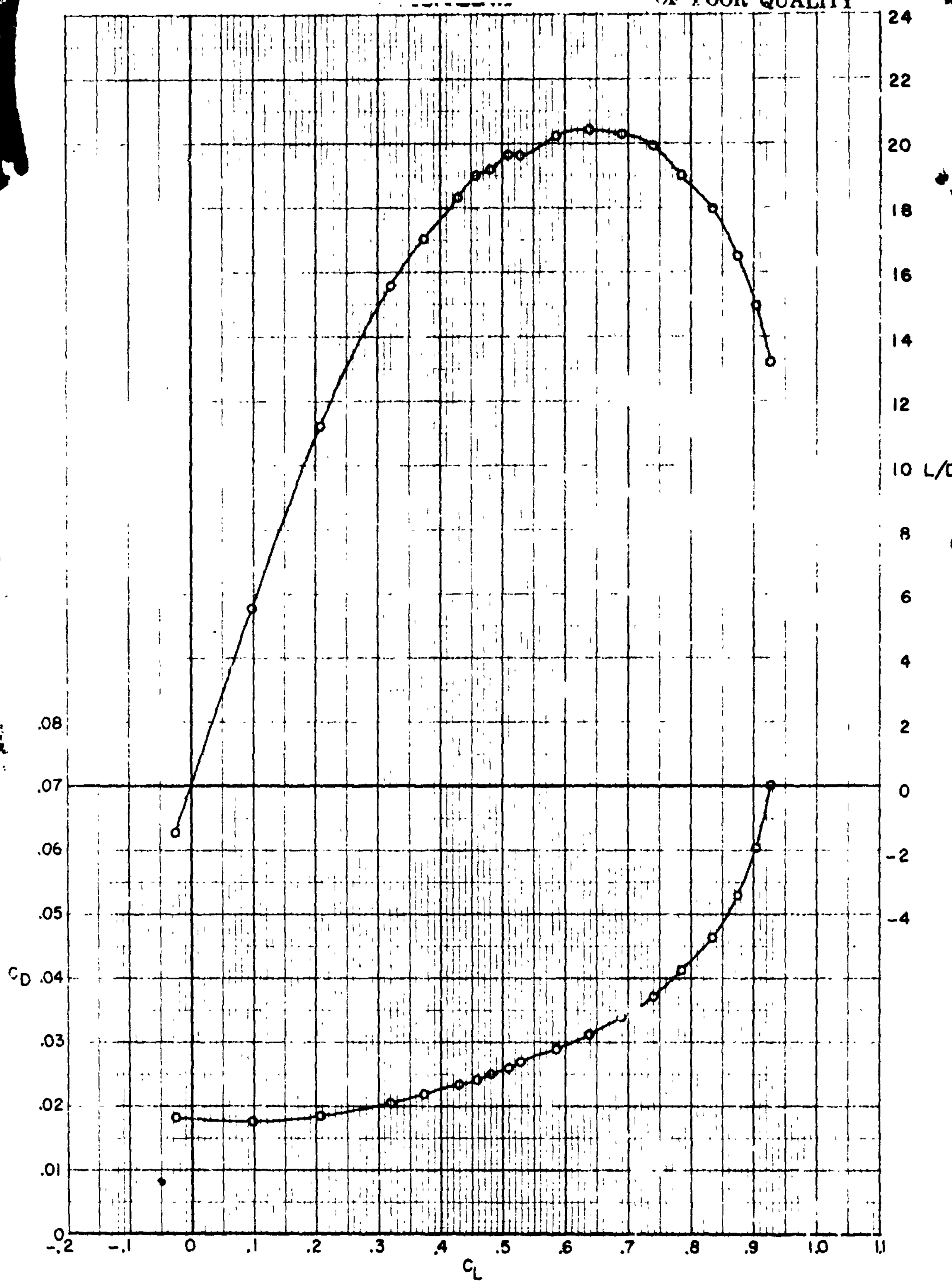

(a) M = 0.60. Continued.

Figure 18. - Continued.

[redacted]

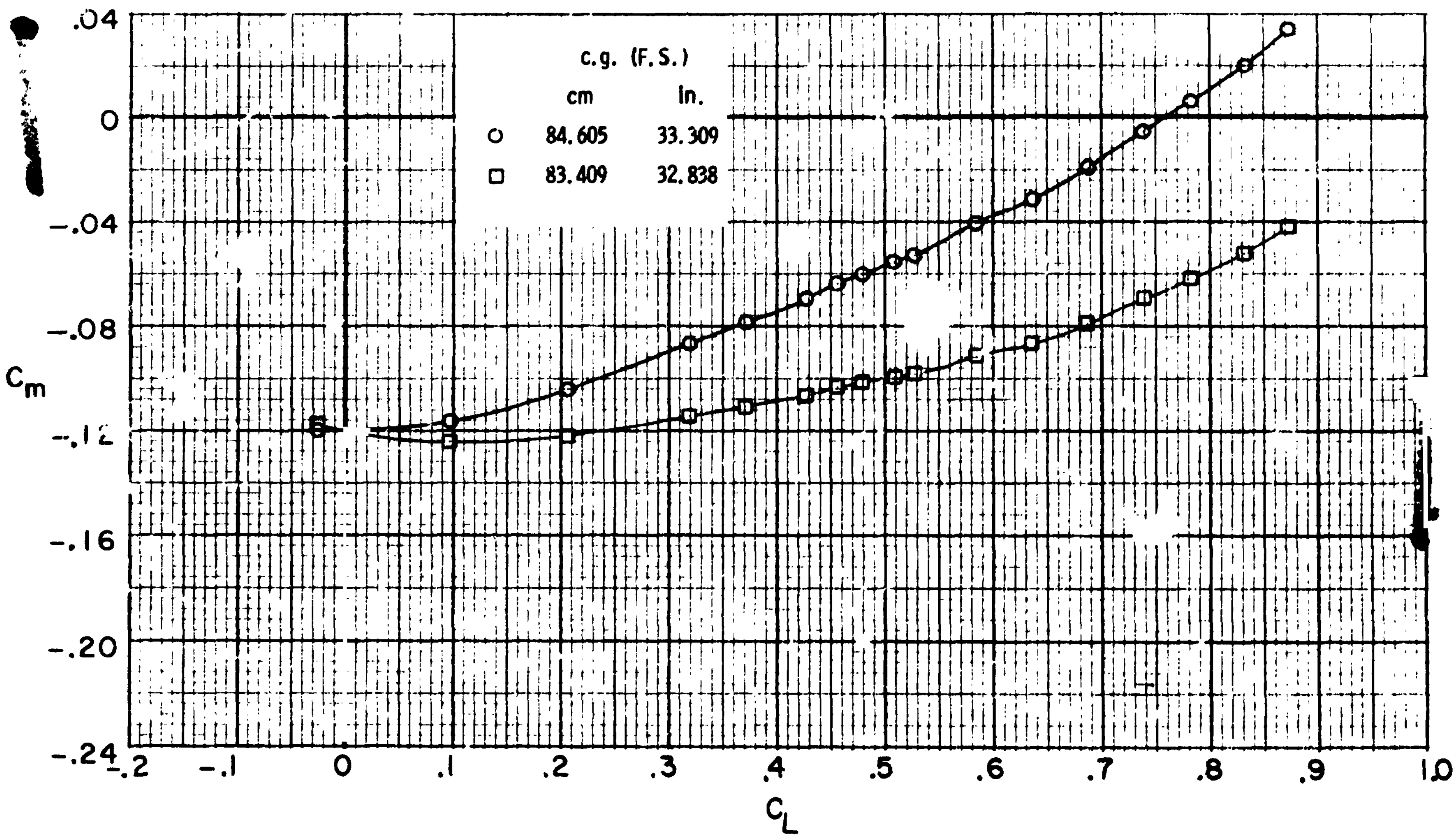

(a) M = 0.60. Concluded.

Figure - Continued.

[redacted]

ORIGINAL PAGE IS
OF POOR QUALITY

[redacted]

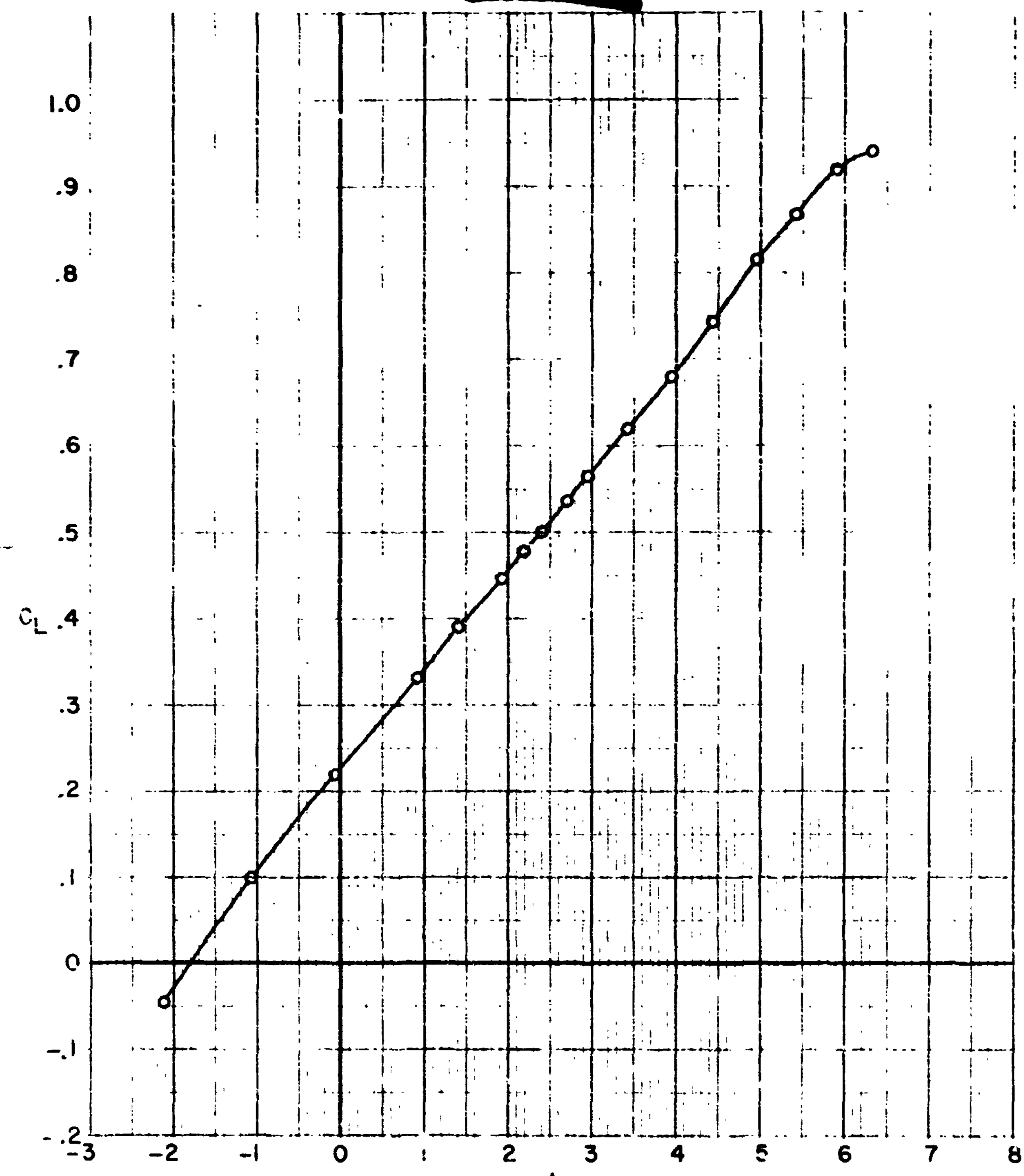

(b) M = 0. .

Figure 18.- Continued.

[redacted]

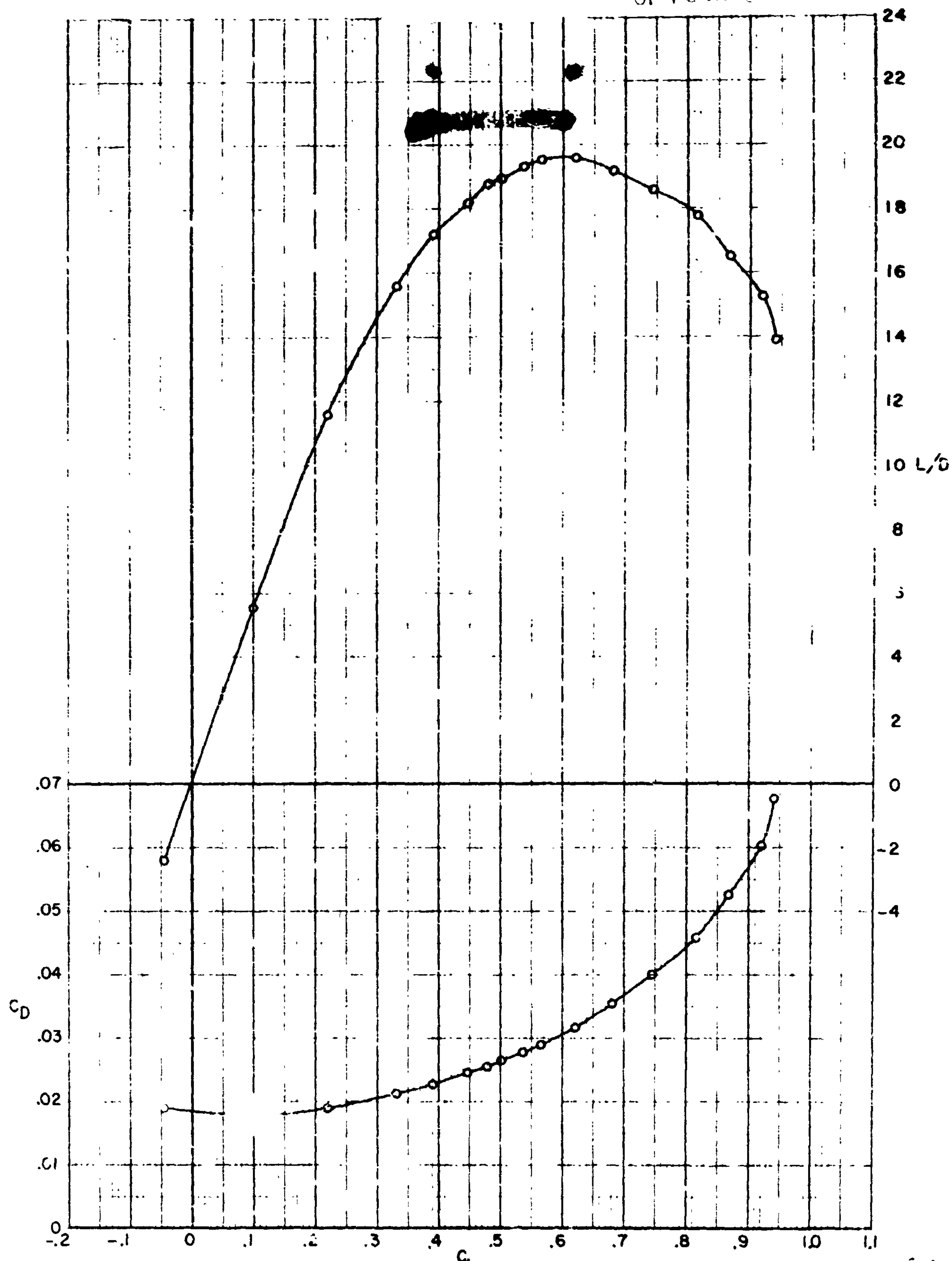

(b) M = 0.70. Continued.

Figure 18. - Continued.

[redacted]

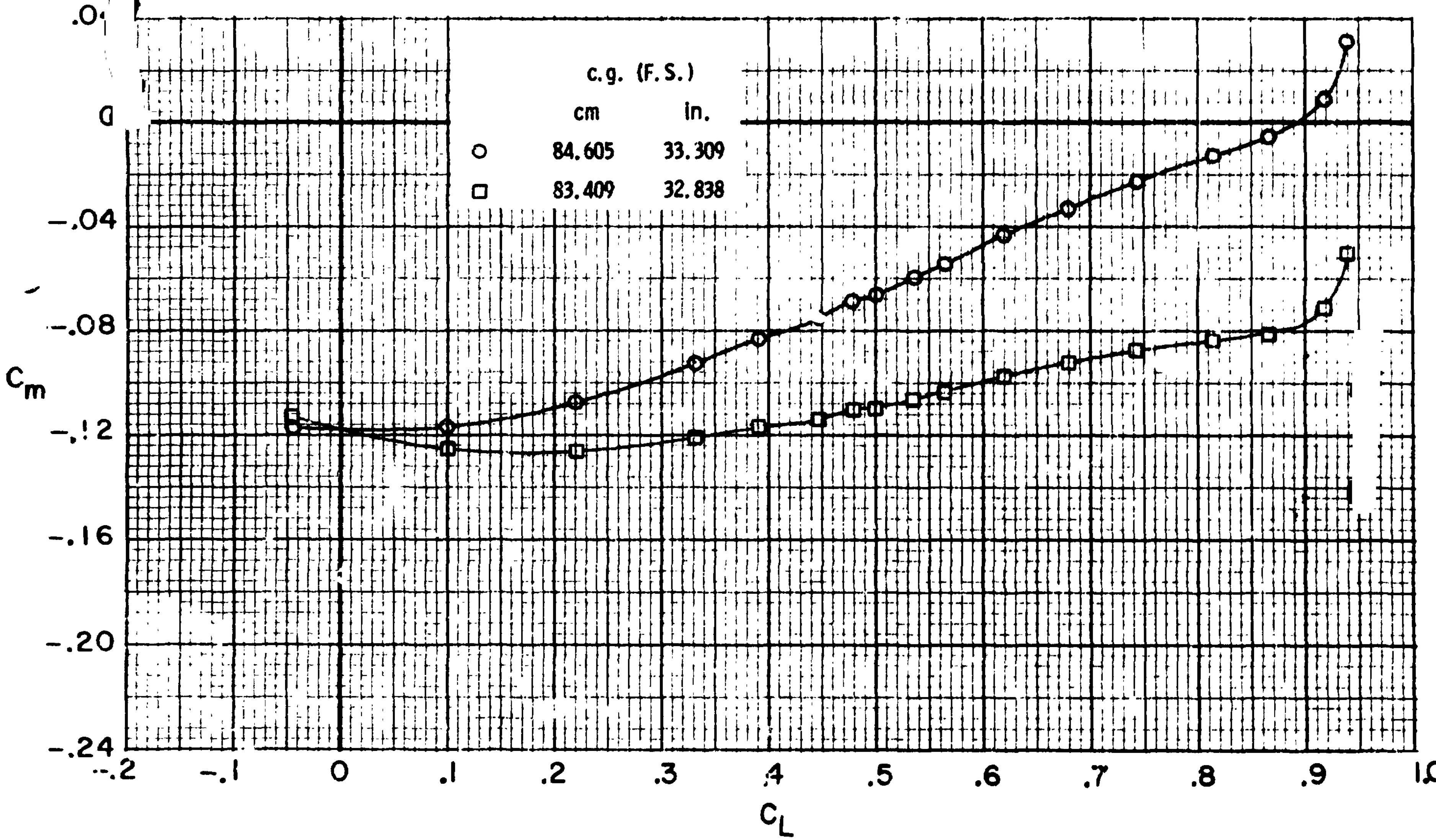

(b) M = 0.70. Concluded.

Figure 18. - Continued.

[redacted]

ORIGINAL PAGE IS
OF POOR QUALITY

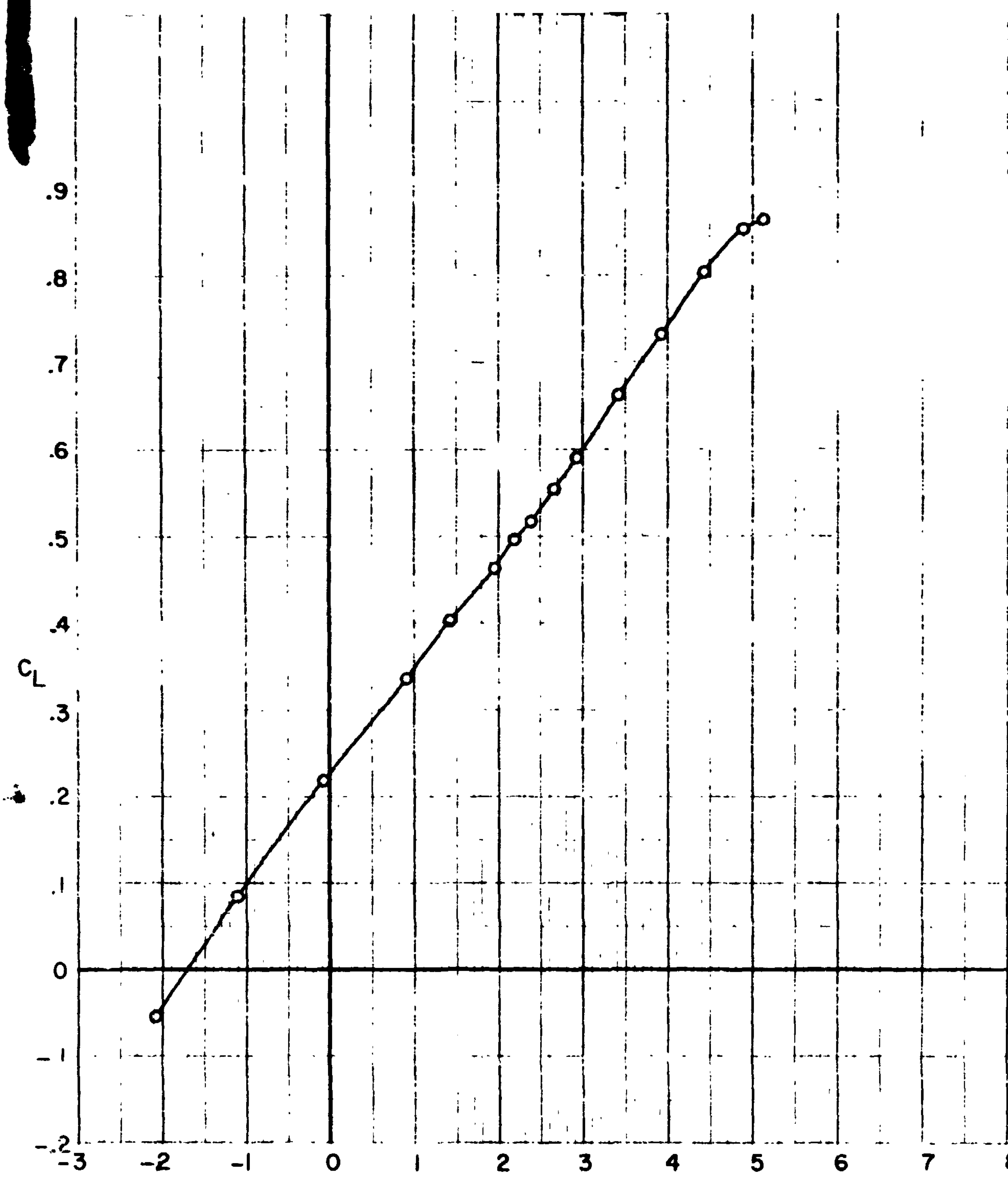

(c) M = 0.75.

Figure 18. - Continued.

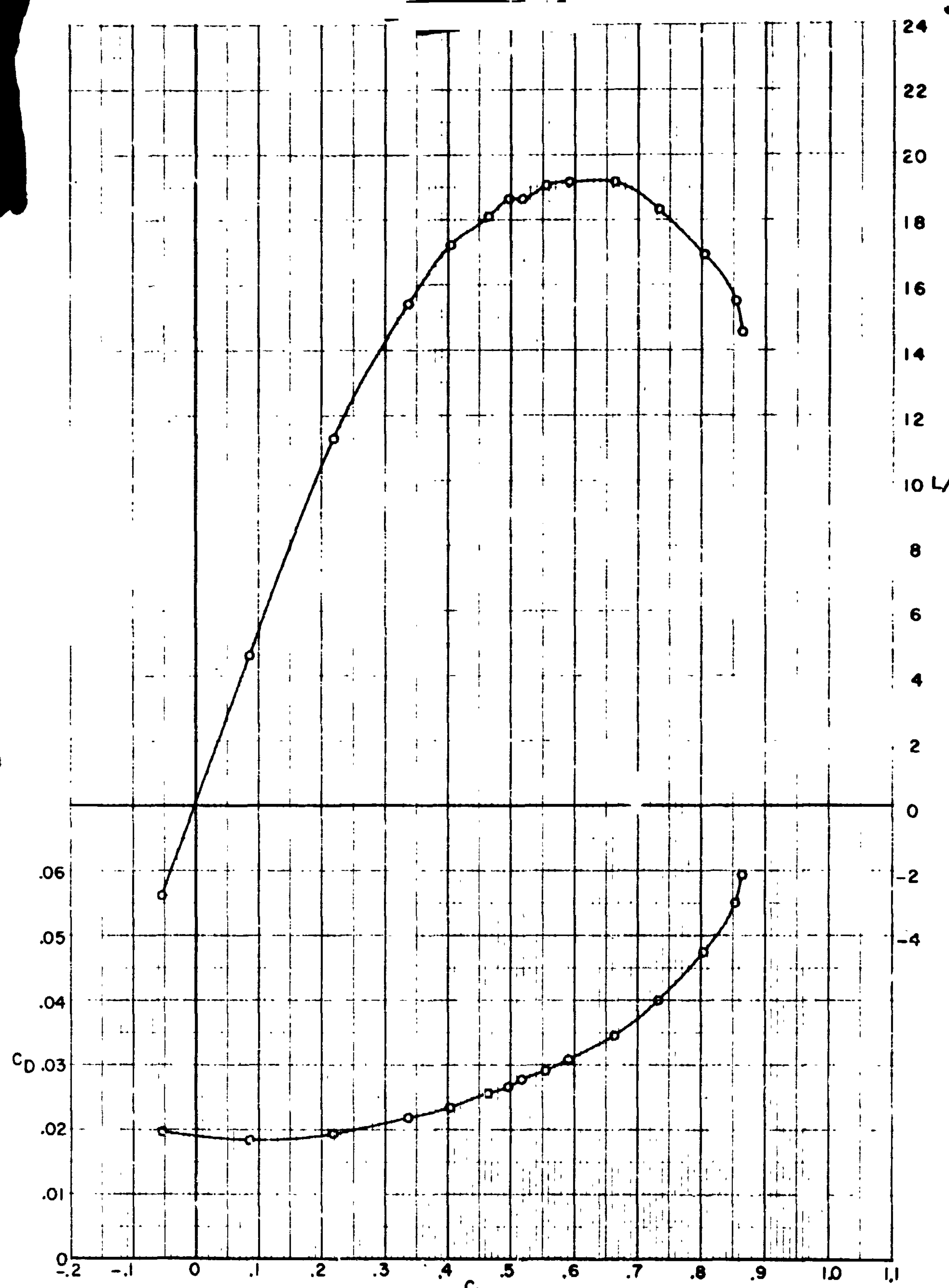

(c) M = 0.75. Continued.

Figure 18.- Continued.

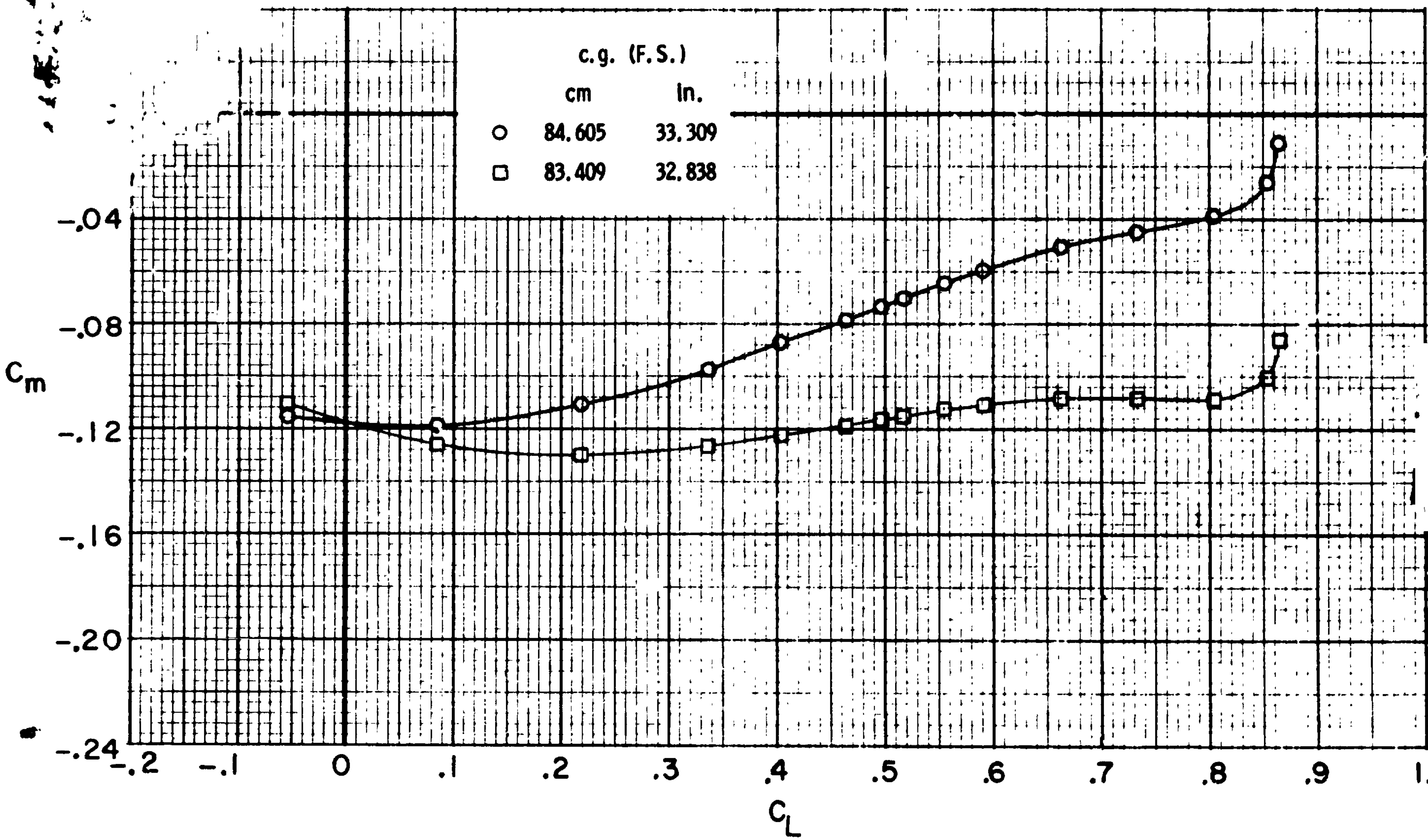

(c) M = 0.75. Concluded.

Figure 18. - Continued.

ORIGINAL PAGE IS
OF POOR QUALITY

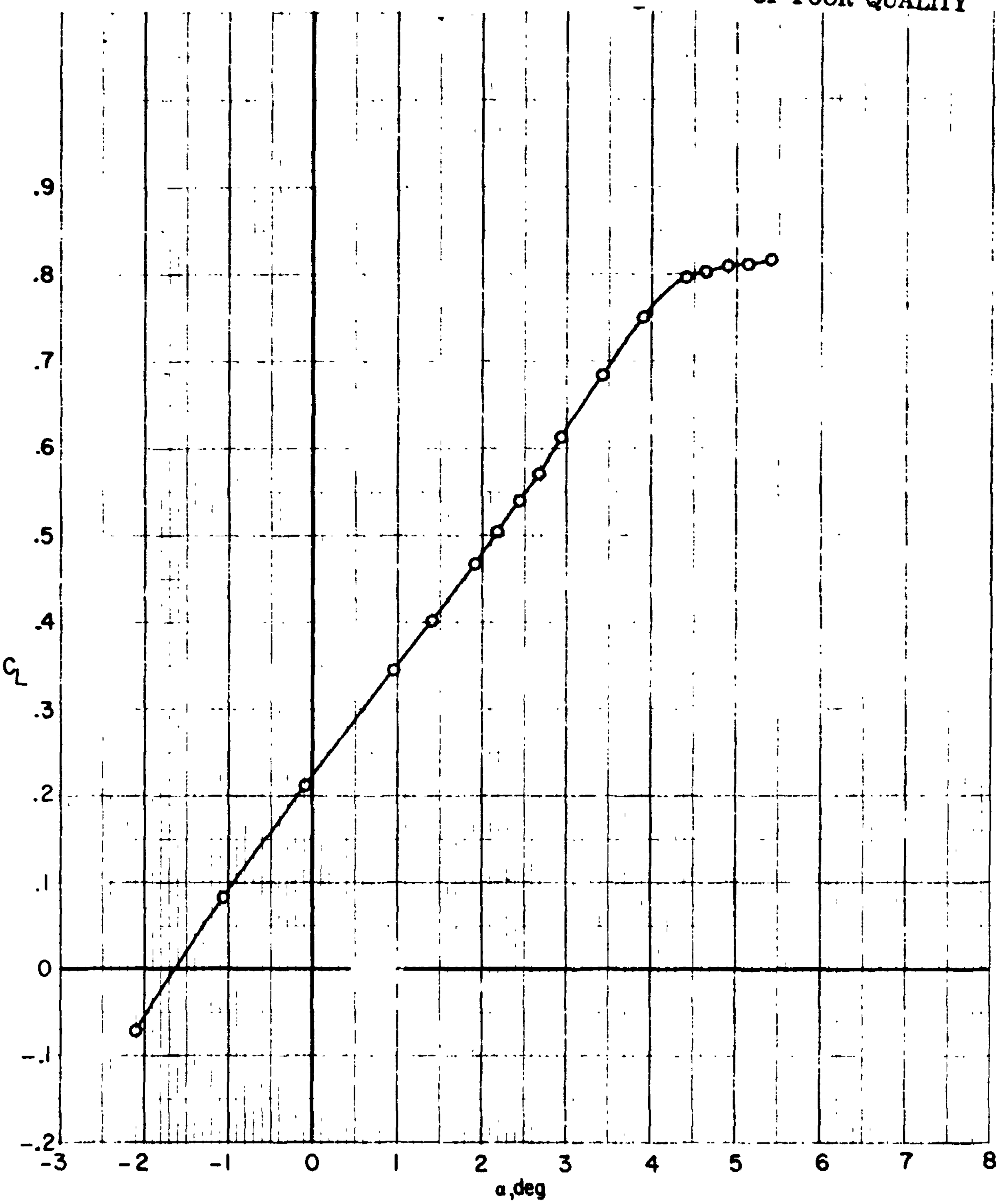

(d) M = 0.77.

Figure 18. - Continued.

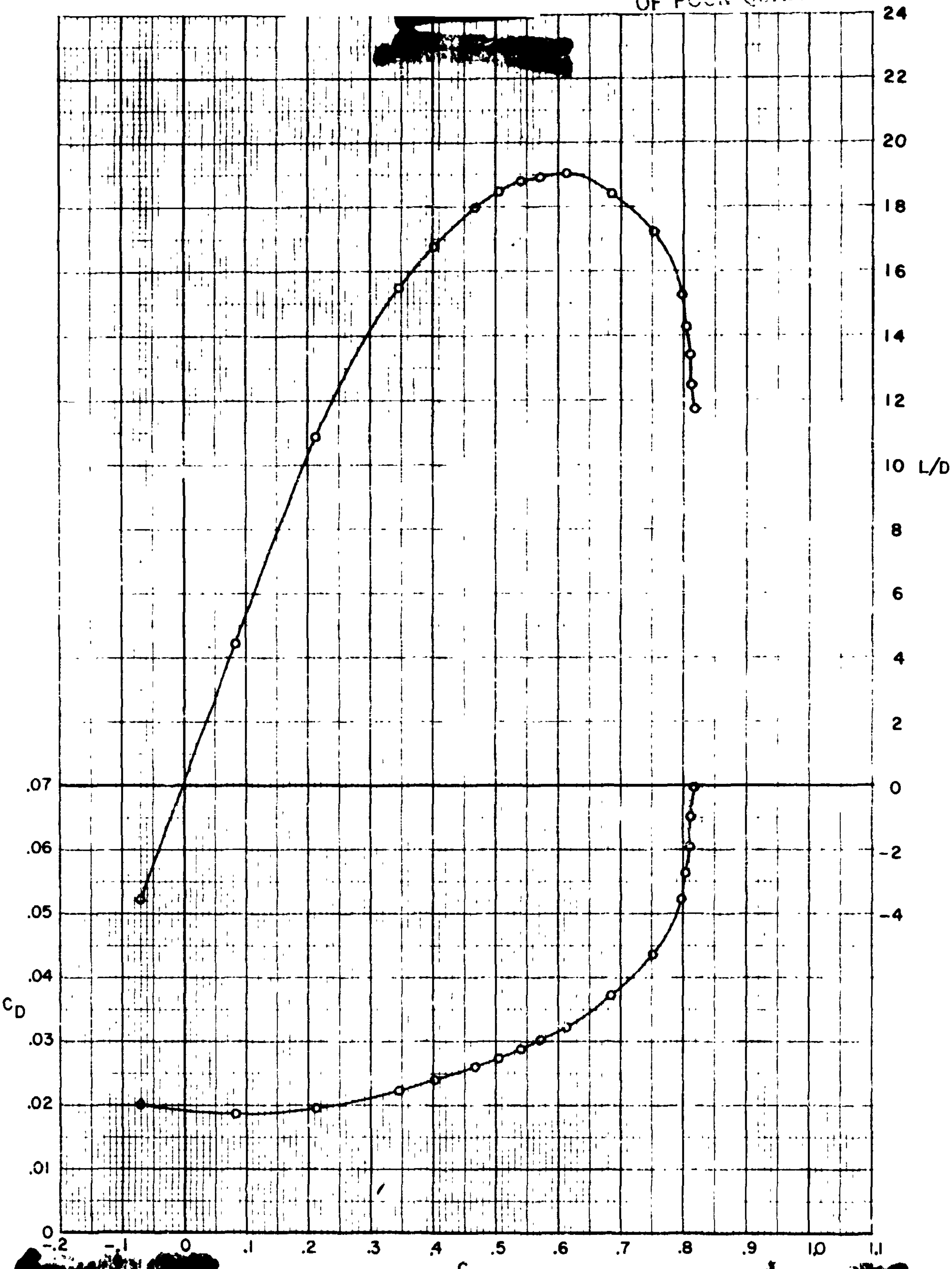

(d) M = 0.77. Continued.

Figure 18. - Continued.

[redacted]

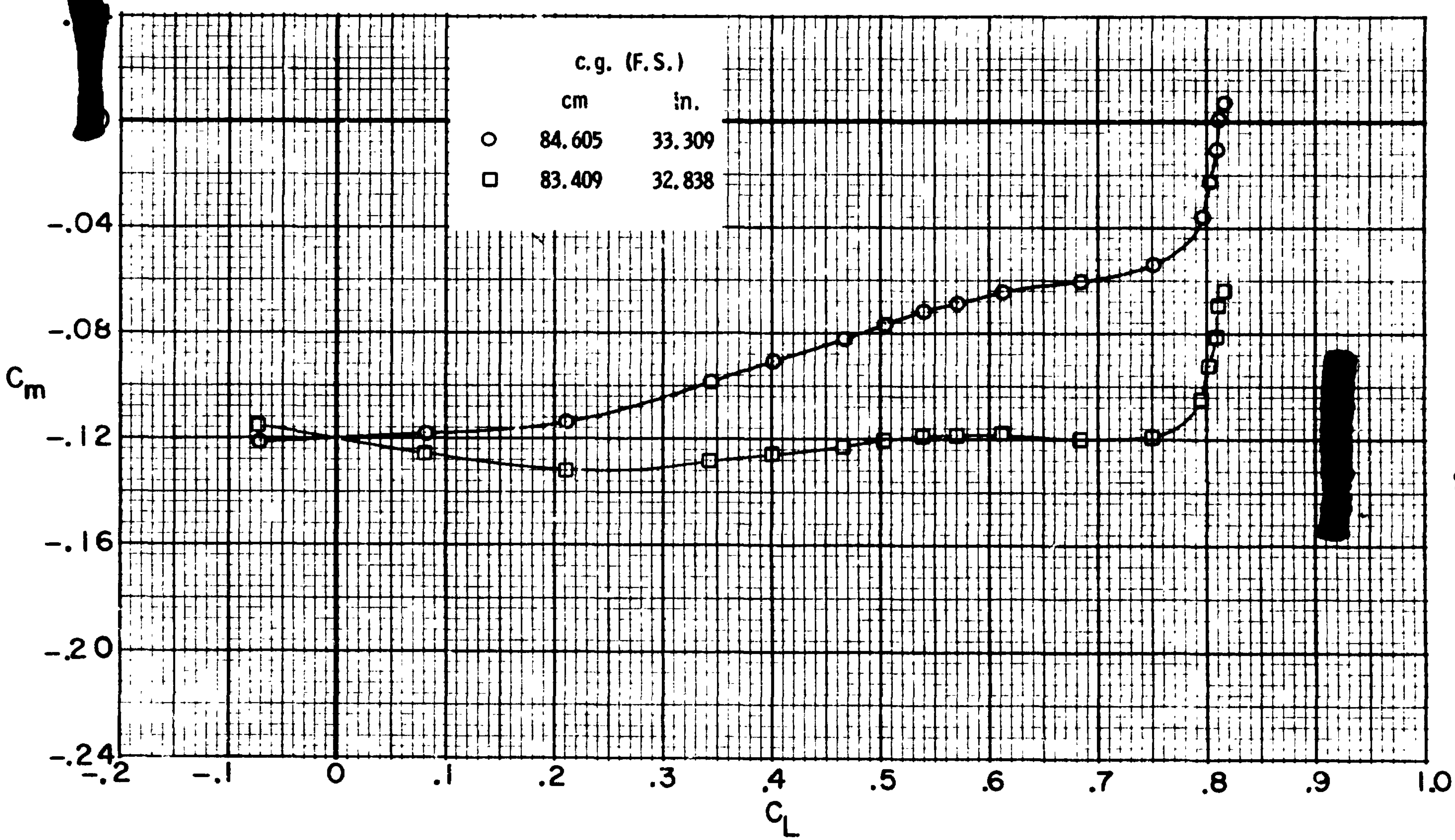

(d) M = 0.77. Concluded.

Figure 18. - Continued.

ORIGINAL PAGE IS
OF POOR QUALITY

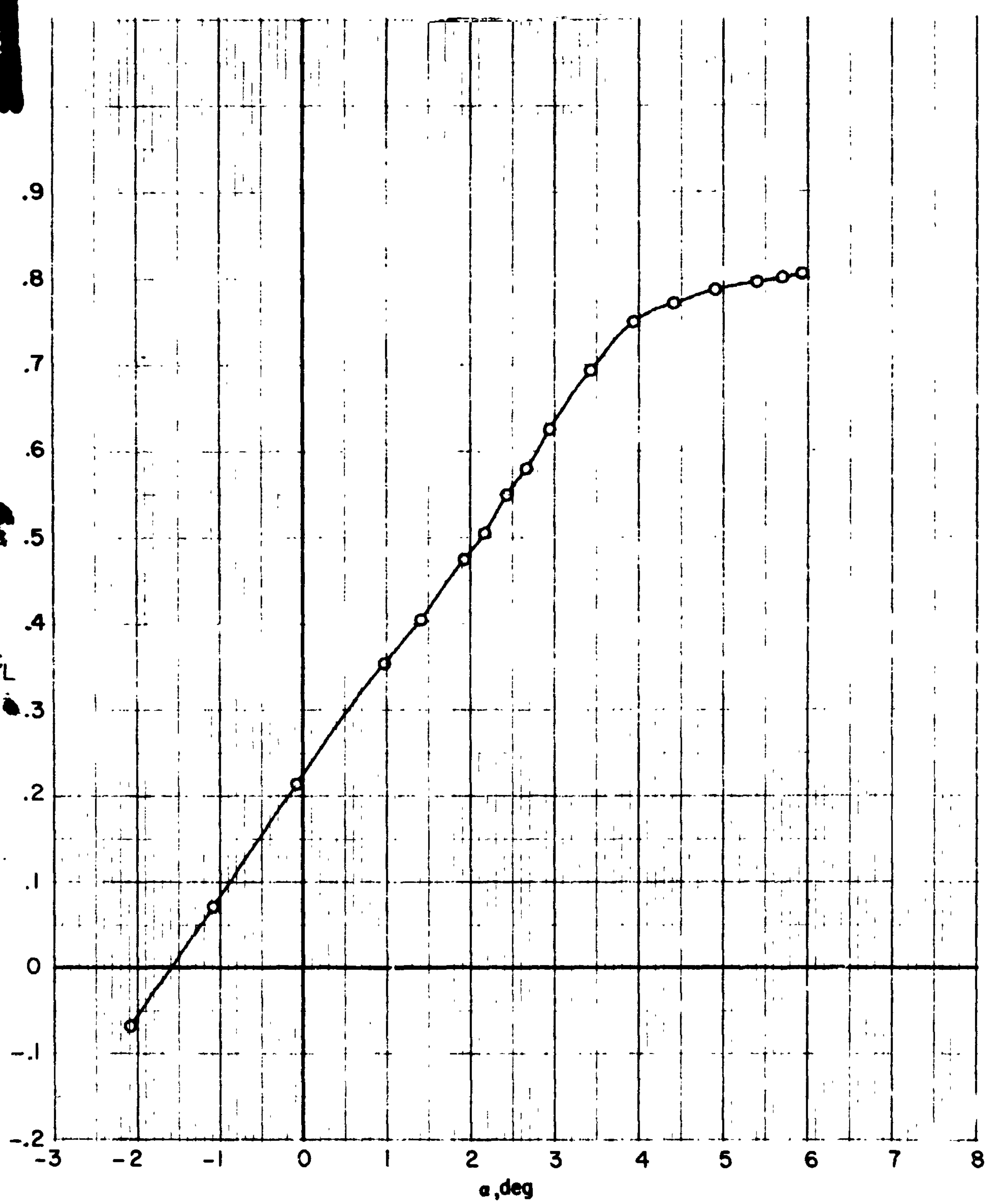

(e) M = 0.78.

Figure 18.- Continued.

ORIGINAL PAGE IS
OF POOR QUALITY

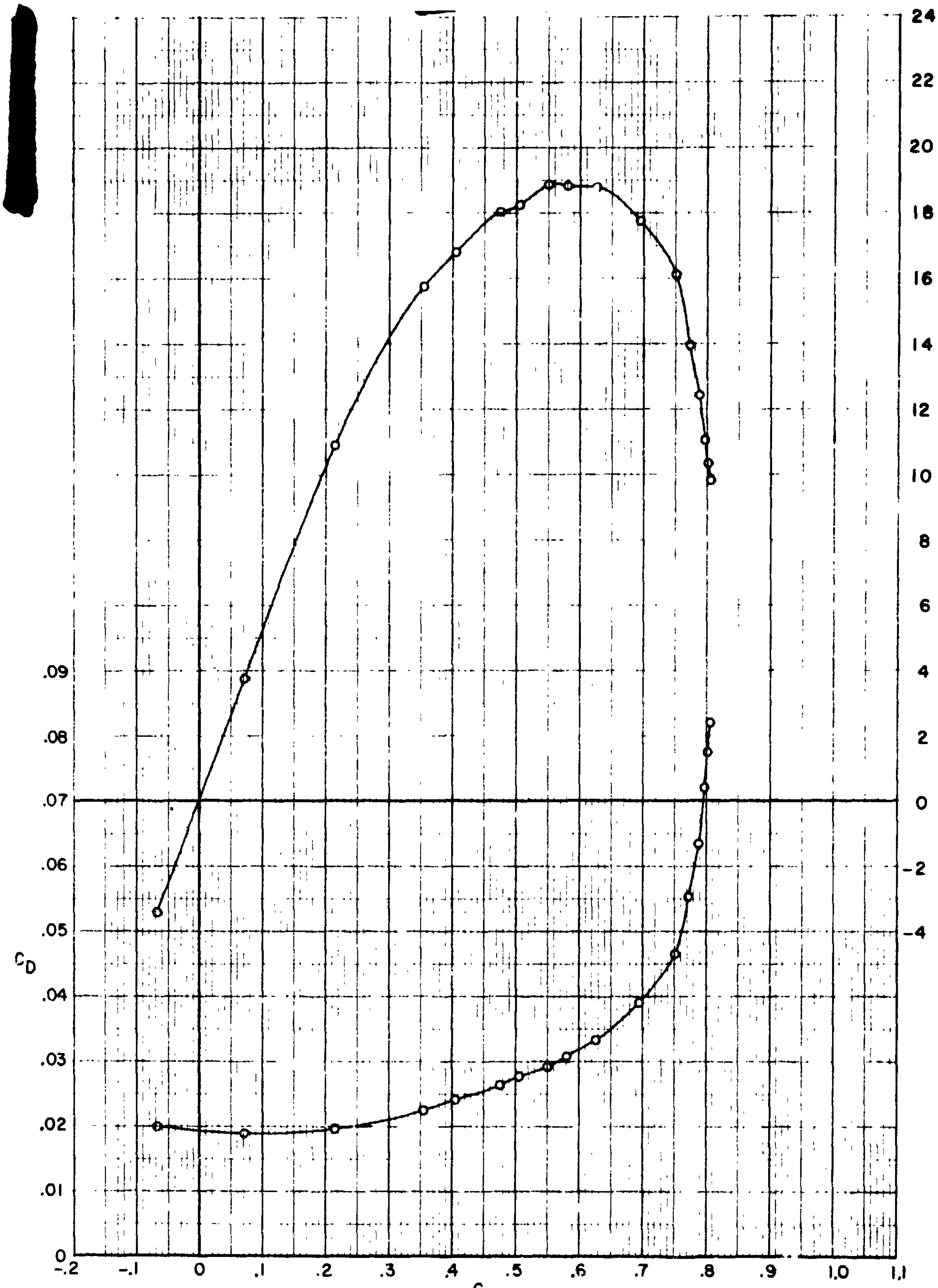

(e) M = 0.78. Continued.

Figure 13.- Continued.

[redacted]

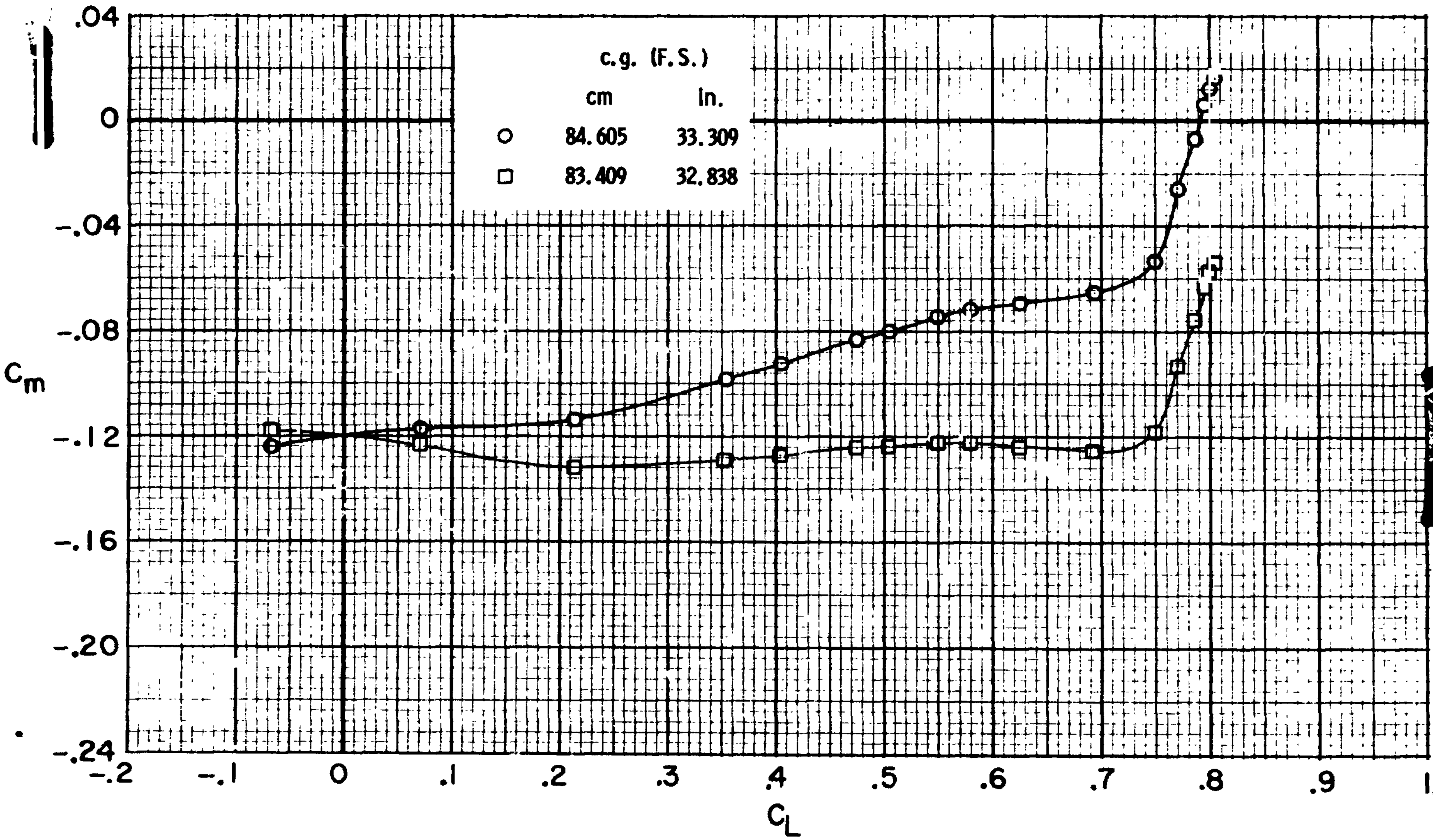

(e) M = 0.78. Concluded.

Figure 18. - Concluded.

[redacted]

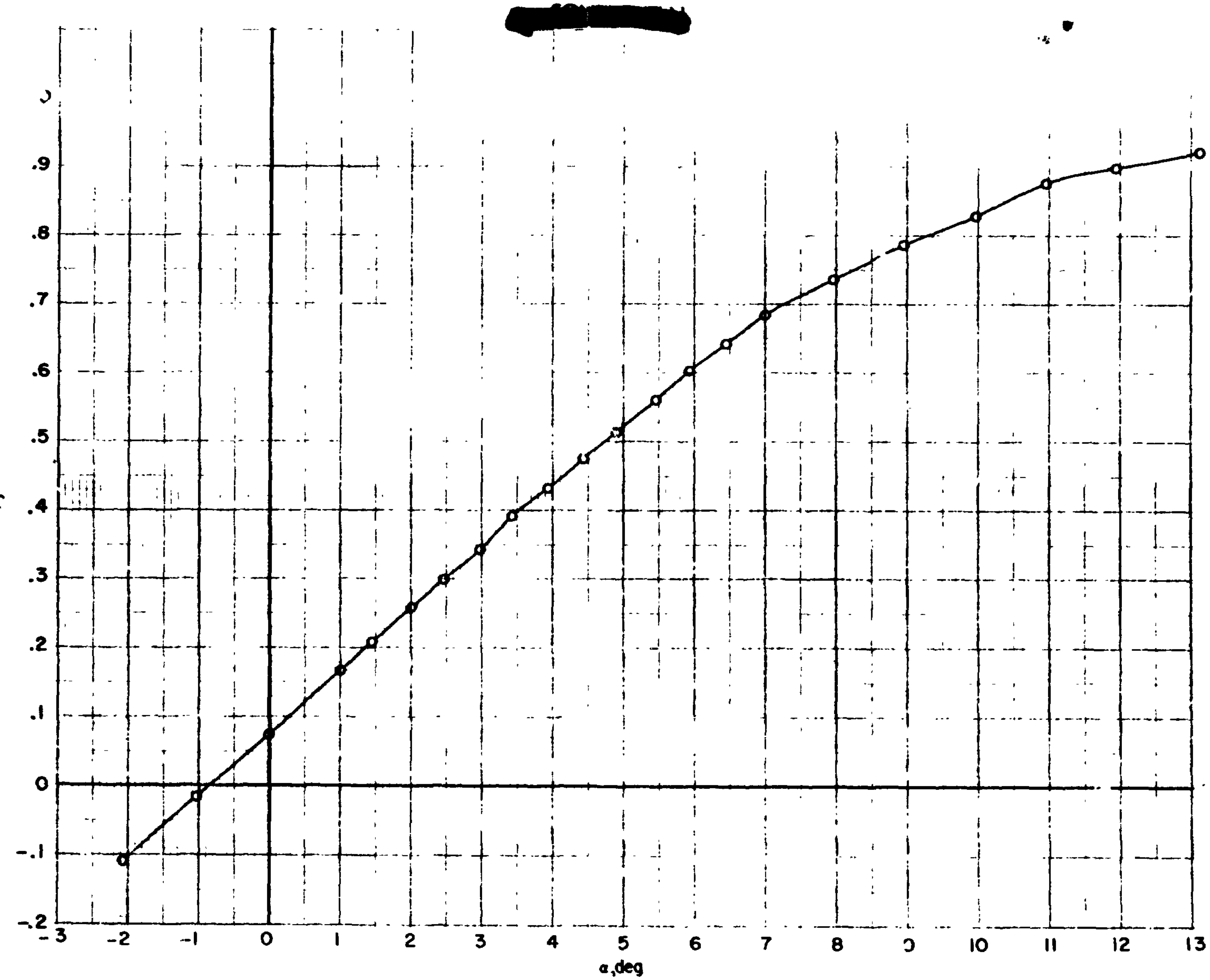

(a) M = 0.60.

Figure 19.- Longitudinal aerodynamic characteristics for simulated current wide-body configuration with wing upper surface grit aft (fig. 5). c.g. (F.S.) = 84.605 cm (33.309 in.); $\Lambda_{c/4} = 35°$.

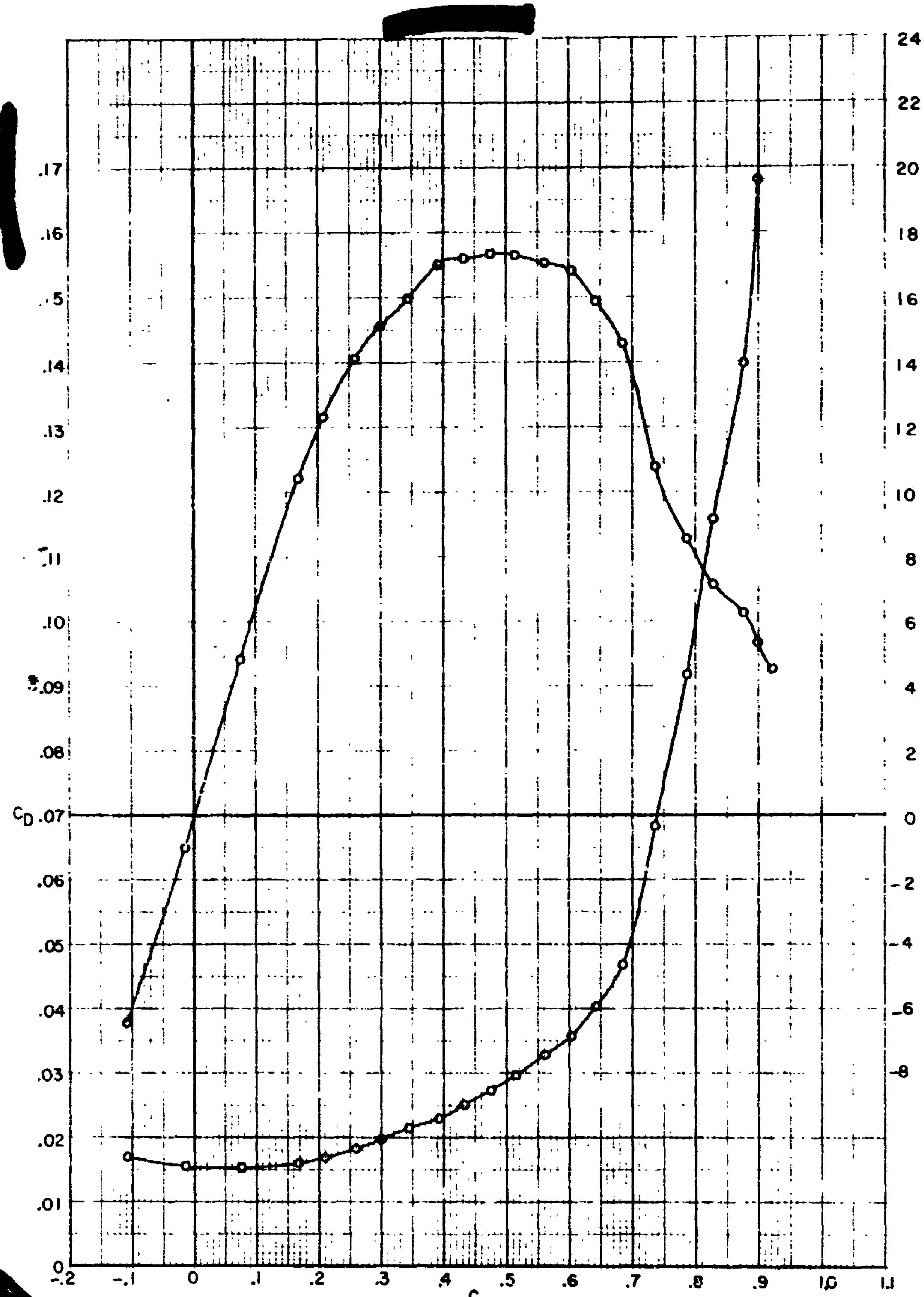

(a) M = 0.60. Continued.

Figure 19. - Continued.

C-4

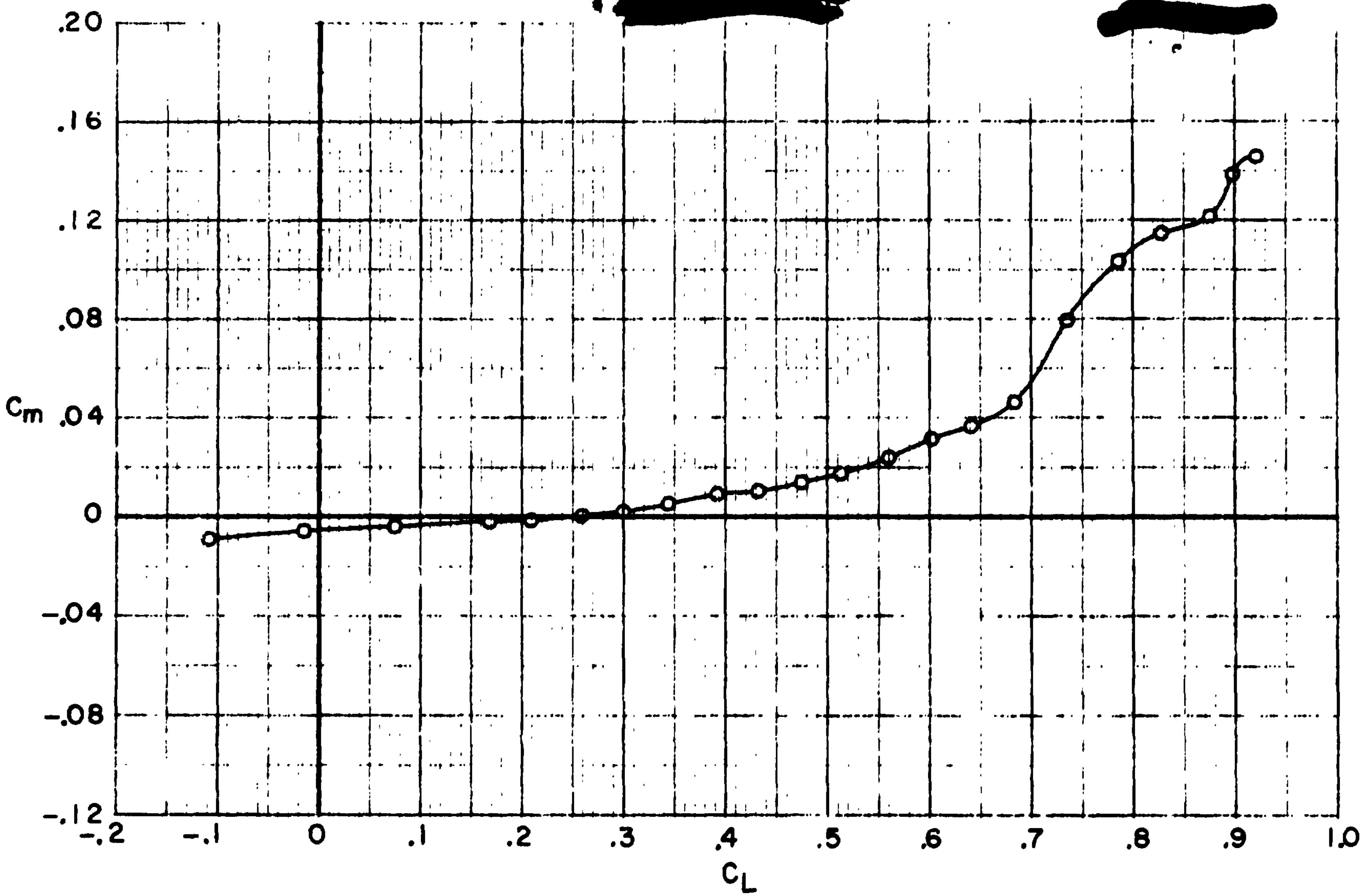

(a) M = 0.60. Concluded.

Figure 19.- Continued.

ORIGINAL PAGE IS
OF POOR QUALITY

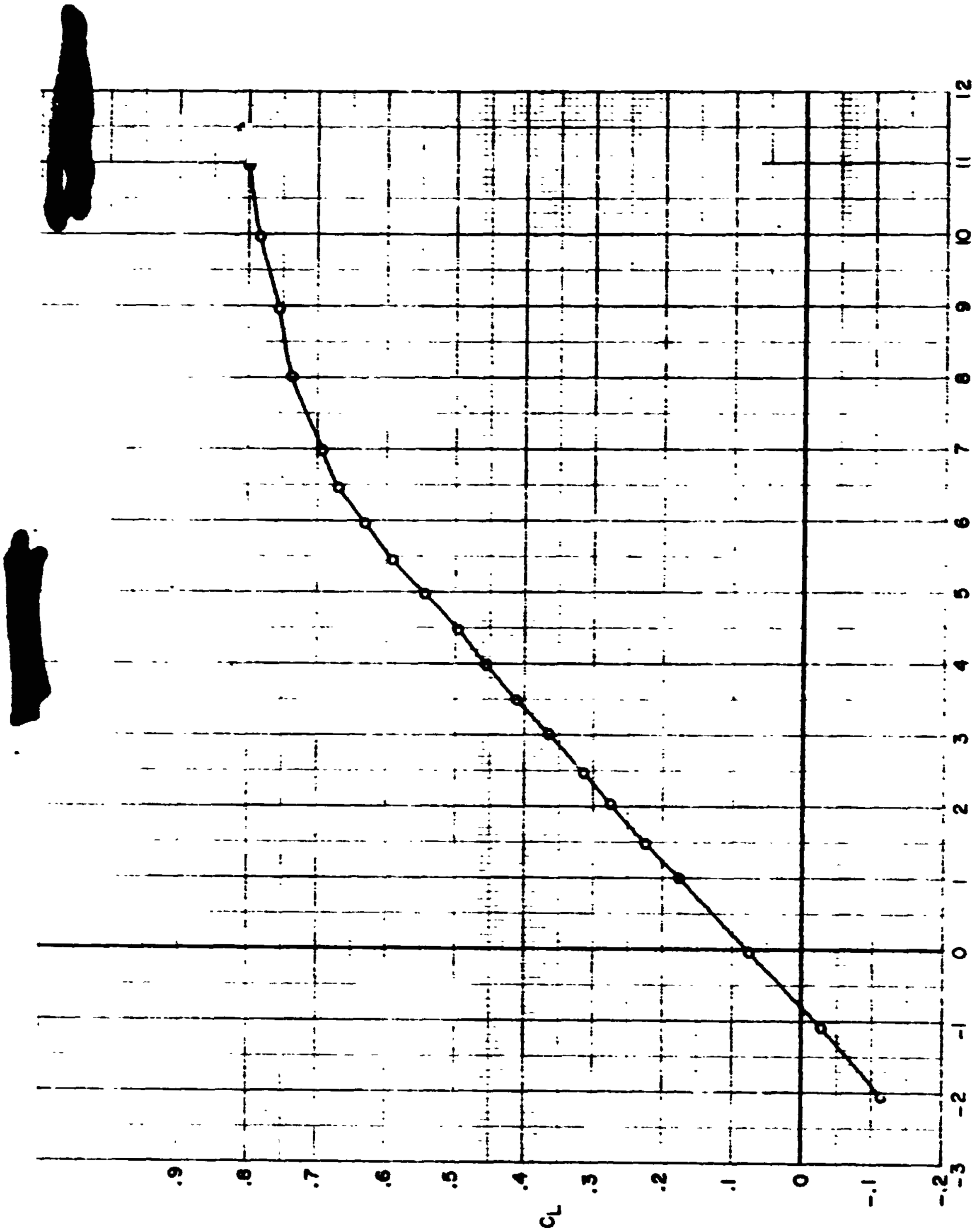

(b) M = 0.70.

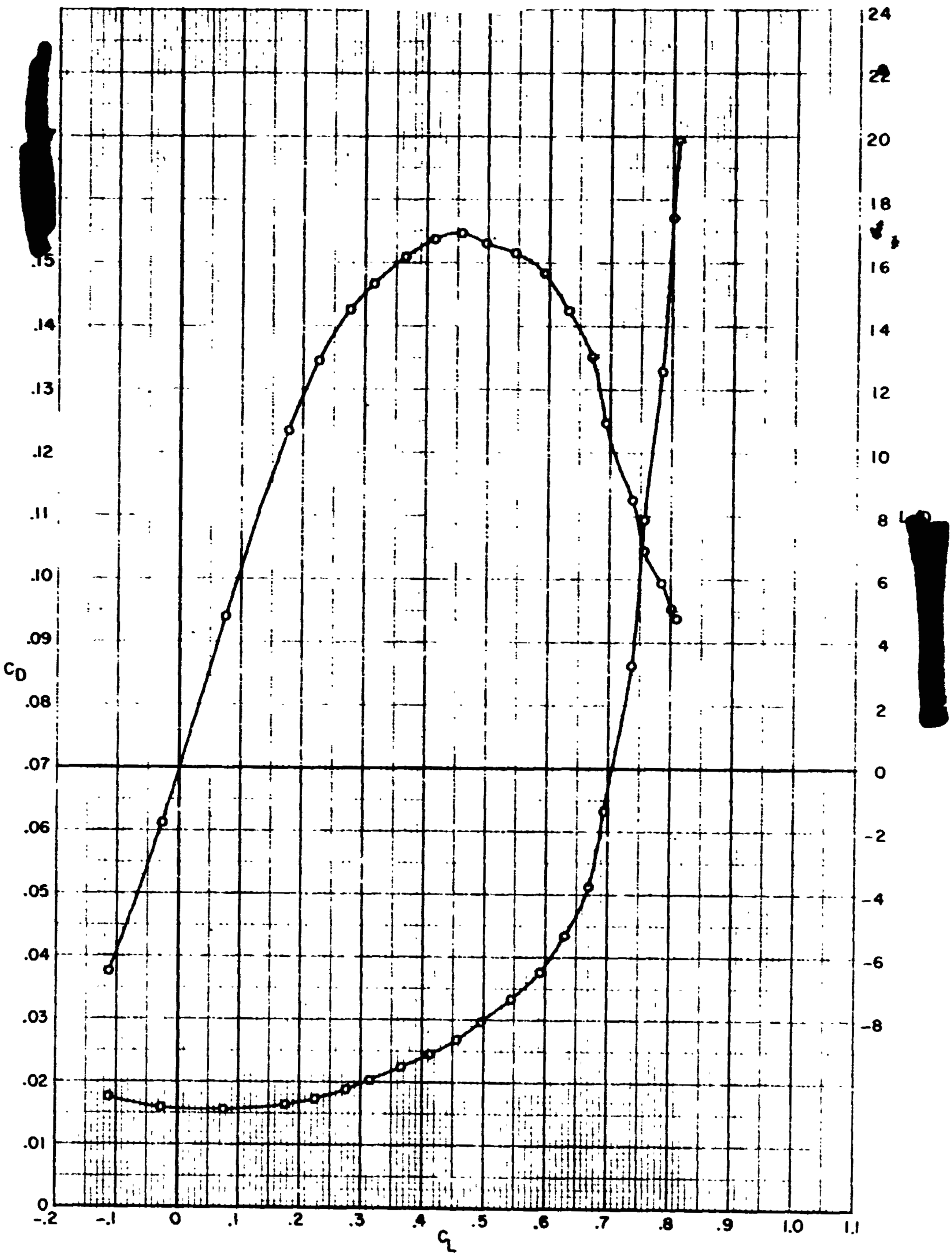

(b) M = 0.70. Continued.

Figure 19. - Continued.

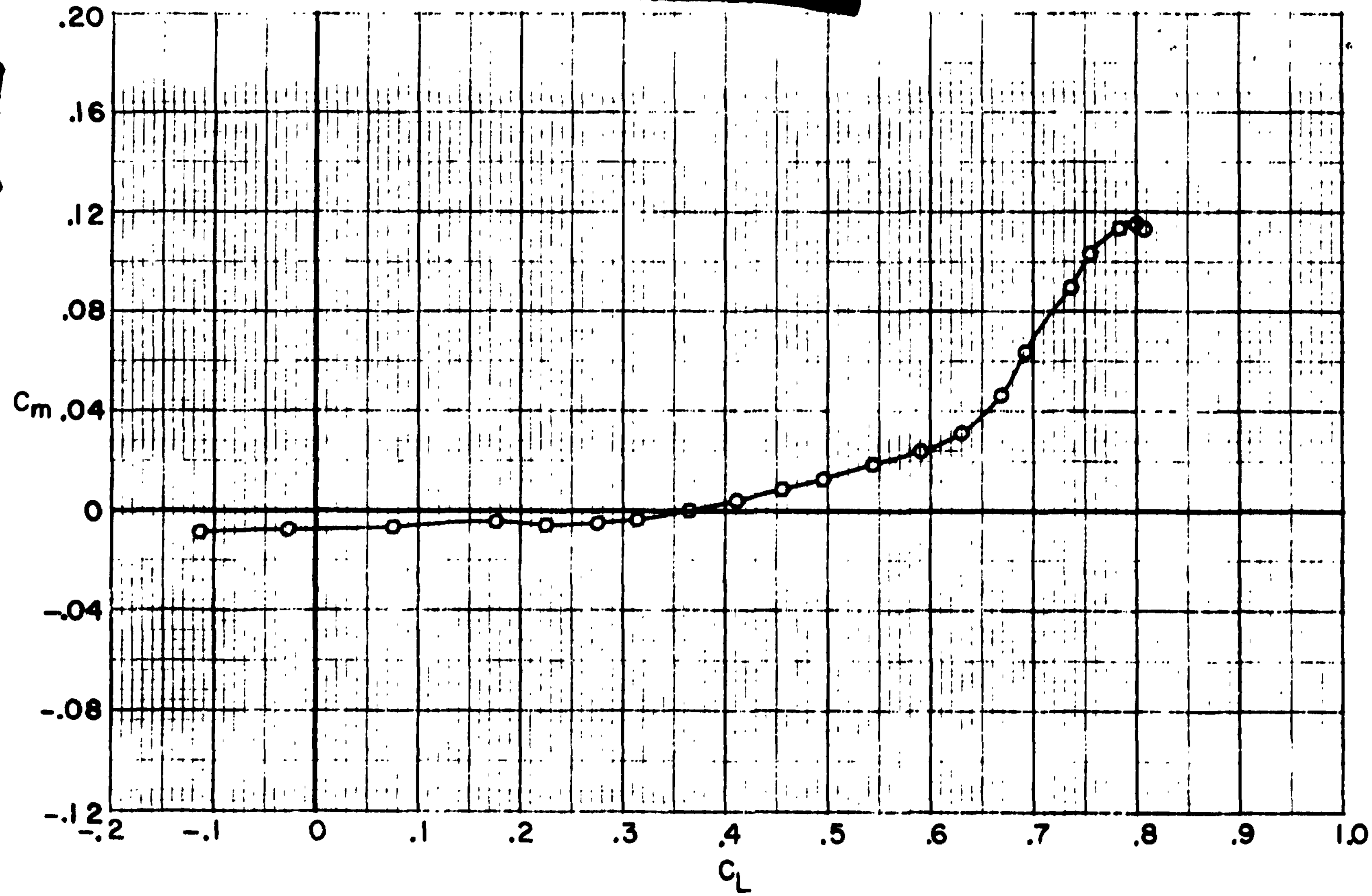

(b) M = 0.70. Concluded.

Figure 19. - Continued.

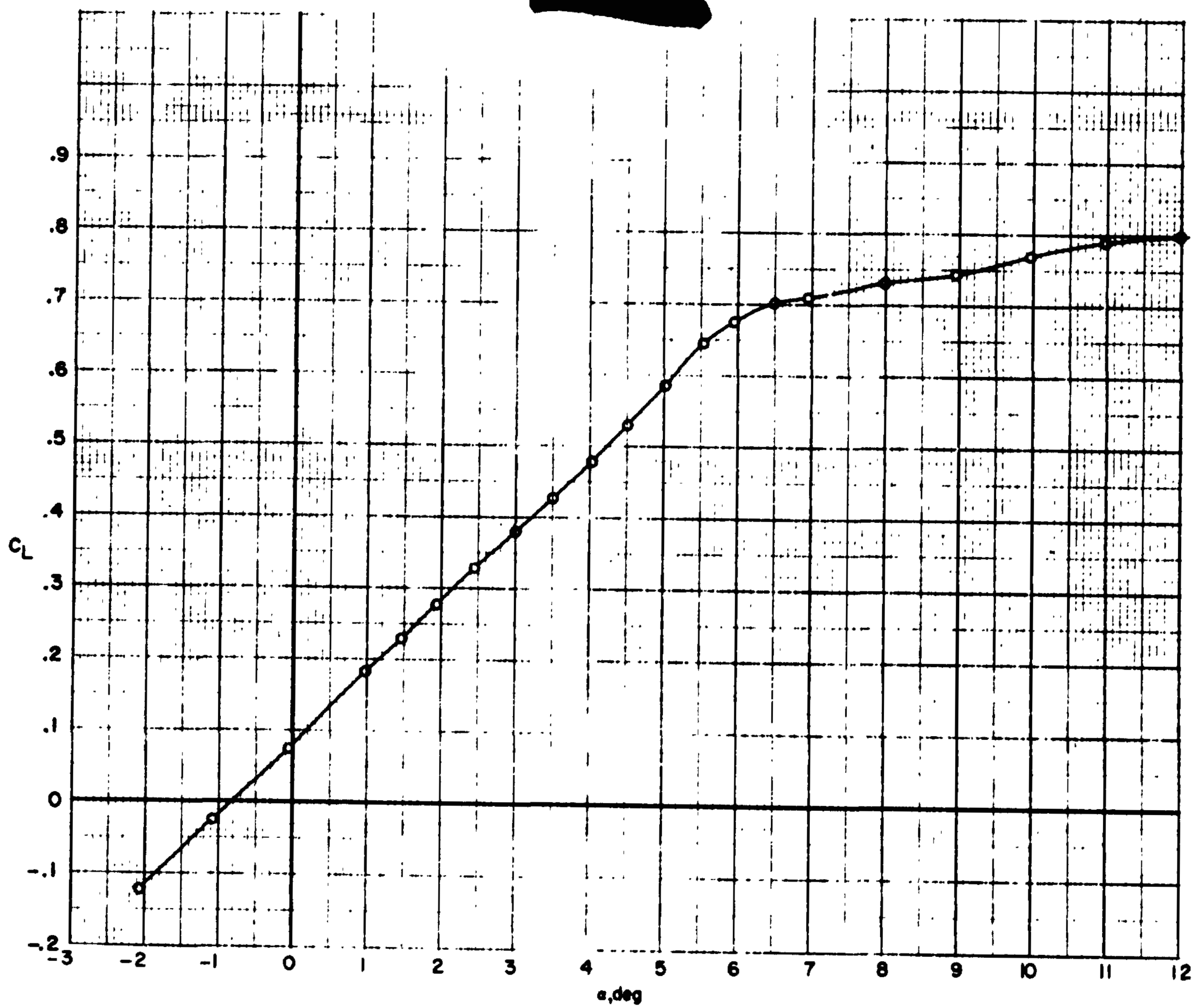

(c) M = 0.75.

Figure 19.- Continued.

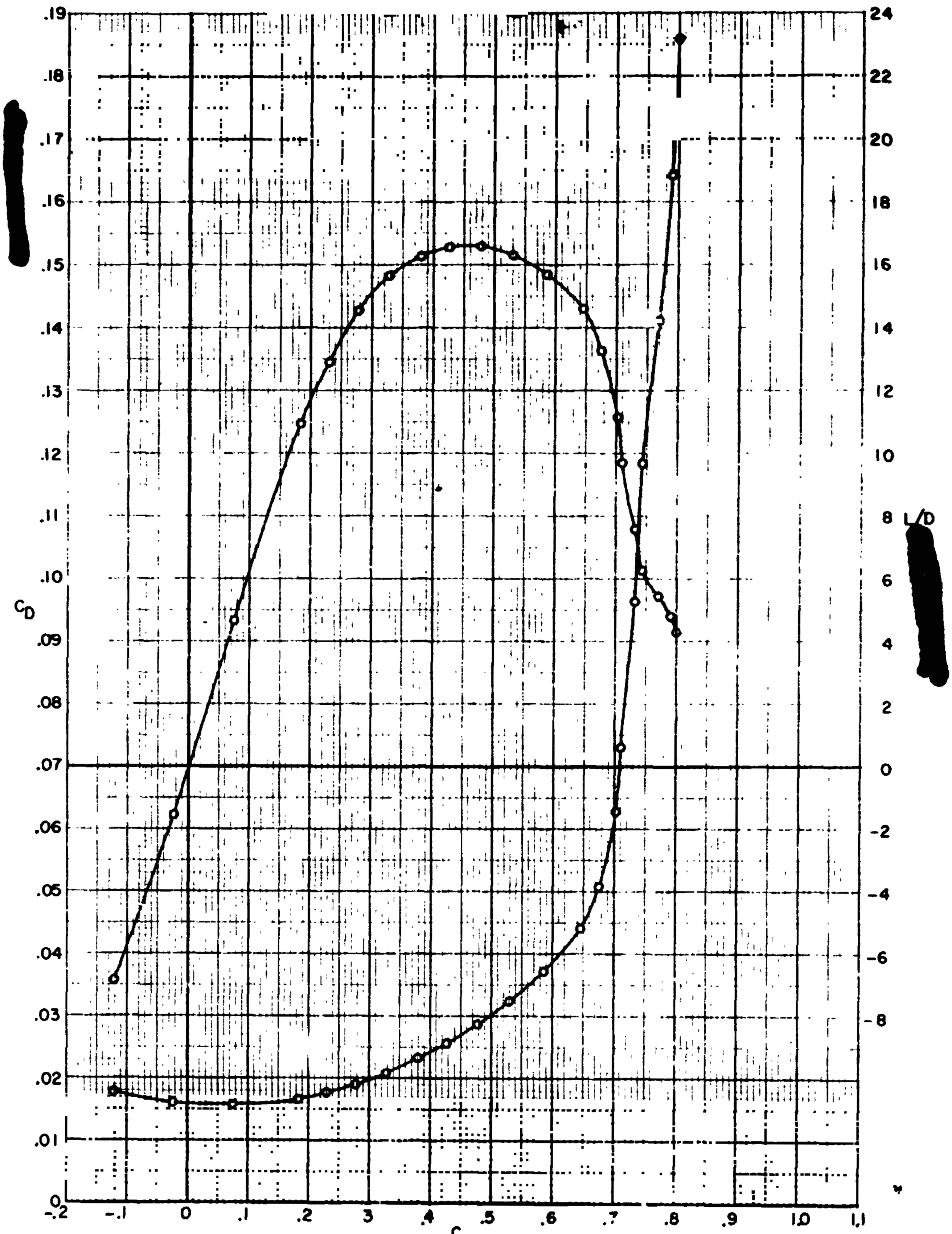

(c) M = 0.75. Continued.

Figure 19.- Continued.

[redacted]

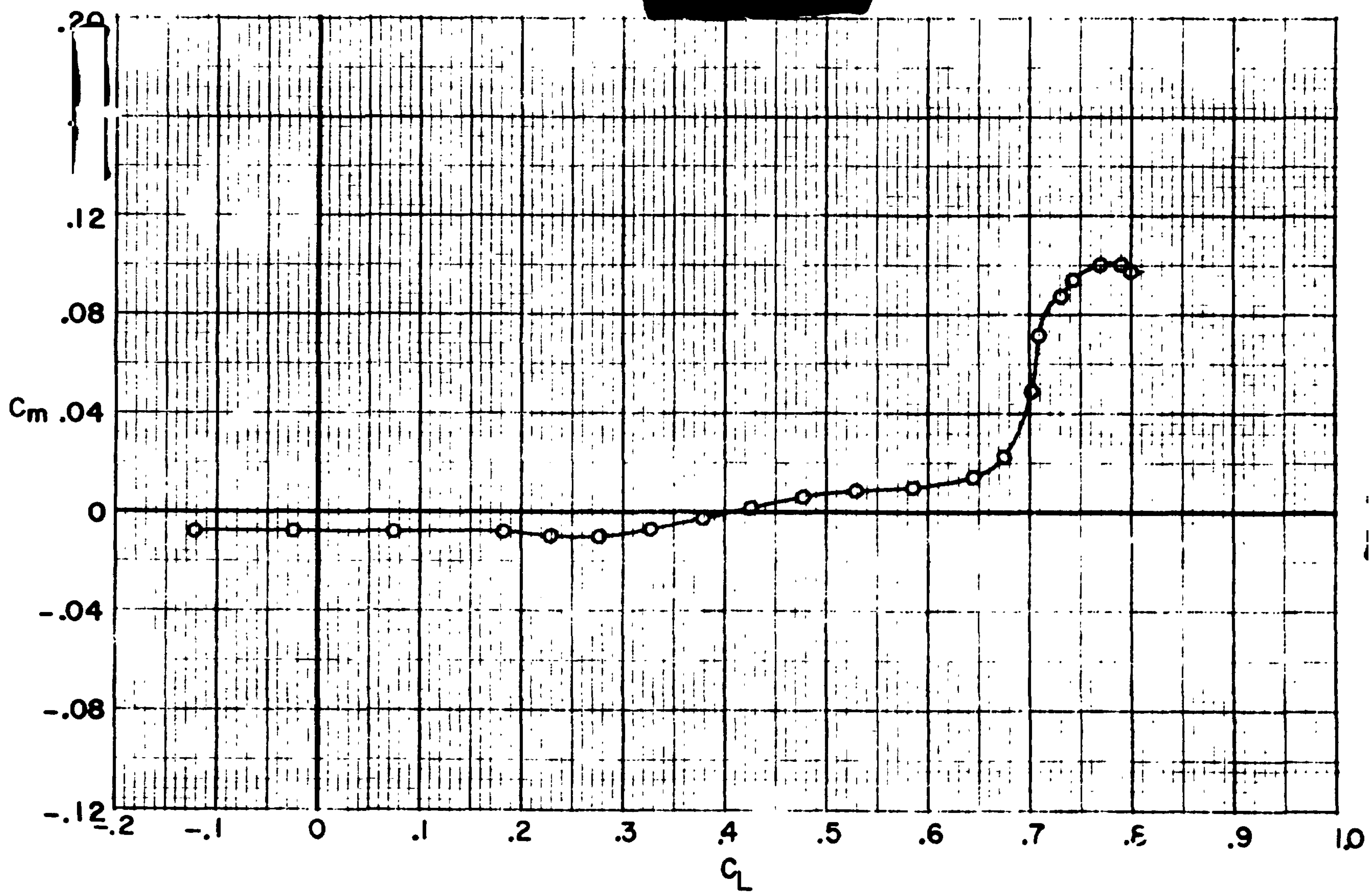

(c) M = 0.75. Concluded.

• Figure 19.- Continued.

[redacted]

ORIGINAL PAGE IS
OF POOR QUALITY

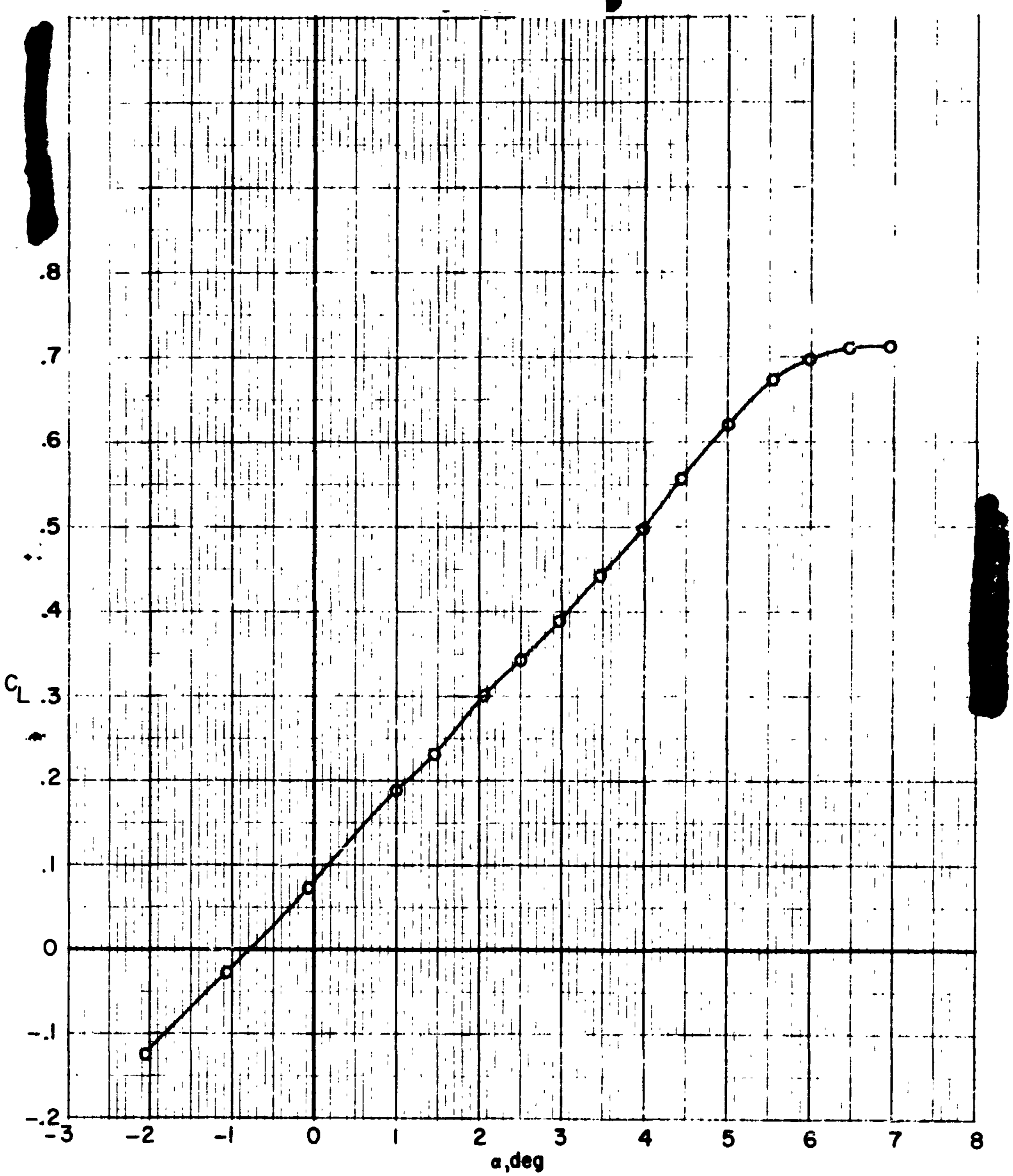

(d) M = 0.78.

Figure 19.- Continued.

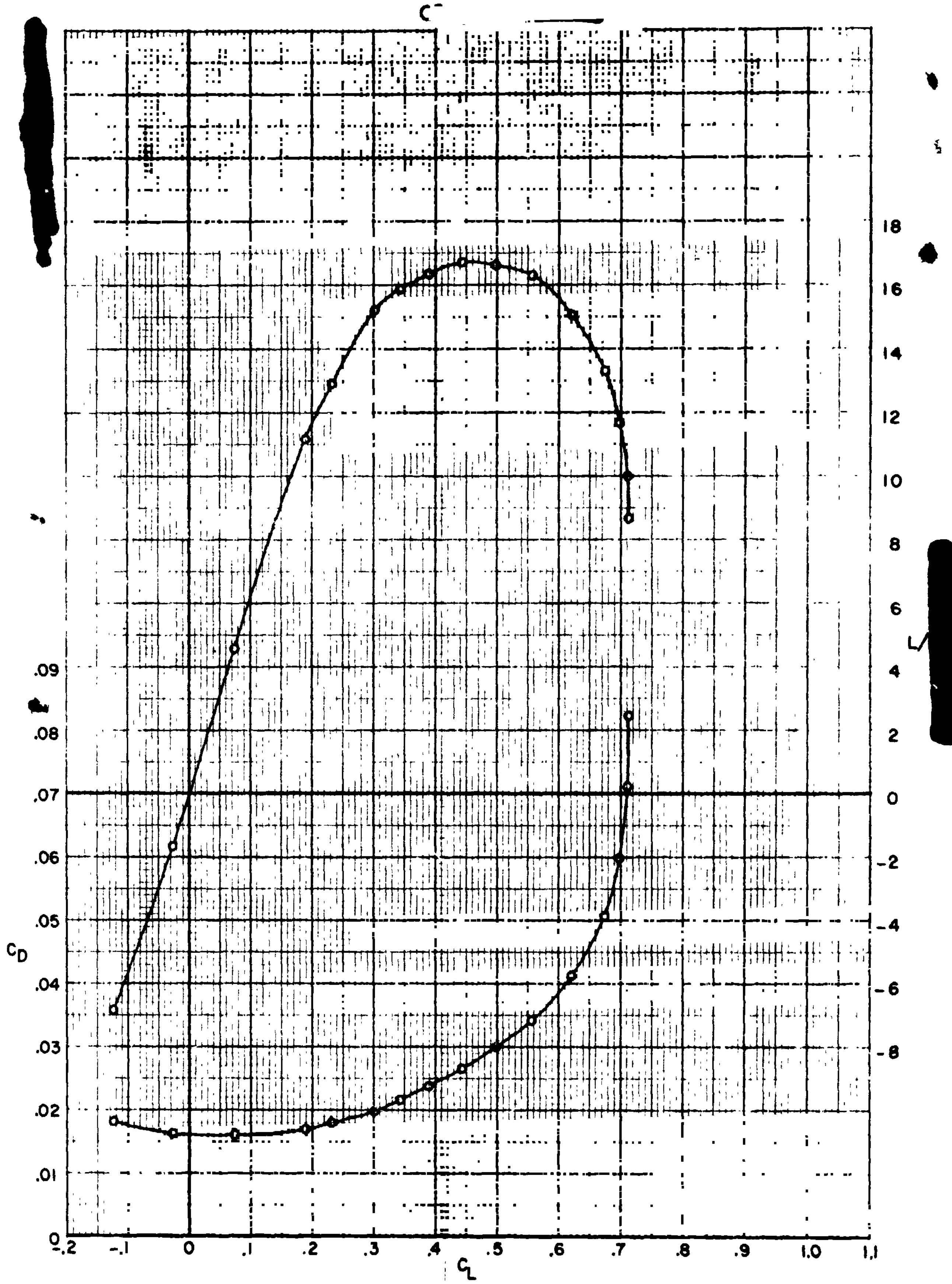

(d) M = 0.78. Continued.

Figure 19. - Continued.

[redacted]

[redacted]

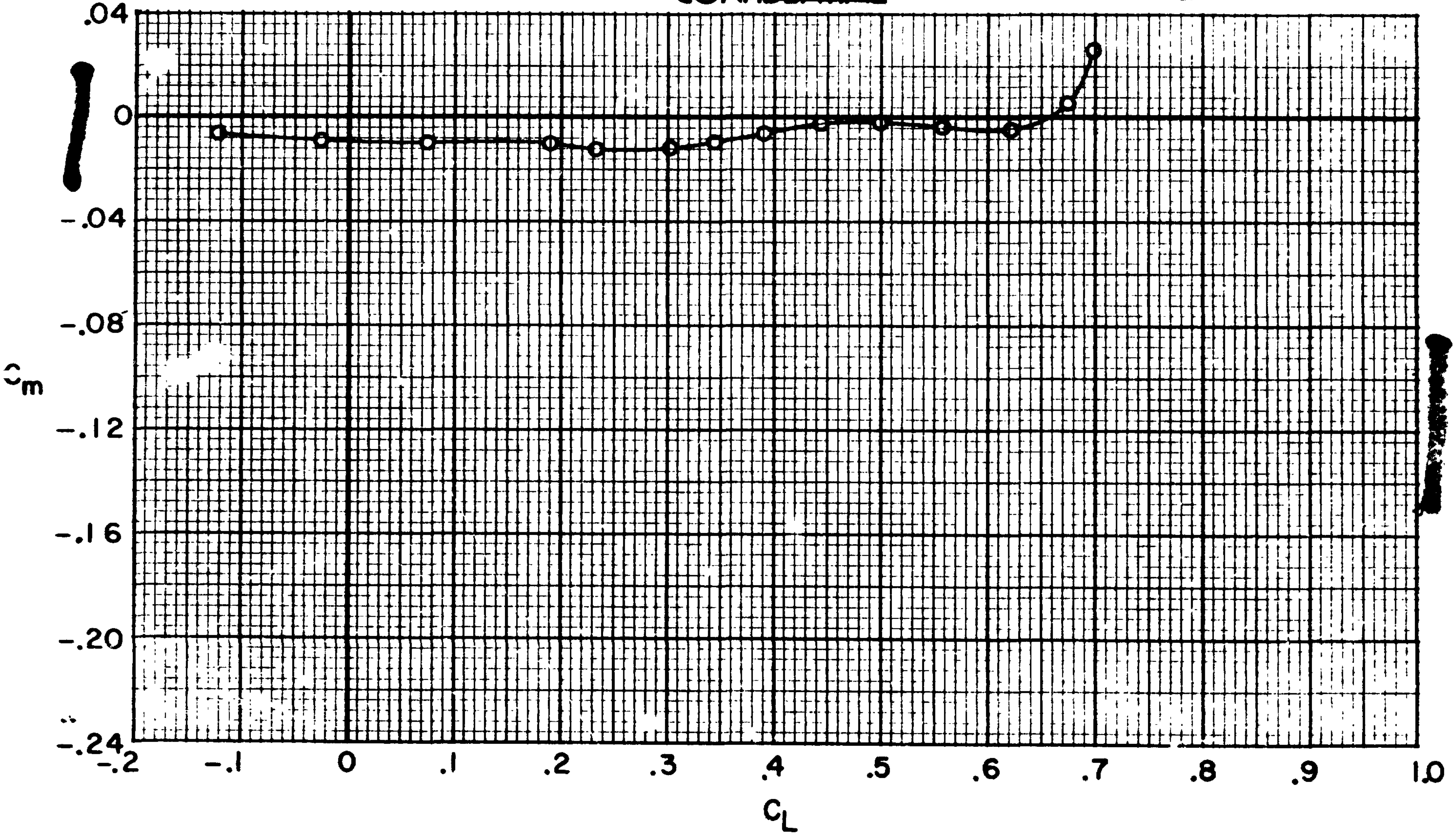

(d) M = 0.78. Concluded.

Figure 19. - Continued.

[redacted]

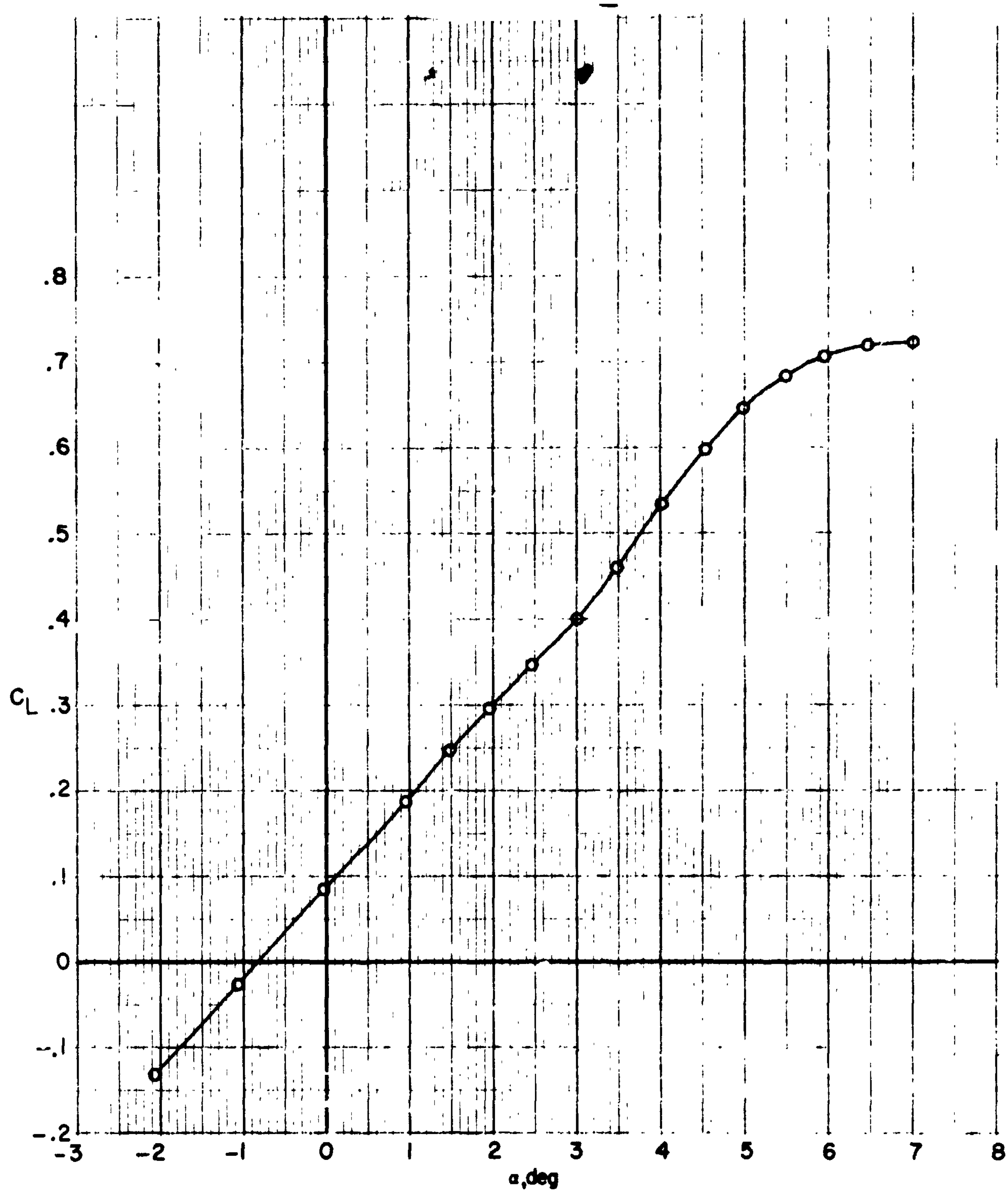

(e) M = 0.80.

Figure 19. - Continued.

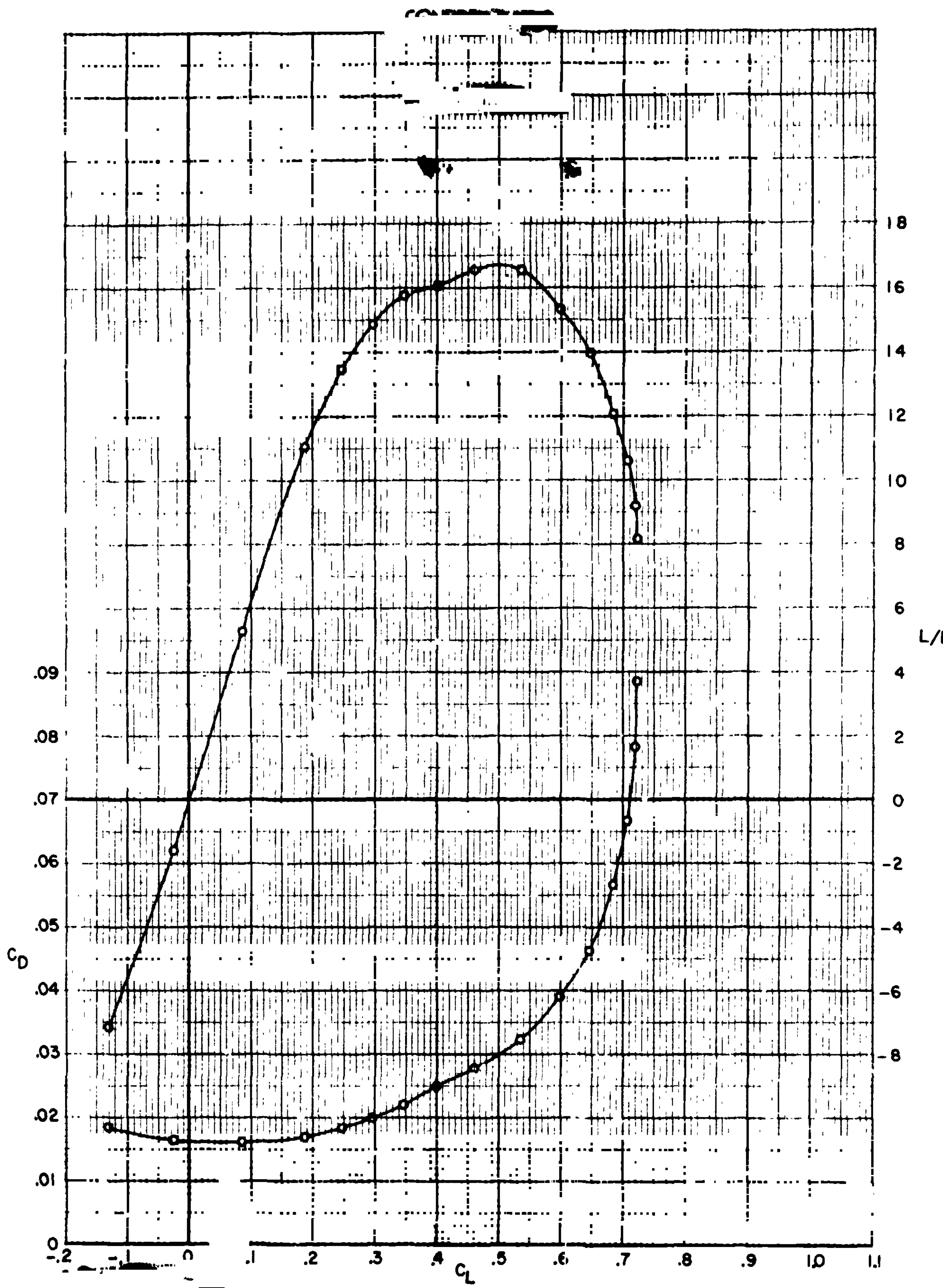

(e) M = 0.80. Continued.

Figure 19. - Continued.

ORIGINAL PAGE IS
OF POOR QUALITY

[redacted]

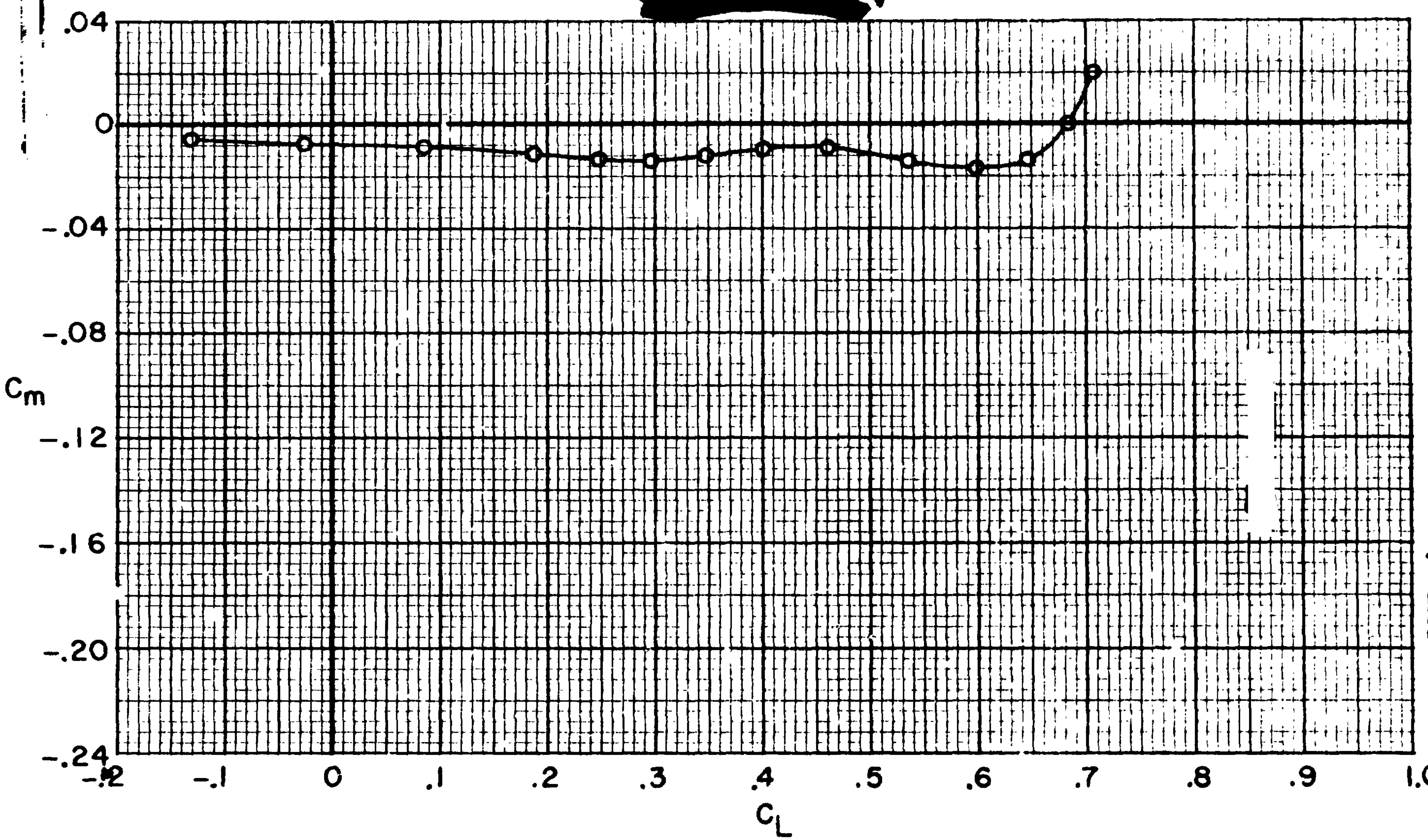

(e) M = 0.80. Concluded.

Figure 19.- Continued.

[redacted]

ORIGINAL PAGE IS
OF POOR QUALITY

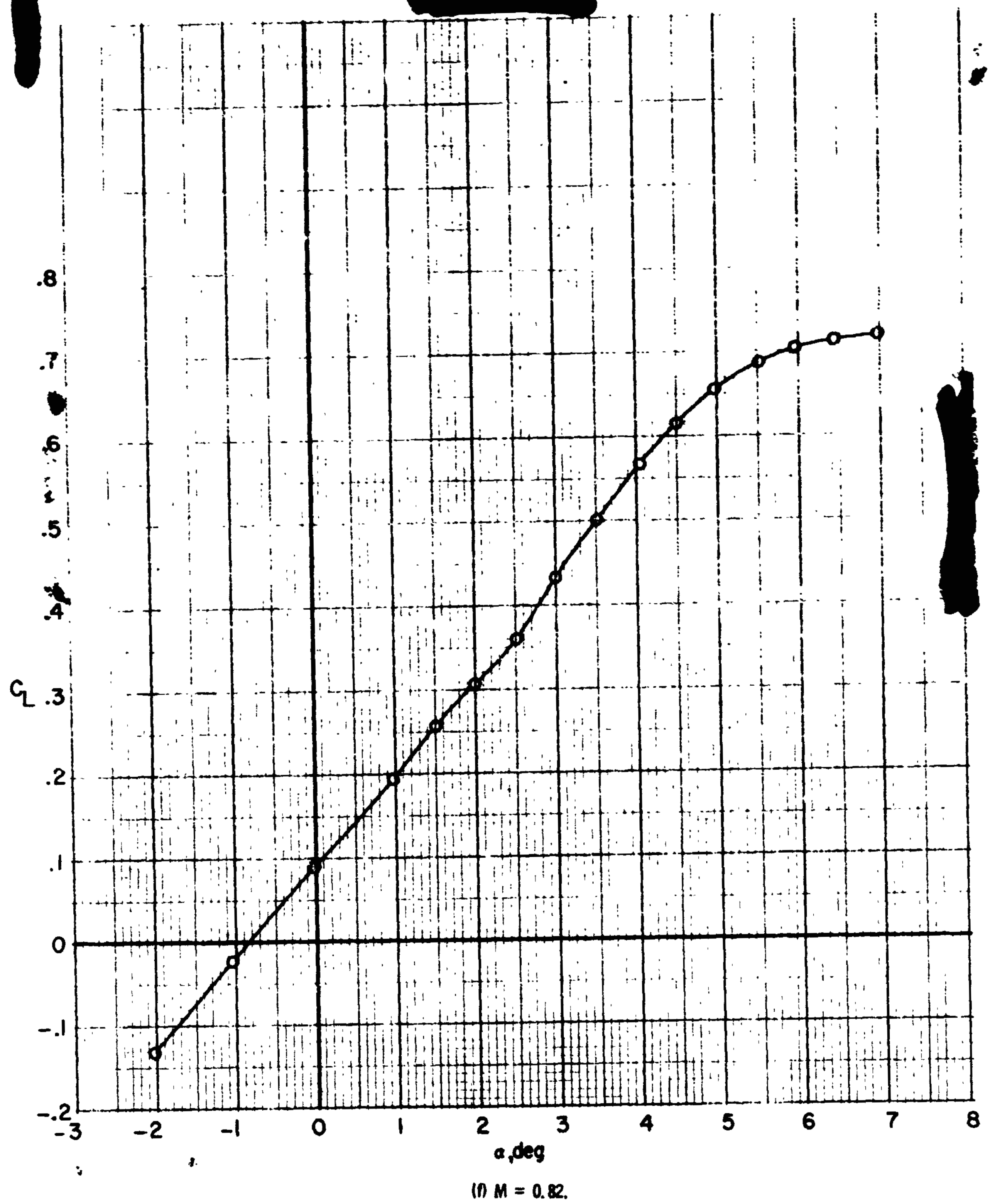

(f) M = 0.82.

Figure 19. - Continued.

ORIGINAL PAGE IS
OF POOR QUALITY

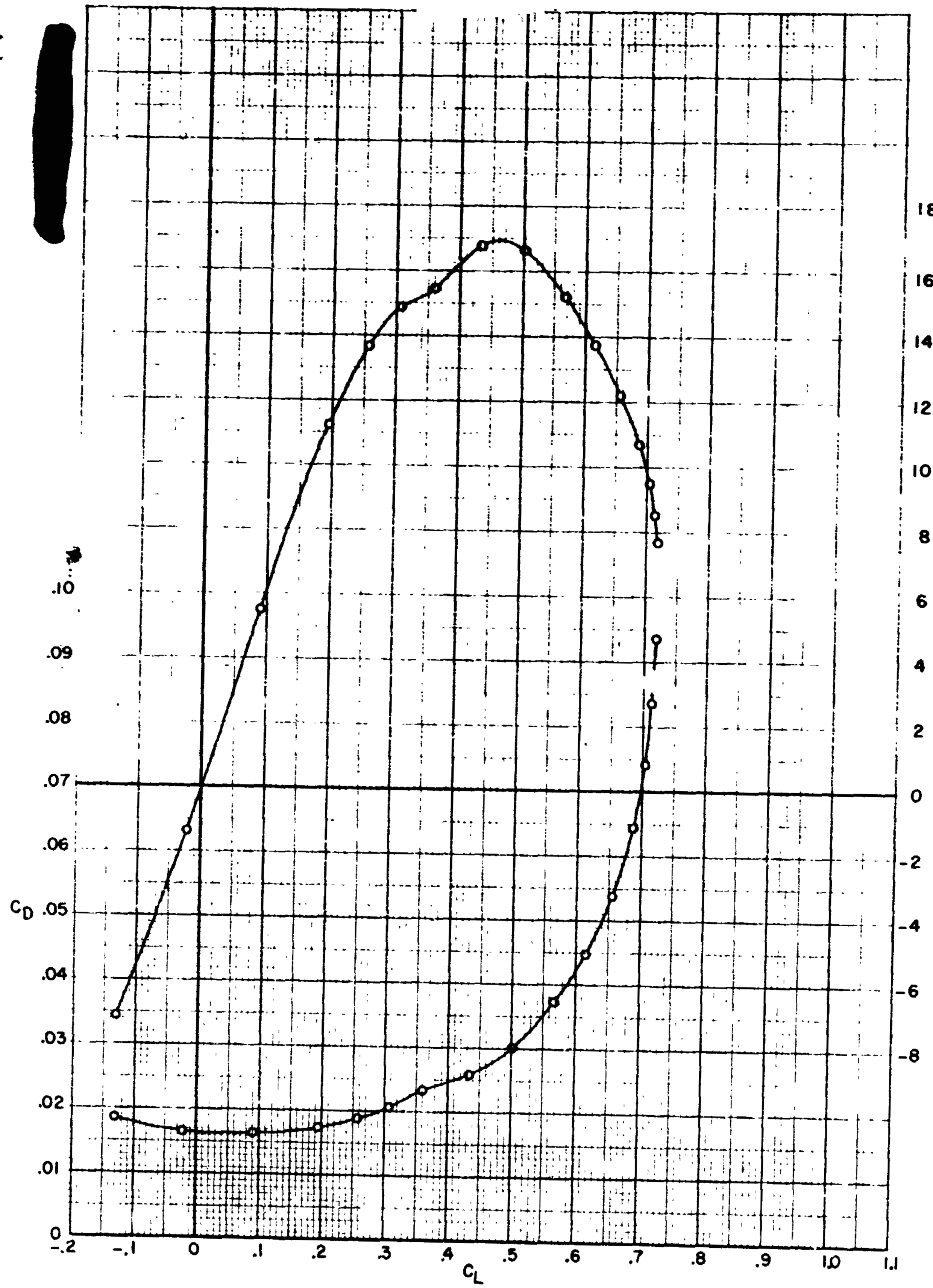

(f) M = 0.82. Continued.

Figure 19.- Continued.

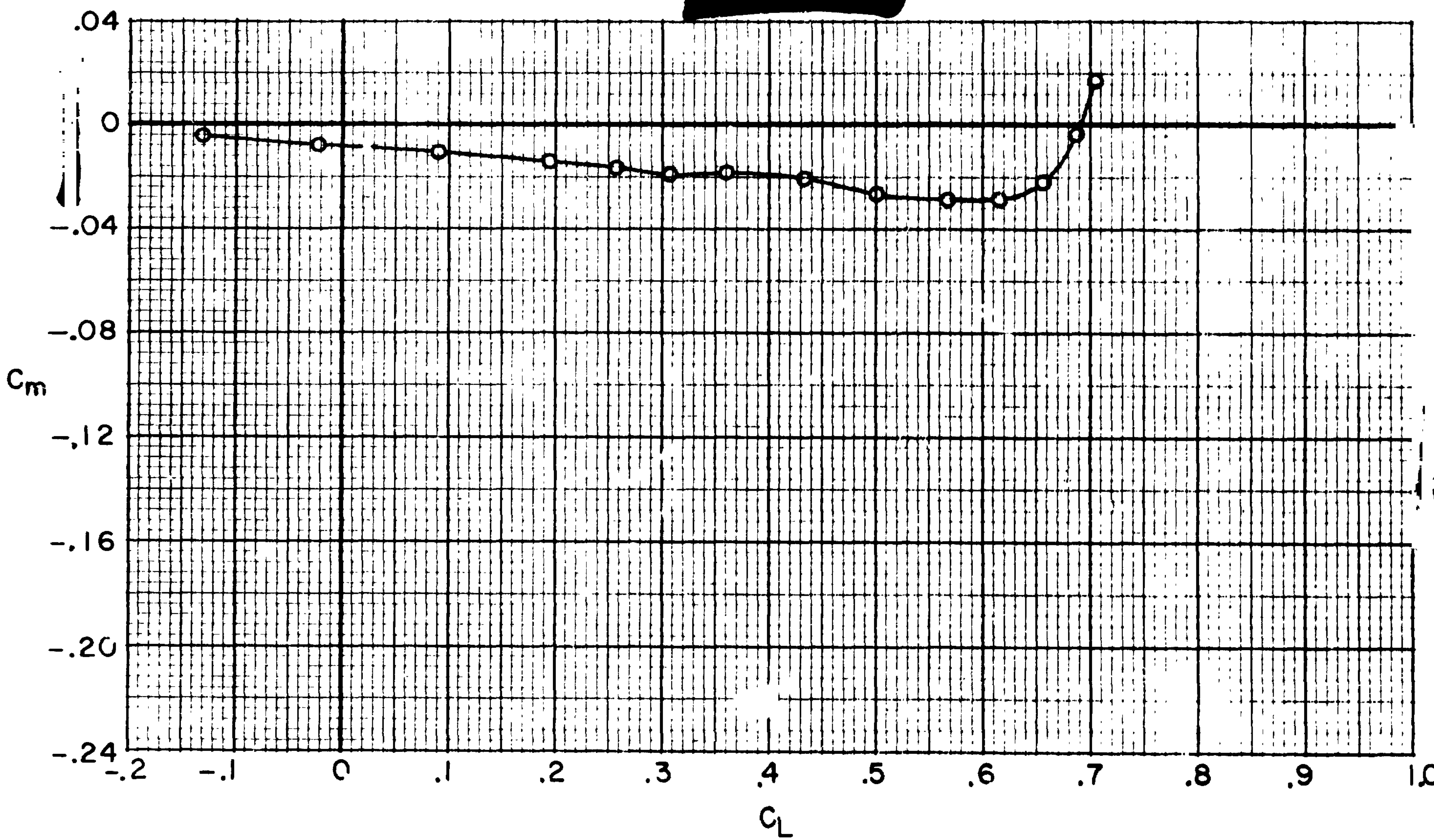

(f) M = 0.82. Concluded.

Figure 19.- Continued.

[redacted]

[redacted]

ORIGINAL PAGE IS
OF POOR QUALITY

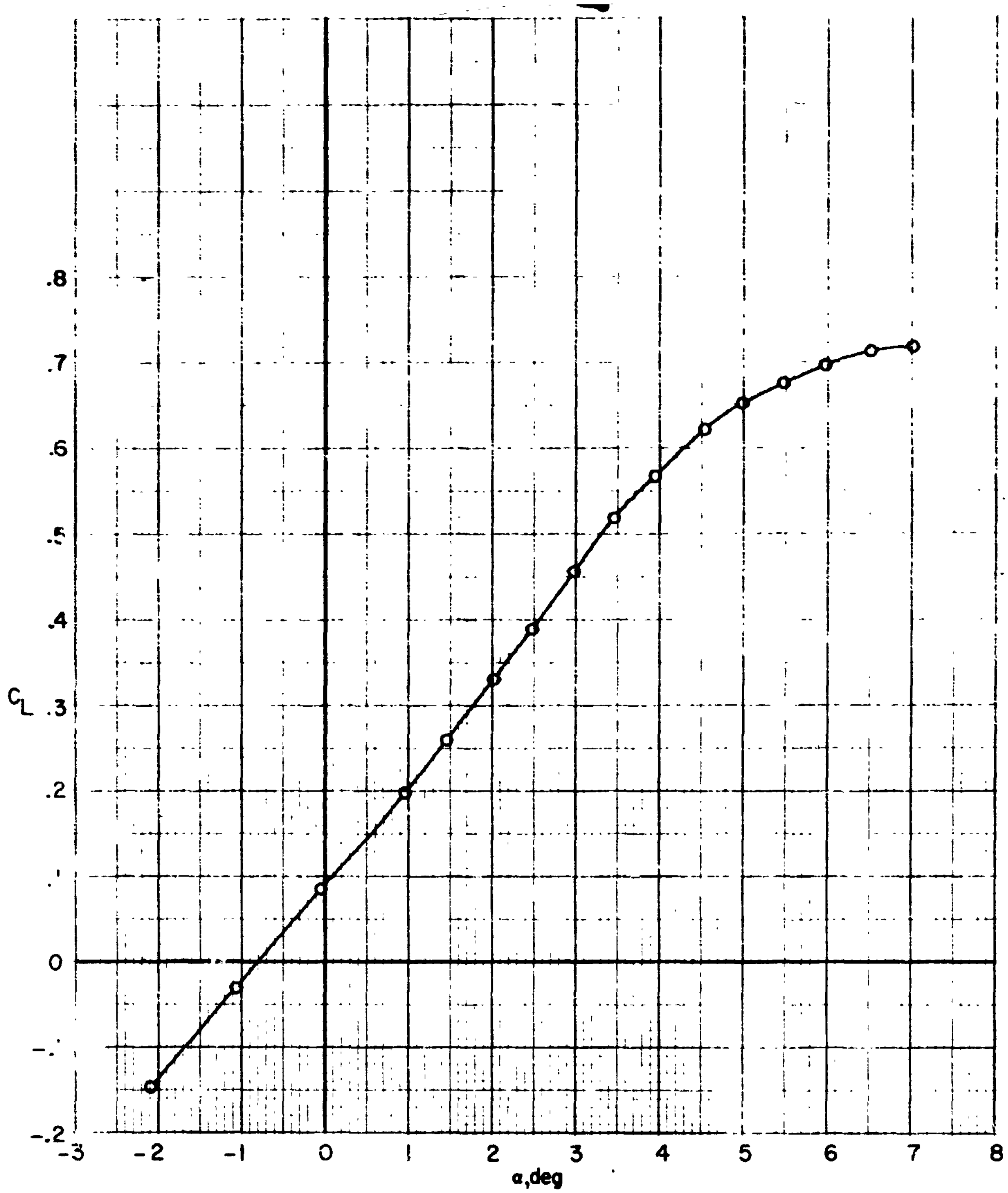

(g) M = 0.84.

Figure 19.- Continued.

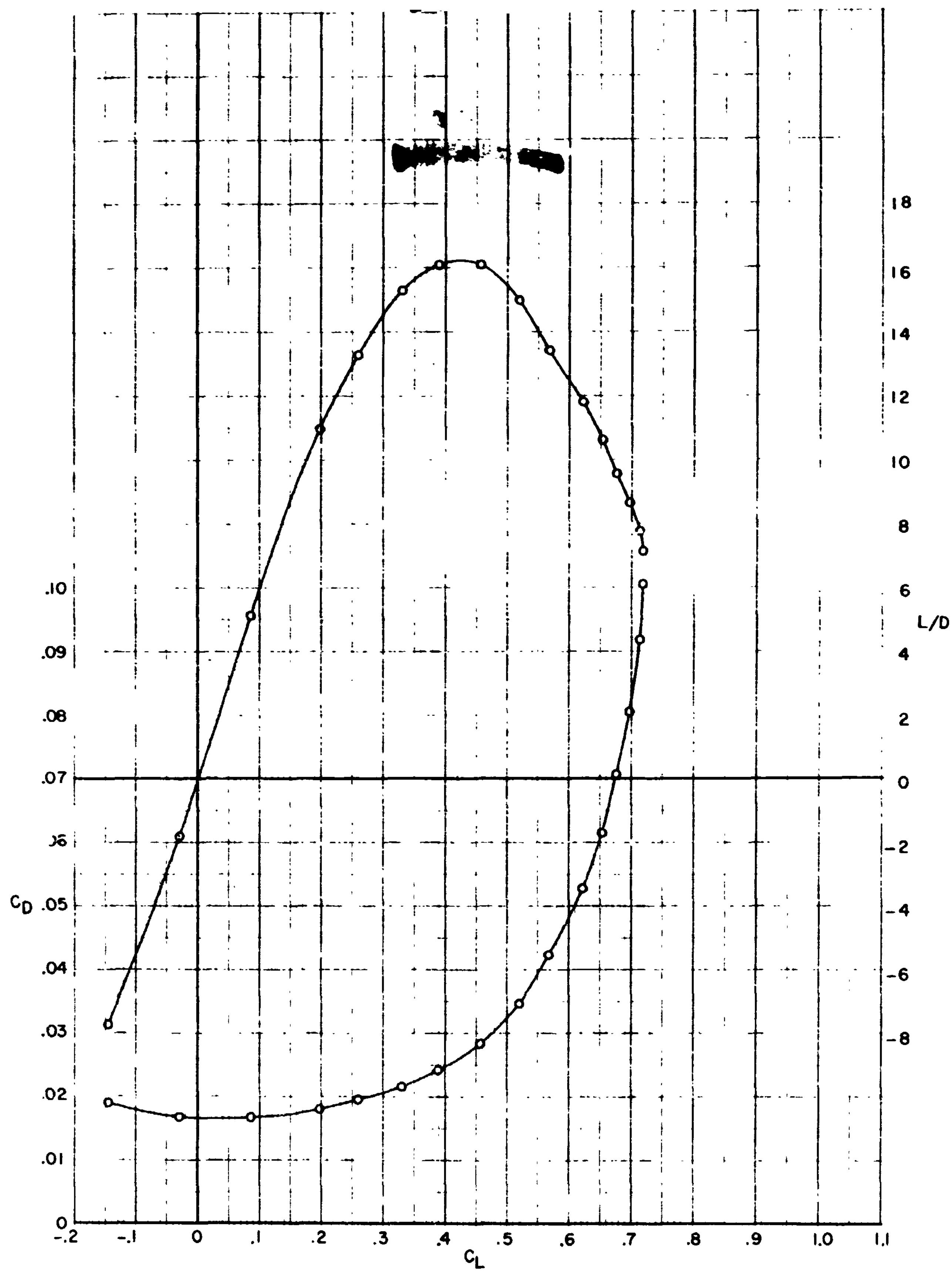

(g) M = 0.84. Continued.

Figure 19. - Continued.

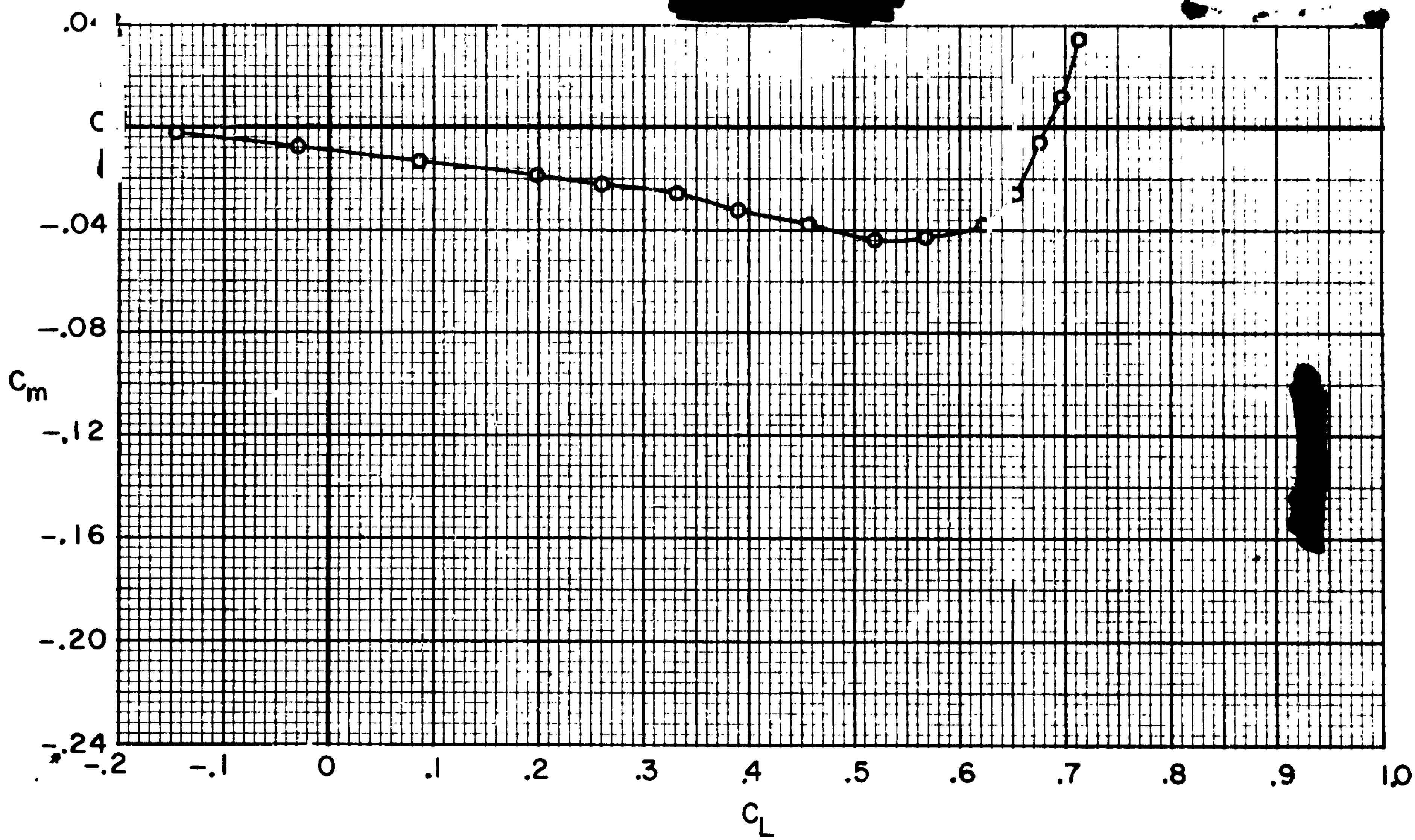

(g) M = 0.84. Concluded.

Figure 19. - Continued.

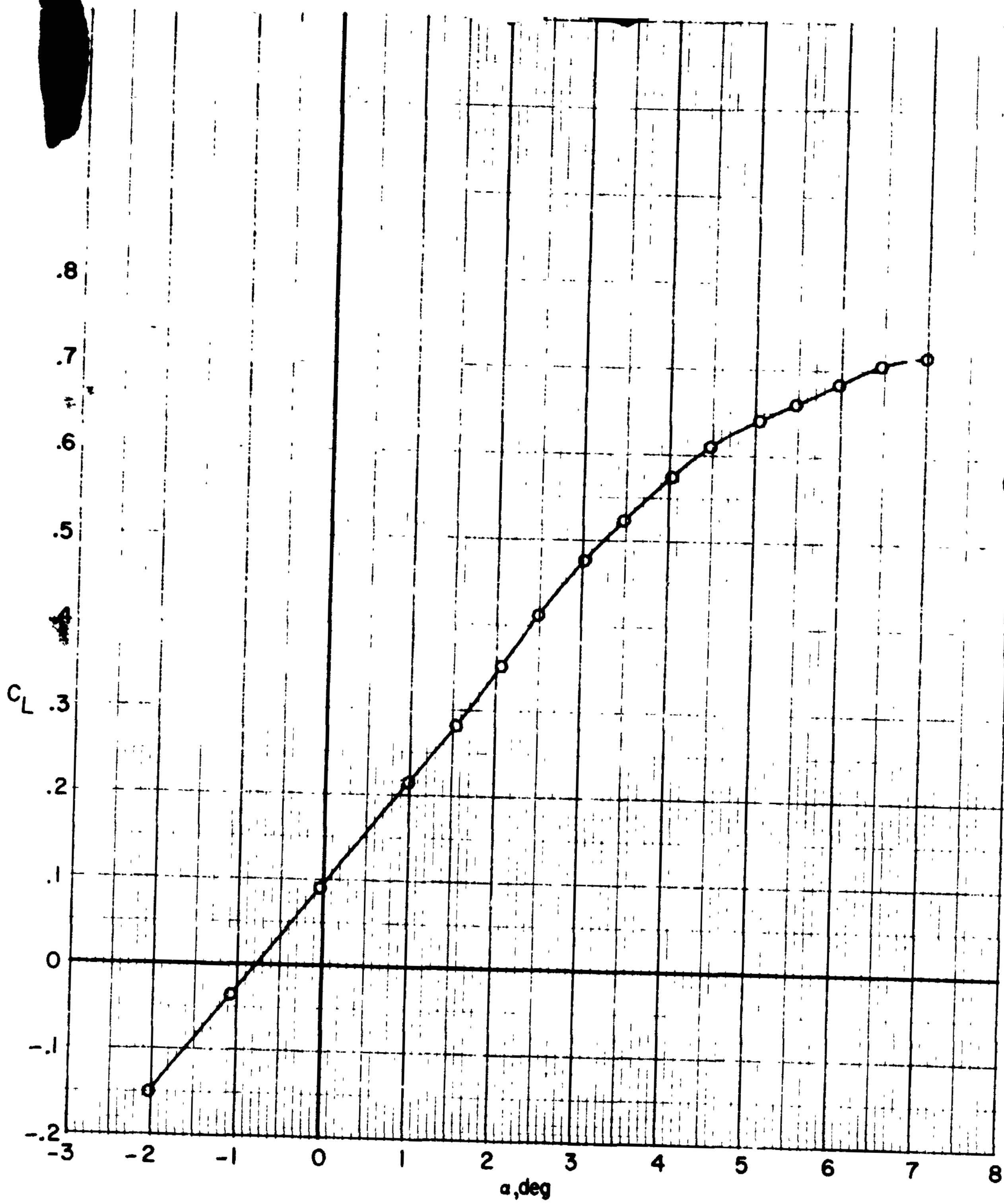

(h) M = 0.86.

Figure 19. - Continued.

[redacted]

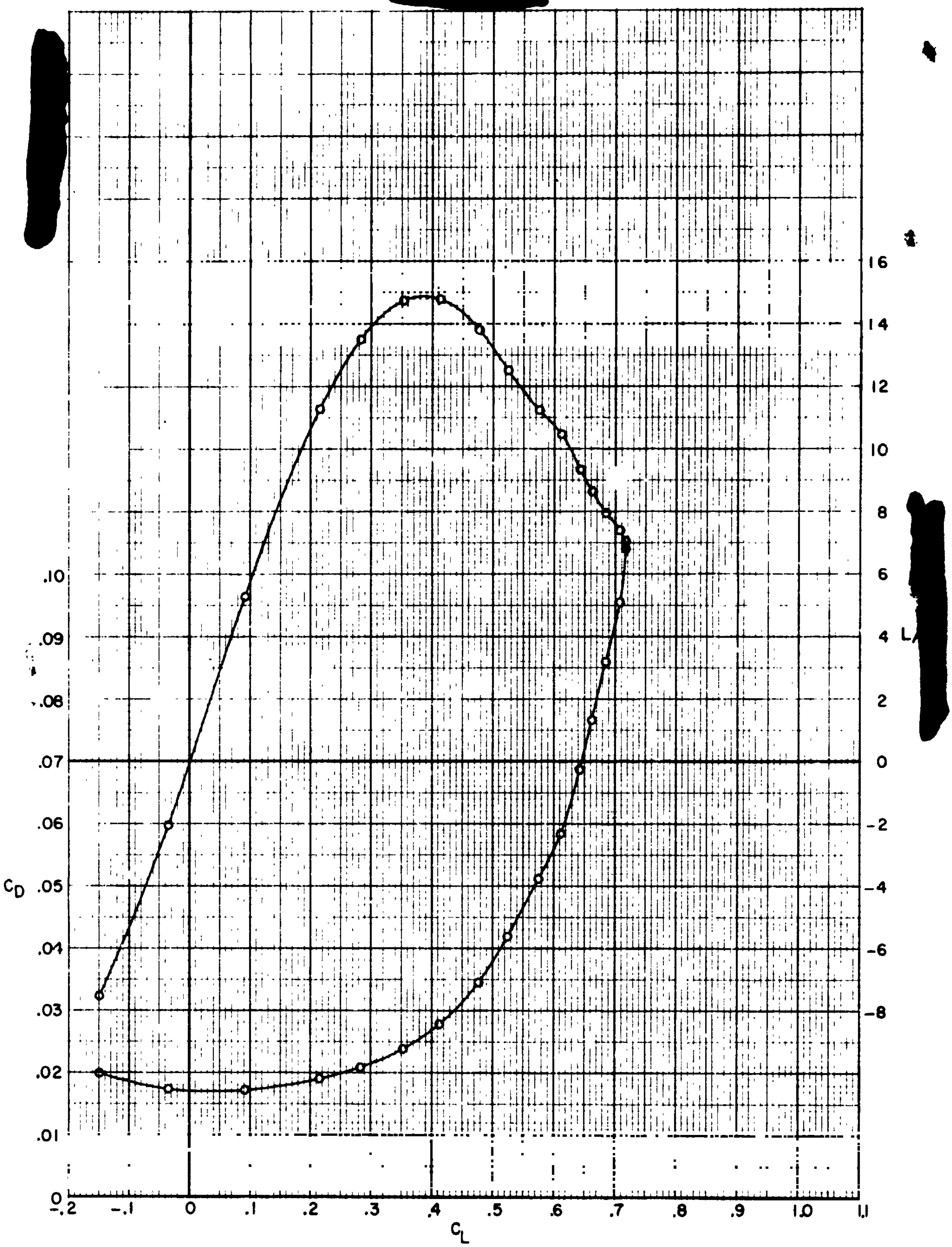

(h) M = 0.86. Continued.

Figure 19.- Continued.

[redacted]

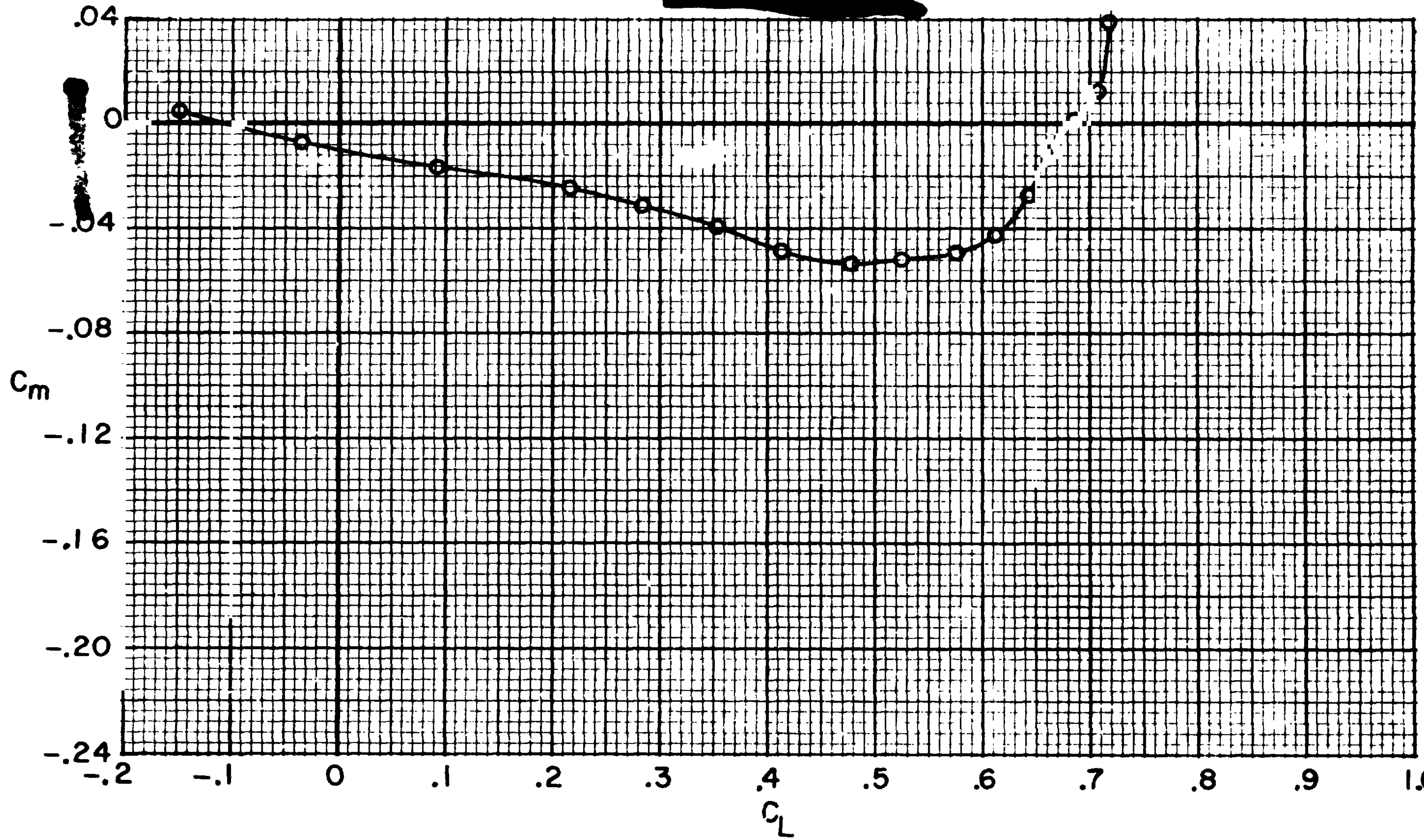

(h) M = 0.86. Concluded.

Figure 19. - Continued.

ORIGINAL PAGE IS
OF POOR QUALITY

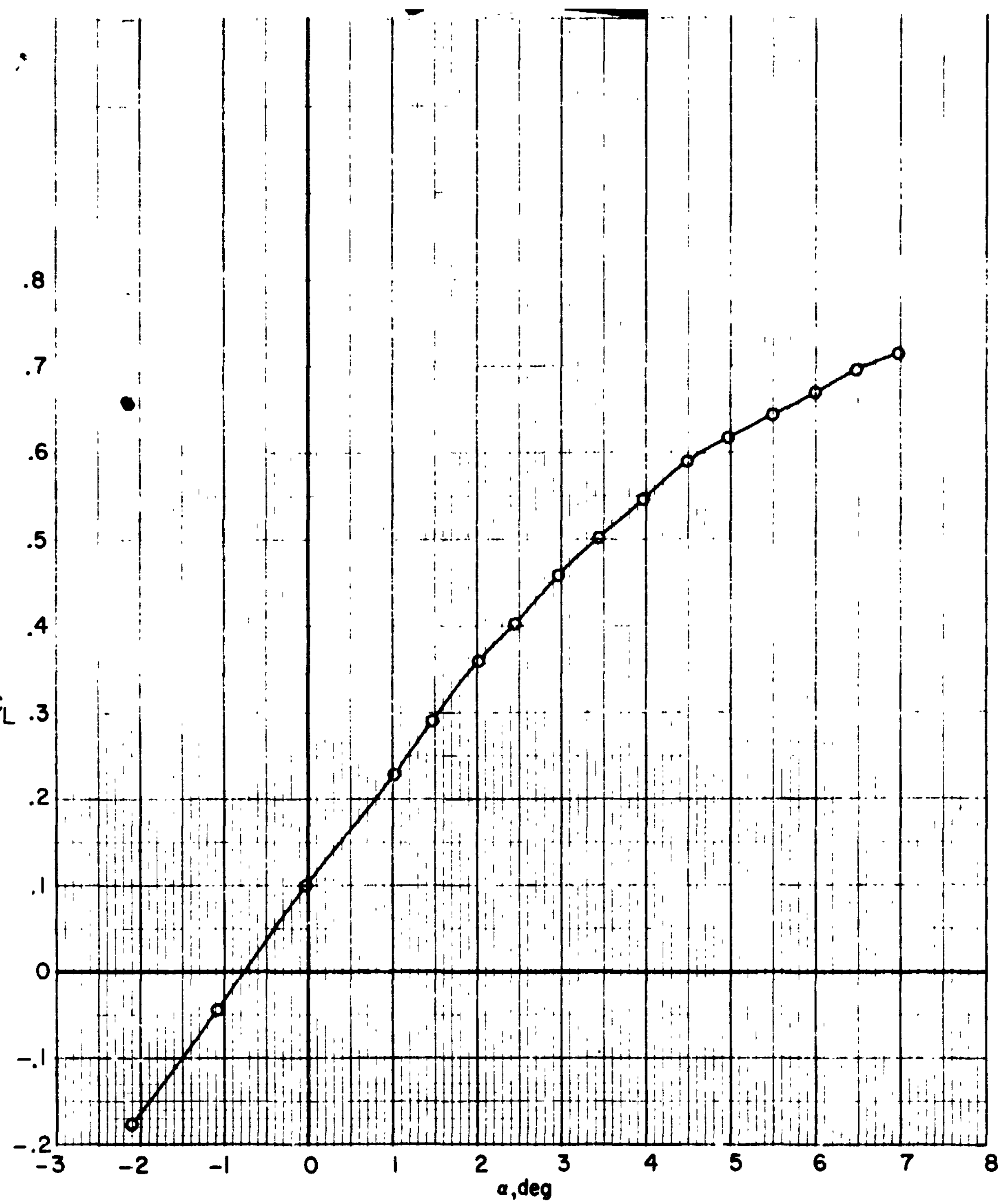

(l) M = 0.88.

Figure 19. - Continued.

[redacted]

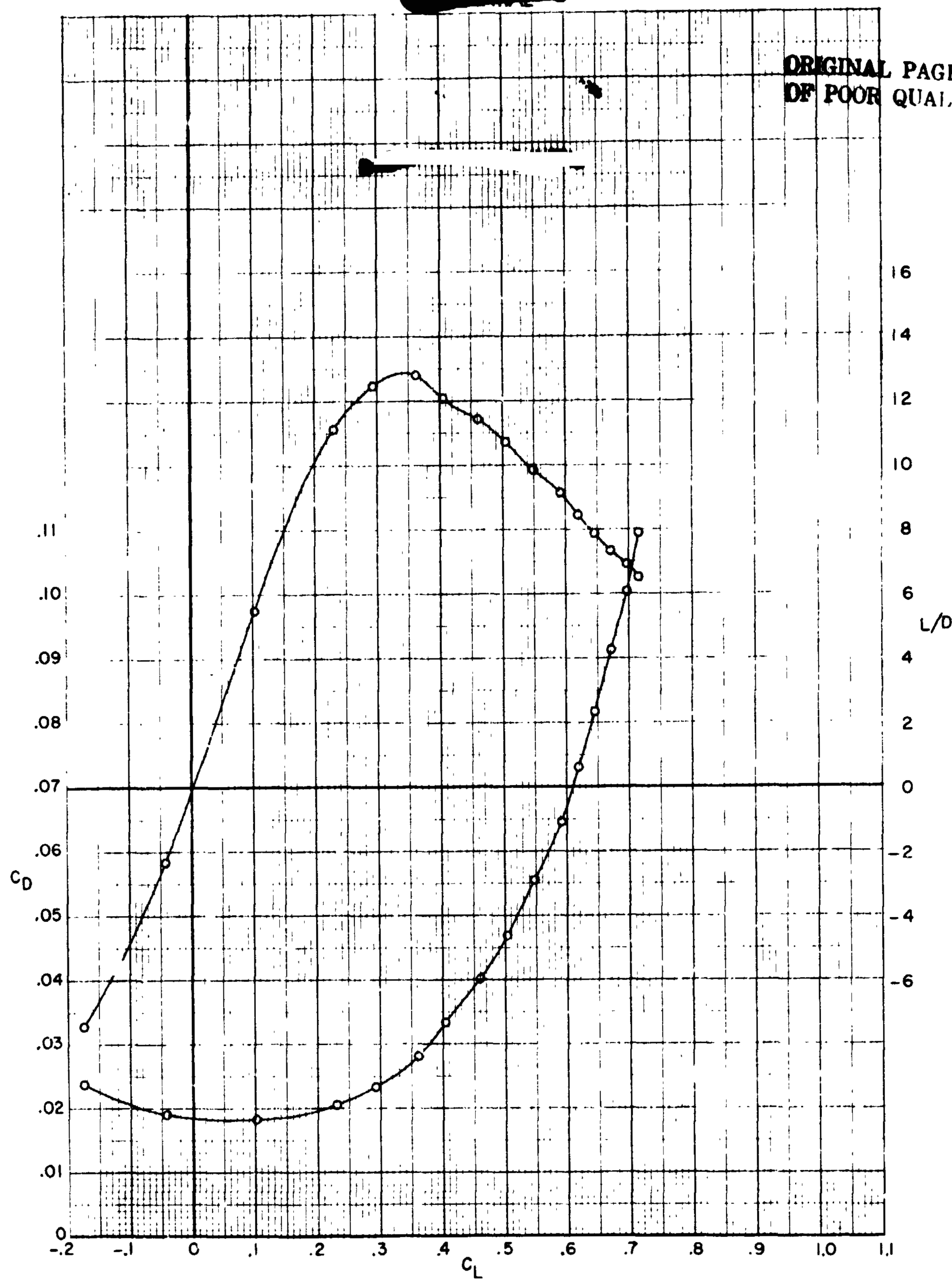

(l) M = 0.88. Continued.

Figure 19.- Continued.

[redacted]

[redacted]

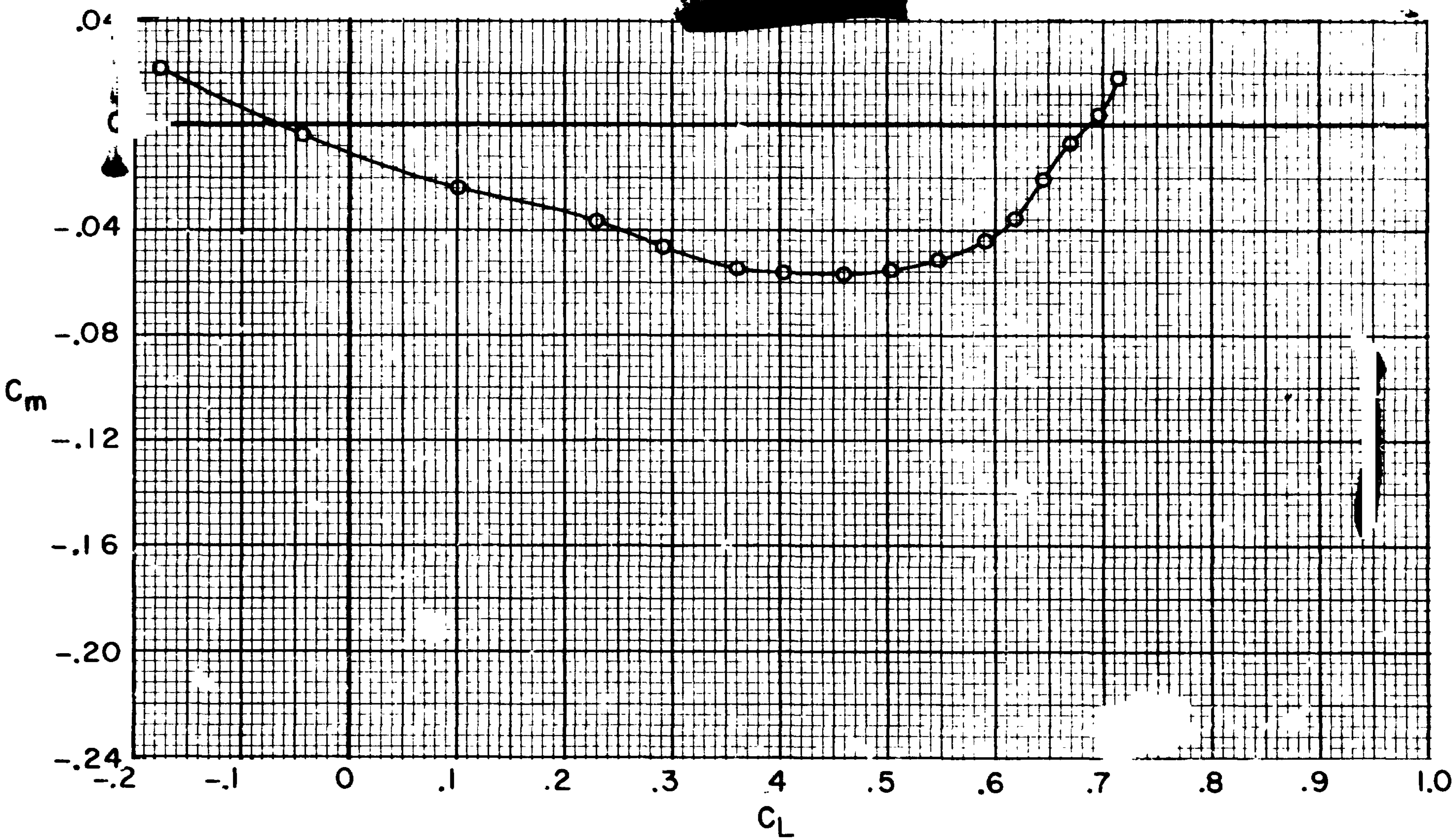

(i) M = 0.88. Concluded.

Figure 19. - Continued.

[redacted]

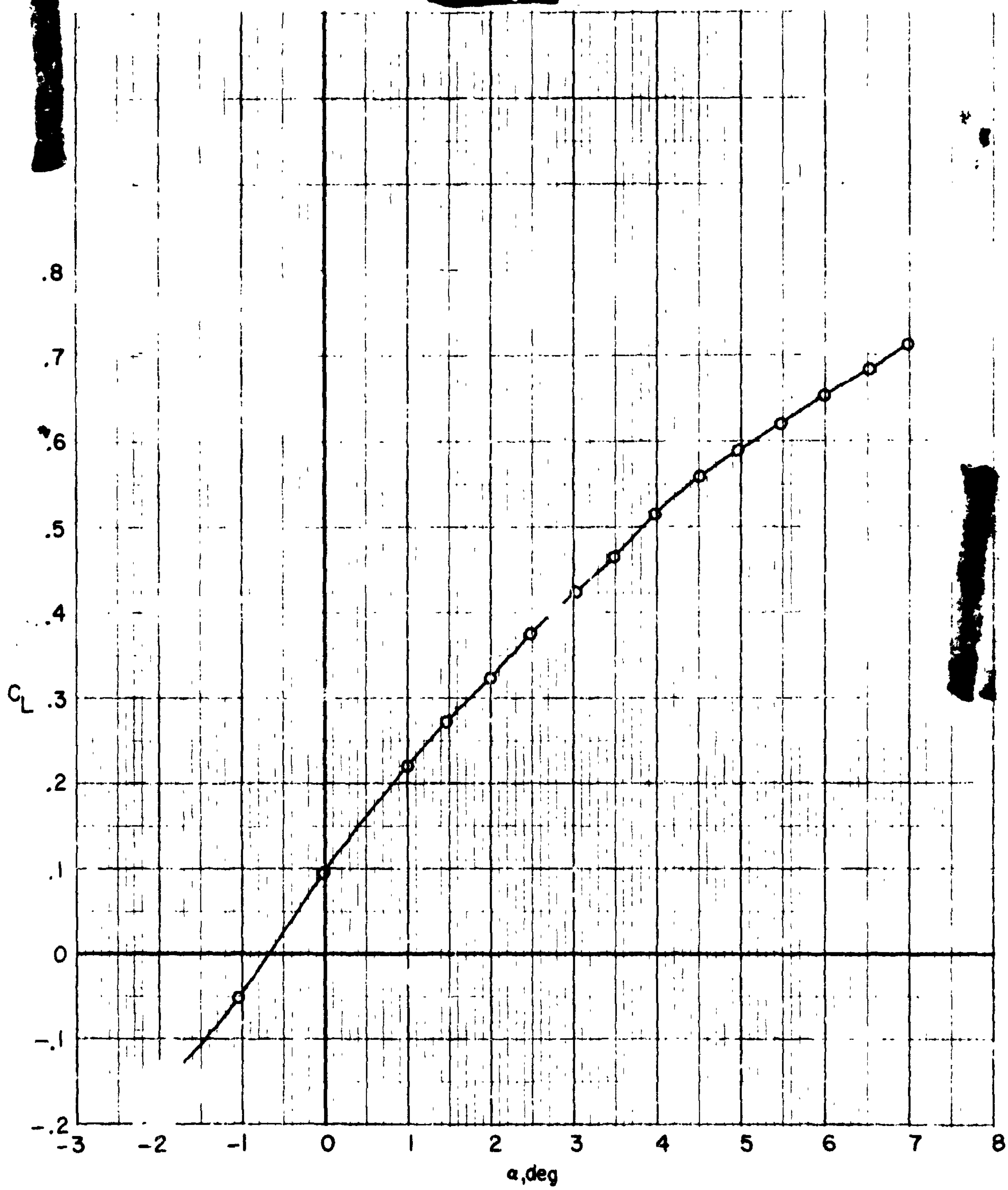

(j) M = 0.90.

Figure 19. - Continued.

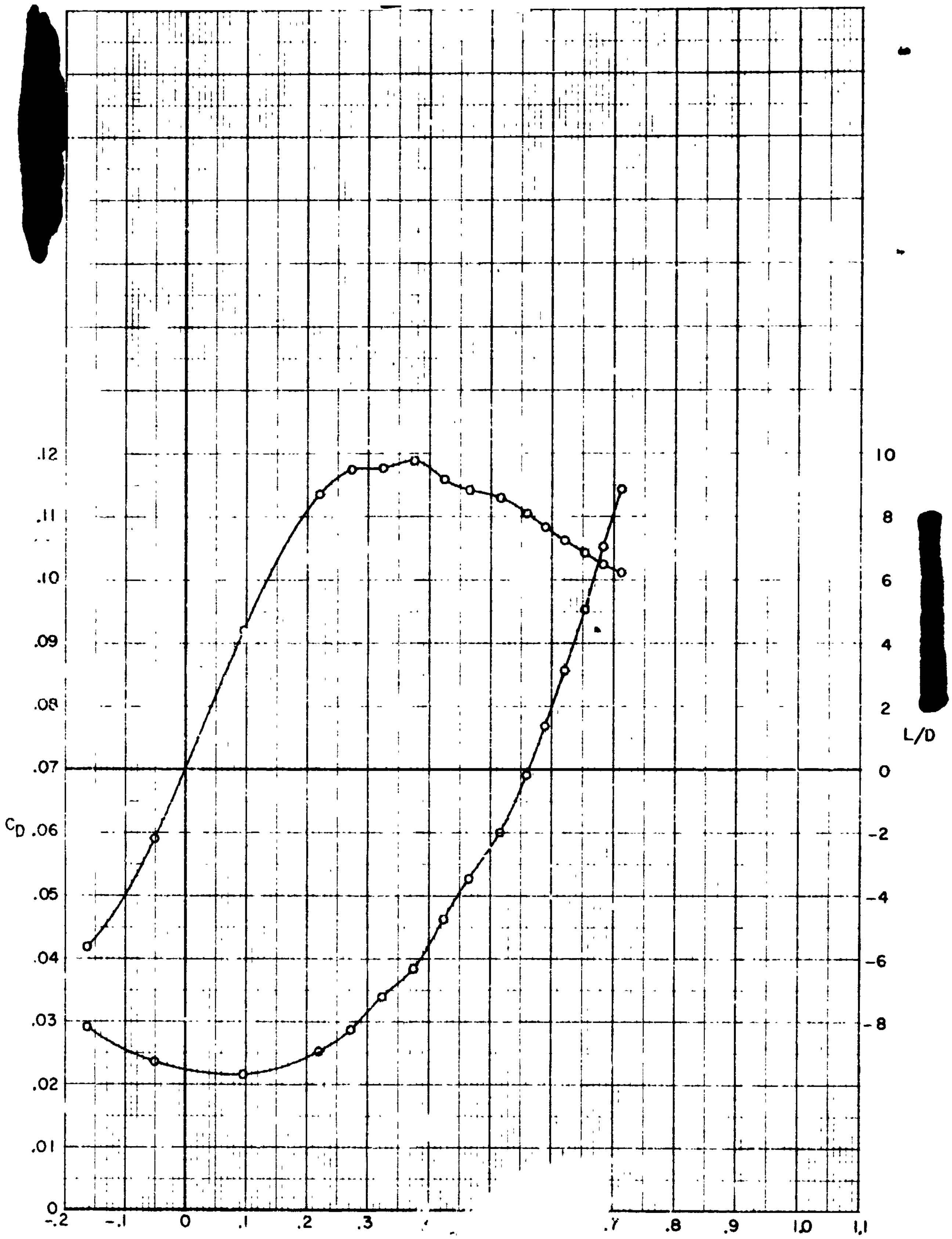

(j) M = 2.9[illegible]. Continued.

Figure 19 - Continued.

[redacted]

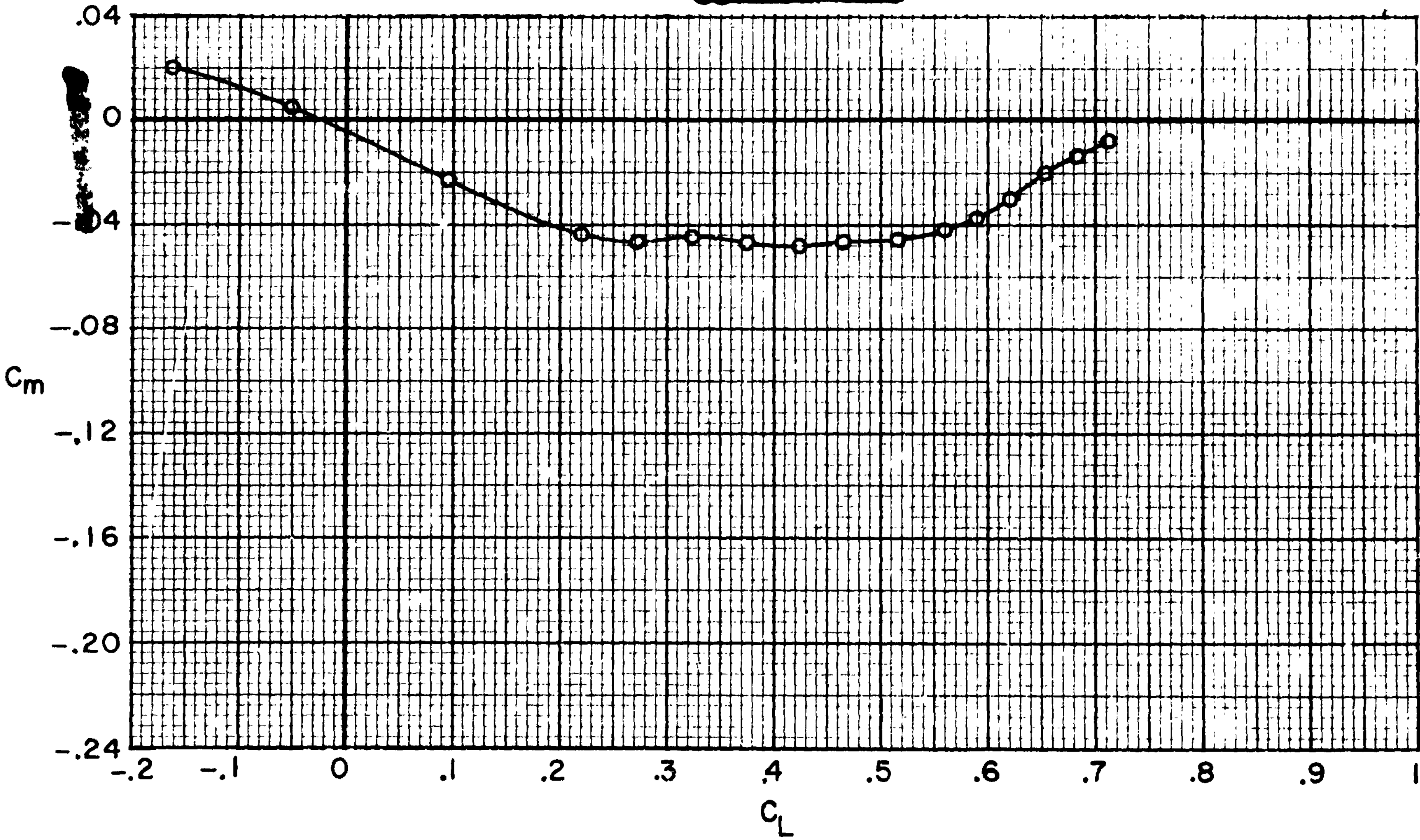

(j) M = 0.90. Concluded.

Figure 19.- Concluded.

[redacted]

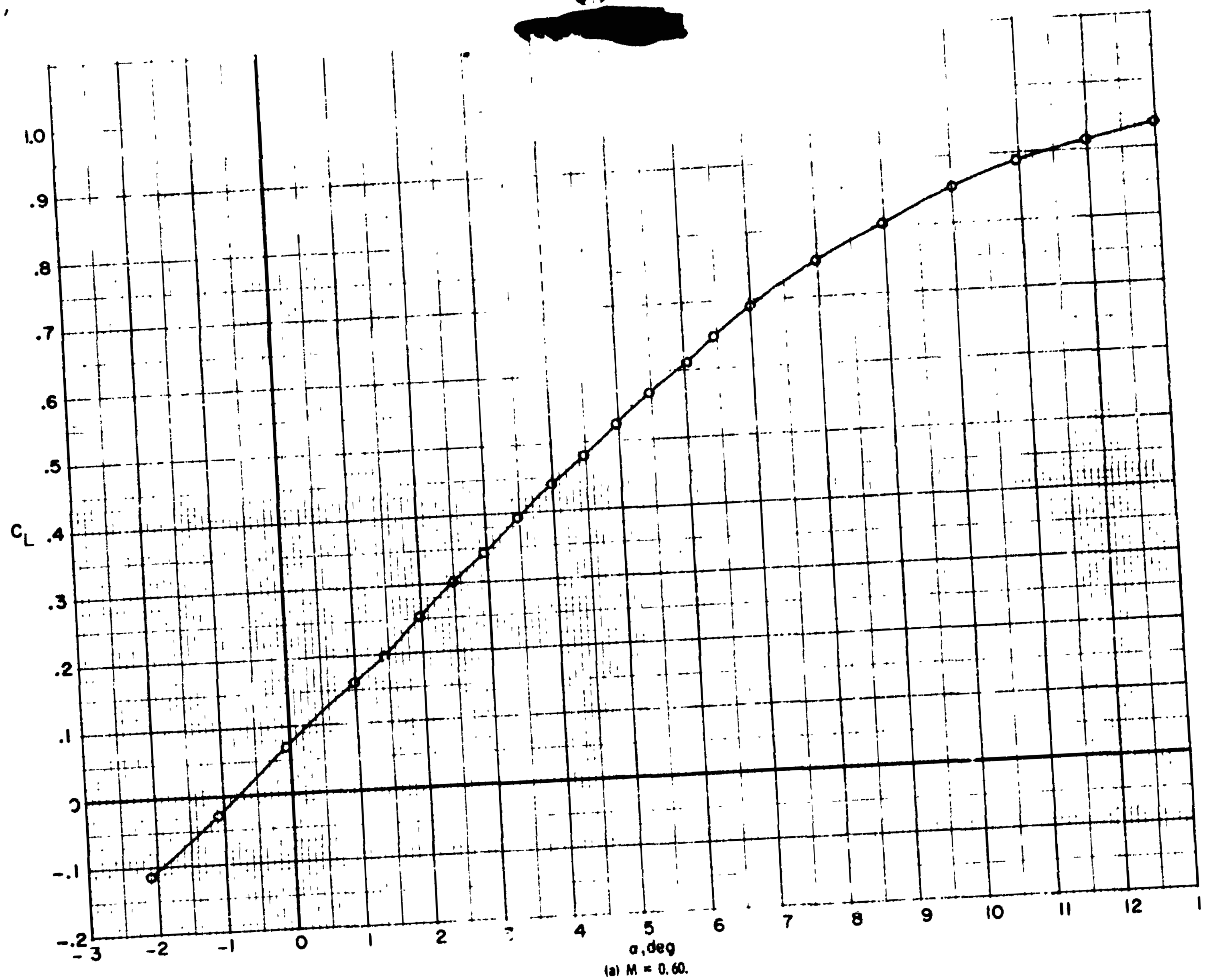

(a) M = 0.60.

Figure 20. - Longitudinal aerodynamic characteristics for simulated current wide-body configuration with wing upper surface grit forward (x_T/c = 0.05). c.g. (F.S.) = 84.605 cm (33.309 in.); $\Lambda_{c/4} = 35°$.

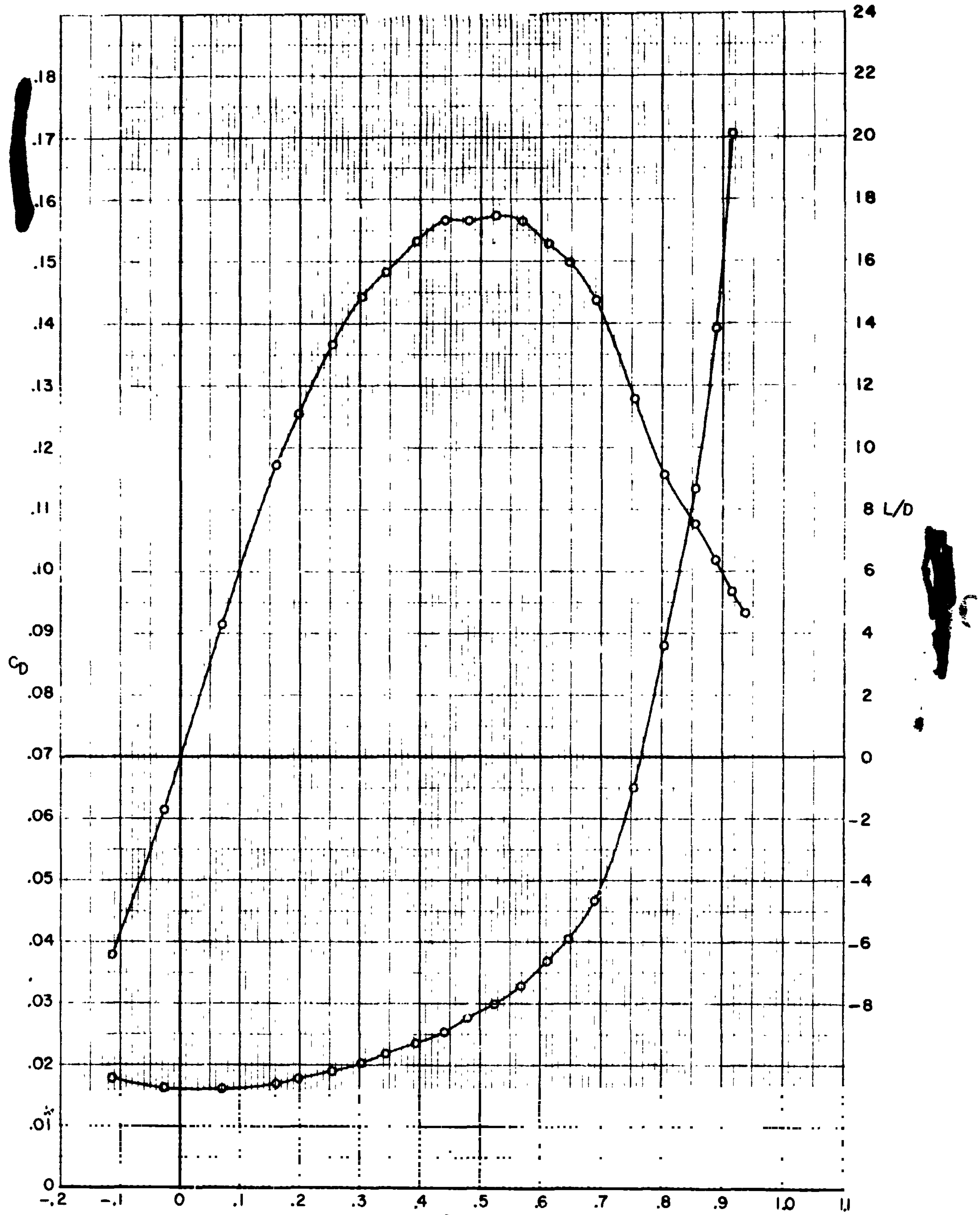

(a) M = 0.60. Continued.

Figure 20. - Continued.

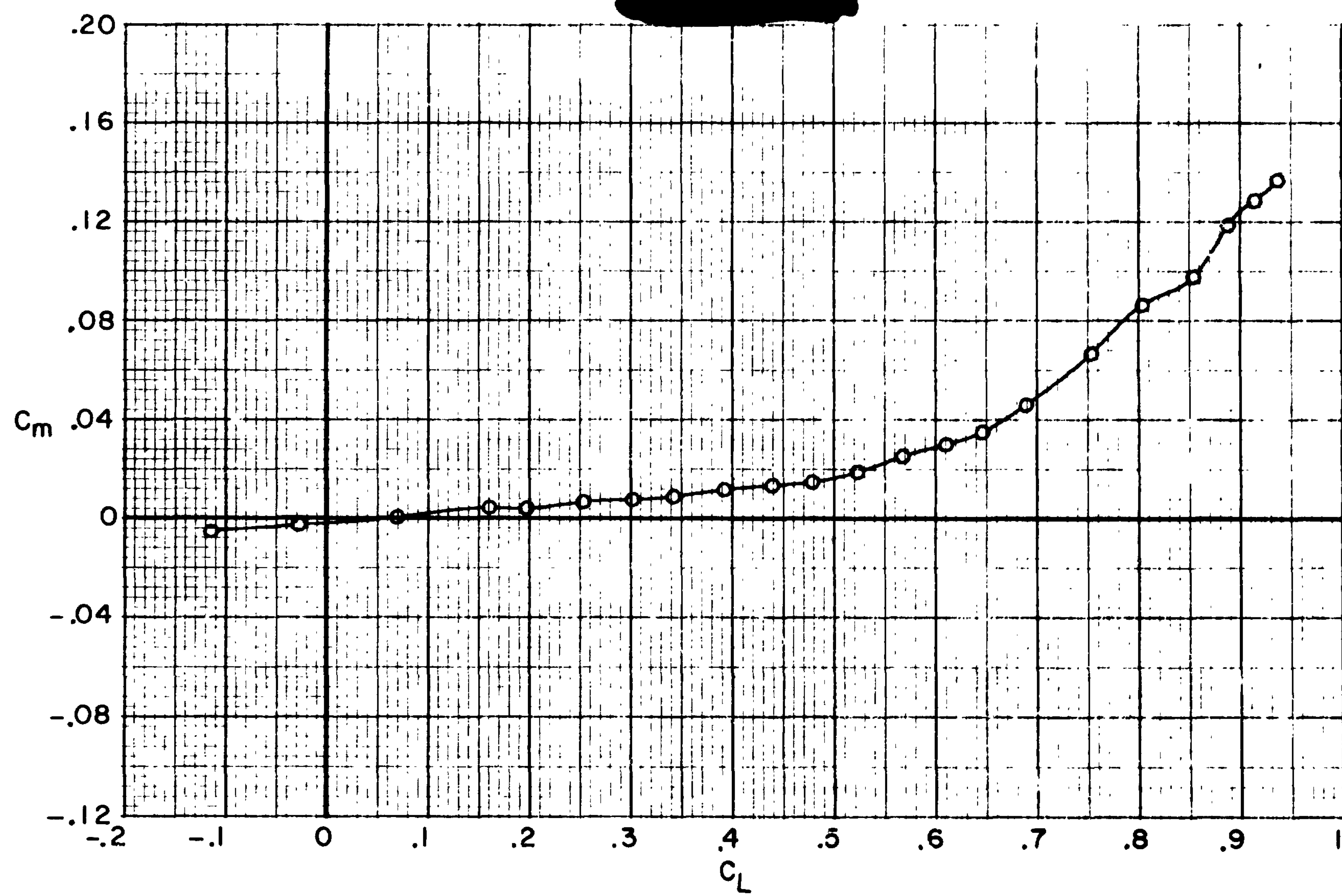

(a) M = 0.60. Concluded.

Figure 20. - Continued.

ORIGINAL PAGE IS
OF POOR QUALITY

ORIGINAL PAGE IS
OF POOR QUALITY

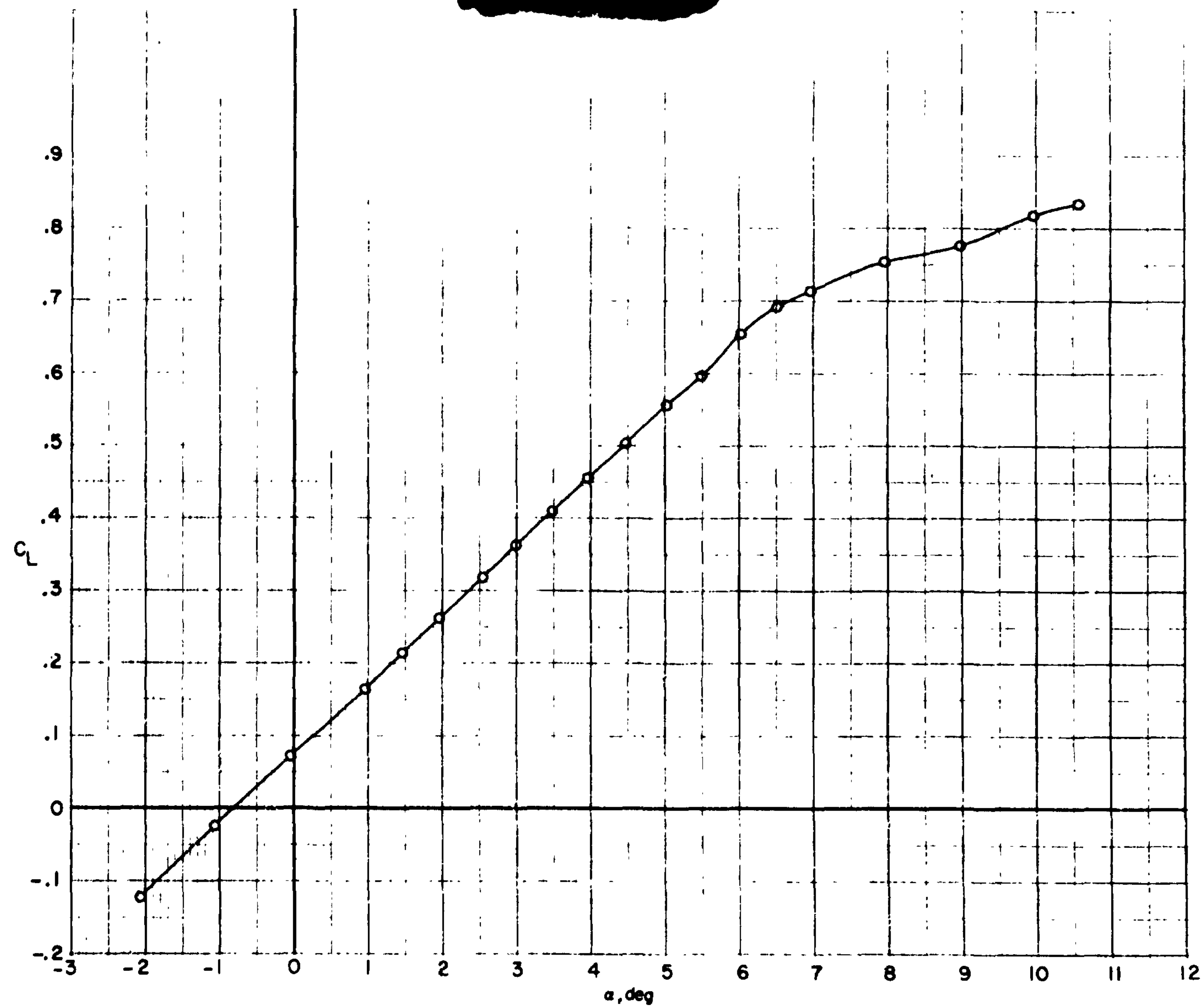

(b) M = 0.70.

Figure 20. - Continued.

ORIGINAL PAGE IS
OF POOR QUALITY

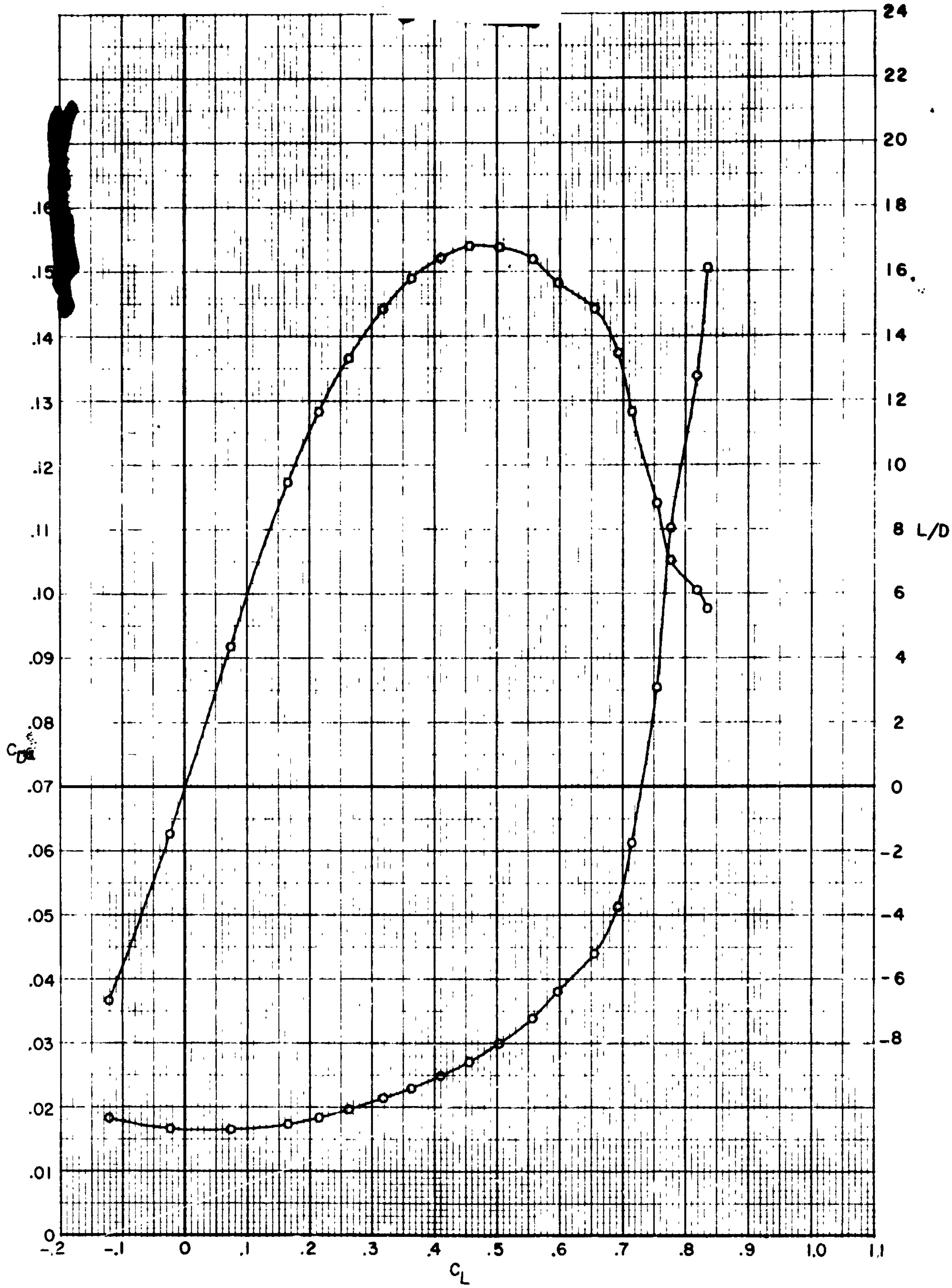

(b) M = 0.70. Continued.

Figure 20.- Continued.

[redacted]

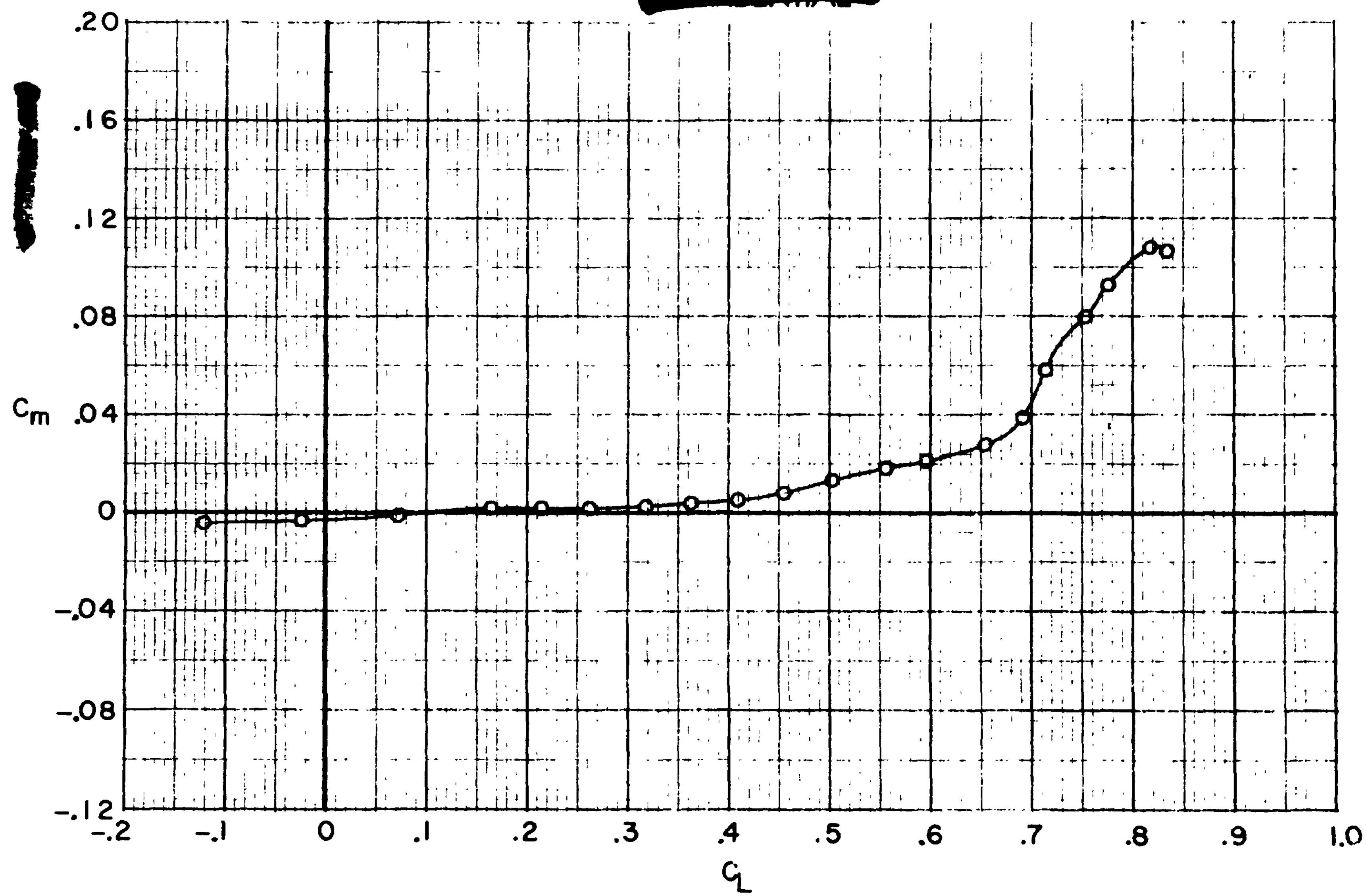

(b) M = 0.70. Concluded.

Figure 20.- Continued.

[redacted]

[redacted]

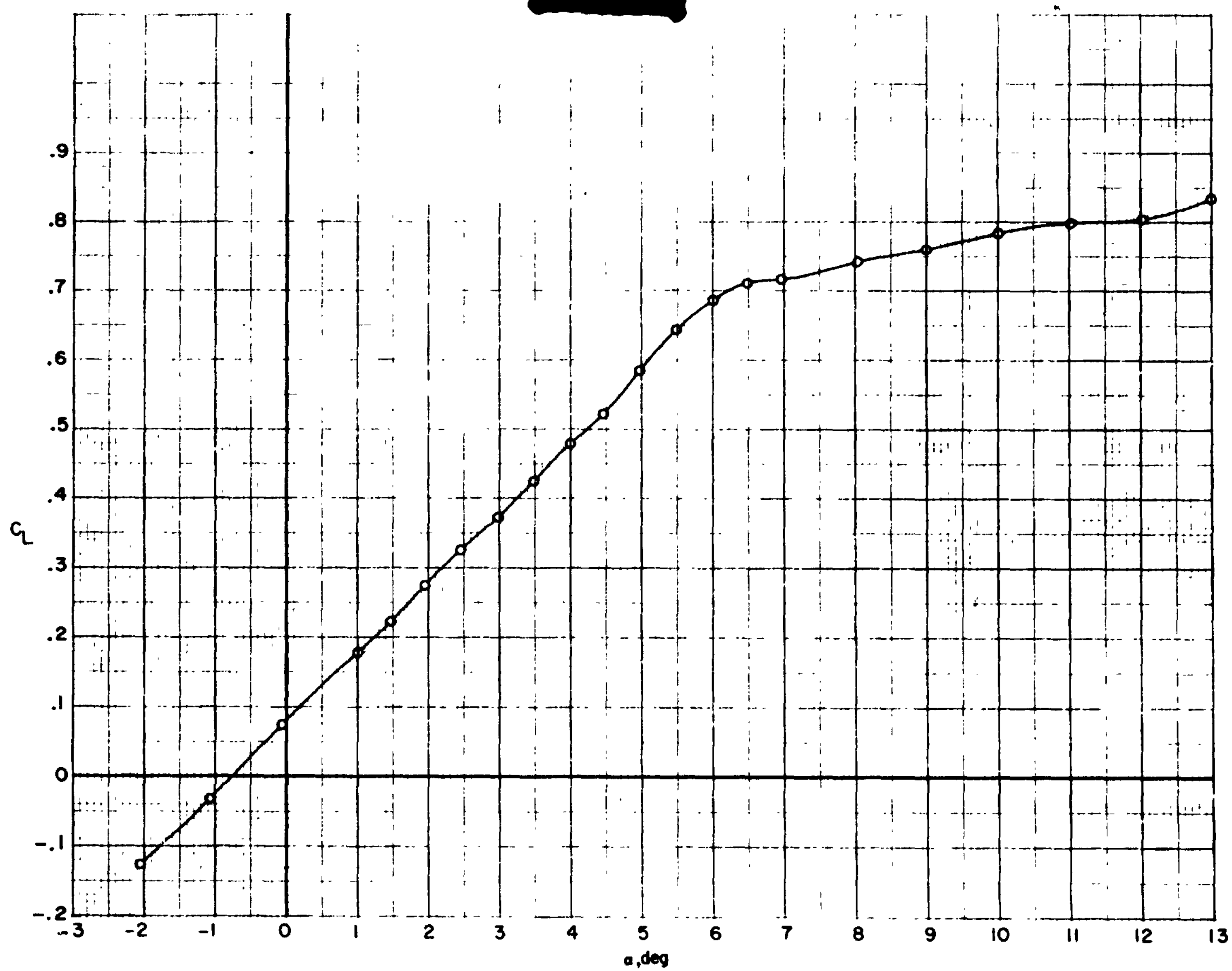

(c) M = 0.75.

Figure 20. - Continued.

[redacted]

ORIGINAL PAGE IS
OF POOR QUALITY

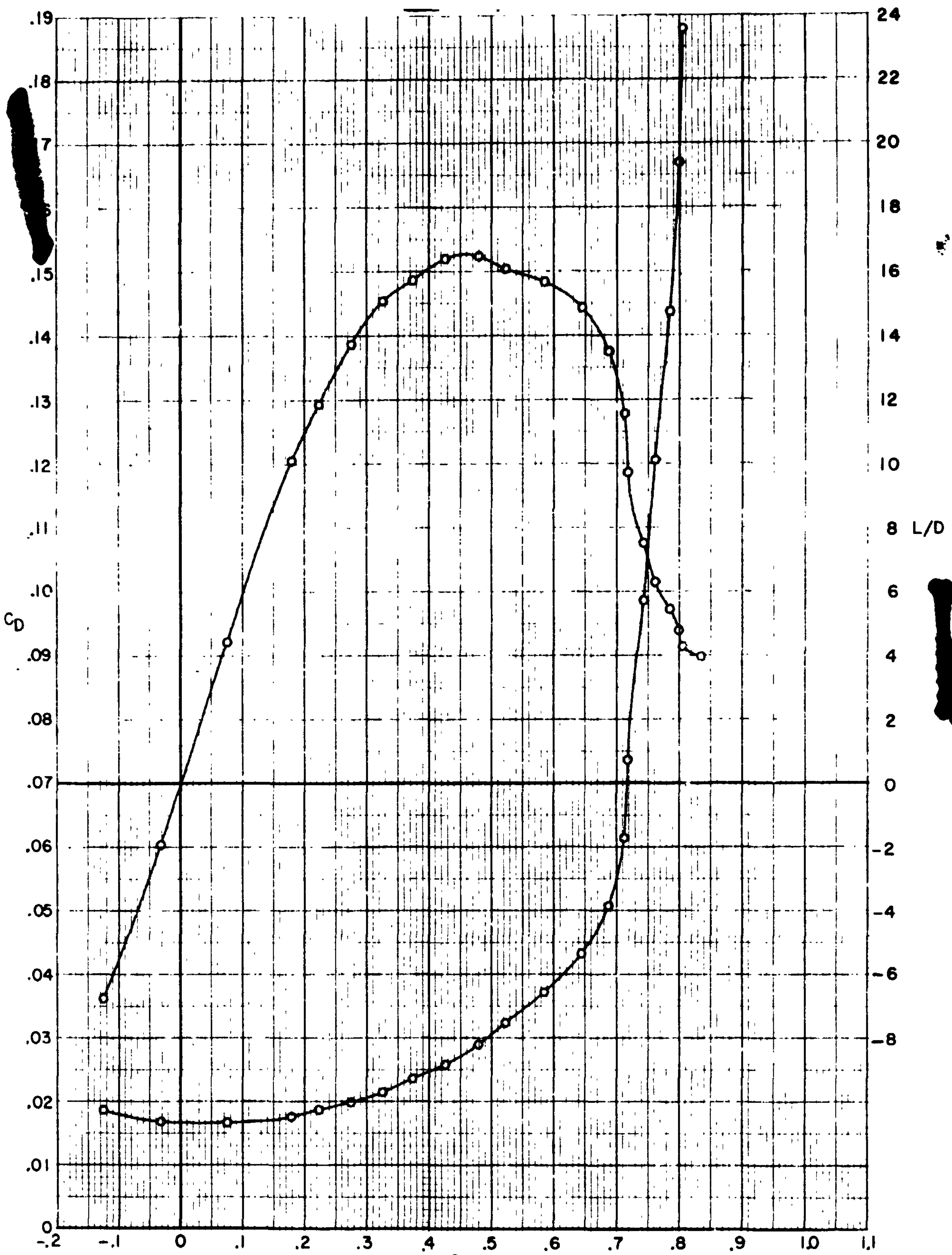

(c) M = 0.75. Continued.

Figure 20.- Continued.

[redacted]

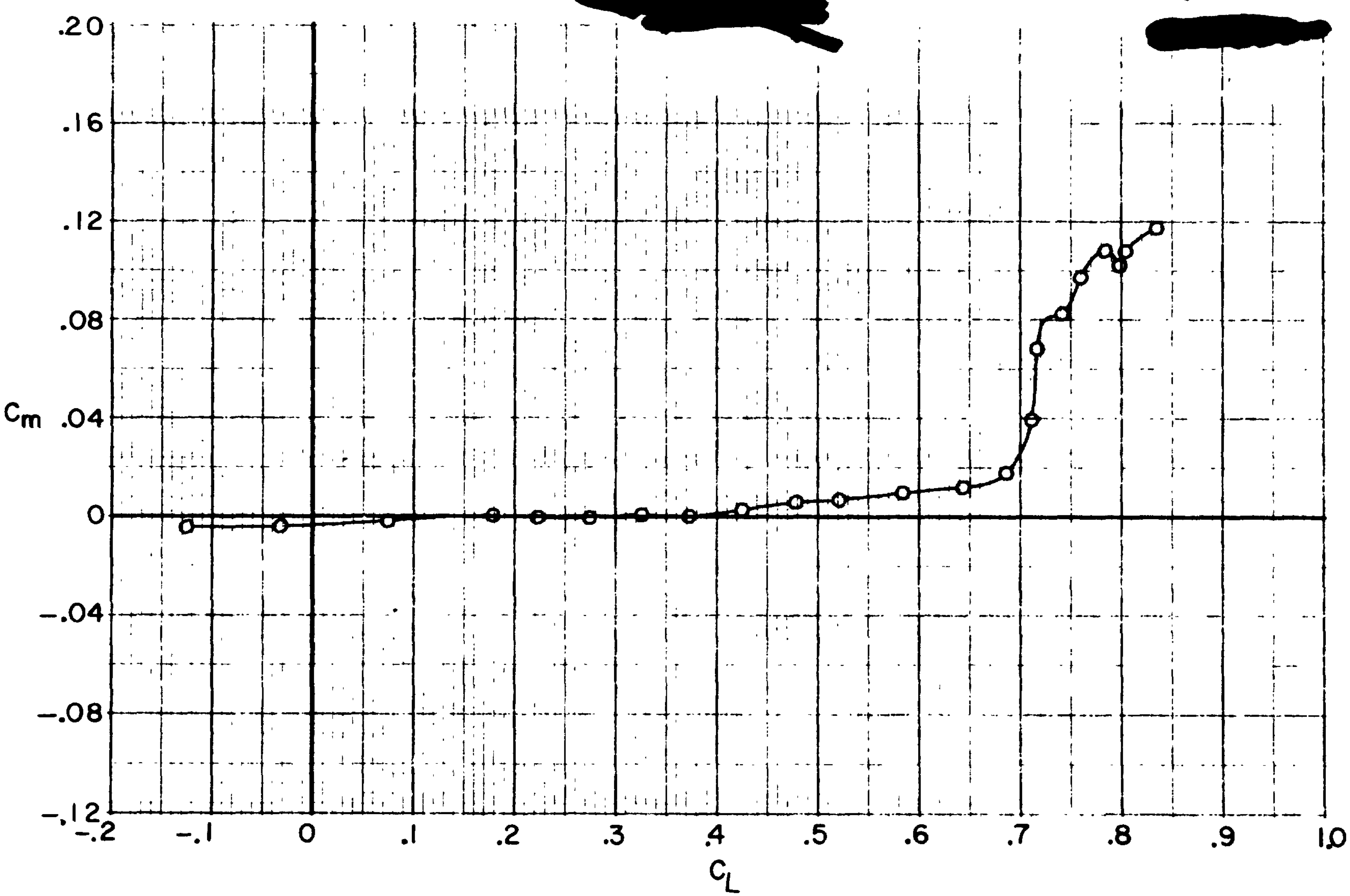

(c) M = 0.75. Concluded.

Figure 20.- Continued.

[redacted]

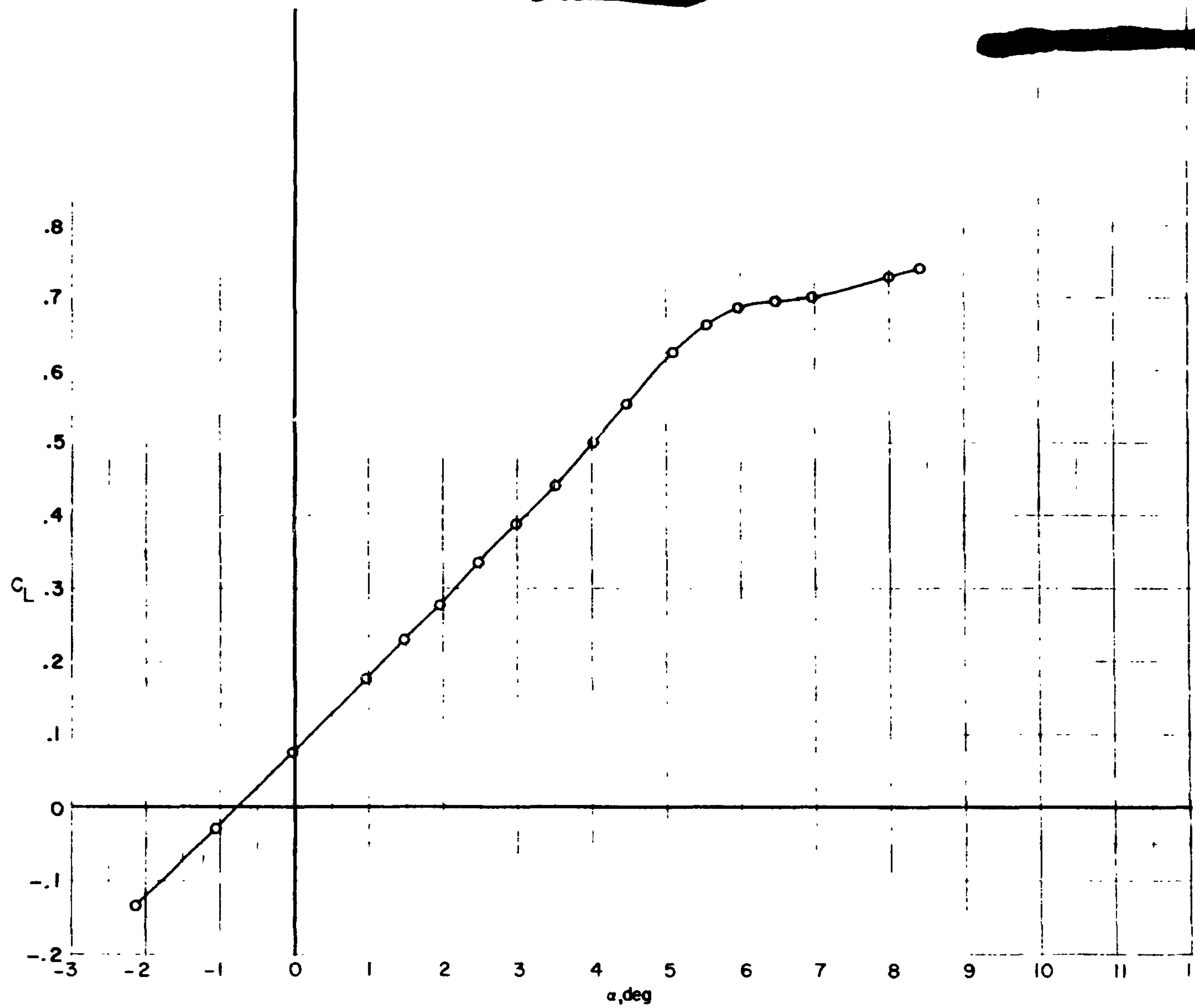

(d) M = 0.78.

Figure 20.- Continued.

ORIGINAL PAGE IS
OF POOR QUALITY

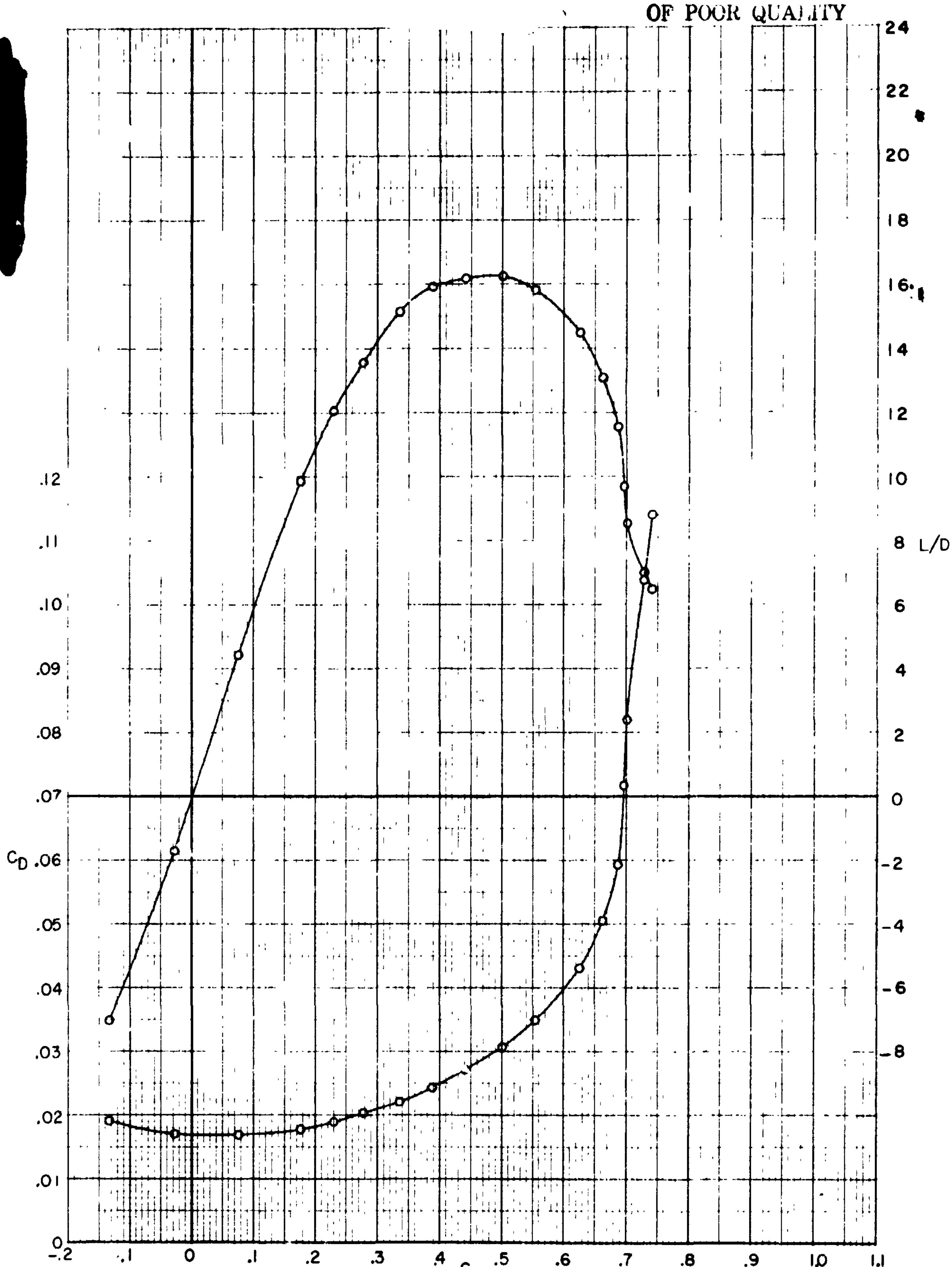

(d) M = 0.78. Continued.

Figure 20. - Continued.

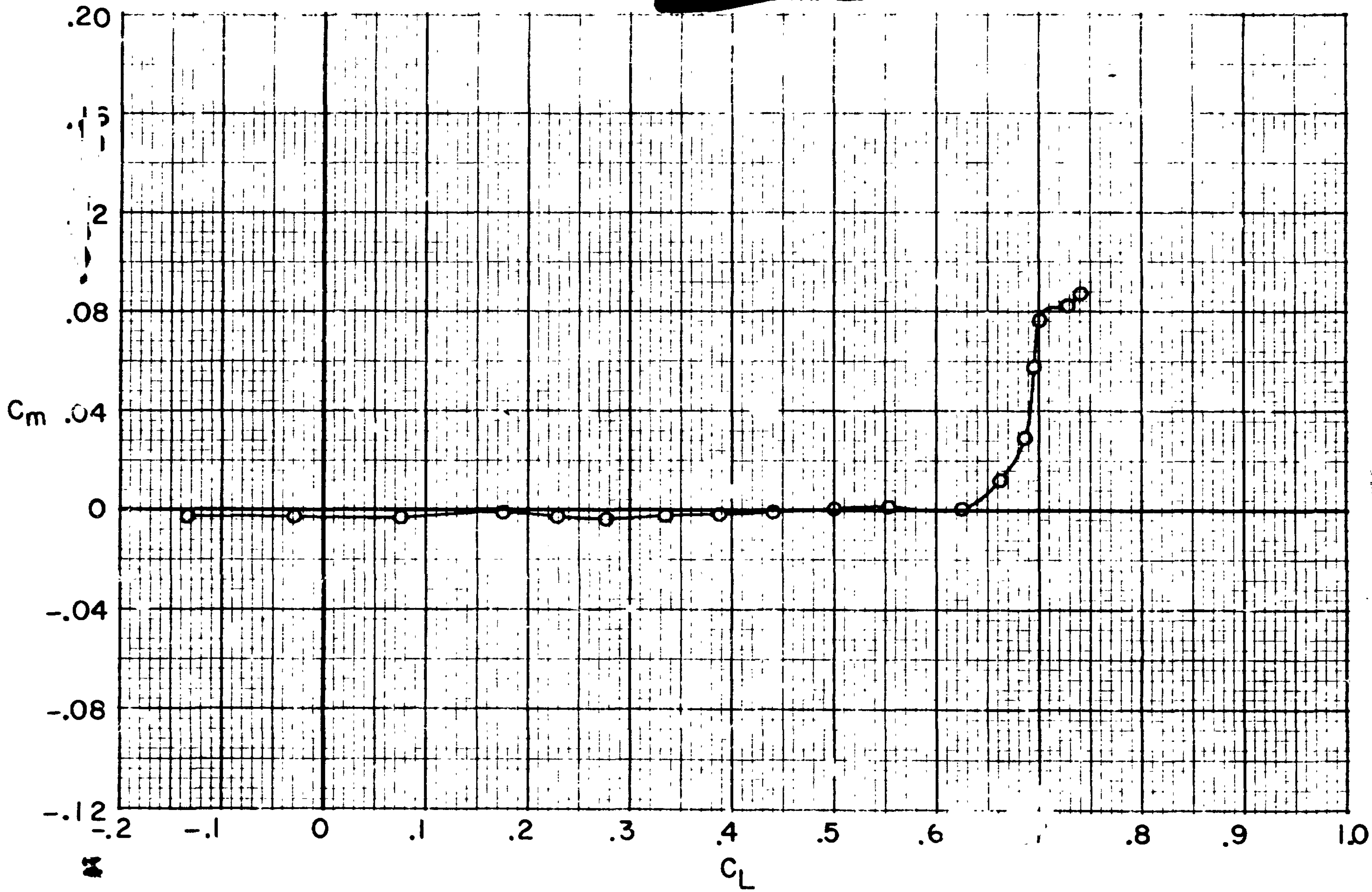

ORIGINAL PAGE IS OF POOR QUALITY

(d) M = 0.78. Concluded.

Figure 20. - Continued.

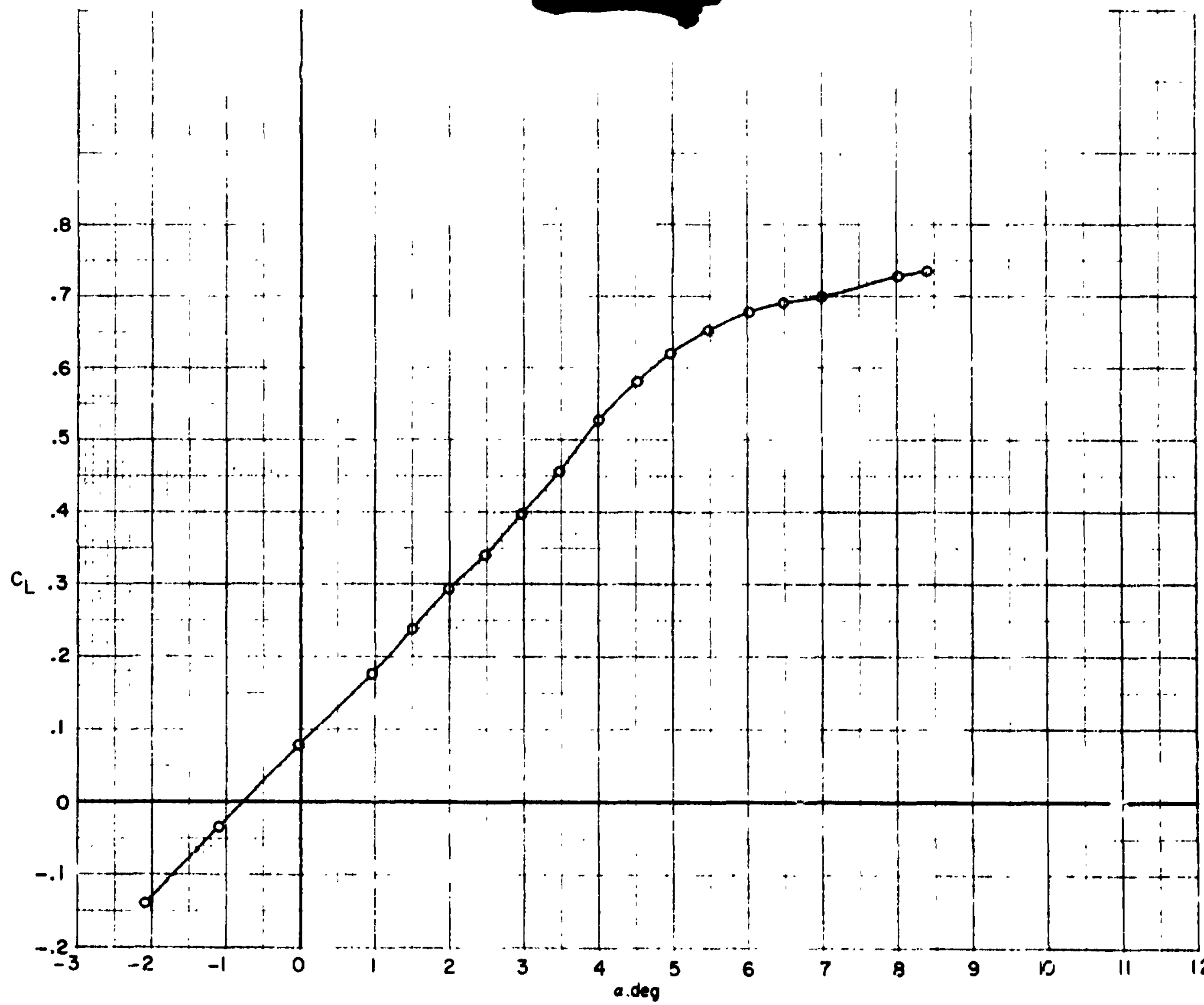

(e) M = 0.80.

Figure 20. - Continued.

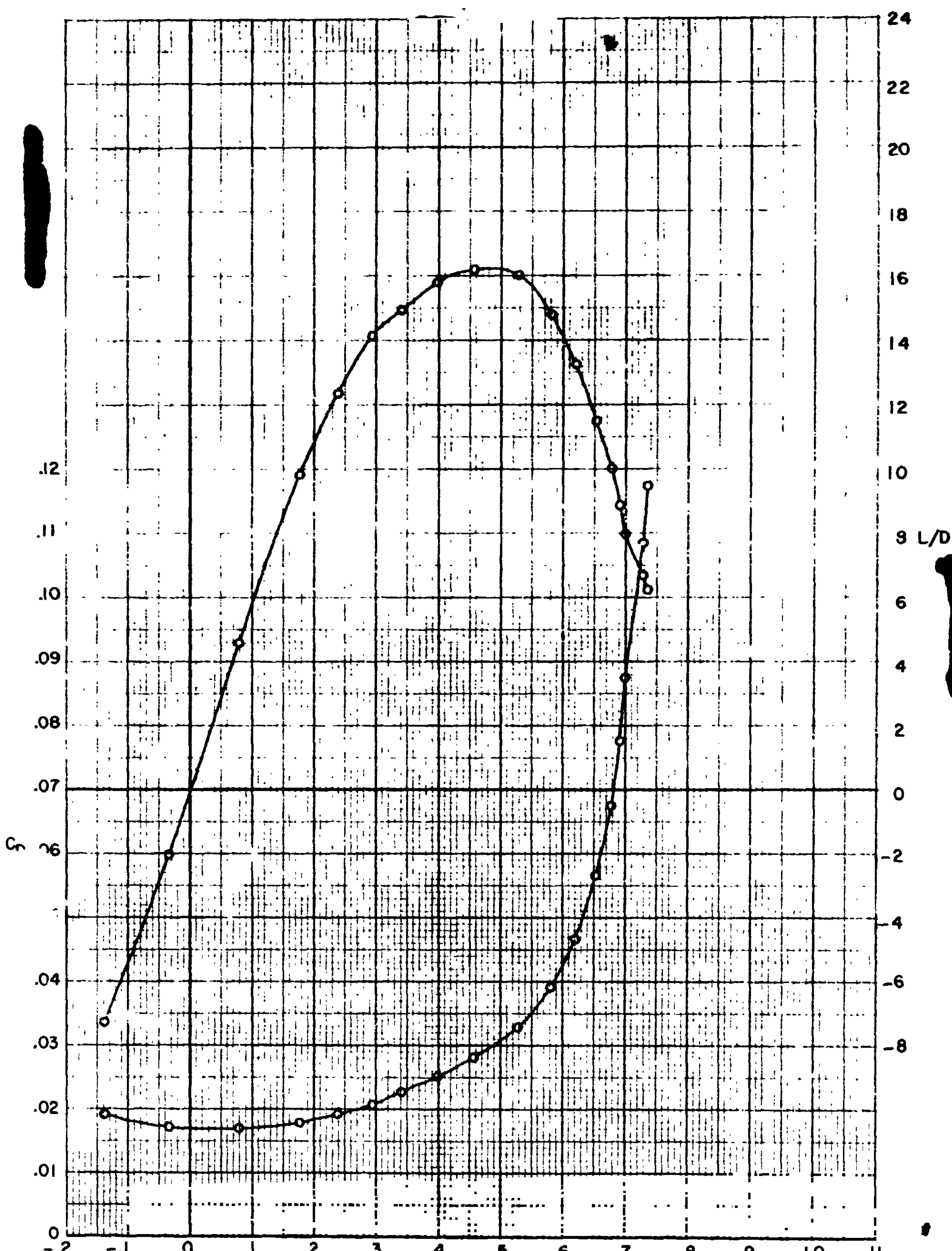

(e) M = 0.80. Continued.

Figure 20.- Continued.

[redacted]

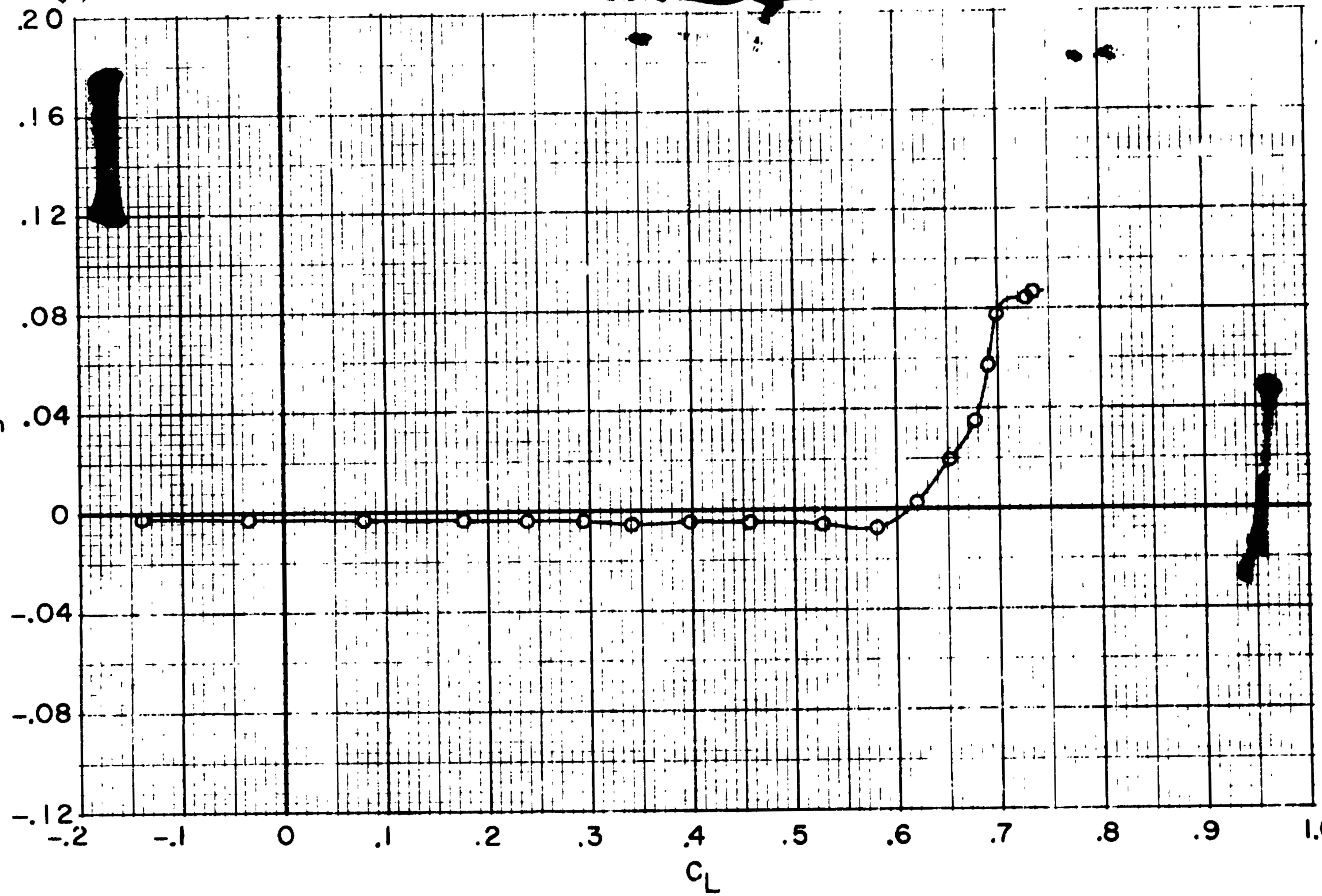

(e) M = 0.80. Concluded.

Figure 20.- Continued.

[redacted]

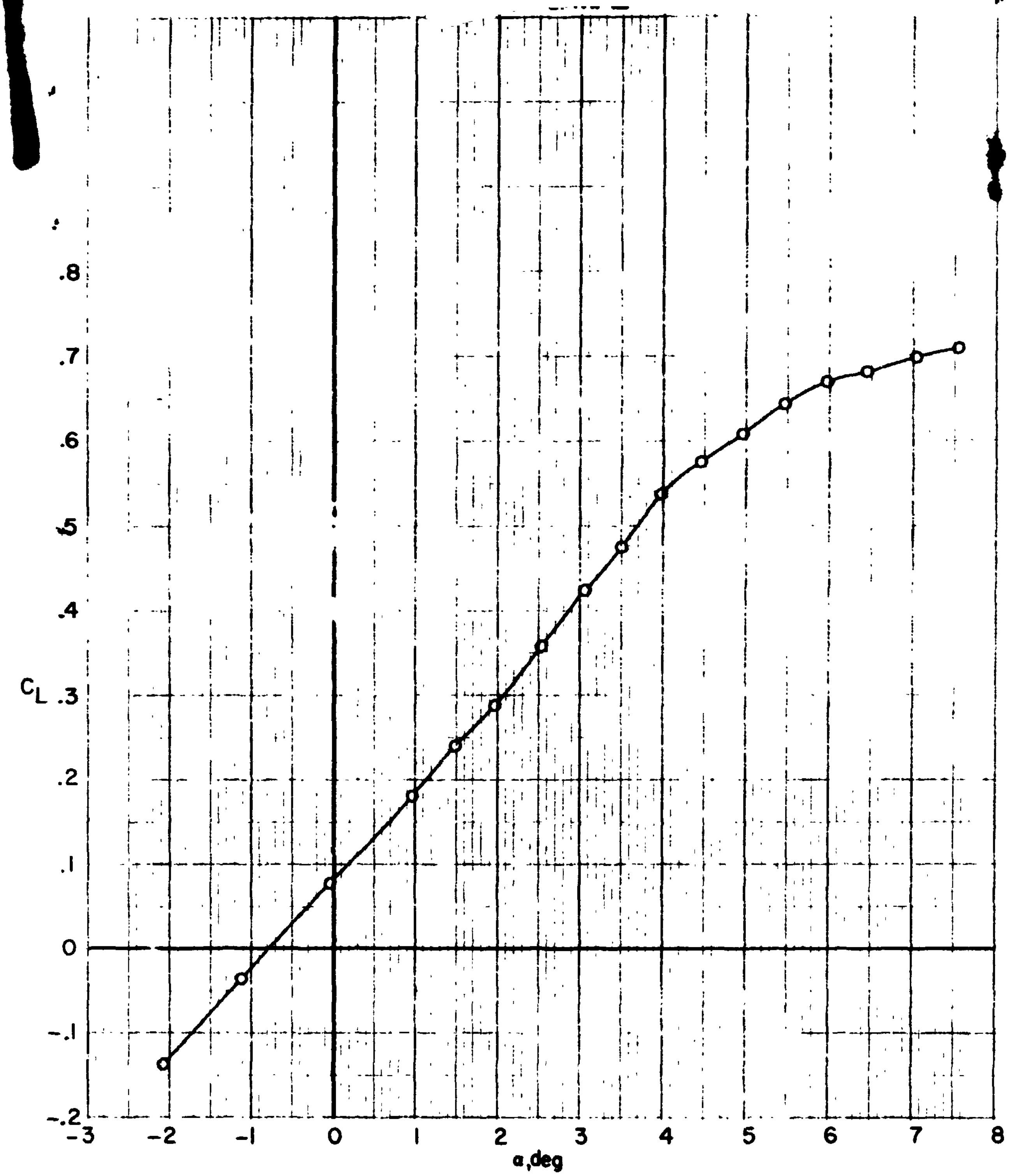

(f) M = 0.82.

Figure 20. - Continued.

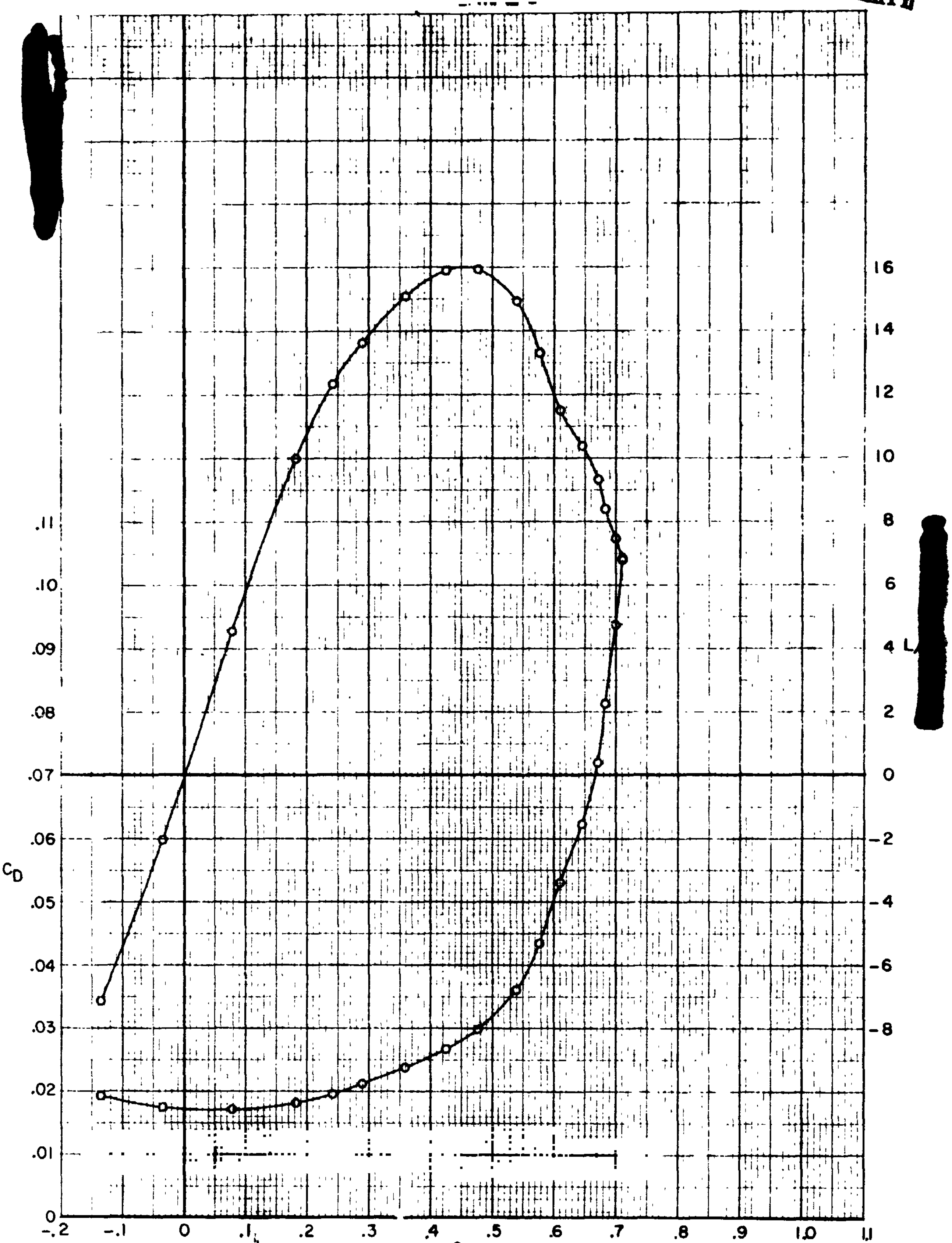

(f) M = 0.82. Continued.

Figure 20.- Continued.

[redacted]

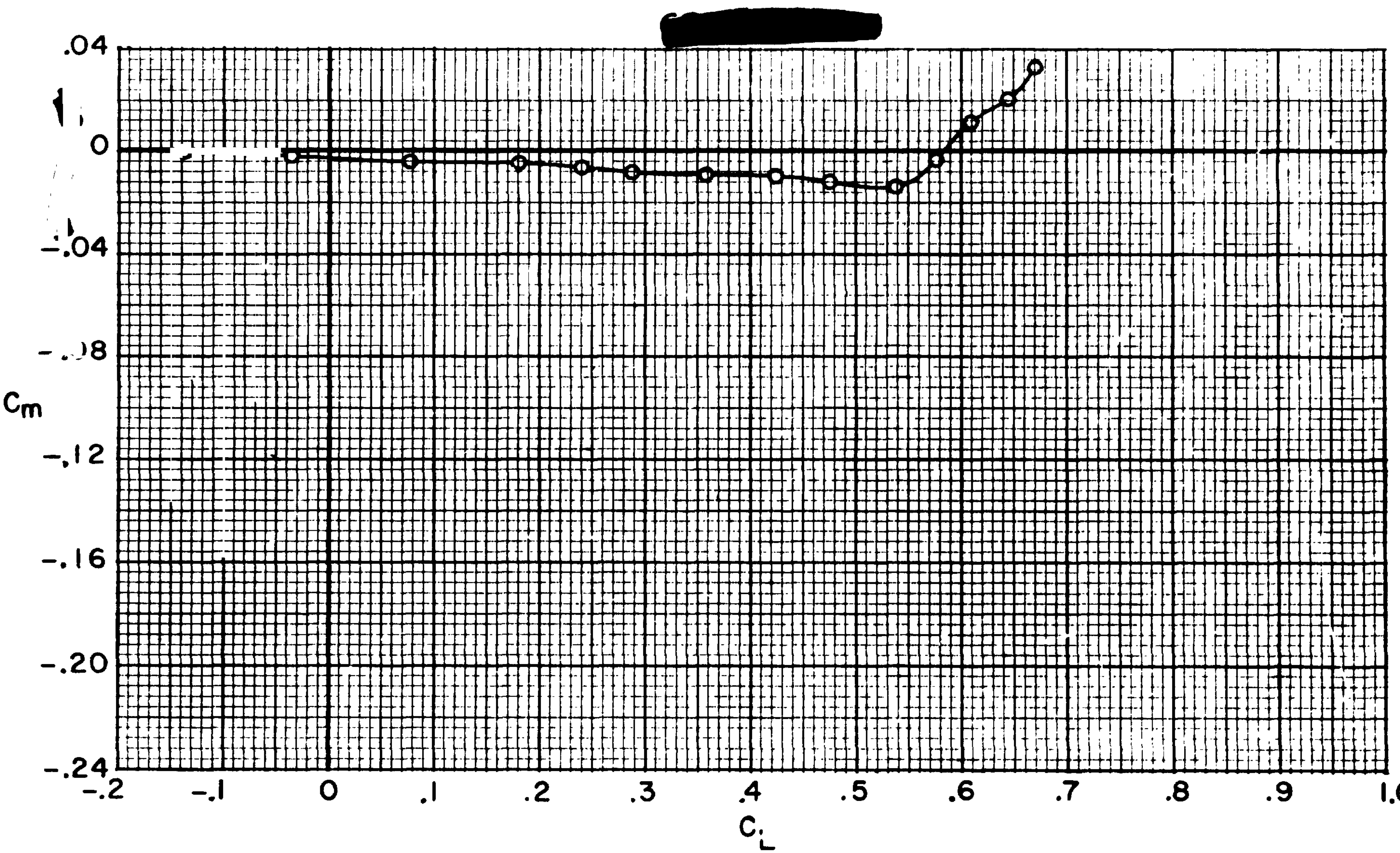

(f) M = 0.82. Concluded.

Figure 20.- Continued.

[redacted]

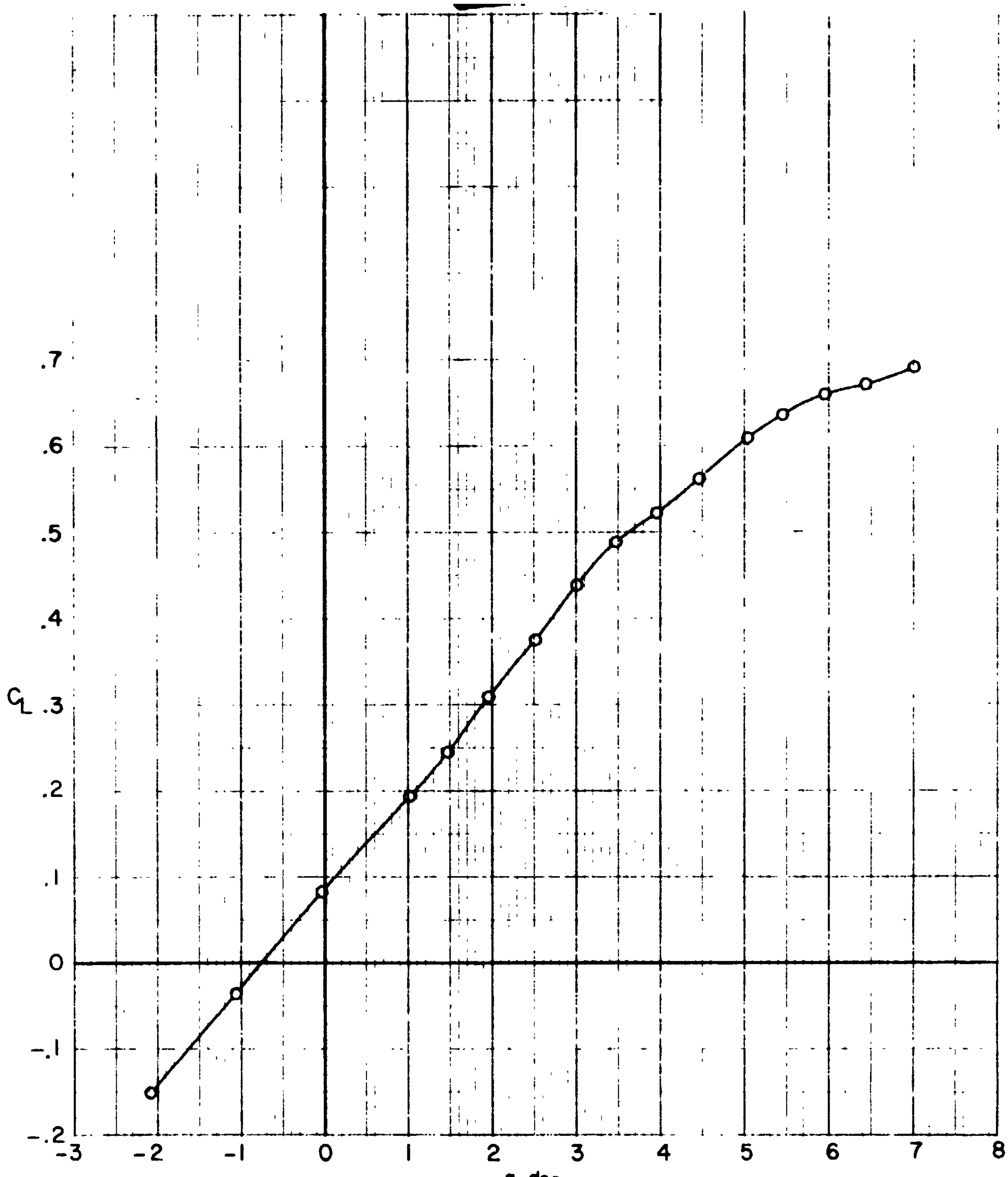

(g) M = 0.84.

Figure 20. - Continued.

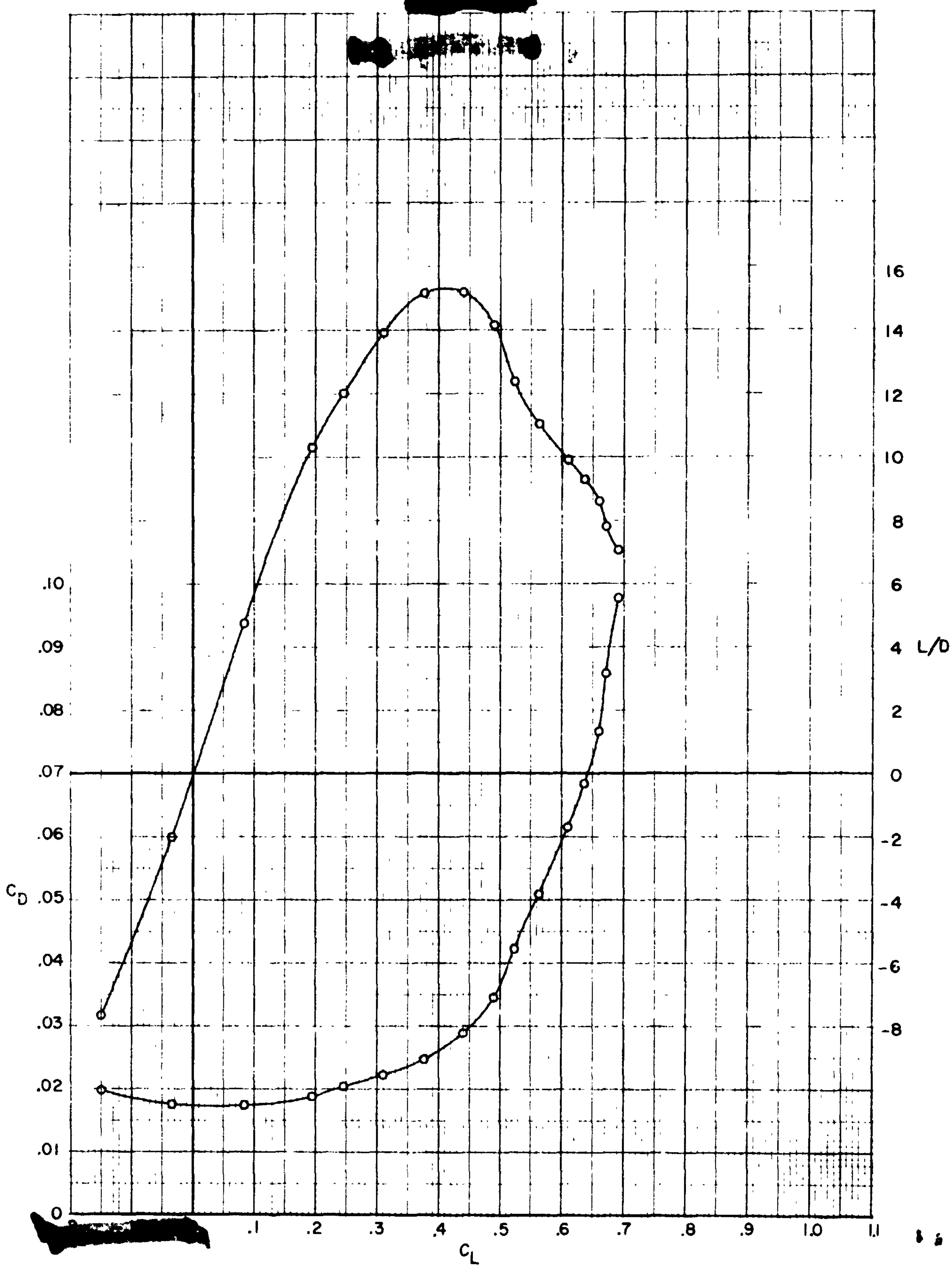

(g) M = 0.84. Continued.

Figure 20. - Continued.

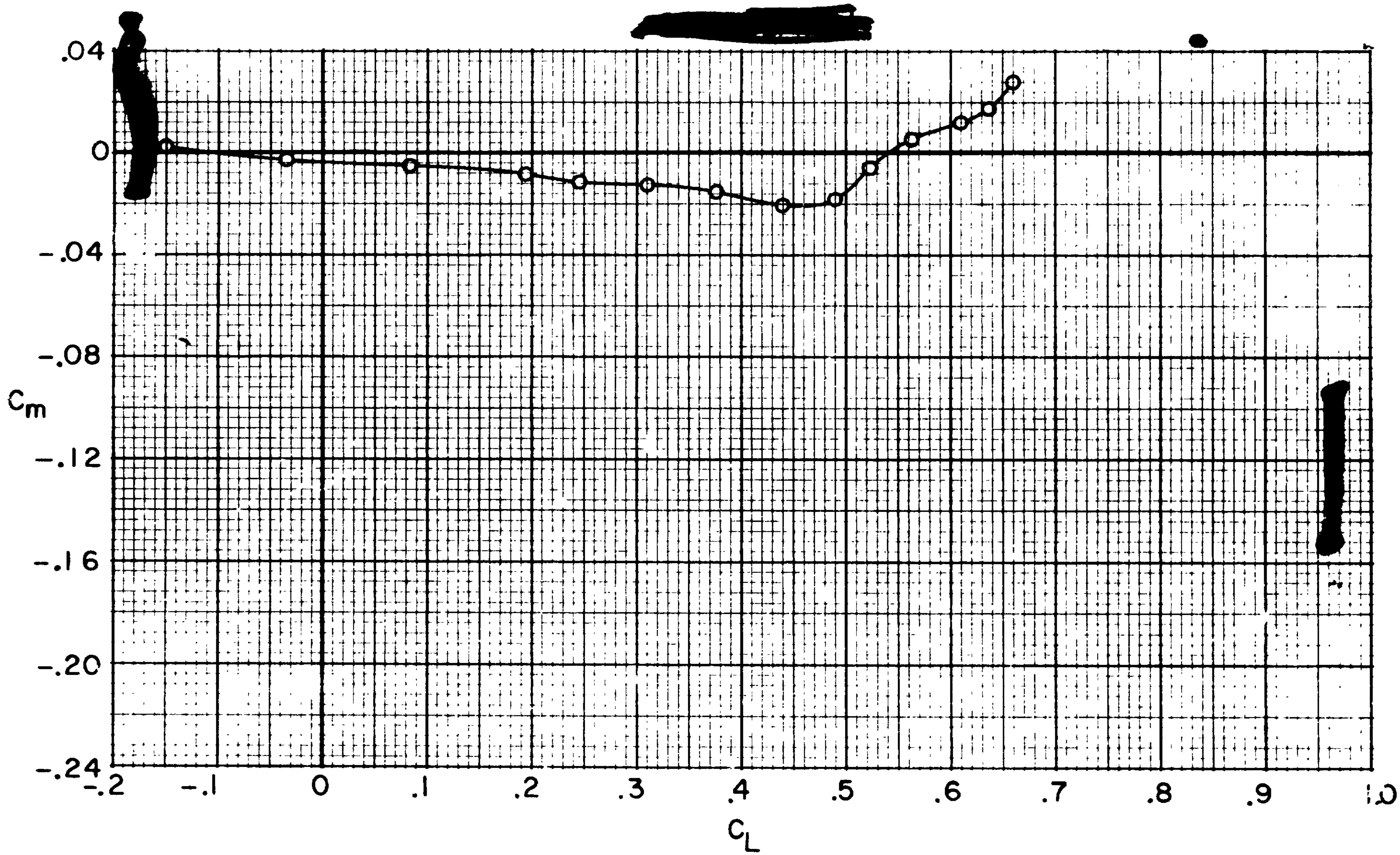

(g) M = 0.84. Concluded.

Figure 20. - Continued.

ORIGINAL PAGE IS
OF POOR QUALITY

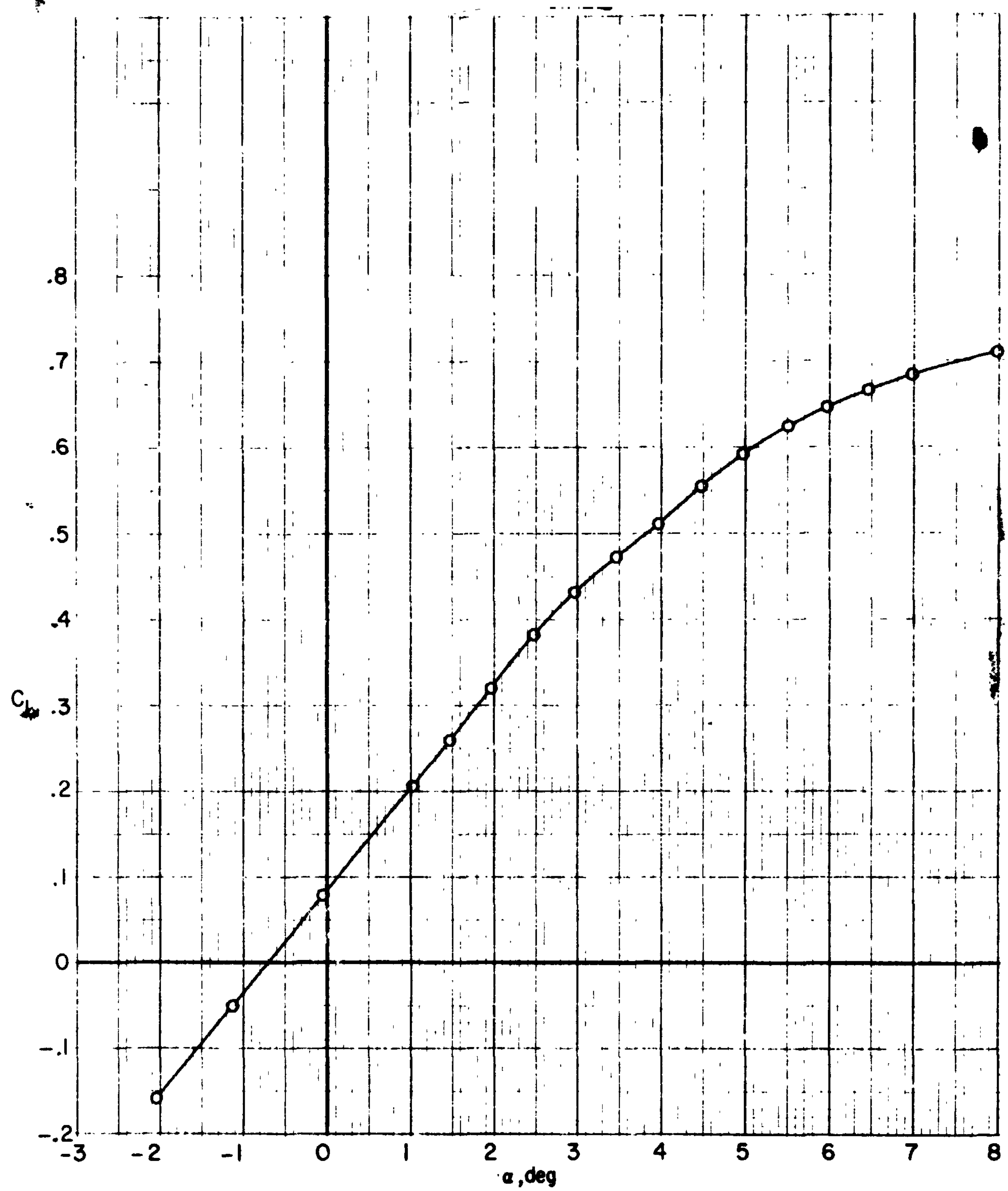

(h) M = 0.86.

Figure 20.- Continued.

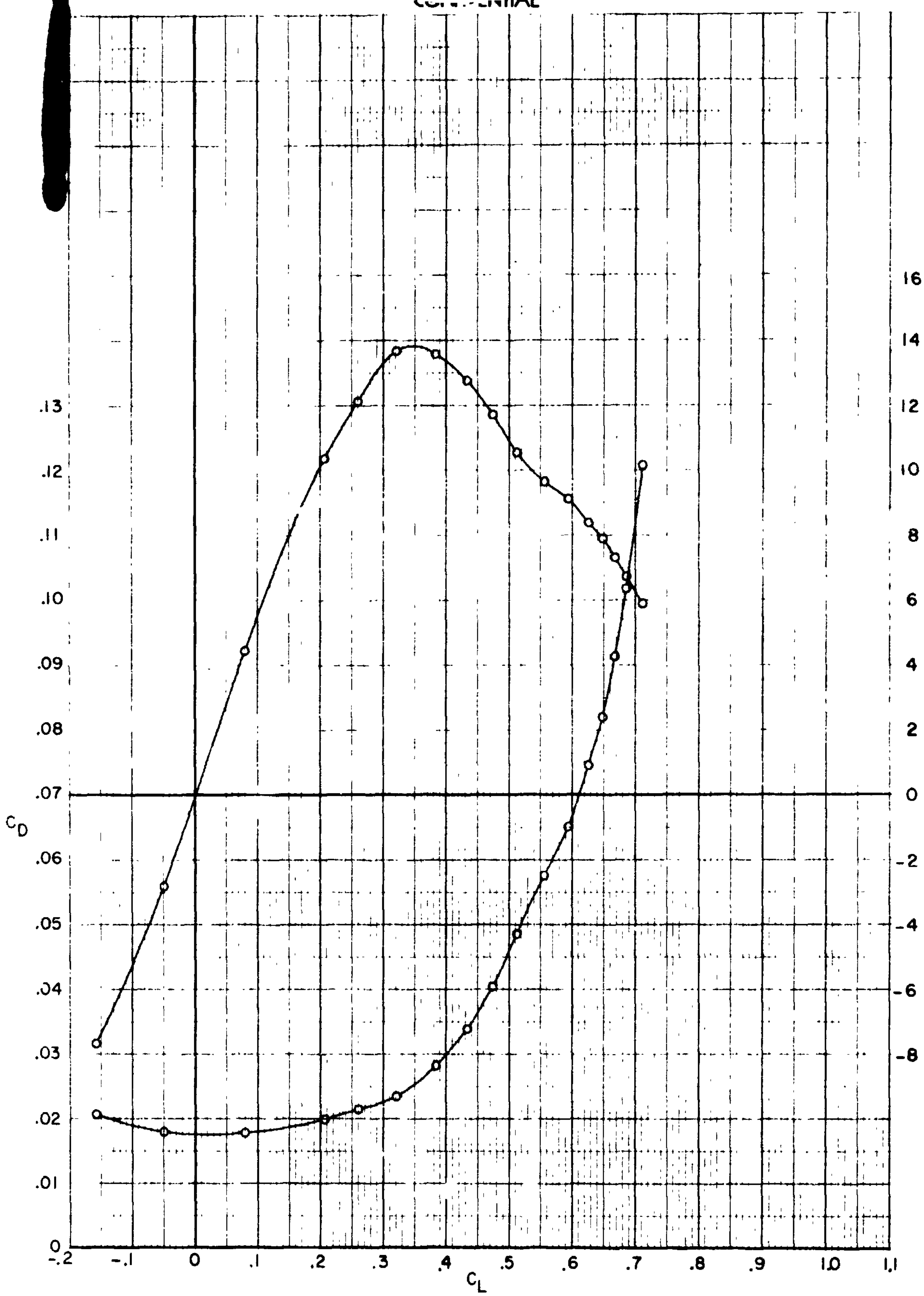

(h) M = 0.86. Continued.

Figure 20. - Continued.

[redacted]

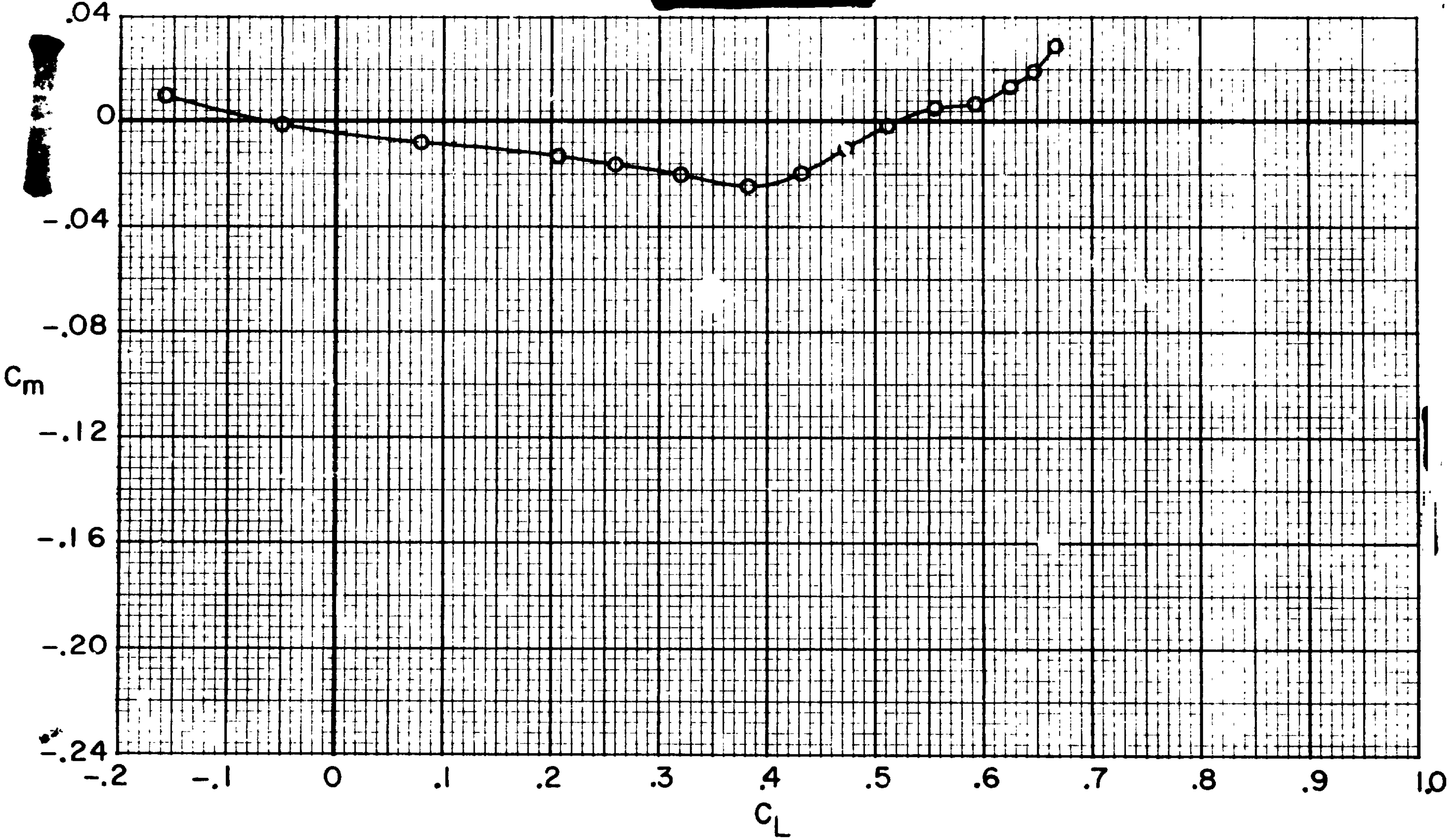

(h) M = 0.86. Concluded.

Figure 20.- Continued.

[redacted]

[redacted]

ORIGINAL PAGE IS
OF POOR QUALITY

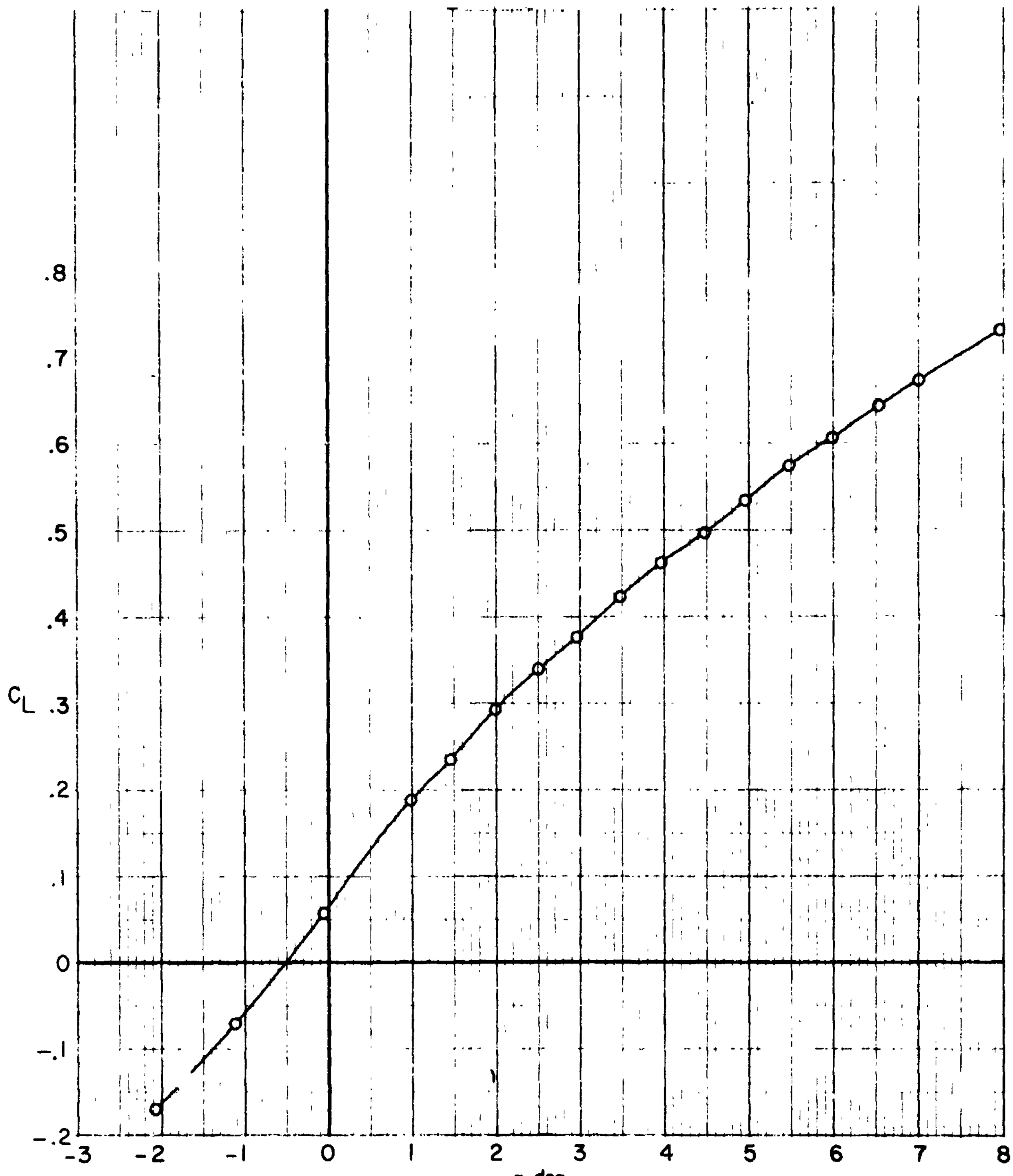

(l) M = 0.90.

Figure 20.- Continued.

[redacted]

[redacted]

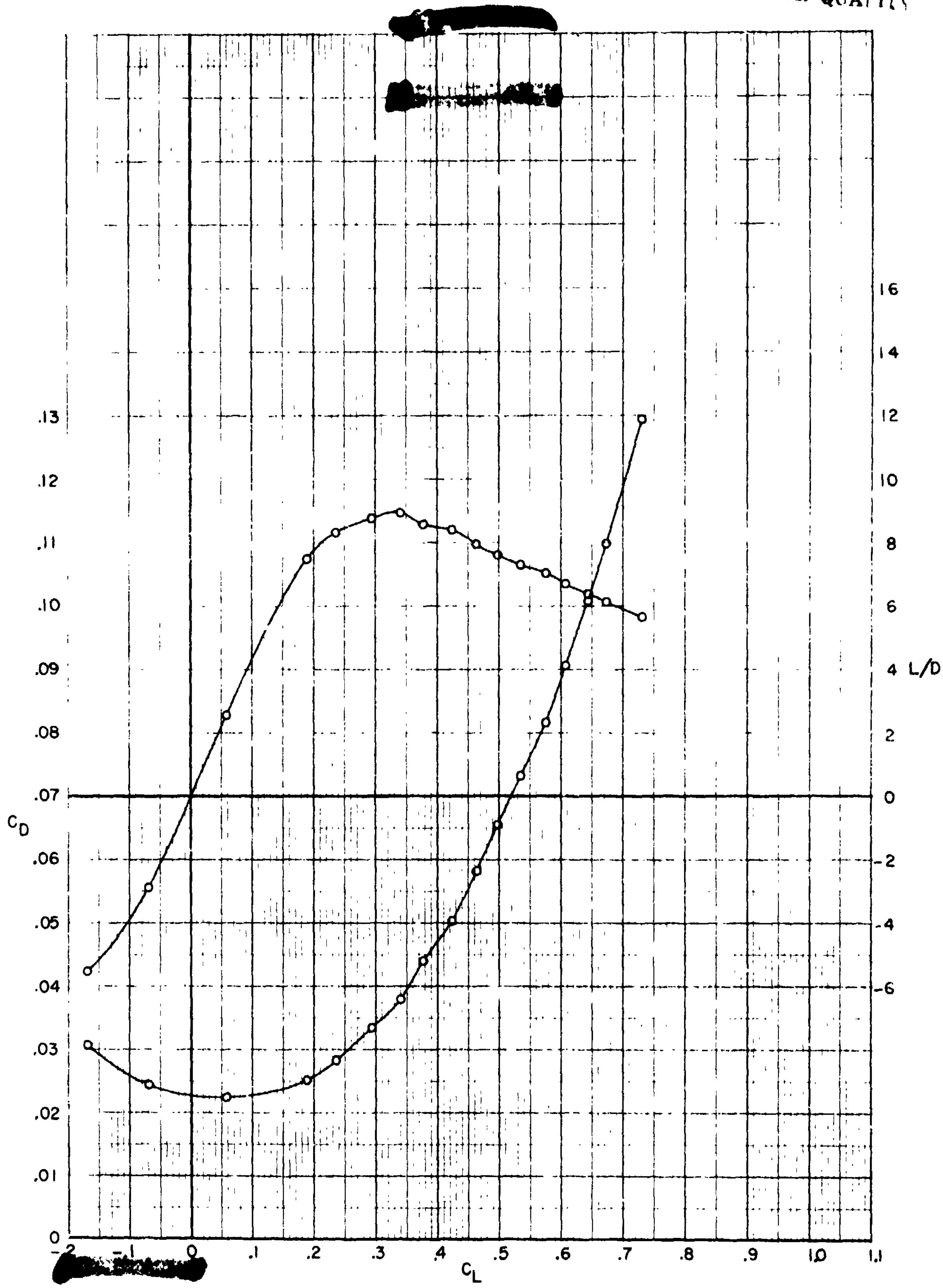

(l) M = 0.90. Continued.

Figure 20. - Continued.

[redacted]

[redacted]

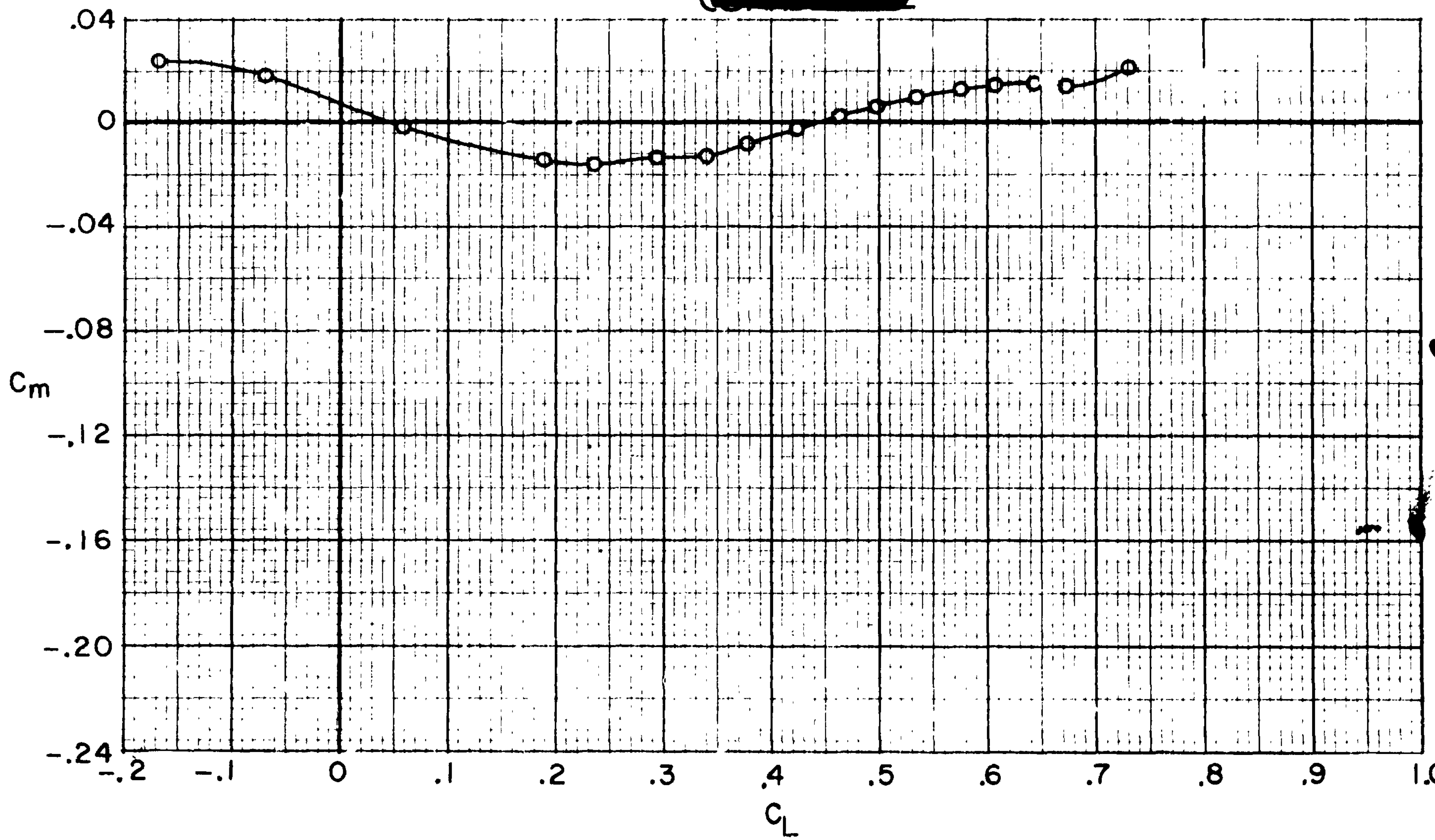

ORIGINAL PAGE IS OF POOR QUALITY

(i) M = 0.90. Concluded.

[redacted]

Figure 20.- Concluded.

ORIGINAL PAGE IS
OF POOR QUALITY

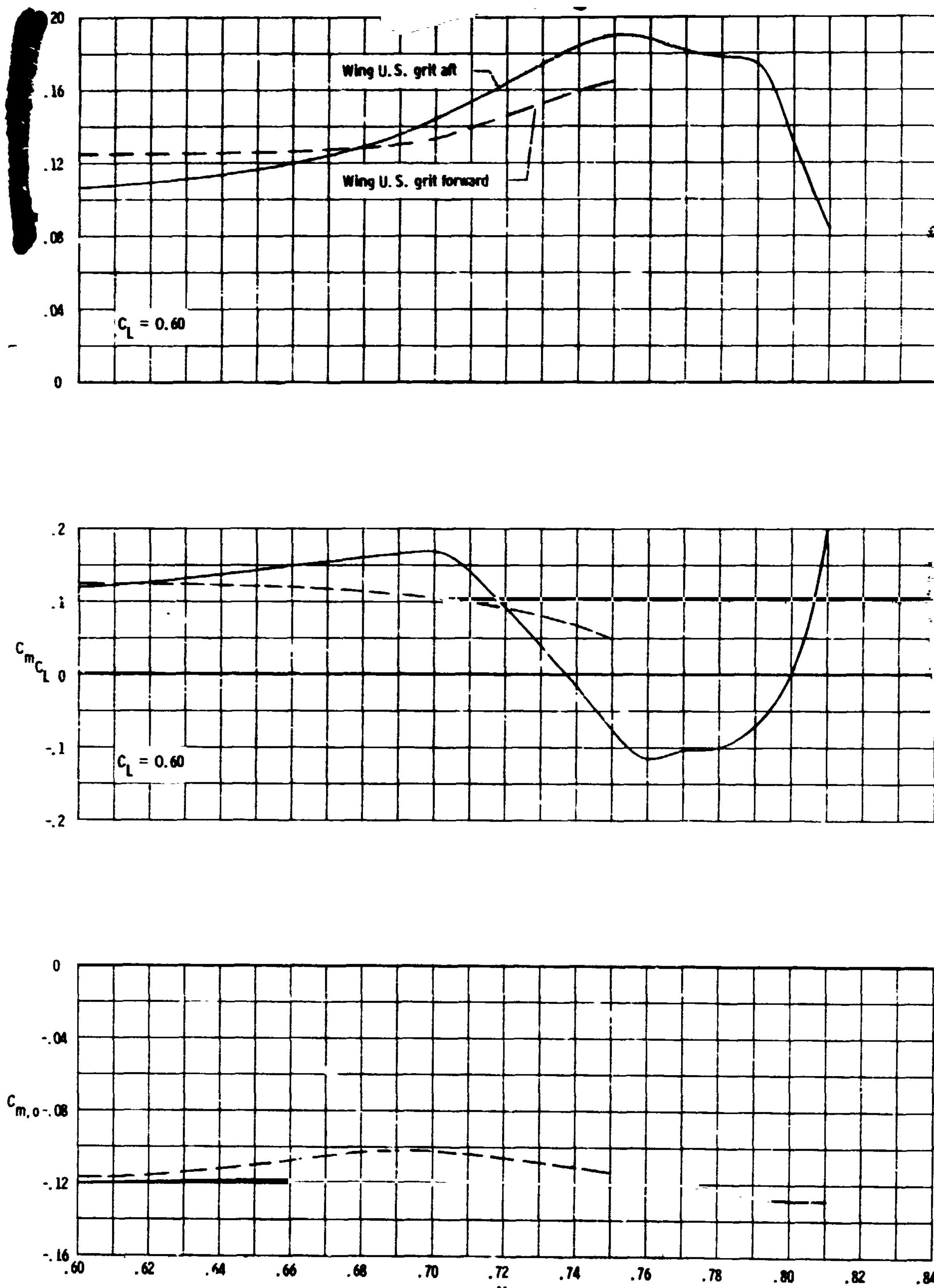

(a) Variation with Mach number of lift-curve slope, longitudinal-stability derivative (c.g. (F.S.) = 84.605 cm (33.309 in.)), and zero-lift pitching-moment coefficient.

Figure 21.- Variation with Mach number of longitudinal aerodynamic characteristics for configuration SCW-Ia. $\beta = 0°$.

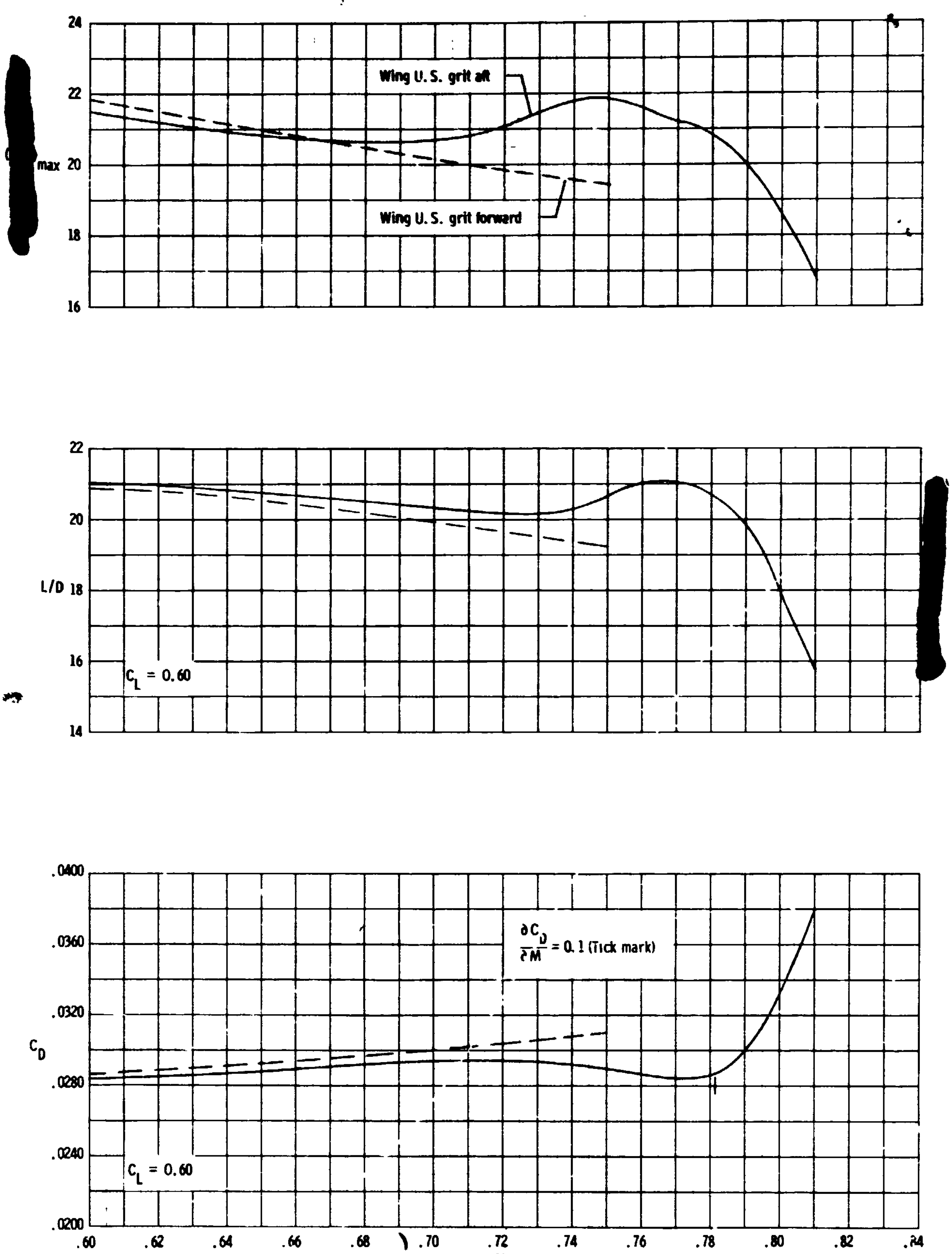

(b) Variation with Mach number of lift-to-drag ratios and drag coefficient.

Figure 21. - Continued.

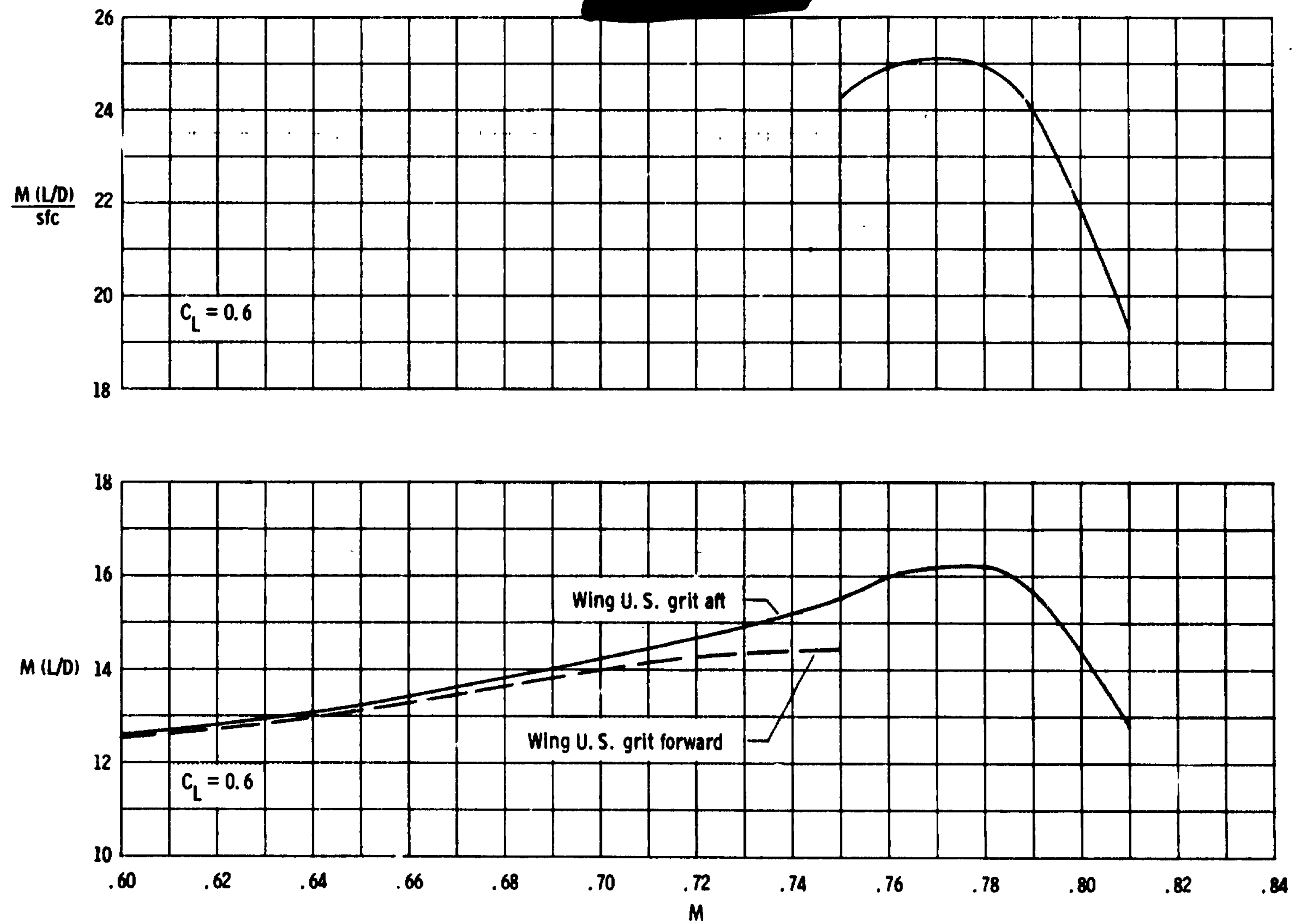

(c) Variation with Mach number of range parameters.

Figure 21. - Concluded.

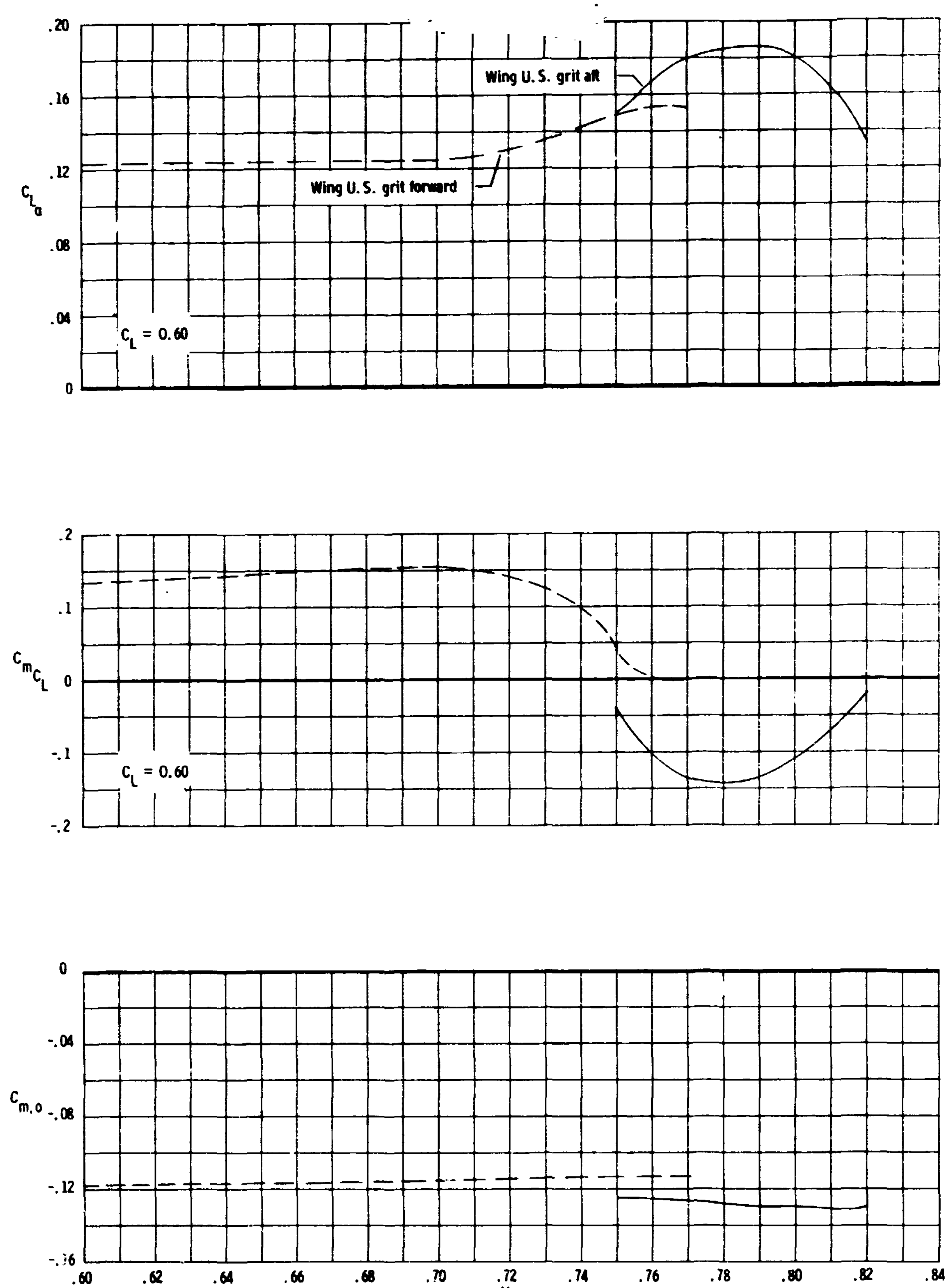

(a) Variation with Mach number of lift-curve slope, longitudinal-stability derivative (c.g. (F.S.) = 86.068 cm (33.885 in.)), and zero-lift pitching-moment coefficient.

Figure 22.- Variation with Mach number of longitudinal aerodynamic characteristics for configuration SCW-Ib. $\beta = 0°$.

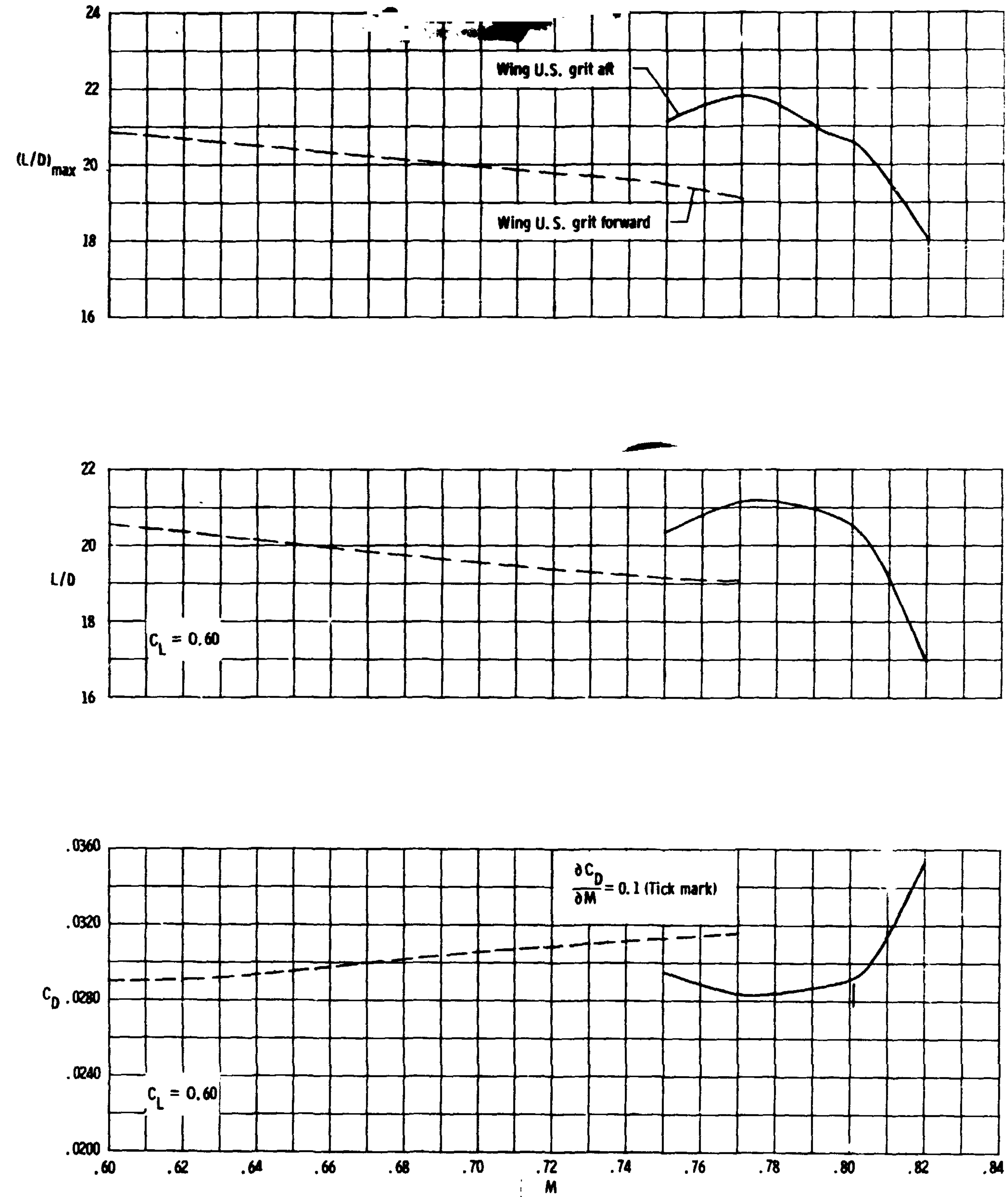

(b) Variation with Mach number of lift-to-drag ratios and drag coefficient.

Figure 22. - Continued.

[redacted]

[redacted]

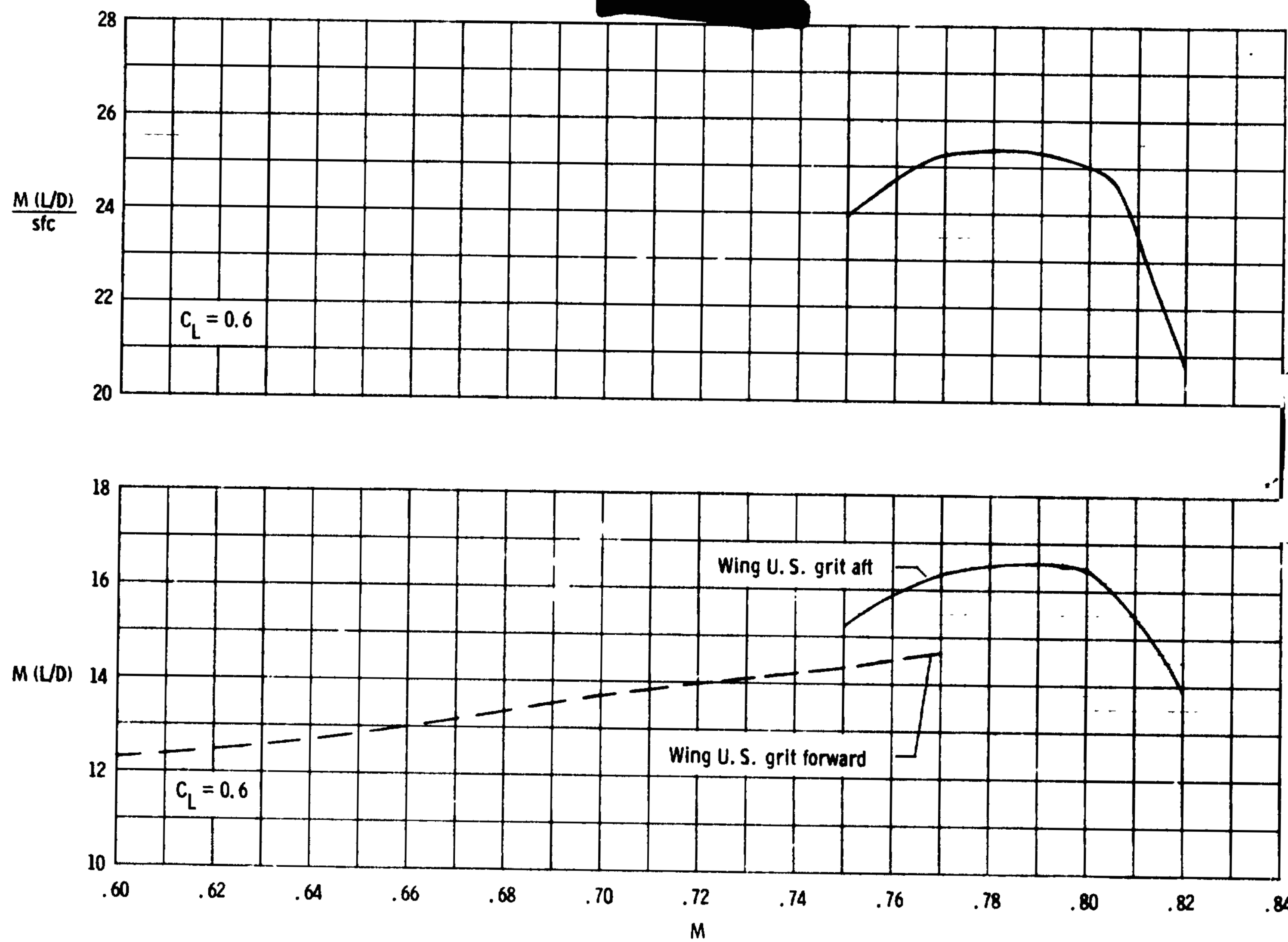

(c) Variation with Mach number of range parameters.

Figure 22. - Concluded.

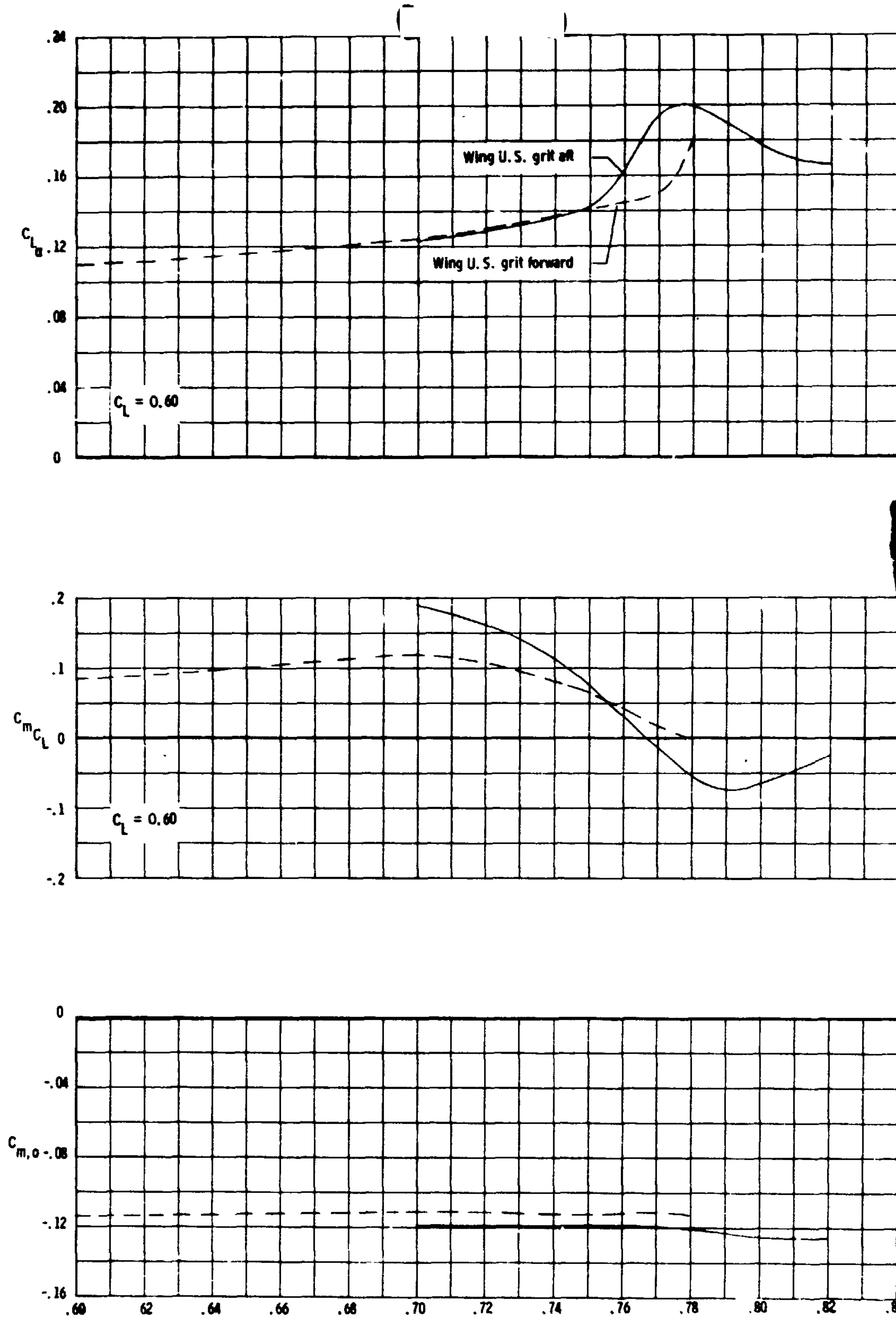

(a) Variation with Mach number of lift-curve slope, longitudinal-stability derivative (c.g. (F.S.) = 84.605 cm (33.309 in.)), and zero-lift pitching-moment coefficient.

Figure 23.- Variation with Mach number of longitudinal aerodynamic characteristics for configuration SCW-2a. $\beta = 0°$.

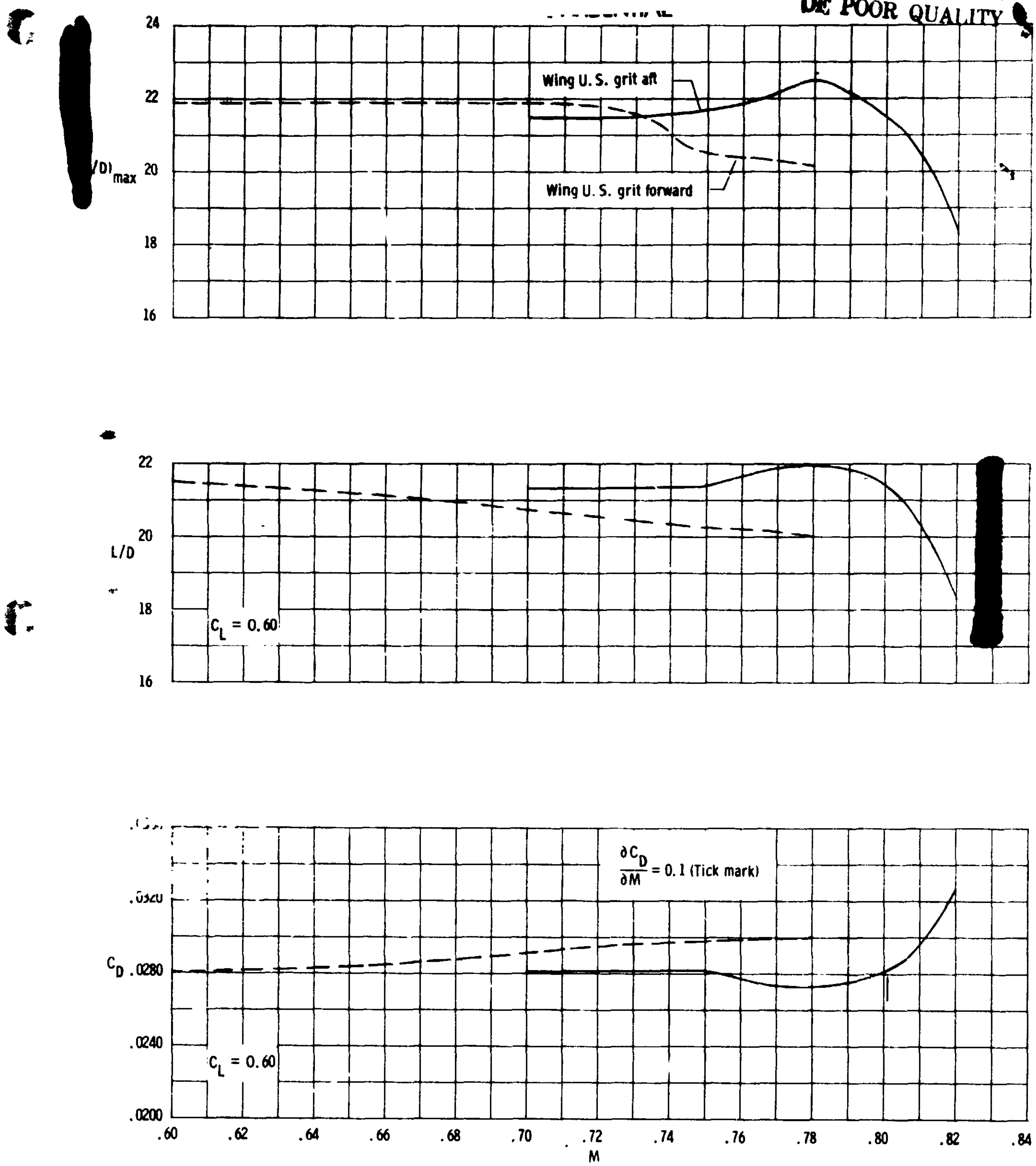

(b) Variation with Mach number of lift-to-drag ratios and drag coefficient.

Figure 23. - Continued.

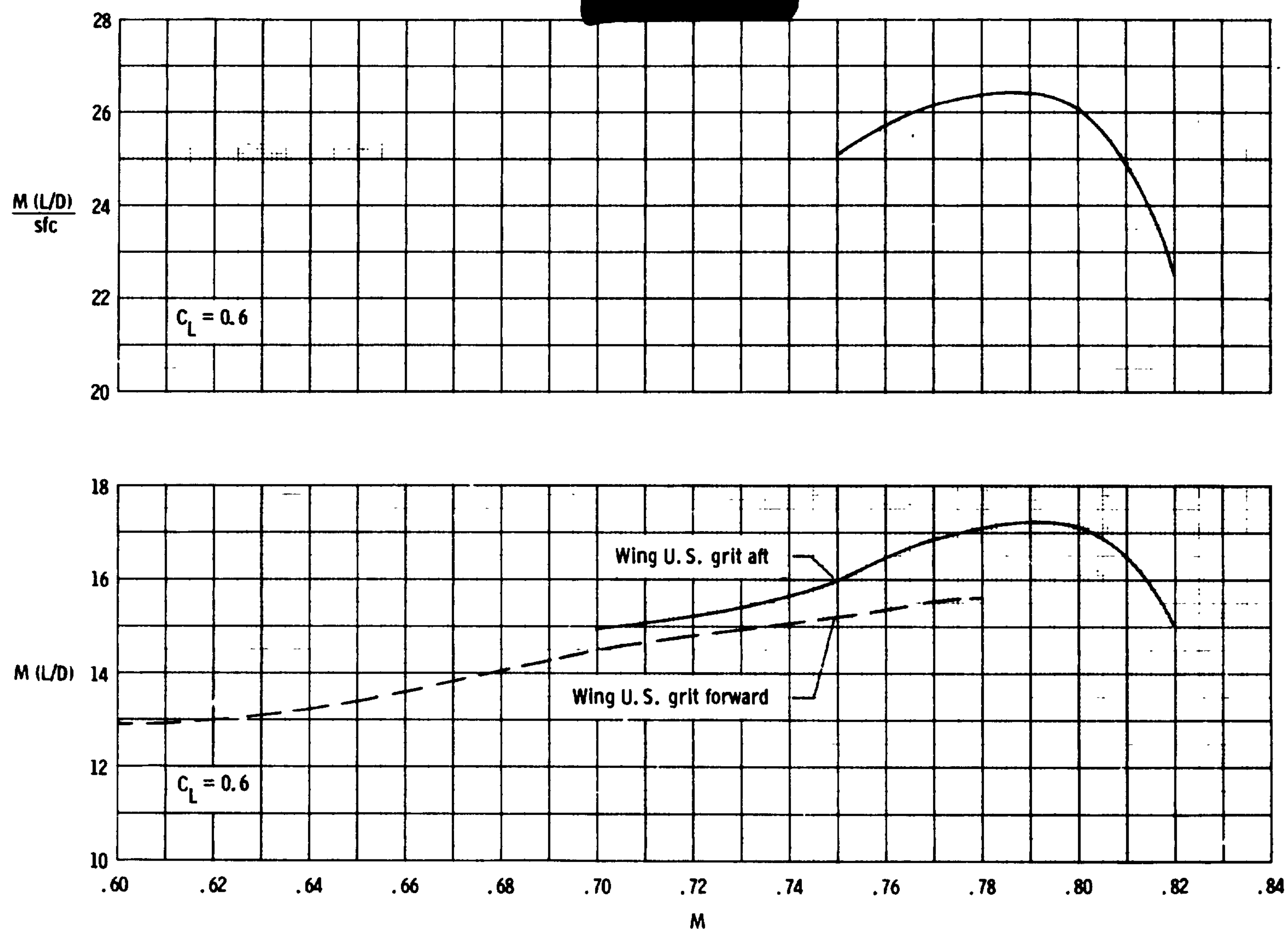

(c) Variation with Mach number of range parameters.

Figure 23. - Concluded.

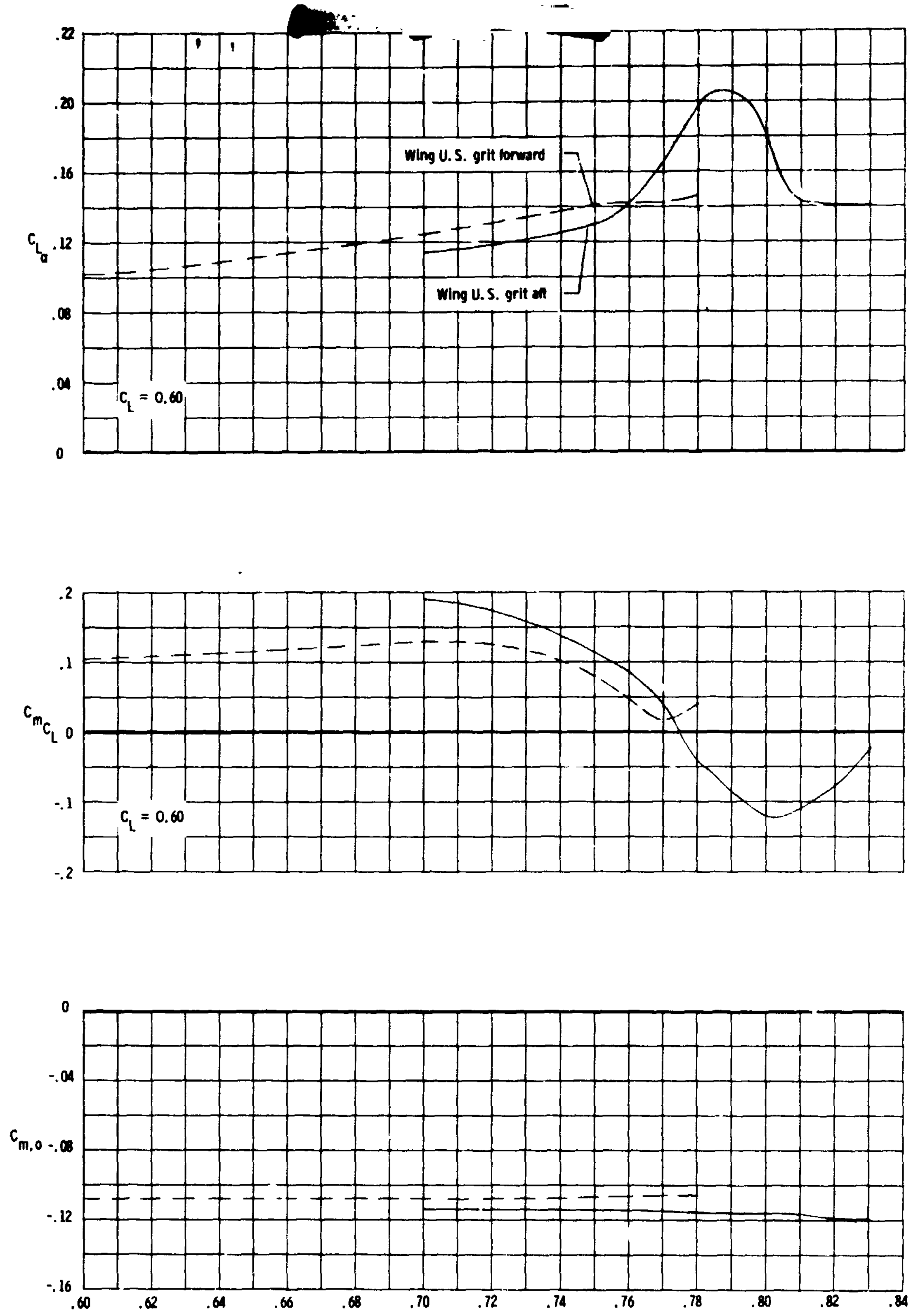

(a) Variation with Mach number of lift-curve slope, longitudinal-stability derivative (c.g. (F.S.) = 86.068 cm (33.885 in.)), and zero-lift pitching-moment coefficient.

Figure 24.- Variation with Mach number of longitudinal aerodynamic characteristics for configuration SCW-2b. $\beta = 0°$.

[redacted]

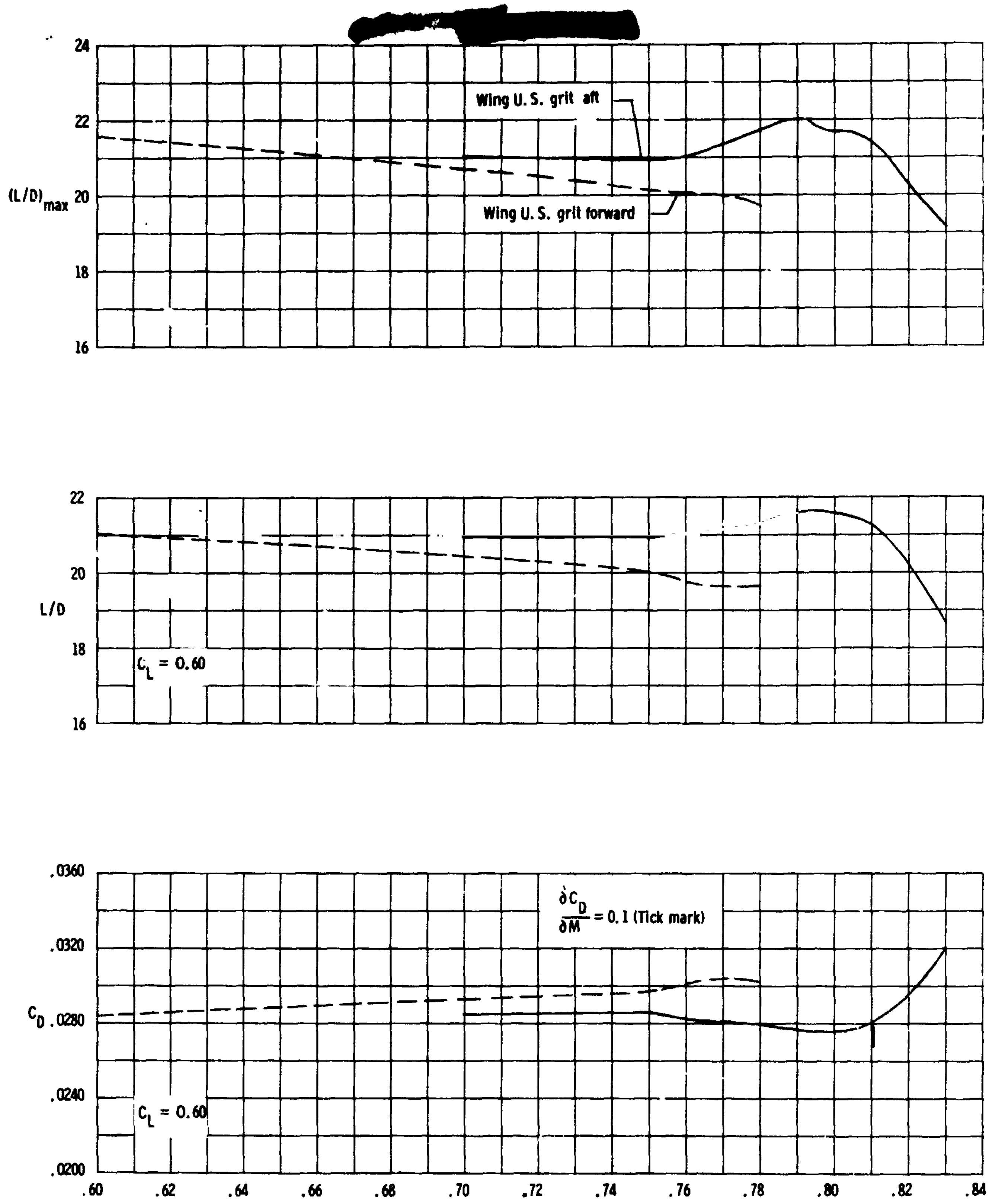

(b) Variation with Mach number of lift-to-drag ratios and drag coefficient.

Figure 24.- Continued.

[redacted]

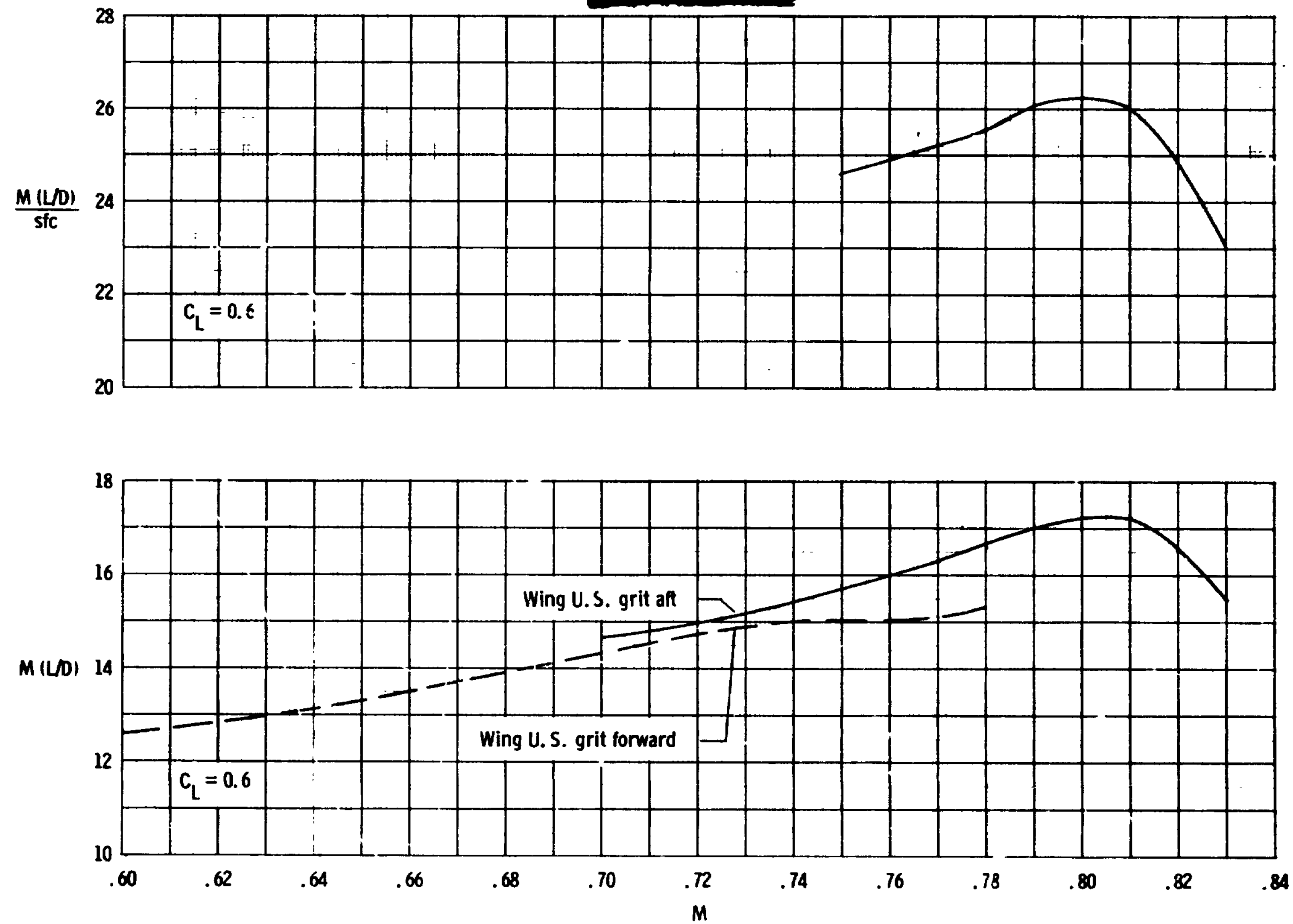

(c) Variation with Mach number of range parameters.

Figure 24. - Concluded.

[redacted]

ORIGINAL PAGE IS
OF POOR QUALITY

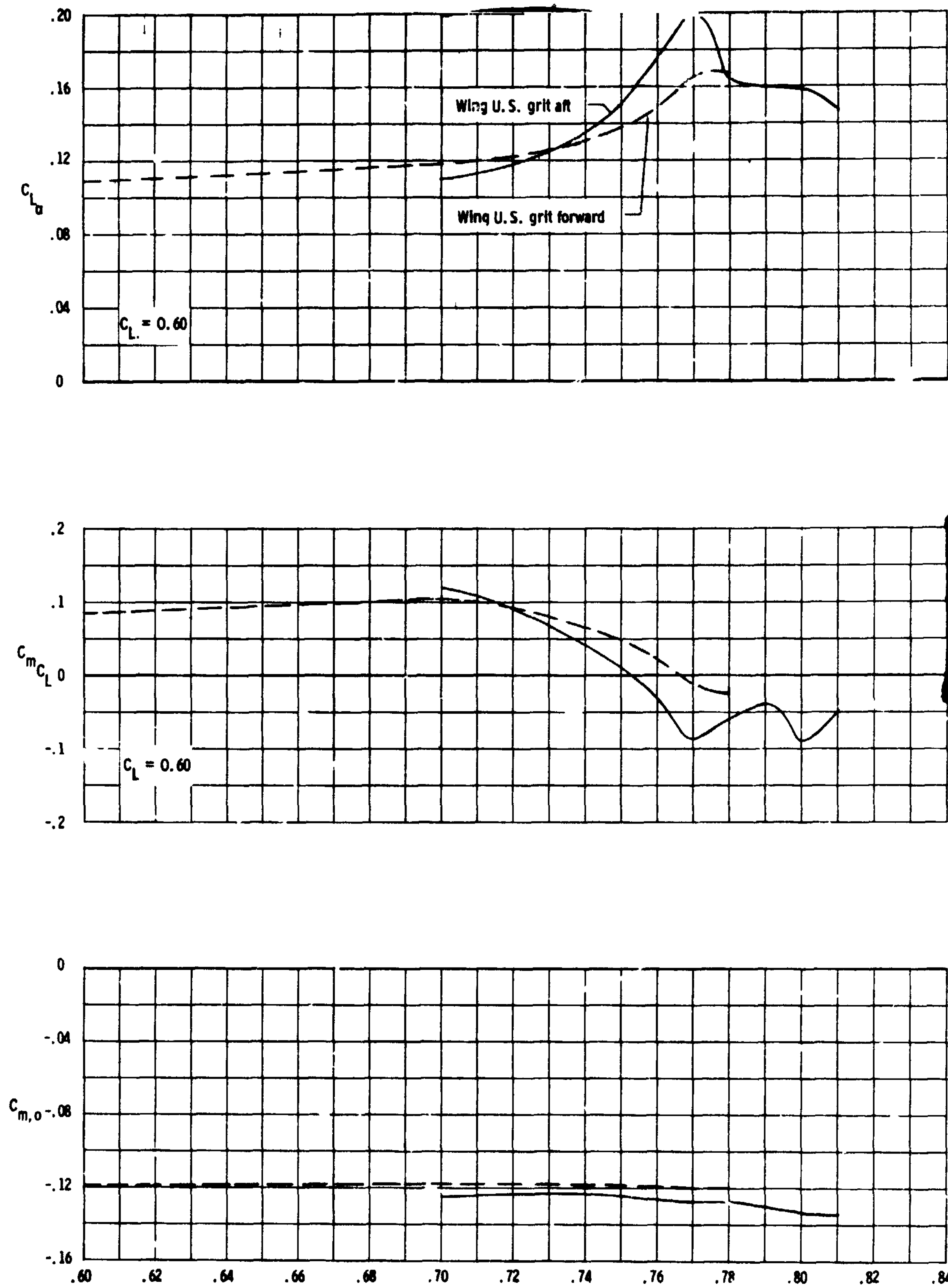

(a) Variation with Mach number of lift-curve slope, longitudinal-stability derivative (c.g. (F.S.) = 83.409 cm (32.838 in.)), and zero-lift pitching-moment coefficient.

Figure 25.- Variation with Mach number of longitudinal aerodynamic characteristics for configuration SCW-2c. β = 0°.

ORIGINAL PAGE IS
OF POOR QUALITY

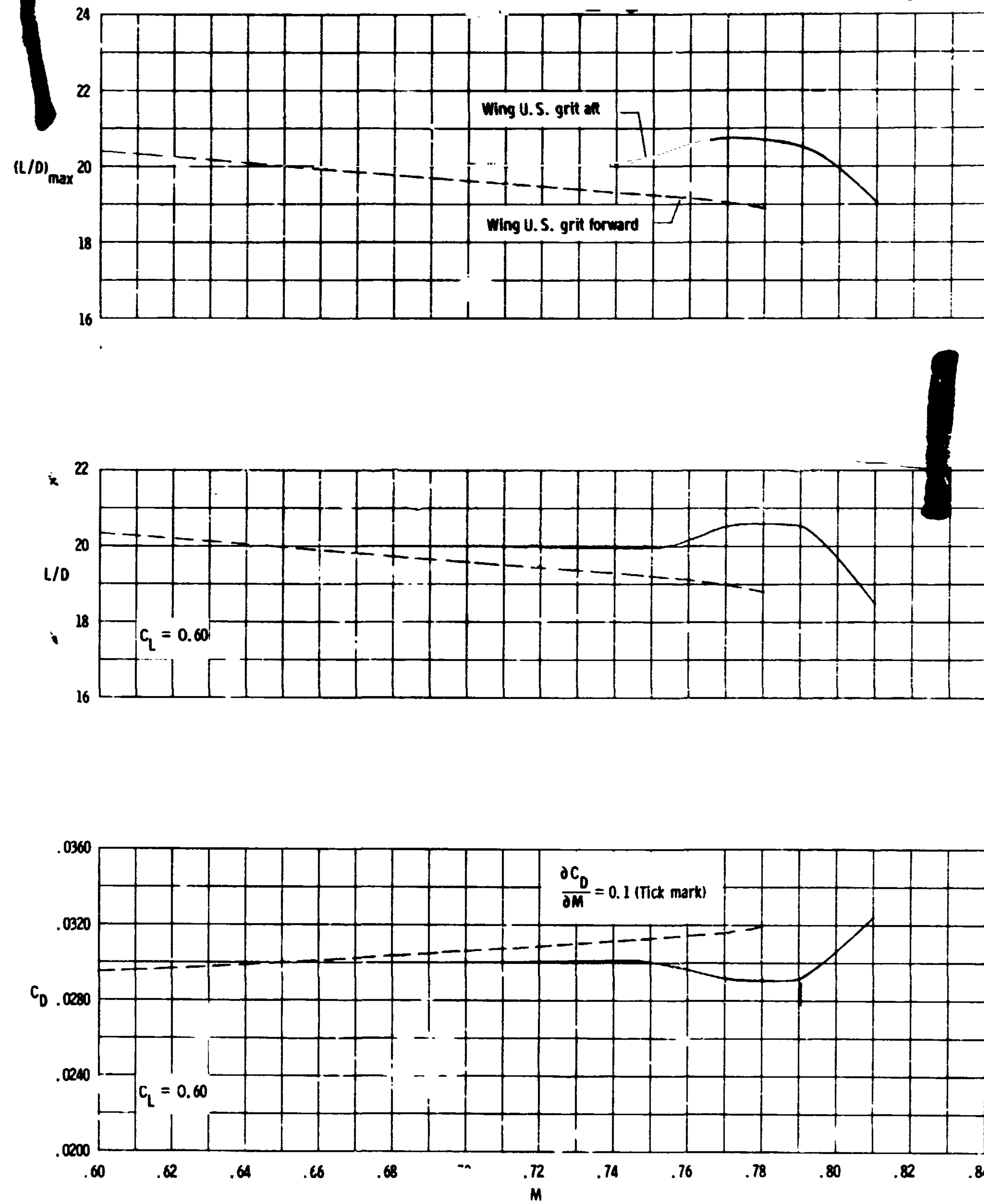

(b) Variation with Mach nu ber of lift-to-drag ratios and drag coefficient.

igure 25. - Continued.

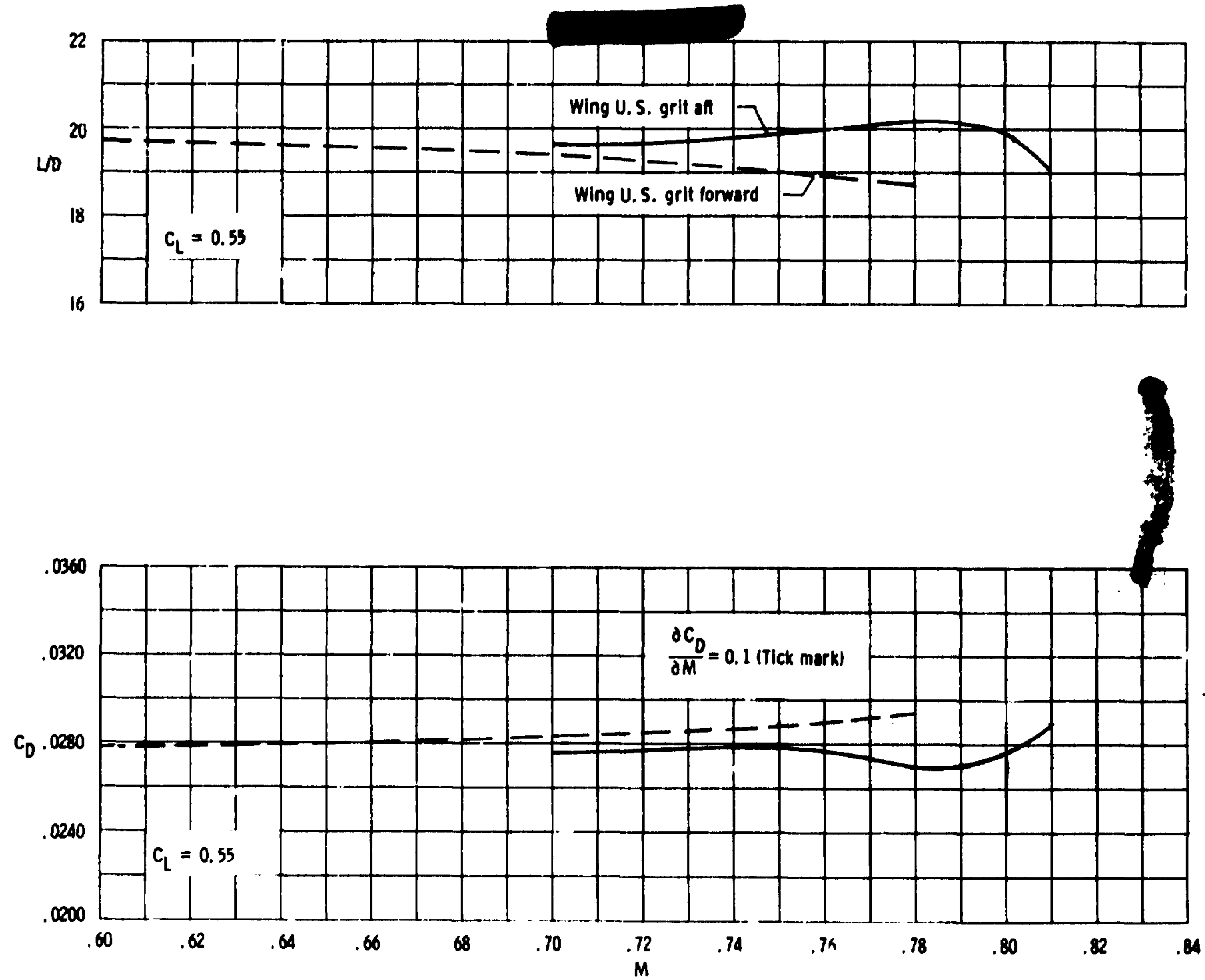

(b) Variation with Mach number of lift-to-drag ratios and drag coefficient. Concluded.

Figure 25.- Continued.

[redacted]

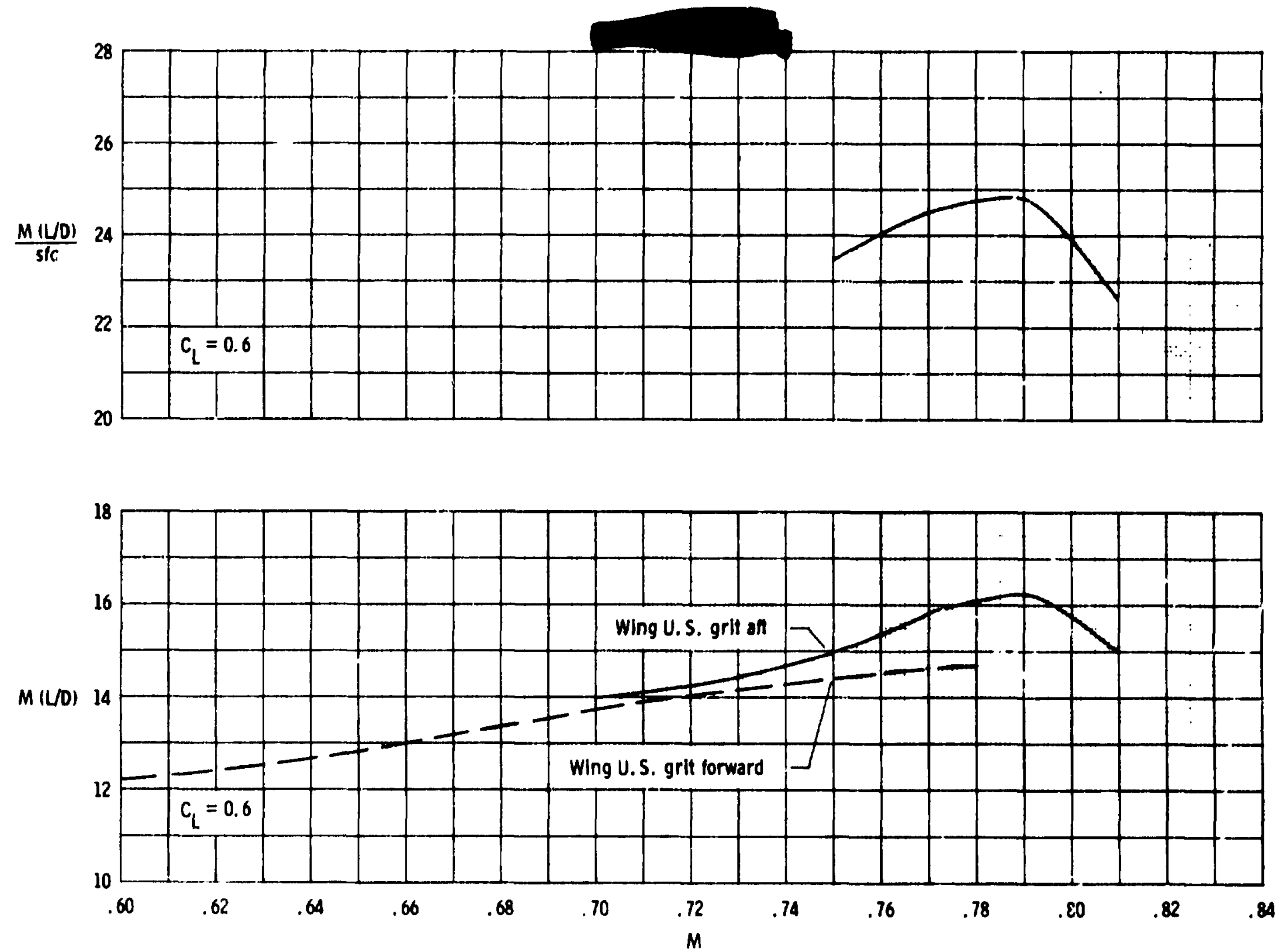

(c) Variation with Mach number of range parameters.

Figure 25. - Concluded

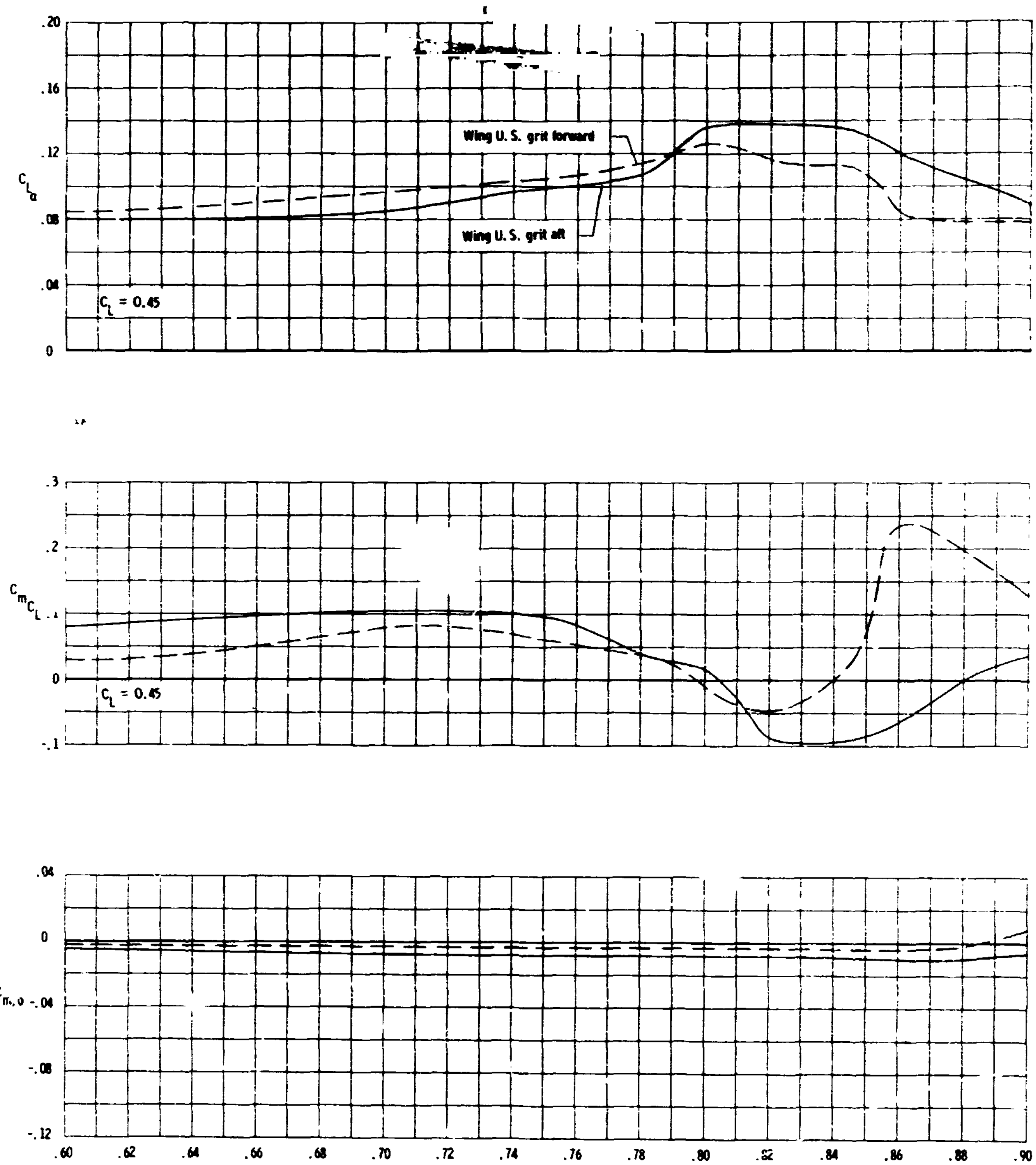

[redacted] (a) Variation with Mach number of lift-curve slope, longitudinal-stability derivative (c.g. (F.S.) = 84.605 cm (33.309 in.)), and and zero-lift pitching-moment coefficient.

Figure 26. - Variation with Mach number of longitudinal aerodynamic characteristics for simulated wide-body configuration. $\beta = 0°$.

[redacted]

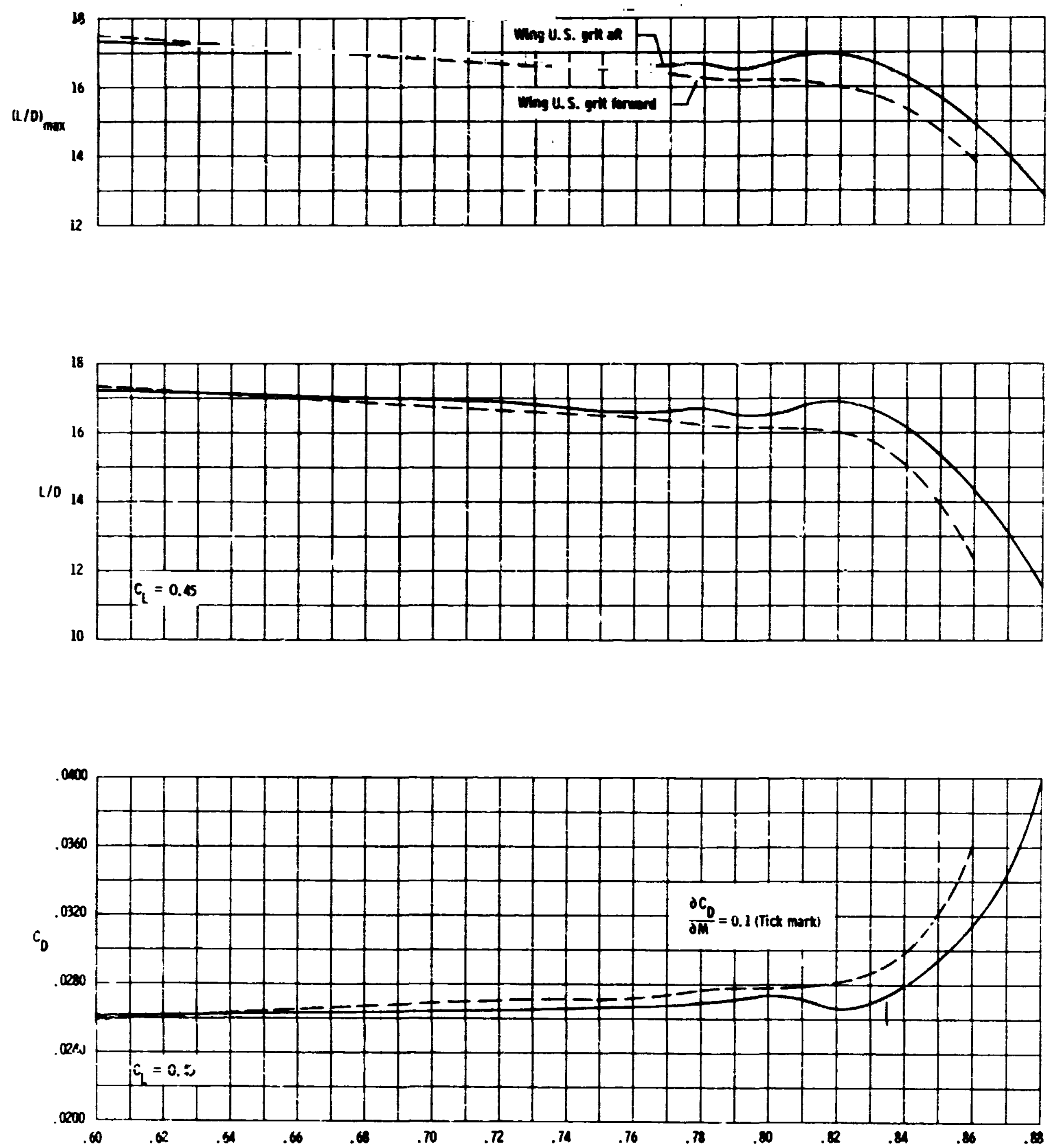

(b) Variation with Mach number of lift-to-drag ratios and drag coefficient.

Figure 26. - Continued.

[redacted]

[redacted]

[redacted]

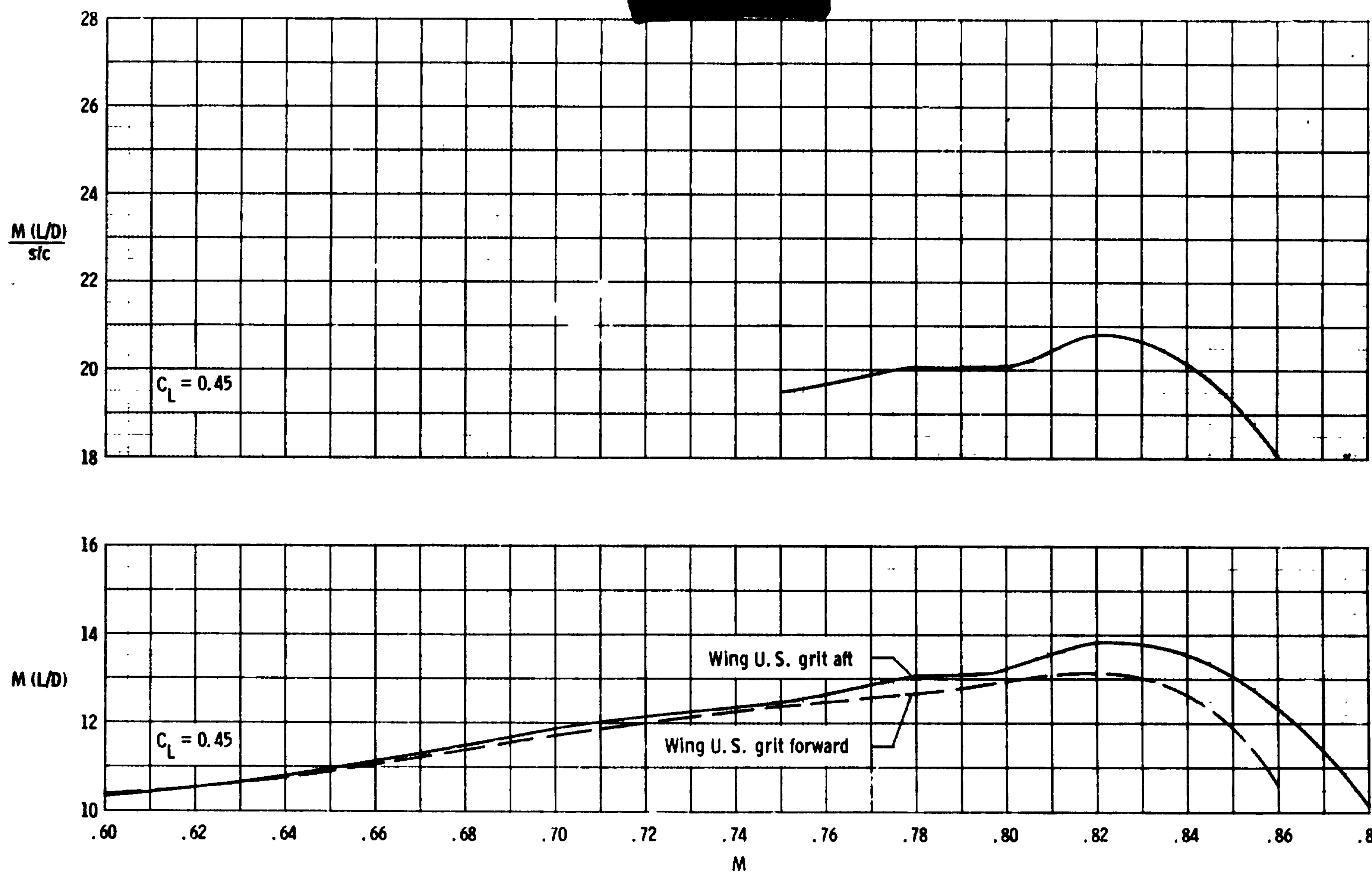

(c) Variation with Mach number of range parameters.

Figure 26. - Concluded.

[redacted]

[redacted]

[redacted]

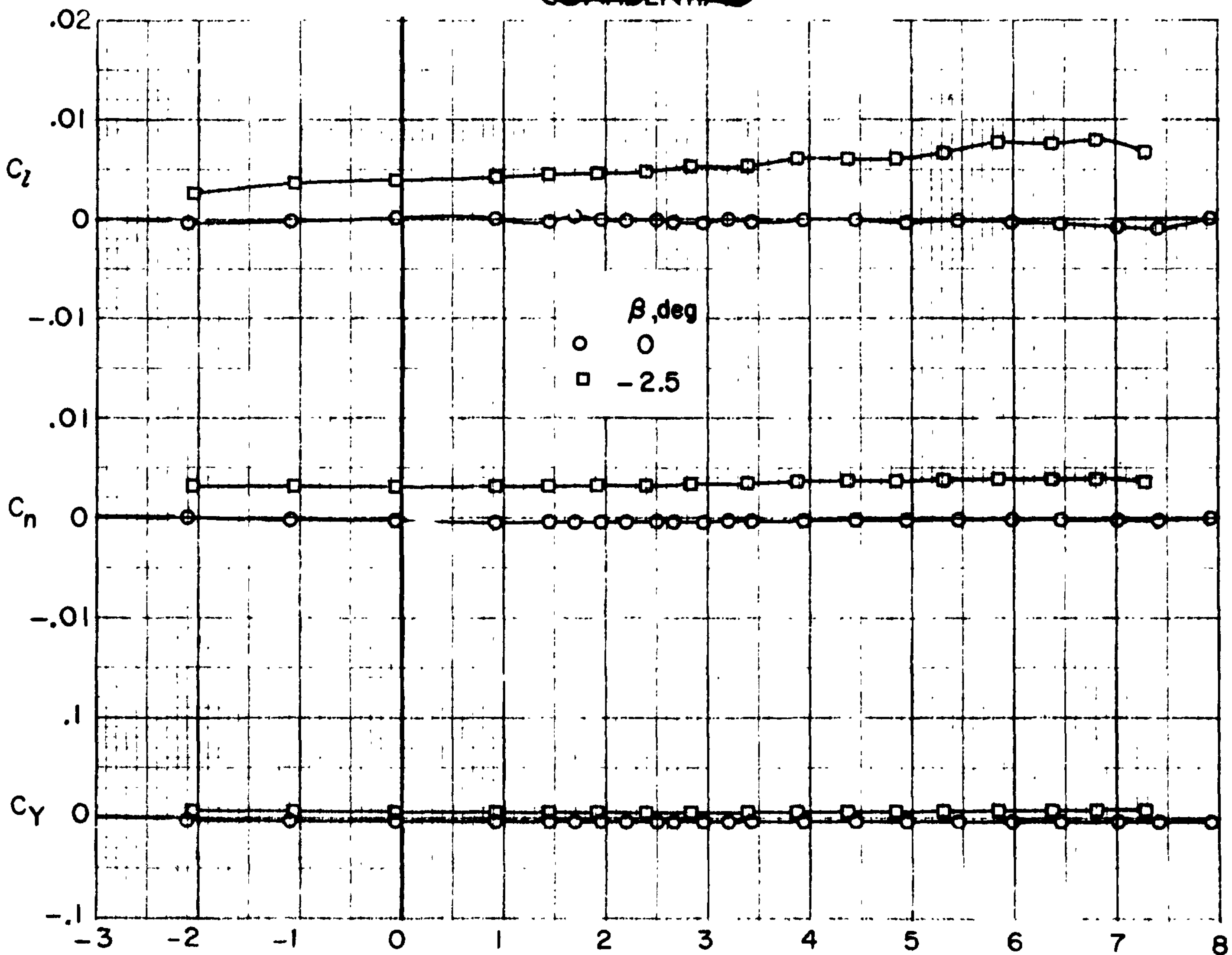

[redacted]

(a) M = 0.60. Wing upper surface grit forward (x_T/c = 0.05).

Figure 27. - Effect of sideslip on lateral-directional aerodynamic characteristics for supercritical wing configuration Ib (SCW-Ib).

[redacted]

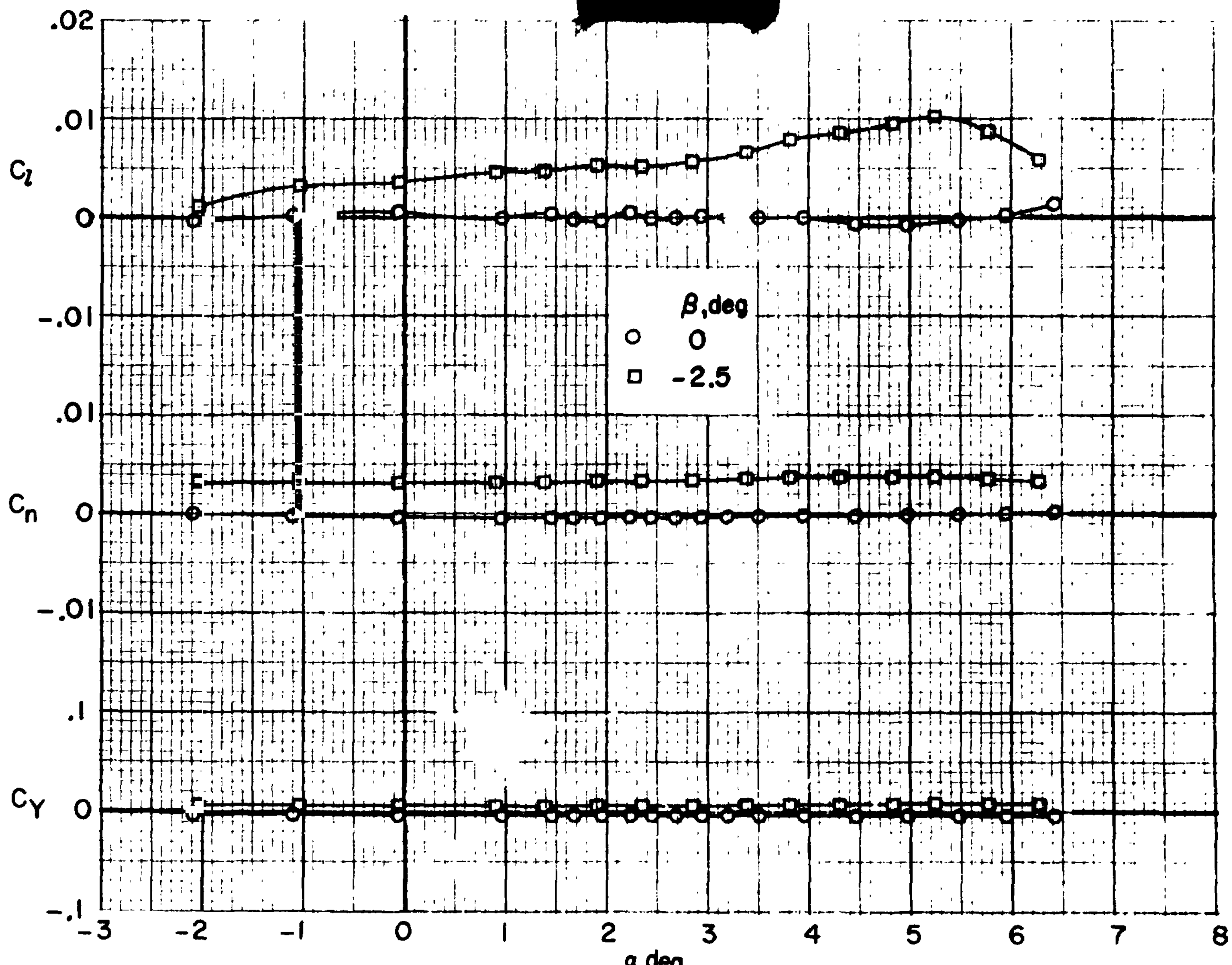

(b) M = 0.70. Wing upper surface grit forward (x_T/c = 0.05).

Figure 27.- Continued.

[redacted]

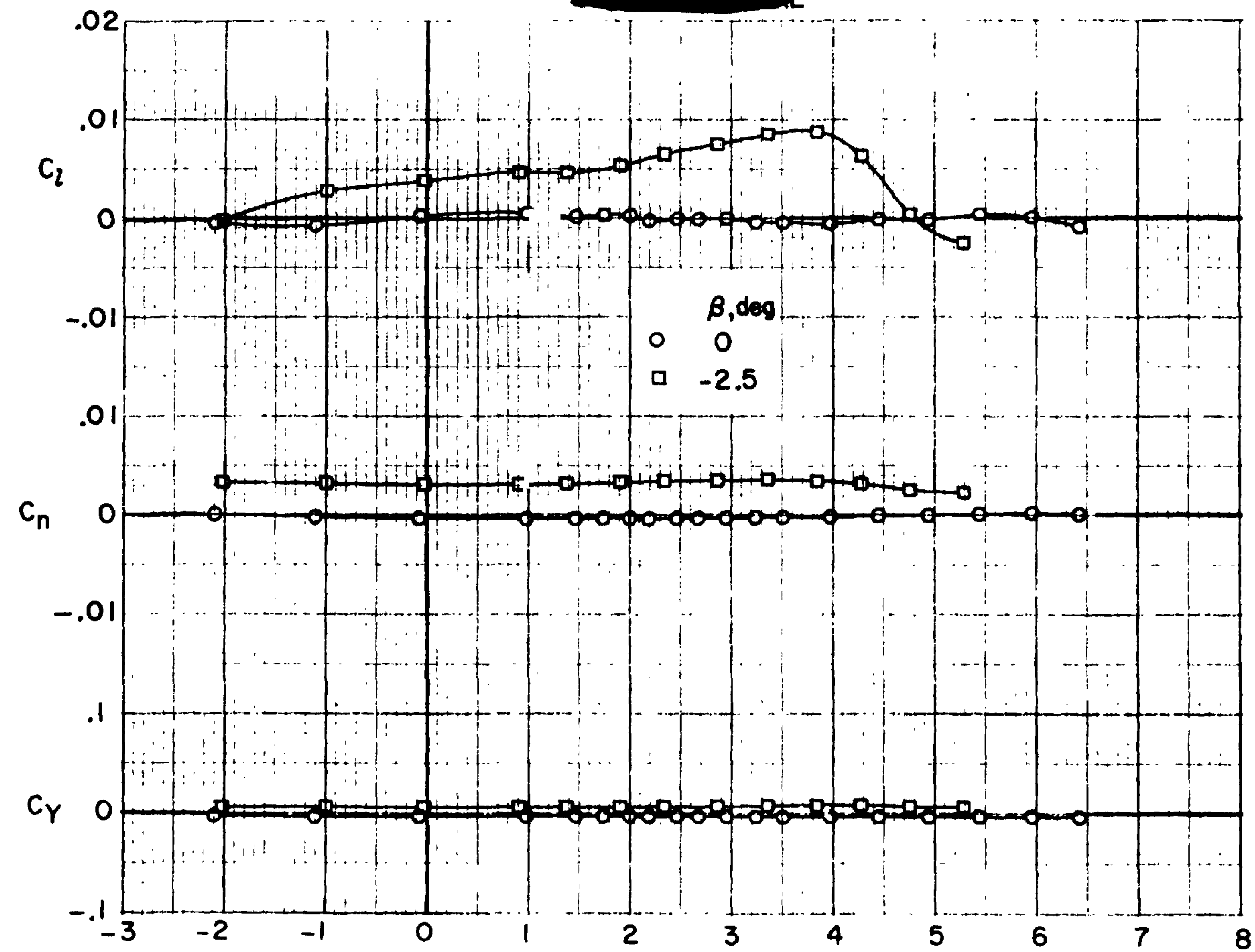

[redacted]

(c) M = 0.75. Wing upper surface grit forward (x_T/c = 0.05).

Figure 27.- Continued.

[redacted]

[redacted]

[redacted]

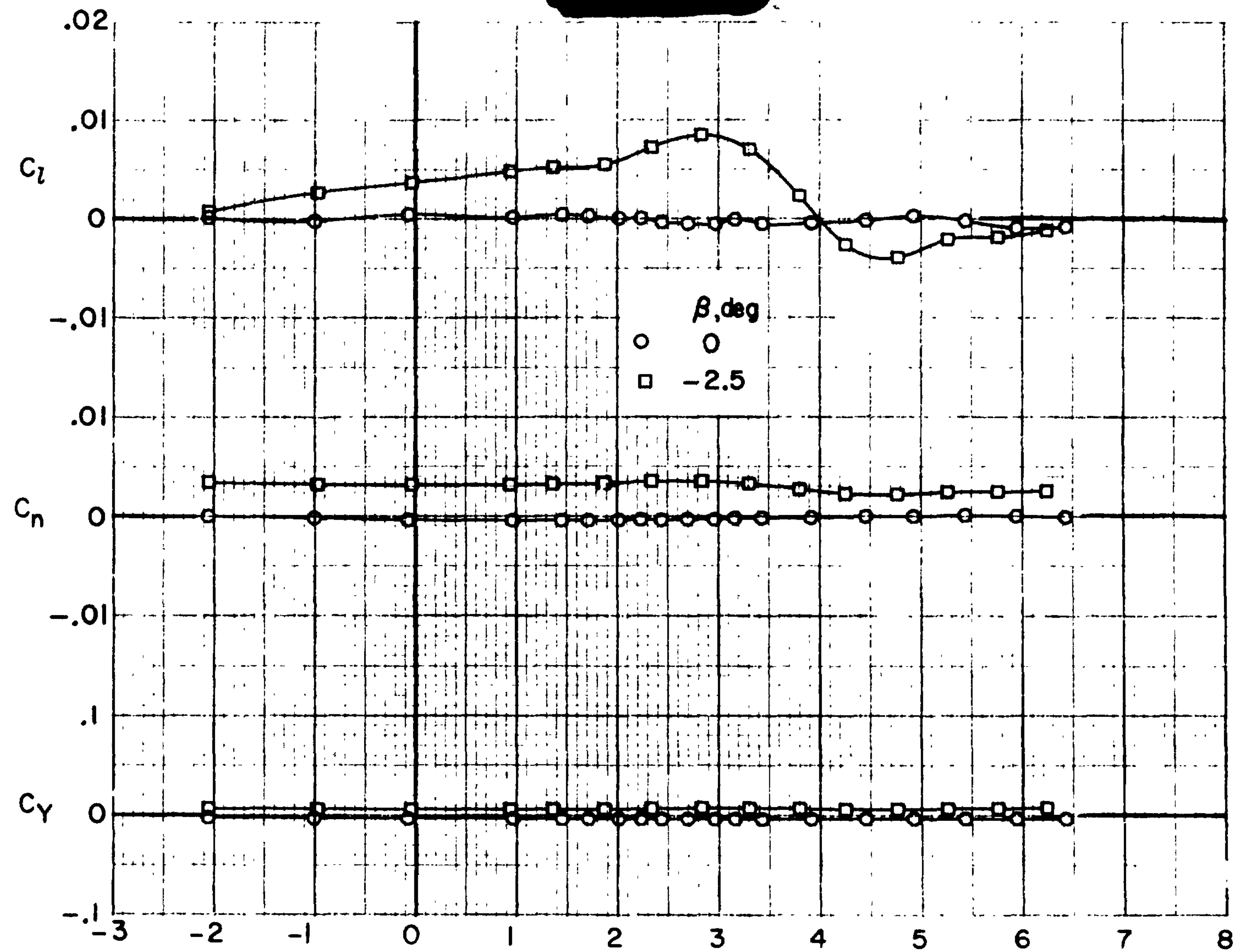

[redacted]

(d) M = 0.77. Wing upper surface grit forward (x_T/c = 0.05).

F' ure 27. - Continued.

CONFIDENTIA.

ORIGINAL PAGE IS
OF POOR QUALITY

[redacted]

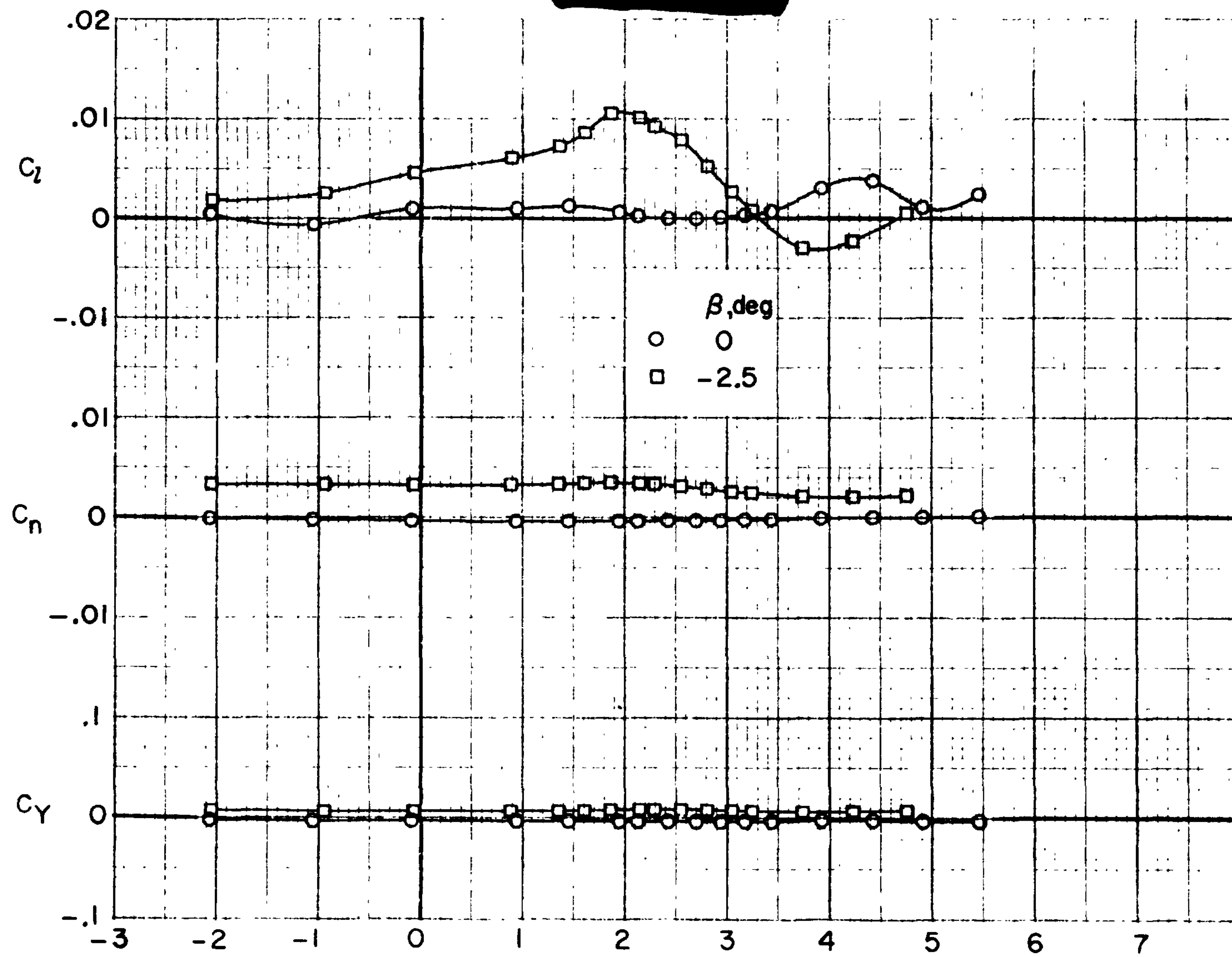

[redacted]

(e) M = 0.79. Wing upper surface grit aft (fig. 5).

Figure 27.- Continued.

[redacted]

[redacted]

[redacted]

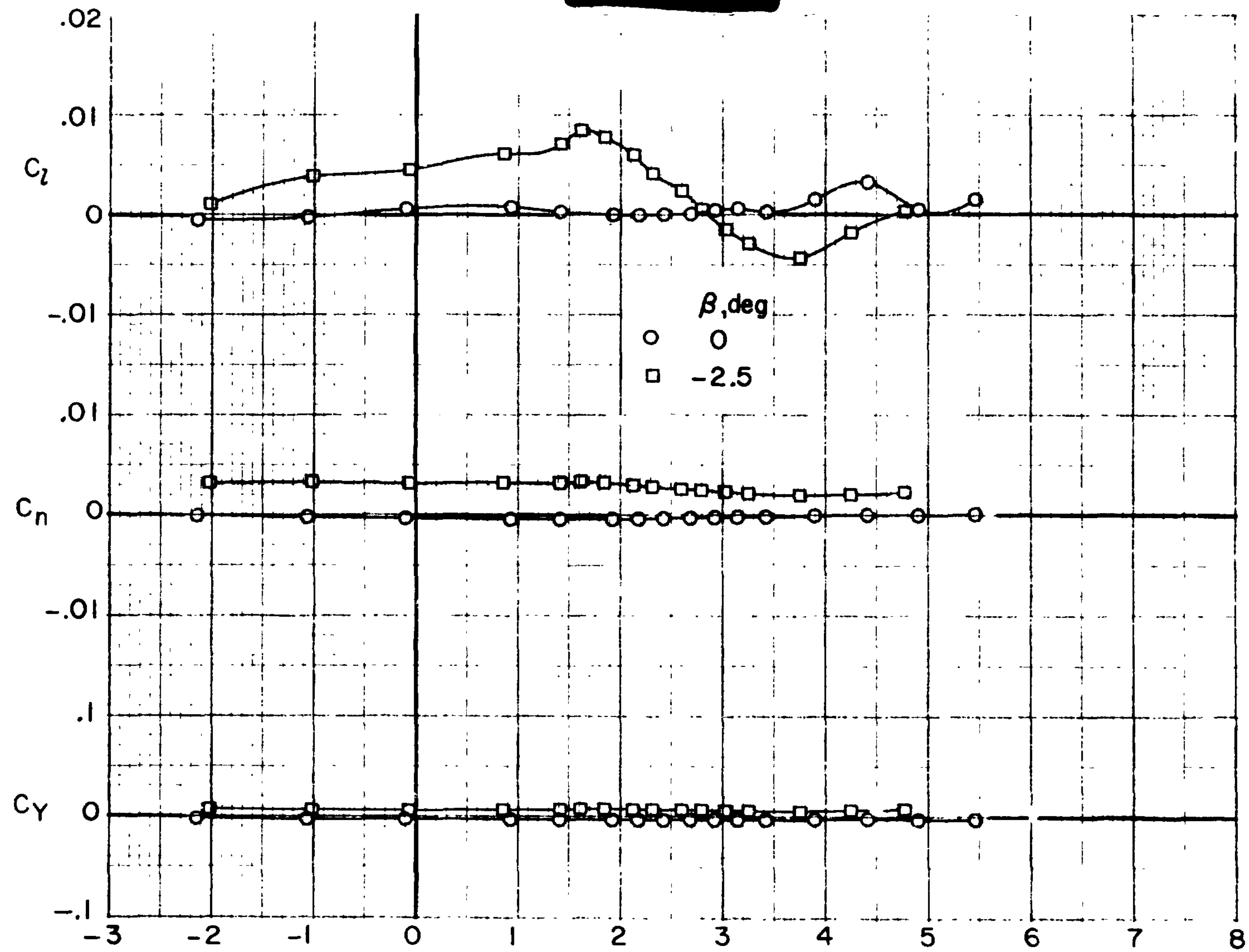

[redacted]

(f) M = 0.80. Wing upper surface grit aft (fig. 5).

Figure 27.- Continued.

[redacted]

[redacted]

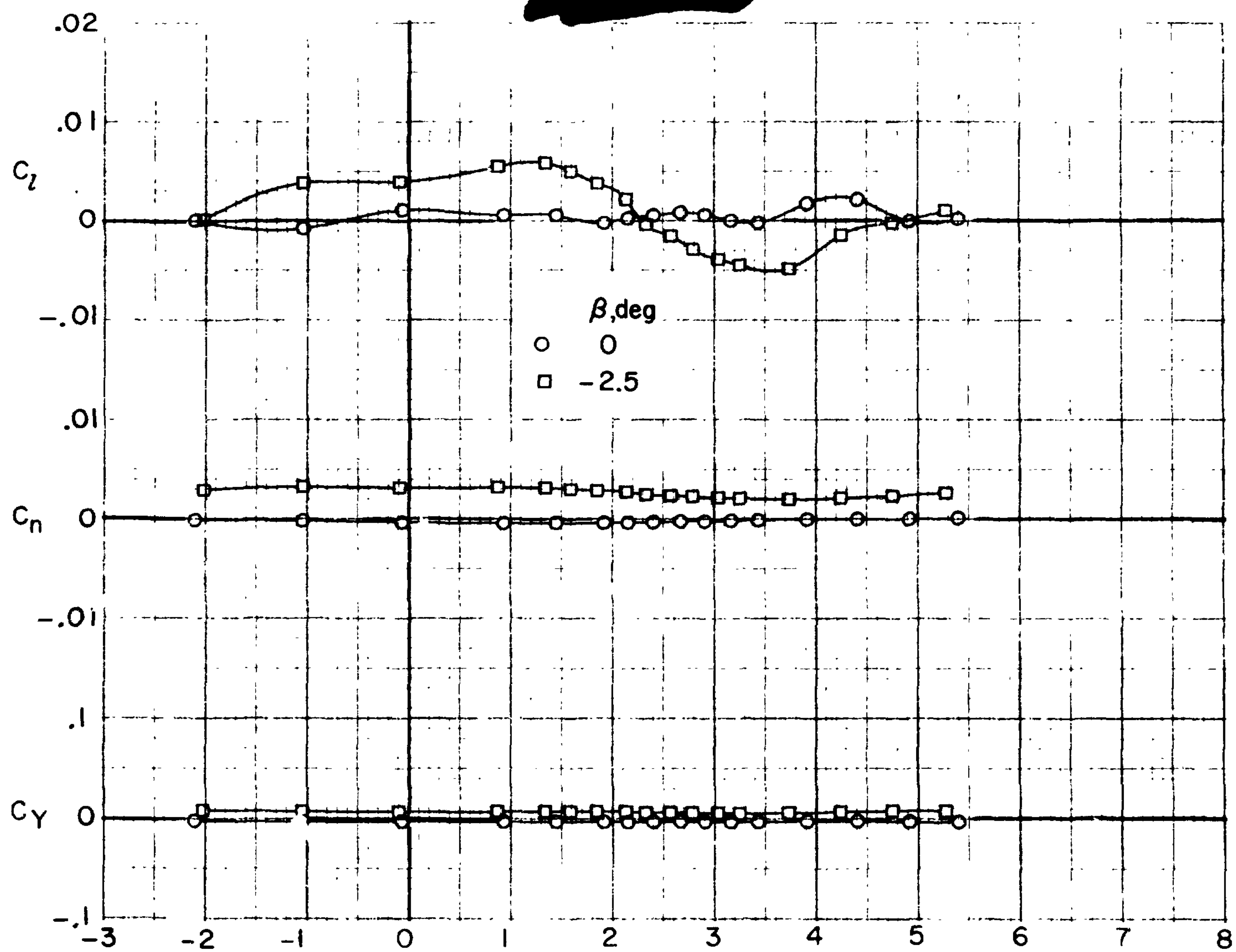

[redacted]

(g) M = 0.81. Wing upper surface grit aft (fig. 5).

Figure 27.- Continued.

[redacted]

[redacted]

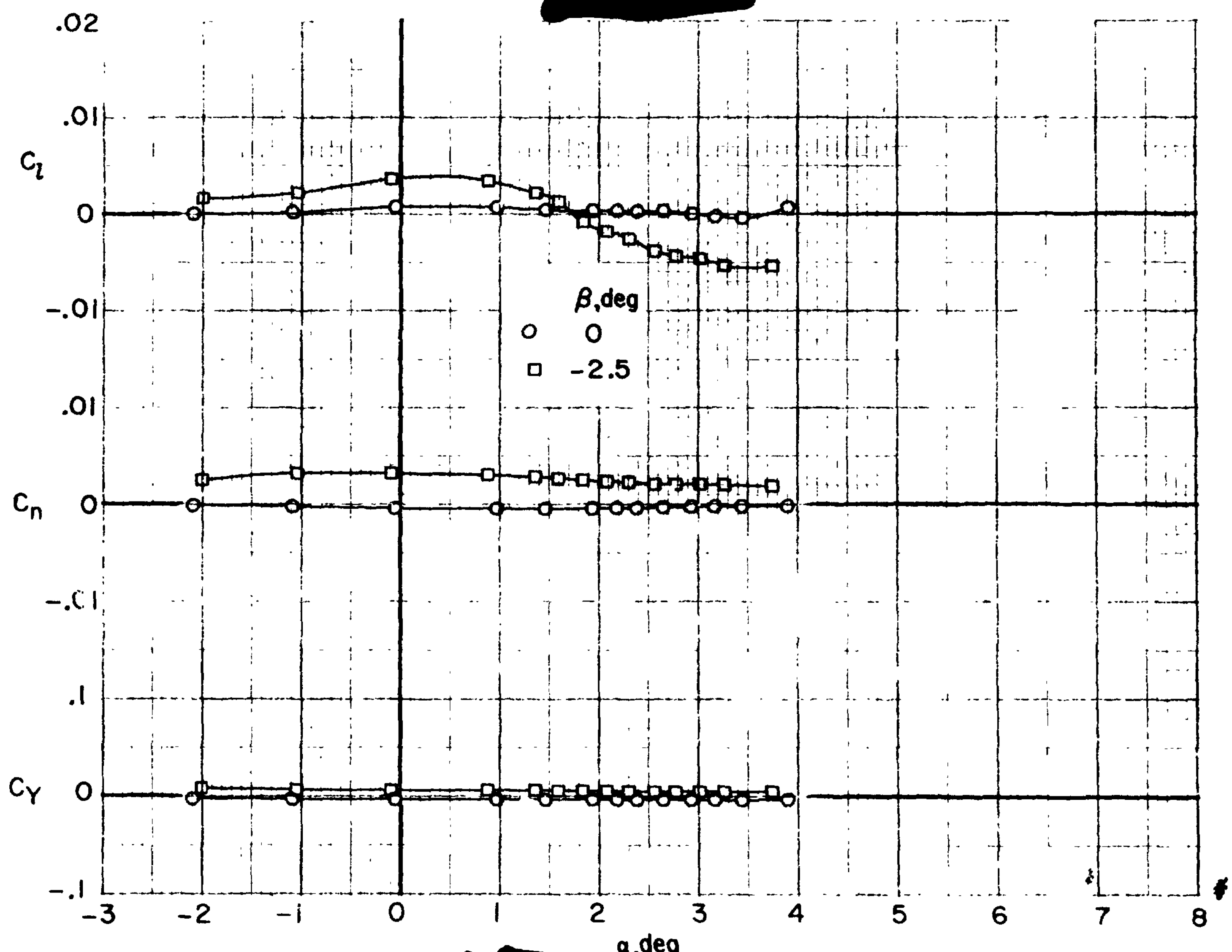

(h) [redacted] surface grit aft (fig. 5).

Figure 27. - Concluded.

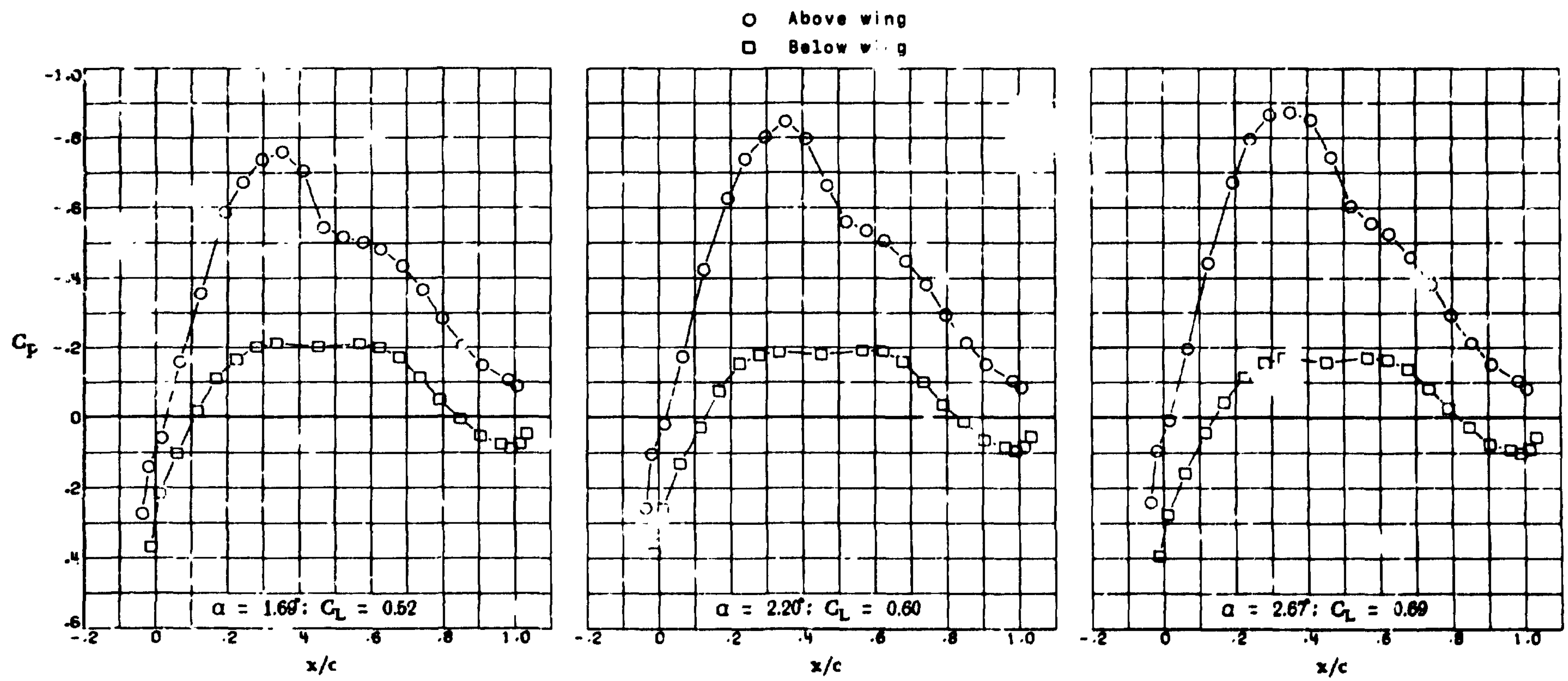

Figure 28. - Fuselage pressure distributions at the wing-fuselage juncture for configuration SCW-1a. (x/c)'s are based on the chord length at the wing-fuselage juncture.

[redacted]

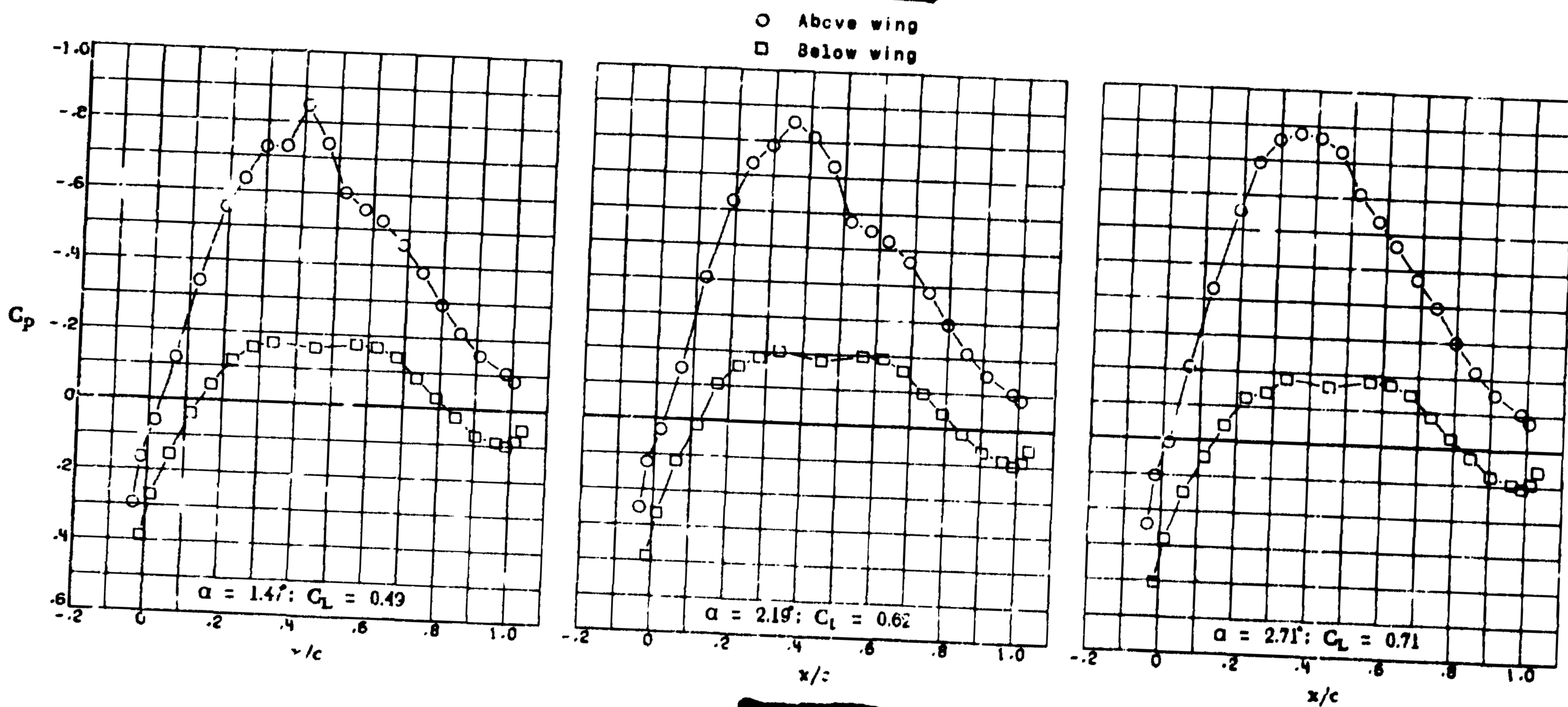

[redacted]

Figure 28. - Continued.

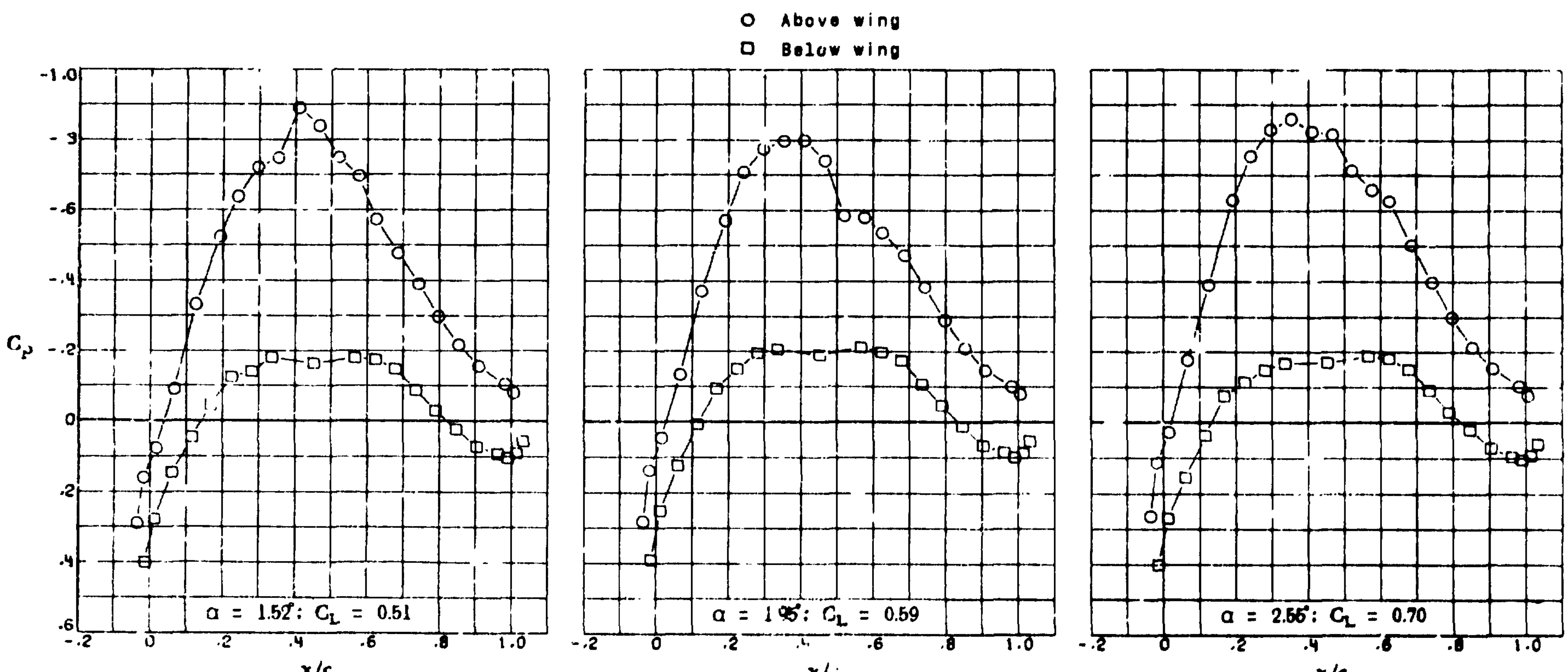

[redacted]

Figure 28. - Continued.

[redacted]

[redacted]

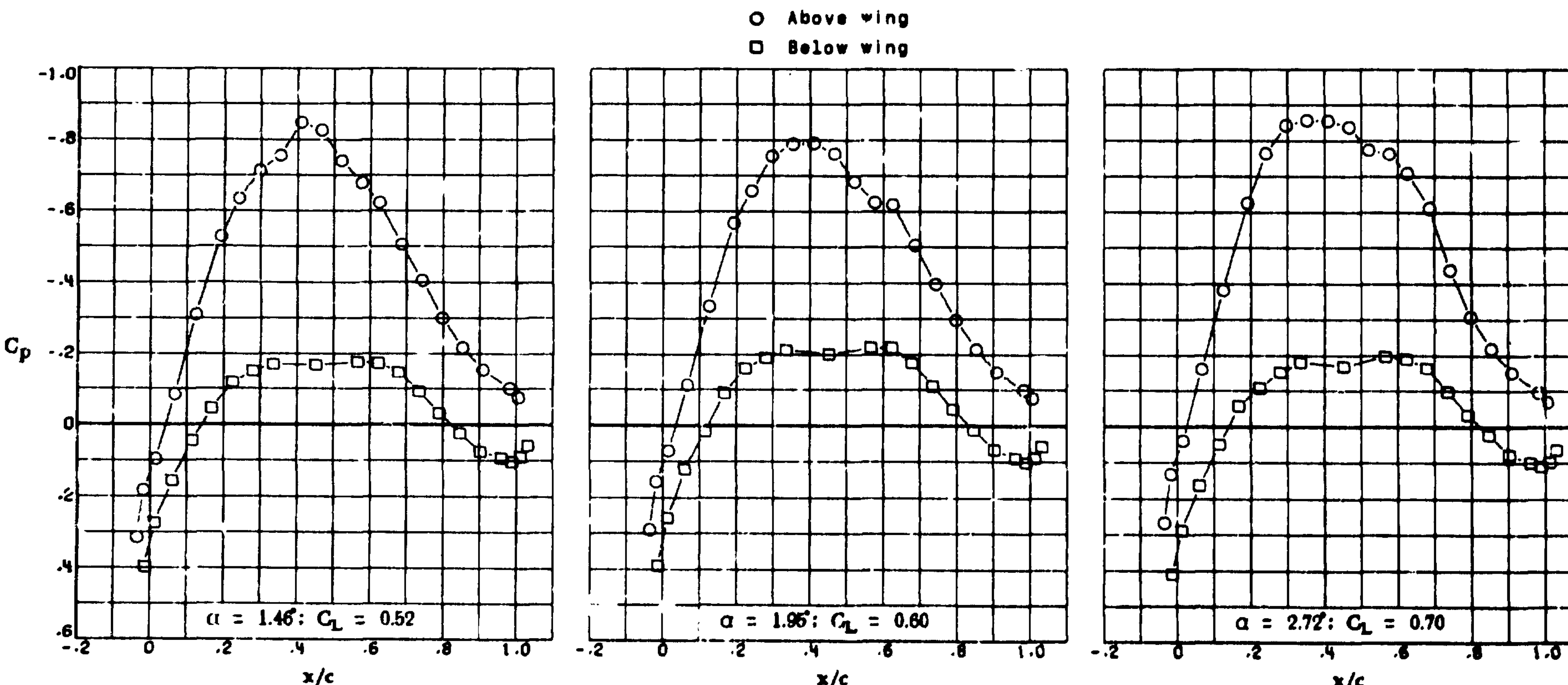

[redacted]

Figure 28. - Continued.

[redacted]

ORIGINAL PAGE IS
OF POOR QUALITY

[redacted]

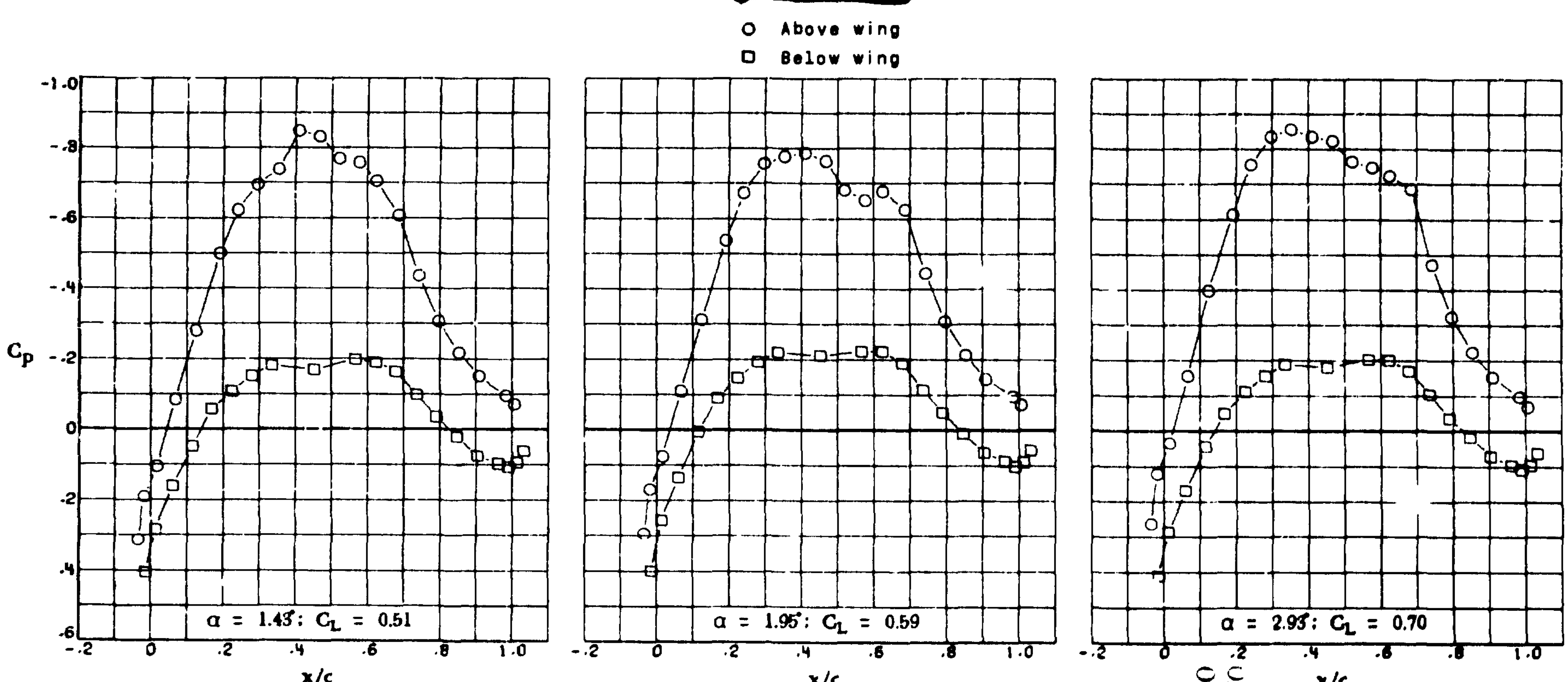

(e) M = 0.80.

Figure 28. - Concluded.

[redacted]

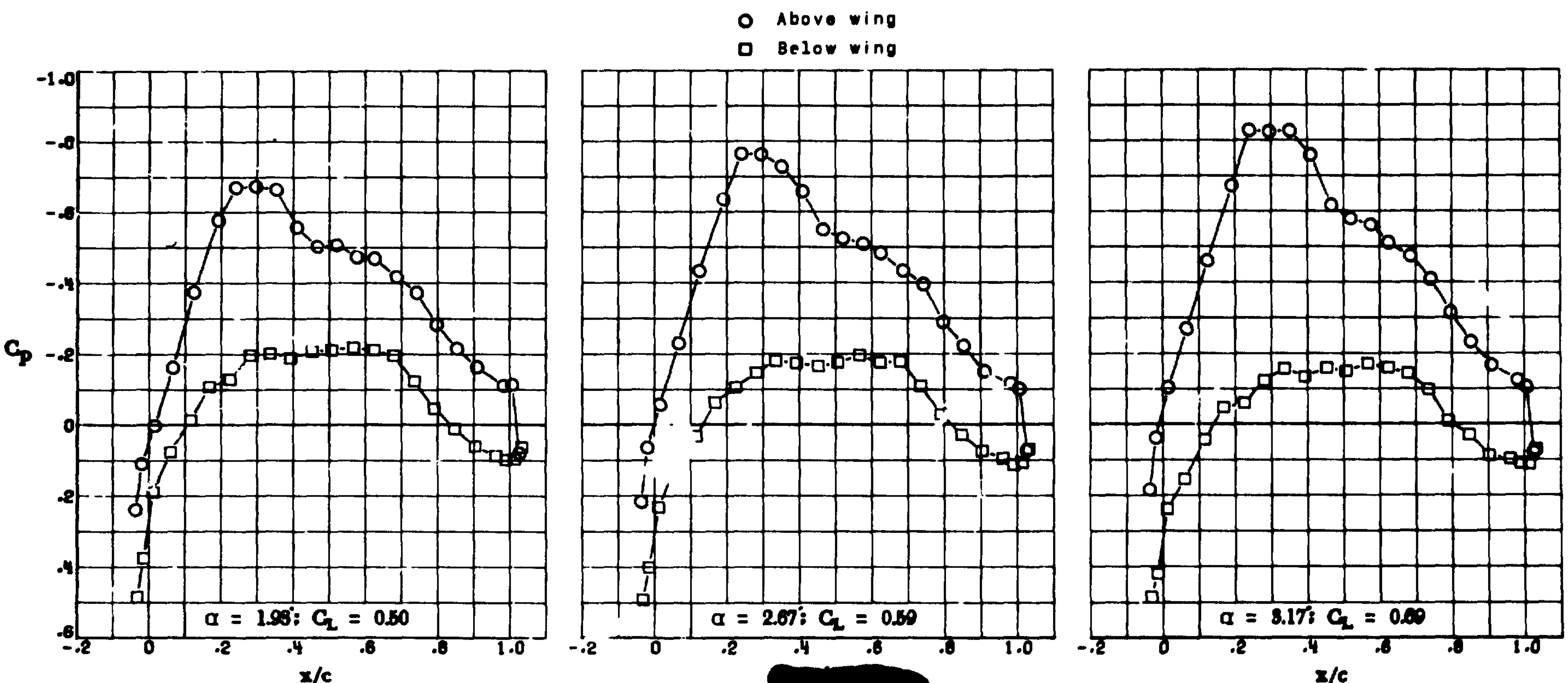

(a) M = 0.75.

Figure 29. - Fuselage pressure distributions at the wing-fuselage juncture for configuration SCW-Ib.

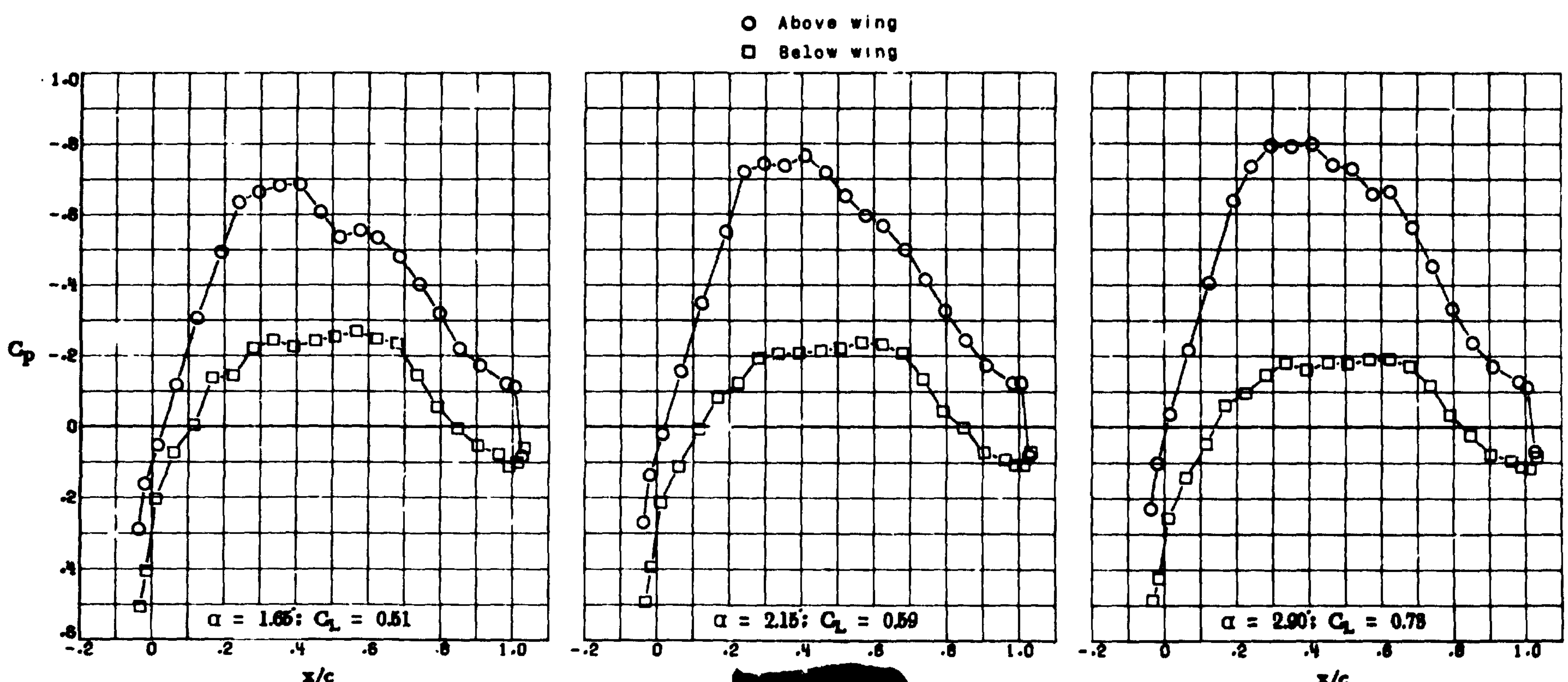

(b) M = 0.79.

Figure 29. - Continued.

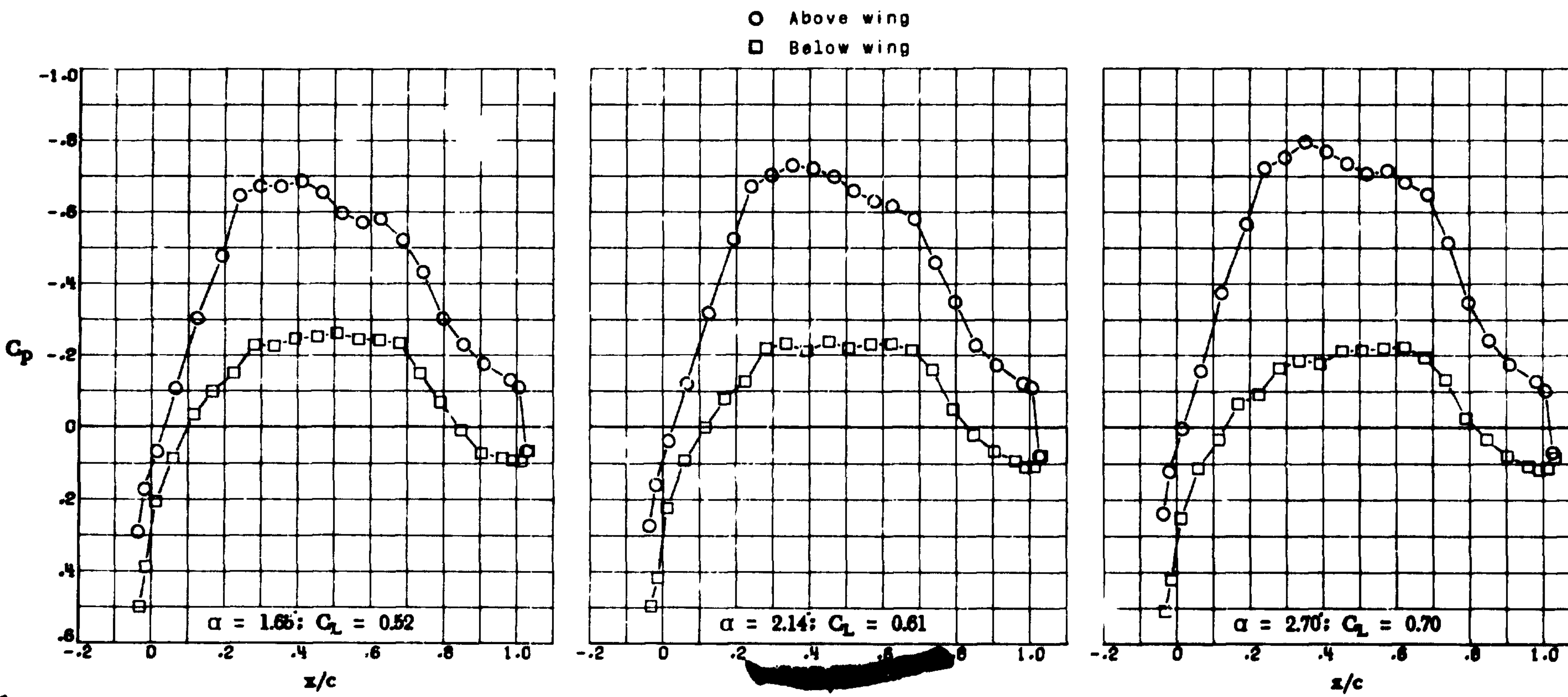

(c) M = 0.80.

Figure 29. - Continued

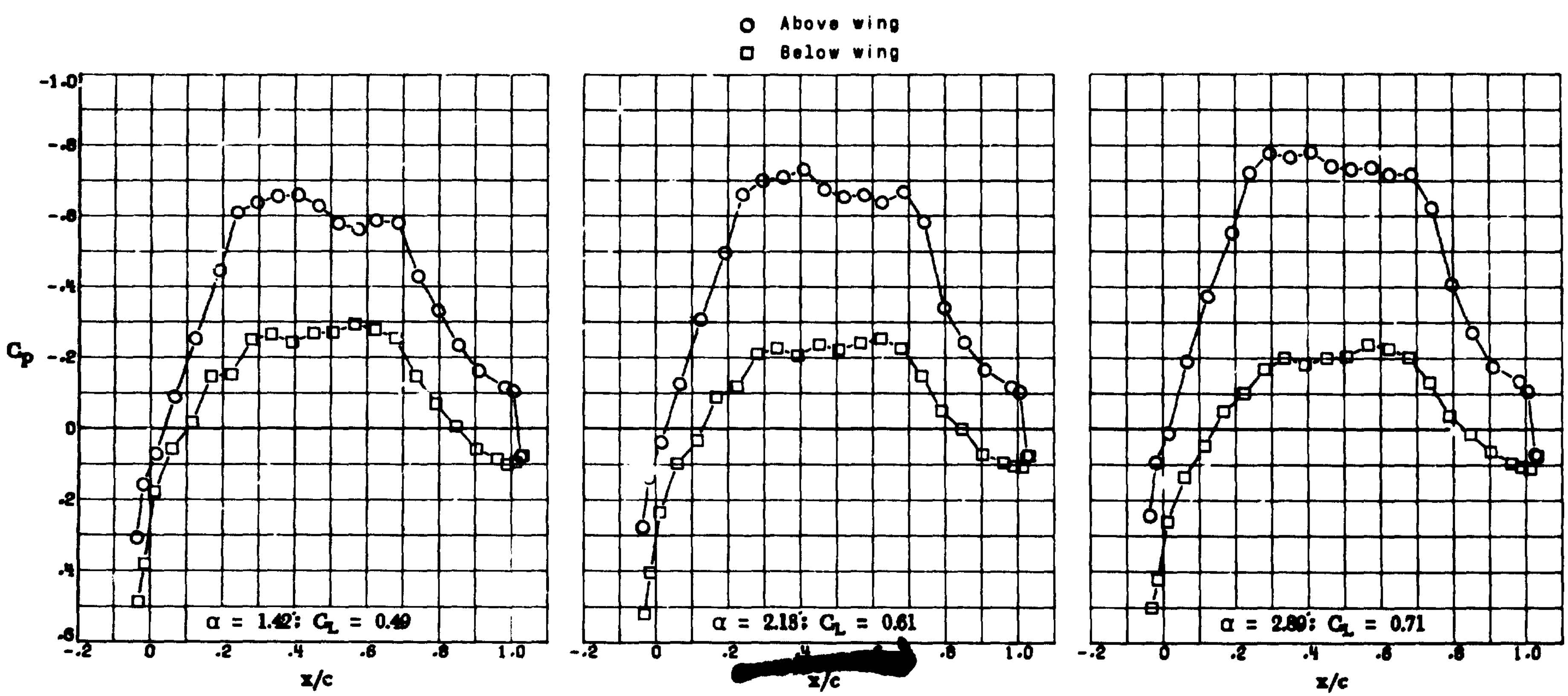

(d) M = 0.81.

Figure 29. - Continued.

[redacted]

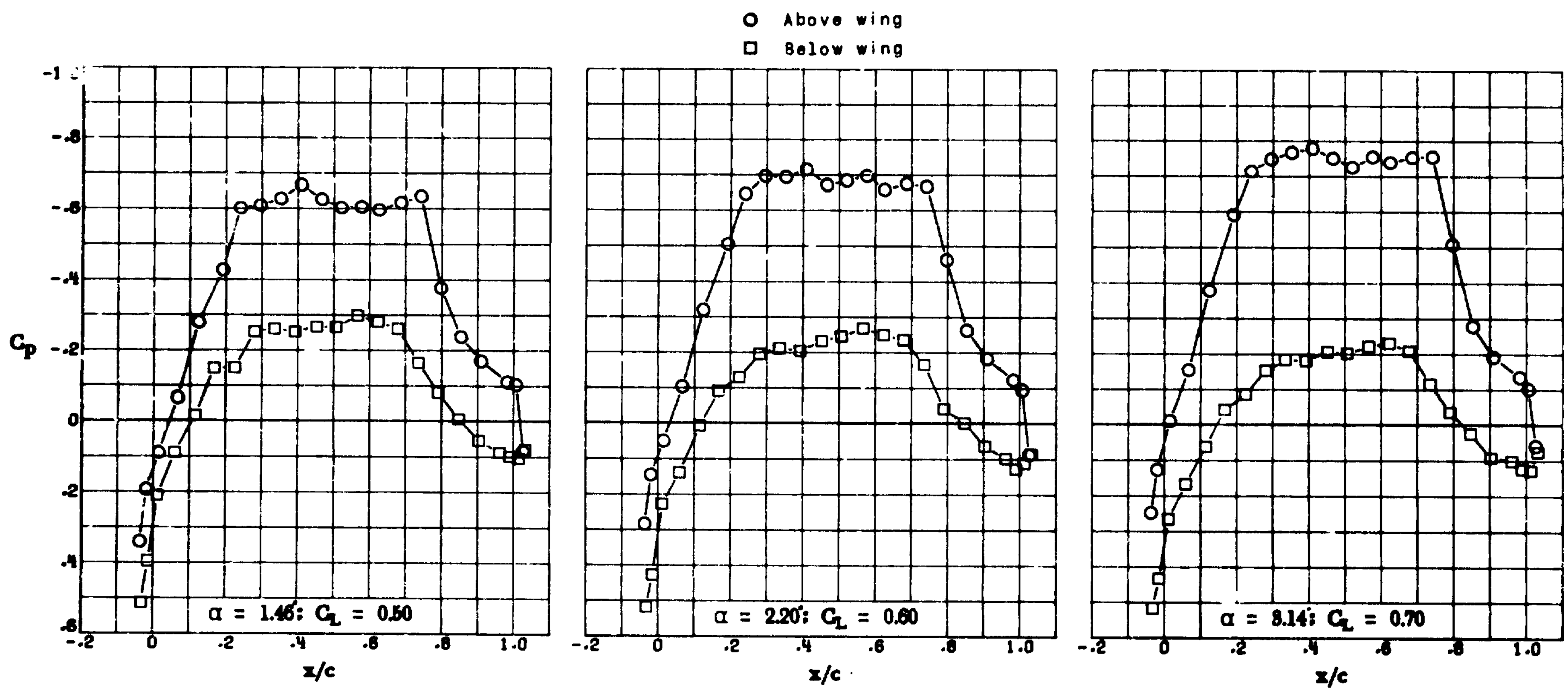

(e) M = 0.82.

Figure 29. - Concluded.

[redacted]

[redacted]

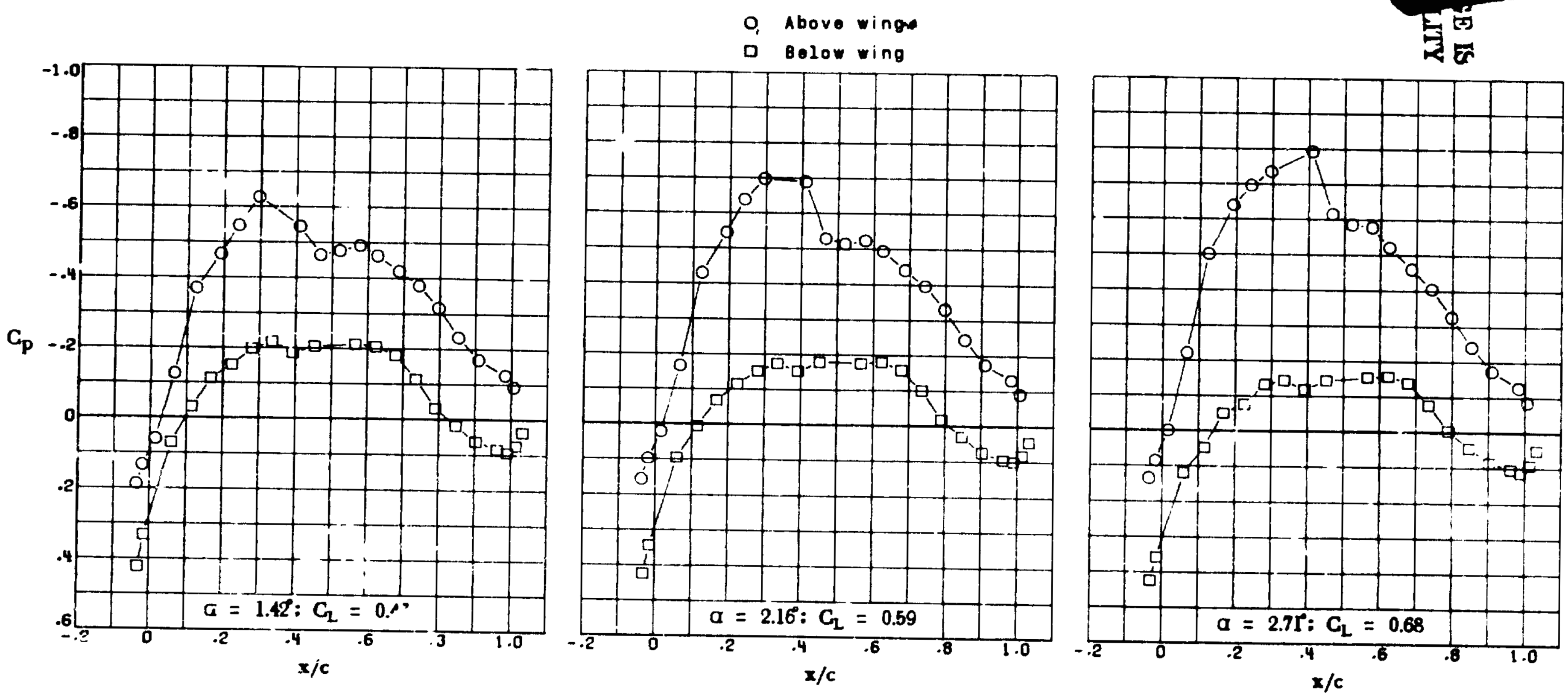

(a) M = 0.78.

Figure 30. - Fuselage pressure distribu[redacted] juncture for configuration SCW-2a.

[redacted]

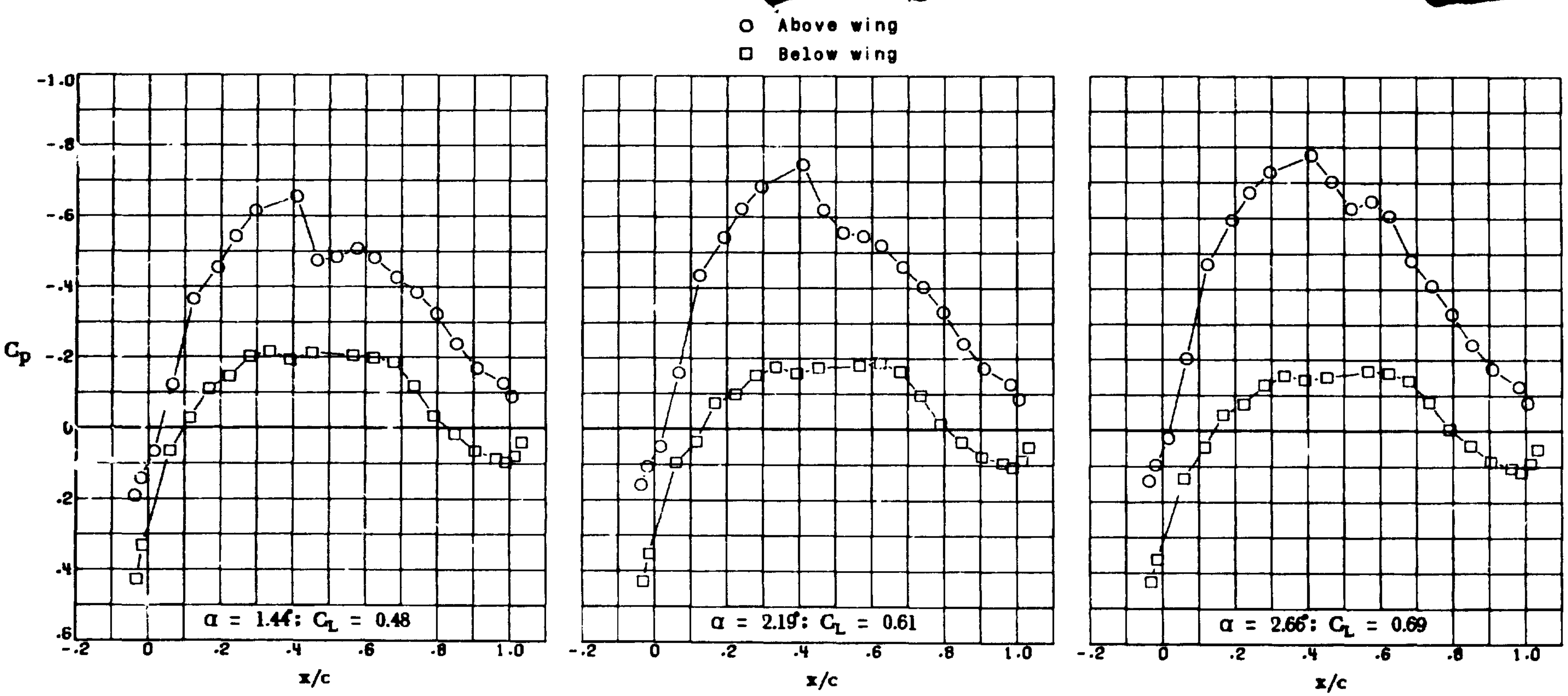

(b) M = 0.79.

Fig[redacted]

[redacted]

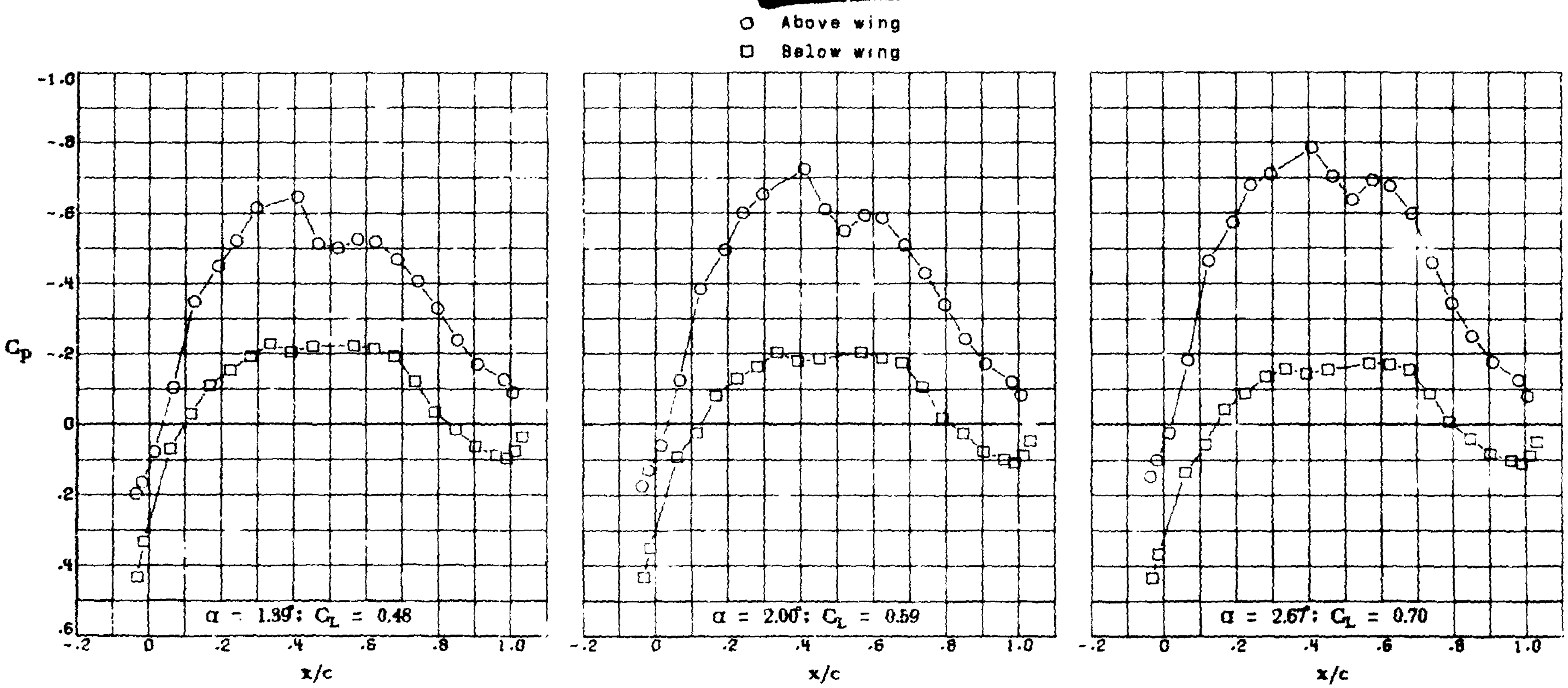

Figure 30 - Continued

ORIGINAL PAGE IS
OF POOR QUALITY

[redacted]

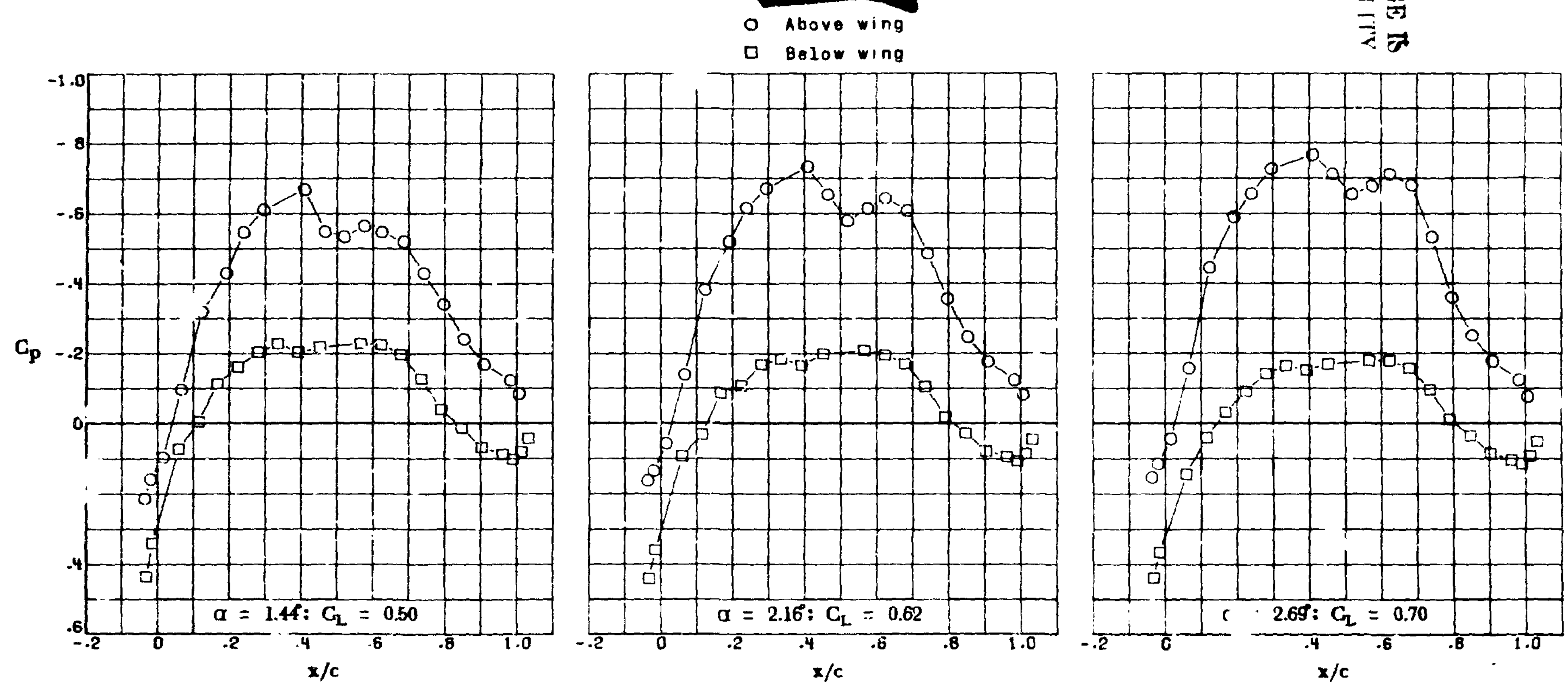

[redacted]

Figure 30 - Continued

[redacted]

[redacted]

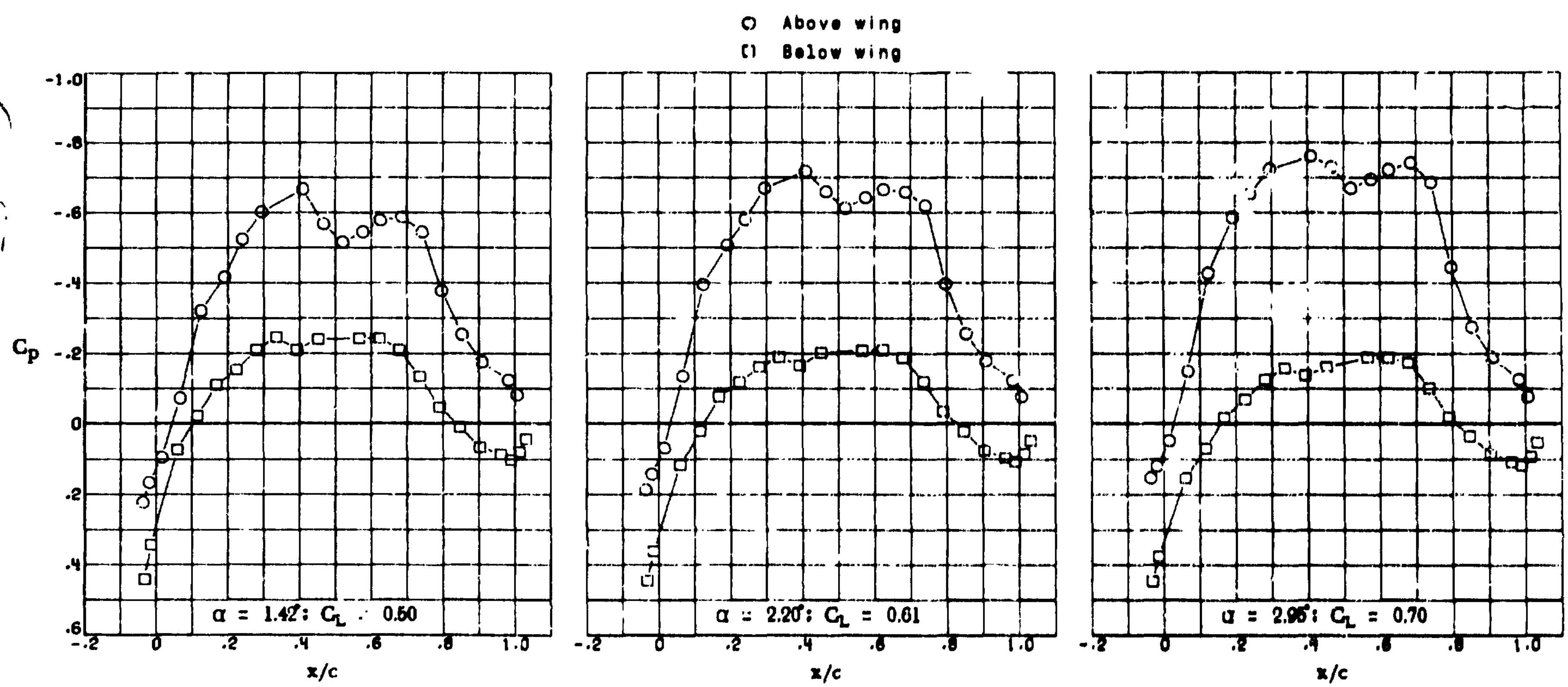

(e) M = 0.82.

Figure 30. - Concluded.

[redacted]

[redacted]

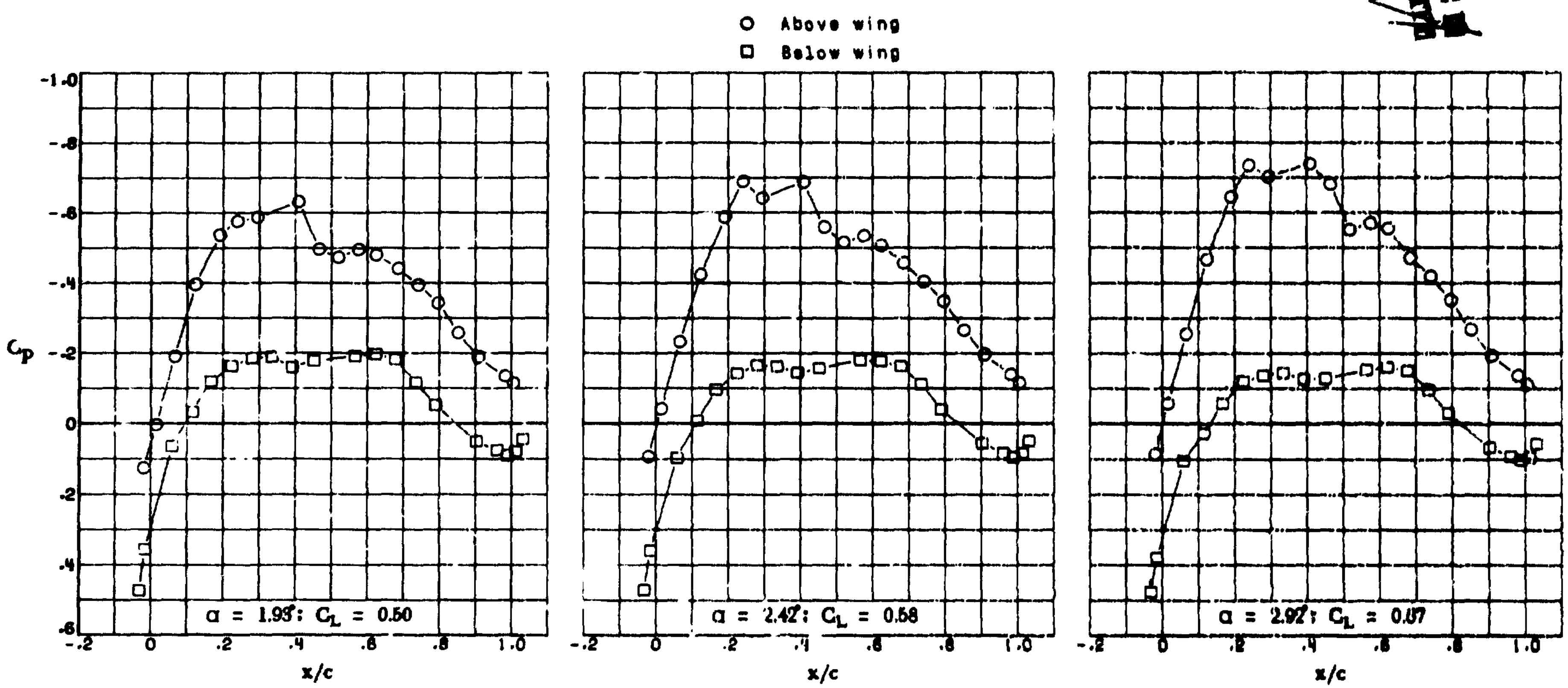

ORIGINAL PAGE IS
OF POOR QUALITY

[redacted]

Figure 31. - Fuselage pressure distributions at the wing-fus[redacted] juncture for configuration SCW-2h.

[redacted]

ORIGINAL PAGE IS
OF POOR QUALITY

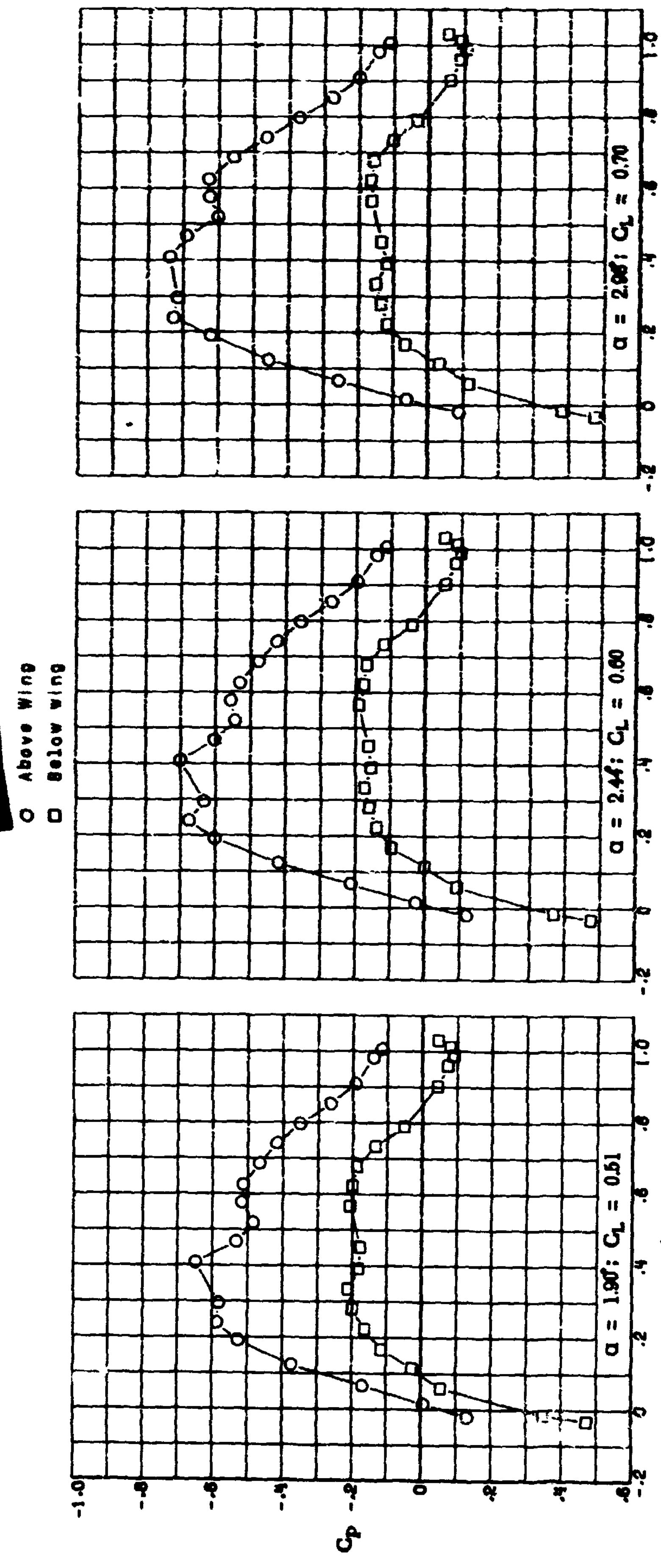

Figure 31. - Continued.

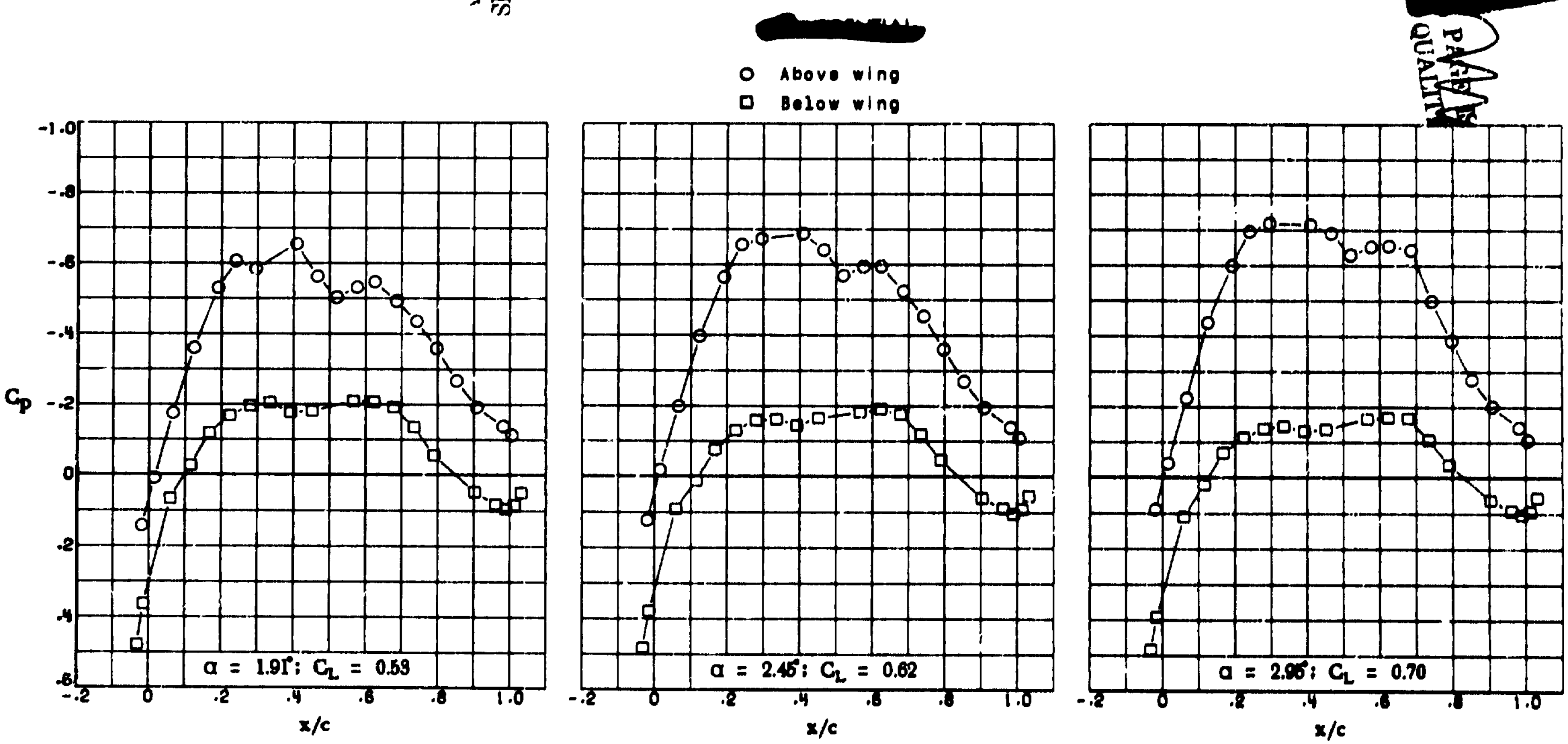

[redacted]

Figure 31. - Continued.

[redacted]

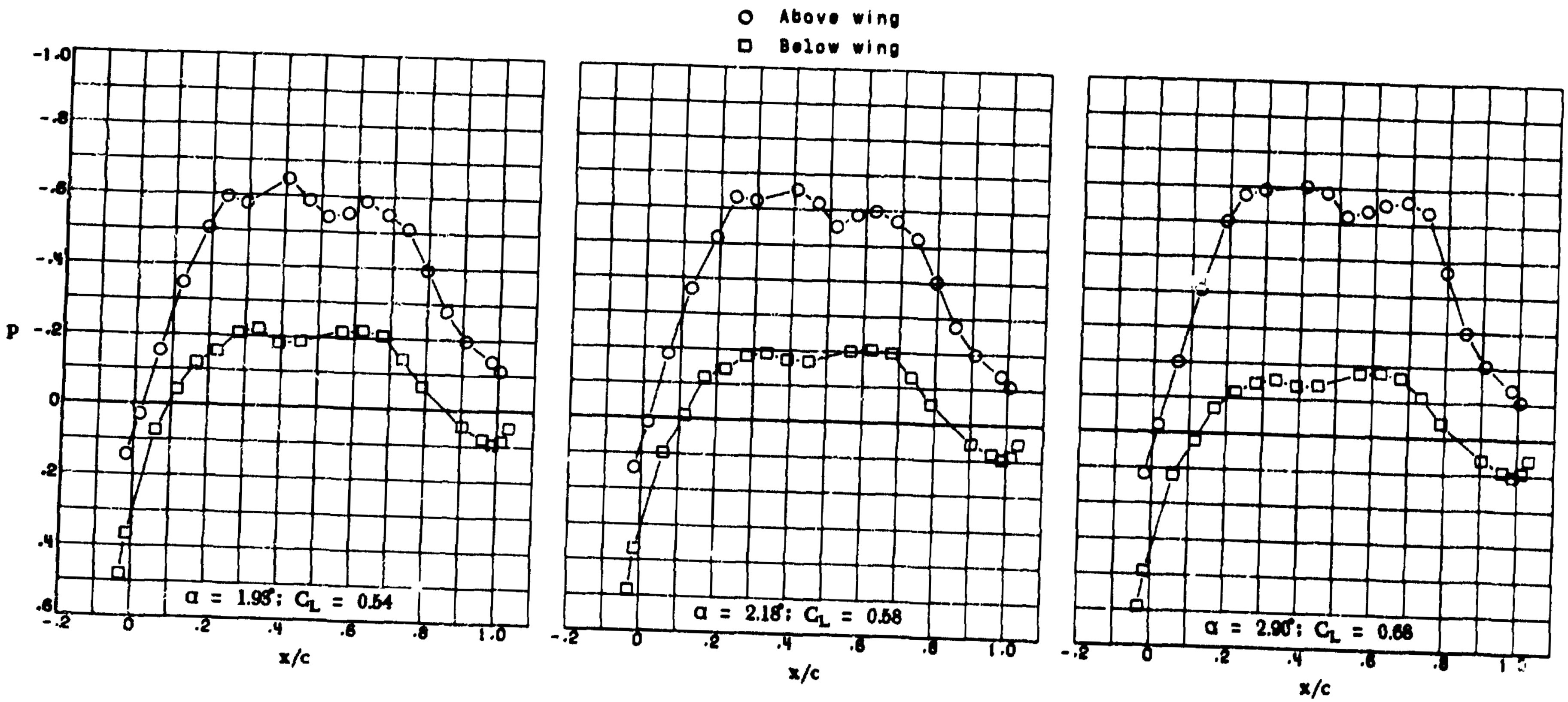

[redacted]

Figure 31. - Continued.

[redacted]

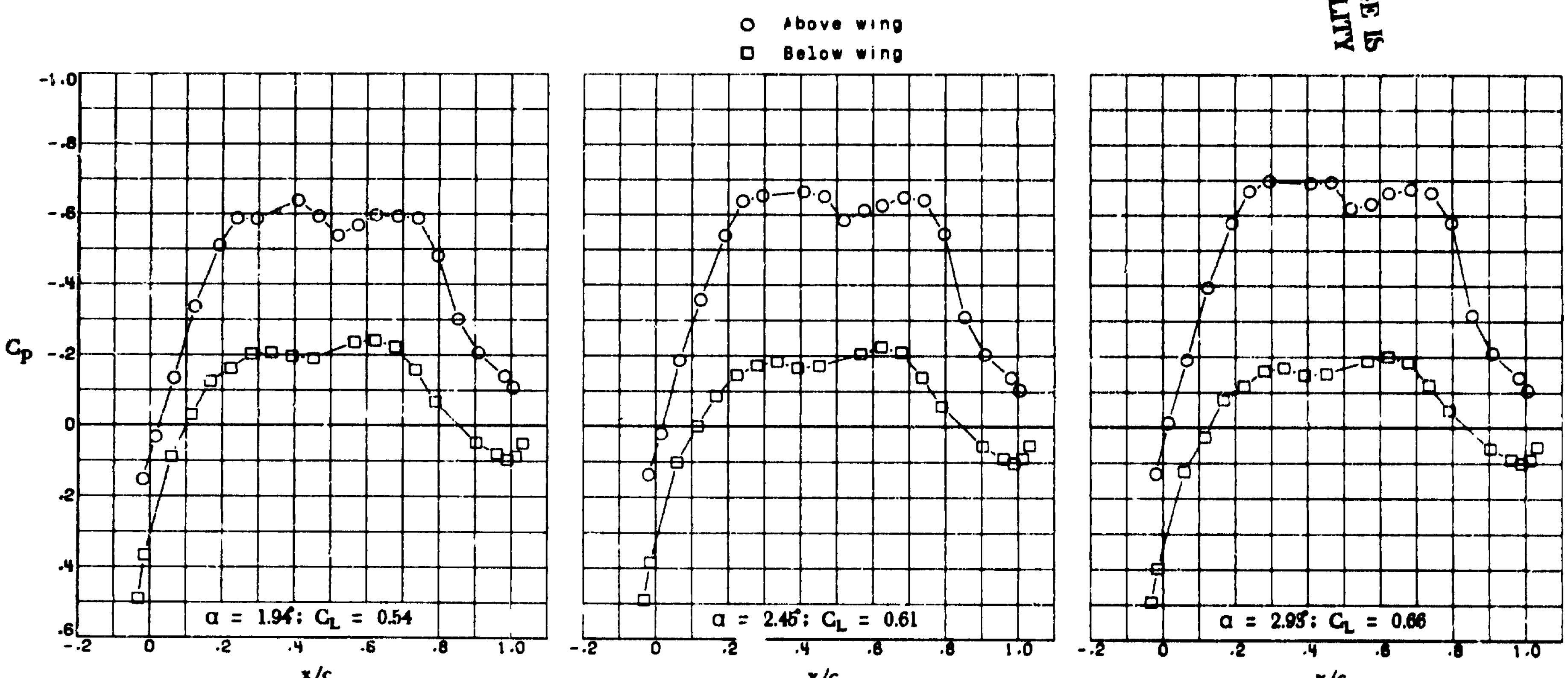

[redacted]

Figure 31 - Continued.

[redacted]

[redacted]

[redacted]

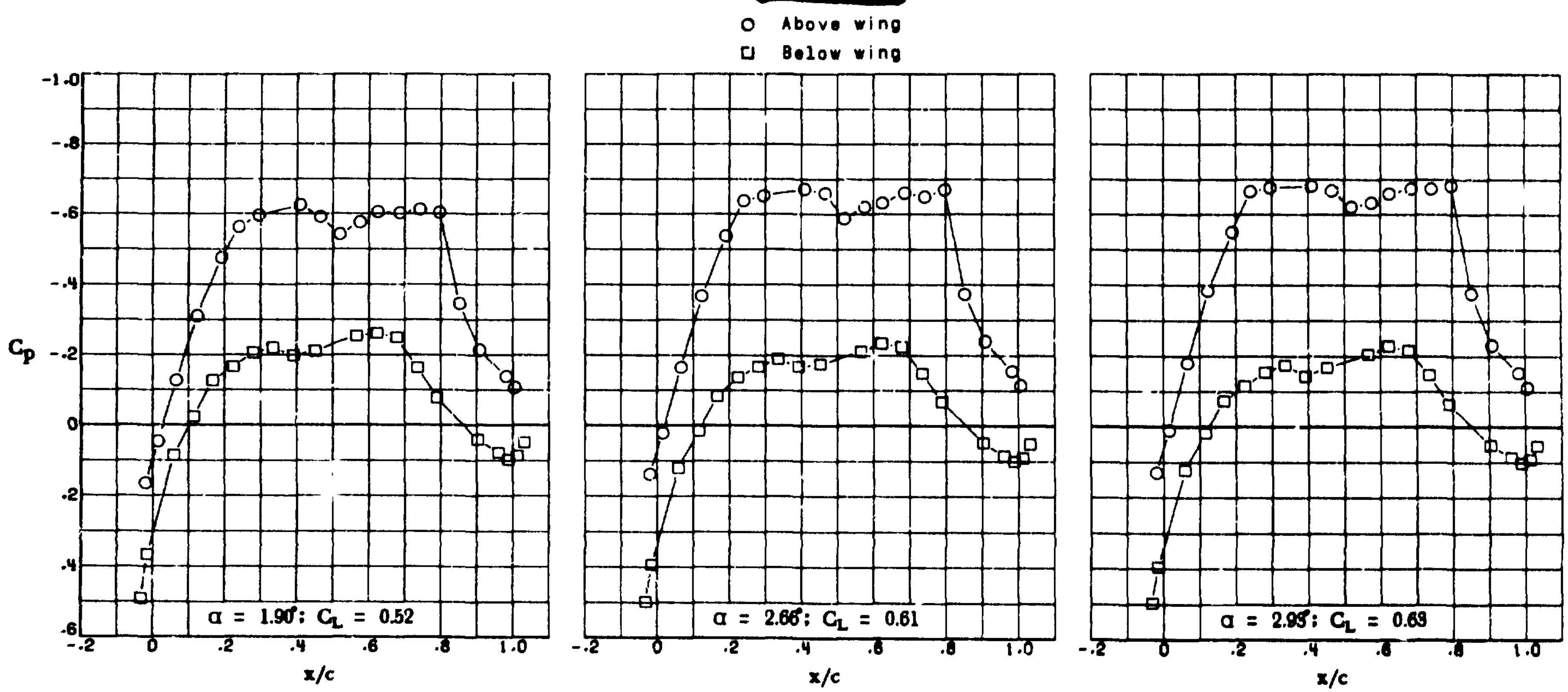

[redacted]

Figure 31. - Concluded.

[redacted]

[redacted]

[redacted]

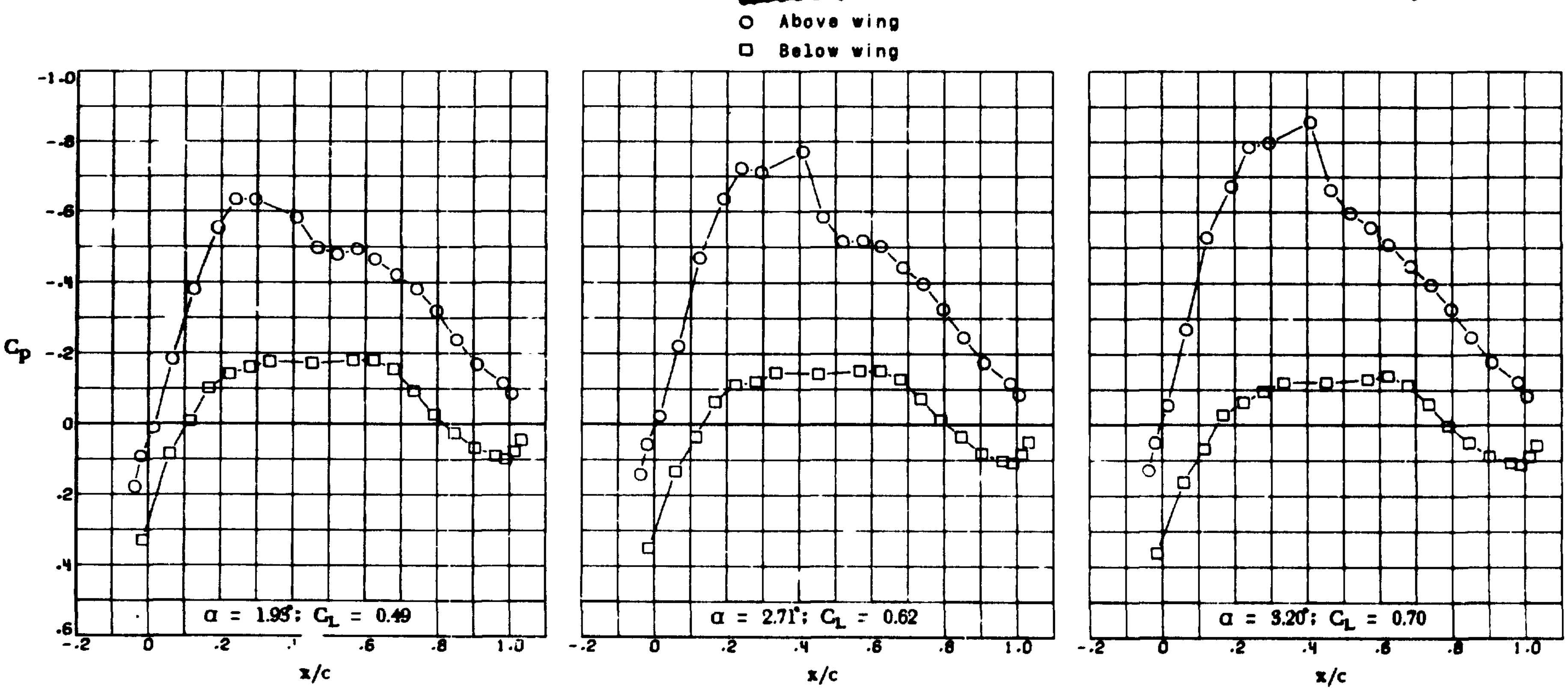

(a) M = 0.77.

Figure 32. - Fuselage pressure distribution [redacted] juncture for configuration SCW-2c.

ORIGINAL PAGE IS
OF POOR QUALITY

[redacted]

[redacted]

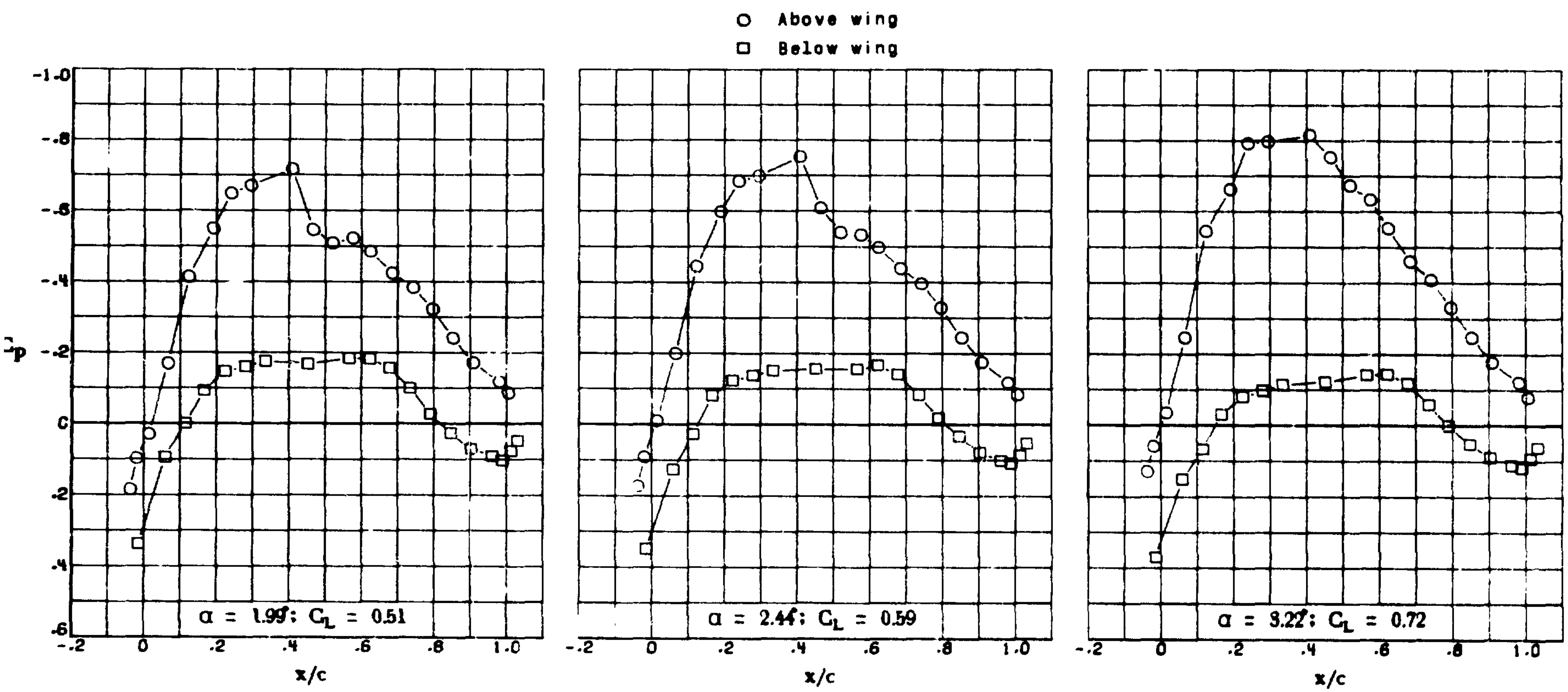

(b) M = 0.78.

[redacted]

ORIGINAL PAGE IS OF POOR QUALITY

[redacted]

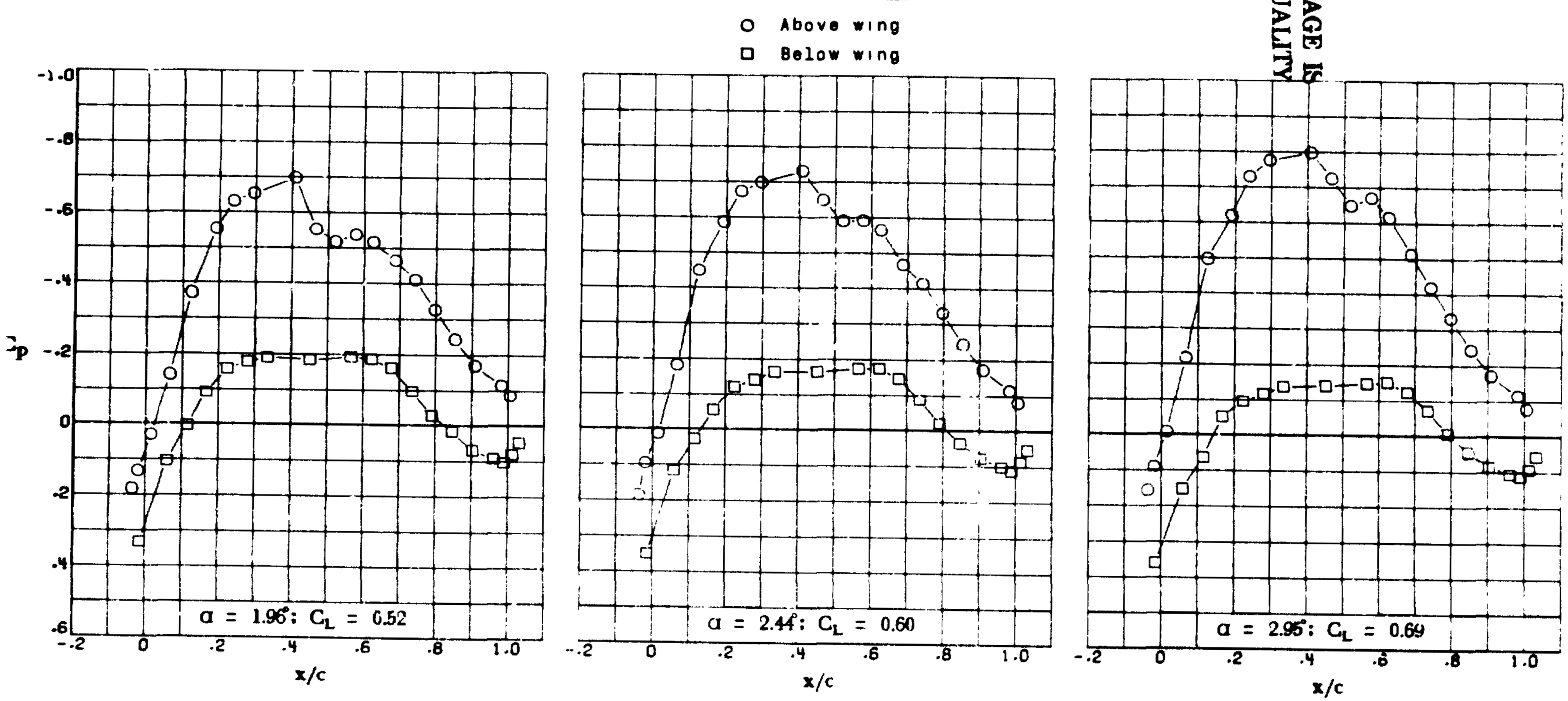

[redacted]

Figure 32. Continued.

[redacted]

[redacted]

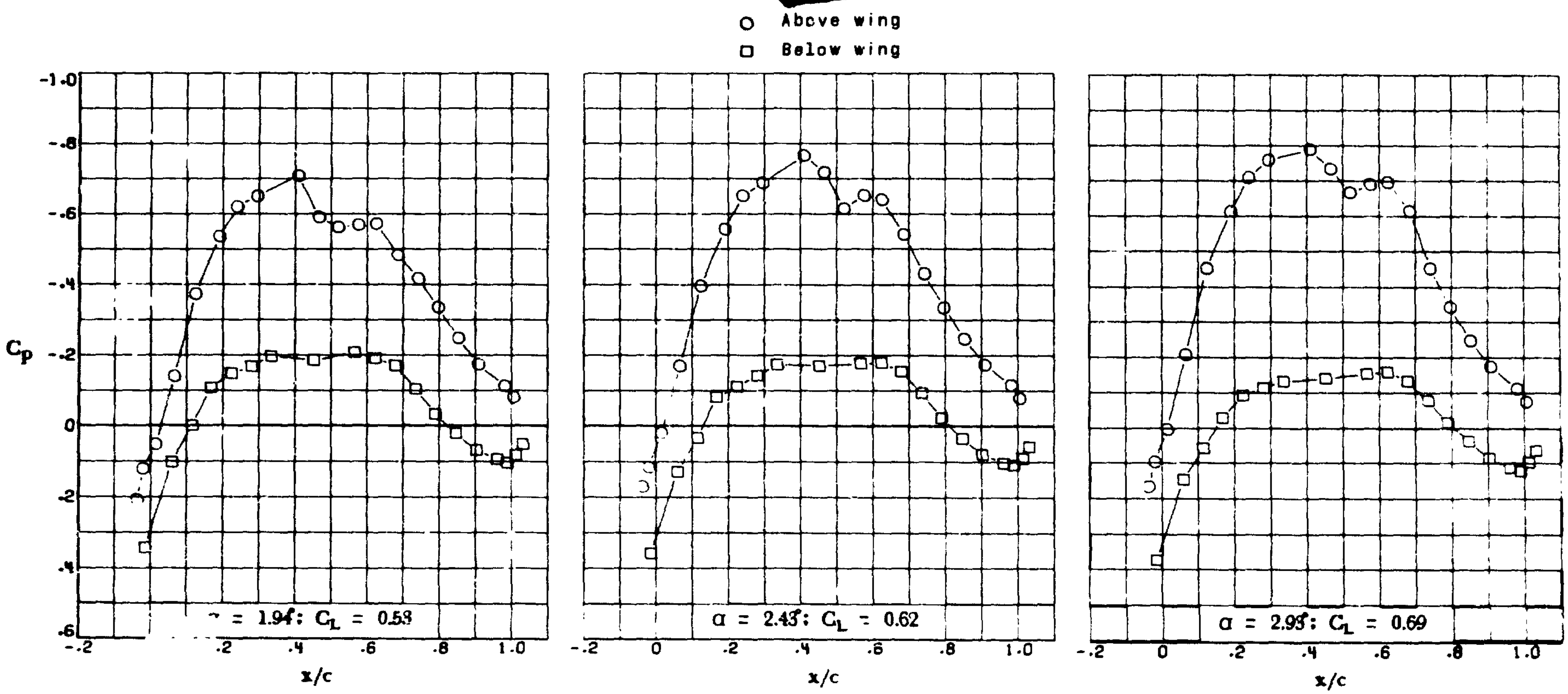

ORIGINAL PAGE IS
OF POOR QUALITY

(d) [redacted]

Figure 32. - Continued.

[redacted]

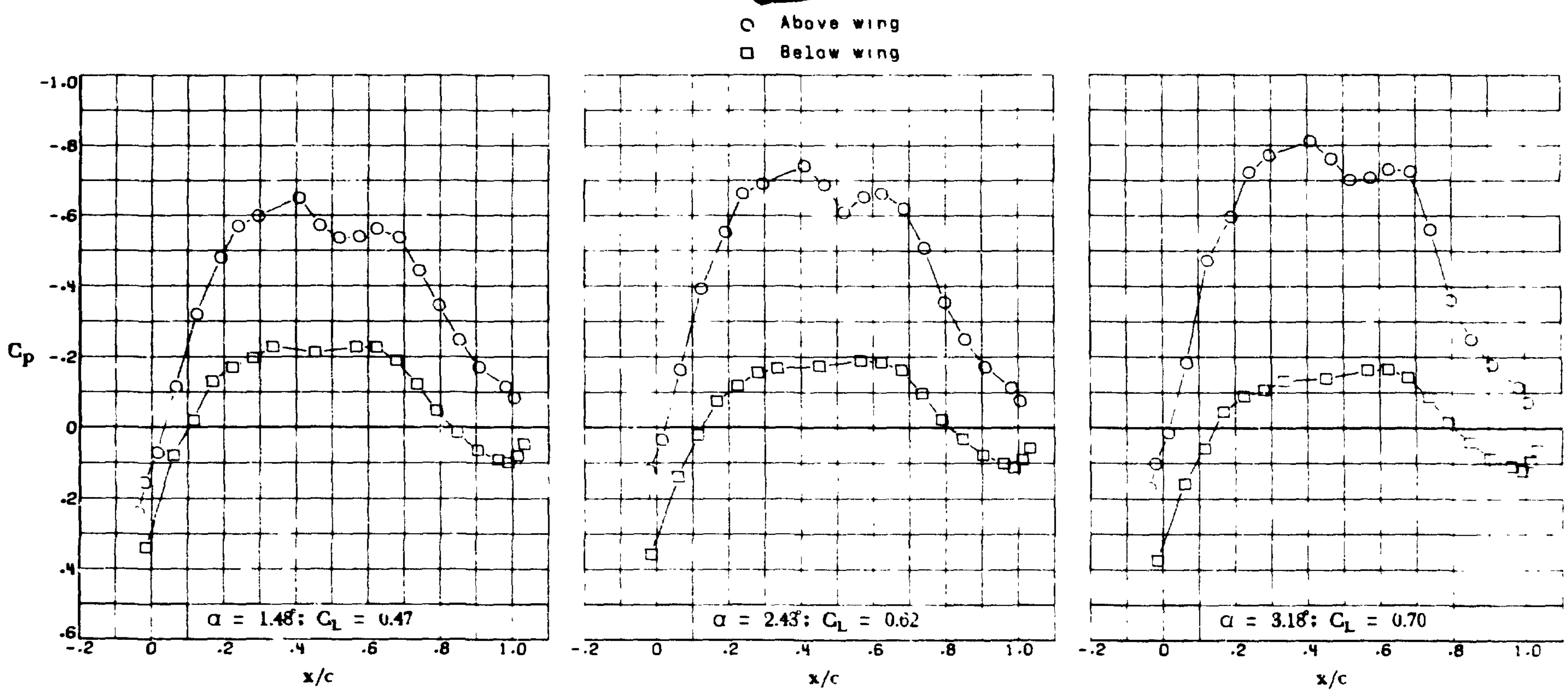

(e) M = 0.81

Figure 32. - Concluded

ORIGINAL PAGE IS
OF POOR QUALITY

[redacted]